POLITEHNICA University of Timisoara, Romania

Faculty of Electrical Engineering

Department of Electrical Machines and Drives

# Wind Turbines using Induction Generators Connected to the Grid

**Ph D Dissertation**



By **Lucian MIHET-POPA**



Supervisor: Professor **Ion BOLDEA**

October 2003

# Content of the thesis

# Preface

This thesis is submitted to the Faculty of Engineering and Science at Politehnica University of Timisoara in partial fulfillment of the requirements of the Ph. D. degree in Electrical Engineering. The most important part of research has been conducting at the Department of Electric Drives and Power Electronics from University Politehnica of Timisoara. Another important part was carried out in the Laboratory of Power Electronics and Drives and High Voltage, at the Institute of Energy Technology, Aalborg University, Denmark and in the laboratory of Power Electronics and Drives at Bee Speed, Timisoara-Romania.

The thesis was started in December 1999 with financial support from University Politehnica of Timisoara.

The project has been followed by my supervisor: Professor Ion Boldea, I would like to thank him for his supervision and his patience. I would also like to thank Professor Frede Blaabjerg, Associate Professor Birgitte Bak-Jensen and Associate Professor Ewen Ritchie, from Aalborg University – Denmark, for their help and suggestions. They hosted my experiments in their laboratories. I spent 4 month (October 2000-January 2001) at Aalborg University, when I visited Prof. Frede Blaabjerg and I worked on a project entitled "Power Plant Characteristic of Wind Farms", and then I spent 15 month (October 2001-December 2002) also at Aalborg University, when I visited Assoc. Prof. Ewen Ritchie and I worked on a project entitled "Condition Monitoring of Wind Generators".

Also thanks to my parents who gave me great support. Special thanks to my wife for giving me the motivation that I needed to actually finish this work.

I would also like to thank to my colleagues and friends from University *Politehnica* of Timisoara who helped me with their valuable advices.

Timisoara,
October, 2003.

Lucian Mihet – Popa.
mihetz@yahoo.com

# List of abbreviations

AC – Alternate Current
ADC – Analog to Digital Conversion
ASD – Adjustable Speed Drive
B – Damping Coefficient
CSI – Current Source Inverter
DAC – Digital to Analog Conversion
DC – Direct Current
DTC – Direct Torque Control
FFT – Fast Fourier Transform
IGBT – Insulated-Gate Bipolar Transistor
IG – Induction Generator
IM – Induction machine
J – Rotor Inertia
P – Proportional Regulator
$P_{el}$ – Electrical Power
PF – Power Factor
PI – Proportional Integrator Regulator
$P_{mec}$ – Mechanical power
PMSM – Permanent Magnet Synchronous Machine
p.u. – per unit
PWM – Pulse Width Modulation
RMS – Root Mean Square value
SM – Synchronous Machine
SVM – Space Vector Modulation
$T_{damp}$ – Damping Torque
$T_{em}$ – Electromagnetic Torque
$T_{sw}$ – Switching Period
$U_{dc}$ – DC-link Voltage
$U_{in}$ – Input Phase Voltage
$V_{LL}$ – Output line-to-line voltage
VSI – Voltage Source Inverter
ZOH – Zero Order Hold
$W_r$ – Rotational energy in the wind turbine rotor
WT – Wind Turbine
WTG – Wind Turbine Generator

# List of Symbols

A – area swept by the wind rotor
$C_p$ – power coefficient of wind turbine
D – rotor diameter of wind turbine
$D_k$, $D_l$, $D_m$ – SVM voltage vector duty cycle ratio
f – grid fundamental frequency
L - length scale
$i_{d,q}$ – d-q currents
Is – stator current
Ir – rotor current
n – rotor speed (rad/sec)
p – number of pole pairs
$P_{el}$ – Electrical Power
$P_{mec}$ – Mechanical Power
$P_s$ – Stator active power
$Q_s$ – Stator reactive power
r – rotor plane radius
$R_s$ – stator resistance
$R_{ex}$ – external resistance
$R_r$ – rotor resistance
s – slip / Laplace operator
t – time
$t_i$ - turbulence intensity
Te – electromagnetic torque
$T_0$ – zero vector on-time
$T_{rot}$ – aerodynamic torque of wind turbine
$T_{damp}$ – damping torque
$u_a$, $u_b$, $u_c$ – three phase voltage system
$u_{d,q}$ – two phase voltage
$u_0$ – mean wind speed
$X_{ex}$ – external reactance
$V_{DC}$ – DC link voltage
w – wind speed
$w_{sfic}$-equivalent wind speed
$w_{spoint}$ – hub wind speed
$\rho$ - air density
$\lambda$ – tip speed ratio
$\lambda_{d,qs}$ – stator d-q flux vectors
$\omega_r$ – electrical angular velocity of the rotor
$\Omega r$ – rotor speed (rpm)
$w_s$ – wind speed
$\theta_{rot}$ – position of the rotor wind turbine
$\theta_e$ – the reference angle

# Romanian Resume – Rezumatul în limba română

## Sumarul Tezei

Teza este structurata pe sase capitole principale si unul de concluzii. Aceasta teza este dedicata sistemelor de conversie a energiei eoliene cu masini de inductie conectate la retea. Generatoarele de inductie antrenate de turbine eoliene au devenit, recent, foarte utile, deoarece se adapteaza perfect pentru uzul acestora datorita constructiei robuste, fiabilitatii, costului redus, facand fata unor conditii dificile de functionare si necasitand o intretinere usoara. Conversia energiei eoliene este sursa de generare a electricitatii cu cresterea ceea mai rapida datorita capacitatii de dezvoltare din intreaga lume, si se estimeaza ca va ramane asa si in urmatoarea decada. In ultimul deceniu sistemele de conversie a energiilor neconventionale si in special sistemele de conversie eoliana au cunoscut o dezvoltare deosebita. Cele mai recente procedee de obtinere a energiei eoliene, utilizand generatoare electrice, au fost realizate in baza avansarii cunostintelor despre reglare si control, utilizand electronica de putere, in special pentru sistemele cu viteza variabila.

***Capitolul 1*** prezinta principalele configuratii ale generatoarelor eoliene, evidentiind componentele principale ale acestor sisteme de conversie a energiei, alaturi de modelul matematic care realizeaza conversia energiei cinetice a vitezei vantului, in energie mecanica prin intermediul unui sistem de transmisie mecanica, iar apoi utilizand un generator electric in energie electrica. In realizarea conversiei energiei un rol important este ocupat de generatorul electric care a devenit o parte semnificativa a sistemului de conversie, fiind utilizat in prezent la puteri de pana la 3 MW/ unitate, in cazul celor de inductie, si pana la 4.5 MW/unitate, in cazul generatoarelor sincrone.

***Capitolul 2*** ilustreaza cele mai raspandite si moderne sisteme eoliene, evidentiind cele mai importante realizari in domeniul masinilor electrice si al electronicii de putere utilizate in acest domeniu. O comparatie intre sistemele de vant cu viteza constantă si viteza variabila, atat pentru generatoarele autonome cat si pentru cele conectate la retea, a fost realizata, evidentind atat avantajele cat si dezavantajele topologiilor respective. Deasemenea, strategiile de control ale turbinelor si tendintele actuale in acest domeniu sunt prezentate pe scurt. Estimarea eficientei a trei sisteme cu generatoare eoliene este facuta cu scopul de a releva pierderile diferitelor parti componente, cum ar fi generatorul electric, cutia de viteze (unde este cazul) sau convertorul static. Pentru determinarea avantajelor diferitelor configuratii de turbine eoliene referitoare la cantitatea de energie produsa intr-un anumit interval de timp pentru un anumit loc este necesara calcularea distributiei energiei anuale. Aceasta analiza poate fi facuta cu ajutorul unor metode statistice cum ar fi metoda de distributie Weibull sau Rayleigh. Aceste metode sunt prezentate pe scurt cu evidentierea diferentei dintre energia anuala produsa de o turbina de vant cu viteza variabila si una cu viteza constanta.

***Capitolul 3*** este dedicat modelarii si simularii turbinelor de vant cu viteza constanta ,care utilizeaza generatoare de inductie cu rotorul in colivie, conectate direct la retea prin intermediul unui transformator. Modelul propus contine modelul vitezei de variatie a vantului, modelul aerodinamic, care include rotor si paletele turbinei, modelul de transmisie mecanic, care,la randul sau include cutia de viteze, modelul generatorului electric, un soft starter pentru conectare la retea, alaturi de o baterie de condensatoare pentru reglarea factorului de putere. Sistemul de conversie eolian a fost implementat „utilizand pachetele de programe dedicate DIgSILENT si Matlab-Simulink, care permit accesul la o librarie vasta, dar care necesita o implementare relevanta a modelului turbinei.

***Capitolul 4*** este dedicat unui sistem de conversie a energiei eoliene cu viteza variabila limitata utilizand un generator de inductie cu rotorul bobinat si impedanta suplimentara. Analiza acestui sistem a fost realizata atat in regim stationar ,cat si in diferite regimuri tranzitorii ,utilizand simulari digitale realizate cu ajutorul unor softuri dedicate Mathcad si Matlab / Simulink. De asemenea un calcul analitic amanuntit pentru studiul regimurilor dinamice a fost dezvoltat si implementat in Matlab / Simulink. Pentru analizarea si validarea rezultatelor de simulare s-a construit si testat un sistem experimental.

***Capitolul 5*** prezinta un sistem de conversie a energiei eoliene cu viteza variabila si generator de inductie dublu alimentat. O strategie de control care realizeaza decuplarea puterilor activa si reactiva este ,deasemenea ,implementata alaturi de comanda si controlul convertorului de frecventa din rotorul masinii. Studiul analitic al buclei de reglare al curentului si puterii este realizat iar regulatoarele corespunzatoare sunt selectate si acordate pe baza simularilor realizate in Matlab-Simulink.

***Capitolul 6*** sintetizeaza un studiu experimental detaliat al unui sistem de masura, monitorizare si achizitie de date a unui sistem de conversie a energiei eoliene cu viteza variabila care utilizeaza masina de inductie dublu alimentata. De asemenea, studiul include dezvoltarea si testarea unor defecte alaturi de diverse tehnici de monitorizare, detectie si diagnoza destinate sistemelor de conversie a energiei eoliene. De asemenea capitolul prezinta o sinteza asupra posibilelor tipuri de defecte dezvoltate in masinile asincrone alaturi de tehnici de monitorizare si detectie existente in literatura. Sistemele de monitorizare, achizitie si detectie trebuie proiectate astfel incat sa poata recunoaste, chiar de la inceput, dezvoltarea unor defecte si prin aceasta preintampinarea unor posibile catastrofe, permitand personalului de intretinere sa programeze repararea sau inlocuirea defectelor. Acest lucru va duce la pastrarea functionarii instalatiei in conditii acceptabile mai mult timp la un pret de cost mult mai scazut.

***Capitolul 7*** prezinta o trecere in revista a acestei teze de doctorat cu concluziile aferente, principalele contributii alaturi de cateva sugestii pentru continuarea cercetarii acestui fascinant subiect. Teza mai contine 5 anexe cu detalii despre modelele matematice implementate, programele de simulare dezvoltate pentru studiul diferitelor regimuri de functionare cat si despre parametrii masinilor electrice si convertoarelor statice implementate si testate in laborator. De asemenea anexa A include lista lucrarilor stintifice ale autorului publicate si prezentate la Conferinte Internationale.

# Contributiile Tezei de Doctorat

Capitolele 3-6 prezinta contributiile acestei teze, reprezentand material original, publicate anterior in patru lucrari stintifice, avandu-l ca prim autor pe autorul acestei teze de doctorat. Aceste lucrari au fost prezentate in reviste si conferinte internationale in anii 2002 si 2003, iar unul dintre articole a fost acceptat pentru publicare in IEEE-IAS Transactions (Appendix A, [64-69]).

***Principalele contributii ale acestei teze de doctorat sunt:***

Modelarea si simularea turbinelor de vant cu viteza constanta care utilizeaza generatoare de inductie cu rotorul in colivie de 500 kW si 2 MW, conectate la retea prin intermediul unui soft-starter si transformator. Modelul turbinei eoliene include: modelul de variatie al vitezei vantului, modelul aerodinamic care cuprinde rotorul turbinei si paletele, modelul de transmisie care include cutia de viteze si modelul generatorului de inductie alaturi de o baterie de condensatoare pentru compensarea factorului de putere. Modelul mai cuprinde controlul soft-starterului si blocul de control al unghiului de modificare al paletelor, utilizand o bucla de control activa bazata pe puterea masurata si puterea de referinta (capitolul 3). Implementarea si simularea acestui sistem a fost realizata utilizand un soft dedicat simularii sistemelor de putere, DIgSILENT care are abilitatea de a simula circulatia de putere, diferite regimuri tranzitorii si regimul stationar incorporate in acelasi mediu de programare. De asemenea, pentru compararea si validarea acestor rezultate, sistemul prezentat anterior a fost implementat si simulat utilizand un alt soft dedicat Matlab-Simulink. Rezultatele comparative ale simularilor digitale dintre aceste 2 softuri au aratat o buna similaritate, atat in regim stationar, cat si in regim tranzitoriu. In studiul si analiza turbinelor eoliene simularile digitale s-au dovedit a fi o unealta valoroasa, oferind un grad ridicat de flexibilitate.

O noua strategie de control al puterii unei turbine de vant cu viteza constanta este implementat pe o turbina de vant de 2 MW (capitolul 3), numita controlul activ al paletelor turbinei, combina avantajele controlului pasiv de reglaj, adica simplitate datorita absentei mecanismului de reglare al pasului relativ al paletelor, cu avantajele controlului puterii prin reglarea pasului paletelor, numit controlabilitate. Astfel, se realizeaza un control suplimentar mai eficient decat controlul pasiv, destinat in special turbinelor de mare putere (> 1 MW / unitate), care face posibila evitarea unui dispozitiv tehnic complex pentru reglarea pasului paletelor rotorului turbinei.

Modelarea, simularea, implementarea si testarea unui generator eolian cu viteza variabila limitata care utilizeaza o masina de inductie cu rotorul bobinat si care are suplimentar in circuitul rotorului amplasata o rezistenta in paralel cu o inductanta pe fiecare faza. Analiza performantelor acestui sistem in regim stationar si in cateva situatii de regim dinamic (conectare la retea la o viteza diferita de ceea sincrona, modificarea brusca a vitezei sau cuplului mecanic la arbore), sa realizat utilizand pachetele de programe dedicate Mathcad si Matlab-Simulink. Implementarea masinii de inductie in regim dinamic s-a realizat cu ajutorul modelului matematic in coordonate rotorice. A fost aratat prin simulari digitale si rezultate experimentale ca aceasta solutie poate functiona pentru un domeniu de variatia al vitezei pana la 130 % (30 % peste viteza sincrona) cu un randament acceptabil de 75 % la incarcare nominala si un factor de putere de 0.81 (capitolul 4).

Modelarea, simularea si testarea unui set-up existent pentru o turbina de vant cu viteza variabila care utilizeaza generatoare de inductie cu alimentare dubla si care are amplasat in rotor un convertor de frecventa bidirectional cu circuit intermediar de tensiune. Implementarea sistemului de control include decuplarea puterilor activa si reactiva, acordardarea regulatoarelor pentru buclele de reglare ale curentului si puterii, traductorii de tensiune si curent, convertoarele de semnal analog-digitale si digital-analogice alaturi de un procesor de semnal cu DSP. Simulatorul de vant format dintr-un convertor de frecventa si un motor de inductie cu rotorul in colivie a fost de asemenea implementat in Matlab-Simulink. Rezultatele experimentale obtinute, atat in regim tranzitoriu cat si in regim stationar, au avut rolul de a valida modelarea si implementarea sistemului utilizand pachetul de programe Matlab-Simulink (capitolul 5).

Proiectarea si comisionarea unui sistem de masura si monitorizare, care include traductori pentru masurarea curentului, tensiunii, turatiei si temperaturii, un card pentru ajustarea semnalelor (conditionarea semnalelor), si un card pentru achizitie si prelucrare a datelor conectat la un computer, utilizat pentru o investigatie experimentala cu scopul detectarii diferitelor tipuri de defecte care apar cel mai frecvent in masina de inductie, cum ar fi scurt-circuite intre spirele infasurarilor statorului sau rotorului, pierderea unei faze sau dezechilibrul de alimentare, excentricitate statica si / sau dinamica. De asemenea, studiul include dezvoltarea si testarea unor defecte alaturi de diverse tehnici de monitorizare, detectie si diagnoza destinate sistemelor de conversie a energiei eoliene cu viteza variabila si care utilizeaza generatoare de inductie dublu alimentate.

## Perspective

Perspectivele acestei tehnologii de conversie a energiei eoliene sunt imense. Dezvoltarea rapida a electronicii de putere ofera noi provocari in acest domeniu la un pret scazut per kW.

Atragerea a cat mai multi cercetatori in acest domeniu este necesar atat pentru studiul si imbunatatirea solutiilor clasice cat si pentru proiectarea si dezvoltarea de solutii si topologii noi.

Generatoarele eoliene cu viteza variabila s-au dezvoltat dramatic in ultimii ani, fiind cele mai raspandite topologii la ora actuala peste tot in lume. Datorita dezvoltarii acestor configuratii cu viteza variabila, generatoarele de inductie cu dubla alimentare si cu convertoare de frecventa cu circuit intermediar de tensiune sunt utilizate pe scara tot mai larga. Oricum sunt inca necesare noi investigatii in controlul, proiectarea optimala sau in detectia si diagnoza acestor topologi.

Noi perspective in acest domeniu ar trebui sa includa dezvoltarea solutiilor propuse, alaturi de noi cercetari in domeniul dezvoltarii de noi alternative in controlul puterii. De asemenea simularea unei configuratii cu viteza variabila utilizand generatoare de inductie cu rotorul in colivie si doua convertoare de tensiune cu circuit intermediar, puse spate in spate, in scopul validarii unor rezultate experimentale realizate pe un set-up existent, implementat utilizand dSPACE DS1103, va fi prezentat intr-un nou articol la o Conferinta Internationala.

# Chapter 1

# Introduction

**Chapter Contents**

## 1.1. Overview

Global environmental concerns and the ever-increasing need for energy spur the search for new opportunities to use renewable energy sources. Harnessing electrical energy from wind power is a cost-effective and cleaner option. Utilizing wind power is one of the cheapest methods of reducing $CO_2$ emissions from electricity production. In the long run, ecologically energy supply can only be guaranteed by the integration of renewable resources. The worldwide potential of wind power means that its contribution to electricity production can be of significant proportions. Wind turbines produce electricity by using the natural power of the wind. The wind is a clean and sustainable fuel source. It does not create pollution and it will never run out.

This thesis deals with the wind energy conversion systems (WECS) with induction generators connected to the grid. The induction generators are suitable for grid-connected as well as standalone applications.

Wind turbines can be classified into two major groups, as depicted in Fig. 1.1:

- Horizontal axis wind turbine (HAWT);
- Vertical axis wind turbine (VAWT).

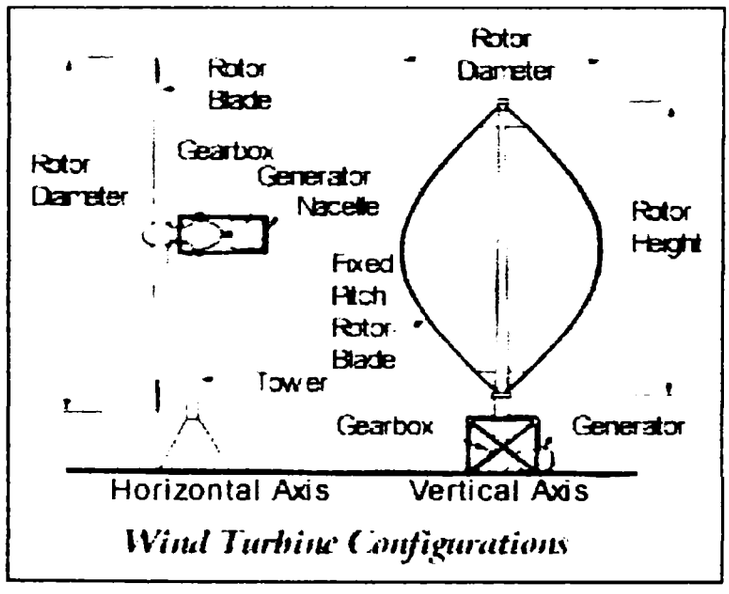


**Figure 1.1**. Wind turbine configurations with horizontal and vertical axis [1].

For the HAWT, the axis of rotation of blades is horizontal with respect to the ground, whereas for the VAWT, it is vertical, as shown in Fig. 1.1. While for the HAWT the turbine is located at higher height to take advantage of greater wind speed, VAWT must be mounted close to the ground.

The most popular WT are of horizontal axis type, three-bladed, down-wind wind turbines connected to three-phase ac grid. Major components of a modern wind turbine as well as the integral parts of these components are shown in Fig. 1.2.

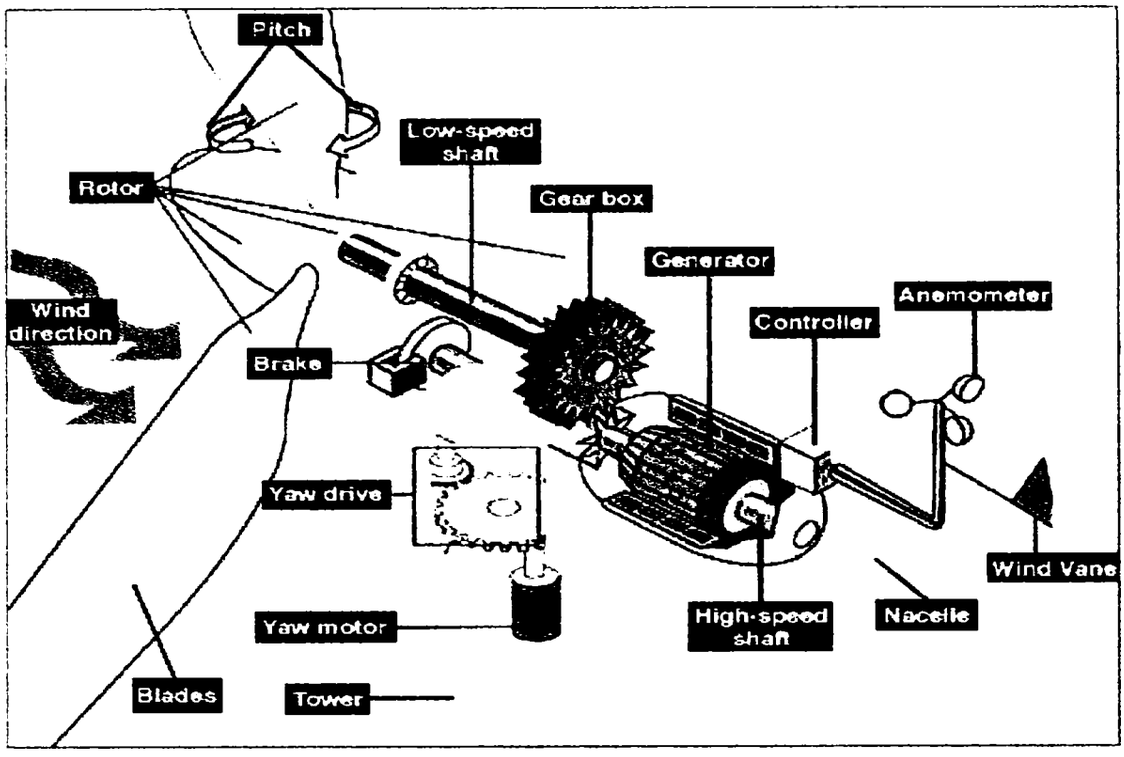


**Figure 1.2.** Assembly diagram of a typical wind turbine [2].

The principal components of a modern wind power plant are the tower, the rotor and the nacelle, which accommodates the transmission mechanisms and the generator, and for a horizontal axis devices, the yaw systems for steering in response to changes in wind directions, as can also be seen in Fig. 1.2.

The wind turbine consists usually of three blades or two or just one rotor blades, mounted on the main shaft. The blades are made of glass-fibre reinforced polyester or wood-epoxy. The nacelle (which houses the gear box, generator and the associated controls) is mounted on the tower. The nacelle is under yaw control and is free to rotate around on a vertical axis to always face the incoming wind as closely as possible. The rotor assembly (including the blades) is connected to the gearbox mechanism. The gearbox converts low speed of the main shaft from about 15-60 rpm to high speed of the generator shaft to about 900-1800 rpm. A disk brake is used to break the shaft in case of over airspeed, when there is no need for energy or in case of maintenance. It can be applied mechanically, electrically or hydraulically.

A generator, usually an AC induction machine converts mechanical power of the shaft to electrical power. The wind turbine controller consists of a number of computers that continuously monitor the condition of the turbine and collect statistics on its operation. The controller also controls a large number of switches, hydraulic pumps, valves, and machines. The controller may check the rotational speed of the rotor and generator, its voltage and currents, the pitch angle of each rotor blade and the power quality. The pitch angle of the rotor blades can be controlled to harness more or less wind, thus optimizing the energy capture and controlling the speed in the event of excessive winds. Hydraulic actuators operating through a mechanical linkage with sufficient capacity to feather the blades control blade pitch.

## 1.2. Basics of Wind Energy Conversion Systems

The block diagram given in Fig. 1.3, showing the links between the most important components and the associated energy conversion stages, may serve as the basis for later detailed observations.

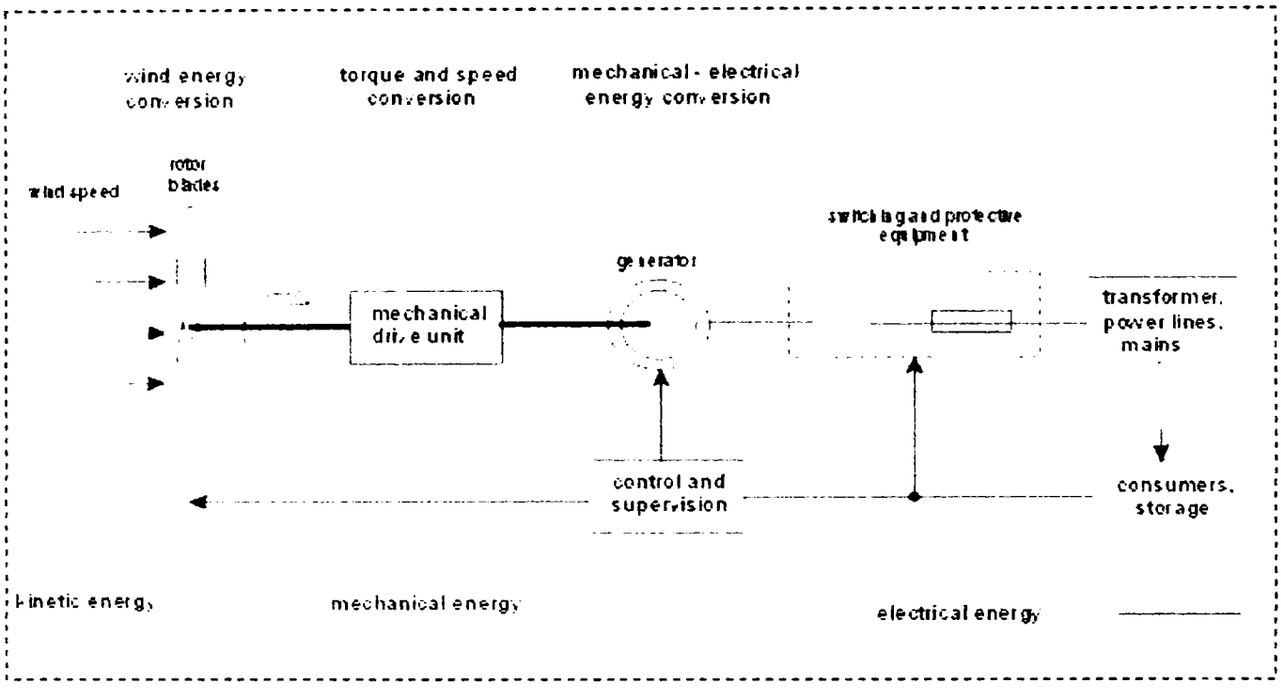


**Figure 1.3**. Power transfer in a wind energy conversion system.

From Fig. 1.3, functional structures for entire wind energy conversion system can be developed. This diagram also gives an idea of how operation can be influenced by control and supervisory processes. Thereafter the central position occupied by the generator becomes particularly significant.

The rotor blades of a wind turbine extract the flow energy from air in motion, convert it into rotational energy, and then deliver it via a mechanical drive unit (shafts and gears) to the rotor and then to the stator of a generator by mechanical-electrical conversion. The electrical energy from the generator is fed via a system of switching and protection devices, leads and any necessary transformers to the mains, to the end user or to some means of storage.

The conversion of wind power into mechanical and thereafter into electrical power may be described by the following equations [6, 7, 8]:

$$P_{mec} = k \cdot C_P(\lambda) \cdot w^3 = \frac{C_P(\lambda) \cdot k \cdot \omega_r{}^3 \cdot r^3}{\lambda^3} \quad \text{.....(1.1)}$$

$$k = \frac{1}{2} \cdot \rho \cdot A \quad \text{.....(1.2)}$$

$$\lambda = \frac{\omega_r \cdot r}{w} \quad \text{.....(1.3)}$$

$$P_{el} = \eta(\omega_R) \cdot P_{mec} \quad \text{.....(1.4)}$$

$$\frac{P_{mec}}{K \cdot \omega_r^{\,3} \cdot r^3} = \frac{P_{el}}{\eta(\omega_r) \cdot K \cdot \omega_r^{\,3} \cdot r^3} = \frac{C_p(\lambda)}{\lambda^3} \quad \text{.....(1.5)}$$

where ($C_p$) is the power coefficient of wind turbine, ($\lambda$) is the tip-speed ratio, (w) is the wind speed, ($\omega_r$) is the rotor speed, (r) is the rotor plane radius, ($\rho$) is the air density, (A) is the area swept by the rotor of wind turbine and ($\eta(\omega_r)$) is the efficiency of the generator and gear-box as a function of the rotor speed. ($P_{mec}$) is the mechanical power on the main shaft and ($P_{el}$) is the electrical power of the generator.

According to (1.1) the mechanical power converted from the power in the wind can be described as a function of the wind speed, (w), or as a function of the rotor speed ($\omega_r$), and the tip-speed ratio, ($\lambda$). The efficiency curve, $C_p(\lambda)$, is a non-linear function of the tip-speed ratio, ($\lambda$). It is determined by the blade design and the pitch angle.

The efficiency of the generator and the gear box, $\eta(\omega_r)$ is different for various rotor speeds. Contribution to the output power comes not only from the wind, but there will also be an extra power contribution, ($P_c$), during a deceleration or acceleration of the rotor speed, due to the change of rotational energy, ($W_r$), in the wind turbine rotor.

$$W_r = \frac{J \cdot \omega_r^2}{2} \quad \text{.....(1.6)}$$

$$P_c = \frac{dW_r}{dt} \approx \frac{\Delta W_r}{dt} = \frac{J\left(\omega_r(t)^2 - \omega_r(t-\Delta t)^2\right)}{2\Delta t} \quad \text{.....(1.7)}$$

where (J) is the rotor inertia and ($\Delta t$) is the sample interval.

## 1.3. The Wind Energy Resources

The wind is an intermittent energy resource, but this does not reduce its value as a source of power. The variable output from wind energy does not pose any difficulty for power system operation. It is very important for the wind industry to be able to describe the variation of wind speed. The wind speed is extremely important for the amount of energy of a wind turbine converted to electricity. Wind Turbine designers need the information to optimize the design of their turbines, so as to minimize generating cost. The energy content of the wind varies with the cube (the third power) of the average wind speed as is describe by equation (1.1), e.g. if the wind speed is twice as high it contains $2^3$ =8 times as much energy [4]. The graph bellow shows that for a wind speed of 8 meters per second (m/s) we get a power (amount of energy per second) of 314 Watts per square meter expose to the wind, where the

wind is coming from a direction perpendicular to the swept rotor area. At 16 m/s we get eight times as much power, i.e. 2509 W/m$^2$, as shown in Fig. 1.4.

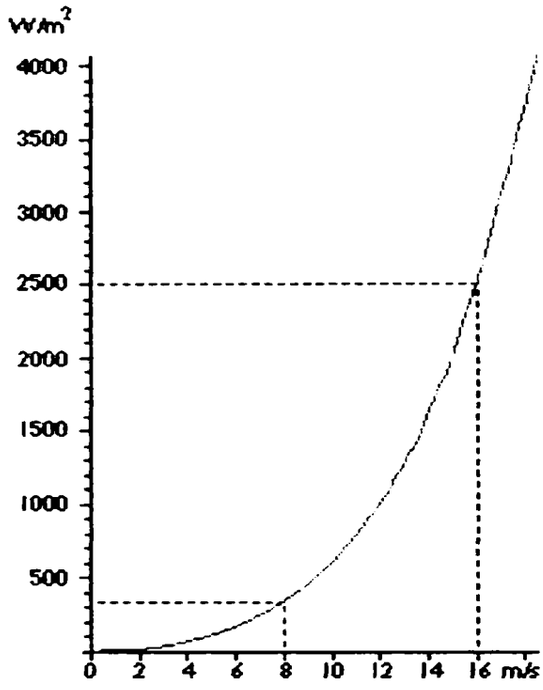


**Figure 1.4.** The power per square meter expose to the wind for different wind speeds [4].

Therefore if the wind blows at twice the speed, its energy content will increase eight-fold. In practice, a turbine at a site where the wind speed averages 8 metres per second (m/s) will produce around 80 % more electricity than those where the wind speed is 6 m/s [1].

## 1.4. Thesis objective

This thesis builds on the previous work of wind energy conversion systems by presenting and implementing the new wind turbine generator control configurations with constant speed and variable speed generators, connected to the grid.

The most important objectives of this thesis are:

- Analysis of the classical wind turbine generators and development of different alternative in the control strategy of constant-speed and variable-speed wind turbines connected to the grid;
- Modeling and simulation of the newest wind turbine configurations using induction generators;
- Building and testing a highly reliable, low maintenance, and low capital cost alternative of wind generator system with acceptable efficiency over a reasonable speed range;

- Analysis of Condition Monitoring of Wind Generators using Doubly Fed Induction Generators (DFIG) focuses on the experimental investigation for incipient fault detection and fault detection methods.

Improvements in wind energy technology mean that the trends which have led to the dramatic fall in the cost of wind energy are set to continue. Wind power is one of the world's fastest growing energy sources.

## 1.5. Description of the individual chapters

In Fig. 1.5 an outline of the structure of this thesis is presented. The thesis is structured in seven chapters and five appendices.

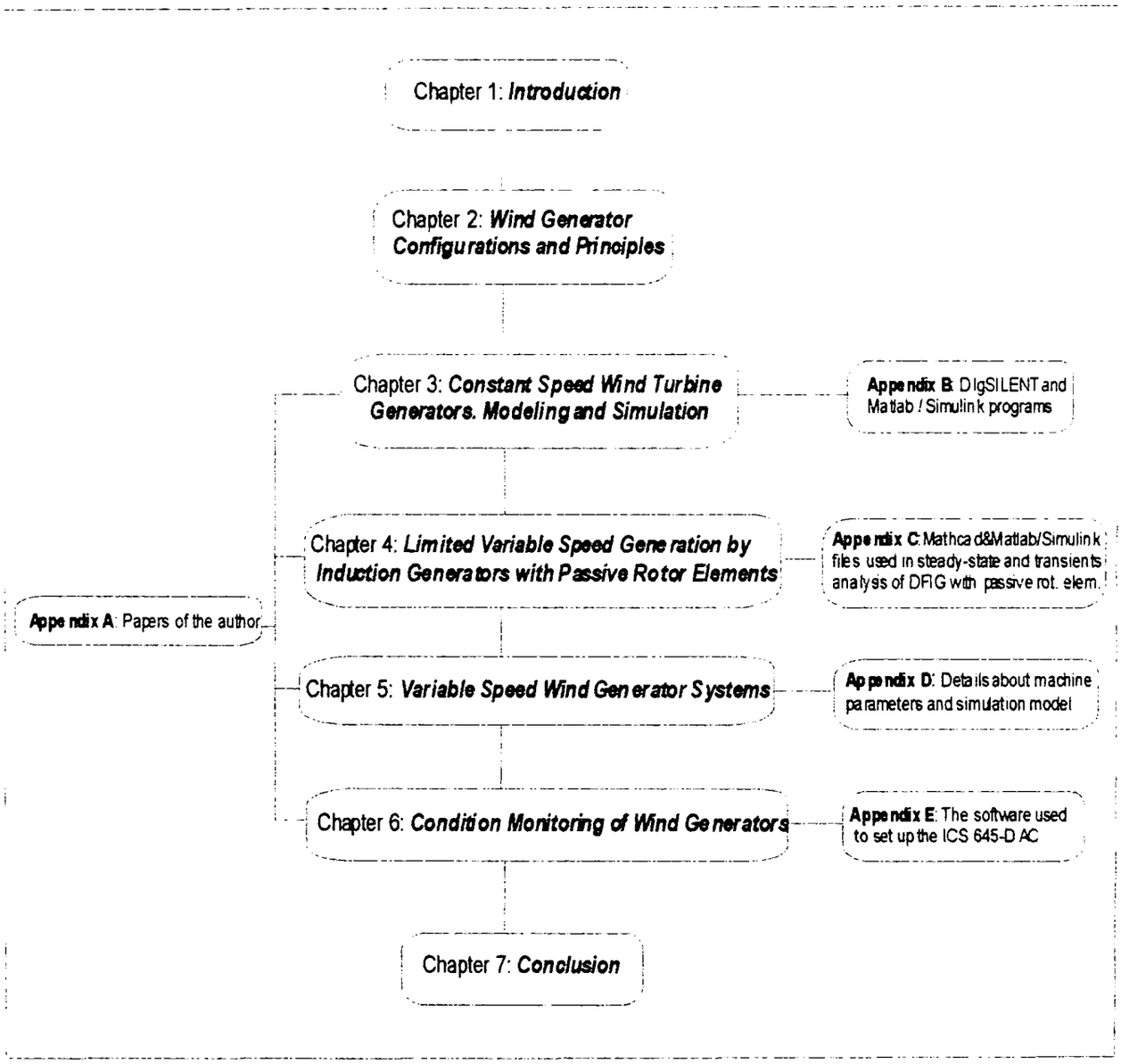


**Figure 1.5.** Overview of the thesis.

***Chapter 2 – Wind Generator Configurations and Principles***

This chapter discusses the development in the area of electric machines and power electronics with respect to wind turbine generators. The generator and power electronics configurations most commonly applied in wind turbines are also presented in details with their advantages and drawbacks. The control strategies and trends in wind turbine design are shortly presented. Estimation of the variable-speed against constant-speed wind generator systems efficiency taking into consideration the loss distribution is analyzed. In order to point out which part of the turbine accounting for the major parts of the energy losses, annual wind distribution and annual energy loss distribution of two variable-speed wind generator system concepts are compared.

***Chapter 3 – Constant Speed Wind Turbine Generators Modeling and Simulation***

In this chapter a complete simulation model of a constant-speed wind turbine with cage rotor induction generators is presented. The system model proposed is developed in the dedicated power system simulation tools DIgSILENT and Matlab-Simulink. The wind turbine model consists of different component models, such as: wind model, aerodynamic model, transmission model and the electrical components that include induction generator model, soft-starter, capacitor bank and transformer. The model developed also includes control of soft-starter, enabling simulation of the power quality characteristics and relatively new alternative control strategy of large constant-speed wind generator systems. The model is intended to simulate the behavior of the wind turbine using induction generators both during transients and during normal operations.

***Chapter 4 – Limited Variable Speed Wound Rotor Induction Generator with Passive Rotor Elements***

In this chapter, the wound rotor induction generator with limited variable-speed generation system is presented. The developed wind generator model with and without additional passive elements is verified through simulations, using Mathcad and Matlab-Simulink packages software, and experiments in steady-state and dynamic conditions as well. A rotor reference frame model has also been developed and implemented using Matlab-Simulink for a viable low-cost, low maintenance, variable-speed wind generator system with passive rotor elements. This wind generator system has also been built and tested in the laboratory.

***Chapter 5 – Variable Speed Wind Generator Systems***

The variable-speed wind turbine configurations investigated in this chapter consist of a doubly-fed induction generator connected to the power grid at the stator terminals, and the rotor is supplied through a back-to-back PWM-VSI converter. A control scheme is developed to decoupling active and reactive power control, modeled and implemented using Matlab-Simulink program package. The PWM-strategy, Stator Flux Asynchronous Vector Modulation is presented and implemented as a modulation function. An analytic analysis of the current loop and the power loop are performed, and the appropriate regulators are selected and compared through simulations. The existing experimental system was analyzed, modeled,

simulated and tested. The simulation results were compared with experiments and good agreement are obtained.

***Chapter 6 – Condition Monitoring of Wind Generators***

This chapter deals with the analysis of Condition Monitoring of Wind Generators using Doubly-Fed Induction Generators. This study focuses on the experimental investigation for incipient faults detection and fault detection methods, suitably adapted for use in wind generator systems. Three main experiments have been performed to study the electrical behavior of the induction machine. Studies also included an overview of condition monitoring pointing out faults and fault detection methods of the induction machines and design and commissioning of a measuring system-comprising signal conditioning box, AD card and transducers for current, voltage, speed and temperature. PC-based data acquisition system is used with advanced computerized data processing and acquisition. The software which controls both the acquisition and analysis of the signals is written in Matlab and has been developed as a sub-part of the monitoring system. Also, this chapter has shown that the detection of different type of faults is possible by time and frequency domain analysis. The frequency spectrum of the stator and the rotor line currents was found to give the best results. The theoretical and experimental results have clearly demonstrated that the machine current signature analysis, the negative-sequence and the instantaneous power detection methods can diagnose turn-to-turn faults and the presence of an unbalance in one stator and rotor phase of doubly-fed induction machine systems.

***Chapter 7 – Conclusion***

The main contributions of this thesis are reviewed and ideas for future work are presented. The final conclusions and some discussions are also drawn in this chapter.

***Appendix A – Publications of the author***

This Appendix includes a list of the published scientific literature by the author of the thesis.

***Appendix B – DIgSILENT and Matlab / Simulink programs***

This appendix contains more details about wind generator system developed in DIgSILENT, including composite models and control slot DSL code of rotor wind model, aerodynamic model, transmission model, asynchronous machines model, pitch control block, soft-starter controller and power factor compensation model and Matlab / Simulink programs with machines parameters.

***Appendix C – Mathcad & Matlab / Simulink files used in steady-state and transient's analysis of DFIG with passive rotor elements***

This appendix contains details about the parameters of three phase wound rotor induction machine and the programs developed in Mathcad for steady-state analysis and in Matlab for dynamic analysis. Also, the complete Simulink scheme are presented.

***Appendix D - Details about machine parameters and simulation model***

This appendix contains more details about DFIG parameters, complete simulation model implemented in Matlab / Simulink, including rotor converter model with details about the control modulation strategy-SFAVM and the control program developed in Ansi C used to control the rotor converter.

***Appendix E - The software used to set up the ICS 645-Data Acquisition Card***

The ICS-645 Matlab Application Software is designed as a starting point from which a user can build application-specific software. This driver software is intended to be used with the Matlab data analysis and graphing software. To access the ICS-645 Matlab Application Software and implicitly to record and process the data it was necessary to build a program for each task using the Matlab software package tool. This program has been performed to plot the spectrum of signals and then to assess the FFT analysis to diagnostic strategy and will be presented in appendix.

## References

[1] http://www.awea.com, The American Wind Energy Association, Wind Turbine Configurations.

[2] http://www.eren.doe.gov/wind/feature.html, *Wind Energy Program-How Do Wind Turbines Work?*, US Department of Energy.

[3] Saifur Rahman, "Green Power. What is it and where can we find it?", IEEE - Power & Energy Magazine, January / February 2003, pp. 30-37.

[4] www.windpower.org/tour/wres/enrspeed.htm, Guided Tour on Wind Energy, Danish Wind Industry Association.

[5] S. Muller, M. Deicke and Rik W. De Doncker, "Doubly Fed Induction Generator Systems for Wind Turbines", IEEE Industry Applications Magazine, May-June 2002, pp. 26-33.

[6] Torbjorn Thiringer and Jan Linders, "Control by Variable Rotor Speed of a Fixed-Pitch Wind Turbine Operating in a Wide Speed Range", IEEE Transactions on Energy Conversion, Vol. 8, No. 3, September 1993, pp. 520-526.

[7] Siegfried Heier, "Wind energy conversion systems", book, John Wiley & Sons Inc., New York, 1998.

[8] Quincy Wang and Liuchen Chang, "An Independent Maximum Power Extraction Strategy for Wind Energy Conversion Systems", Proceedings of the 1999 IEEE Canadian Conference on Electrical and Computer, Engineering Shaw Conference Center, Edmonton, Alberta, Canada, May 9-12, 1999, pp.1142-1147.

# Chapter 2

# Wind Generator Configurations and Principles

**Chapter Contents**

## 2.1. Overview

The installation of wind turbines in power systems has developed rapidly through the last 20 years. During 1999, 3920 MW of wind turbine capacity was installed in the world, making up a total accumulated installation of 13.932 MW of wind power at the end of 1999 [1]. At the end of 2000, the worldwide wind energy capacity was 17.500 MW, of which about 12.800 MW was in Europe, or 70% of the total. These wind energy projects across Europe produce enough electricity to meet the domestic needs of 5 million people [5]. The European Wind Energy Association has a target of 60.000 MW of installed capacity by 2010 and 150.000 MW by 2020 [5]. The aim of wind turbine systems development is to continuously increase output power. A few years ago, the rated output power of production-type units reached 200 kW. By 1999, the average output power of new installations climbed to 600 kW [4]. The largest series production units today are specified to deliver 1.5-2 MW output power. It is anticipated that in the near future, power rating of wind turbines will increase further. During the last years the wind turbines have grown in size up to 3 MW per unit and this trend in size up scaling is expected to continue. Furthermore, a huge expansion of wind power is planned in the near future.

In the recent years, the development in the area of electric machines and power electronics with respect to wind turbines has been vigorous. Due to this development, it is necessary to point out the present state of the art on wind turbine systems, as follows.

## 2.2. Concepts and Wind Turbine Configurations

By nature a large number of consistent system solutions exist. The electrical part of a wind turbine is becoming more and more important. Therefore, it is very important to have this system highly integrated into the overall wind turbine design. Due to rapid development of power electronics, offering both higher power and handling capability and lower price/kW, the application of power electronics in wind turbines will increase further. Another interesting issue is the efforts, which have been put into research and development of new motor/generator concepts for some years. Because of their robust constructional possibilities, the generators used in wind power plants have been almost exclusively synchronous or asynchronous.

The generator and power electronics configurations most commonly applied in wind turbines are displayed in Fig. 2.1.

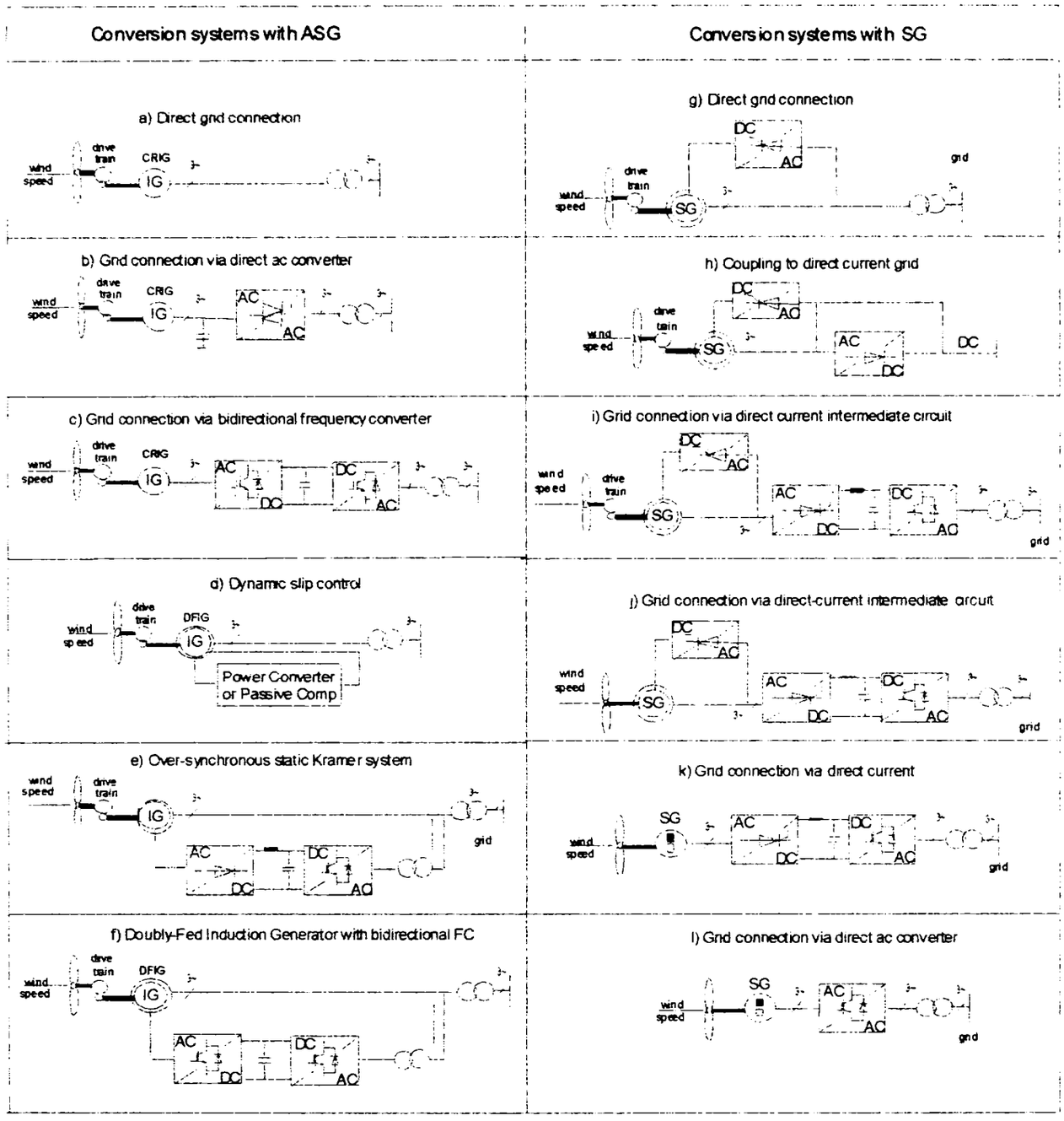


**Figure 2.1**. Standard wind turbine configurations using asynchronous and synchronous generators [2, 3].

The configurations depicted in Fig. 2.1 present an outline of typical electrical topologies used in wind generators. As listed in Table 2.1, these configurations cover a wide range of the applied power control concepts for wind turbines.

The configurations (a) and (g) in Fig. 2.1 show extremely rigid grid coupling. In all the other systems shown, design allows the mechanical speed of rotation to be dissociated from the electrical frequency and voltage in AC or DC systems in varying degrees by the incorporation of power electronics and the associated regulation procedures. The configuration (c) is the conventional concept applied by many Danish wind turbine manufacturers during the 1980's and 1990's, an upwind, stall regulated, three-blades wind turbine concept using an induction generator with cage rotor [2, 3, 4, 5]. During the 1980's this concept was extended with a capacitor bank (for reactive power compensation) and a

soft-starter (for smoother grid connection). In the variant (b), the capacitor bank and soft-starter are replaced by either a full scale frequency converter or a "low wind" region sized frequency converter, where the frequency converter is by-passed and used only for reactive power compensation when the wind speed exceeds the design wind speed. This concept uses a small frequency converter (20-30) % of nominal generator power. On the other hand the full scale concept (approximately 120 % of nominal generator power) enables variable speed operation at all wind speeds. The configuration depicted in Fig. 2.1 d) employs a wound rotor and it has been used by Vestas since the mid 1990's known as OptiSlip. The basic idea of this concept is to control the total rotor resistance using a variable external rotor resistance by means of a power electronic (PE) converter. With the PE converter mounted on the rotor shaft, it is possible to control the slip (by controlling the external rotor resistance) over a 10 % range [2, 3]. Control of the slip implies control of the power output in the system. An alternative control concept it is possible using passive components instead of a PE converter, which also achieves a range of 10 % slip variation [7]. Other configurations in wind turbines employ a doubly fed induction generator (DFIG), as can be seen in Fig. 2.1 (e, f). A frequency converter directly controls the currents in the rotor windings. This enables control of the whole generator output, using a PE converter, rated at (20-30) % of nominal generator power. Introduction of this concept is mainly motivated by two reasons: 1) variable speed in a wide speed range compared to the variant (d) and 2) less expensive compared to the full power control concept. Variants (f) and (g), in addition to the requisite performance control, also allow a controlled delivery of reactive power. These systems can therefore be used as primary grid supply or as grid support for AC grids, as can variant (h) for DC supplies. Synchronous generators delivering power via grid-commutated inverters (models (i), (j) and (k)) must draw their reactive power from the grid. Self commutated inverters such as designs (f) and (g) are, on the other hand, able to provide the reactive power necessary themselves and to control the voltage in grid branches. For the gearless systems (j), (k) and (l), only synchronous generators are used, excited either electrically (j) or by permanent magnets (k, l). A gearless two or three bladed upwind wind turbine using permanent magnet generators (PMG), configurations (k, l), typically less than 1 kW, are used to charge a battery energy storage through a rectifier. These configurations are also applied in wind turbines for home wind systems and hybrid systems (stand-alone configurations), i.e. wind turbines larger than 1 kW and smaller than approximately 20 kW. A future concept-the *Windformer* – using these configurations has been suggested in year 2000 by ABB [3], with the following specifications: multi-pole 3.5 MW PMG which together with a diode-rectifier produces 21 kV DC. The configurations (g), (h) and (i) are not widely used in wind turbines due to their drawbacks such as: the need for an exciter circuit, the need for slip rings and a more complex wind turbine safely strategy, which makes these configurations less attractive [3].

Because of their extremely short reaction times (2-20 ms), the use of frequency converters to couple generators to the grid allows very effective and dynamically efficient torque limiting. This is the case in systems that feed their entire output power to the grid via rectifiers and inverters (See Fig. 2.1, models (b), (h), (i), (j) and (k)), and in configurations that feed only part of their output to the grid via power converters (Fig. 2.1 models (e) and (f)) or take off slip power via supplementary resistors (model d) [2].

**Table 2.1**. The generally applied control concepts for wind turbines (refer to Fig. 2.1) [3].

| Config. | Power Converter | Multi-pole or Gear box | Power Control Features | Comments |
|---|---|---|---|---|
| a) | | Gearbox | Passive Stall | Constant speed |
| b) | Frequency Converter | Gearbox | Passive Stall or Active Stall | Variable speed |
| c) | Soft Starter | Gearbox | Passive Stall or Active Stall | One or two speed machine |
| d) | PE converter or passive components | Gearbox | Pitch Control | Limited variable speed |
| e) | Frequency Converter | Gearbox | Pitch Control | Variable speed (DFIG) |
| f) | Frequency Converter | Gearbox | Stall Control or Pitch Control | Variable speed |
| g) | Rectifier | Gearbox | Stall Control or Pitch Control | Variable speed |
| h) | Rectifier and | Gearbox | Pitch Control | |
| i) | Rectifier and Frequency Converter | Gearbox | Pitch Control | Variable speed with gearbox |
| j) | Rectifier and Frequency Converter | Multi-pole | Pitch Control | Variable speed without gearbox |
| k) | Frequency Converter | Multi-pole | Passive Stall, Pitch Control or Active Stall | Variable speed |
| l) | Frequency Converter | Multi-pole | Passive Stall, Pitch Control or Active Stall | Variable speed |

The configurations (a) and (c) are the only commonly applied control concept, which does not support variable speed operation. Excluding these configurations a road map for conversion of mechanical energy into electrical energy may be drawn, as presented in Fig. 2.2. The focus in this figure is the applied generator concept used in the conversion of a mechanical torque input at variable speed to an electrical power output at fixed frequency.

Figure 2.2 also summarizes the variable-speed mechanical to fixed-frequency electrical energy conversion process. Most of these processes need to sense machine speed and/or output frequency to control power electronic converters, many of which are large (of system rating) and highly expensive.

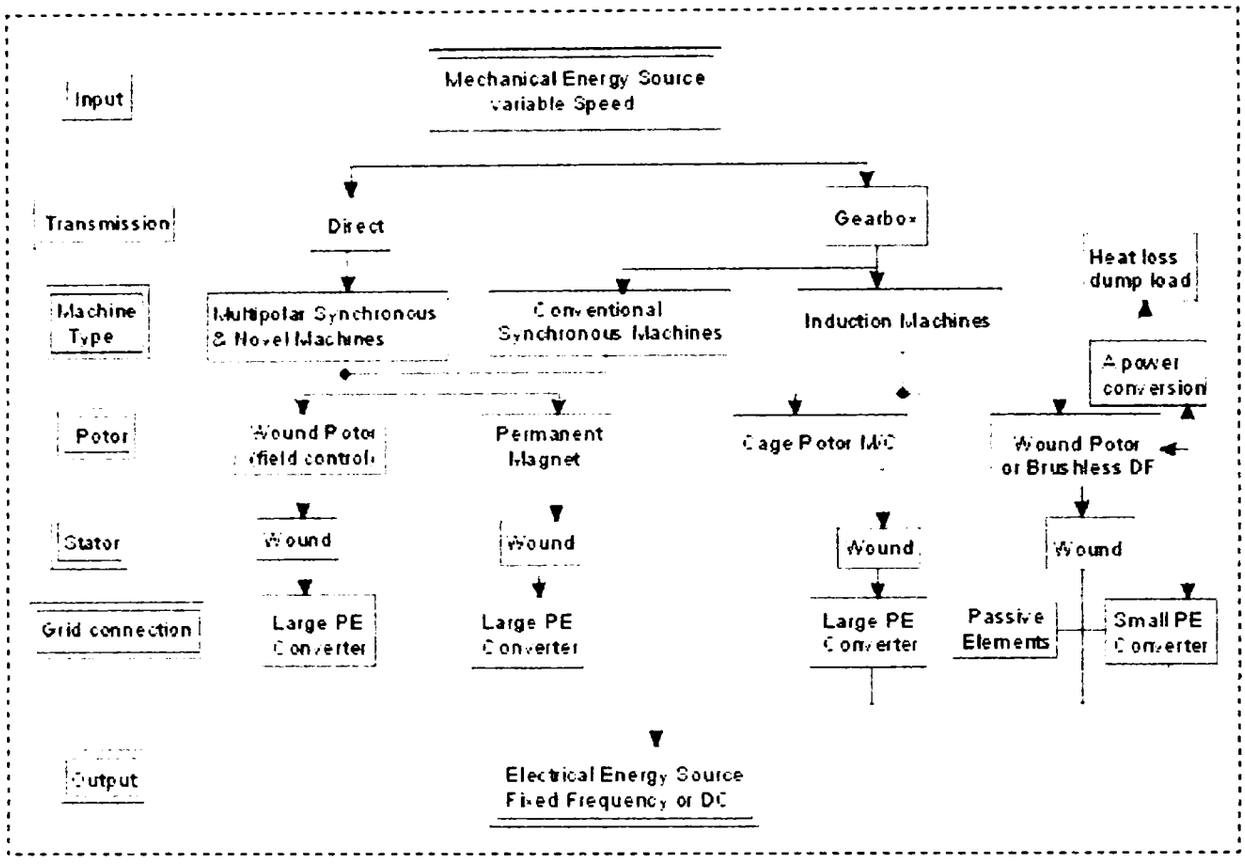


**Figure 2.2**. Conversion process of mechanical energy to electrical energy using power electronic converter (inspired by [3] and [7]).

As it may be observed in Fig. 2.2, the DFIG has two possible implementations, where 1) the rotor is connected to the grid through a small frequency converter or 2) the rotor is connected to an external power conversion unit (PE converter or passive components). The term "Novel Machines" is used here to cover the reluctance machine, the *Windformer* concept (from ABB).

Extracting power from the wind can be realized by means of one of the following methods [8]:

- Constant Speed Constant Frequency (CSCF) System, where a synchronous generator is employed, and the speed is kept constant;
- Almost Constant Speed Constant Frequency (ACSCF) System, where a squirrel cage induction machine is employed with a small slip of one to five percent;
- Variable Speed – Constant Frequency (VSCF) System, where a doubly fed induction generator with a frequency converter may be employed, in which the control needs speed controller to obtain maximum power from the wind and converter to change variable frequency of the generator to constant frequency of output voltage;
- Variable Speed Variable Frequency (VSVF) System, which employs a double output induction machine to feed frequency insensitive loads.

Some of advantages of VSCF-WTG against CSCF-WTG are [5]:

- Generates more energy by operating on a larger wind speed range
- It reduces stresses in the drive train due to flywheel effect of the rotor
- It minimizes the audible noise when operating in light winds

- It simplifies the mechanical design and reduces mechanical stress.

Regarding the connection to the consumers of electrical energy, WT can be used in three modes of operation:

1. Grid connected mode, where Wind Generator is connected directly to the grid;
2. Indirect grid connected mode, where Wind Generator is connected to the grid through a power electronic converter (frequency converter);
3. Standalone mode, where Wind Generator is not connected to the grid and acts as single voltage source.

Most WTs run at almost constant speed with direct grid connection. With indirect grid connection, the WTG runs in its own, separate mini AC grid so that the current from the generator passes through a series of electrical devices which adjust it to match that of the grid. This grid is controlled electronically (using an inverter), so that the frequency of the alternating current in the stator of the generator may be varied. In this way it is possible to run the wind turbine at variable rotational speed. The generator may be either a synchronous or an asynchronous generator, and the turbine may have a gearbox, or run without a gearbox if the generator has many poles. The advantage of indirect grid connection is that it is possible to reduce the peak torque, and the fatigue loads on the tower and rotor blades. The secondary advantage is that with power electronics may control the reactive power, so as to improve the power quality in the electrical grid. The variable speed wind turbine may also give a slight advantage in terms of annual production, since it is possible to run the turbine at an optimal rotational speed, depending on the wind speed. The basic disadvantage of indirect grid connection is the cost. Other disadvantage is the energy lost in the AC-DC-AC conversion process, and the fact that power electronics may induce harmonic distortion of the alternating current in the electrical grid, thus reducing the power quality.

There are two main categories of wind turbine generators, those that are large enough to be used for power generation by public utilities and are typically deployed as "wind farms" and smaller units for residential and small business power generation that usually stand alone and generate less than 50 kW of power. Much of the small system installation was for buildings or communication facilities that were in remote areas where a connection to the power grid was impossible or prohibitively expensive.

## 2.3. Autonomous (Stand Alone) Systems

Reliable, cost-effective and environmentally friendly, wind energy is the ideal power source for many applications. Stand-alone systems are totally independence with no connection to the utility grid system. They generate electricity during daylight hours, and store excess for nighttime use. Most stand-alone systems fall into one of three categories [10]: micro systems (100 W or less), mini systems (100 W to 10 kW) and small systems (10 kW to 50 kW). The wind is not always present with enough velocity to power a wind energy system. This is why many systems are used in combination with another energy source such as solar panels or a diesel generator. In remote communities where diesel generators often supply electricity, the use of wind energy not only makes environmental sense, it makes economic sense. A stand alone system may have a method for storing energy when wind conditions are not good. Usually, batteries are used for storage. Other types of wind energy systems are connected to batteries. When the wind falls bellow the "cut in" speed, the batteries are used.

When the wind is sufficient, the turbines charge the batteries. There are also mechanical systems which are used to aerate ponds or pump water for livestock, irrigation or household water supplies. Such systems, such as mechanical water pumps, do not need a back up power supply or batteries.

For rural areas where grid connection is comparatively expensive there is a trend towards stand-alone wind generators becoming an example of a more up market partial solution to power supply for some flagship industrial developments.

### 2.3.1. Concepts for stand-alone wind turbines

There are several types of wind energy systems regarding stand-alone applications, which provide power solely from the wind. There are hybrid systems, which use another source of power, such as solar panels or a diesel generator, to supplement the energy provided from the wind. Stand-alone (SA) systems may be of the following categories [10]: SA Photo-Voltaic with battery storage for DC load or AC loads, SA Hybrid Photo-Voltaic (PV) with Diesel Generators (DG) and battery storage for DC loads or AC loads, SA Hybrid PV with DG and Wind Generators with battery storage for DC loads or for AC loads.

Autonomous squirrel-cage three-phase induction generators driven either by constant or variable speed prime movers with capacitive excitations are being commissioned as power sources for many stand-alone AC and DC applications. The adjustable speed generators (ASG) system with squirrel cage induction machine is commonly used in low power variable-speed wind turbines replacing the classical direct grid connected fixed speed drives. The goals that can be achieved by using ASG are to increase the energy production especially in the low wind range, eliminate the capacitor bank for reactive power compensation and allow both grid connection and stand-alone operation modes. There is an increase demand on the market for low power stand-alone wind turbines that can be used in remote places. But in order to achieve these goals, relative complex control strategies needs to be developed and power converter need to be used to process the power.

The most common configurations of power converters for stand-alone wind turbines are depicted in Fig. 2.3. The diode rectifier (Fig. 2.3a)) can only be used in one quadrant and is not possible to control it, but it is a simple and cheap solution. This configuration is suitable for fixed-pitch, fixed-speed wind turbines. However, using a DC-DC converter between the diode rectifier and the voltage source inverter this configuration can be used for variable-speed wind turbines. The back-to-back voltage source converter is a bidirectional power converter consisting of two conventional voltage source inverters as shown in Fig. 2.3 b). To achieve full control of the output, the DC-link voltage must be boosted to a level higher than the amplitude of the isolated grid voltage. The power flow of the grid side converter is controlled in order to keep the DC-link voltage constant, while the control of the generator side is set to suite the magnetization demand and the reference speed or torque [9]. A technical advantage of this topology is the capacitor decoupling between the grid converter and the generator converter. Besides affording some protection, this decoupling offers separate control of two converters, allowing compensation of asymmetry both on the generator side and on the grid side, independently. One drawback of this topology is the presence of the DC-link capacitor, which is bulky and has a relative reduced overall lifetime. The matrix converter solution (Fig. 2.3 c)) should be an all silicon solution with no passive

components in the power circuit. The basic idea of this converter is that a desired input current, a desired output voltage and a desired output frequency may be obtained by properly connecting the output terminals of the converter to the input terminals. Some advantages of this topology are: less thermal stress of the semiconductors for a low output frequency compared with the back-to-back solution, the absence of the DC-link capacitor may increase the efficiency and the life-time, depending on the realization of the bi-directional switches, the switching losses may be less than those of the back-to-back voltage source converter. As drawbacks can be mentioned: the intrinsic limitation of the output voltage and the unavailability of a true bi-directional switch. There is no decoupling between the input and the output of the converter and problems can arise for unbalanced or distorted input voltages, or unbalanced load.

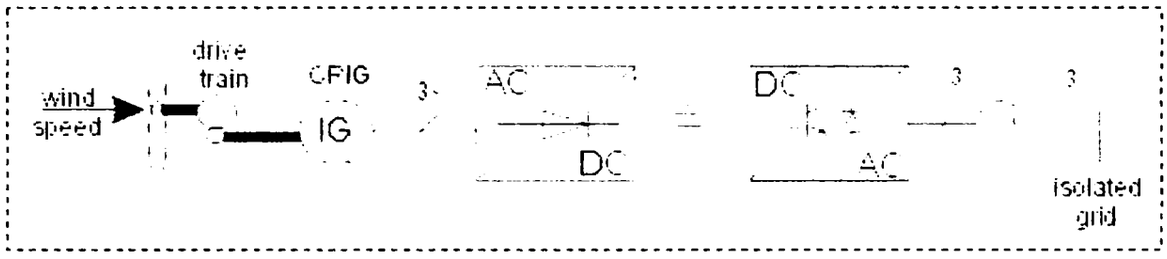


a)

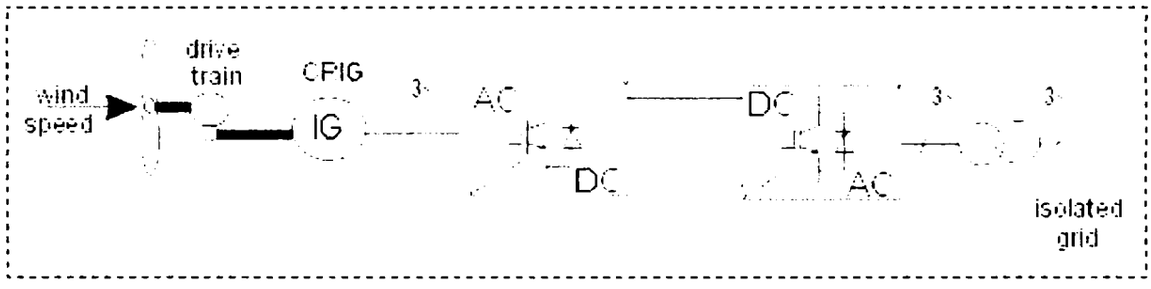


b)

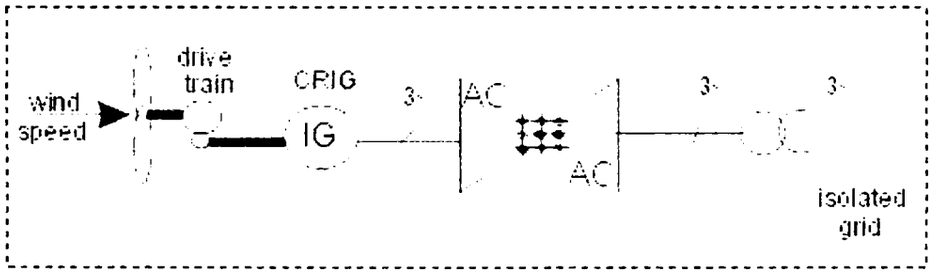


c)

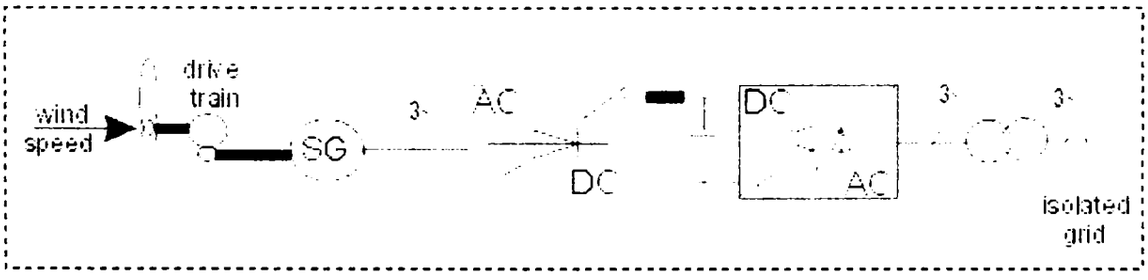


d)

**Fig. 2.3**. Stand-alone wind turbine configurations using, a) IG and diode bridge rectifier and voltage source inverter (vsi), b) back-to-back vsi, c) matrix converter and d) SG with diode bridge rectifier and IGBT inverter.

The implemented system (Fig. 2.3 d) includes a synchronous generator, a three phase diode bridge rectifier, a DC inductor and an IGBT inverter. The DC inductor is used to smooth the ripple of the direct current and the inverter controls the active and reactive power of the wind energy converter system. Higher energy capture, lower transient torque and a cheaper gear-box are the advantages and the higher capital cost is a disadvantage of this system.

## 2.4. Wind Generators connected to the grid

Wind Turbines may be designed with either synchronous or asynchronous generators, and with various forms of direct or indirect grid connection of the generator. The vast majority of the installed power of wind turbines in the world is grid connected, i.e. the turbines feed their electricity directly into the public electrical grid. Most wind turbines run at almost constant speed with direct grid connection. One of the simplest methods of running a wind generation system is to use an induction machine connected directly to the power grid. This very common method of operation forcing the machine to run at a constant frequency and therefore at nearly constant speed. Because the wind is highly variable, it is desirable to operate a wind turbine at variable speeds. With variable speeds the turbine is able to operate at it maximum power producing point for a given wind speed.

Most of wind turbines installed at present are based on one of the three main wind turbine types:

1. fixed speed with directly grid coupled squirrel cage induction generator (Danish concept), Fig. 2.4;
2. variable speed with doubly fed induction generator (Fig. 2.5);
3. variable speed based on a direct drive synchronous generator (Fig. 2.6).

Apart from these three mainstream designs, a number of manufacturers have developed other technologies over the time.

**Table 2.2**. Wind turbine manufacturers-current design and power ranges, based on information found on the internet at February 2003.

| Manufacturer | Design | Power range | Comments |
|---|---|---|---|
| Bonus (Dk) | CT/CS; CT/AS | 600 kW | (1-2.3) MW |
| De Wind (UK/Germany) | VTDI | (0.6-2) MW | |
| Enercon (Germany) | VTDD | (0.3-4.5) MW | |
| GE Wind Energy (Germ./US) | CT/CS; VTDI | 600 kW | (0.9-3.6) MW |
| Lagerway (Netherlands) | VT/AGP; VTDD | 250 kW | (0.75-2) MW |
| Jeumont Industrie (Fr.) | VTDD | (0.75-1.5) MW | |
| MADE (Spain) | CT/CS; VTSGP | (0.66-2) MW | |
| NEG Micon (Dk) | CT/CS; CT/AS; VTDI | (0.6-2.75) MW | |
| Nordex (Germany) | CT/CS ; VTDI | (0.6-1.3) MW; (1.5-2.5) MW | |
| RE Power systems (Germany) | CT/CS; CT/AGP; VTDI | (0.6-0.75) MW | 1050 MW |
| Vestas (Dk) | SVT/OSP; VTDI | (0.66-2.75) MW; (0.85-3) MW | |

CT/CS = fixed speed, classic stall (fixed blade angle)

CT/AS = fixed speed, active stall (negative variable blade angle, 3-5 degrees)

VTDI = variable speed (+ pitch), doubly fed induction generator

VTDD = variable speed, direct drive synchronous generator combined with pitch (Enercon + Lagerwey + 1.5 MW Jeumont) combined with classic stall (Jeumont J48 (750 kW))

VTSGP = variable speed / pitch combined with (brushless) synchronous generator

VT/AGP = variable speed /pitch combined with asynchronous generator (100 % current via converter)

CT/AGP = nowadays unusual combination of fixed speed /pitch with directly connected asynchronous generator. This used to be Vestas' standard system, including 225 and 500 kW

SVT/OSP = semi-variable speed / pitch combined with OptiSlip (maximum +10 % variation in nominal speed)

### 2.4.1. Constant Speed Wind Turbine Configurations

Many wind turbines built to date were constructed according to the "Danish concept", in which wind energy is transformed into electrical energy using a simple squirrel-cage induction machine directly connected to a three-phase power grid, as shown in Fig. 2.4. The rotor of the wind turbine is coupled to the generator shaft with a fixed-ratio gearbox. This conventional concept applied by many Danish wind turbine manufacturers during 1980's and 1990's was extended with a capacitor bank for reactive power compensation and a soft-starter for smoother grid connection at more than 500 kW induction machine (see chapter 3). Some induction generators use pole-adjustable winding configurations to enable operation at different synchronous speeds (Table 2.1). However, at any given operating point, this wind turbine configuration basically has to operate at constant speed. The generator slip varies with the generated power, so the speed is not, in fact, constant; however, as the speed variations are very small (just 1-2%), it is commonly referred to as a fixed-speed wind turbine.

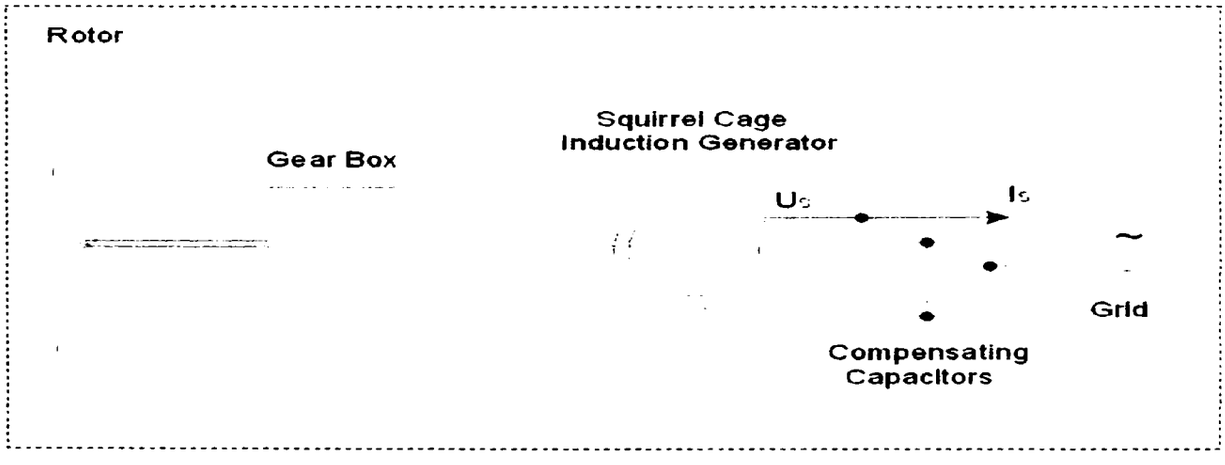


**Figure 2.4**. Fixed speed wind turbine with squirrel cage induction generator.

The construction and performance of fixed-speed wind turbines depends on the characteristics of mechanical sub-circuits, e.g. pitch control time constants, main breaker maximum switching rate [5]. The response time of some of these mechanical circuits may be in the range of tens milliseconds. As a result, each time when the wind gusts hits the turbine, a fast and strong variation of output electrical power may be observed. These loads required a sturdy mechanical design to absorbed high mechanical stresses. This strategy leads to expensive mechanical construction, especially at high-rated power. To do this topology more efficiently and cheaper a control strategy called "active stall constant speed" may be implemented, as will be describe in details in chapter 3.

Each of the wind turbine designs has its own benefits and drawbacks. The advantage of a fixed-speed turbine is that it is relatively simple; therefore the price tends to be slightly lower. These turbines have to be more mechanically robust than other designs, because of the higher structural loads involved - since the rotor speed cannot be varied, fluctuations in wind speed translate directly into drive train torque fluctuations. Depending on the strength of the grid connection, the resulting power fluctuations may result in grid voltage fluctuations, which can cause unwanted fluctuations in bulb brightness ('flicker').

### 2.4.2. Variable Speed Wind Turbine Configurations

Variable speed wind turbine generators have progressed dramatically in recent years. They are a spreading, dominating design principle of power converters applied in wind power turbines today. Up to 75 % of all wind turbines built in 2001 and up to 80 % of those that were built in 2002 are variable speed wind turbines [13]. Variable speed operation can only be achieved by decoupling electrical grid frequency and mechanical rotor frequency. To this end, power electronic converters are used, such as an AC-DC-AC converter combined with advanced control systems. Because of the improved reliability of power electronic converters, it is possible to vary the frequency to the ac generator and thereby allow for variable-speed operation. By adjusting the speed, the wind turbine can be optimized to run at near peak power production for various wind speeds.

The advantages of variable speed turbines are that they generate more energy for a given wind speed regime, and that the active and reactive power generated can be easily controlled [3, 5, 17-21]. There is also less mechanical stress, and rapid power fluctuations are scarce, because the rotor acts as a flywheel [14, 15] (storing energy temporarily as a buffer). In general, no flicker problems occur with variable speed turbines. Variable speed turbines also allow the grid voltage to be controlled, as the reactive power generation can be varied [5, 9].

Variable speed wind turbines can use more wind, due to the fact that they adapt to the particularity of the wind power itself-the changeable force of the wind. They start at lower wind speeds, and increase the power with speed. The design itself may be more demanding than classic, constant-speed turbine, but the reported energy increase of up to 10 % is rewarding [5, 13].

The drawbacks of variable speed wind generators are that the built-in power electronics are sensitive to voltage dips caused by faults and/or switching and that they are more expensive. On the other hand, using variable speed systems can also give major savings elsewhere, such as lighter foundations in offshore applications [12].

The existing topologies of variable speed wind turbines include solutions for asynchronous generators and for synchronous generators as well. As in the case of the adjustable speed electrical drives, the variable speed operation of the WTs is achieved using suitable power electronic converters. Several alternative configurations exist, regarding the type of the converters and the electrical generators. To optimize wind turbine operation, some control scheme require a method of searching techniques to find the maximum power for a given wind operation [26, 28, 33, 34]. Other controllers use field-oriented control techniques to determine the power flow in the machines [5, 9, 14-20]. Quite often, control techniques use simple V/f converters to adjust the speed of the turbine [31, 32].

### 2.4.2.1. Variable Speed Wind Turbine Configurations with Induction Generators

Typically variable speed wind turbine configurations are considered, using induction generators and different types of power electronics converters, including voltage and current source inverters or matrix converters.
Commonly used circuits for variable speed:
*1. Solution with the induction machine and squirrel cage rotor*
The power electronics circuit is with machine side voltage source inverter, DC link, line side voltage source converter and filter, all for full generated power, as shown in Fig. 2.5.

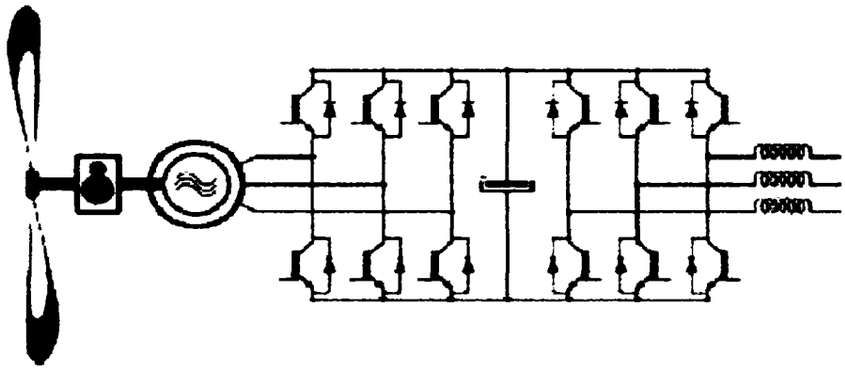

**Figure 2.5.** 4-Q AC Drive: Induction generator with the full line side converter and machine side inverter, both for full generated power.

This scheme presents significant advantages [13, 16], such as the inherent bi-directional power flow capability (required for motor starting of stall regulated WTs), no minimum and maximum turbine speed limits, generated power and voltage increase with the speed, reactive power control, the reduced harmonic injection to the grid and continues operation at network disturbances. As drawbacks of this scheme can be mention: two full-power converters in series, high dv/dt applied at generated windings, power loss of up to 3% of generated power and big DC-link capacitors.
Other possibility for power electronics circuit can be a current source inverter cascade [2, 3, 16]. These existing solutions of variable speed wind turbines use a thyristor current source converter at the generator side and a conventional 6-pulse phase controlled inverter at the line-side.

As it will be shown in the following, much more suitable is the application of the "slip control" principle with doubly fed machine.

*2. Solutions with the doubly-fed induction machine*

In a variable speed turbine with doubly fed induction generator, the converter feeds the rotor winding, while the stator winding is connected directly to the grid, as can be seen in Fig. 2.6. The electrical rotor frequency can be varied by this converter, thus decoupling mechanical and electrical frequency and making variable speed operation possible.

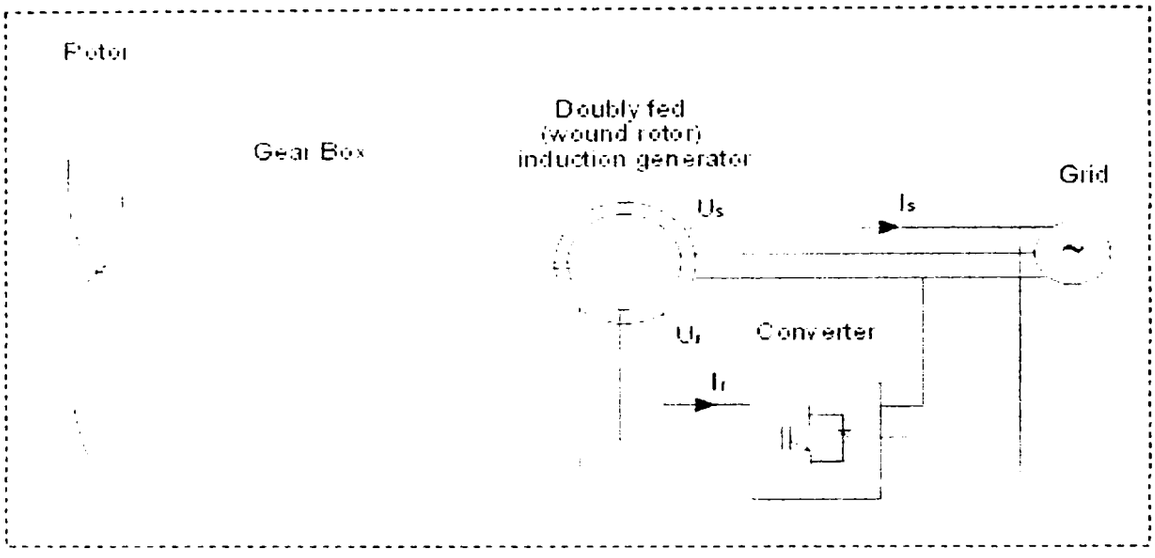


**Figure 2.6.** Variable speed wind turbine with double fed induction generator.

Doubly output induction machines permit operation in the over-synchronous and under-synchronous range, where their speed can be varied by [2]:

- up to around 10 % with dynamic slip control;
- approximately 30 % using power converter cascades in over-synchronous operation;
- around 40 % under and over-synchronous in doubly fed operation.

For the principle circuit, three different modes of operations are possible [2, 16].

*2.1.* The stator winding has to be connected to the grid, only when the rotor speed is near synchronous speed. The rotor circuit is always connected to the grid, over the frequency converter. For lower generator speed, that is 80%, only 20% of the generator power will be supplied from the grid to the rotor. For higher rotor speed (120%), 20% of the generator power will be supplied to the grid via rotor circuit. This circuit is also known as the cascade circuit. In this system, the slip output of the rotor can be drawn from the rotor via an uncontrolled rectifier and via a grid or self-commutated inverter, and supplied to the three-phase current grid (Scherbius principle).

*2.2.* The stator and rotor circuits with inverter and converter are always connected together and at the beginning disconnected from the grid. Wind starts the rotation, and for lower speed than the rated one, the rotor inverter produce the frequency ($f_r$), so that the frequency corresponds to the speed $f_{rotation} + f_r = 50$ Hz. Stator winding and rotor converter will be connected to the grid, when the generator voltage is synchronized with the grid. The principle of operation is used for the generator which has to supply constant frequency, and is driven with variable shaft speed.

For both solutions, the rotor side inverter operates at lower output frequency, between 10 Hz and near to zero Hz. The connection between rotated rotor and inverter is made via slip rings. Maximum power is (120-130) % of the machine power. Semiconductor power losses are up to (0.6-0.9) % of the generated power.
Advantages: only two power converters in series for rotor power exchange (usually 20-30% of the generated power), active and reactive power control, and line side inductance is only 3-4.5% (12-15% of the rotor power).

Disadvantages: minimum and maximum turbine-speed limits corresponding to the rotor power exchange (usually 20-30% of generated power), the rotor size converter operates at low frequency, and therefore double size semi-conductors are needed.

*2.3. **Dynamic slip control***. By connecting resistors in the three-phases of the rotor circuit, high slip values and thus high elasticity of speed can be achieved if the resistors are correctly dimensioned. whereby increased slip brings better dynamic characteristics but worse efficiency. The complete redesign of the power section with additional resistors, power electronics and regulation in the rotating part of the generator was realized by Vestas for their wind turbines called OptiSlip system. The generators specifically designed for the OptiSlip function are fitted with a wound rotor and an integrated current regulation system in the rotor-side. This is installed at the rear of the generator on the end of the shaft, and consists of additional resistors, power electronics, current sensors and a microprocessor controller. A recently developed alternative variable-speed generation system employs a wound rotor induction machine with passive rotor connected elements. This system provides acceptable efficiency over a reasonable speed range. In consequence, it offers a highly reliable, low maintenance, and low capital cost alternative, more detailed can be found in chapter 4.

The asynchronous machine with wound rotor and speed control by slip-power recovery is a very cost effective and a widely successful solution. More than 50 % variable speed windmills today are built using this principle [13].

### 2.4.2.2. Variable Speed Wind Turbines using Synchronous Generators

As it may be observed in section 2.2, the wind turbines with synchronous generators are used with and without gearing via frequency converters in grid operation. For the gearless systems, only synchronous generators are used, excited either electrically or by permanent magnets. The permanent magnet synchronous generators are proposed as a wind turbine due to its property of self-excitation. The utilization of permanent magnets in a multi-pole rotor reduces the rotor losses significantly and makes it possible to eliminate the gear box.

In a variable speed turbine with direct drive synchronous generator, the generator and the grid are completely decoupled by means of a power electronic converter, also allowing variable speed operation, as shown in Fig. 2.7.

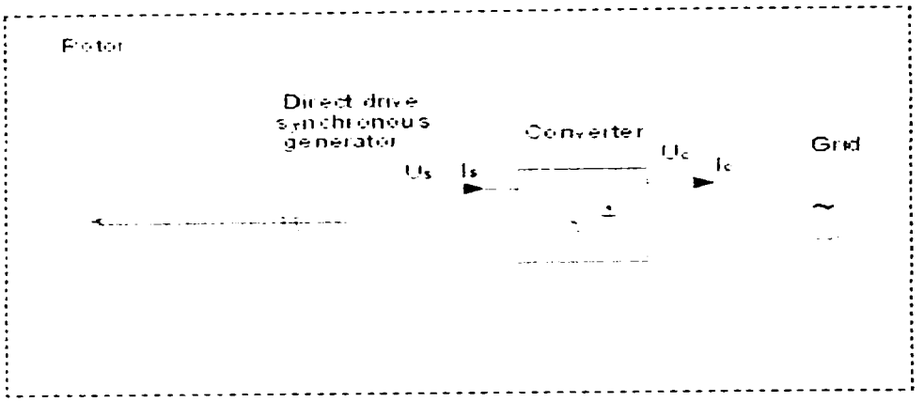


a)

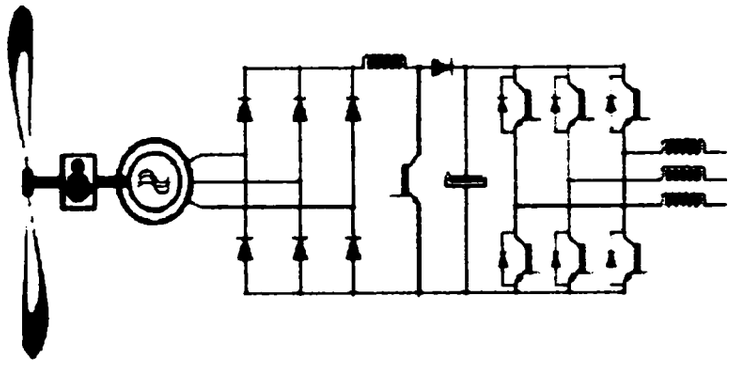

b)

**Figure 2.7.** Variable speed based on direct drive synchronous generator, a), and equipped with a gear and a frequency converter, b).

The typical arrangement of variable speed direct drive synchronous generator is often used without a gear box, using a low speed synchronous generator. In order to achieve variable speed operation, a power electronics converter interface is used to connect the generator to the grid. The converter may consist of an uncontrolled 3-phase diode rectifier, a DC/DC boost converter and a 3-phase PWM voltage source inverter or two back-to-back PWM-VSI converters [25, 26, 29]. The output voltage of the synchronous generator is lower at lower speed; therefore one boost chopper is built-in between the rectifier and the DC-link capacitors. At the lower speed the boost chopper pumps the rectified generator voltage up to the DC link value necessary for the line side converter operation ($V_{DC}>V_{line\text{-}peak}$).

The power electronic circuits without a boost chopper are also used [13]. In this case the DC link voltage control is achieved due to excitation control of the synchronous generator. There is no need for an inverter on the generator side; therefore a simple rectifier may be used. Use of a diode bridge rectifier will cause harmonics in the current waveforms, giving a high peak current in relation to the RMS value of the load [3]. This will increased eddy current losses in the rotor, and also the danger of demagnetizing the magnets at a small load. The use of a controlled rectifier allows several advantages, such as the current may be controlled to be sinusoidal, the amplitude of the voltage may be controlled to match the grid voltage, independent of shaft speed. The use of the inverter effectively decouples the generator from the grid. The inverter performance, such as the voltage regulation, reactive

power control and power quality depend mainly on the grid-side inverter [22, 23, 24]. This system may operate at any power angle, without losing synchronism.

Another variable-speed wind turbine topology employs a self excited brushless synchronous generator (SG) with automatic voltage regulator (AVR) [27, 28]. The SG supplies power to a diode rectifier chosen for its simplicity, low cost and low losses. The use of the diode rectifier is possible since the voltage control of the DC-link is achieved through the AVR of the SG. The rectifier generates non-sinusoidal generator currents which increase the generator losses and decrease the rating of the generator by about 5%. Also the commutation of the diodes leads to a voltage drop of about 5-10%. The DC inductor is used to smooth the ripple of the direct current. The IGBT inverter controls the active and reactive power of the variable speed wind energy conversion system supplied to the grid. The small grid filter is used to eliminate the high order harmonics.

The advantages of these topologies are [13]: no minimum and maximum turbine-speed limits, generated power and voltage increase with speed, VAR-reactive power control is possible, simple generator side converter and control and continues operation when network disturbances occur. As disadvantages should be mentioned: two (three) full-power converters in series, power loss of up to (2-3) % of the generated power, large DC-link capacitors and line-side inductance of (10-15) % of the generated power.

A directly driven variable-speed generator can be more efficient than a conventional gear and generator, even if the generator efficiency at rated load is low. The reasons for that is the elimination of the gear box losses and that a large part of the generator losses at rated load are copper losses and they are very much reduced at low wind speed [29].

#### 2.4.2.3. A comparison between asynchronous and synchronous generators based on variable speed wind turbine applications

Whether the trend towards variable speed systems will eventually mean a greater role for synchronous generators with gearboxes and grid coupling via frequency converters is hard to say as yet. This will depend amongst others on whether the stability problems, which can occur when a short circuit occurs in grids with large numbers of wind turbines based on the doubly fed induction generators, appear to be soluble in the near future.

The trend is towards advanced designs, especially for wind turbines in the megawatt class. Currently, the two trend-setting technological designs in this category (> 1.5 MW) are variable pitch turbines with doubly fed induction generators, and direct drive systems. The first segment now includes almost all leading names of companies opting for turbines with gearboxes. The second segment so far is more or less exclusively the domain of Enercon (300 kW - 4.5 MW), although there are a number of promising potential direct drive suppliers taking off.

Comparing the two variable speed designs, one advantage that can be observed in designs based on the doubly fed induction generator, is that a fairly standard generator and a small - and hence cheaper - power electronics converter can be used. The cost of the semiconductor components used in AC-DC-AC converters has, however, fallen spectacularly in the last five to seven years, reducing the latter advantage. A drawback of designs with the doubly fed induction generator, when compared with direct drive variable speed turbines, is

that they still need a rather maintenance-intensive - and potentially unreliable - gearbox in the drive train. The drawbacks of the direct drive design are the large, and relatively heavy and complex ring generator and a larger electronic converter, through which the full 100% of the power generated has to pass, compared with about one third of the power in the case of the doubly fed induction generator-based wind turbine.

## 2.5. Control Strategies for Wind Turbines

Wind turbines are designed to produce electrical energy as cheaply as possible. Wind turbines are therefore generally designed so that they yield maximum output at wind speeds around (12-15) meters per second. In case of stronger winds it is necessary to waste part of the excess energy of the wind in order to avoid damaging the wind turbine. All wind turbines are therefore designed with some sort of power control. There are two different ways of doing this safely on modern wind turbines [4]: pitch control and stall control.

### 2.5.1. Pitch controlled wind turbines

On a pitch controlled wind turbine the turbine's electronic controller checks the power output of the turbine several times per second. When the power output becomes too high, it sends an order to the blade pitch mechanism which immediately pitches (turns) the rotor blades slightly out of the wind. Conversely, the blades are turned back into the wind whenever the wind drops again. The rotor blades thus have to be able to turn around their longitudinal axis (to pitch). During normal operation the blades will pitch a fraction of a degree at a time - and the rotor will be turning at the same time. Designing a pitch controlled wind turbine requires some clever engineering to make sure that the rotor blades pitch exactly the amount required. On a pitch controlled wind turbine, the computer will generally pitch the blades a few degrees every time the wind changes in order to keep the rotor blades at the optimum angle in order to maximize output for all wind speeds. The pitch mechanism is usually operated using hydraulics.

### 2.5.2. Stall controlled wind turbines

Passive stall controlled wind turbines have the rotor blades bolted onto the hub at a fixed angle. The geometry of the rotor blade profile however has been aerodynamically designed to ensure that the moment when the wind speed becomes too high; it creates turbulence on the side of the rotor blade which is not facing the wind This stall prevents the lifting force of the rotor blade from acting on the rotor. As the actual wind speed in the area increases, the angle of attack of the rotor blade will increase, until at some point it starts to stall. If you look closely at a rotor blade for a stall controlled wind turbine you will notice that the blade is twisted slightly as you move along its longitudinal axis. This is partly done in order to ensure that the rotor blade stalls gradually rather than abruptly when the wind speed reaches its critical value. The basic advantage of stall control is that one avoids moving parts in the rotor itself, and a complex control system. On the other hand, stall control represents a very complex aerodynamic design problem, and related design challenges in the structural

dynamics of the whole wind turbine, e.g. to avoid stall-induced vibrations. Around two thirds of the wind turbines currently being installed in the world are stall controlled machines [4]

#### 2.5.2.1. Active Stall Controlled Wind Turbines

An increasing number of larger wind turbines (1 MW and more) are being developed with an active stall power control mechanism. Technically the active stall turbines resemble pitch controlled turbines, since they have pitch able blades. In order to get a reasonably large torque (turning force) at low wind speeds, the wind turbines will usually be programmed to pitch their blades much like a pitch controlled wind turbine at low wind speeds. (Often they use only a few fixed steps depending upon the wind speed). When the turbine reaches its rated power, however, it will notice an important difference from the pitch controlled wind turbines: If the generator is about to be overloaded, the turbine will pitch its blades in the opposite direction from what a pitch controlled wind turbine does. In other words, it will increase the angle of attack of the rotor blades in order to make the blades go into a deeper stall, thus wasting the excess energy in the wind. One of the advantages of active stall is that one can control the power output more accurately than with passive stall, so as to avoid overshooting the rated power of the turbine at the beginning of a gust of wind. Another advantage is that the wind generator can be run almost exactly at rated power at all high wind speeds. A normal passive stall controlled wind turbine will usually have a drop in the electrical power output for higher wind speeds, as the rotor blades go into deeper stall.

The pitch mechanism is usually operated using hydraulics or electric stepper motors. As with pitch control it is largely an economic question whether it is worthwhile to pay for the added complexity of the machine, when the blade pitch mechanism is added.

### *2.5.3. Rotor Efficiency under Stall and Pitch Controlled Wind Turbines*

The output of wind turbines varies with wind speed, but is not proportional to it, as the energy that the wind contains increases with the cube of the wind speed. At low wind speeds (1-3 m/s), wind turbines are shut down, as they would be able to generate little or no power (Fig. 2.8). Wind turbines only start up at wind speeds between 2.5 and 5 m/s, known as the "cut-in" wind speed. "Nominal" or "rated" wind speed, at which nominal output is reached, is normally between 12 and 15 m/s. The precise value depends on the ratio of generator capacity to rotor surface area, and is a design variable. Finally, any wind turbine has a "cut-out wind speed": this is the wind speed at which the turbine is shut down to avoid structural overload. Its value is around 25 m/s for IEC Wind class I and II turbines [4]. For IEC Wind Class III turbines, which generate maximum output at lower wind speeds, the cut-out value is in the range of 17-20 m/s. Wind turbines are shut down if the 10-minute average of the wind speed is above this design value.

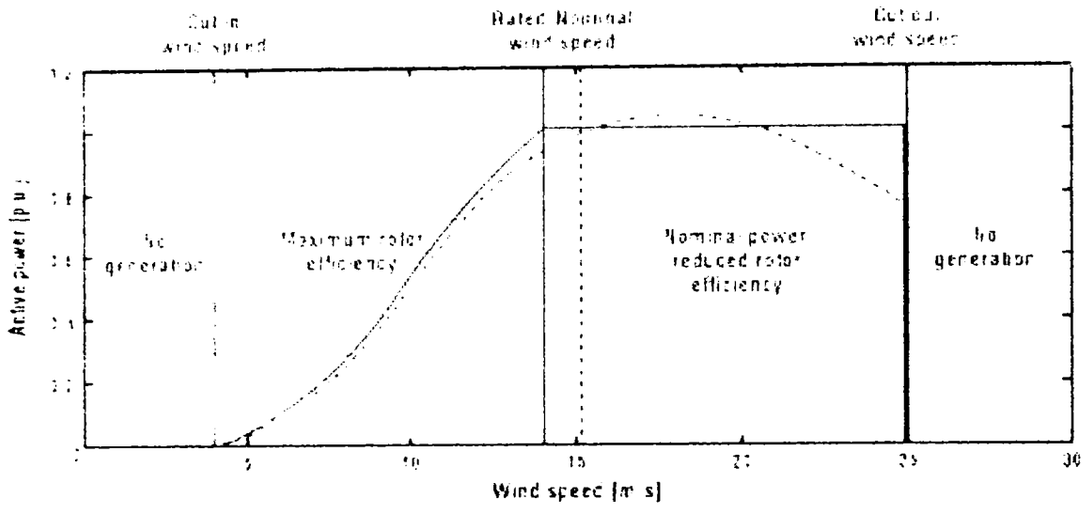


**Figure 2.8.** Typical power curves and operation areas of a stall (dashed line) and pitch controlled (solid line) wind turbines [13].

Below nominal wind speed, the aim is to maximize rotor efficiency (Fig. 2.8). The rotor efficiency depends on the ratio of the rotor blade tip speed and wind speed, known as the "tip speed ratio". The tip speed ratio of a fixed speed wind turbine cannot be controlled, as the rotor speed (and thus the blade tip speed) is fixed. Nevertheless, the tip speed ratio varies with wind speed, and thus reaches the optimum value at one wind speed only in case of fixed speed designs (or at two speeds if the wind turbine can operate at two different, but constant, rotor speeds), more details can be found in chapter 3.

With a variable speed wind turbine, the tip speed ratio varies, and depends both on wind speed and rotor speed. For maximum rotor efficiency, the tip speed ratio must be maintained at the value that corresponds to optimum rotor efficiency (usually 6-8) at all times. This is achieved by controlling the rotor speed accordingly. The higher aerodynamic efficiency that is thus achieved explains why a variable speed turbine generates more energy for the same wind speed regime. At wind speeds below nominal, the aim is to extract energy from the wind as efficiently as possible; however, this ceases to apply above nominal wind speed, as this would overload the generator and/or the converter system. Above nominal wind speed, therefore, the mechanical power extracted from the wind must remain constant. To achieve this, the aerodynamic rotor efficiency must be reduced when the wind speed increases, as can also be seen in Fig. 2.8.

Two methods can be applied to this end: stall power limitation and pitch control. With stall control, the blades are designed such that the rotor efficiency "collapses" at high wind speeds. Due to the blade design, this behavior is intrinsic, and no active control systems are required to achieve the aerodynamic efficiency reduction. With pitch control, the blade is gradually turned out of the wind, so the wind impact angle changes and the aerodynamic efficiency is reduced. In this case active stall control is applied, by means of hydraulics or an electric drive system. The input variable for the pitch controller is the rotor speed. The higher the rotor speed, the more the blades are turned out of the wind. The blades are turned back into the wind when the rotor speed falls (Fig. 2.9. In general, fixed speed turbines use stall control for technical reasons, while variable speed turbines are usually equipped with pitch control.

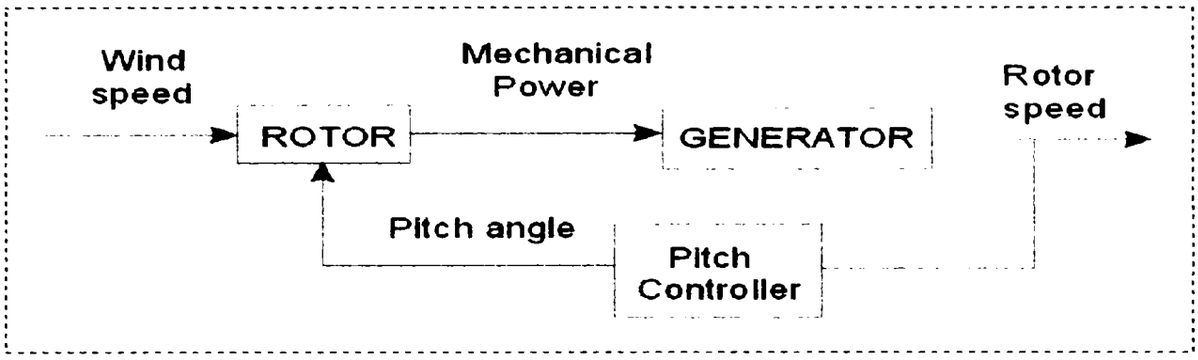


**Figure 2.9.** Rotor speed control principle for wind speeds above nominal.

A relatively recent innovation is the active-stall concept. This is similar to normal stall power limitation, except that the whole blade can be rotated backwards (in the opposite direction as is the case with pitch control) by a few (3-5) degrees at the nominal speed range in order to give better rotor control. The result is known as the 'deep stall' effect, which leads to the power curve bending sharply to a horizontal output line at nominal power and keeping this constant value for all wind speeds between nominal and cut-out. The application of this concept is more or less restricted to fixed speed turbines. Typical active-stall representatives are the Danish manufacturers Bonus (1 MW and over) and NEG Micon (1.5 and 2 MW) [4]. The difference from active pitch control is not only that the range of blade angle variation is less, but also that the direction of the variation is opposite. Further, the blade angle is only varied during the start-up phase and nominal speed range, while active pitch control is sometimes also used continuously from a threshold value as a second controller to optimize aerodynamic rotor efficiency.

## *2.6. Trends in Wind Turbine Design and Prices*

Based on the previous section the present "state of the art" large wind turbine may be summarized as a 3-bladed upwind turbine using:

- active stall with two speeds asynchronous generator with constant speed
- pitch control combined with variable speed. Moreover, the variable speed concept is mainly realized using a doubly-fed induction generator with a rotor connected IGBT based frequency converter
- only one of the top-10 manufacturers offers a gearless (variable speed) wind turbine [3].

Meanwhile, it should be mentioned that a number of alternative wind turbine designs exist.

To obtain an overview of the wind turbine prices, the well known concepts have been evaluated using publicly available data obtained from the internet. The results are presented in Table 2.3, to ascertain the standard prices for the largest wind turbines of almost each top-10 manufacturer.

**Table 2.3**. Nominal power, typical rotor diameter and wind turbine prices. The wind turbine price also includes installation and start-up and excludes foundation costs. (Year 2000)

| Manufacture | Wind Turbine | Power (kW) | Hub height (meters) | Wind turbine price (EU) |
|---|---|---|---|---|
| NEG Micon | NM 2000/72 | 2000 | 68 | 1.715.000 |
| | NM 1500/64 | 1500 | 60 | 1.140.000 |
| Vestas | V80 | 2000 | 78 | 1.810.000 |
| | V66 | 1650 | 67 | 1.340.000 |
| Enercon | E-66/70 | 1800 | 65 | 1.550.000 |
| Enron Wind | 1.5 s/70.5 | 1500 | 80 | 1.375.000 |
| Bonus | 1.3/62 | 1300 | 60 | 900.000 |
| Nordex | N80/2500 | 2500 | 70 | 1.850.000 |
| | N60/1300 | 1300 | 60 | 875.000 |

The specific wind turbine price has decreased from 1600 EU / kW for 20-30 kW machines down bellow 800 EU / kW for 450-600 kW machines, as reported in [3]. The Megawatt machines have an increasing specific price. This fact is partly explained by the development in offshore wind turbines, which are generally Wind Farms. It seems to be the technical performance, measured at the swept rotor per nominal power, or the yearly energy production per unit swept rotor area, that is the optimizing criterion-rather than the economic performance, measured as the cost per nominal power, or the cost per yearly energy unit production.

Improvements in wind energy technology mean that the trends which have led to the dramatic fall in the cost of wind energy are set to continue.

## 2.7. Estimation of the wind generator systems efficiency

Modern wind turbines typically have availabilities exceeding 98% and perform with capacity factor of (35 to 45) % in good wind resource areas.

Different wind energy systems are compared mainly regarding cost per kWh. Therefore, several things should be investigated: the average power captured by the turbine, the system cost, the efficiency and the availability of the systems. The efficiency is very important when comparing different systems the losses reduce the average power produces by the wind energy converter and, thereby, they reduce the incomes. The average power production is determined by the average efficiency and not by the efficiency of rated load [29].

In this section the three compared 500 kW wind generator systems are presented. The systems represent three different concepts which are interesting for actual and future wind energy conversion systems. The first one is the conventional constant-speed wind generator system with a step-up gear and a directly grid-connected induction generator. The second system is a variable-speed synchronous generator equipped with a gear and a frequency converter. The frequency converter consists of a diode-rectifier, a DC step-up converter and an IGBT inverter. The rectifier is chosen for its low price and low losses and the inverter because it produces high quality power to the grid. The synchronous generator has almost the same efficiency as the induction generator, only 0.4% lower because of current harmonics

from the diode rectifier. The third system is a directly-driven variable-speed permanent magnet synchronous generator with a frequency converter as the same type as the one presented before.

### 2.7.1. Loss distribution: losses in the generator, gear box and power converter

In this section the losses for different systems will be estimated and discussed. The losses of the wind generators can be divided into several types depending on different variables.

The gear losses can be divided into the gear mesh losses and the no load losses. The gear mesh losses only depend on the transmitted power and not on the turbine rotor speed. The no load losses are bearing losses, oil churning losses and wind age losses [29]. They are independent of load but are speed-dependent. The estimated losses at rated of 500 kW gear for wind turbines are shown in Table 2.4.

**Table 2.4**. Losses in the gear at rated load [29].

| | |
|---|---|
| Friction, wind age and oil churning losses | 1 % included turbine bearing |
| Gear mesh load | 1.7 % |
| Total losses at rated load | 2.7 % |

The generator losses are calculated according to the conventional electric machine theory. The losses are: copper losses, hysteresis and eddy current core losses, wind age and friction losses and additional losses. The copper losses are dependent on the currents, the histeresis and eddy current core losses depend on the flux linkage and the frequency, the friction losses only depend on the generator speed and the additional losses can be assumed to depend only on the current. The losses of the induction generator are based on data from a commercial induction generator and the losses of the direct driven generator are from a design study of a 500 kW synchronous generator with permanent magnet. The losses of the synchronous generator are estimated for a generator with the same stator rating as the induction machine and with salient pole rotor excited by a brushless exciter and are shown in Table 2.5.

**Table 2.5**. Losses in the generators at rated load [29].

| Losses | Induction generator | Synchronous generator | Directly driven PM synchronous generator |
|---|---|---|---|
| Core losses | 1.5 % | 1.5 % | 1.2 % |
| Copper losses and additional losses | 1.5 % stator & rotor | 1.15 % stator | 3.5 % stator |
| Friction, windage and cooling losses | 0.5 % | 0.5 % | 1 % incl. turbine bearing |
| Excitation losses | - | 0.75 % | - |
| Total losses | 3.5 % | 3.9 % | 5.7 % |

In the variable speed wind generators the losses of the frequency converters have to be included. The converter losses are copper losses, voltage drop losses and no load losses for

the rectifier, the dc step-up converter, and the inverter. For a 500 kW diode/IGBT converter the losses at rated load are shown in Table 2.6 [29].

**Table 2.6.** Losses in the frequency converter at rated load.

| | |
|---|---|
| Voltage drop losses of the diode rectifier | 0.4 % |
| Resistance losses of rectifier and inductor | 0.2 % |
| Step up converter transistor losses | 0.75 % |
| Step up converter diode losses | 0.25 % |
| No load converter losses | 0.1 % |
| Inverter load losses at cosφ=1 | 1.5 % |
| Inverter and inductor resistive losses | 0.3 % |
| Total losses at rated generator voltage | 2.75 % |

## 2.7.2. Calculation Method

Because one of the compared systems is a constant speed wind generator system while the other two are variable-speed wind generator systems, the energy captured by the turbine differs. Therefore, the comparison should be made only on the average efficiency from wind turbine shaft to the grid. This means that the results does not include that a variable-speed wind turbine will capture a few percentage more energy than a constant-speed turbine.

To find the average efficiency, the average power production of the turbine ($P_{Tav}$) and average losses ($P_{Lav}$) must be calculated. This can be done by using a probability density distribution (w) for the wind speed (v). The aerodynamic power of wind turbine ($P_T(v)$) is multiplied by the probability density and integrated from the wind speed $v_{min}$, at which the turbine starts, to the wind speed $v_{max}$, at which it is stopped. By definition the integral of the probability density function over wind speeds from zero to infinity is exactly one. The value of this integral is the average power captured by the turbine:

$$P_{Tav} = \int_{v\min}^{v\max} P_T(v) \cdot w(v) \cdot dv \quad \text{.....(2.1)}$$

The average losses can be calculated in the same way as the average power. The average efficiency can then be calculated as:

$$\eta_{av} = 1 - \frac{P_{Lav}}{P_{Tav}} \quad \text{.....(2.2)}$$

The probability density of different wind speeds is approximated by a Weibull distribution. A typical wind speed probability density distribution and typical losses of a wind energy converter are shown in Fig. 2.10. In Fig. 2.11 the product of the probability density and the losses is shown.

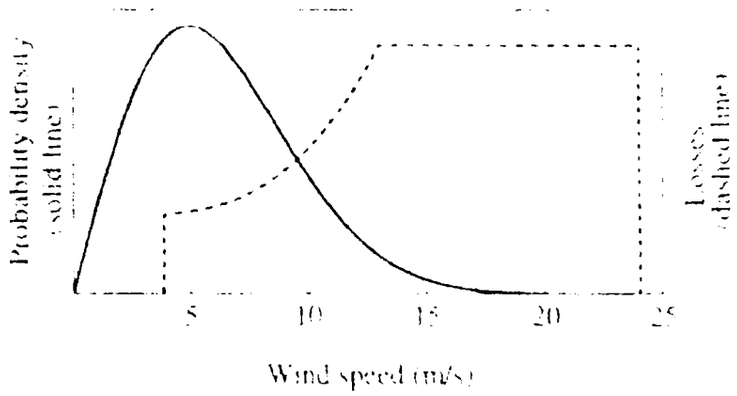


**Figure 2.10**. Wind speed probability density and losses of a constant speed wind energy converter [29].

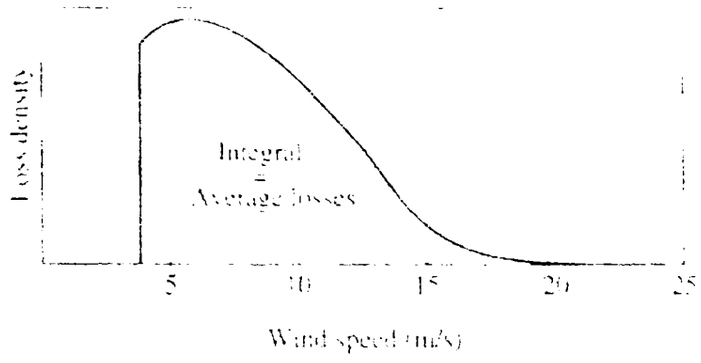


**Figure 2.11**. The loss density and average losses [29].

The losses at wind speeds bellow 8 m/s are much more important for the average losses than the losses above rated wind speed, 13 m/s, because the loss density is much higher at low wind speed than above the rated wind speed.

### 2.7.3. The average losses

To be able to use the proposed method to calculate the average losses, the losses must be expressed as a function of the wind speed. By defining the parameters that determine the losses as functions of the wind speed, all the losses can be expressed as a function of wind speed. In Fig. 2.12 the different losses are plotted separately for all three compared wind generators.

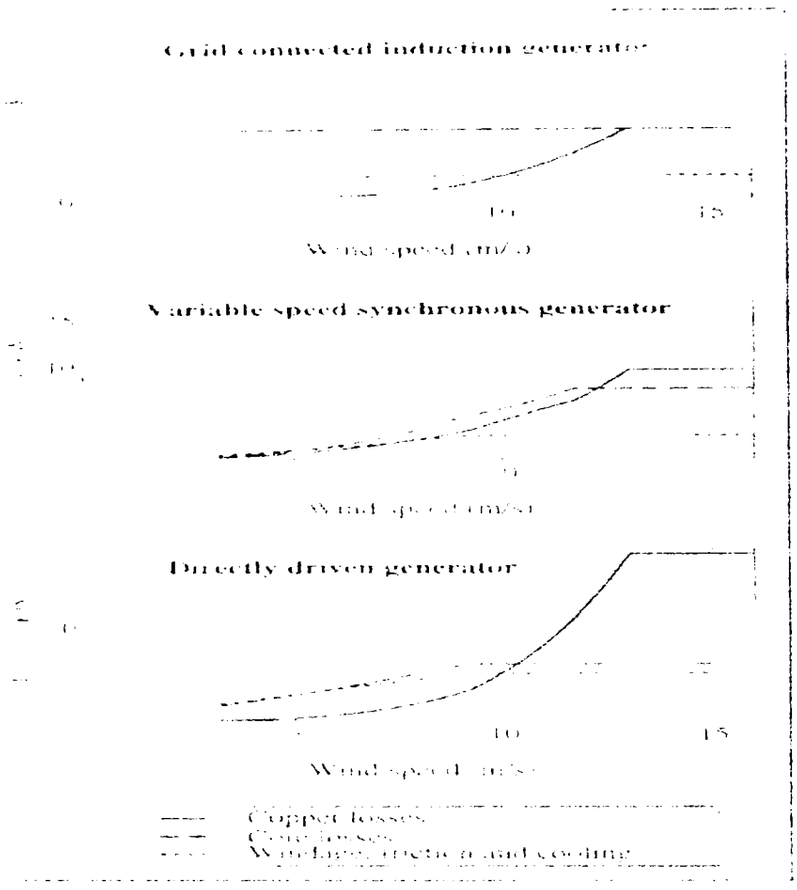


**Figure 2.12**. The wind generator losses for three different systems [29].

In Fig. 2.12 it also can be seen that the copper losses decrease in all the generators as the wind speed decreases. The core losses and the friction losses are not reduced in the grid connected induction generator because the flux linkage and the speed remain approximately constant. In both the variable-speed wind generator systems the wind age and friction losses decrease when the generator speed decreases, below 9 m/s. The core losses of the directly driven PM generator do not decrease before the speed is decreased, since the flux linkage is constant. The core losses of the conventional synchronous generator decrease when the wind speed is below 12 m/s, since the flux linkage is reduced by the excitation control. It can be seen that the copper losses decrease much faster than the other types of losses in all the generators. Because of that, the core losses and friction losses are more important for average losses than the copper losses, especially in grid-connected generator but normally also in variable-speed configurations. Even in the directly-driven generator, which has three times higher copper losses at rated load, the average core losses are still somewhat higher than the average copper losses.

### 2.7.4. The average efficiency

In this section the average efficiency of the different wind generator systems are compared. This is done for three different wind energy converter sites, the low wind speed site (average wind speed 5.3 m/s), the medium wind speed site (6.6 m/s) and the high wind speed site (7.8 m/s).

The calculated average efficiency at different sites and the efficiency at rated load for the three systems are compared in Table 2.7

**Table 2.7**. Average and rated efficiency of the systems [29].

| | Low wins speed site | Medium wind speed site | High wind speed site | Rated load |
|---|---|---|---|---|
| Grid connected induction generator and gear | 82 % | 87.3 % | 89.7 % | 93.8 % |
| Synch. Generator, gear and F.C. | 84 % | 86.8 % | 88.1 % | 90.6 % |
| Directly driven synch. generator and F.C. | 86.4 % | 88.8 % | 89.9 % | 91.6 % |
| Average wind speed | 5.3 m/s | 6.6 m/s | 7.8 m/s | - |
| Weibull parameters (C=2) | A=6 | A=7.4 | A=8.85 | - |
| Average turbine power (Capacity factor) | 15 % | 25 % | 35 % | - |

The comparison shows that the variable-speed wind generators can be about as efficient as the constant wind generator system even though the efficiency at rated load is 3.2 % lower. At a typical site the variable-speed system is 0.5 % less efficient, at a low-wind speed sites it is 2 % more efficient, and at a high-wind speed sites it is 1.6 less efficient than the constant-speed system. It is also found that the directly-driven variable-speed generator is more efficient than the generator equipped with gear box both at low and high-wind speed sites.

The difference in efficiency between constant-speed and variable-speed systems is depending on how efficient the frequency converter (FC) is. If a higher harmonic content is acceptable in the grid current an IGBT inverter can be used and the efficiency of the variable-speed system will be higher.

## 2.8. Generated Power

The cost of wind-generated electricity has declined about 90 % over the last 20 years. Today, large new wind farms at excellent wind sites generate electricity at a cost of 4 to 0.06 US dollars / kWh [6]. That places the cost of power from the most efficient wind farms in a range that is competitive with that of electricity from new conventional power plants.

Using the calculated power transmitted to the hub and subtracting all losses (generator losses, converter losses, and gear box losses), the generated power versus wind speed can be found.

### 2.8.1. Annual wind distribution

To determine the advantages of a specific configuration of a wind turbine, the annualized energy production of the turbine needs to be considered. This involves looking at a standard distribution of wind and combining that with the characteristic of the turbine control to estimate the annual energy production. This may be done by using a probability distribution to determine the number of hours of a particular wind speed which occur in a given year, such as the Weibull distribution or the Raileigh distribution [4, 30, 36]. This distribution may be used with the aero-dynamic power generated at a given average wind speed to determine the total energy generated during the year.

The Weibull distribution is a generalized gamma distribution, and the Rayleigh is a special condition of the Weibull distribution. The Weibull distribution allows for more parameter adjustments, making it more flexible than the Rayleigh distribution, but at the price of being more complicated. It is often suggested for use when estimating the cost of energy [30, 36]. Because of the additional flexibility, wind data for the specific site is required. For a generic wind study, it is more practical to use a Rayleigh distribution, where the variance is directly tied to the mean [30].

The procedure for calculating the total energy produced for a given wind distribution is performed by first finding the total number of hours per year for a particular wind speed. This is possible by finding the probability of a particular wind speed for the desired distribution and multiplying it by the numbers of hour per year. The probability that the wind lies between two wind speeds is given by:

$$P_r(u+\Delta u) - P_r(u-\Delta u) = p(u)\Delta u \quad \text{.....(2.3)}$$

where $P_r(u)$ is the probability function, and p(u) is the probability density function. For the Rayleigh distribution, the probability distribution function is given by:

$$p(u) = \frac{\pi \cdot u}{2 \cdot u_a} \cdot \exp\left[-\frac{\pi}{4}\left(\frac{u}{u_a}\right)^2\right] \quad \text{.....(2.4)}$$

where $u_a$ is the average wind velocity. From this, the number of hours when a wind turbine is operated at a given speed is estimated as:

$$H(u) = 8760 \cdot p(u) \cdot \Delta u \quad \text{.....(2.5)}$$

where 8760 represents the total number of hours in a 365-day year. Once the hours a particular wind speed occurs is determined, the amount of power is calculated for the given turbine control at the particular wind speed. The power is then multiplied by the time for the wind speeds for a given year to find the total energy production:

$$E(u) = P(u) \cdot H(u) \quad \text{.....(2.6)}$$

where P(u) is the developed power for a given wind turbine. This procedure is repeated through all the wind speeds, and the sum will give the estimate of the total annualized wind energy [30]:

$$E_t = \sum_u E(u) \quad \text{.....(2.7)}$$

The calculation for the annual energy production is based on an annual wind distribution, where it is assumed that the turbine has a total availability of 8760 hours per year, as shown in Fig. 2.13.

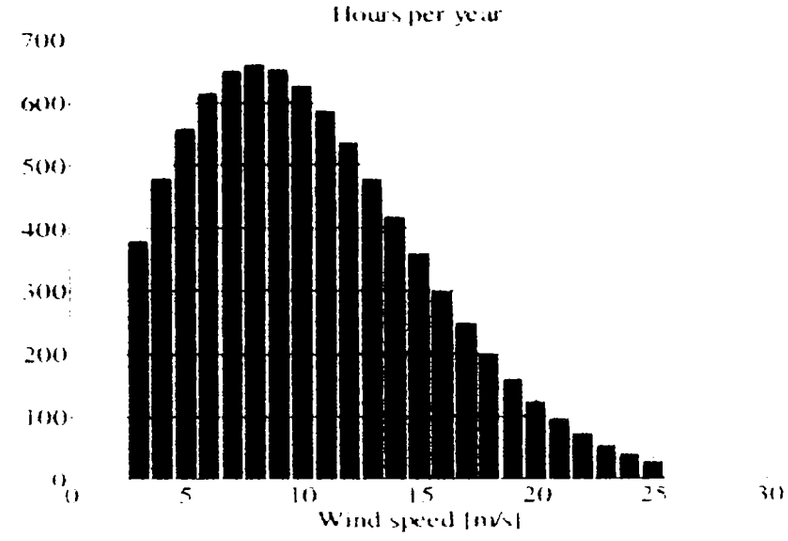


a)

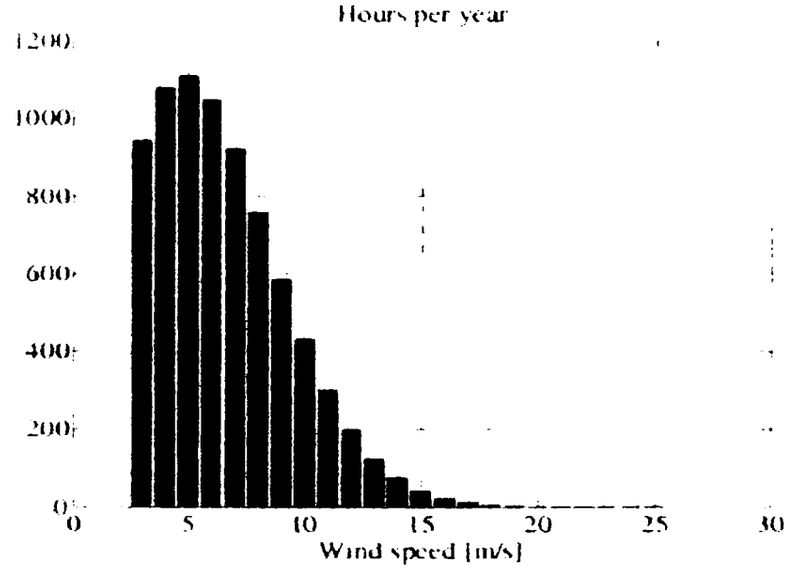


b)

**Figure 2.13**. Comparison between annual wind distribution for a site in IEC class 1,a) with an average wind speed of 10 m/s and for a site in IEC class 4, b) with an average wind speed of 6 m/s [4].

## 2.8.2. Annual energy production

Constant speed turbines must be concerned with limitations of the overall system. Since the speed is held essentially constant, there is not a concern that the system will be running above rated speed under normal operation conditions. Since the power generated is related to the tip speed ratio, the amount of the energy produced would depend on the speed of turbine rotor, as well as the average wind speed. With a generator operating at constant speed, the turbine's speed would depend on the gear ratio chosen. When choosing a gear ratio it is therefore important to consider the average wind speed of the site.

The annual energy production for a variable-speed wind system was calculated over the same range of average annual wind speeds as the constant-speed systems. For these computations, a Rayleigh distribution was assumed for the wind speed [30]. The speed limit was set to match the speed of a system operating at constant speed with a gear ratio of 25:1. The power limit was set at 30 kW, the same as the constant-speed systems. The graph is shown in Fig. 2.14 and may be concluded that the variable-speed system generates more total energy at any wind speed. For example, for an average annual wind speed of 7 m/s, the energy produced by the variable speed wind system was 75.8 MWh, while the energy produced by a fixed-speed system with a 25:1 gear ratio was 54.6 MWh.

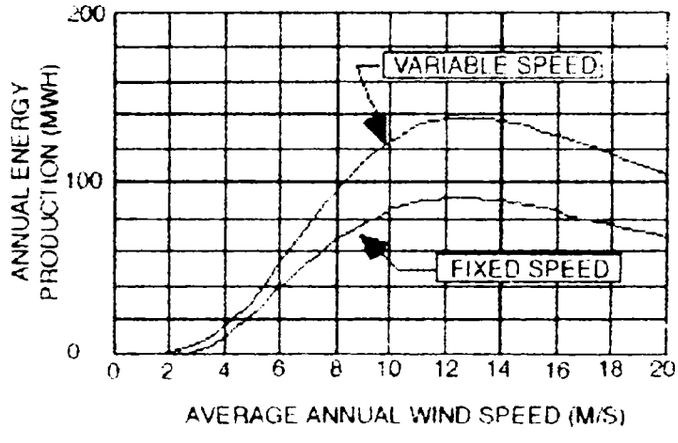


**Figure 2.14.** Annual energy production versus average annual wind speed [30].

The comparison between annual energy production with constant-speed and variable-speed wind turbines points out that although improvements can be made by matching the gear ratio to the wind profile, while the variable speed operation can improve the wind production further. The variable-speed operation thus gives a more flexible system under various wind conditions. The variable-speed wind turbines also show improved energy production over the constant-speed systems.

### 2.8.3. Annual energy loss distribution

Nowadays there is a trend towards application of variable speed wind turbines, in particular for turbines in the MW range. Therefore, for optimal energy extraction, the wind turbines should operate at variable speed.

In this section the losses of the different components of two variable speed wind generator systems are evaluated, with regards to their annual energy production. Besides paying attention to the annual energy production, the evaluation has to point out in which part of each turbine concept the main part of the energy is dissipated. The candidates are 3 MW variable speed wind turbines based on the DFIG with two PWM-VSI Frequency Converters and with passive external elements in the rotor side.

Having the wind distribution for a given site (see section 2.8.1) and the models of the system components, it is possible to predict the annual wind energy production. The Figure 2.15 shows a general model for calculating the produced power for a given wind power.

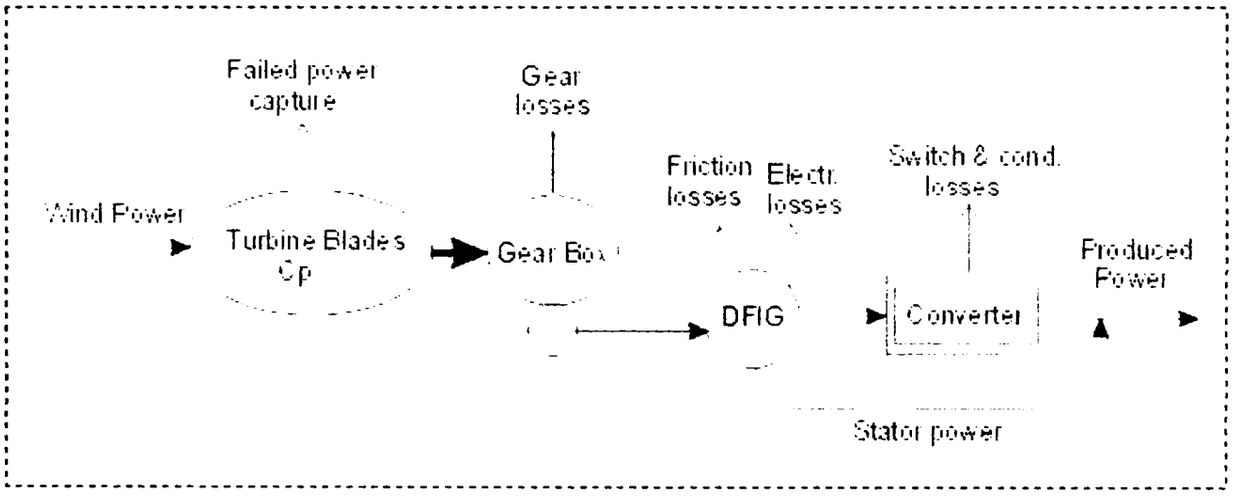


**Fig. 2.15.** The model for calculating the produced power for a given wind power of a wind turbine with DFIG.

In order to point out which part of the turbine accounting for the major parts of the energy losses, the annual energy loss distribution for both configurations are calculated as depicted in Fig. 2.16. The calculations included power losses due to the Cp coefficient variation, losses in the gear train, mechanical and electrical losses in the generators and finally converter losses.

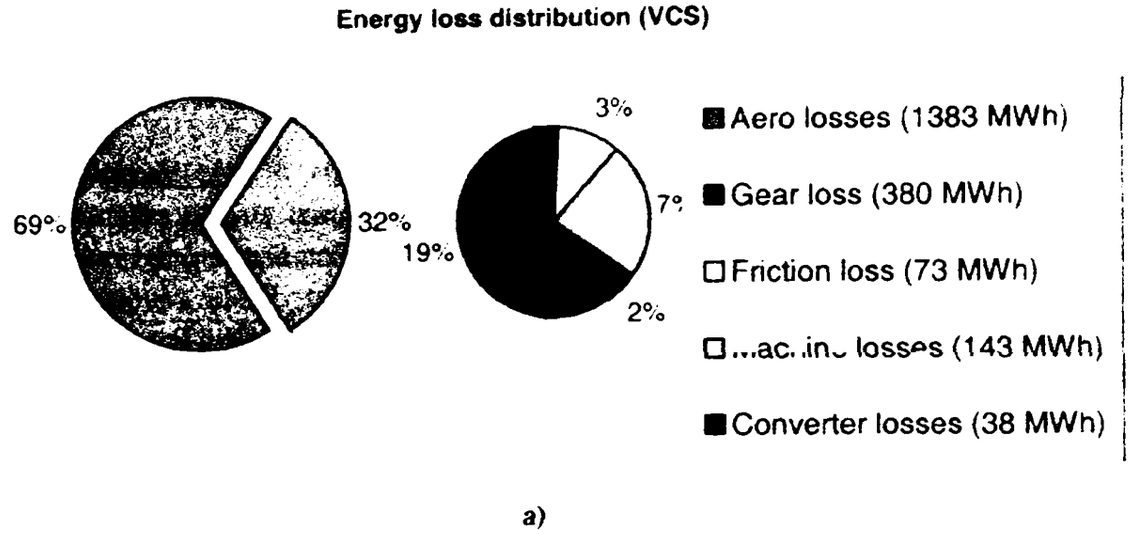


a)

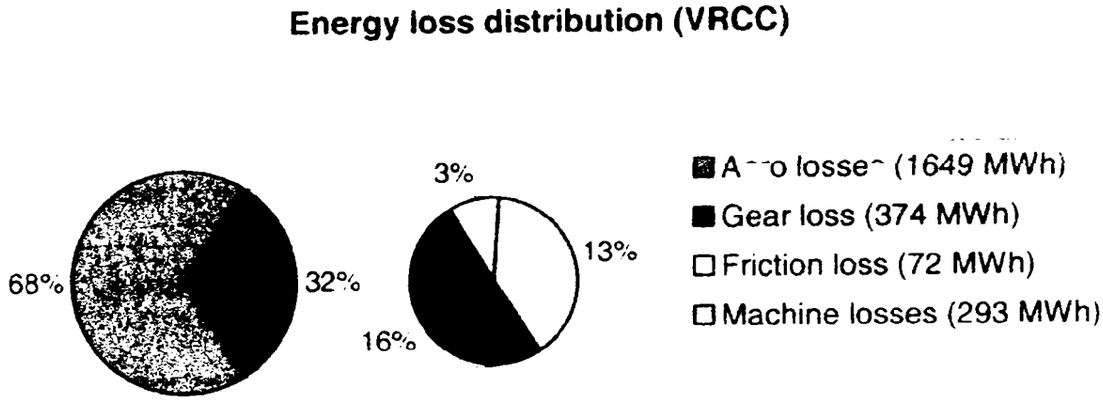


b)

**Figure 2.16**. Annual energy loss distribution for different components of a variable-speed wind turbines of 3 MW with DFIG and back-to-back frequency converter a) (Vestas-OptiSpeed concept), and with DFIG with passive elements, b) (Vestas-OptiSlip concept) [35].

The calculations of the aero-dynamic losses assume a theoretical maximum utilization of the wind energy of 0.59 whenever the produced output power is below 3 MW. The aero losses and friction losses are equals for both concepts while the gear drive losses (16 % and 19 %). and machine losses (7 % and 13 %) are different, as can also be seen in Fig. 2.16. The machine losses are different due to the fact that the OptiSlip concept includes the losses of the external controllable rotor resistance. Regarding to the loss distribution it is concluded that the energy losses due to the turbine blades accounted for the major part of the losses for both systems. The losses in the gear drive are the second largest while the losses in the converter and the friction losses are the least significant for the considered topologies.

The comparison between both topologies presented before, point out that the OptiSpeed concept has a very high utilization of the wind energy while the OptiSlip concept has a slightly lower utilization of the wind energy.

## 2.9. Discussion and Conclusion

The state of the art of wind turbines seen from electrical point of view includes old and new potential concepts of generators and power electronics based on technical aspects and market trends. Several generic types of generator are possible candidates in wind turbines. The squirrel cage induction generator has been frequently applied commercially. A second popular type is the induction generator with wound rotor, while the third is the current excited synchronous generator.

A large number of alternative wind turbine designs exist but the state of the art wind turbine may be summarized as a 3-bladed upwind turbine using active stall control with constant speed using a two speed asynchronous generator or pitch control combined with variable speed. Moreover the variable speed concept is mainly realized using a double-fed induction generator with a rotor connected IGBT based frequency converter (two back-to-back PWM-VSI Converters). Because of these both configurations have been chosen to be analyzed, modeled, simulated and tested in the next chapters.

More research is also necessary in the classical solutions using power electronics. Especially, it is important to be able to predict the losses in order to keep a high reliability. As the back-to-back converter is state of the art today in wind turbine applications it can be used as a reference in a benchmark of the other converter topologies regarding the number of the components and their ratings, the efficiency, the harmonic performances and implementation.

The doubly fed induction generator is now widely used but still research is needed in diagnosis, control and even more optimized design in order to reduce the overall prices of the generator system.

In wind power systems in the range of more than 1.5 MW per unit, the DFIGs are used as a viable alternative to adjust rotor speed and to keep system costs of the power converter minimal. In power systems with a high level of wind energy penetration it is necessary to adapt the wind turbines (or the wind farms) and the rest of the power system in order to ensure optimal operation of the combined system. Optimal operation in this context means the lowest operating cost of the complete system as well as utilization of the wind energy. Wind power installations with blade angle control and/or power converters are able to control the active power supply to the power system. Moreover, wind power installations with power converters are able also to control the reactive power supply to the power system. The active power control in these power installations (wind farms) normally serve to obtain maximum production, and limit the power to avoid only overloading and stress of the wind turbine components, whereas the reactive power control serves to obtain a constant, high power factor, e.g. at unity.

The main challenges related to technology development are to reduce the technical uncertainties relating to production and durability for future wind energy project all over the world, to maintain the development towards a more optimal, reliable and cost-optimized technology, to improve the power plant characteristics of the wind turbine plants, developed the wind turbine technology for future applications, such as hybrid systems for smaller/isolated communities, the integration of a variable energy source into the energy system (HVDC transmission system), energy storage technologies, power flow control, compensation units and production forecasting and control of the power plants.

## References

[1] ∴ International Wind Energy Development. "World Market Update 1999". *BTM Consults Aps. Ringkobing, Denmark 2000 ISBN 87-987788-0-3.*

[2] Siegfried Heier. "Wind energy conversion systems", book. John Wiley & Sons Inc., New York. 1998.

[3] L.H. Hansen, L. Helle, F. Blaabjerg, E. Ritchie, S. Munk-Nielsen, H. Bidner, P. Sorensen and B. Bak-Jensen, "Conceptual Survey of Generators and Power Electronics for Wind Turbines", Riso-R-1205 (EN). December 2001.

[4] ∴ www.windpower.org, Danish Wind Industry Associations, Guided Tour on Wind Energy.

[5] S. Muller, M. Deicke and R.W. De Doncker, "Doubly Fed Induction Generator Systems for Wind Turbines". IEEE Industry Applications Magazine, May-June 2002, pp. 26-33.

[6] Saifur Rahman, "Green Power. What is it and where can we find it?", IEEE power & energy magazine, January/February 2003, pp. 30-37.

[7] A.K. Wallace and J.A. Oliver, "Variable-speed generation controlled by passive elements", International conference on electric machines, 1998, Istanbul, pp. 1554-1559.

[8] Francois Giraud and Ziyad M. Salameh, "Wind-Driven, Variable-Speed, Variable-Frequency, Double-Output, Induction Generators", Electric Machines and Power Systems, vol. 26, 1998, pp. 287-297.

[9] R. Pena, R. Cardenas, R. Blasco, G. Asher, J. Clare, "A Cage Induction Generator using back-to-back PWM Converters for Variable Speed Grid Connected Wind Energy System", Proceedings of IECON'01, pp. 1376-1381.

[10] www.NREL.gov, National Renewable Energy Lab.

[11] J.G. Slootweg., S. W. H De Haan., H. Polinder, and W.L. Kling, "Voltage Control Methods with Grid Connected Wind Turbines: a tutorial review", *Wind Engineering*, Vol. 25, no. 6, 2001, pp. 353-365.

[12] J.G. Slootweg, and W.L. Kling, "Modelling and Analysing Impacts of Wind Power on Transient Stability of Power Systems", *Wind Engineering*, Vol. 26, no. 1, 2002, pp. 3-20.

[13] Dejan Schreiber, "Applied Designs of Variable Speed Wind Turbines and New Approaches", PCIM 2002.

[14] H. Akagi and H. Sato, "Control and Performance of a Doubly-Fed Induction Machine Intended for a Flywheel Energy Storage System", IEEE Transactions on Power Electronics, Vol. 17, No. 1, January 2002, pp. 109-116.

[15] R.Cardenas, R. Pena, G.M. Asher and J.C. Clare, "Experimental emulation of wind turbines and flywheels for wind energy applications", Proceedings of IEEE-EPE 2001, Graz.

[16] S.A. Papathanassiou and M.P. Papadopoulos, "Dynamic Behavior of Variable Speed Wind Turbines under Stochastic Wind", IEEE Transactions on Energy Conversion, Vol. 14, No. 4, December 1999, pp. 1617-1623.

[17] R. Pena, J.C. Clare and G.M.Asher, "Doubly fed induction generator using back-to-back PWM converters and its application to variable-speed wind energy generation", IEE Proc.-Electr. Power Appl., Vol. 143, No. 3, May 1996, pp. 231-241.

[18] A. Tapia, G. Tapia, J.X. Ostolaza, J.R. Saenz and J.L. Berasategui, "Reactive Power Control of a Wind Farm made up with Doubly Fed Induction Generators", Paper accepted for presentation at PPT (Porto Power Tech Conference)-IEEE 2001, 10th - 13th September, Porto-Portugal.

[19] V. Akhmatov, "Modelling of Variable-Speed Wind Turbines with Doubly-Fed Induction Generators in Short-Term Stability Investigations", 3rd Int. Workshop on Transmission Networks for Offshore Wind Farms, April 1-12, 2002, Stockholm, Sweden.

[20] Rajib Datta and V.T. Ranganathan, "Direct Power Control of Grid-Connected Wound Rotor Induction Machine without Rotor Position Sensors", IEEE Transactions on Power Electronics, vol. 16, no. 3, May 2001, pp. 390-399.

[21] L. Helle and S. Nielsen, "Comparison of Converter Efficiency in Large Variable Speed Wind Turbines", IEEE Transaction on Power Electronics, Vol. , No. , 2001, pp. 628-634.

[22] Z. Chen, E. Spooner, "Grid Interface for a Variable-Speed, Permanent-Magnet, Wind Turbine Generator", International Conference on Electric Machine-ICEM'96, Vol. 3, pp. 347-352.

[23] Z. Chen, E. Spooner, "Wind Turbine Power Converters: A comparative study", IEE International Conference – PEVD'98, London, September, pp. 471-476.

[24] Z. Chen, S. Arnalte Gomez and M. Mc Cormick, "A fuzzy logic controlled power electronic system for variable speed wing wind energy conversion systems", Power Electronics and Variable Speed Drives, 18-19 September 2000, Conference Publication No. 475, IEE 2000, pp. 114-119.

[25] D.C. Aliprantis, S.A. Papathanassiou, M.P. Papadopoulos and A.G. Kladas, "Modeling and control of a variable-speed wind turbine equipped with permanent magnet synchronous generator", ICEM 2000, 28-30 August, Espoo-Finland, pp. 558-562.

[26] I. Schiemenz and M. Stiebler, "Maximum power point tracking of a wind energy system with a permanent-magnet synchronous generator", ICEM 2000, 28-30 August, Espoo-Finland, pp. 1083-1086.

[27] A.S. Neris, N.A. Vovos and G.B. Giannakopoulos, "A variable speed wind energy conversion scheme for connection to weak ac systems", IEEE Transactions on Energy Conversion, Vol. 14, No. 1, March 1999, pp. 122-127.

[28] S. Mpekos, E. Tsimplostephanakis, E. Tatakis and A. Safacas, "Control technique for a variable speed WECS using a synchronous generator", ICEM 2000, 28-30 August, Espoo-Finland, pp. 1092-1096.

[29] Anders Grauers, "Efficiency of three wind energy generator systems", IEEE Transactions on Energy Conversion, Vol. 11, No. 3, September 1996, pp. 650-657.

[30] Donald S. Zinger and Eduard Muljadi, "Annualized Wind Energy Improvement using Variable Speeds", IEEE Transactions on Industry Applications, Vol. 33, No. 6, November/December 1997, pp. 1444-1447.

[31] A. Miller, E. Muljadi and D.S. Zinger, "A variable speed wind turbine power control", IEEE/PESC Summer Meeting, Denver-CO, July 1996.

[32] D.S. Zinger, E. Muljadi and A. Miller, "A simple control scheme for variable speed wind turbines", IEEE-IAS Annual Meeting, October 1996, pp. 1613-1618.

[33] R. Spee, S. Bhowmik and J.H.R. Eslin, "Adaptive control strategies for variable speed doubly-fed wind power generation systems", Proc. IEEE-IAS Annual Meeting, 1995, pp. 545-552.

[34] Q. Wang and L. Chang. "An Independent Maximum Power Extraction Strategy for Wind Energy Conversion Systems", Proceedings of the 1999 IEEE Canadian Conference on Electrical and Computer Engineering Shaw Conference Center, Edmonton-Alberta, Canada, May 9-12, 1999, pp.1142-1147.

[35] ∴ www.vestas.com, Vestas Wind Systems.

[36] ∴ http://www.awea.com, The American Wind Energy Association, Wind Turbine Configurations.

# Chapter 3

## Constant Speed Wind Turbine Generators Modeling and Simulation

**Chapter contents**

## 3.1. Overview

In this paper a complete simulation model of a constant speed wind turbine with rotor cage induction generators is presented using data from a new wind farm. A model of the wind turbine with 2MW and 0.5 MW induction generators are presented in detail. A set of simulations is performed and they show that it is possible to simulate a complete wind turbine as a part of wind farm from wind to the grid. The simulation tool can be used to simulate bigger wind generators connected to the grid.

This chapter also describes a model, which is being developed to simulate the interaction between a wind turbine and the power system. The model is intended to simulate the behavior of the wind turbine using induction generators both during transient grid fault events and during normal operation. Sample simulation results for two induction generators (2 / 0.5 MW) validate the fundamental issues.

This paper also presents the measured and simulated power quality performances of wind turbines during normal operation. The motivation for this investigation is still increasing wind energy penetration in the power system. In the last few years the trend has moved from installations including few wind turbines to planning of large wind farms with capacity over hundreds of MW, e.g. in Denmark five new wind farms with approximately 150 MW each, has been already installed offshore [1, 3]. These wind farms are only the beginning of an offshore wind energy development with thousands of MW concentrated in a few appointed offshore areas.

The system model proposed in this paper is developed in the dedicated power system simulation tools MATLAB-Simulink and DIgSILENT, which gives access to an extensive library of grid components, but requires implementation of the relevant wind turbine model, more details can be found in Appendix B. The model also includes wind speed fluctuations and control of soft–starter, enabling simulation of the power quality characteristics of the wind turbine. Finally, the model can be used to study alternative control strategies for wind turbine and additional equipment such as compensation units and storage systems [12, 13].

## 3.2. Wind turbine modeling

The purpose of the model is to simulate the dynamic behavior and the electrical properties of a wind turbine. The modeling of the wind turbine should create a model as simple as possible from a mechanical point of view, but capable of providing a good description of the electrical characteristics of a wind turbine. The wind turbine model consists of different component models: wind model, aerodynamic model, transmission model and the electrical components that include induction generator model, soft-starter, capacitor bank and transformer [12, 13 and 14].

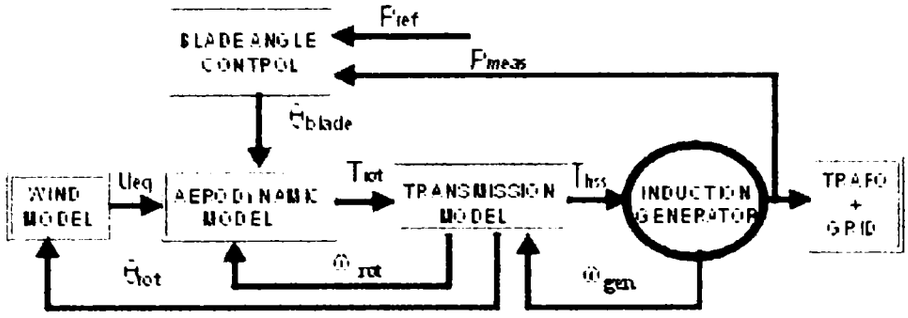


**Fig. 3.1**. Simplified scheme of the wind turbine model.

As shown in Fig. 3.1, the wind model generates an equivalent wind speed ($u_{eq}$), which, together with the blade pitch angle ($\theta_{blade}$) and rotor speed ($\omega_{rot}$), are input to the aerodynamic block. The output of the aerodynamic model is the aerodynamic torque ($T_{rot}$), which is the input for the transmission system together with the generator speed ($\omega_{gen}$). The transmission system has as output the mechanical torque ($T_{hss}$) on the high-speed shaft, which is used as an input to the generator model. Finally, the blade angle control block models the active control loop, based on the measured power and the set point.

## 3.2.1. The Wind Model

The wind acting on the rotor plane of a wind turbine is very complex and includes both deterministic effects (mean wind, tower shadow) and stochastic variations due to turbulence [10, 14 and 18]. To model this coherence, Mann wind field method [18] is applied. The Mann model can be used in 3 dimensions, but in our case, only two dimensions are used, because the wind speed is only simulated in hub height, as depicted in Fig. 3.2.

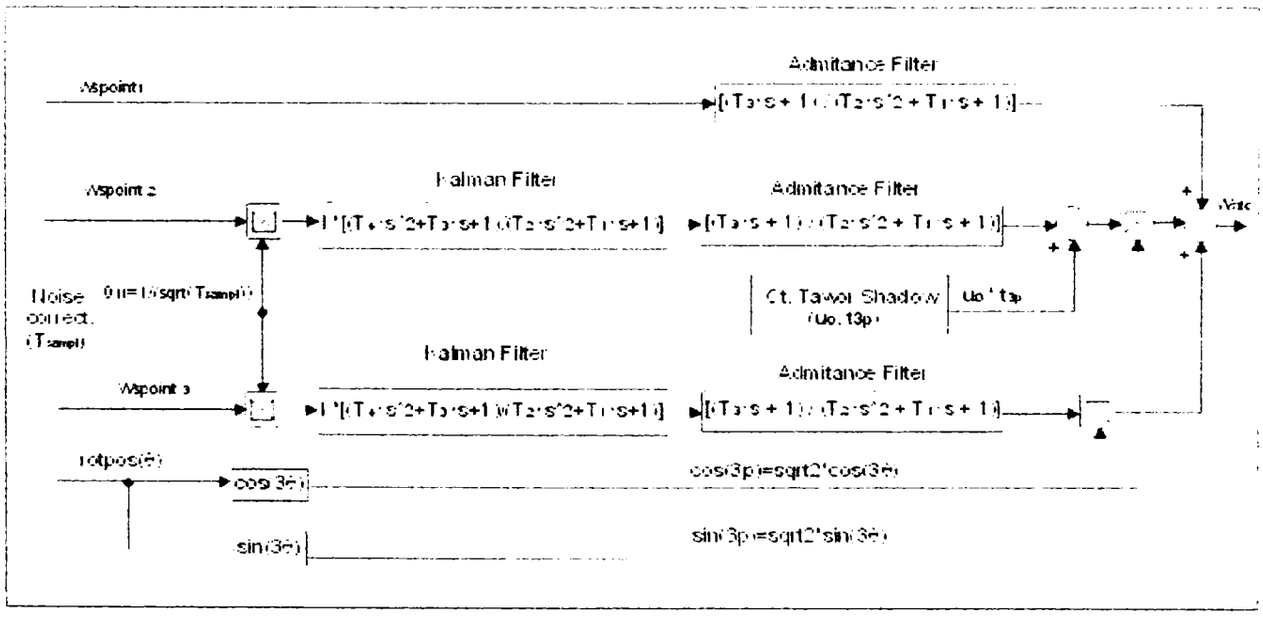


**Fig. 3.2**. Rotor wind speed model- block diagram.

The Mann model has been developed using second order Kalman Filters which contains the correlation coefficient (k) and the time constants ($T_1$-$T_4$) for two time series wind speeds with the same standard deviation. The transfer function of Kalman Filter is given by:

$$H_{KF}(s) = k \cdot \frac{T_4 \cdot s^2 + T_3 \cdot s + 1}{T_2 \cdot s^2 + T_1 \cdot s + 1}; k = 0.007 * t_i * \sqrt{L * u_0} \quad \text{.....(3.1)}$$

Where, $t_i$-turbulence intensity [%], L-length scale [m], $u_o$-mean wind speed [m/s] and s-Laplace operator. Time constants are expressed by:

$$T_1 = 3.76 \cdot c; T_2 = 1.346 \cdot c^2; T_3 = 1.387 \cdot c; T_4 = 0.0185 \cdot c^2; c = \frac{L}{2 \cdot \pi \cdot u_0} \quad \text{.....(3.2)}$$

The rotor wind speed model includes the effect of rotational sampling of turbulence and the tower shadow effect that provide fluctuations in the wind speed with three times the rotational speed of wind turbine, i.e. so called 3p effect. To include the 3p effect, the position of the rotor ($\theta_{rot}$) is used as input to the rotor wind speed model, as is also illustrate in Fig. 3.2. The idea of the rotor wind model is therefore to produce a single equivalent wind speed ($w_{sfic}$-$u_{eq}$), using an Admitance Filter, which includes the effect of different wind speeds in the wind turbine rotor plane. At the same time it can be used as input to a simplified aerodynamic model based on the aerodynamic efficiency ($C_p$). The transfer function of Admitance Filter is given by:

$$H_{AF}(s) = \frac{T_3 \cdot s + 1}{T_2 \cdot s^2 + T_1 \cdot s + 1} \quad \text{.....(3.3)}$$

Where time constants ($T_1$-$T_3$) in (3.3) are expressed by:

$$T_1 = 1.77 \cdot d; T_2 = 0.369 \cdot d^2; T_3 = 9.01 \cdot d; d = \frac{D}{2 \cdot u_0} \quad \text{.....(3.4)}$$

In which ($D$) represents rotor diameter of wind turbine. More details about rotor wind model and parameters (variables) can be found in *Appendix B1*.

The wind model describes the fluctuations in the wind speed ($w_{spoint}$) that generates a hub wind speed ($w_{sfic}$), as depicted in Fig. 3.3 a). Actually there are two types of wind models, combined as also shown in Fig. 3.3 a). The first is the hub wind model, which models the fixed point wind speed at hub height of wind turbine. The second one is the rotor wind model. The hub wind speed ($u_{hub}$-$w_{spoint}$) is used as input to the rotor wind model to produce an equivalent wind speed ($u_{eq}$-$w_{sfic}$), which accounts for the rotational sampling on each of the blades, where an averaging of the fixed speed over the whole rotor, the rotational turbulence and the tower shadow influence are taken into account.

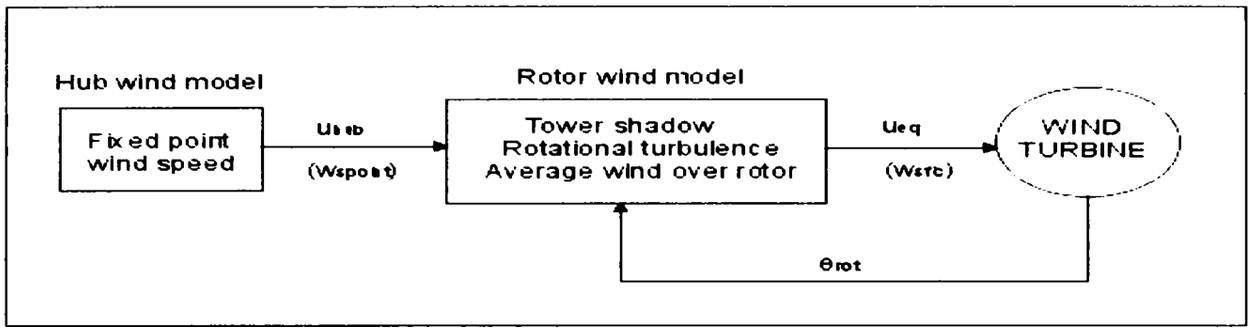


a)

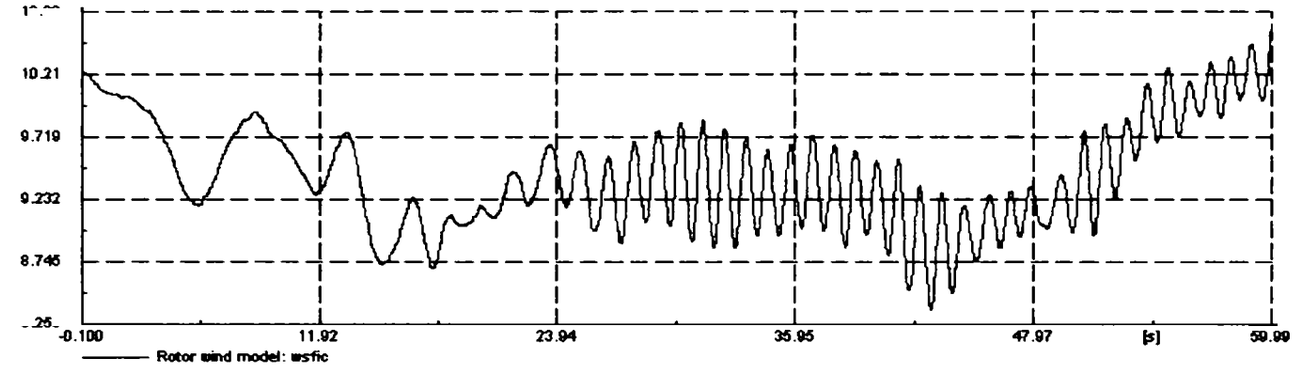


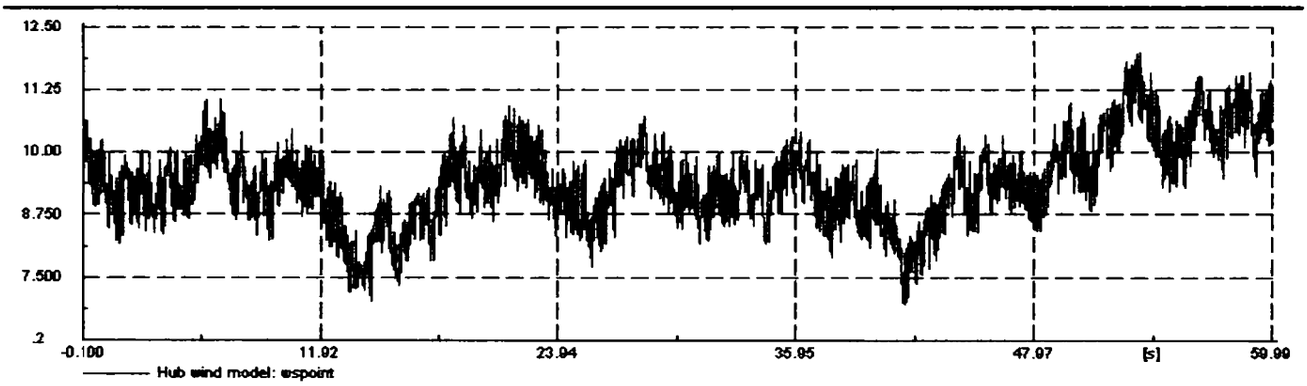


b)

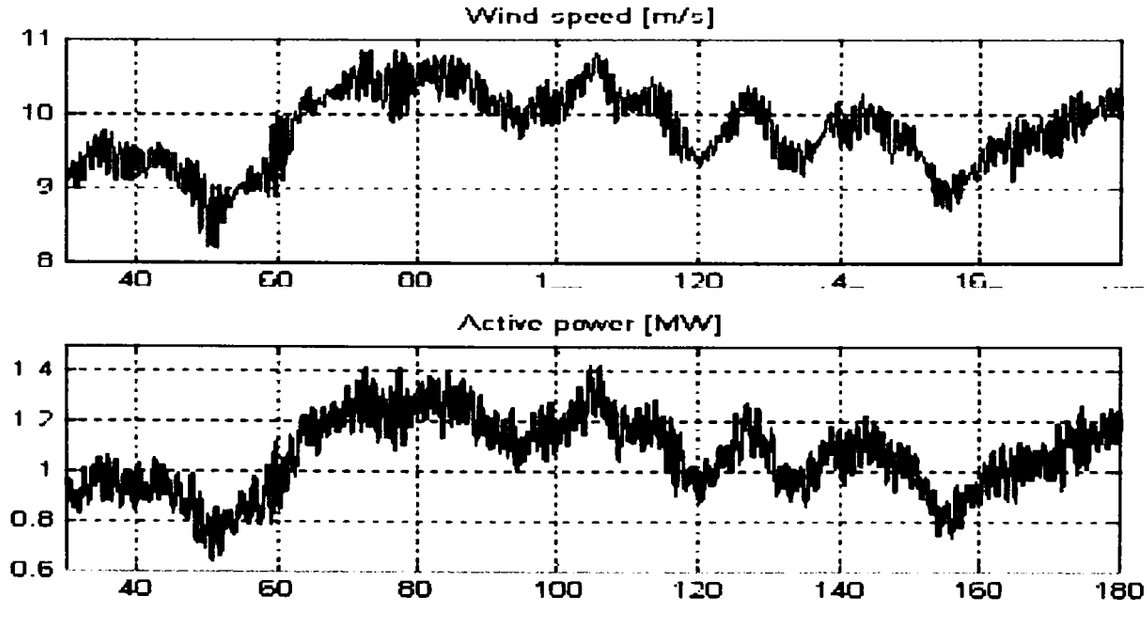


c)

**Fig. 3.3**. Simplified scheme of wind model (a) and simulated rotor wind model ($w_{sfic}$) and hub wind model ($w_{spoint}$) as a function of time (b) and simulation results of wind speed and active power waveforms versus time (c) for a 2 MW wind turbine.

The wind models describe the fluctuations in the wind speed, which influence the power quality and control characteristics of the wind turbine. Thus, the wind speed model simulates the wind speed fluctuations that influence the fluctuations in the power of the wind turbines [10, 18], as is shown in Fig. 3.3 c). Figure 3.3 c) also shows a simulation result for 2 MW wind turbine, at an average wind speed of 10 m/s.

The simulations shown in Fig. 3.3 b) illustrate the effect of the rotational sampling, which is a consequence of fluctuations in the wind speed seen by the rotating of the blades. The rotational sampling causes fluctuations in the power with three times the rotational frequency (3p), both due to the tower shadow effect and due to the turbulence [10, 19].

## 3.2.2. The Aerodynamic Model

A wind turbine is essentially a machine that converts the kinetic energy of the moving air (wind) first into mechanical energy at the turbine shaft and then into electrical energy [3].

The Figure 3.4 describes the conversion of wind power ($P_{WIND}$) into mechanical ($P_{MEC}$) and thereafter into electrical power ($P_{EL}$).

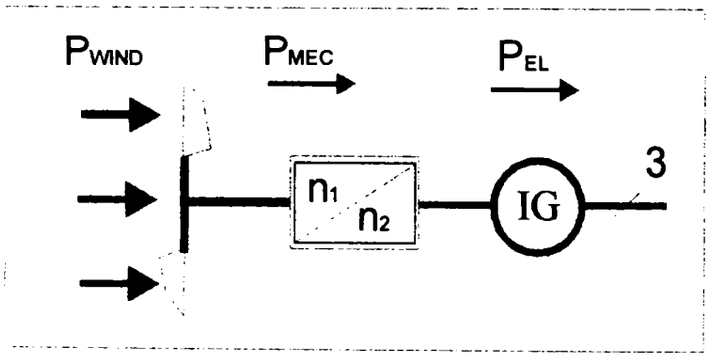


**Fig. 3.4.** A block diagram of the wind turbine.

The interaction of the turbine with the wind is complex but a reasonably simple representation is possible by modelling the aerodynamic torque or the aerodynamic power as described below.

The force of the wind creates aerodynamic lift and drag forces on the rotor blades, which in turn produce the torque on the wind turbine rotor [3].

The aerodynamic torque is given by:

$$T_{rot} = \frac{P_{aero}}{\omega_{rot}} = \frac{1}{2\lambda} \rho \pi R^3 C_p(\lambda, \theta_{pitch}) \quad \text{.....(3.5)}$$

Where ($P_{aero}$) is the aerodynamic power developed on the main shaft of a wind turbine with radius ($R$), at a wind speed ($u_{eq}$) and air density ($\rho$). It is expressed by:

$$P_{aero} = \frac{1}{2} \rho \pi R^2 u_{eq}^{\ 3} C_p(\lambda, \theta_{pitch}) \quad \text{.....(3.6)}$$

The air density ( $\rho$ ) is depending on the temperature and on the pressure of the air.

The dimensionless power coefficient $C_p(\lambda,\theta_{pitch})$ represents the rotor efficiency of the turbine, as can be seen in Fig. 3.5 (its upper bound is known as Betz' limit: $C_p<16/27=59.3$ %). It is taken from a look-up table, which contains the specific aerodynamic characteristics for the 2 MW wind turbine.

Figure 3.5 a) shows how this coefficient depends on the tip speed ratio $\lambda = \omega_{rot} \cdot R / u_{eq}$ and on the blade angle ($\theta_{pitch}$), ($\omega_{rot}$) denotes the rotor speed. For a constant speed wind turbine, the power coefficient decreases when the wind speed $u_{eq}$ increases ( $\lambda$ small). This fact is used in the passive stall control wind turbine, and can be seen in Fig. 3.5 b).

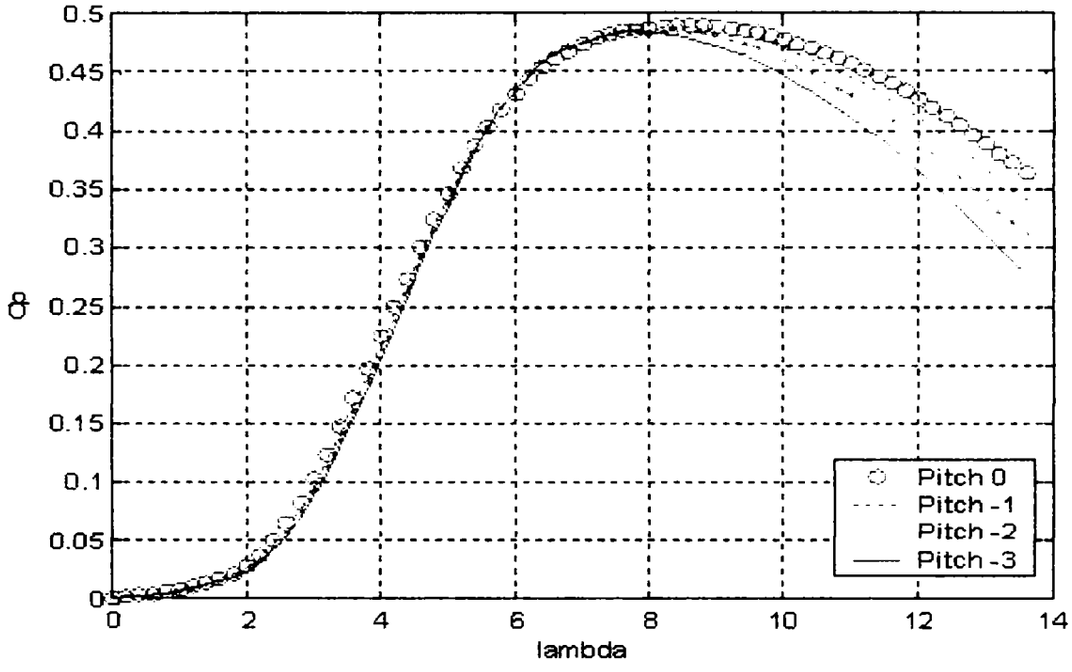


(a)

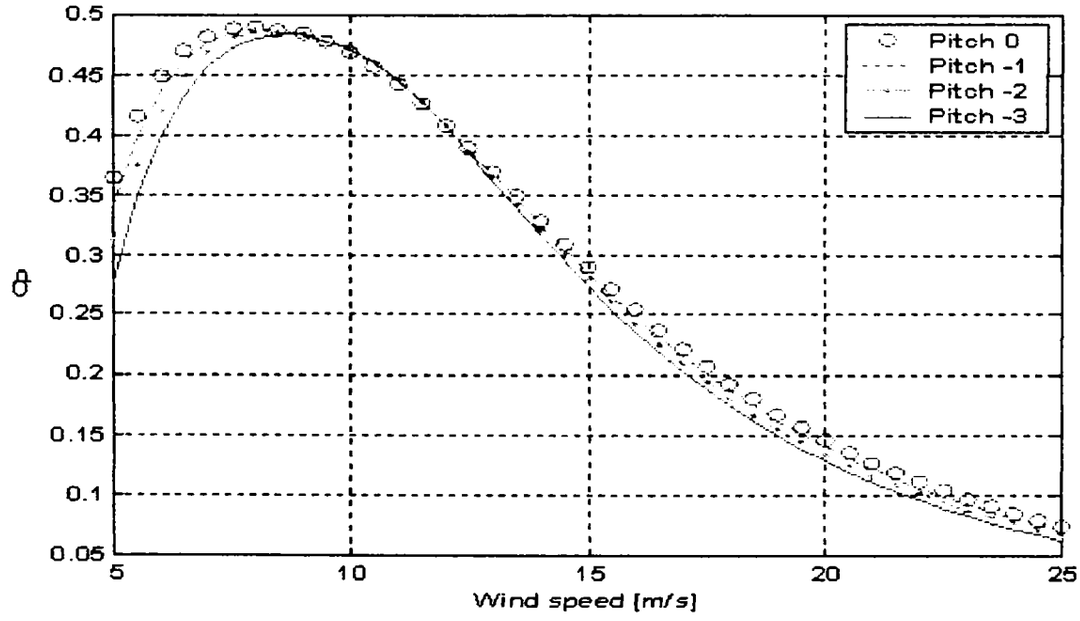


(b)

**Figure 3.5.** Power coefficient (Cp) of the 2MW wind turbine against ( $\lambda$ )

(a), and versus wind speed (b), for different pitch angles.

The efficiency coefficient ($C_p$) changes with different negative values of the pitch angle ($0^0$, $-1^0$, $-2^0$, and $-3^0$) every time when the wind changes, in order to keep the rotor blades at the optimum angle, but the best efficiency is obtained for $\theta_{pitch} = 0^0$.

The aerodynamic model is based on $C_p$ curves for the given rotor blades and the aerodynamic power and torque given by (3.5) and (3.6), as can be seen in Fig. 3.6. The representation of the $C_p$ curves, Fig. 3.5, based on a look-up table, is done by using aerodynamic measurements on rotating blades of 2 MW wind turbine (for example with the rated rotational speed). Therefore, the variation of $C_p$ coefficient at low values or rotor speed is not appropriate, because it corresponds to a zero aerodynamic torque for a not rotating wind turbine. When $\omega_{rot}$ is close to zero, the aerodynamic torque is not zero, while the aerodynamic power is. In order to overcome this inaccuracy, in the simulation model is made the approximation that for rotor speeds less than a certain value $\omega_{low}$ the aerodynamics are computed considering $\omega_{rot} = \omega_{low}$.

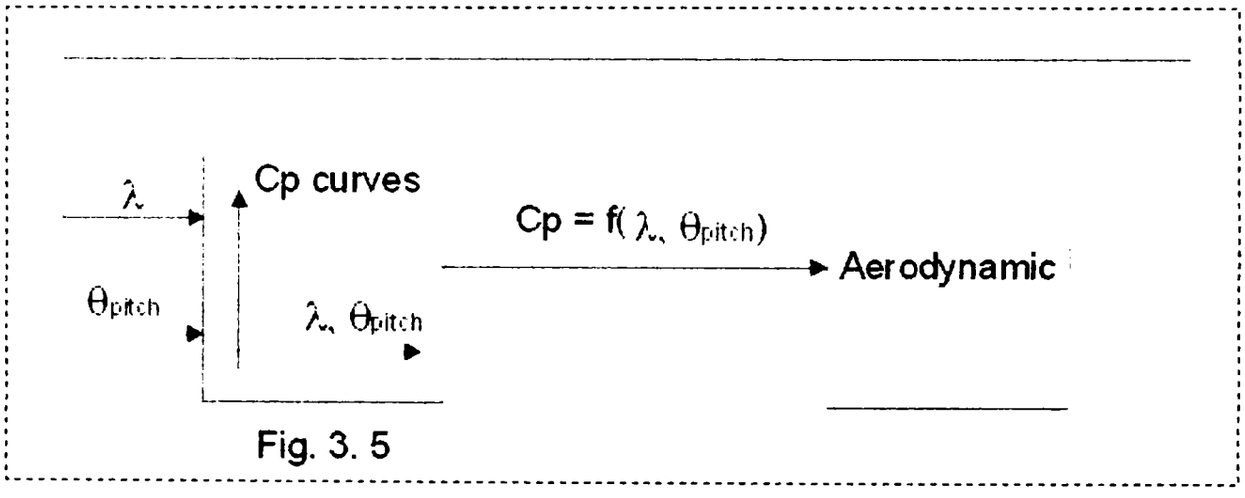


**Figure 3.6**. Aerodynamic model based on aerodynamic efficiency Cp of wind turbine.

## 3.2.3. Transmission System Model

To describe the impact of the dynamic behavior of the wind turbine, a simple model is considered, where the tower bending mode and the flap-bending mode of the wind turbine are neglected. It is assumed that all the torsion movements are concentrated in the low speed shaft, as ($T_{lss}$). Emphasis is placed on the parts of the dynamic structure of the wind turbine, which contributes to the interaction with the grid, i.e. which influence the power. Therefore only the drive train is considered in the first place because the other parts of the wind turbine structure have less influence on power.

The drive train model is illustrated in Fig. 3.7. The input to the model is the aerodynamic torque ($T_{rot}$). This is converted into the torque on the low speed shaft ($T_{lss}$), which is further scaled down through the gearbox to the torque on the high-speed shaft ($T_{hss}$). The generator inertia is implemented as part of the generator model, not as a part of the transmission system. The output of the model is the torque on the high-speed shaft ($T_{hss}$).

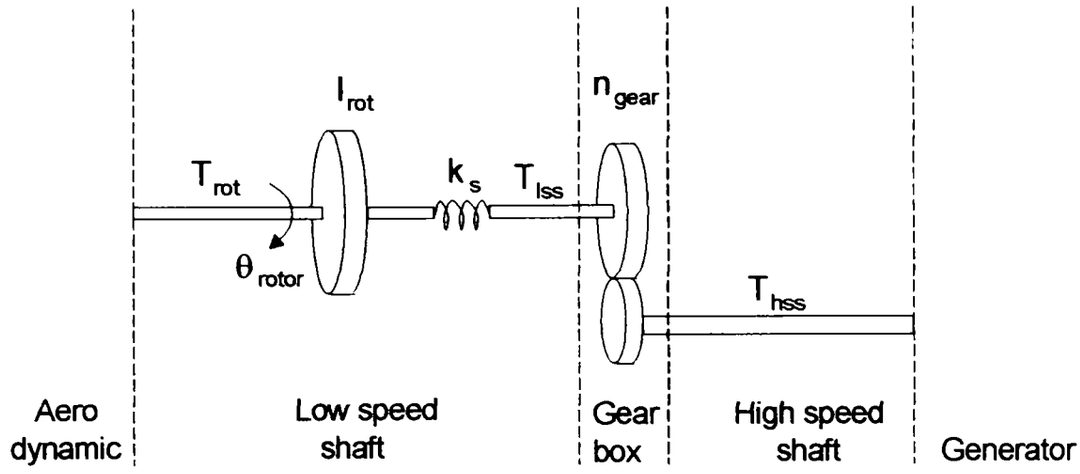


**Figure 3.7**. Drive train model in the wind turbine.

The rotor is modelled by inertia ( $I_{rot}$ ), low speed shaft only by a stiffness $k_s$ (the torsion damping is neglected), while the high-speed shaft is assumed to be stiff. Thus the transmission is described by the following equations:

$$I_{rot} \cdot \frac{d\omega_{rot}}{dt} = T_{rot} - T_{lss} \quad \text{.....(3.7)}$$

$$\frac{dT_{lss}}{dt} = k_s \left( \omega_{rot} - \frac{\omega_{gen}}{n_{gear}} \right) \quad \text{.....(3.8)}$$

It is also assumed that the losses in the gearbox are zero, thus the gear transmits ideally from the low speed to high speed. The output of the model is:

$$T_{hss} = \frac{T_{lss}}{n_{gear}} \quad \text{.....(3.9)}$$

where $n_{gear}$ is ratio of the gear box.

## 3.2.4. The Induction Generator Model

The induction generator model is a combined mechanical and electro-magnetic model. The mechanical model includes the inertia of the generator rotor in the generator model.

The generator wind turbine is of squirrel cage induction type. Based on the existing generator data (*Appendix B2*), a preliminary study has been made in MATLAB-Simulink using the power system block-set built in induction machine model and a custom d–q model, as shown in Fig. 3.8, simulating different dynamic behaviour as seen in Fig. 3.9.

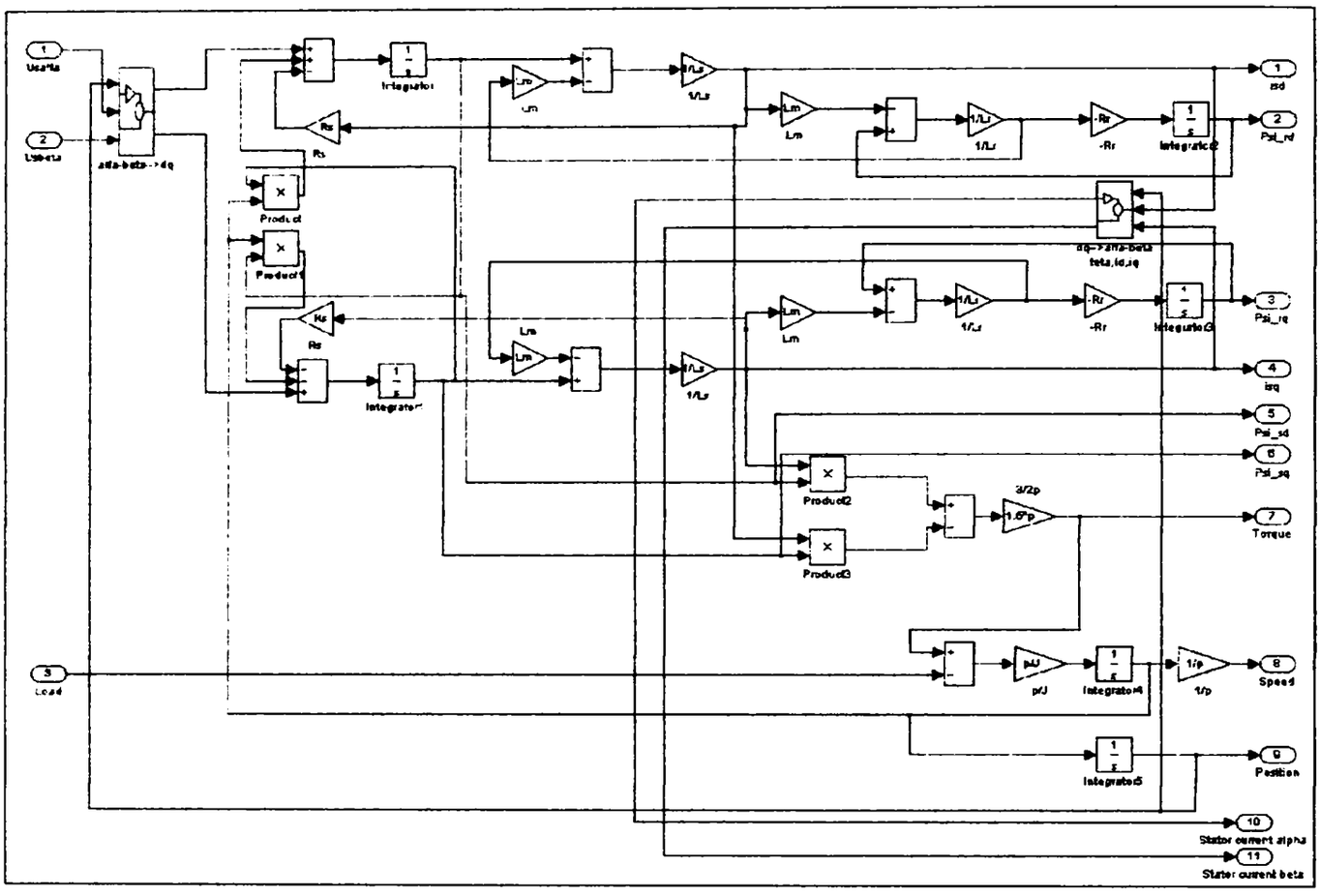


**Figure. 3.8**. Asynchronous machine d – q model implemented in MATLAB-Simulink (constant parameter approach).

The equations used to build up the Matlab–Simulink induction machine d-q model are:

$$\bar{i}_s R_1 - \bar{U}_s = -\frac{d\bar{\psi}_s}{dt} - j\omega_b \bar{\psi}_s \quad \text{.....(3.10)}$$

$$\bar{i}_r R_2' - \bar{U}_r = -\frac{d\bar{\psi}_r}{dt} - j(\omega_b - \omega_r)\bar{\psi}_r \quad \text{.....(3.11)}$$

$$M_e = p_1 \, \text{Real}\left[j\bar{\psi}_s \bar{i}_s^*\right] \quad \text{.....(3.12)}$$

Where the stator and the rotor fluxes have the following expression:

$$\bar{\psi}_s = L_{1\sigma}\bar{i}_s + L_m\left(\bar{i}_s + \bar{i}_r\right) \quad \text{.....(3.13)}$$

$$\bar{\psi}_r = L_{2\sigma}'\bar{i}_r + L_m\left(\bar{i}_s + \bar{i}_r\right) \quad \text{.....(3.14)}$$

The parameters in these equations are: $R_1$, $R_2$' – stator resistance and rotor resistance;
$L_{1\sigma}$, $L_{2\sigma}$ – stator and rotor leakage inductance;
$L_m$ – magnetizing inductance;
$\omega_b$ – speed of the reference system;
$p_1$ –pole pairs of the machine
$\bar{i}_s, \bar{i}_r$ – stator and rotor current phasors
(Note: all the rotor quantities are reduced to the stator).

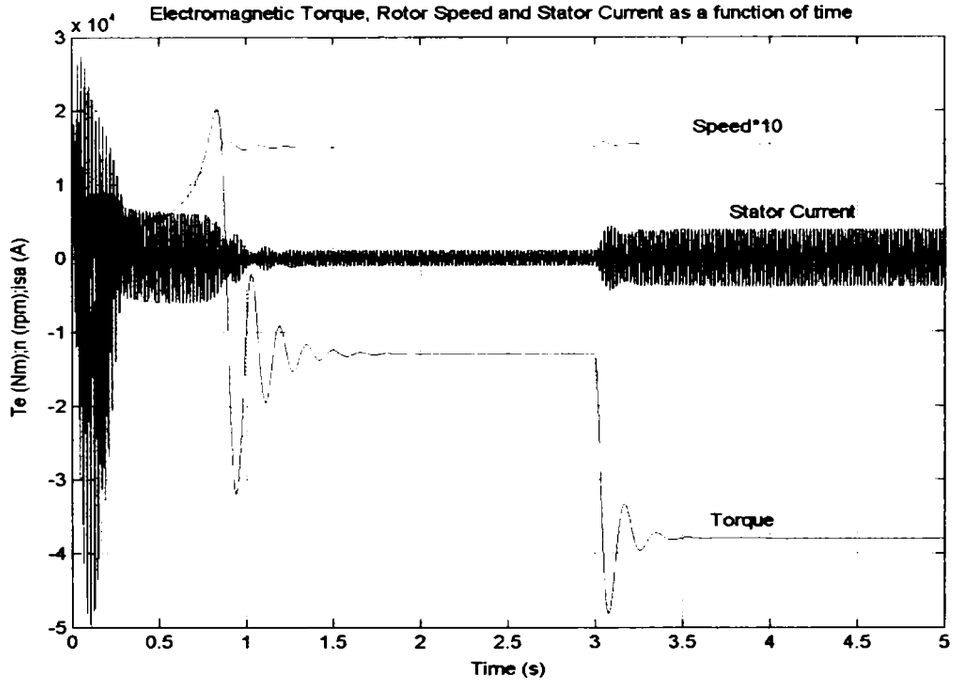


**Fig. 3.9**. Simulated torque, speed and stator current transients versus time during generator startup. Turbine torque steps up at t=3 s, from [full load torque-13.050 Nm] to [pull out torque-38.000 Nm].

The Figure 3.9 shows a full load start-up and steady-state performance of 2 MW induction generator, directly connected to the grid and then at t=3 s the mechanical input torque was changed from full load to pull out torque to simulate dynamic behaviour of the machine.

Later the induction generator was defined using the DIgSILENT 12.0.116 built in improved induction (asynchronous) machine model [7]. The reasons why the built in DIgSILENT model (squirrel cage with current displacement) has been used are:

1. Different cage rotors can be considered with rotor current displacement;
2. The machine can be defined based on its measured torque – slip curve, short-circuit test and nameplate values;
3. Electrical parameter variations can also be considered;

An eventual implementation of a new d-q model in DIgSILENT can be done by some controlled voltage sources and parameter variation cannot be considered, as there is no measured data for that.

The single line equivalent circuit built in DIgSILENT is presented in Fig. 3.10:

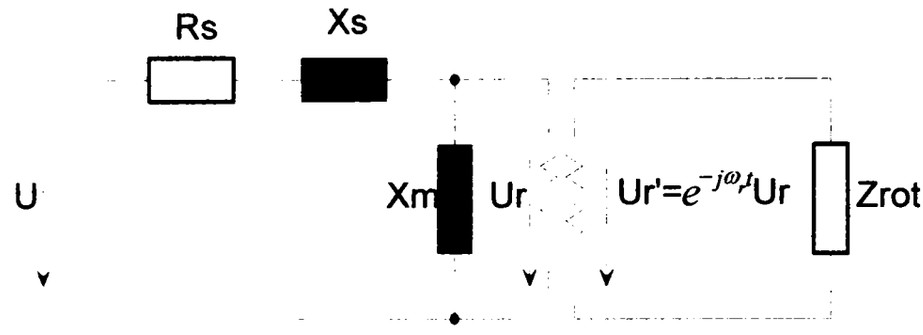


**Fig. 3.10.** Induction Machine Model built up in DIgSILENT Power Factory [7].

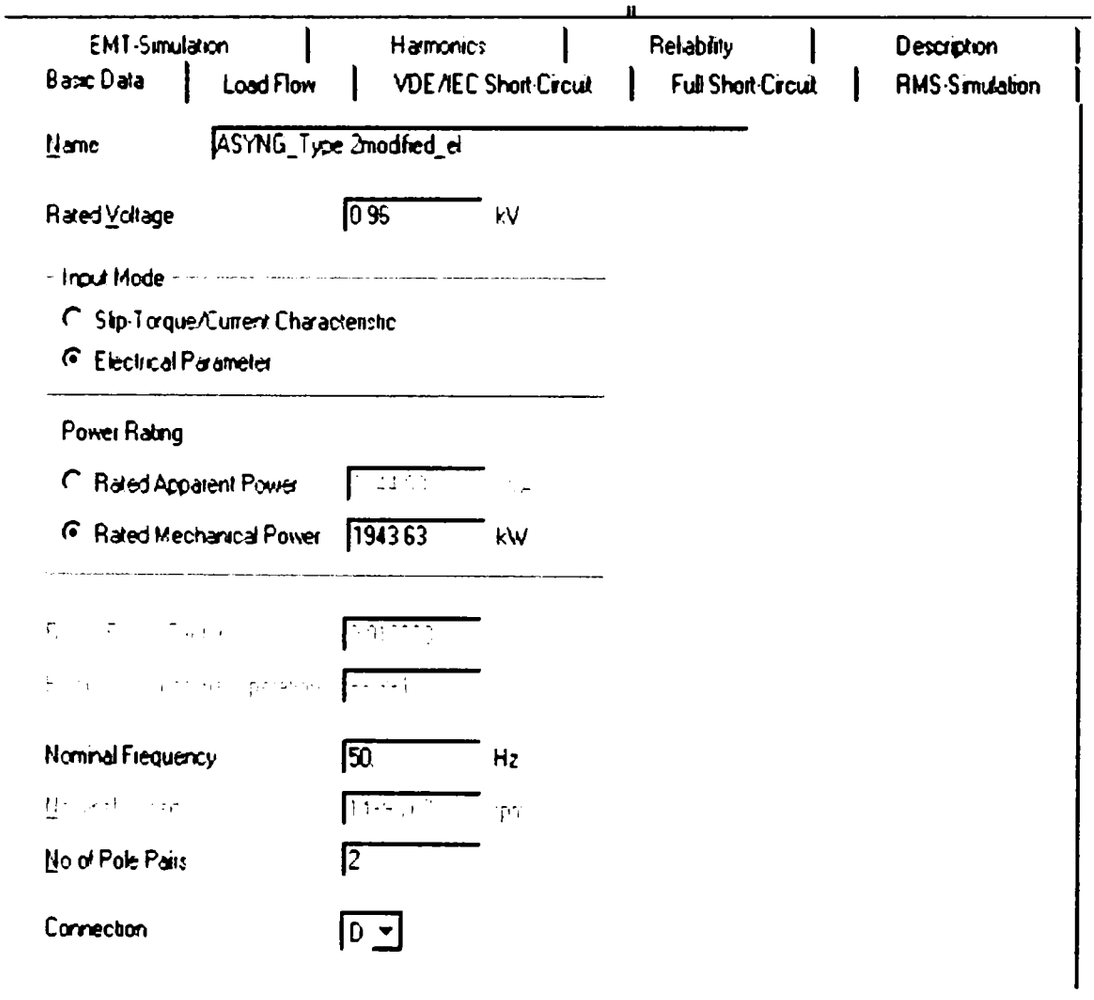


a)

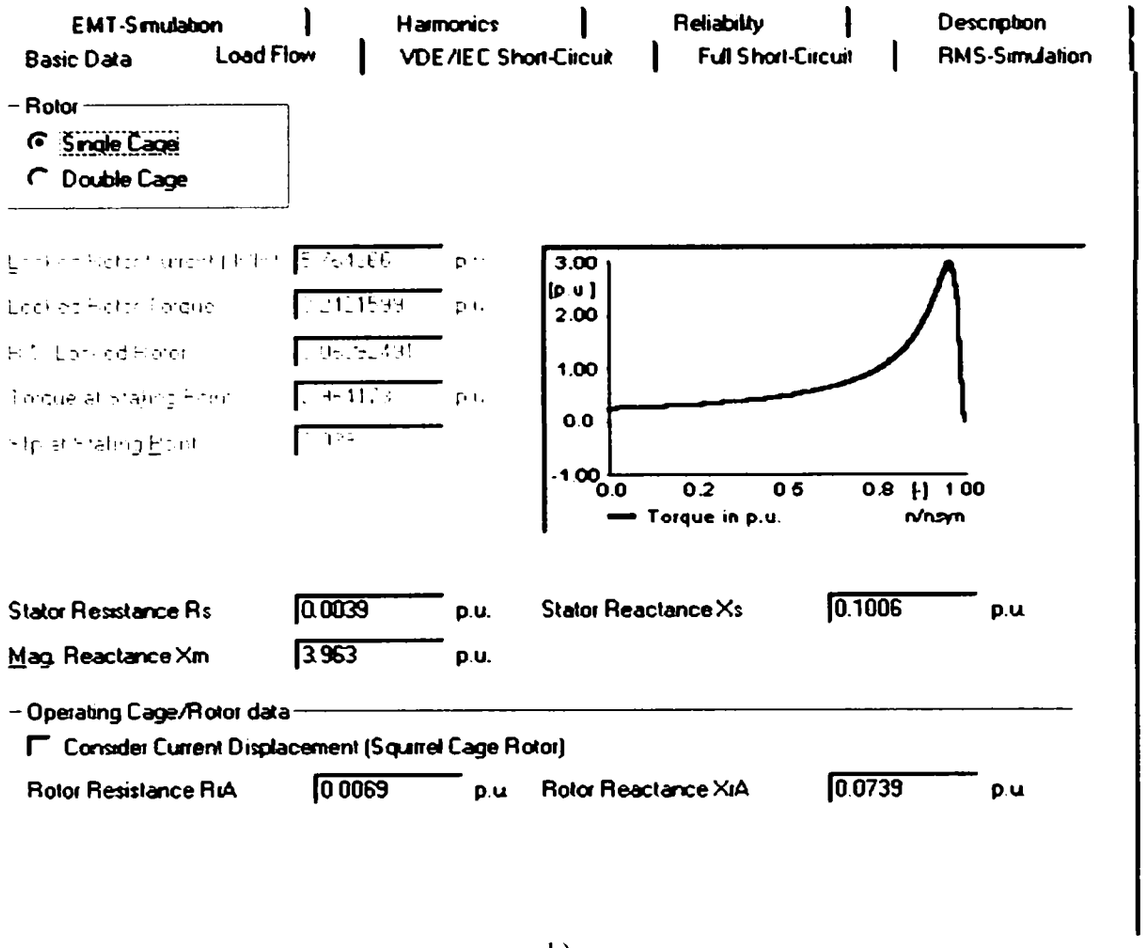


b)

**Fig. 3.11**. Induction generator data of 2 MW implemented in DIgSILENT simulation tool [7].

The induction machines can be defined in DIgSILENT software package based on its measured torque-slip curve, short circuit test and name plate values, as shown in Fig. 3.11 a).

Electrical parameter variations and different cage rotors with rotor current displacement can also be considered (Fig. 3.11 b). In our simulation model the induction generators are single cage machines implemented using their nominal nameplate parameters.

DIgSILENT combines the traditional transient EMT simulation tool for power systems with RMS simulations of longer-term dynamics. This makes the developed models useful for the power quality studies as well as for the grid fault studies. In this paper, the power quality performance during normal operation is the goal of the analysis and therefore simulations of RMS values are performed. The RMS simulations are based on electro-mechanical transient models, which are simplified models than those used in EMT simulations. They are more appropriate for the most studies of power quality and control issues. They are much faster than the instantaneous value simulation compared to the period, which is simulated. The EMT simulations, as they are based on detailed electromagnetic transient models, are appropriate for studies of the behaviour during grid faults.

For performance comparisons simulation results in MATLAB-Simulink and DIgSILENT are presented in Fig. 3.12 for a 2MW induction generator under three-phase short-circuit at generator terminals at nominal operation point, and for a start-up at nominal load and under mechanical power steps, in Fig. 3.13.

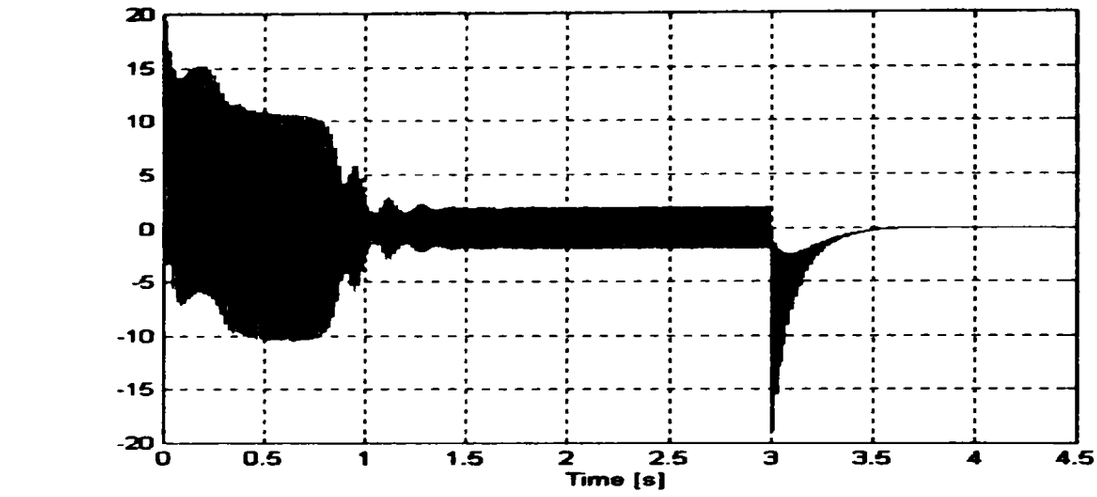
20
15
10
5
0
-5
-10
-15
-20
0
0.5
1
1.5
2
2.5
3
3.5
4
4.5
Time [s]

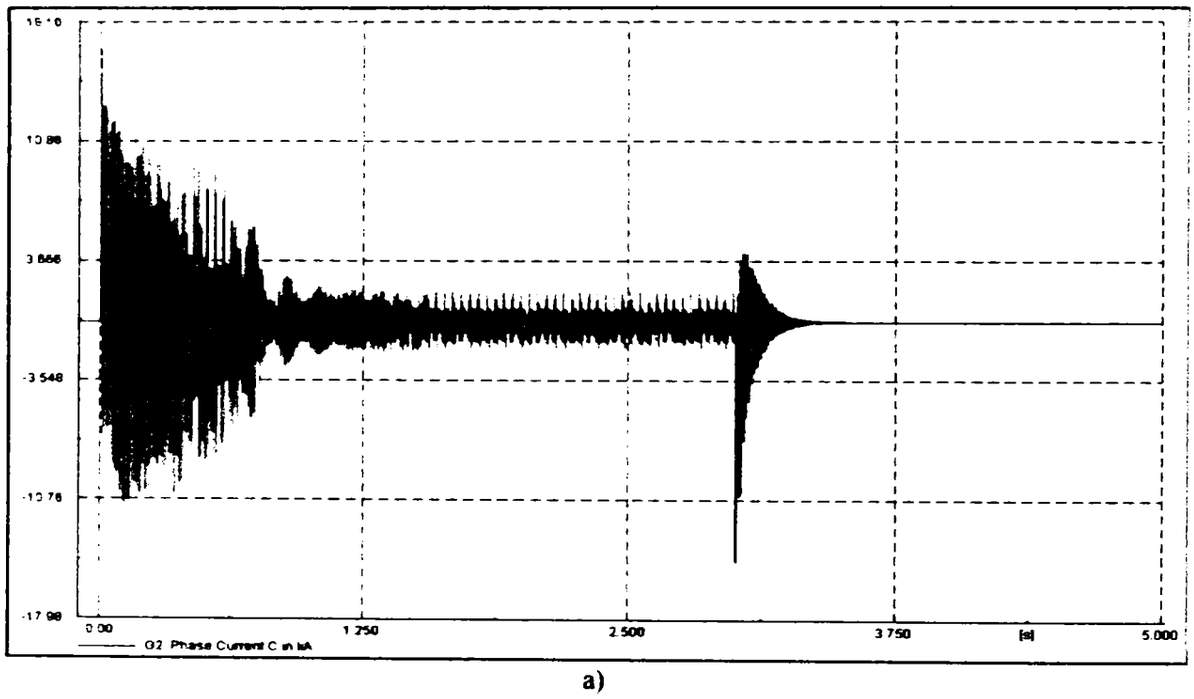
10.88
3.868
-3.548
-10.76
-17.98
0.00
1.250
2.500
3.750
[s]
5.000
G2 Phase Current C in kA

a)

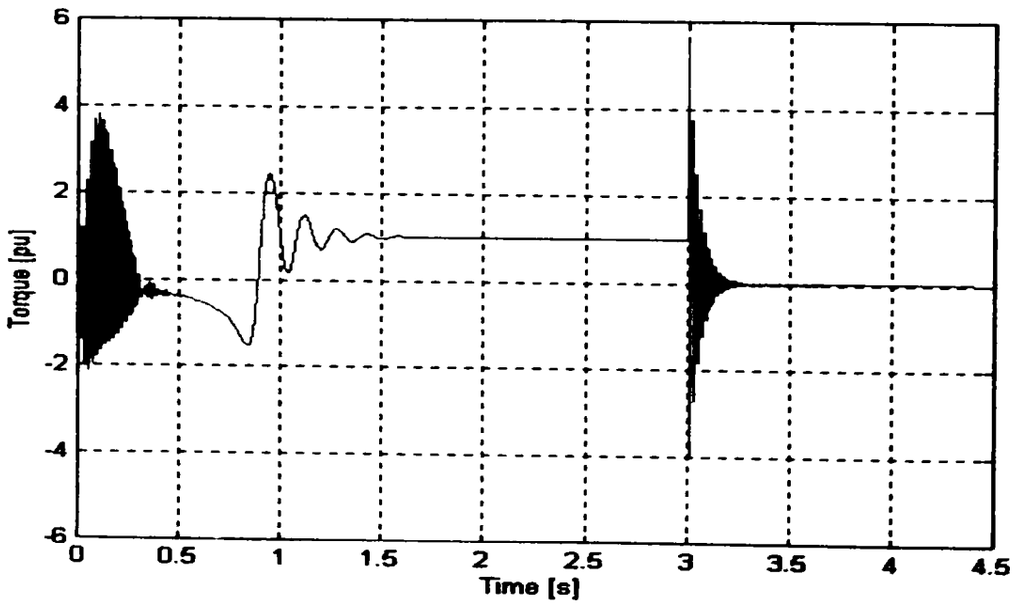
6
4
2
0
-2
-4
-6
Torque [pu]
0
0.5
1
1.5
2
2.5
3
3.5
4
4.5
Time [s]

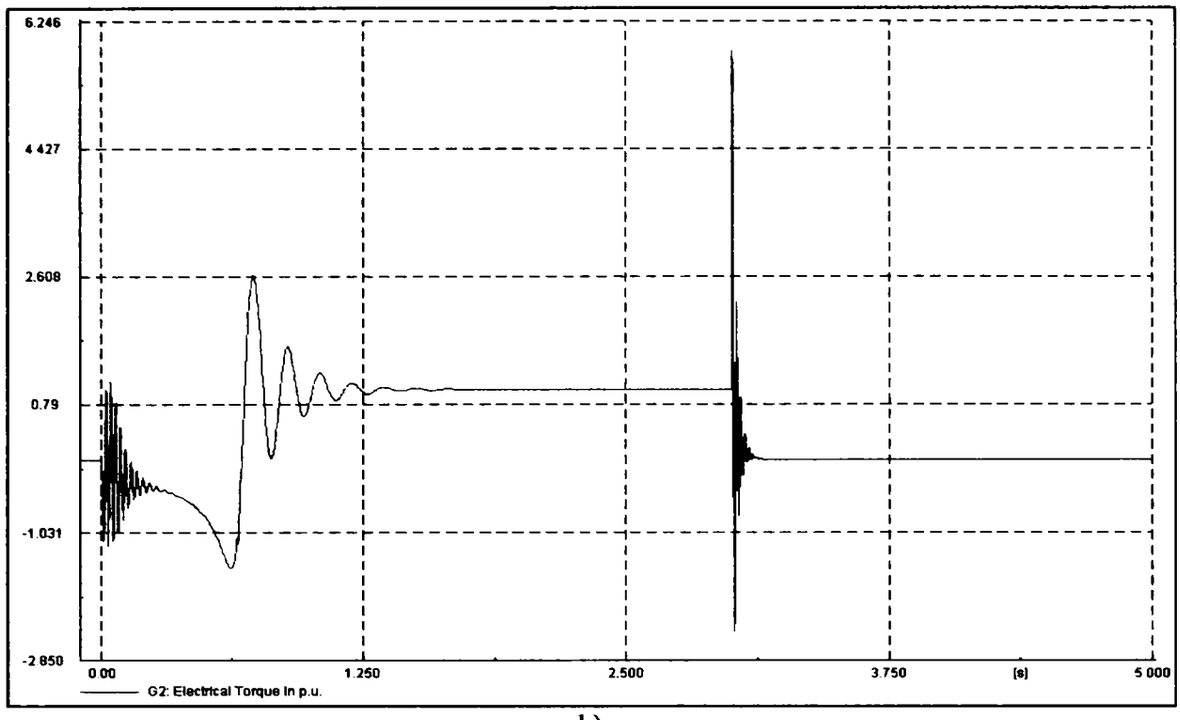


b)

**Figure 3.12.** Comparative simulation results of phase current (a) and electromagnetic torque (b) transients under 3~ short-circuit at t=3s using Matlab-Simulink and DIgSILENT packages software.

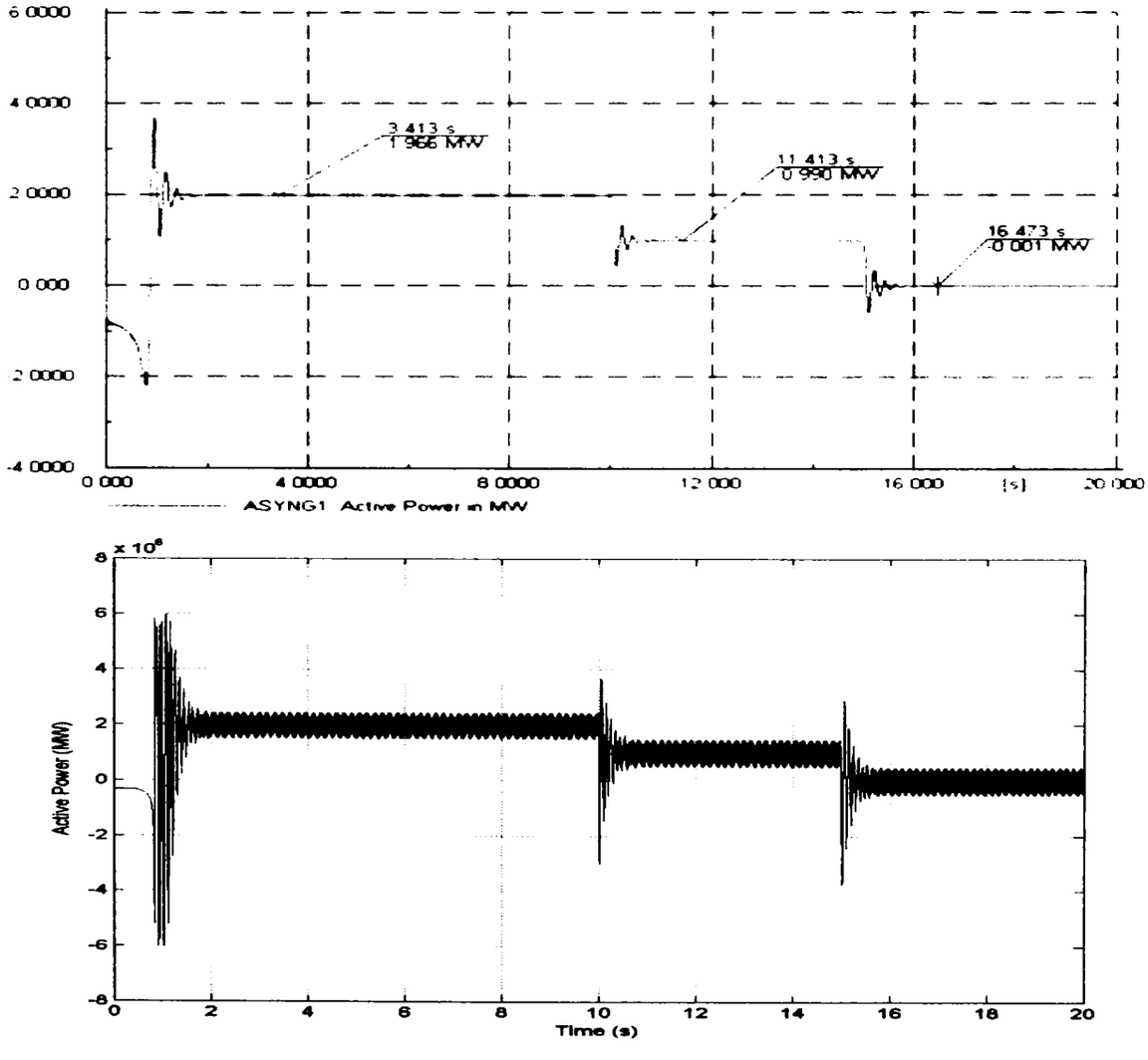


a)

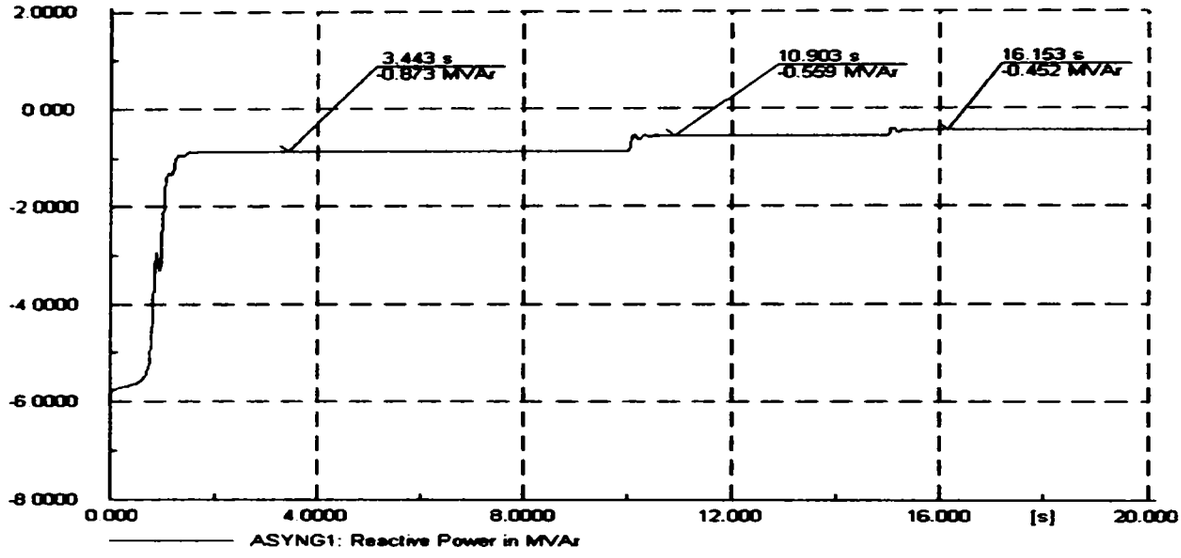


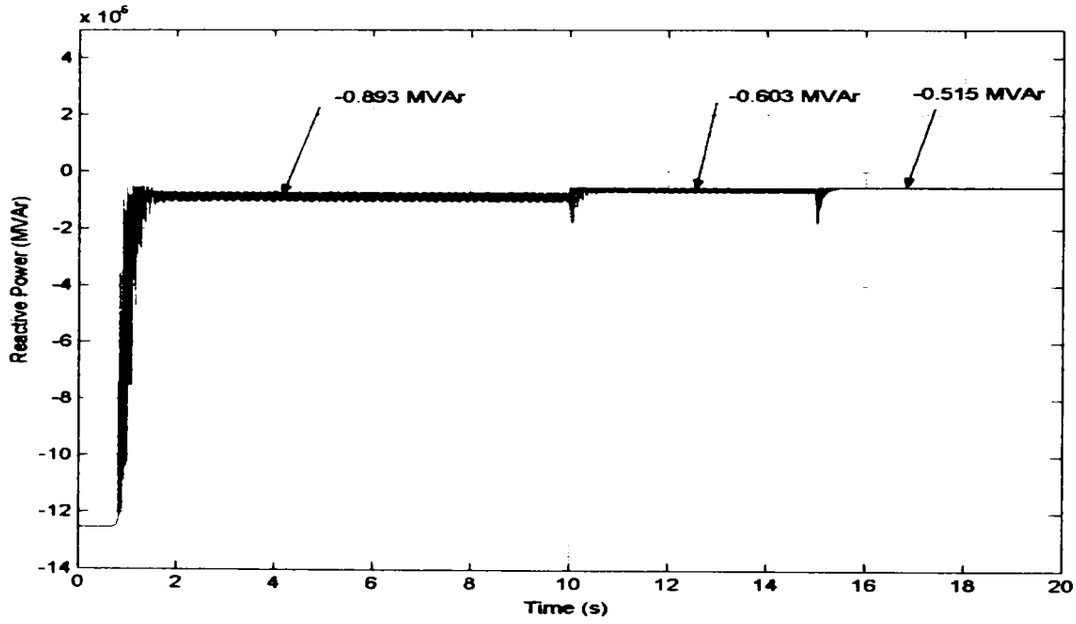


b)

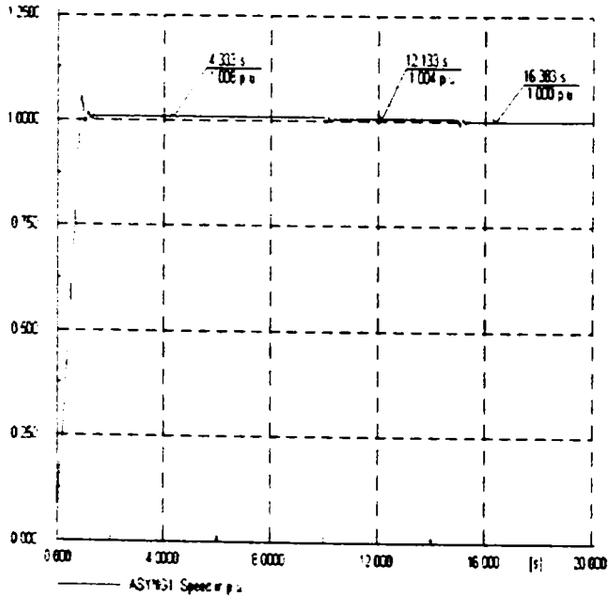

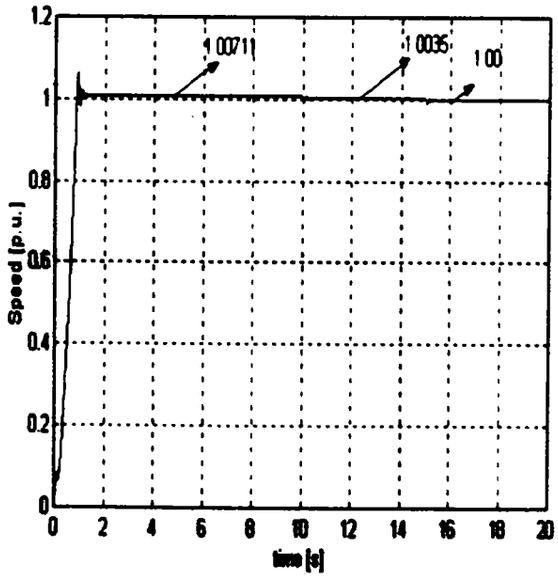


c)

**Figure 3.13**. Comparative simulation results of active power (a), reactive power (b), and speed (c) of 2 MW induction generator under start-up at nominal load and mechanical power steps at t=10s from 100 % to 50 % and at t=15 s from 50 % to 0 % using DIgSILENT and Matlab-Simulink packages software.

These comparative results show a good similarity between a custom d – q Matlab-Simulink model and DIgSILENT built in model of the induction machine for transient events such as start-up at nominal load, 3-phase short-circuit and mechanical power steps. It is thus concluded that here the proposed MATLAB Simulink program is validated and thus trust worthy for further applications.

### 3.2.5. The Soft Starter Model

In order to reduce the transient current during connection of generator to the 0.96kV grid a soft starter is used. When the induction machine speed increases above the synchronous speed at 1450 rpm the soft starter is connected and using firing angle control (α) the machine is connected over the grid, as shown in Fig. 3.14 a).

The connection diagram of soft starter with induction machine is presented in Fig. 3.14 a):

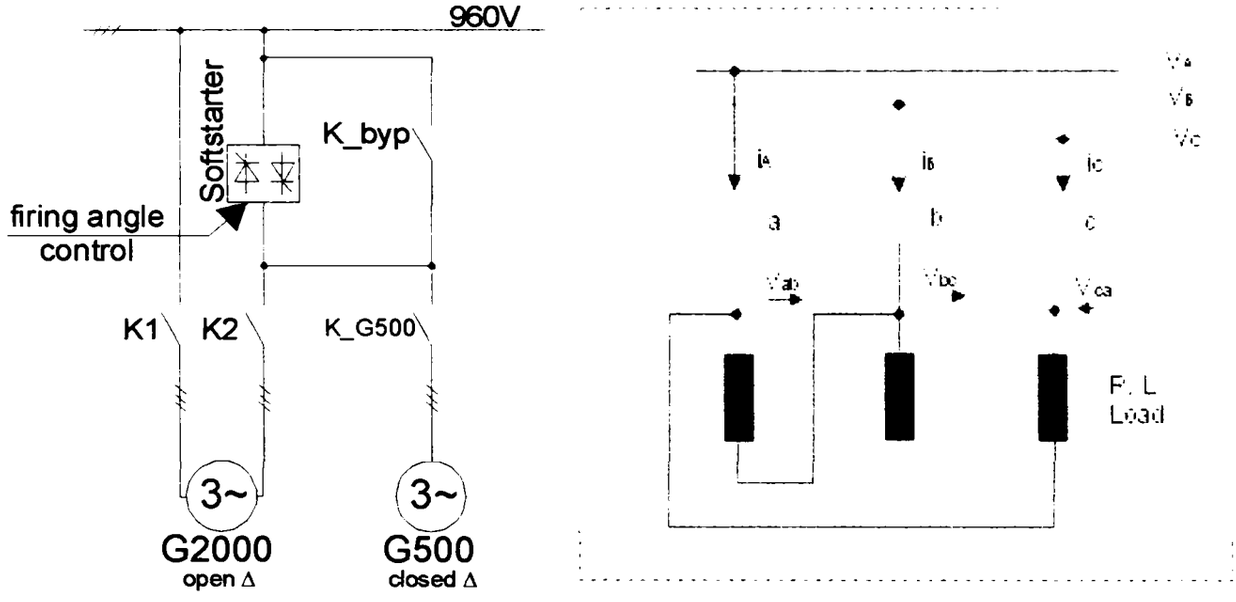


a) b)

**Figure 3.14**. Connection diagram of soft-starter with induction generators. a) and schematic diagram of soft-starter with delta connected load. b).

Figure 3.14 b) shows the fully controlled topology with a delta-connected load. If thyristors are delta-connected, their control is simplified and their ratings considerably reduced. The delta arrangements generate, in the load, all the odd harmonics, but no triple harmonics. Harmonics of order 5, 7, 11, 13 ... remain.

To get the controller started, two or three switches must be fired simultaneously to provide the path for current necessary to maintain the on-state. Switching variables *a*, *b* and *c* may be introduced for 2 thyristors connected in anti-parallel for each phase and defined as equal to 1 when a given thyristor is conducting and equal to 0 otherwise. It can easily be demonstrated that the output voltages ($V_{ab}$, $V_{bc}$ and $V_{ca}$) of the controller (soft-starter) are given by (3.15):

$$\begin{bmatrix} V_{ab} \\ V_{bc} \\ V_{ca} \end{bmatrix} = \begin{bmatrix} ab & -\frac{1}{2}a & -\frac{1}{2}b \\ -\frac{1}{2}c & bc & -\frac{1}{2}b \\ -\frac{1}{2}c & -\frac{1}{2}a & ca \end{bmatrix} \cdot \begin{bmatrix} V_{AB} \\ V_{BC} \\ V_{CA} \end{bmatrix} \quad \text{.....(3.15)}$$

Where $V_{AB}$, $V_{BC}$ and $V_{CA}$ are the line-to-line voltages (input voltages).

Depending on the firing angle, three modes of operation of the soft-starter can be distinguished, with a purely resistive load:

1. $0^\circ \le \alpha < 60^\circ$ : 2 or 3 switches conducting (in either direction)
2. $60^\circ \le \alpha < 90^\circ$ : 2 switches conducting
3. $90^\circ \le \alpha < 150^\circ$ : *none or two switches conducting*

Analysis of operation of the controller with RL load is difficult since the extension angle and the so-called limit angle ($\alpha_{lim}$) must be known. Mode 2, characterized by rapid changes of the output currents is impossible due to the load inductance. The ranges of the two remaining operation modes are $\varphi \le \alpha < \alpha_{lim}$ for *mode 1* and $\alpha_{lim} \le \alpha < 150°$ for *mode 3*. The limit angle ($\alpha_{lim}$) can be determined numerically from eq.3.16 [8]:

$$\frac{\sin(\alpha_{lim} - \varphi - \frac{4}{3}\pi)}{\sin(\alpha_{lim} - \varphi)} = \frac{2e^{-\frac{\pi}{3tg(\varphi)}} - 1}{2 - e^{-\frac{\pi}{3tg(\varphi)}}} \quad \text{.....(3.16)}$$

The equations for the rms output voltage, $V_{out}$, of the fully controlled soft-starter with purely resistive and inductive loads are provided bellow [8, 15]:

*Resistive load*

$$V_{out} = V_{in} \cdot \sqrt{\frac{1}{\pi}\left[\pi - \frac{3}{2}\alpha + \frac{3}{4}\sin(2\alpha)\right]}; \text{ for } 0^\circ \le \alpha < 60^\circ \quad \text{.....(3.17)}$$

$$V_{out} = V_{in} \cdot \sqrt{\frac{1}{\pi}\left[\frac{\pi}{2} + \frac{3\sqrt{3}}{4}\sin(2\alpha + \frac{\pi}{6})\right]}; \text{ for } 60^\circ \le \alpha < 90^\circ \quad \text{.....(3.18)}$$

$$V_{out} = V_{in} \cdot \sqrt{\frac{1}{\pi}\left[\frac{5\pi}{4} - \frac{3}{2}\alpha + \frac{3}{4}\sin(2\alpha + \frac{\pi}{3})\right]}; \text{ for } 90^\circ \le \alpha < 150^\circ \quad \text{.....(3.19)}$$

*Inductive load*

$$V_{out} = V_{in} \cdot \sqrt{\frac{1}{\pi}\left[\frac{5\pi}{2} - 3\alpha + \frac{3}{2}\sin(2\alpha)\right]}; \text{ for } 90° \le \alpha < 120° \quad \text{.....(3.20)}$$

$$V_{out} = V_{in} \cdot \sqrt{\frac{1}{\pi}\left[\frac{5\pi}{2} - 3\alpha + \frac{3}{2}\sin(2\alpha + \frac{\pi}{3})\right]}; \text{ for } 120° \le \alpha < 150° \quad \text{.....(3.21)}$$

The envelope of control characteristics given by eq. (3.17) through (3.21) is shown in Fig. 3.15. The relationship between the firing angle ($\alpha$) and the resulting amplification of the soft starter is highly non-linear and depends additionally on the power factor of the connected element. In the case of a resistive load $\varphi$ can vary between 0 (full on) and 90 (full off) degrees. While in the case of a purely inductive load $\varphi$ varies between 90 (full on) and 180 (full off) degrees. For any power factor in between, it will be somewhere between these limits [8, 15], as can also be seen in Fig. 3.15.

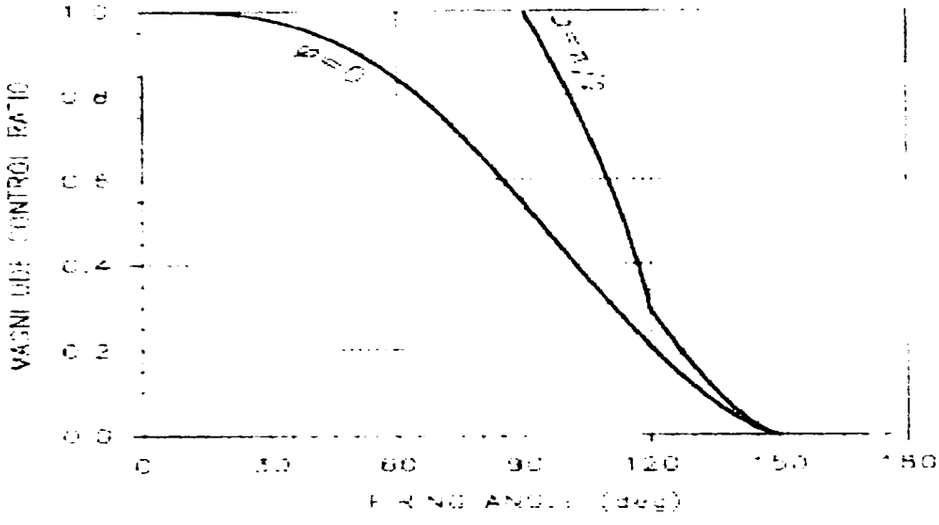

**Figure 3.15**. Control characteristic, $V_{out}=f(\alpha)$, for a fully controlled soft starter [8, 15].

In DIgSILENT the soft starter is a stand-alone element. The commutation devices are 2 thyristors connected in anti-parallel for each phase. A complete control in details of the soft starter using the firing angle as input is possible just in EMT (electromagnetic transient) simulation mode, where every thyristor switching is modeled in detail, while the RMS simulation uses a simplified model (as a controlled voltage source). More details about soft starter control implementation in DIgSILENT will be presented in *Appendix B1.3*.

Figure 3.16 presents the phase currents and phase voltages under a connection of 2 MW induction machine to the grid through the soft-starter, driven with mechanical load of 0.1 p.u. The soft-starter was connected at a firing angle ($\alpha$) of 120° and by-passed after 0.3 seconds at a firing angle of 106°. When the machine accelerates and goes from motor area to generator area the difference between firing angle ($\alpha$) and load angle ($\varphi$) becomes smaller, therefore the current will increase, as can also be seen in Fig. 3.16.

For a complete representation of machine behavior with different values of phase angle ($\alpha$) as 110° (Fig. 3.17 a), 90° (Fig. 3.17 b) and 70° (Fig. 3.17 c) the phase current (output current), phase voltage (output voltage) and input phase voltage are presented. With a firing angle larger than $105^0$ (Fig. 3.17 a) the machine is working with a lower output phase voltage and current then the nominal supply voltage (input phase voltage). It can also be seen, in Fig. 3.17 a), that when the firing angle increases the current pulses become smaller and shorter. Consequently, the RMS value of the current decreases, as does the RMS value of output voltage. Note that the current is always discontinuously and waveforms of both the current and output voltage are strongly distorted in comparison with pure sinusoids as the input voltage, especially with high firing angles ($120^0$).

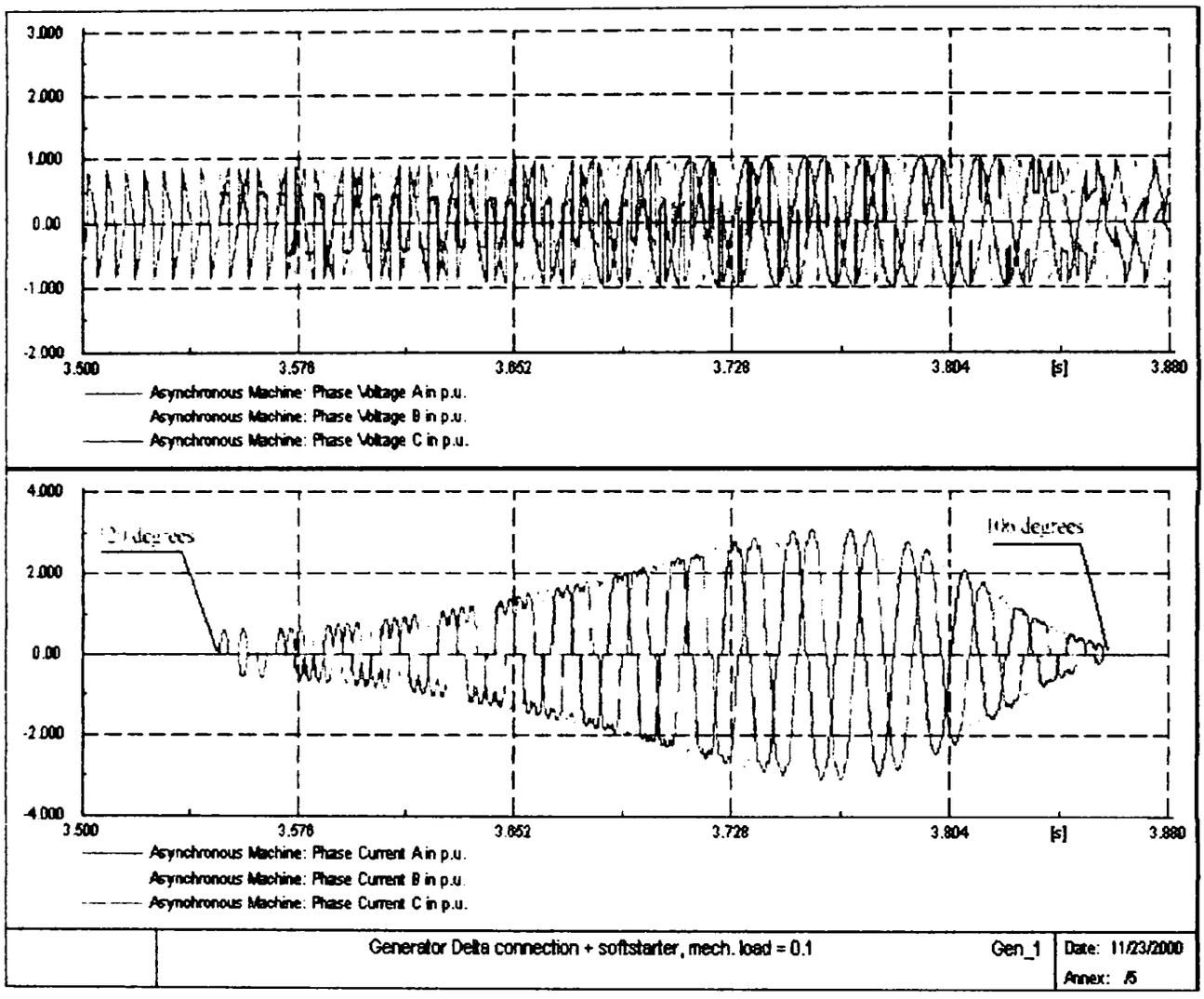


**Fig. 3.16**. Simulation of 2 MW induction generator connected to the grid through soft-starter to a mechanical load of 0.1 p.u., using DIgSILENT software.

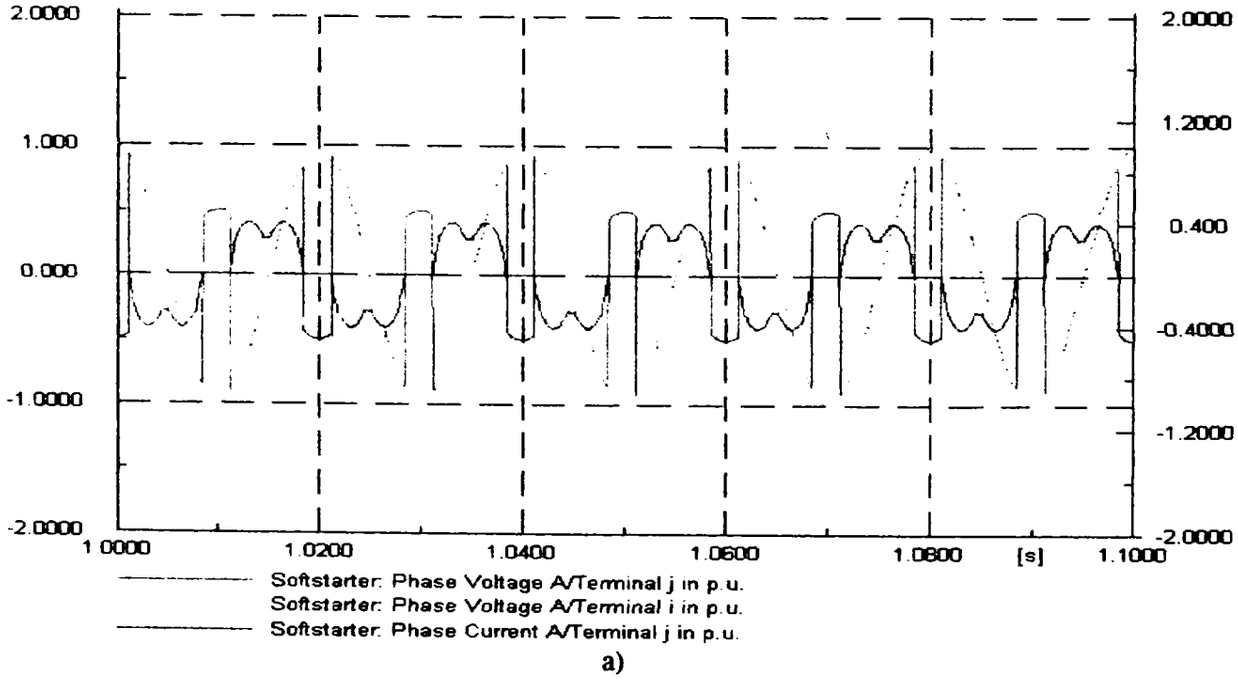


a)

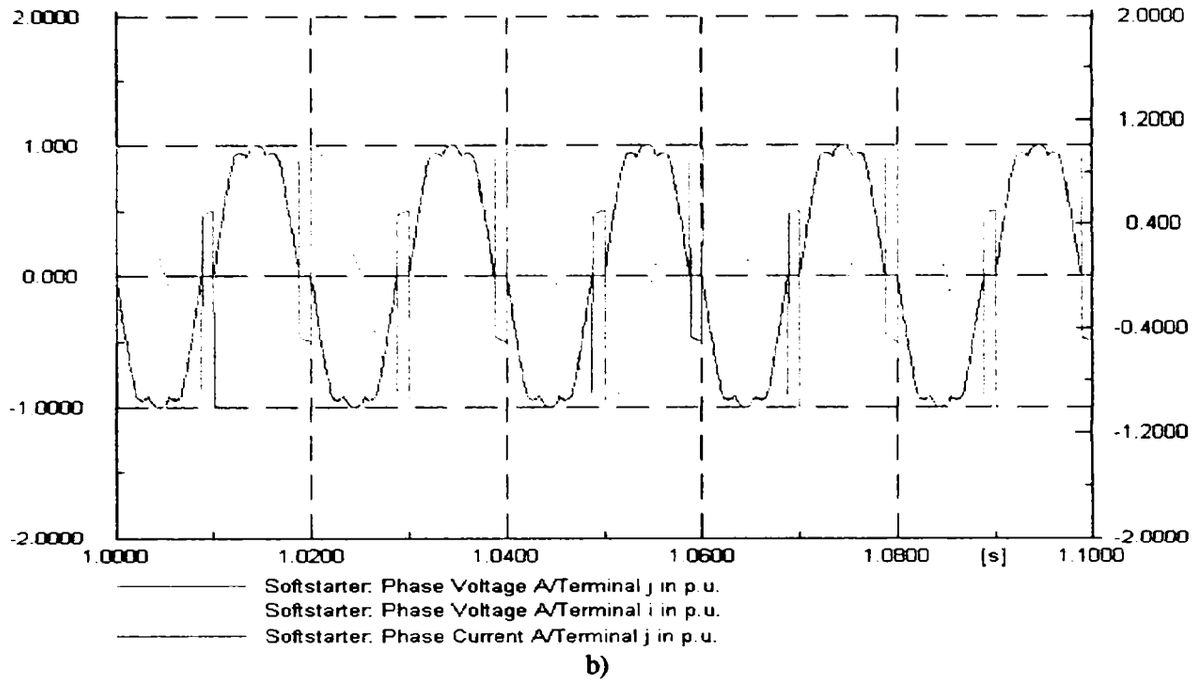


b)

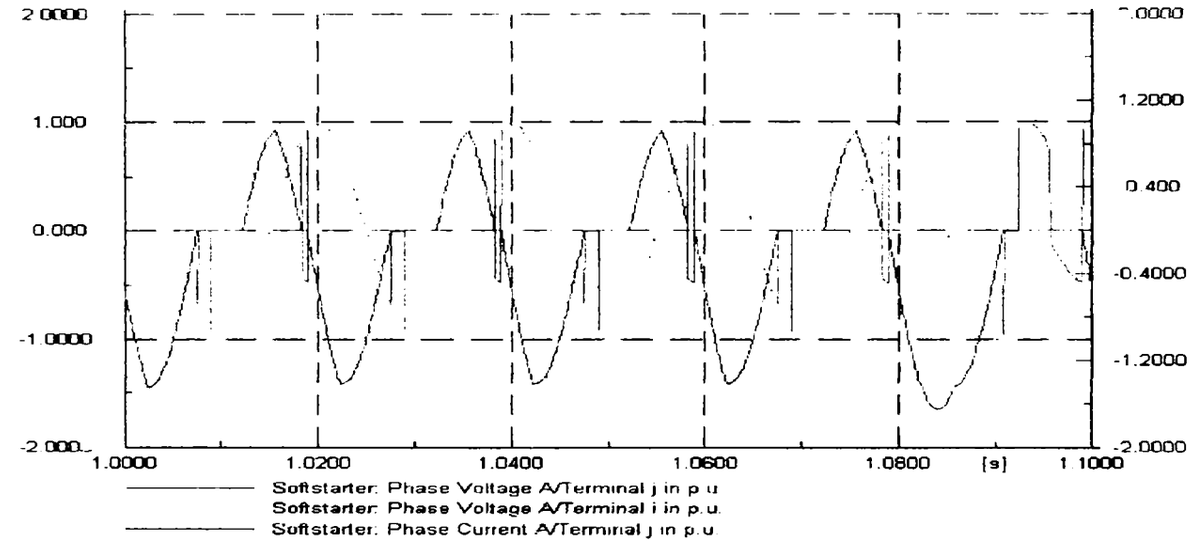


c)

**Fig. 3.17.** Phase voltage and current waveforms for alpha = $110^0$, (a), for alpha = $90^0$, (b) and for alpha = $70^0$ (c).

## 3.2.6. The Capacitor Bank Model

For power factor compensation capacitor bank is used, as shown in Fig. 3.18. The 2 MW induction generator is full load compensated. The switching of capacitors is done as a function of average value of measured reactive power during a certain period of time. Two $PT_1$ filters ($T_1$=0.33 s and $T_2$=20 s) are implemented in DIgSILENT for 1 second and 1 minute averaging of reactive power measured at soft-starter terminal. Internal variables are defined for each step of connection of capacitors with a delay time of 1s between two connections of capacitors, see Appendix B1.3 for details.

The capacitor bank is mounted in the nacelle, in the top of wind turbine.

In order to reduce the current at connection/disconnection of capacitors a coil (L) is connected in series.

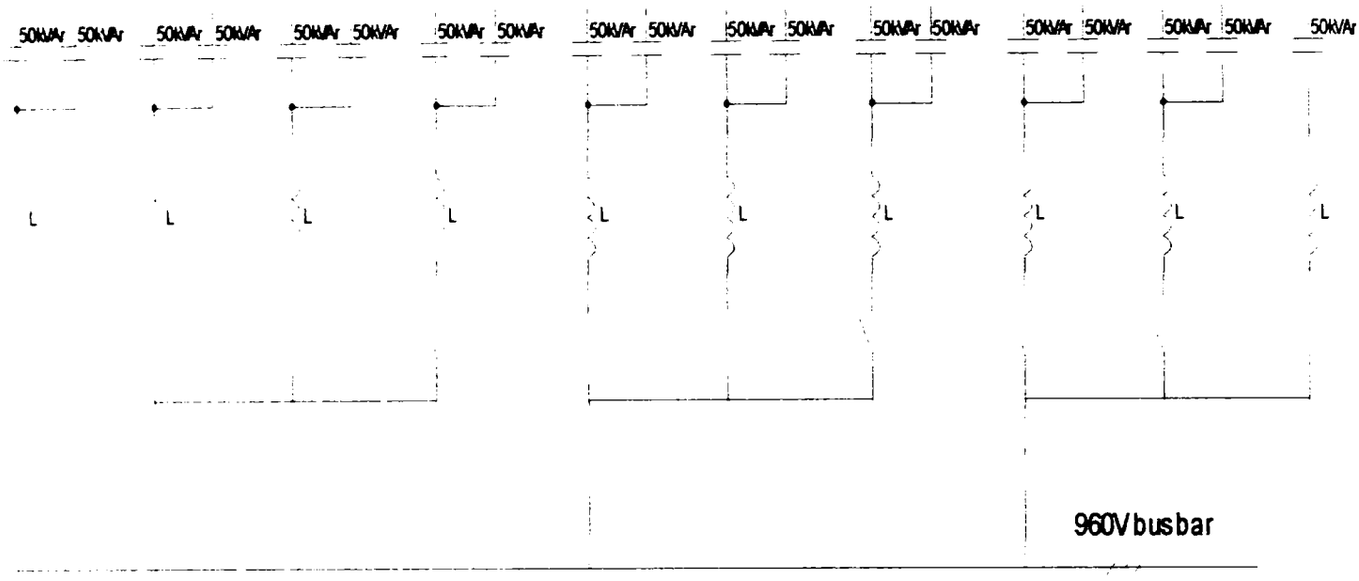


**Figure 3.18**. Capacitor bank configuration for power factor compensation.

The steady state voltage is dependent on the reactive power consumption of induction generator (IG). Therefore it is important to supply the IG with a reactive power compensation unit to provide the reactive power balance and to improve the voltage stability.

## 3.2.7. The Transformer Model

The transformer type is a 2MVA, 10kV/0.96kV mounted in the top of the wind turbine tower next to the induction generator and transmission system.

The implementation in DIgSILENT is presented as follows. The representation of the positive sequence equivalent diagram is shown in Fig. 3.19 and includes a generalized tap – changer model (phase and magnitude). The tap-changer in this figure has been drawn at the LV side by choice.

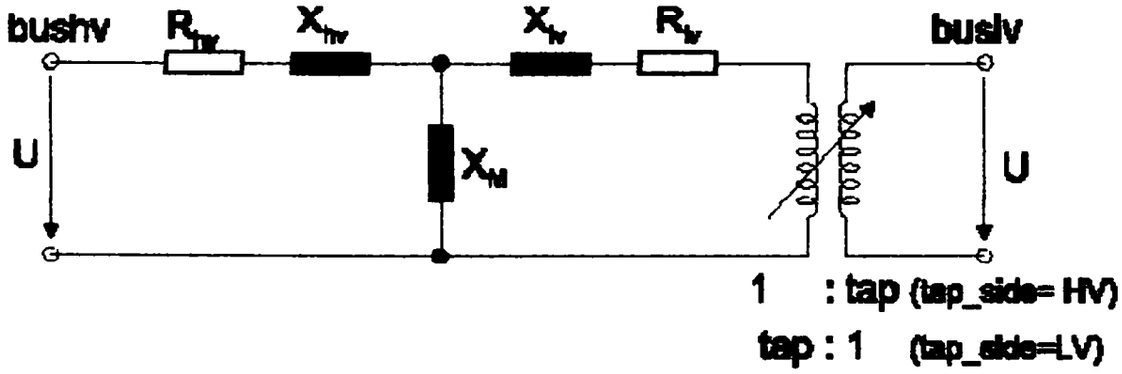


**Figure 3.19**. Transformer equivalent model developed in DIgSILENT.

The mathematical parameters which describe the transformer model implemented in DIgSILENT are presented in the next equation set (3.22).

$$
\begin{array}{lll}
R_s & R_{s_1} + R_{s_2} & p.u. \\
X_s & X_{s_1} + X_{s_2} & p.u. \\
Z_s & ukt_r / 100 & p.u. \\
R_s & pcutr / (1000 \cdot strn) & p.u. \\
X_s & \sqrt{Z_s^2 - R^2} & p.u. \\
X_{s_2} & itrdl \cdot X_s & p.u. \\
X_{s_1} & (1 - itrdl) \cdot X_s & p.u. \\
R_{s_2} & itrdr \cdot R_s & p.u. \\
R_{s_1} & (1 - itrdr) \cdot R_s & p.u. \\
X_m & 100 / curmg & p.u.
\end{array}
\qquad \text{.....(3.22)}
$$

Where (*strn*) is rated power, (*uktr*) is short circuit voltage, (*pcutr*) is copper losses, (*curmg*) is no load current, (*itrdl*) distribution of leakage reactances.

## 3.3. The Control Strategy of Wind Turbine

Wind turbines are designed to produce as much electrical energy as possible. Wind turbines are therefore generally designed so that they yield maximum output at wind speeds around 12-15 metres per second [3].

In case of stronger winds it is necessary to waste part of the excess energy of the wind in order to avoid damaging the wind turbine. All wind turbines are therefore designed with some sort of power control such as pitch control or stall control (passive stall and active stall).

Passive stall control relies on inherent machine characteristics in the way that the aerodynamic power is limited when the wind speed increases [11, 20].

A common control concept for new megawatt-size turbines without power electronic converters (as in our case) is the active stall regulation (i.e., a stall regulated wind turbine with adjustable pitch angle). At high wind speeds, the pitch angle is adjusted to obtain the desired rated power level. When connecting the turbine to the grid, the pitch angle also is adjusted in order to obtain a smooth connection. The use of active stall control also facilitates the emergency stopping of the turbine.

Active stall constant speed combines the advantages of passive stall, namely simplicity due to the absence of a pitch mechanism, with the advantages of pitch control, namely controllability. Thus it provides additional control capabilities beyond passive stall, required for offshore & large utility developments, while it makes possible to avoid additional technical complexity of pitch control turbines [2, 3]. The blade angle control is shown in Fig. 3.20.

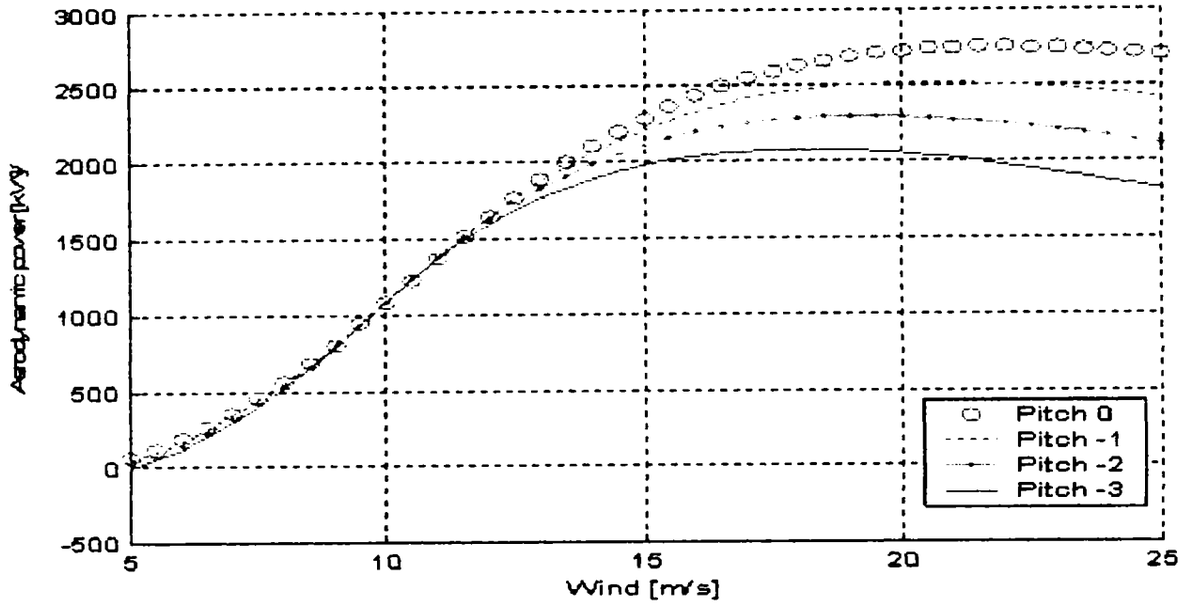


a)

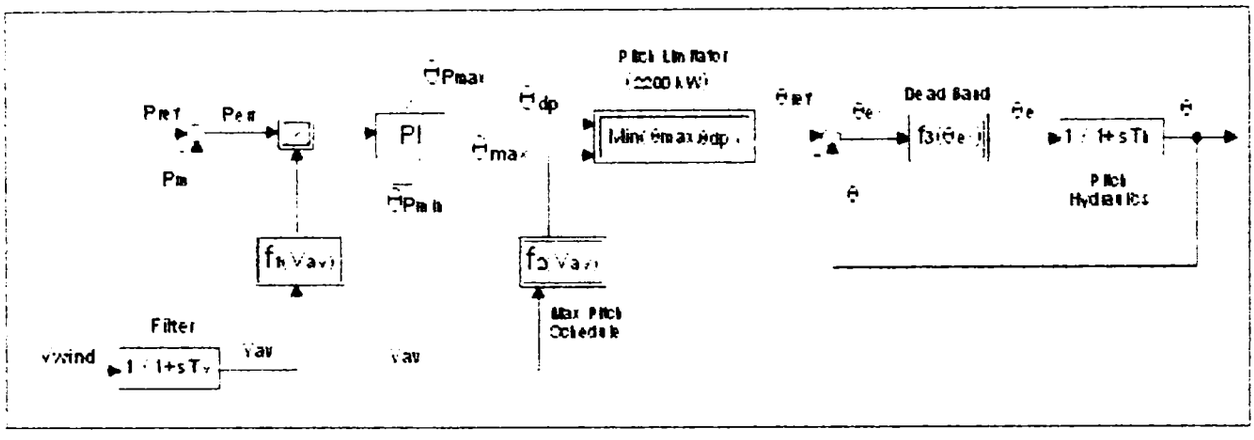


b)

**Figure 3.20**. Aerodynamic power of 2 MW wind turbine versus wind speed for different pitch angles, a) and blade pitch angle control system, b).

The model of the pitch control system, depicted in Fig. 3.20 b), is based on the measured generator power ($P_m$) and the aerodynamic power of wind turbine as a function of measured wind speed ($v_{wind}$) at different pitch angles, shown in Fig. 3.20 a). The measured power is compared with its reference ($P_{ref}$=2000 kW) and the error signal ($P_{err}$) multiply by pitch angle of power control ($f_1(v_{av})$) is sent to the PI-controller producing the pitch angle demand ($\theta_{dp}$), which together with maximum pitch angle-upper limit ($\theta_{max}$) are sent to the pitch limitation non-linear block producing the reference value of the pitch angle ($\theta_{ref}$). The reference value is in the range between the optimised pitch ($\theta_{dp}$) and the maximal pitch angle ($\theta_{max}=90^0$). The maximum value is defined as a function of average wind speed ($f_2(v_{av})$). The reference value is, further, compared to the actual pitch angle ($\theta_{pitch}$) and the error signal ($\theta_{e2}$) is corrected by the pitch hydraulics.

The control strategy used in the present paper called active stall constant speed involves the combined interaction between wind model, pitch control and the aerodynamics of the wind turbine, as shown in Fig. 3.21 a). The blade angle control block (Fig. 3.20 b) models the active stall control of the wind turbine, based on the measured power and the set point, where

rotational speed is the controlled variable. This control strategy takes its origin in the Cp-curves (Fig. 3.6), i.e. to operate the wind turbine at maximum Cp and thereby maximising the energy capture. In fact, the control strategy is characterised by two terms: the optimal region and the power limiting region. In the optimal region, the output power is designed to fulfil the criterion of maximal Cp, which corresponds to the optimal energy capture, by keeping the tip speed ration (λ) constant. In the power limiting region, the speed is kept constant, while the wind turbine will pitch the blades a few degrees every time when the wind changes in order to keep the rotor blades at the optimum angle.

When the wind turbine reaches its rated power, and the generator is about to be overloaded, the turbine will pitch its blades in the opposite direction. In this way, it will increase the angle of attack of the rotor blades in order to make the blades go into a deeper stall, thus wasting the excess energy in the wind.

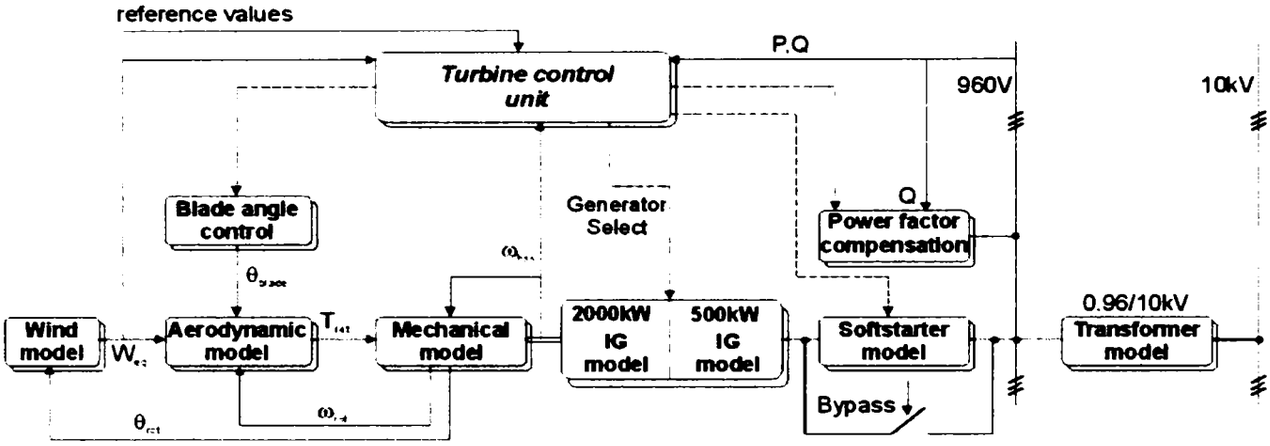


a)

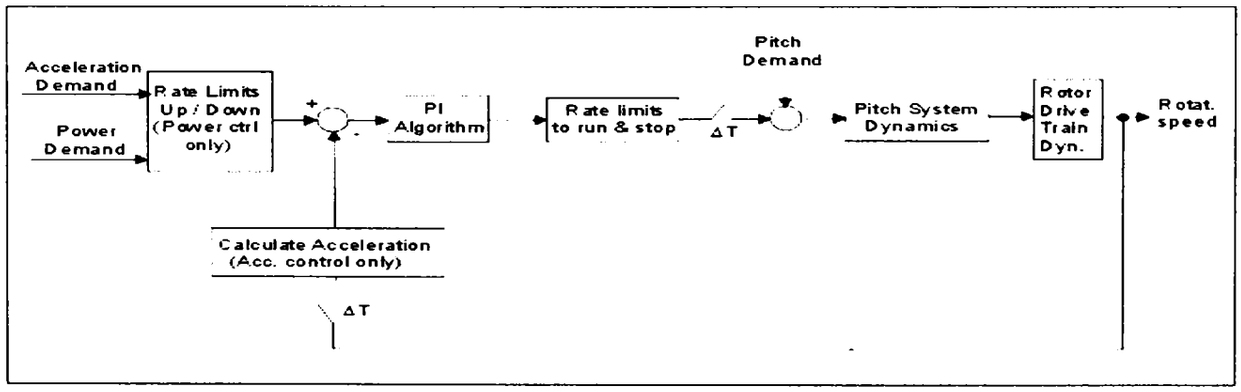


b)

**Fig. 3.21**. Wind turbine control block scheme, a) and block diagram of acceleration and power control loops, b).

Three modes of operation are implemented in the pitch controller developed in DIgSILENT (Appendix B1): acceleration control (speed control), power control and direct pitch control, as can be seen in Fig. 3.21 b). The acceleration and pitch control systems are used during start up, shut down and emergency conditions.

The acceleration demand changes linearly between ($speed_1$=0, $acc._1$=25 rpm/s) and ($speed_2$=1500 rpm, $acc._2$=3 rpm/s) and can be calculated using eq. (3.23):

$$\text{acc. demand}=[\text{rotational speed} * (acc._2-acc._1) / (speed_2-speed_1)] + acc._1 \quad \ldots\ldots\ldots(3.23)$$

The acceleration loop is reseted before generator speed reaches to 1000 rpm. If speed is above 1504 rpm, acceleration demand is set at 2 rpm/s. Direct pitch control is active until generator speed is smaller than 1000 rpm. Pitch value at direct pitch control until soft starts is $-0.5^0$ and in rest is read from a look up table (pitch_table). More details can be found in *Appendix B1*.

The power control is used during normal operations. In the power control system the blade pitch command is provided to the pitch hydraulics by an algorithm with output power error and rotational speed versus average wind speed as inputs. This system has been shown in Fig. 3.20 b).

A few advantages of active stall constant speed control versus passive stall control are: improved output power (see Fig. 3.22), reduced synchronisation transients, lower pitch system / blade bearing activity, and provides additional control capabilities with large utility developments avoiding additional technical complexity and cheaper tower and foundations.

One of the advantages of active stall regulated, point out in Fig. 3.23, is that it can control the power output more accurately than with passive stall, so as to avoid overshooting the rated power of the induction generator of the beginning of a gust of wind. Another advantage is that the machine can be run almost exactly at rated power at all high wind speeds. A normal passive stall controlled wind turbine will usually have a drop in the output power for higher wind speeds, as the rotor blades go into deeper stall, as can be seen in Fig. 3.22.

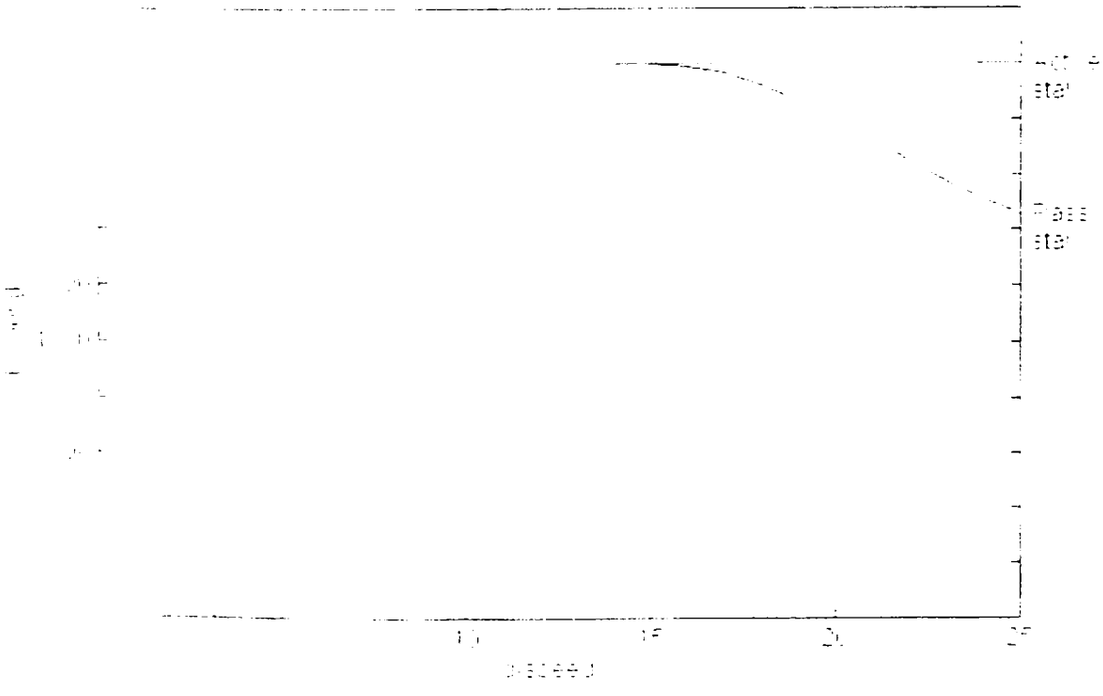

**Fig. 3.22**. Active stall control versus passive stall control of 2 MW wind turbine.

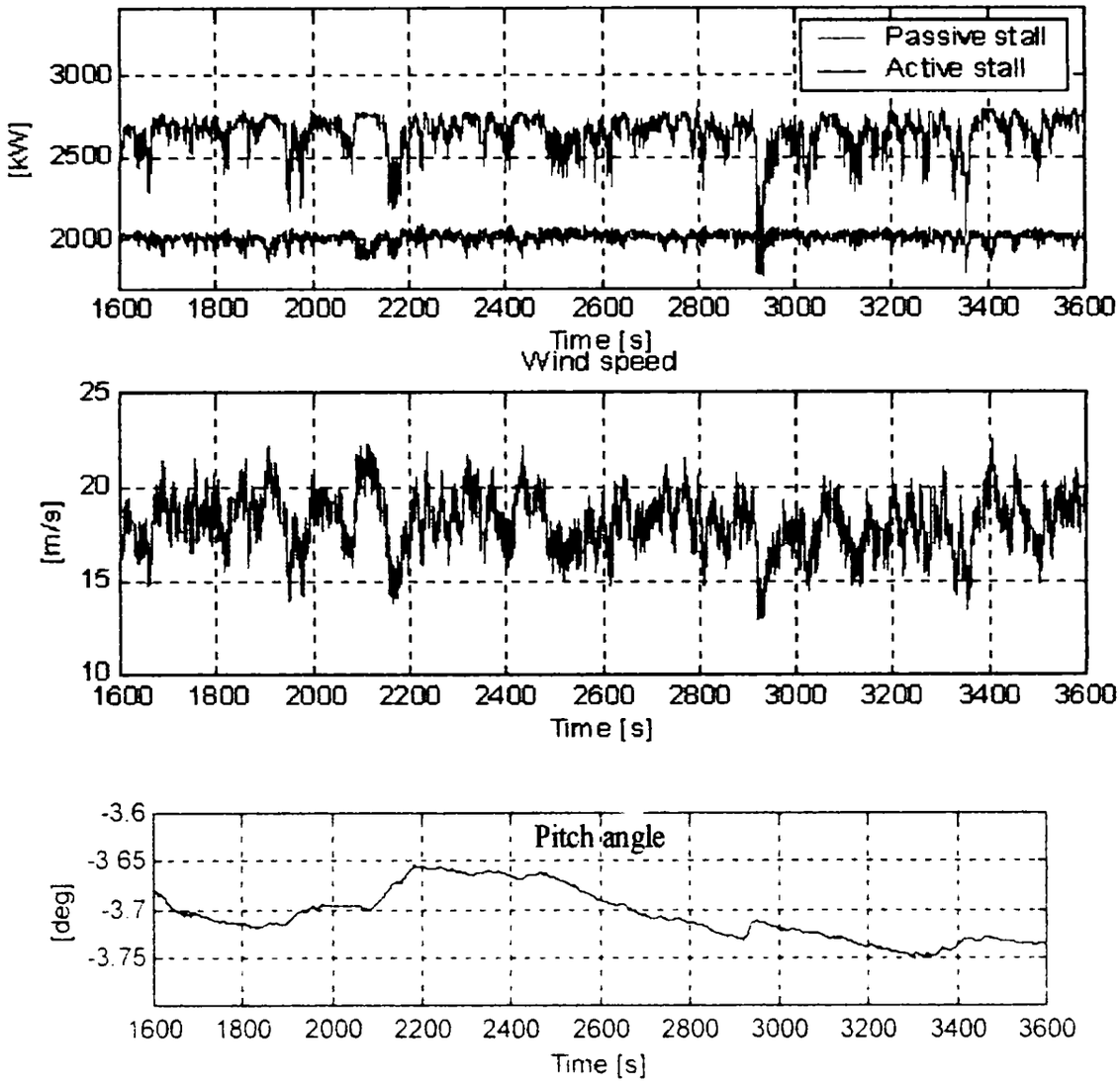


**Fig. 3.23**. Comparison between simulated active power with active and passive stall control at an average wind speed $u_{eq}$=18 (m/s) and with pitch angle control at turbulence intensity of ti=0.12.

## *3.4. Simulation Results*

Simulation results on constant-speed wind turbines with 2 MW and 0.5 MW induction generators are presented. The scheme also presents a case of load flow simulation, when the wind generator works at nominal conditions and full power factor compensation is used. In order to limit the starting current transients during the 2 MW generator connections to the grid, a soft starter startup is used. The generators are connected when the generator speed is higher than the synchronous speed.

To simulate the wind turbine, models have been developed for each element and implemented in the dedicated power system simulation tool DIgSILENT, which provides the ability to simulate load flow, RMS fluctuations and transient events in the same software environment. The DIgSILENT simulation tool therefore has a dedicated model for induction generators, which take into account the current displacements in the rotor, the torque – slip and short circuit test curves. Also models of synchronous machines, transformers, bus bars, grid models, static converters etc are provided.

The grid model and the electrical components of the wind turbine are built on standard component models from DIgSILENT library. The models of the wind speed and of the mechanical, aerodynamics and control parts of the wind turbine are written in the dynamic simulation language DSL of DIgSILENT, more details will be presented in *Appendix B1*.

Fig. 3.24 contains the grid representations from 50 kV double bus-bar systems down to the wind turbine. The wind turbine contains the tower cable making the connection to the 0.96 kV / 10 kV transformer and the 10 kV cable at the bottom of the tower. The 10 kV cables are modeled using the existing DIgSILENT model toolbox.

The power factor compensation units are represented by a capacitor bank on this scheme and a Static Var System (SVS) unit. The switching of capacitors is done as a function of average value of measured reactive power. The generators are full load compensated.

The block diagram represents a case of load flow simulation, from induction generator to the grid, when the 2 MW wind generator is working at nominal conditions and full power factor compensation is used, as can be seen in Fig. 3.25.

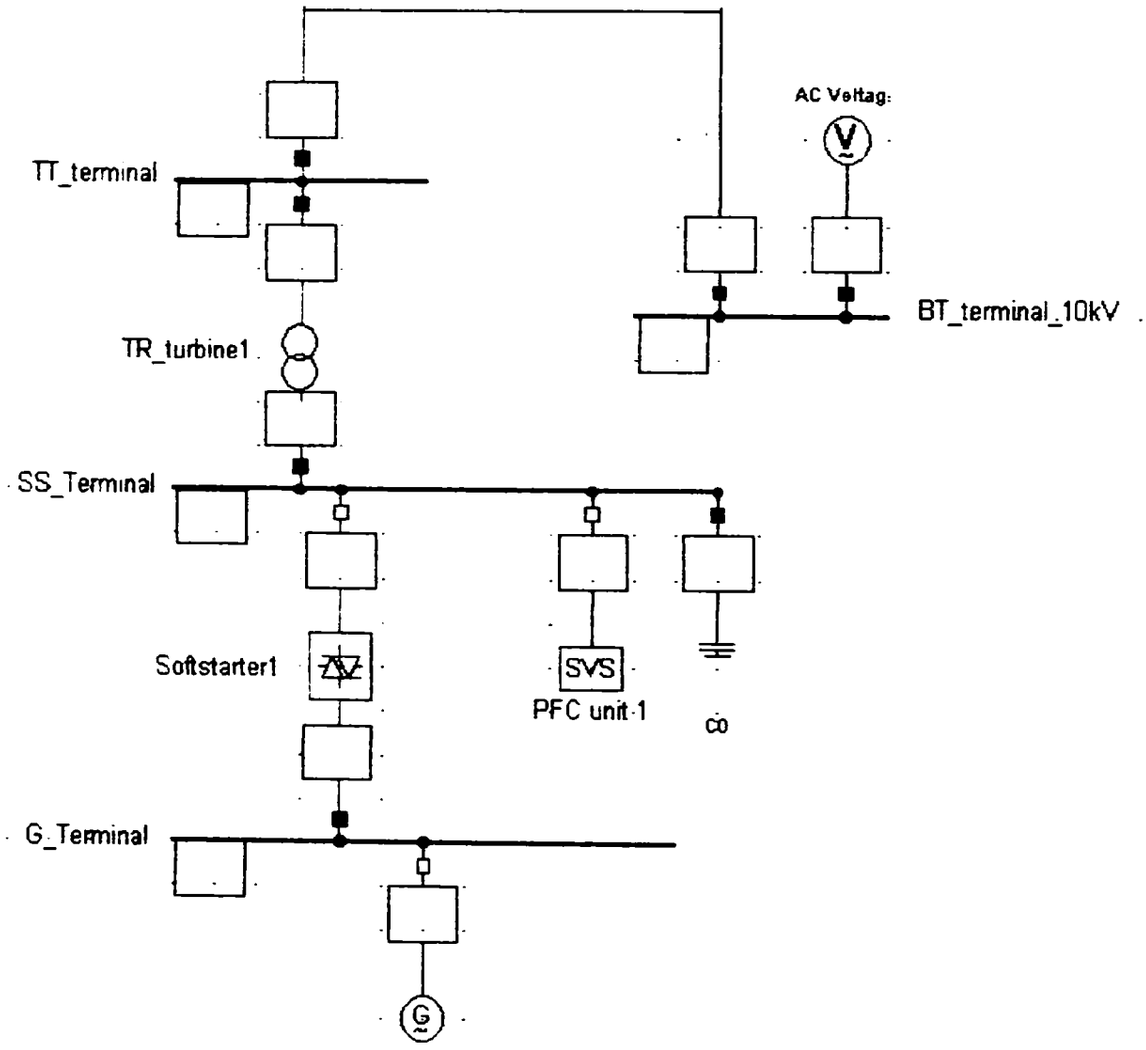


**Figure 3.24**. Electrical diagram of 2 / 0.5 MW wind generators.

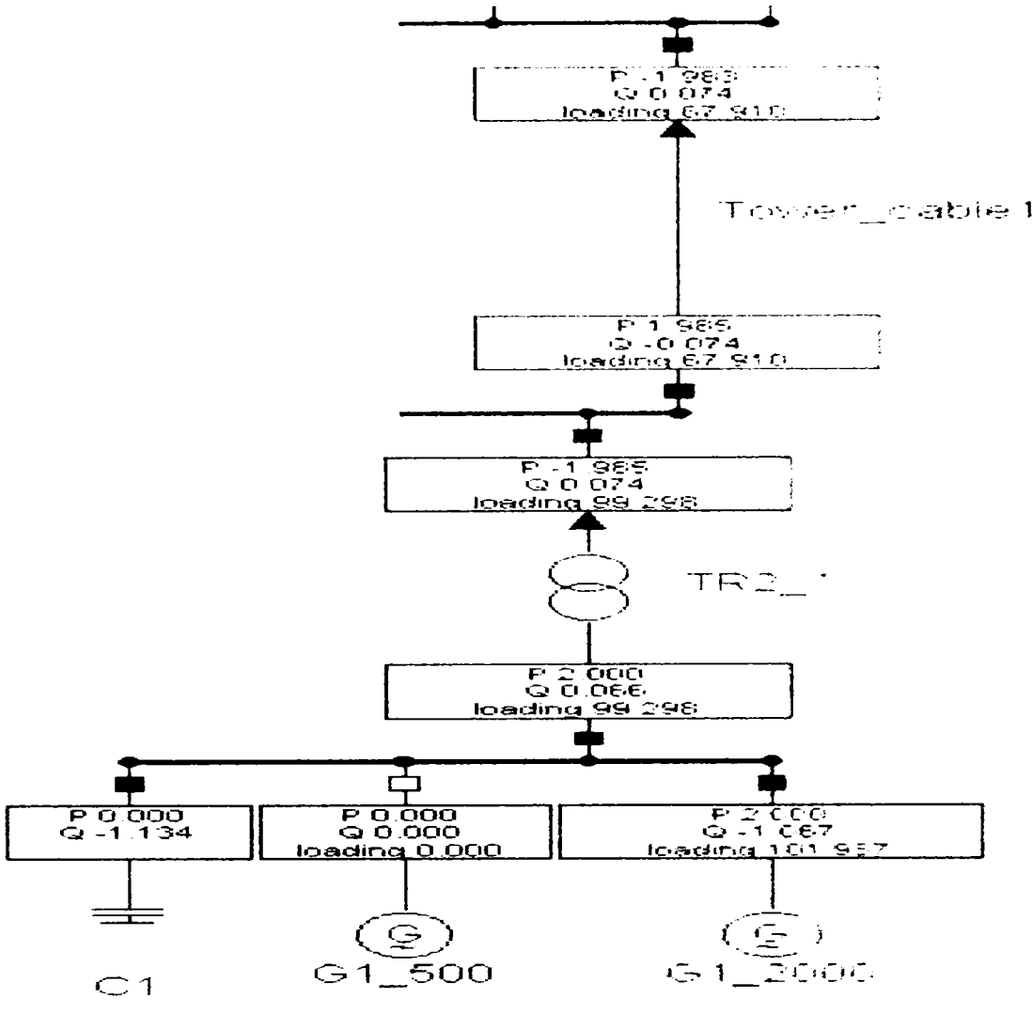


**Fig. 3.25**. Load flow block diagram of wind turbine with 2 MW induction generator connected to the grid.

The aerodynamic torque (torque_rot-$T_{rot}$) accelerates the wind turbine rotor, with the generator disconnected from the grid, until the rotor speed (omega rot-$\omega_{rot}$) is close to its nominal value. Then the generator is connected to the grid as seen in Fig. 3.26. The basic idea is to control the rotational speed using only measurement of the power (or torque), as it is depicted in Fig. 3.1 and by equations (3.5) and (3.6) as well.

Results for two induction generators (0.5 and 2 MW) are presented in Fig. 3.27 and Fig. 3.28. These figures contain traces of rotor speed, current magnitude, and total active and reactive power for start-up of the wind turbine with directly connected induction generators, at 1505 rpm (1.007 p.u.).

The starting current of 0.5 MW machine is 3 times higher than the rated current, while the starting current of the large induction machine (2 MW) is 8 times higher than its rated value. It is clear that for 2 MW machine it is imperative to reduce the start-up current.

As it can also be seen in Fig. 3.27 and Fig. 3.28, the induction generators have a peak consumption of reactive power right after connection to the grid. The reactive power is required to magnetize the generators. The steady state voltage is dependent on the reactive power consumption of induction generator (IG). Therefore it is important to supply the IG with a reactive power compensation unit to provide the reactive power balance and to improve the voltage stability.

In Fig. 3.29 the connection of the 2 MW generator to the grid is realized by a soft-starter. The soft starter limits the current and torque transients and implicitly reduces the reactive power peak value. When the induction machine of 2 MW was connected to the grid through soft-starter, the starting current has been reduced at 1.1 times of rated current, while the reactive power peak became 13.5 times smaller than when the machine was directly connected to the grid.

When the soft-starter is bypassed and thus the 2 MW induction generator is connected, the power factor compensation is performed by the capacitor bank (Figs.3.30). It is also seen in Fig. 3.30 how the capacitor banks are connected in steps after the 2 MW generator is connected to the grid. The capacitors can be switched on and off individually as a function of average value of reactive power during a certain period of time.

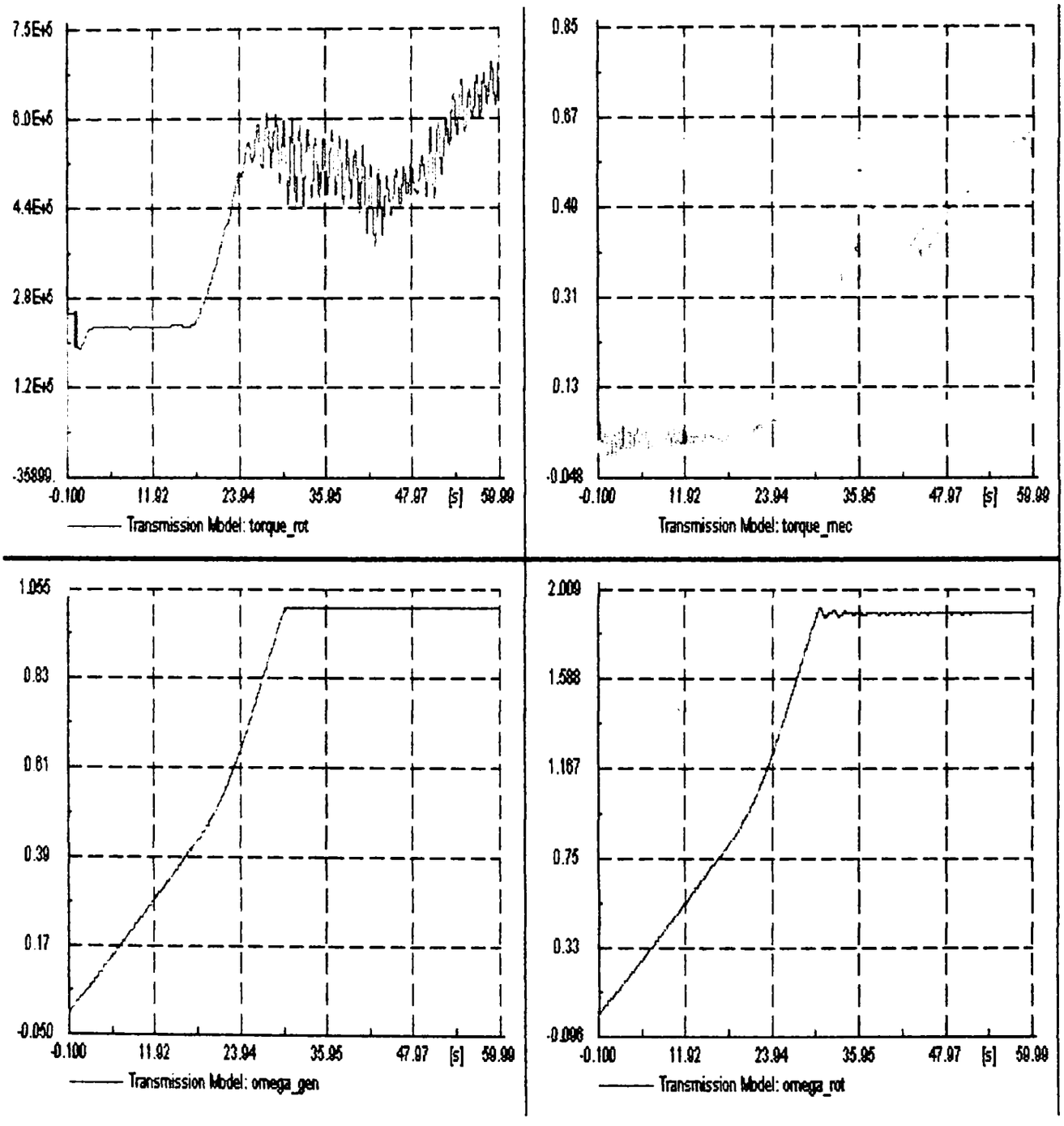


**Fig. 3.26**. Transmission model during start-up. Aerodynamic torque (torque_rot), mechanical torque (torque_mec), generator speed (omega_gen) and rotor speed (omega_rot) of wind turbine system.

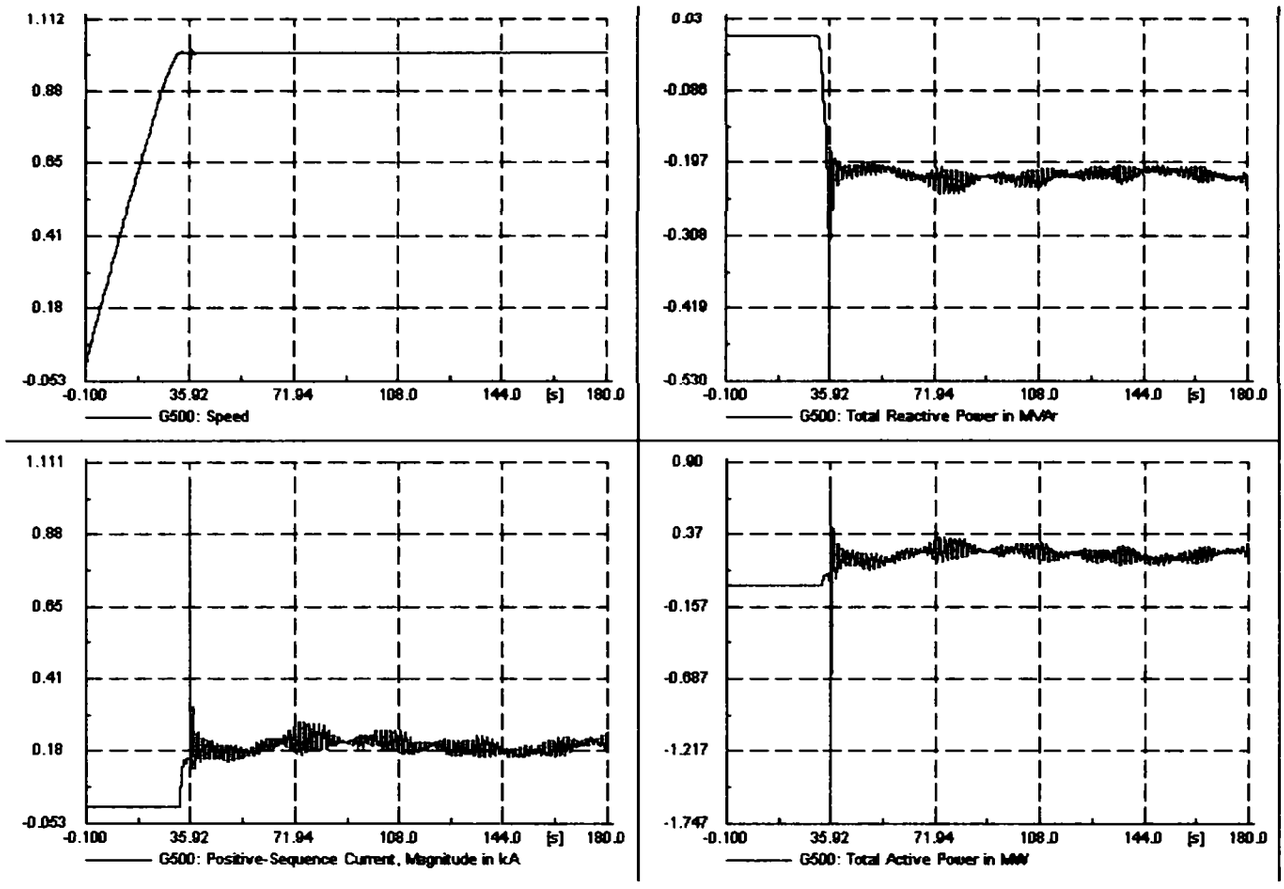


**Figure 3.27**. Start-up with directly connected and operation of 0.5 MW induction generator. Speed, reactive power, current and active power of the generator.

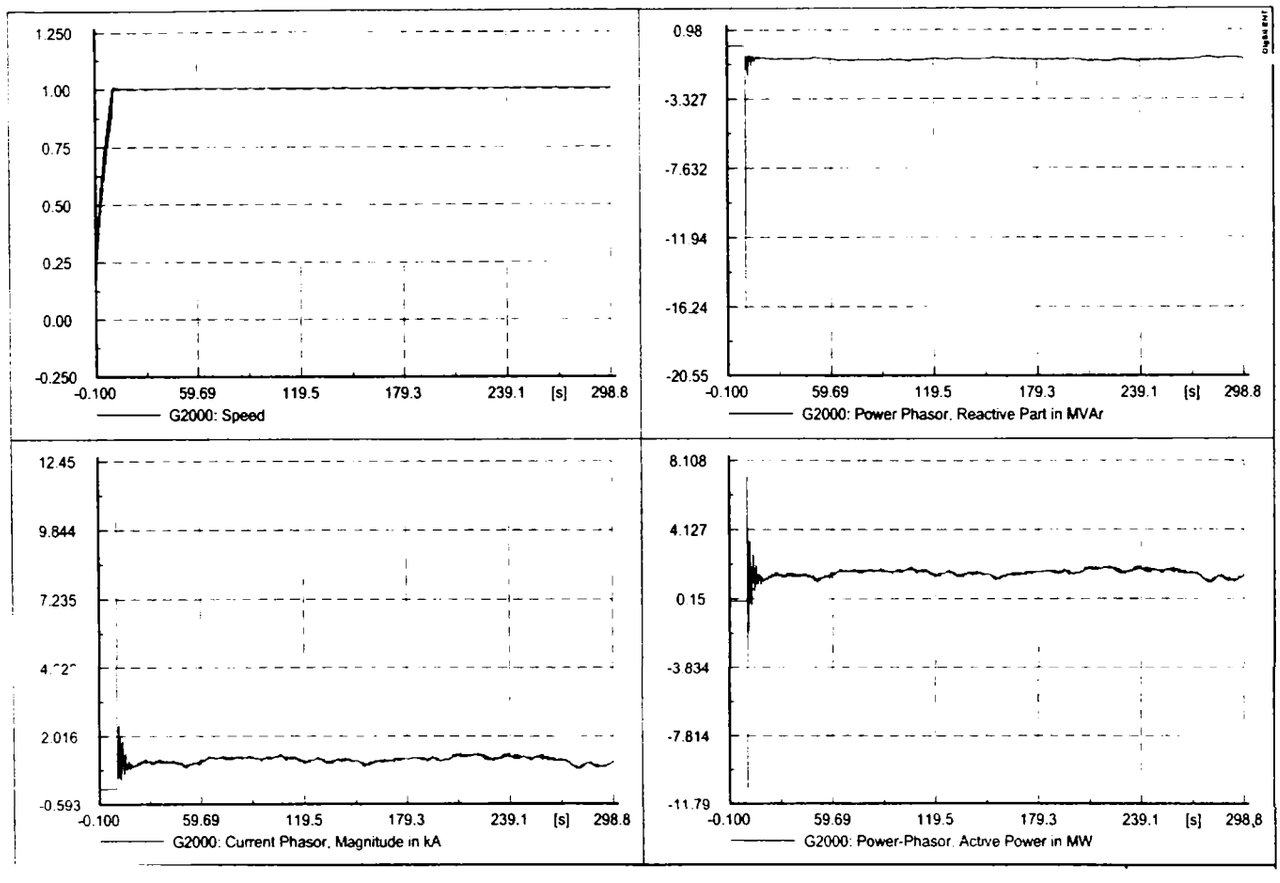


**Figure 3.28**. Start-up with directly connected and operation of 2 MW induction generator. Speed, reactive power, current and active power of the generator.

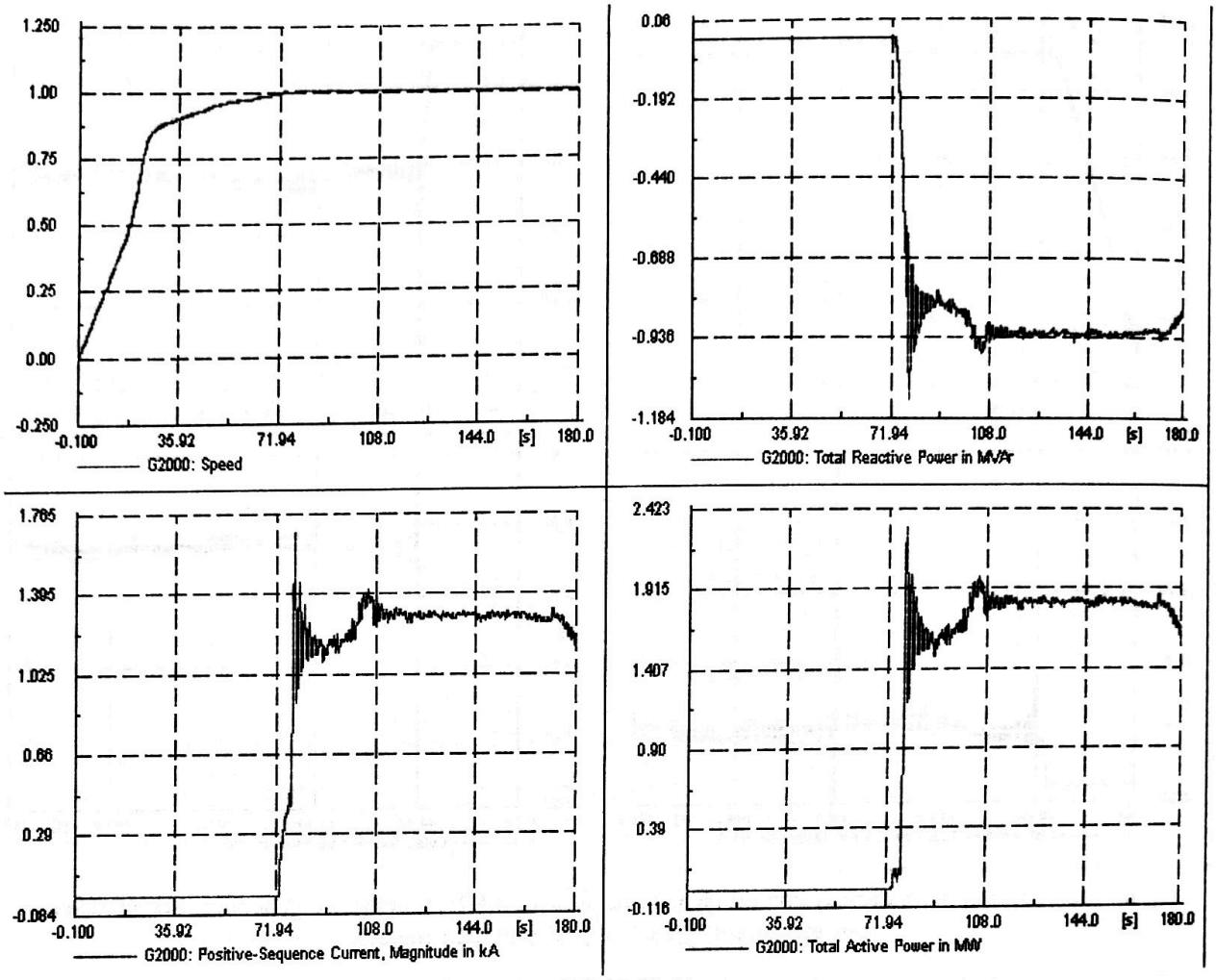


**Figure 3.29**. Start-up with soft-starter and operation of 2 MW induction generator. Speed, reactive power, current and active power of the generator.

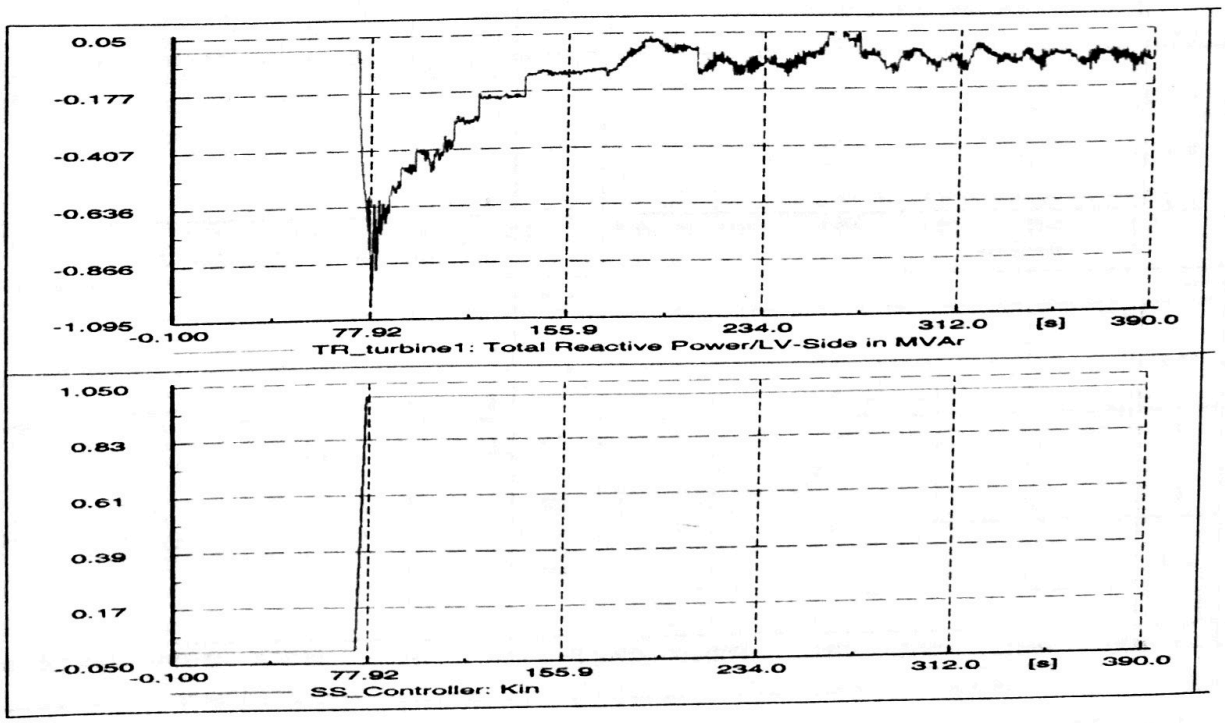


**Figure 3.30**. Reactive power compensation with capacitors connected in steps and the soft-starter by-passed controller (SS_controller: $K_{IN}$).

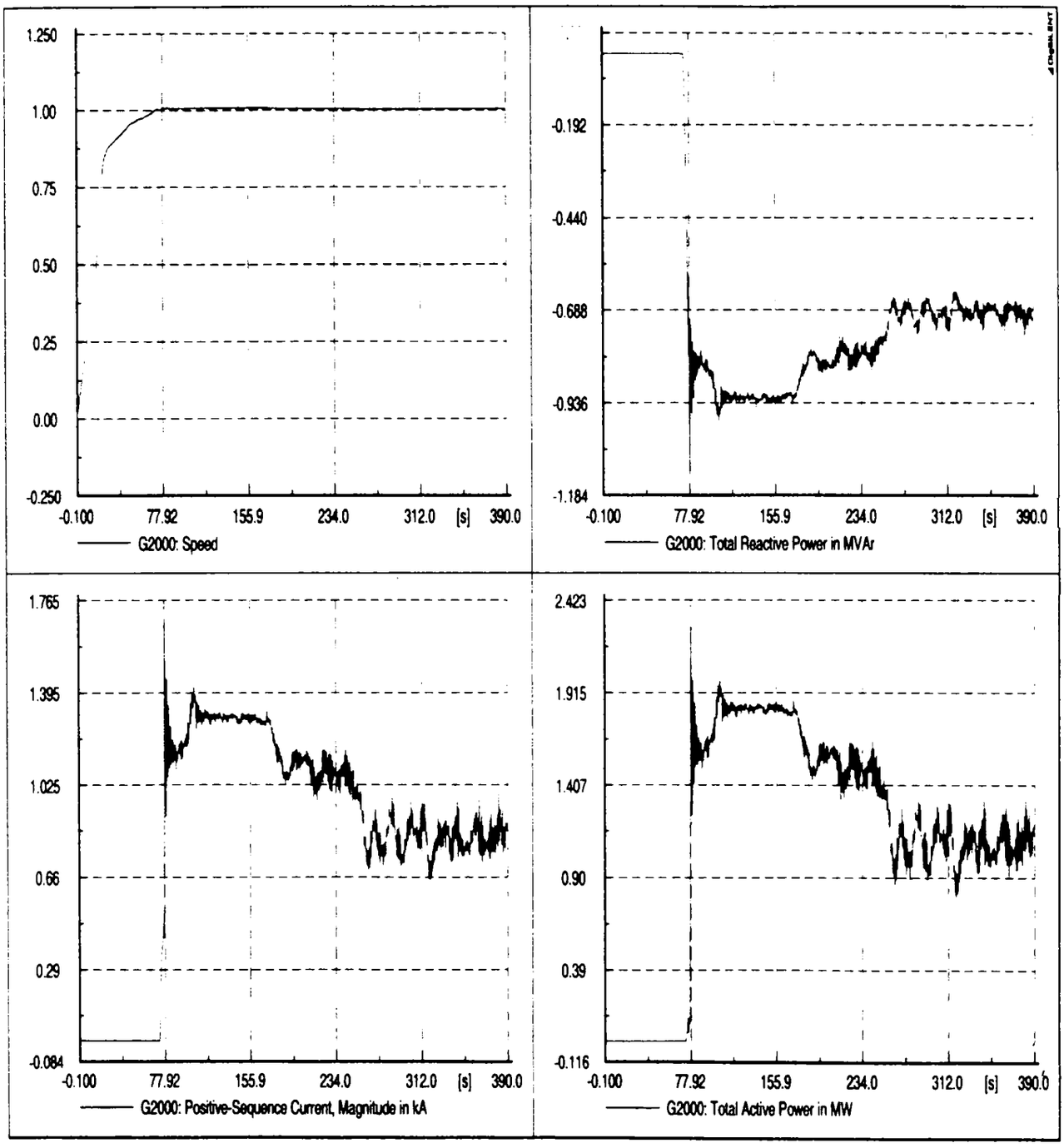


**Figure 3.31**. Simulated speed, active and reactive power and stator current of 2 MW induction generator under sudden changes in wind speed from 12 m/s to 18 m/s at 100 s and then from 18 m/s to 11 m/s at 170 s.

In Fig. 3.31 the 2 MW induction generator was connected to the grid through soft-starter at t=73 seconds and then the soft-starter was by-passed at t=77 seconds (see Fig. 3.30). In the same time the power factor compensation unit started to work using capacitor switching. The mean wind speed was 12 m/s. At t=100 seconds the mean wind speed was modified to 18 m/s and at t=170 seconds mean wind speed was modified again at 11 m/s to simulate sudden changes in wind speed and to test the system performance and implemented control strategy. The active and reactive powers have been able to follow these changes in both situations. It is concluded that the wind turbine absorbed the transients very fast and the control strategy offers a good stability of the system during transition of dynamic changes.

## 3.5. Comparison between measurements and simulations

The comparison between simulations and measurements will be done to validate the model. The validation of the developed model in DIgSILENT is performed for the case of continuous operation, and is based on power quality measurements for one of the 2 MW wind turbine from an existing new wind farm in Denmark. The wind speed measurement was provided by the anemometer of the control system on the top of the nacelle of wind turbine, as shown in Figs. 3.32 and 3.33. Power quality measurements are performed as sampling of instantaneous values of three-phase currents and voltages with a sampling frequency of 3.2 kHz.

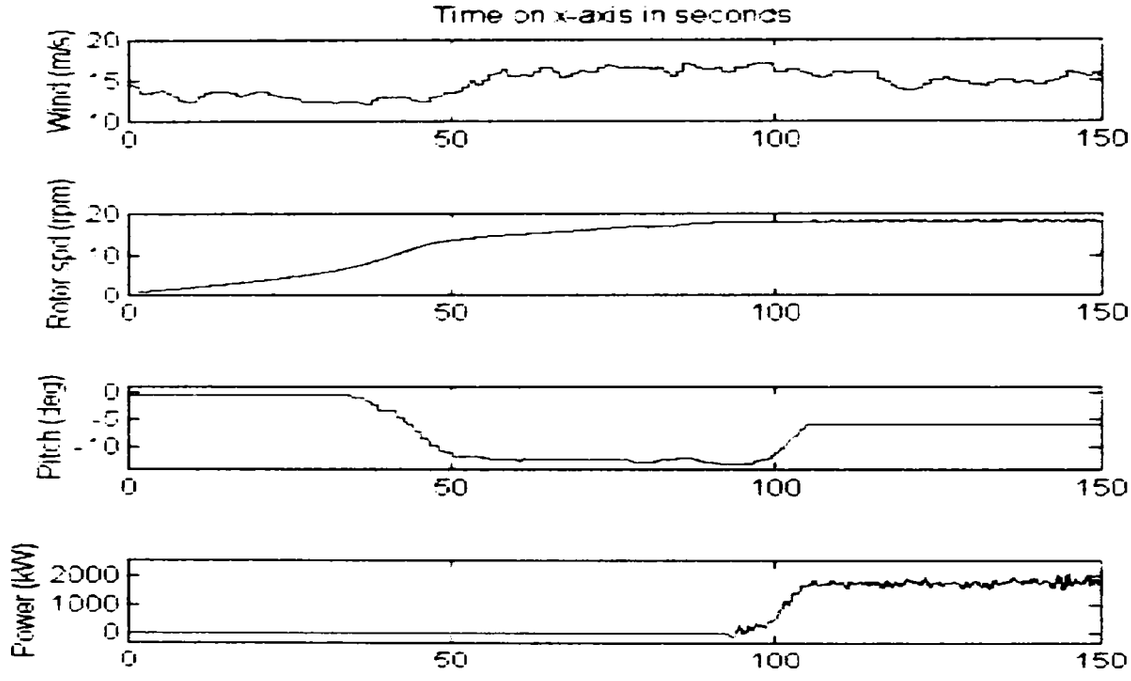


**Fig. 3.32.** Acceleration control mode in a 2 MW wind turbine. Measured wind, rotor speed and active power.

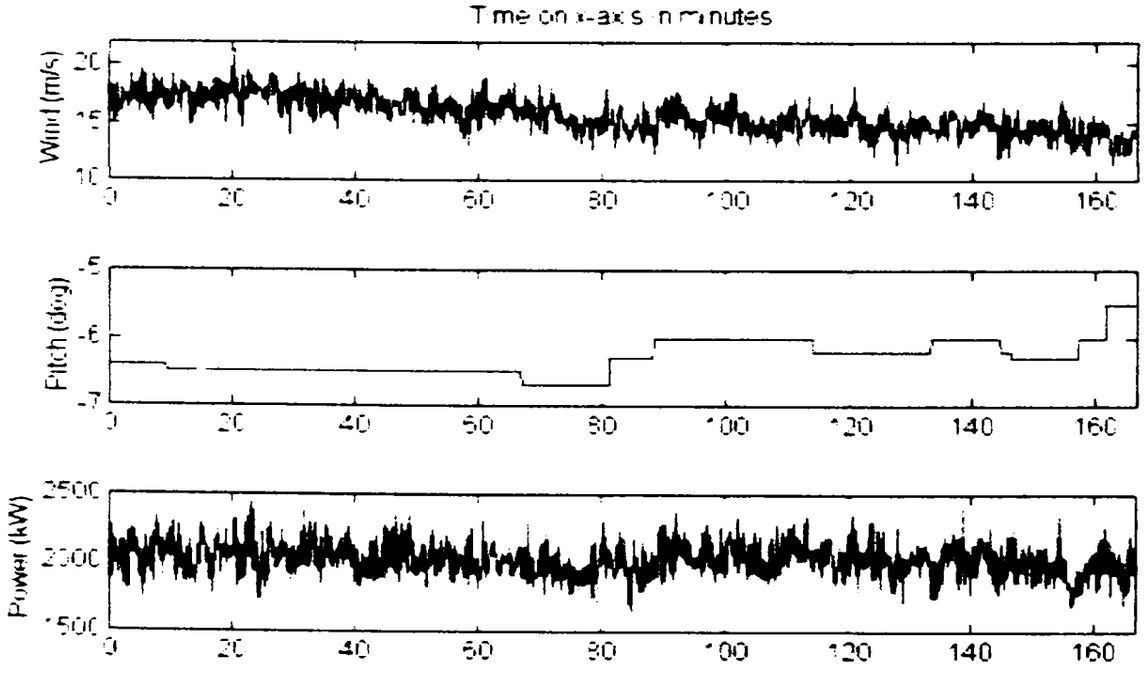


**Fig. 3.33.** Power control mode of 2 MW Wind Turbine. Measured wind speed and active power under pitch control regulated during 170 minutes.

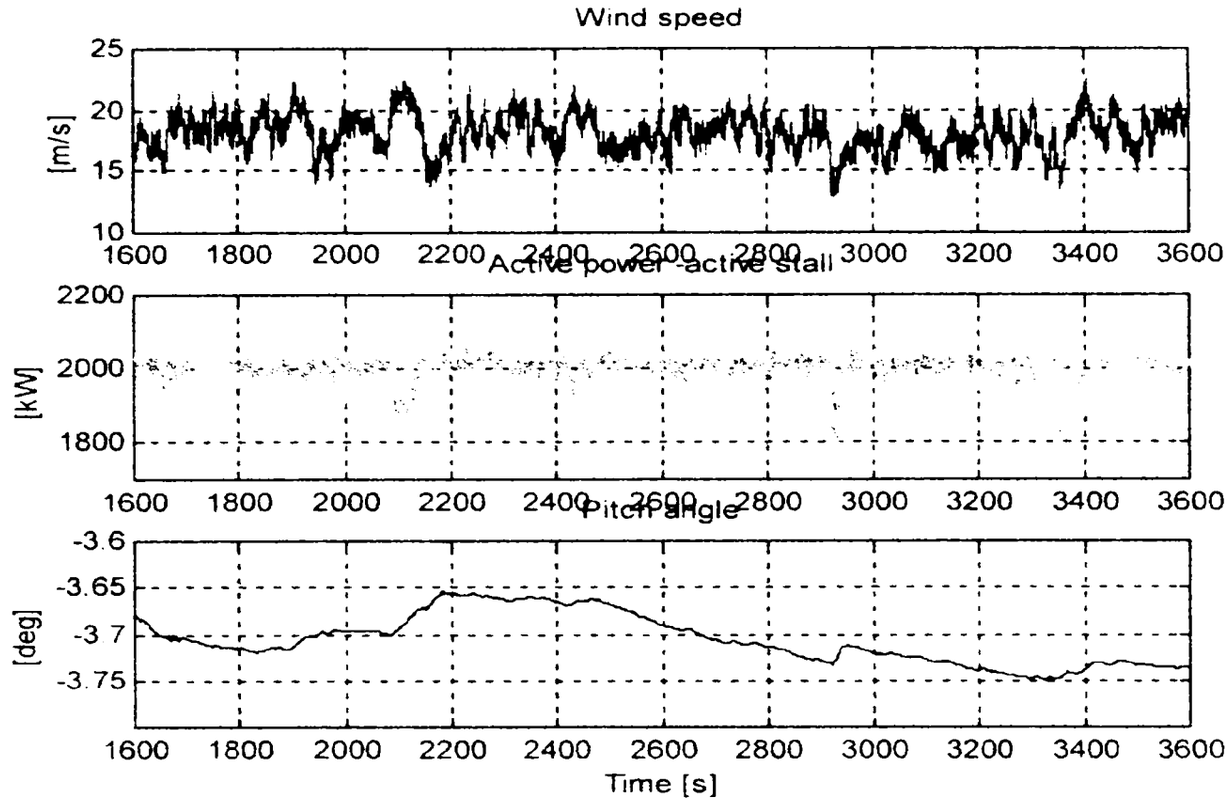


**Fig. 3.34**. Simulation of power control mode of 2 MW Wind Turbine Generator. Wind speed, active power and pitch angle versus time.

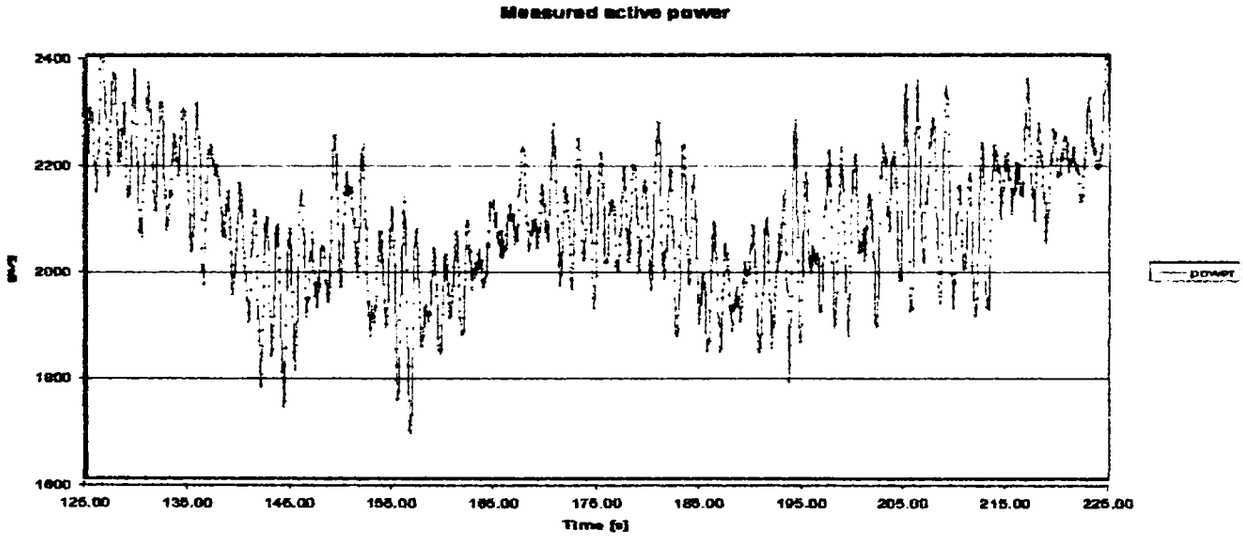


a)

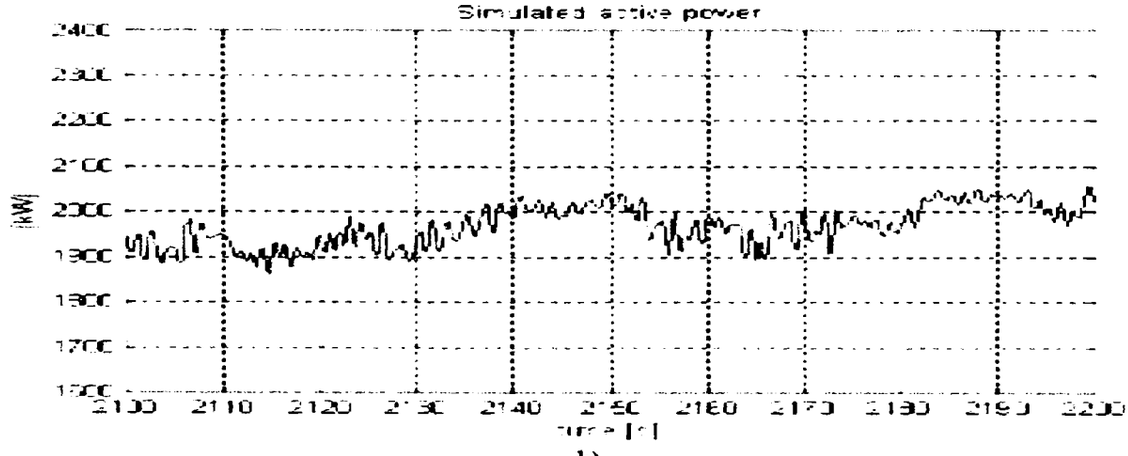


b)

**Fig. 3.35**. Measured (a) and simulated (b) active power versus time of 2 MW Wind Generator.

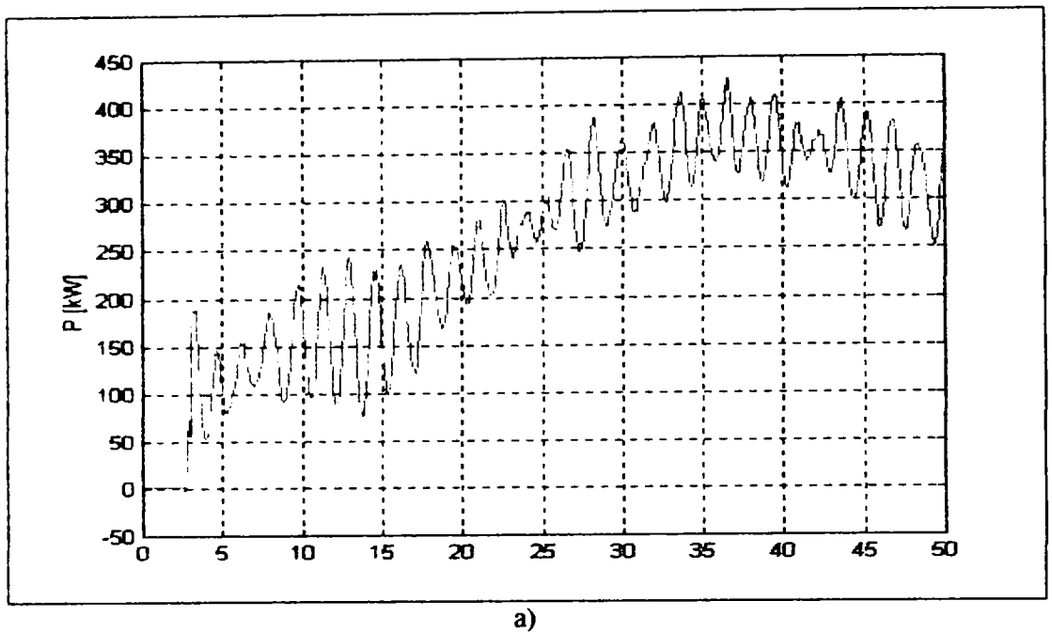


a)

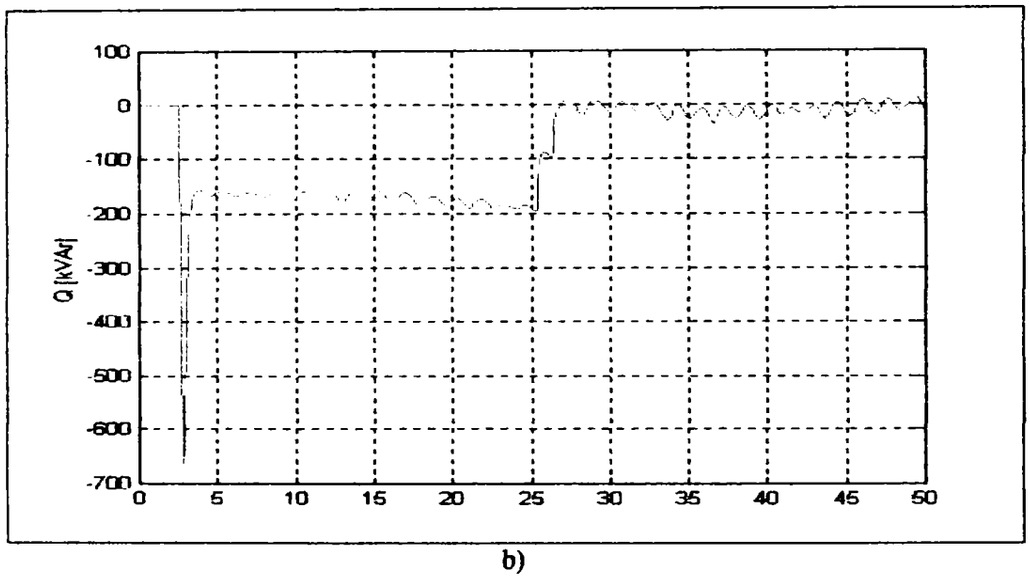


b)

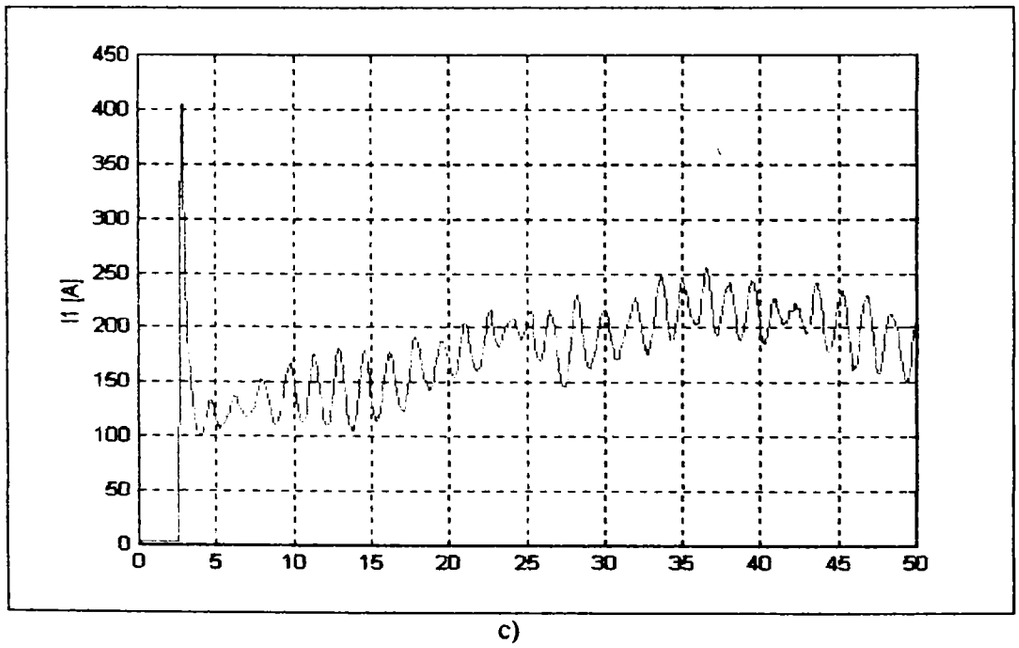


c)

**Fig. 3.36**. Measured active power (a), reactive power (b) and stator current (c) of 0.5 MW Wind Turbine generator versus time [s].

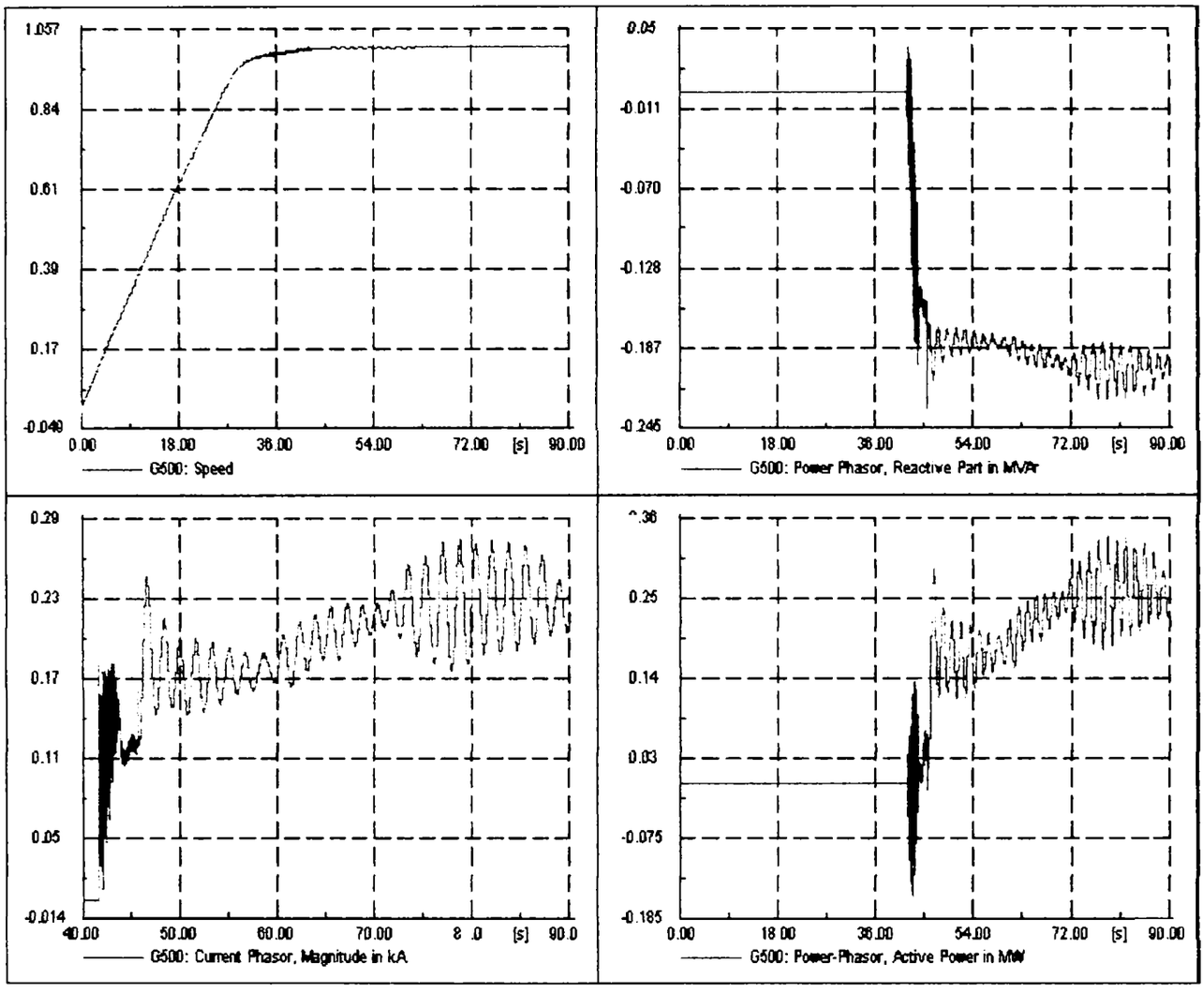


**Fig. 3.37**. Simulated speed, active and reactive power and stator current of 0.5 MW Induction Generator versus time.

Figs. 3.36 and 3.37 present the measured and simulated power quality performances of a 500 kW Constant-Speed Wind Generator during normal operation. Focus is on the maximum value of active and reactive power consumption and flicker emission which influence the power quality. A comparison between Fig. 3.36 and Fig. 3.37, point out that the measured (Fig. 3.36) and simulated (Fig. 3.37) active and reactive power and stator current from a 0.5 MW wind turbine generator, there is a good correspondence. It is observed that the reactive power compensation is used in measurements only.

Figures 3.33 and 3.34 present a comparison between measured (Fig. 3.33) and simulated (Fig. 3.34) of wind speed, pitch angle and active power of 2 MW wind generator under power control mode. The power control mode is used during normal operations. It is clear that at high wind speed (around 18 m/s), using the active stall regulation, the pitch angle is continuously adjusted to obtain the desired rated power level (2 MW). The results show a good agreement between measurements and simulations.

The acceleration control mode (Fig. 3.32) and direct pitch control are used during a start up of generator. Direct pitch control is active until rotor speed is smaller than 18 rpm.

## 3.6. Conclusions

This chapter presents details about modeling and simulation of constant-speed wind turbines using cage rotor induction generators.

A wind turbine model has been built to simulate the influence on the transient stability of power systems. The model of the wind turbine includes the wind fluctuation model, which will make the model useful also to simulate the power quality and to study control strategies of a wind turbine. The control scheme has been developed for wind turbine generator control including soft starter start-up, and power factor compensation.

The constant speed wind turbine has to be operated at the optimum tip speed ratio, which gives the maximum power transfer. The control strategy used – active stall constant speed, is a relatively recent innovation in the power control strategy of a large wind turbine, and provides simple pitch control improving power quality and system efficiency. This eliminates electrical power variations (fewer flickers) and reduced torque pulsations due to elasticity of wind turbine system. Also, this alternative control strategy, involves the combined interaction between wind model, pitch control and the aerodynamics of wind turbine rotor blades.

The comparative results between MATLAB-Simulink and DIgSILENT show a good similarity during generator start-up and steady state performance. Especially in wind power applications, DIgSILENT Power Factory has become the de-facto standard tool, as all required models and simulation algorithms are providing unmet accuracy and performance.

The computer simulations prove to be a valuable tool in predicting the system behavior.

The above-presented model can be a useful tool for wind power industry to study the behavior and influence of big wind turbines on power distribution networks.

The power quality impact of wind turbines with 0.5 and 2 MW induction generators has been investigated through the comparison of the computed characteristics from simulations with measured power quality characteristics. The implemented model is able to simulate a whole wind turbine system. The results show a good agreement between measurements and simulations.

**ACNOWLEDGEMENT**

This work was carried out with the support of the Danish Technical University of Aalborg. I would like to thanks Professor Frede Blaabjerg for his suggestions and useful discussions.

# References


[1] "International Wind Energy Development. "World Market Update 1999". *BTM Consults Aps. Ringkobing, Denmark 2000 ISBN 87-987788-0-3.*

[2] S. Muller. M. Deicke and R.W. De Doncker. "Doubly Fed Induction Generator Systems for Wind Turbines". IEEE Industry Applications Magazine. May-June 2002. pp. 26-33.

[3] "Guided Tour on Wind Energy". *Danish Wind Turbine Manufacturers Association, Denmark.*

[4] E. Muljadi. P.C. Butterfield. "Pitch controlled variable–speed wind turbine generator". *Industry Applications Conference, 1999. IAS Annual Meeting. Conference Record.* Vol. 1. pp. 323 – 330.

[5] S.A. Papathanassious. M.P.Papadopoulus. "Dynamic Behaviour of Variable Speed Wind Turbines under Stochastic Wind". *IEEE Trans. on Energy Conversion,* vol. 14. no.4 1999. pp. 1617-1623.

[6] A. Miller. E. Muljadi. D.S. Zinger. "A Variable Speed Wind Turbine Control". *IEEE Trans. on Energy Conversion.* vol.12. no 2. June 1997. pp. 181-186.

[7] DiGSILENT Power Factory user manuals. *DiGSILENT GmbH, Germany.*

[8] G. Seguier. *Power Electronic Converters-AC/DC Conversion*. New York: McGraw-Hill. 1986.

[9] L.H. Hansen. P. Sorensen. U.S. Paulsen. "Variable Speed Wind Turbine using Full Conversion". *Contribution to the NORpie-2000, Aalborg, Denmark*. pp. 115-119. June 13th to 16th. 2000.

[10] P.A.C. Rosas. P. Sorensen and H. Bindner. "Fast wind modelling of wind turbines". *Special topic conference. Wind power for the 21st Century.* Kassel. Germany. September 2000.

[11] Torbjorn Thiringer. "Grid-Friendly Connecting of Constant-Speed Wind Turbines Using External Resistors", IEEE Transactions on Energy Conversion. vol. 17. no. 4. pp. 537-542. December. 2002.

[12] **Lucian Mihet-Popa**. F. Blaabjerg and I. Boldea. "Simulation of Wind Generator Systems for the Power Grid". OPTIM 2002. vol. 2. pp. . 16-18 May. 2002.

[13] **Lucian Mihet-Popa**. F. Blaabjerg and I. Boldea. "Wind Turbine Generator Modeling and Simulation where Rotational Speed is the Controlled Variable". IEEE Transactions on Energy Conversion. vol. . no. . pp. . January / February 2004.

[14] Anca D. Hansen. Poul Sorensen. L.Janosi and J. Bech. "Wind farm modelling for power quality". *IECON'01: The 27th Annual Conference of the IEEE Industrial Electronics Society*. vol. 3. pp.1959-1964.

[15] C. Rombaut. G. Seguier and R. Bausiere. "Power Electronic Converters". McGraw-Hill Book Company. vol. 2 AC-AC Conversion. 1987.

[16] W. Deleroi. J.B. Woudstra. "Connecting an asynchronous generator on the grid using a thyristor switch". IEEE Transactions on Industry Application. vol. 2. March 1991. pp. 55-60.

[17] W. Deleroi. J.B. Woudstra and A.A. Fahim. "Analysis of thyristor controlled three-phase induction motor with alternation of symmetrical and unsymmetrical operation". EM&PS. vol. 16. 1989. pp. 59-76.

[18] Jakob Mann. "Wind field simulation". Prob. Eng. Mech.. Vol. 13. no. 4. Elsevier 1998.

[19] P. Madsen and J. Rasmussen. "Rotor loading on a three-bladed wind turbine". European Wind Energy Conference. Glasgow EWEC. 1989.

[20] Torbjorn Thiringer. Jan Linders. "Control by variable rotor speed of a fixed-pitch wind turbine operating in a wide speed range". IEEE Transactions on Energy Conversion. September 1993. vol. 8. no. 3. pp. 520-526.

# Chapter 4

## Limited Variable Speed Generation by Induction Generators with Passive Rotor Elements.

**Chapter Contents**

## 4.1. An overview of DFIG with limited variable speed based Wind Turbines

Since the start of modern wind turbine development in 1957, marked by the innovative Gedser Wind Turbine (200 kW), the main aerodynamic concept has been a horizontal axis, three bladed, downwind wind turbine, connected to a three-phase AC-grid. Many different concepts have been developed and tested since, [S. Heier, pg. 6].

During the last two decades, the production of wind turbines has grown in size from 20 kW to 3 MW per unit. Due to the rapid development of power electronics, offering higher power handling capability and lower price / kW, the application of power electronics in wind turbines will increase further.

The most commonly concepts using the wound rotor asynchronous generator with limited speed variation applied in wind turbine configurations are displayed in Fig. 4.1. [1, 2]

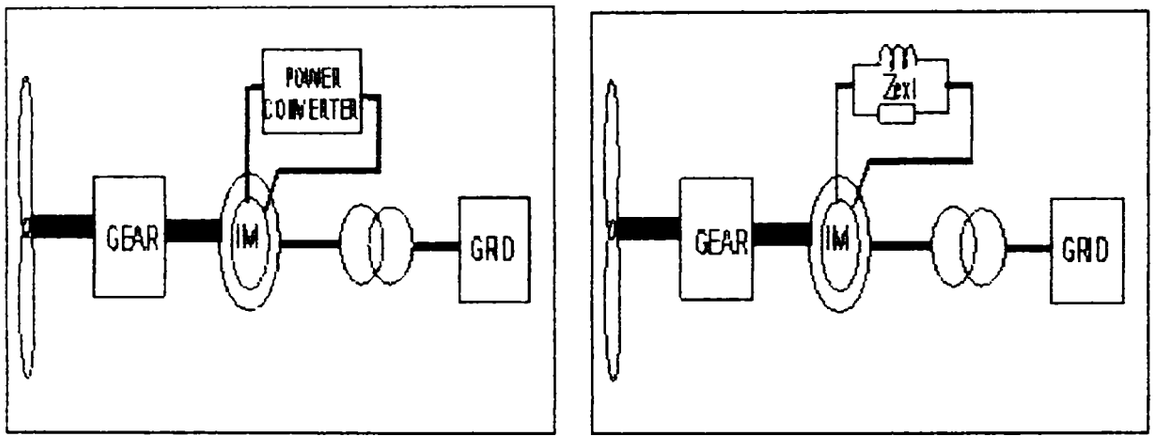


a) b)

**Figure 4.1**. Standard wind turbine configurations using slip ring rotor machines;
a) Dynamic slip control using power converter, b) Dynamic slip control using external impedance.

The configurations depicted in Fig. 4.1 present an outline of typical electrical topologies used in wind turbines with wound rotor induction generators with limited variable speed. These configurations cover a relatively wide range of the applied power control concepts for wind generators.

The doubly-fed induction generator, involved in these concepts, has two possible implementations: the rotor is connected to an external power electronics converter (Fig. 4.1a) or the rotor is connected to external passive components (Fig. 4.1b). To rigidly setting slip values by using extra resistances in the rotor circuit, slip-ring machines offer the possibility of dynamically adjusting or controlling slip to adapt to output power variations. In this way, by varying the resistance of the rotor, the slip value and thus the proportional loss in power are

kept low and system efficiency is increased. To achieve a high total efficiency, the rotor slip should be kept as low as possible in this relatively simple system.

The configuration in Fig. 4.1a) employs a wound rotor and it has been used by Vestas since the mid 1990's – known as OptiSlip [2]. The basic idea of this concept is to control the total rotor resistance using a variable external rotor resistance by means of a Power Electronics (PE) converter. With the power electronic converter mounted on the rotor shaft, it is possible to control the slip (by controlling the external rotor resistance) over a 10 % range [6]. Control of the slip implies control of the power output in the system. This concept will be considered below.

## 4.2. OptiSlip Control Scheme

The Wind Turbines, with additional resistors, power electronics and regulation in the rotated part of the generator, from Vestas Wind Systems A/S are equipped with a system called OptiSlip, for suppressing wind gusts are reducing power fluctuations fed into the power grid. These wind turbines are equipped with two types of control. Pitch control is used for limiting and controlling the average active power. The additional control system, called OptiSlip control, is used for damping power fluctuations due to wind gusts.

The OptiSlip switches external rotor resistance in and out of the rotor circuit of the generator and thereby varies the speed of the generator. The scheme is depicted in Fig. 4.2.

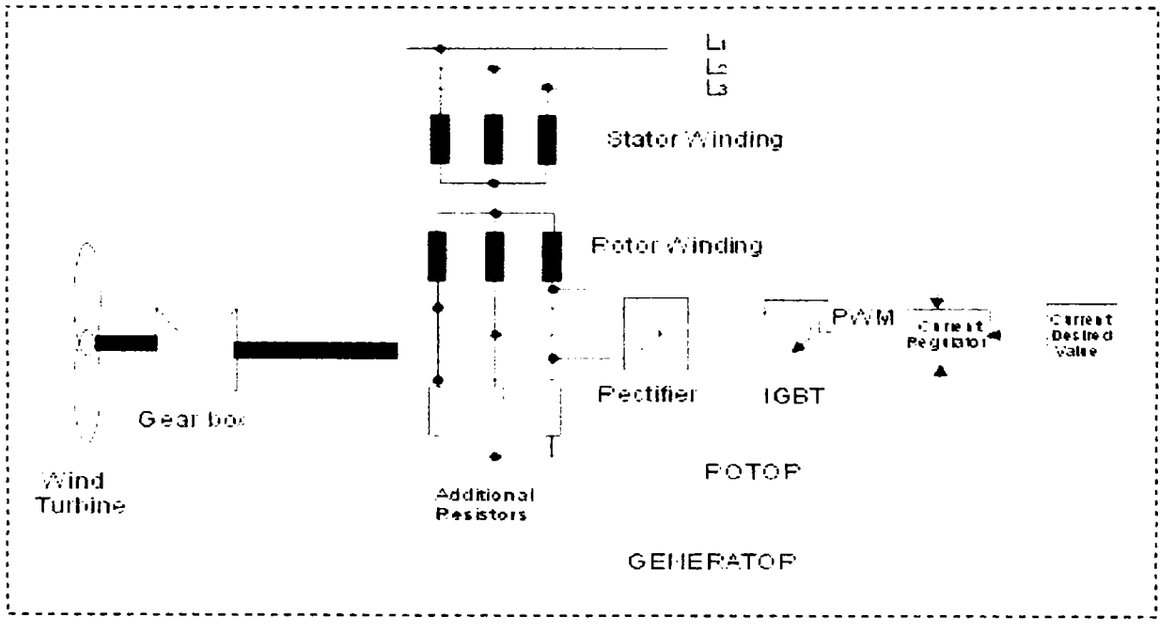


**Figure 4.2.** Dynamic slip regulation of wind power plants using asynchronous machines without slip-ring system for power section and regulation in the rotor (OptiSlip-Vestas V 42/44-600 kW, V 57/63-1.5 MW and V 66-1.65 MW Turbine) [1, 6].

The generators specifically designed for the OptiSlip function are fitted with a wound rotor and an integrated current regulation system (rotor current controller) in the rotor. This is installed at the rear of the generator on the end of the shaft, and consists of additional resistors, power electronics, current sensors and a microprocessor controller. The communications signals between the control system (Vestas multi processor) and the current regulation are carried via a maintenance-free fibre-optic cable [S. Heier, 1998, pg. 300].

The current regulator controls the rotor current by use of a power electronic device chopping the additional rotor resistances in and out of the rotor circuit. The power regulator generates a current reference for keeping the output power constant. Generator output is adapted to the momentary operating state (partial or full load), with the aid of slip via current regulation, pulse with modulation and the power output adjuster in the rotor. Thus, in the partial load region, small slip values (e.g. 2 %) and, at nominal operation, large slip values (e.g. 5 %) can be set, so that the generator speed can be varied to smooth output power and drive train torque.

By use of the OptiSlip scheme described above, it is possible to operate the generator with semi variable speed. The external rotor resistances enable variable speed operation above synchronous speed. The power control is improved compared to systems without OptiSlip. However, the reactive power cannot be controlled satisfactory because no power is fed into the rotor circuit. Therefore capacitor batteries are still required for reactive power compensation. By the application of OptiSlip additional losses are introduced in the system.

Wallace & Oliver [3], in 1998 describe an alternative concept using passive components instead of a PE converter, which also achieves a range of (10-20) % slip variation. Though this concept does not allow active control of slip, it produces a slip-driven self-regulated rotor resistance and will be analyzed and described in details in the following sections. The simplicity of the solution made us pursue it further in this chapter to investigate both its steady and transient performance.

## 4.3. Variable-Speed Generation Controlled by Passive Elements

In order to optimize energy capture from renewable energy sources, such as wind energy, significant recent interest has been directed towards variable-speed generation systems. Numerous schemes have been suggested and evaluated, employing both conventional and novel machine configurations, both direct drives and via gearboxes [1, 2]. Most of these

processes need to sense machine speed and / or output frequency to control power electronic converters, many of which are large (of system rating) and highly expensive.

A recently developed alternative variable-speed generation system employs a wound rotor induction machine with passive, fixed, rotor connected elements [3-5]. This system provides acceptable efficiency (approx 90 %) over a reasonable speed range (1200-1400 rpm) without the use of sensors, feedback system, or power electronics for normal operation. In consequence, it offers a highly reliable, low maintenance, and low capital cost alternative.

The physical system, in which parallel passive elements control the effective rotor impedance as a function of speed, is shown schematically in Fig. 4.3.

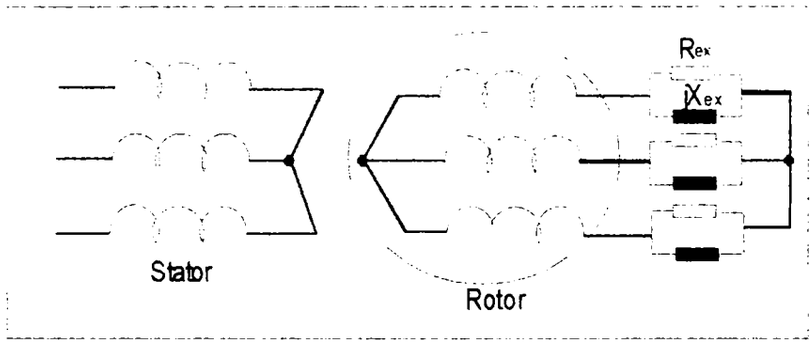


**Figure 4.3.** Wound rotor machine with fixed passive control elements. [3-5]

Selection of the passive element values is dictated by the rating of the generator and the required speed range.

Suitable values for external resistance $R_{ex}$ and reactance $X_{ex}$ can be determined by iterative simulations. Initially a value for $R_{ex}$ alone is determined by the generator reaching rated current at the upper speed limit. Value of $X_{ex}$ is then determined in accordance with its modifying effect, as will be presented in the next section.

### *4.3.1. Steady State Analysis*

For steady-state operation, it has been shown that the DFIG can be simulated, on a per-phase basic, by an equivalent circuit such as this depicted in Fig. 4.4. From the induction machine equivalent circuit, it is also possible to obtain torque-speed curves for various values of rotor resistance.

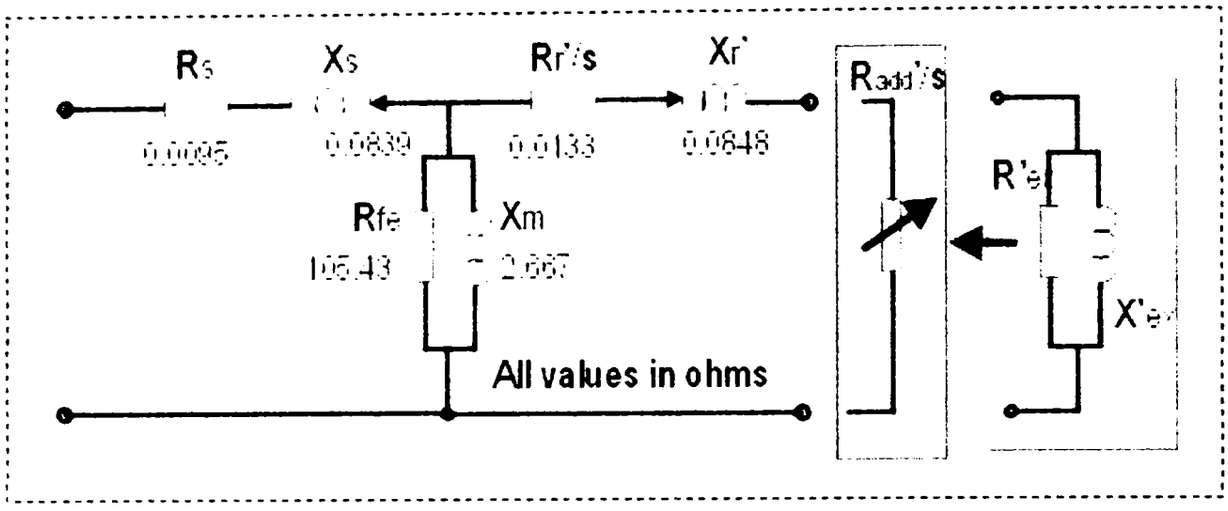


**Figure 4.4.** Equivalent circuit of DFIG with passive control.

The single phase equivalent circuit offers an excellent tool to analyze the performance of the induction generator in steady state. In our case the generator is a 10 kW, 380 V, 920 rpm, 23.5 A at full load. $R_{ex}$ and $X_{ex}$ are the external resistance and reactance to be connected to rotor windings via slip rings and brushes.

The use of adjustable resistors for the starting and speed control of wound-rotor slip-rings induction machines, as shown in Fig. 4.4, can be found in numerous papers [4, 8-12] and is well known to be effective.

The effect of inserting an external resistance in series with the rotor winding is first examined and simulated in MathCAD as shown in Fig. 4.5 for both motoring and generating regions with a copy of the script file shown in the appendix C1. Then the variable resistance ($R_{add}$) was replaced for analysis by an external resistance ($R_{ex}$) in parallel with a reactance ($X_{ex}$).

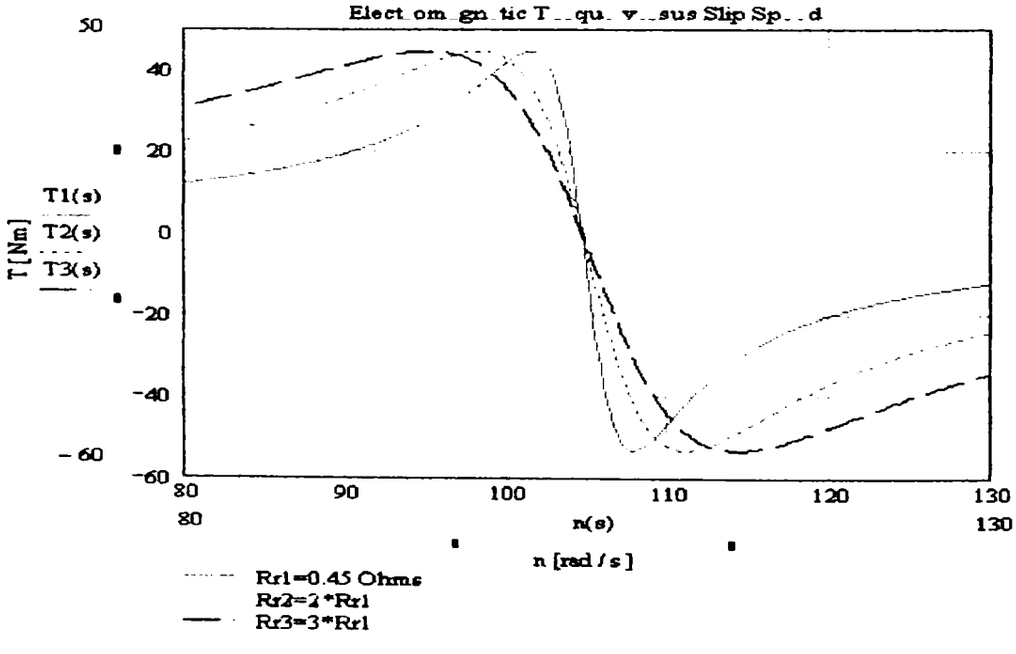


**Figure 4.5.** Simulated effects of external rotor series resistance on Torque-Speed curves.

For the torque-speed curves shown in Fig. 4.5, it is quite apparent that the speed of operation can be continuously varied by controlling the external resistance in the rotor circuit.

When both torque and speed act in the same angular direction, the speed torque curve of Fig. 4.5 applied to the motor mode of operation. If the speed were greater than synchronous speed, the torque acts opposite to speed direction, giving generator mode of operation.

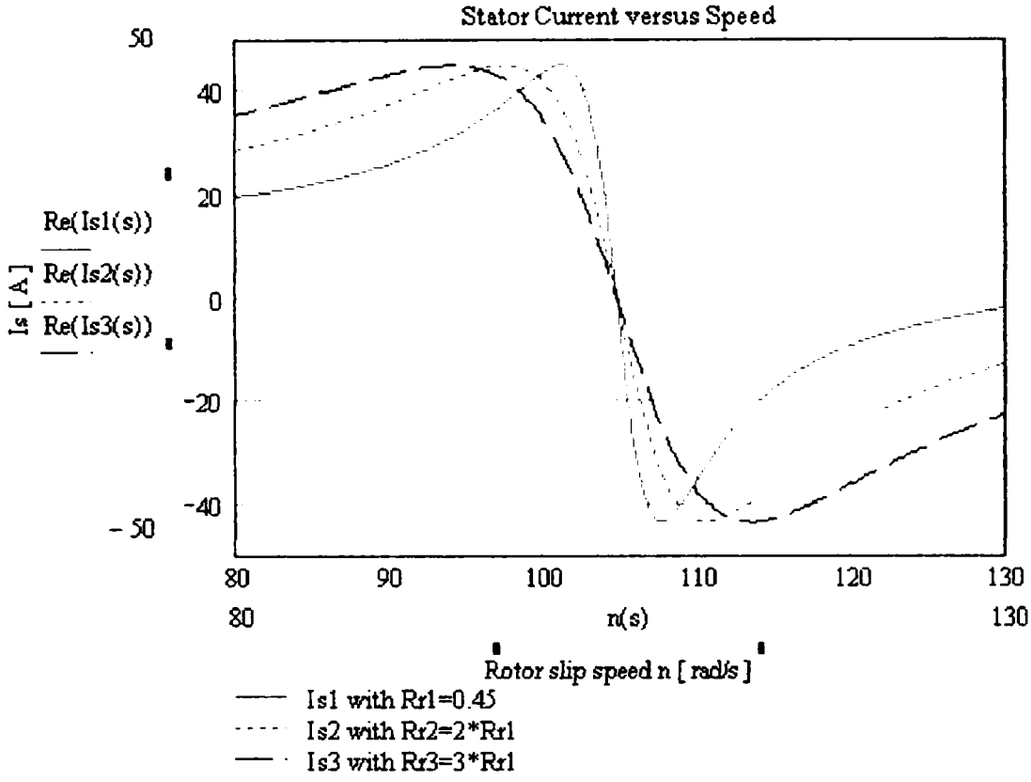


**Figure 4.6.** Simulated effects of external rotor resistance on starting current using Mathcad software.

It is obvious that only the position of maximum torque is shifted with no change on the maximum value itself. The rotor resistance was doubled and then tripled and hence the operating point at which the generator would deliver the rated output is shifted to the right in case of generating which means higher rotor speed.

Higher starting torque for motoring is obviously achieved as it shown in Fig. 4.5 but at the higher starting current as can be seen in Fig. 4.6.

Series resistors inserted in the three rotor phases are sometimes used to limit the starting current. These resistors are shorted out when the machine has gained speed. This method has the obvious disadvantage of being inefficient because of the extra losses in the external resistances during the starting period.

An analysis of the rotor power of this system shows that the slip at which peak torque value of the machine occurs can be modified according to the equation (4.1):

$$s \cong \pm \frac{R_T}{X_T} \qquad \text{.....(4.1)}$$

In which $R_T=R_r'+R_{ex}'$ and $X_T=X_S+X_R'$.

Equation (4.1) is linear and may be solved analytically. If the machine parameters of $X_S$, $X_R$' (stator and stator-referred rotor leakage reactance's) and $R_r$' (stator-referred rotor resistance) are known, a suitable value of $R_{ex}$ may be determined to provide the required slip. Modification of the machine performance in this way is inefficient, due to the increased losses in the external resistor, and the maintenance problem of mechanical switches used to modify the resistance can be considerable. Alternatively, use of power electronic switching to modify the effective external resistance may lead to power quality issues.

The effect of a simple fixed resistor connected to the rotor circuit can be modified by the use of parallel reactive elements, as shown in Fig. 4.4.

It can be shown that for parallel resistor and inductor at slip frequency ($sf_1$), taking in consideration that the external inductance has also its own resistance ($R_{Lex}$) we obtained:

$$R_{eff}(sf_1)=\frac{a^2\cdot[s^2\cdot R_{ex}\cdot X_{Lex}^2+R_{ex}\cdot R_{Lex}(R_{ex}+R_{Lex})]}{(R_{Lex}+R_{ex})^2+(s\cdot X_{Lex})^2};\ X_{eff}(sf_1)=\frac{a^2\cdot s\cdot R_{ex}^2\cdot X_{Lex}}{(R_{Lex}+R_{ex})^2+(s\cdot X_{Lex})^2} \quad (4.2)$$

Where $s$ is the fractional slip, $(a)$ is the stator-rotor turns ratio, and $X_{Lex}$ is the impedance of inductor at line frequency.

Hence, it is evident that in this case the reactive elements are more effective in the determination of the effective resistance than is the external resistance itself. As the slip plays a significant role in the effective resistive impedance, this may be employed to provide generator characteristics that match the output of variable speed energy sources.

For machine control by this technique, equation (4.1) is still valid but the total resistance and reactance values are extended to:

$$R_T=R_r'+R_{eff};\ X_T=X_s+X_r'+X_{eff}/s;\ Z_T=R_T/s+jX_T \quad (4.3)$$

In this case, equation (4.1) becomes non-linear with respect to the slip and cannot be used directly to design a speed control algorithm. However, suitable values for $R_{ex}$ and $X_{ex}$ may be determined by iterative simulations [3, 4].

An external inductance is required in parallel with $R_{ex}$ to stabilize the power output over a wide range of speed, as can be seen in Fig. 4.9.

The reasonable values were found as follows:

$R_{ex}$=1.8 Ω, $L_{ex}$=0.56 H which has its own resistance $R_{Lex}$=0.28 Ω.

Figure 4.8 presents a simulation of equivalent induction machine resistance and reactance as a function of slip speed and as a function of slip as well, using Math cad software.

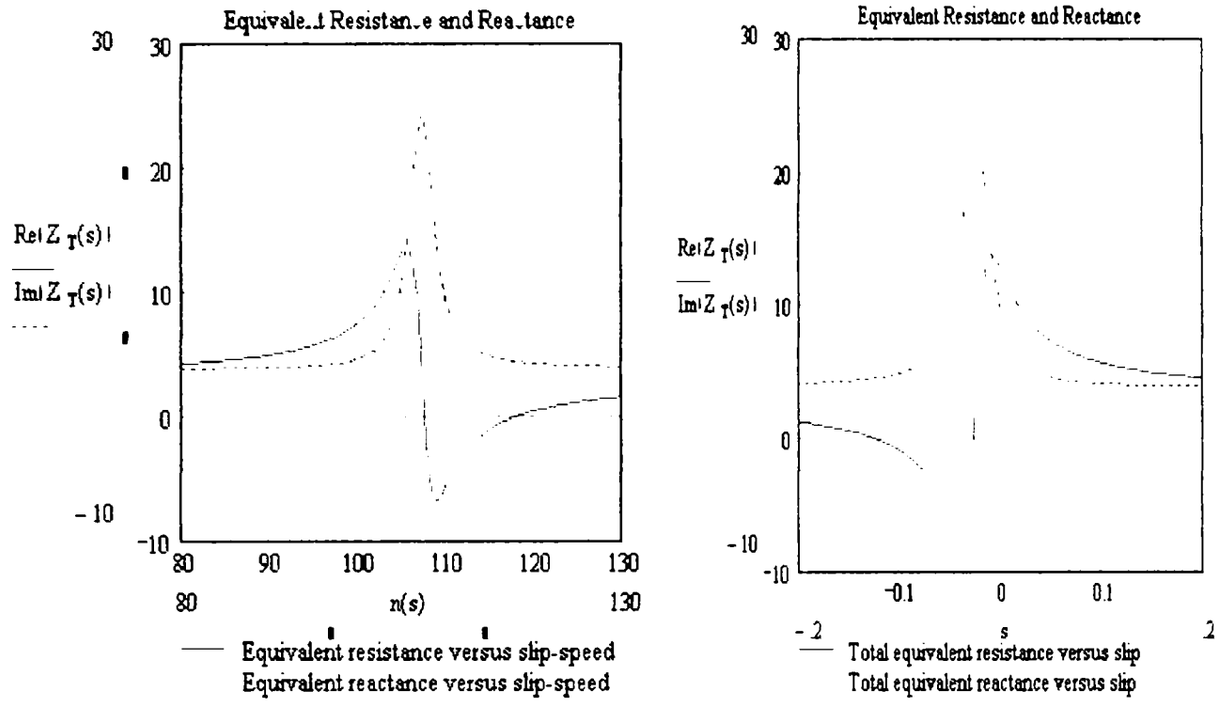


**Figure 4.8.** Simulated Induction Machine equivalent resistance and reactance with $R_{ex}$ in parallel with $L_{ex}$.

It may be seen that the equivalent resistance and reactance, as seen from the power grid, vary with slip as shown in Fig. 4.8. The equivalent reactance comes down with slip and speed in generating mode, while the equivalent resistance increases when the speed also increase. It should be noted that the equivalent reactance remains positive at all slips; this means that the induction machine draws reactive power in any conditions. The equivalent resistance of induction machine becomes negative due to slip in generating mode; this means it delivers active power to the power grid. Because a positive resistance absorbs electrical power, a negative resistance may be considered as a source of power.

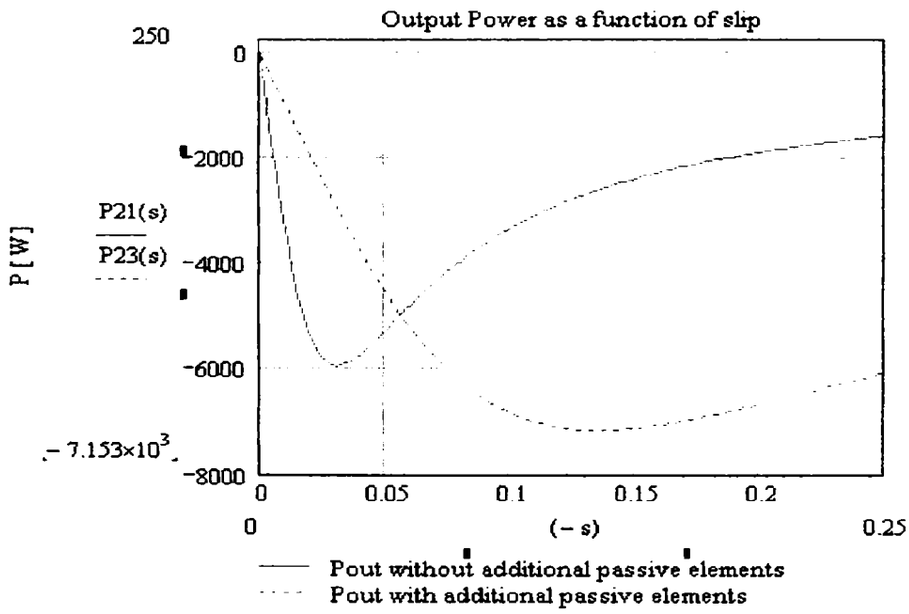


**Fig. 4.9.** Simulated generator output power with and without rotor external elements.

The power factor may be defined in relation to the equivalent circuit as:

$$\cos\varphi_1 = \frac{|R_e|}{Z_e} \quad \text{.....(4.4)}$$

Figure 4.8 shows that the equivalent resistance ($R_e$) is negative for generating mode. This explains why in equation (4.4) the absolute value of $R_e$ is used.

The generator efficiency may be written as:

$$\eta = \frac{ElectricPower\_output}{Shaftpower\_input} = \frac{P_{21electric}}{P_{1shaft}} \quad \text{.....(4.5)}$$

Plots for induction machine power factor and efficiency versus slip are shown in Fig. 4.10. The simulations were performed using Mathcad software package.

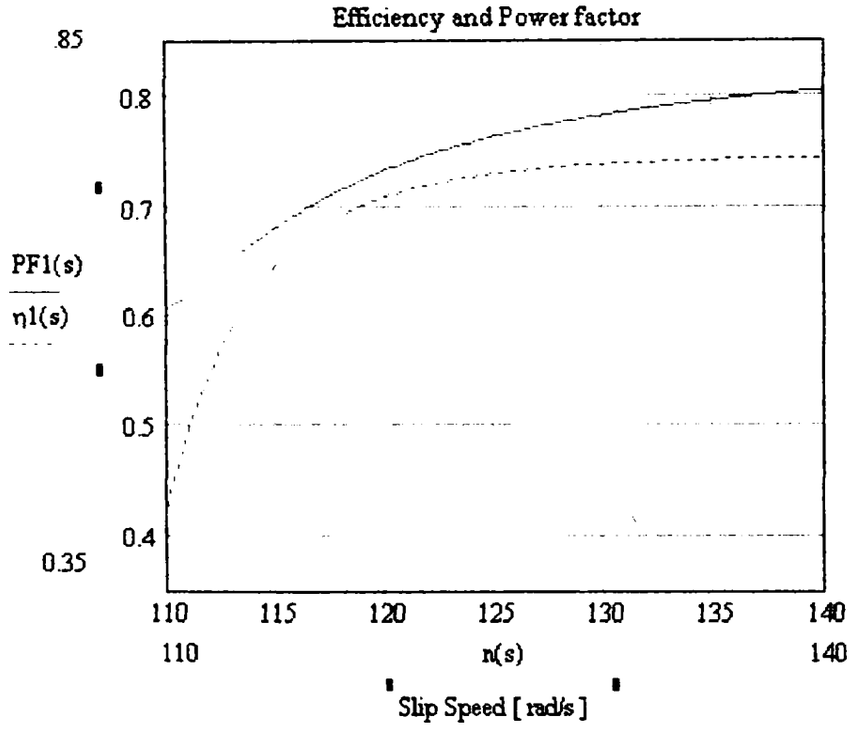


**Figure 4.10.** Efficiency and Power factor of the induction machine with additional resistance and reactance.

The dependence of efficiency and power factor on load (slip or speed) is essential when the induction machine is used for variable load.

The curves in Fig. 4.10 may be calculated strictly based on the equivalent circuit (Fig. 4.4) with known parameters, and given values of slip.

### 4.3.2. Dynamic Operations of the System

For dynamic operation, a simulation of the equivalent d-q model is required. In addition, as there is a need to examine the actual performance of the rotor quantities and the connected elements, the rotor reference frame is appropriate.

In order to be viable, the variable-speed generation system (VSGS) must provide adequate response to sudden changes in speed (due to wind gusts) and to repeated fluctuations in input torque (due to the "tower shadow" effect). In addition, the effect of connecting the generator to the grid at speeds other than synchronism is investigated.

The dynamic operation of the induction generator is most suitably represented by transforming the three phase machine equations to two axes, d-q model. Clarke's transformation is used to converter the stator voltages to the stationary rotor frame as given by Krause et al. [7], operating on the rotor referred voltages:

$$\begin{aligned} V_a &= V_m \cdot \cos(\omega t - \theta_r) \\ V_b &= V_m \cdot \cos(\omega t - \theta_r + \frac{2\pi}{3}) \\ V_c &= V_m \cdot \cos(\omega t - \theta_r - \frac{2\pi}{3}) \end{aligned} \quad \text{.....(4.6)}$$

Where $\theta_r$ represents the rotor position in electrical degrees.

The flux linkage equations in the rotor reference frame for the d-q axis are shown in equations (4.7)-(4.9):

$$\frac{d\lambda_{ds}^r}{dt} = V_{ds}^r + \frac{R_s}{L_{ls}} \cdot \left(\lambda_{md}{}^r - \lambda_{ds}{}^r\right) + \omega_r \cdot \lambda_{qs}^r$$

$$\frac{d\lambda_{qs}^r}{dt} = V_{qs}^r + \frac{R_s}{L_{ls}} \cdot \left(\lambda_{mq}{}^r - \lambda_{qs}{}^r\right) - \omega_r \cdot \lambda_{qs}^r \quad \text{.....(4.7)}$$

$$\frac{d\lambda_{dr}^{'r}}{dt} = V_{dr}^{'r} + \frac{R_r^{'}}{L_{lr}^{'}} \cdot \left(\lambda_{md}^r - \lambda_{dr}^{'r}\right)$$

$$\frac{d\lambda_{qr}^{'r}}{dt} = V_{qr}^{'r} + \frac{R_r^{'}}{L_{lr}^{'}} \cdot \left(\lambda_{mq}^r - \lambda_{qr}^{'r}\right) \quad \text{.....(4.8)}$$

$$\lambda^{r}_{md} = L_{M} \cdot \left( \frac{\lambda^{r}_{ds}}{L_{ls}} + \frac{\lambda'^{r}_{dr}}{L'_{lr}} \right)$$

$$\lambda^{r}_{mq} = L_{M} \cdot \left( \frac{\lambda^{r}_{qs}}{L_{ls}} + \frac{\lambda'^{r}_{qr}}{L'_{lr}} \right) \quad \text{.....(4.9)}$$

Where

$$L_{M} = \frac{1}{\frac{1}{L_{m}} + \frac{1}{L_{ls}} + \frac{1}{L'_{lr}}} \quad \text{.....(4.10)}$$

The stator and rotor current equations are shown in the equations (4.11) and (4.12) respectively:

$$i^{r}_{ds} = \frac{\lambda^{r}_{ds} - \lambda^{r}_{md}}{L_{ls}}$$

$$i^{r}_{qs} = \frac{\lambda^{r}_{qs} - \lambda^{r}_{mq}}{L_{ls}} \quad \text{.....(4.11)}$$

$$i'^{r}_{dr} = \frac{\lambda'^{r}_{dr} - \lambda^{r}_{md}}{L'_{lr}}$$

$$i'^{r}_{qr} = \frac{\lambda'^{r}_{qr} - \lambda^{r}_{mq}}{L'_{lr}} \quad \text{.....(4.12)}$$

To include the external rotor elements in the simulation process we should introduce a third state variable. This is the rotor current that flows through the external inductor $L_{ex}$, $i_{d-qr\_Lex}$. The rotor currents ($i_{dr}^{r}$ and $i_{qr}^{r}$) are the sum of the current flowing through the external resistor and inductor:

$$i'^{r}_{dr} = i'^{r}_{dr\_Rex} + i'^{r}_{dr\_Lex}$$

$$i'^{r}_{qr} = i'^{r}_{qr\_Rex} + i'^{r}_{qr\_Lex} \quad \text{.....(4.13)}$$

The voltage equations of the external rotor circuit may be written as equation 4.14:

$$V_{dr}^{'r} = -(R_{ex}^{'} \cdot i_{dr\_Rex}^{'r}) = -\left( L_{ex} \cdot \frac{di_{dr\_Lex}^{'r}}{dt} + R_{Lex}^{'} \cdot i_{dr\_Lex}^{'r} \right)$$

$$V_{qr}^{'r} = -(R_{ex}^{'} \cdot i_{qr\_Rex}^{'r}) = -\left( L_{ex} \cdot \frac{di_{qr\_Lex}^{'r}}{dt} + R_{Lex}^{'} \cdot i_{qr\_Lex}^{'r} \right) \quad \text{.....(4.14)}$$

Substituting equations (4.13) into equations (4.14) and solving for $\frac{di_{d-qr\_Lex}^{'r}}{dt}$ yield to the third state variable equations which are to be implemented in MATLAB-Simulink model:

$$\frac{di_{dr\_Lex}^{'r}}{dt} = \frac{R_{ex}^{'}}{L_{ex}^{'}} \cdot i_{dr}^{'r} - \frac{R_{Lex}^{'} + R_{ex}^{'}}{L_{ex}^{'}} \cdot i_{dr\_Lex}^{'r}$$

$$\frac{di_{qr\_Lex}^{'r}}{dt} = \frac{R_{ex}^{'}}{L_{ex}^{'}} \cdot i_{qr}^{'r} - \frac{R_{Lex}^{'} + R_{ex}^{'}}{L_{ex}^{'}} \cdot i_{qr\_Lex}^{'r} \quad \text{.....(4.15)}$$

We have now the equations expressed with the stator and rotor flux and the rotor current which flows through external rotor inductive branch as state variables for the d-q axis. In the computer simulation, equations (4.7), (4.8) and (4.15) are implemented as a subsystem and are used to solve for $\lambda_{d\text{-}qs}^{r}$, $\lambda_{d\text{-}qr}^{'r}$ and $i_{d\text{-}qr\_Lex}^{'r}$ and equations (4.9) are used to solve for $\lambda_{d\text{-}qm}^{r}$. From eqs. (4.11), (4.12) and (4.13) the currents can then be obtained, as it is depicted in Fig. 4.11.

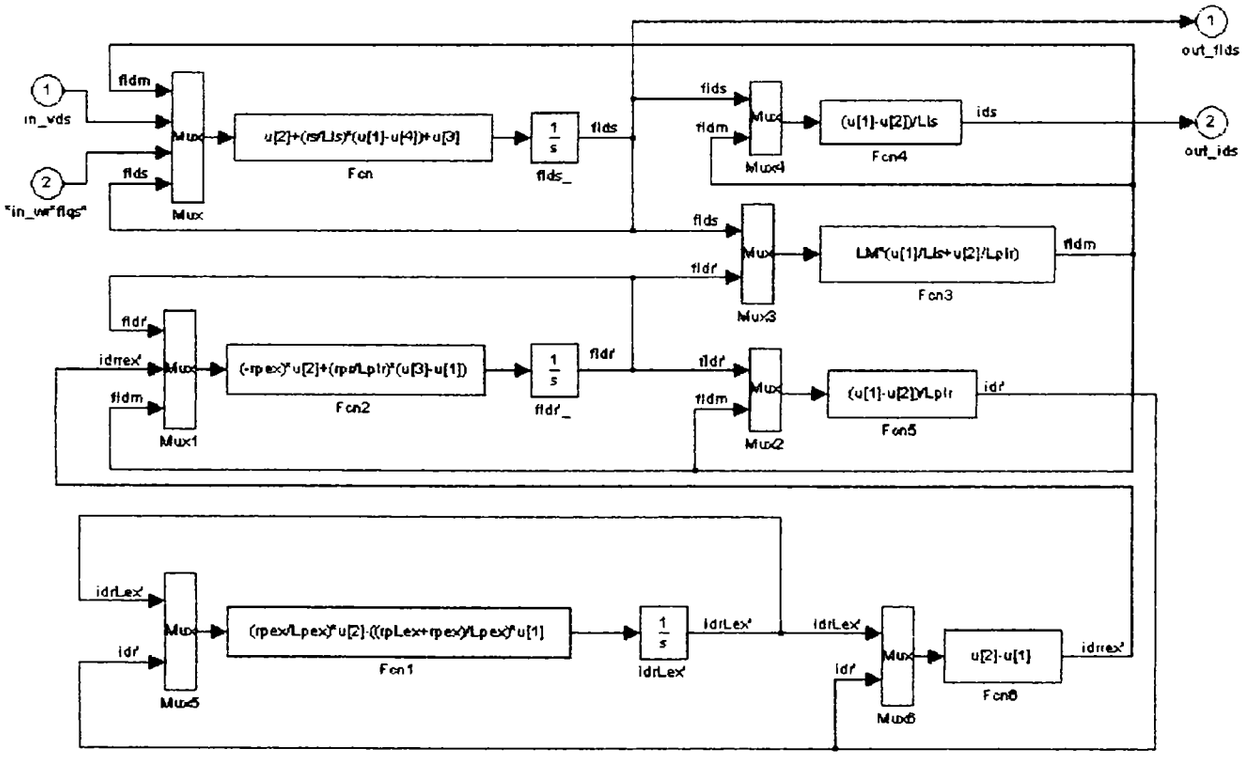


**Figure 4.11.** Block representation of the d-axis subsystem. Figure illustrates the principles of how the flux and current equations are implemented in Simulink.

With the derived equations of the d-q flux linkages and currents we are able to compute the electromagnetic torque $T_{em}$ of the induction machine:

$$T_{em} = \frac{3}{2} \cdot \frac{p}{2} \cdot \left( \lambda_{ds}^{r} \cdot i_{qs}^{r} - \lambda_{qs}^{r} \cdot i_{ds}^{r} \right) \quad \text{.....(4.16)}$$

In which (p) represents the number of poles of the machine.

During dynamic operation the relation of electromagnetic torque ($T_{em}$) and mechanical torque ($T_{mech}$) may be found in the equation of motion of the rotor, which depends on the inertia (J), rotor speed ($\omega_r$), poles (p) and the damping torque $T_{damp}$ of the machine.

$$T_{em} - T_{mech} - T_{damp} = J \cdot \frac{2}{p} \cdot \frac{d\omega_r}{dt} \quad \text{.....(4.17)}$$

Details of the rotor block implemented in Simulink are presented in Fig. 4.12:

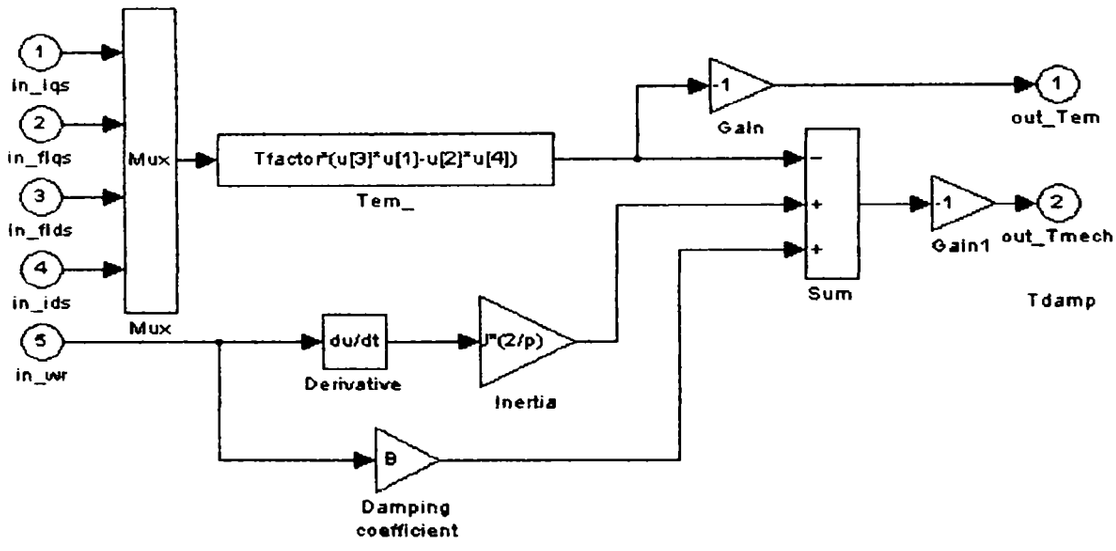


**Figure 4.12.** Details of the rotor block implemented in Simulink according to (4.16) and (4.17).

Where the damping torque may be expressed as: $T_{damp} = B \cdot \omega_r$ in which (B) represents the damping coefficient in [N*m*s] associated with the mechanical rotational system of the machine and mechanical load.

The stator abc currents may be determined from the stator d-q currents using the inverse of Clarke's transformation.

Solution of these equations requires a repeated integration process using a Runga-Kutta technique. As has been described by Ong [8], sets of simultaneous equations such as these for electrical machines may be readily formulated diagrammatically by the Simulink representation for solution in the MATLAB suite of computer tools. The complete Simulink model for the above system of equations is shown in Fig. 4.13.

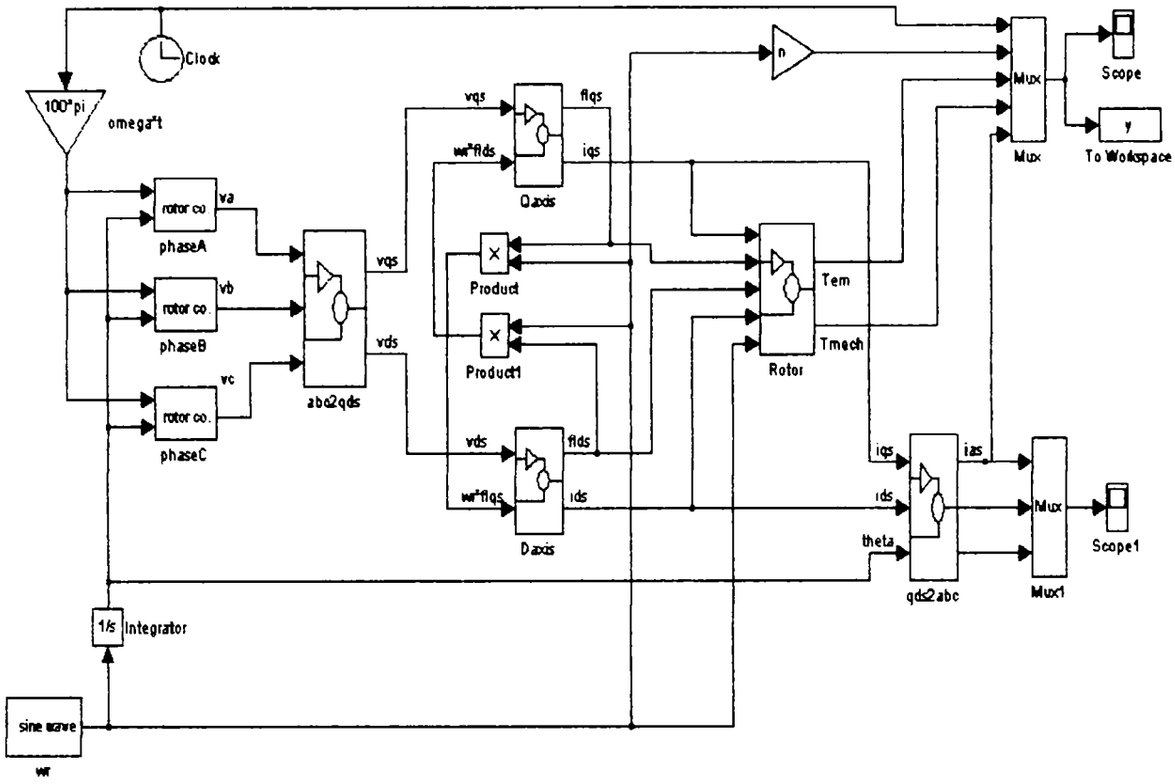


**Figure 4.13.** The complete system simulation diagram of induction machine simulated in the rotor reference frame.

A rotor reference frame model has been developed for the passively controlled variable-speed generation system which, when implemented in MATLAB-Simulink, provides good correlation of predicted performance in both dynamic and steady-state conditions. The generator system is shown to have good response characteristics for a wide range of dynamic changes. This favorable performance is valid for a generator of 10 kW rating operating at a range of 30 % of base speed. More details about parameters of the machine used in simulations can be found in *Appendix C*.

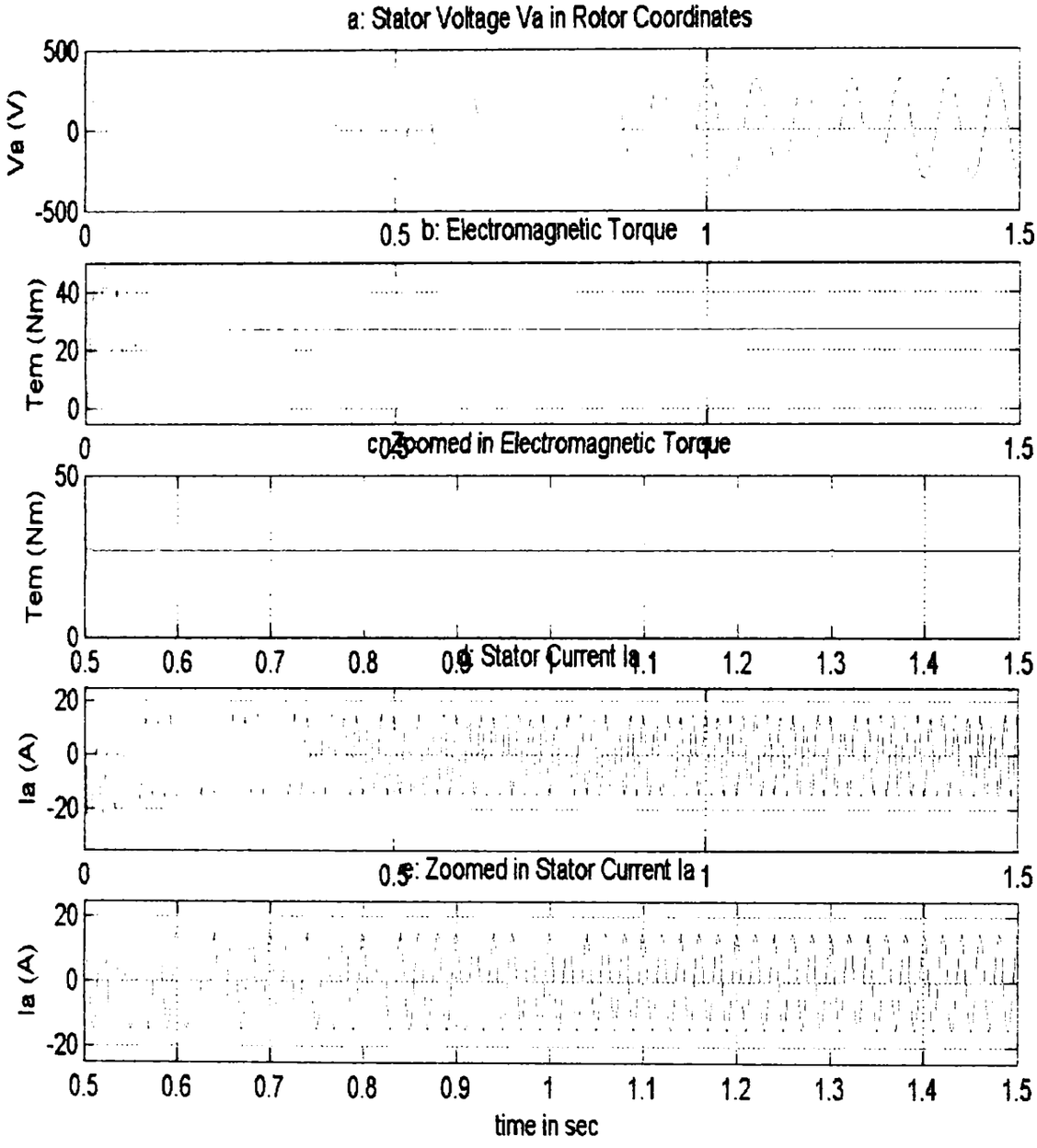


**Figure 4.14.** Predicted effects of non-synchronous connection to power system.

Figs. 4.14-4.16 show the calculated torque and current transients that occur when the induction generator of 10 kW is connected to the power supply at 1015 rpm (super-synchronous speed).

An initial electromagnetic torque pulsation, reaching 50 Nm approx, reduces to a steady-state of just below 25 Nm. The 6-pole, 50 Hz machine used in this study was connected to the 400 rated line to line voltage. It should be noted that the transient current peak increased at 30 A and then in steady-state becomes 15 A.

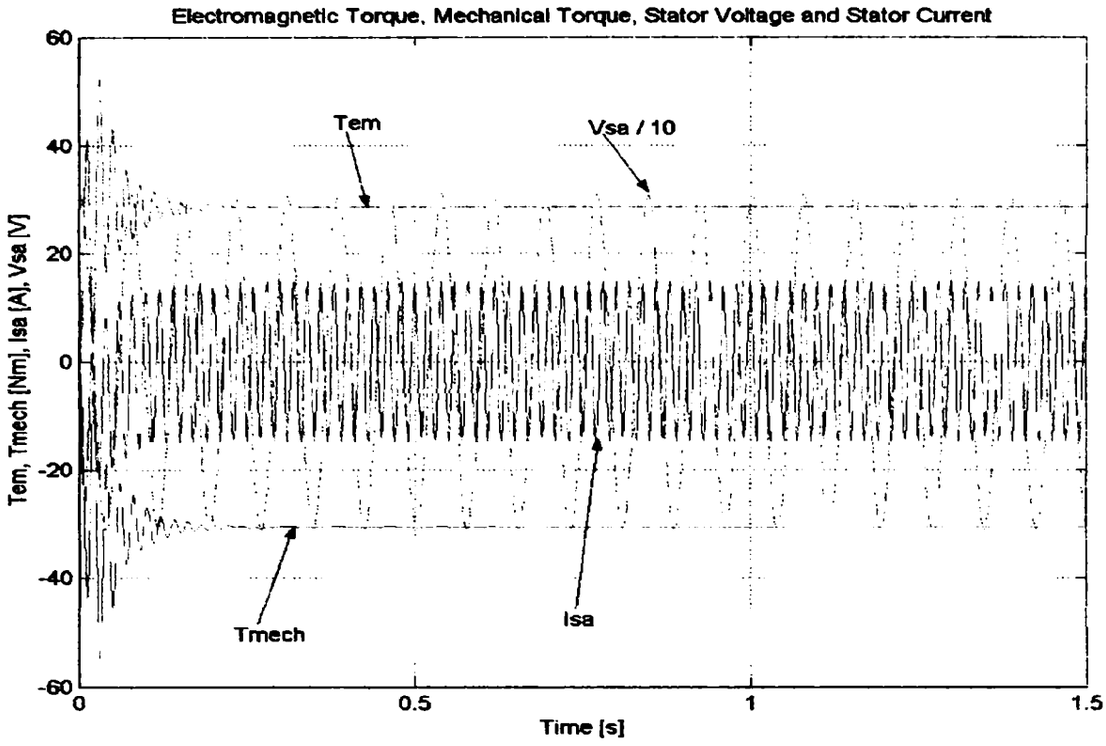


**Figure 4.15 .** Simulation of Electromagnetic Torque, Mechanical Torque, Stator Voltage and Stator Current to a non-synchronous connection of power system.

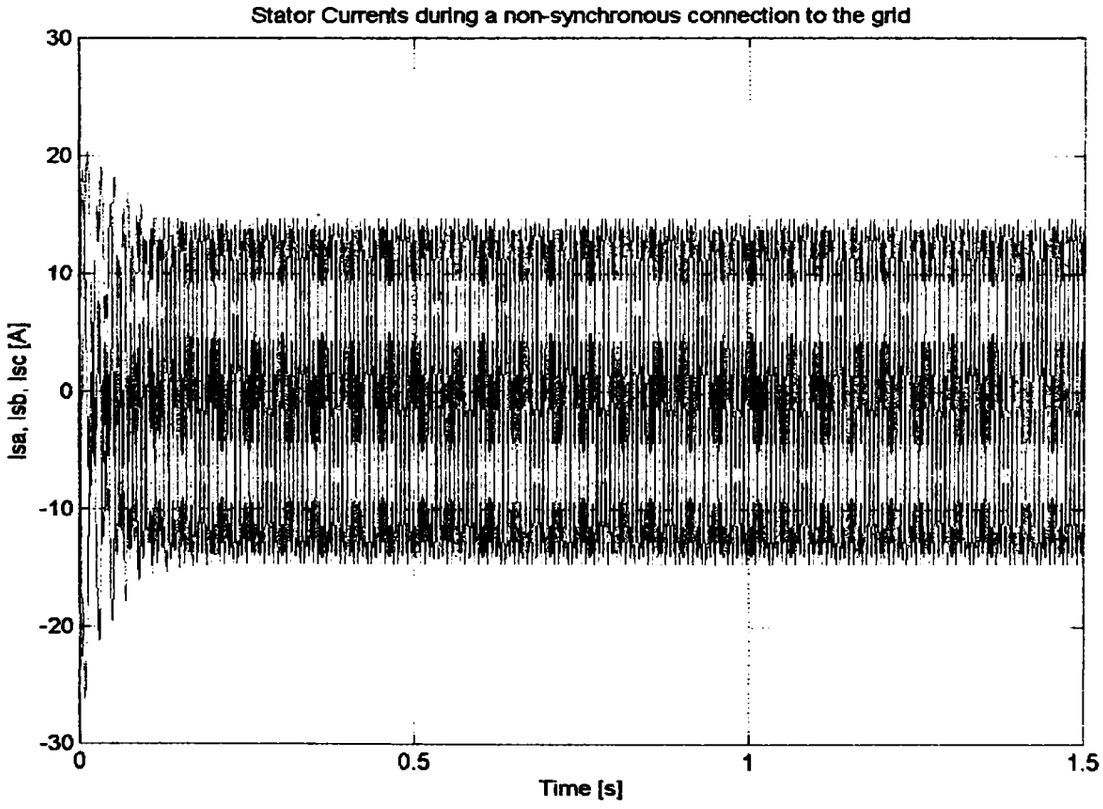


**Figure 4.16.** Simulation of Stator Currents when the induction generator of 10 kW is connected to the power supply at 1015 rpm.

Figs. 4.17-4.18 show the simulated response of the generator to a mechanical input cycling. From a synchronous 1000 rpm the generator is targeted to oscillate between upper and lower limits of 1015 and 985 rpm. However, the inertia of the system prevents reaching these limits.

When operating at a steady 1000 rpm, with an applied mechanical torque 30 Nm and a generated current of 15 A peak, the generator was subjected to a torque reduction to 25 Nm resulting in a new condition of 975 rpm, and 12 A peak, as can be seen in Figs. 4.19 and 4.20. This is followed after 3 seconds by a torque increase to 35 Nm, resulting in a change in speed to 1025 rpm and a current of 18 A peak. The simulation of these changes was intended to represent effects of wind gusts on the turbine. The Figs. 4.19 and 4.20 also indicate that the generator system quickly reaches new stable operating conditions following such changes. Hence, the passively controlled generator system exhibits adequate stability and natural damping.

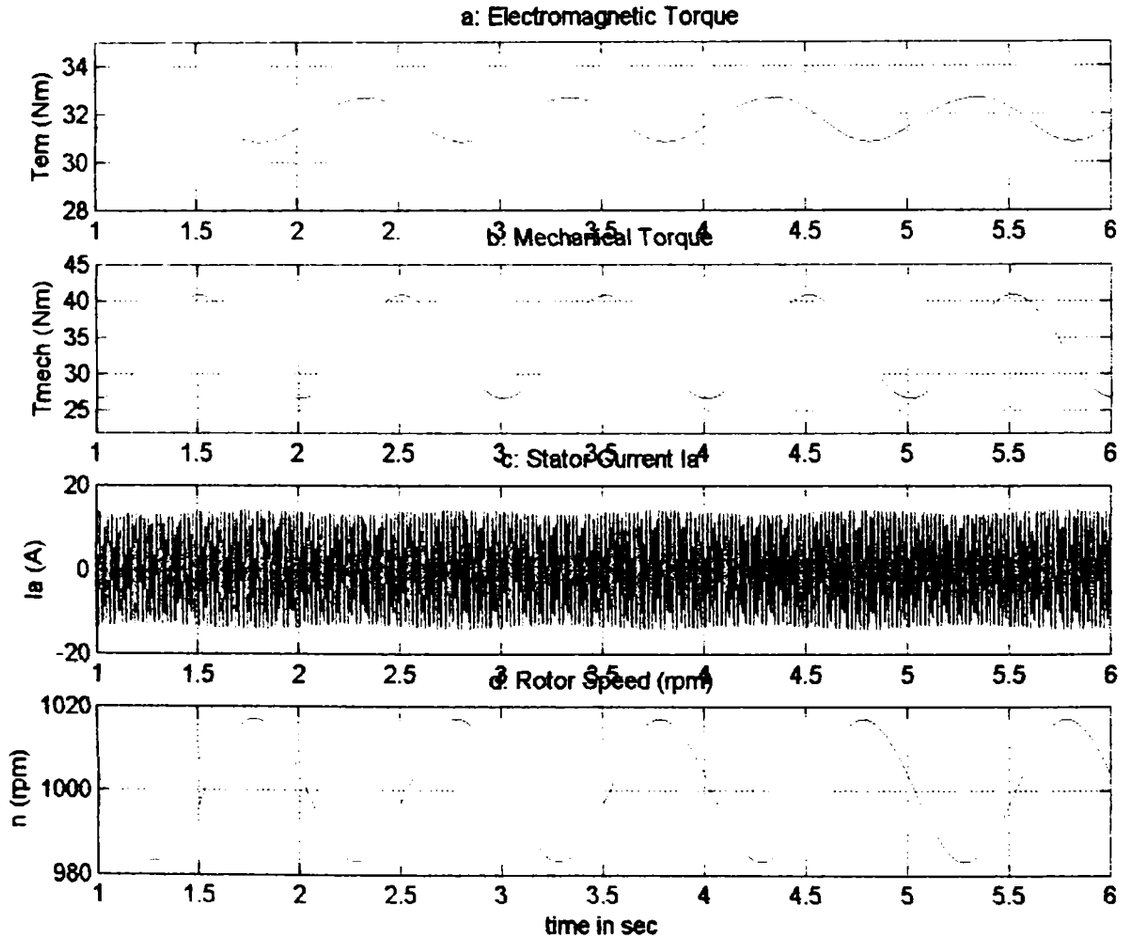


**Figure 4.17.** Predicted effect of repeated fluctuations in input torque to investigate the tower shadow effect.

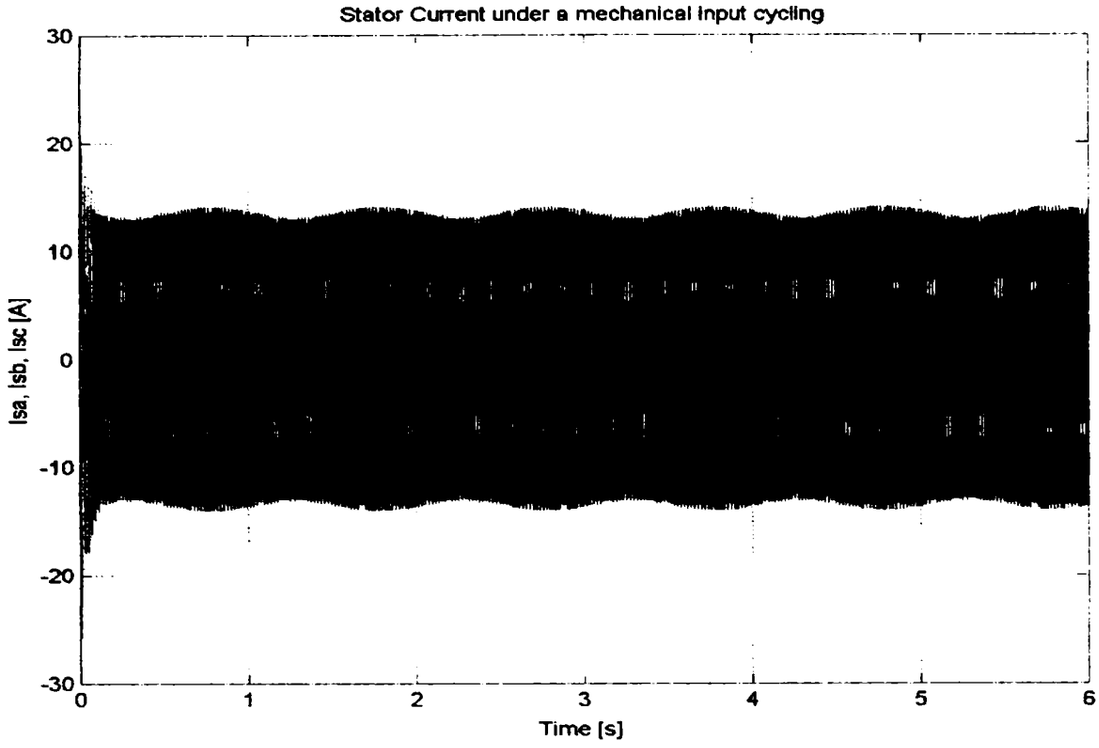


**Figure 4.18**. Simulation of Stator Currents at a mechanical input cycling.

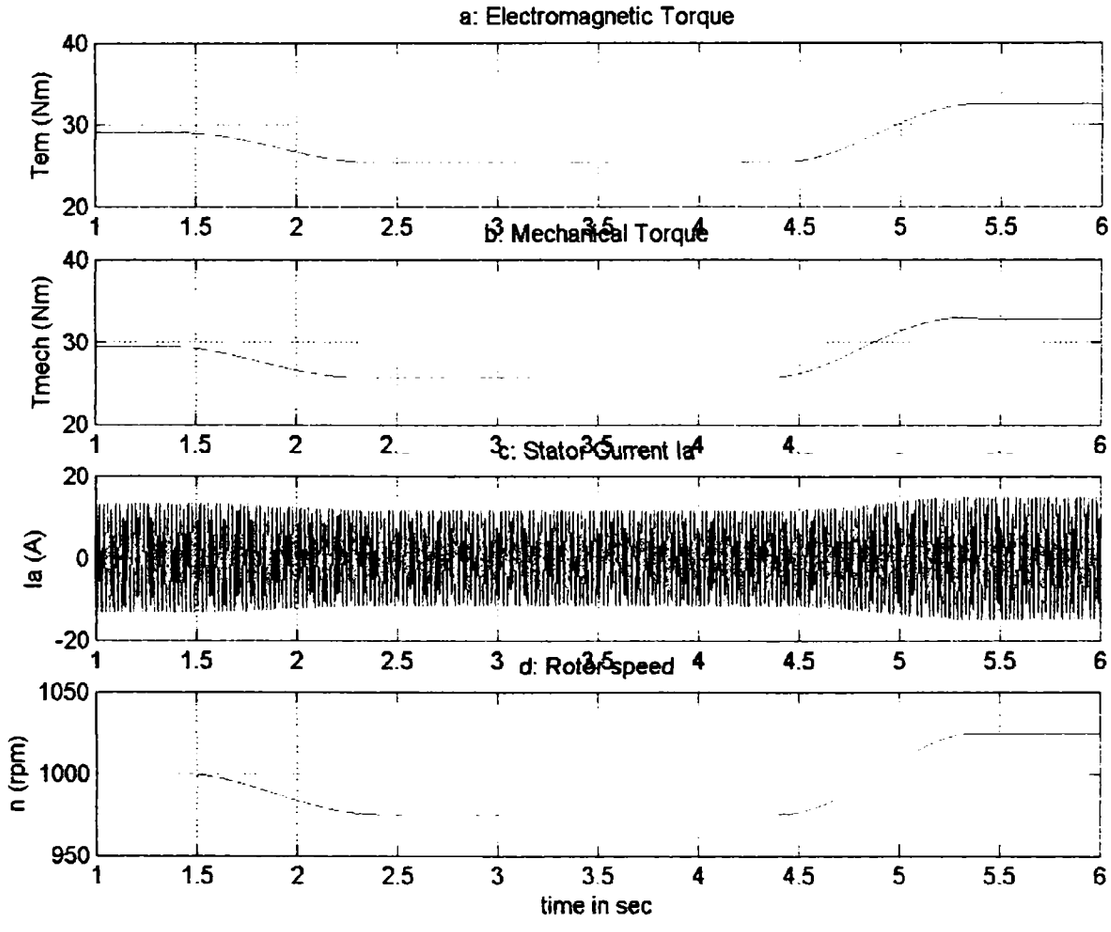


**Figure 4.19.** Predicted response to sudden changes: electrical torque, mechanical torque, current and speed.

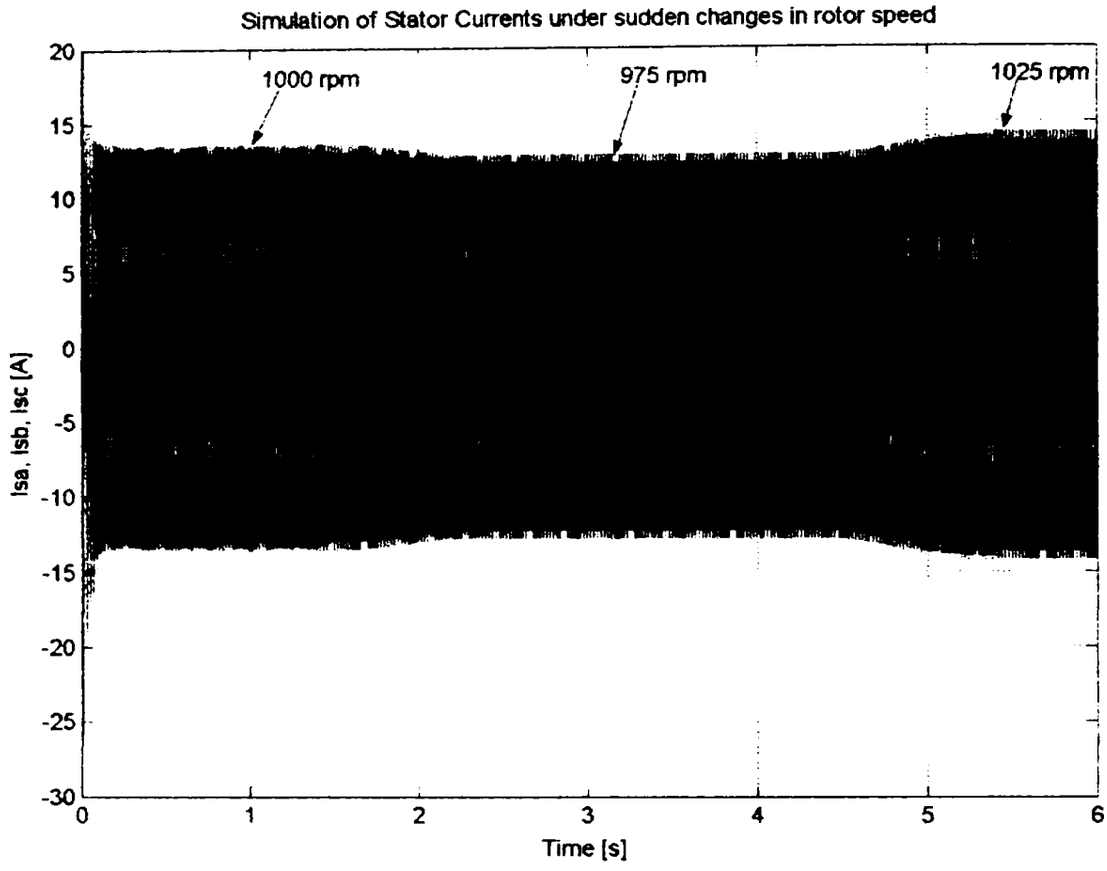


**Figure 4.20**. Simulation of Stator Currents under sudden changes in rotor speed, from a synchronous 1000 rpm the generator is targeted to oscillate between upper and lower limits of 975 and 1025 rpm.

## 4.4. The Experimental Procedure and Results

The circuit diagram of the experimental set-up consisting of a Wind Turbine Simulator (WTS) and the wound rotor induction machine slip-ring terminals as is shown in Fig. 4.21.

The WTS is composing of a 10 kW rotor cage induction machine (RCIM) and a bidirectional power converter of 25 kVA.

The induction machine is a doubly fed induction generator (DFIG) rated at 10 kW, with additional passive elements inserted in the rotor side and the stator is direct connected to the power supply. More details about technical data can be found in *Appendix C*.

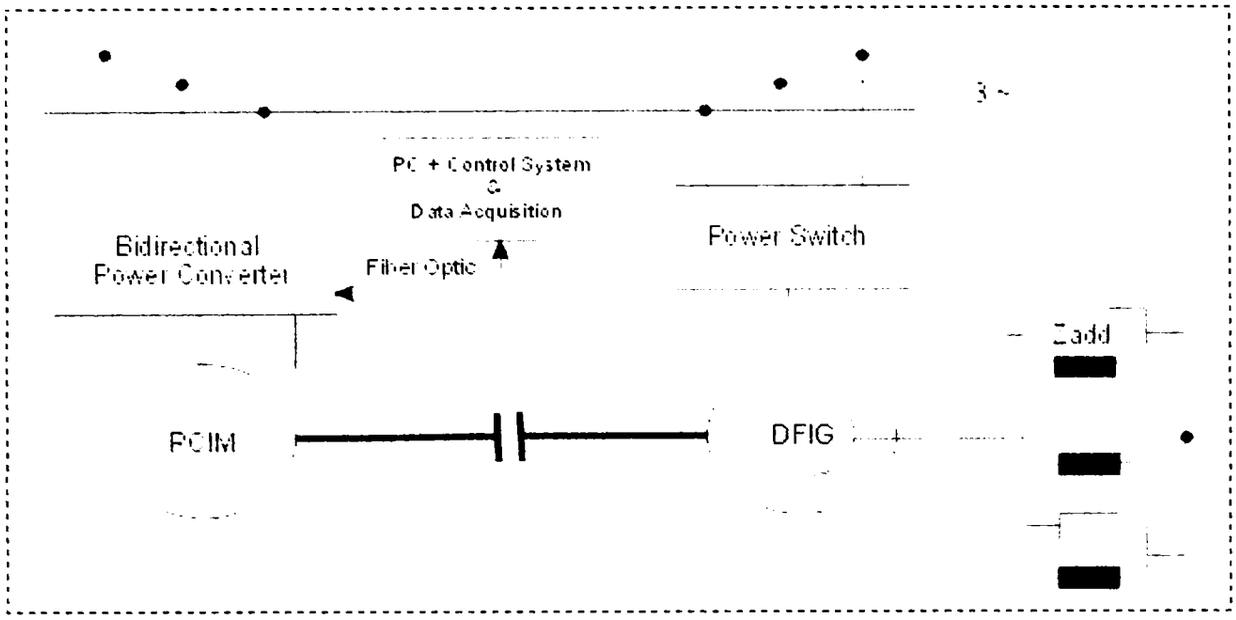


**Figure 4.21**`. Schematic diagram of the experimental set-up.

The basic component of the proposed generation system is a wound-rotor induction machine. As is well documented in numerous papers [7-12], the torque-speed characteristics of this machine may be modified to provide an extended speed range as a generator, the resistance to reactance ratio of the rotor circuit. Typically, the operating speed range of a high efficiency induction generator is approx 1 % [3]. To extend this range to (10-30) % requires substantial resistance to be added. Selection of the passive elements values is dictated by the rating of the generator and the required speed range.

To simulate the adjustable speed prime mover, a squirrel cage induction motor supply by an ACS 611 Frequency Converter is employed in the experiments. The ACS 611 is a four-quadrant drive. The main circuit consists of two IGBT converters, a line-side converter and a motor side converter, integrated into a same frame. The line-side and motor-side converters consist of six insulated gate bipolar transistors with free wheeling diodes. The ACS 611 can be controlled from the Local control location. The control commands are given from the Control Panel keypad or from the Drive Window PC tool.

Drive Window is a Windows Application for commissioning and maintaining drives equipped with fiber optic communication. Drive Window provides the commissioning personnel with a powerful tool, which provides also remote connection possibility. Using Drive Window is possible to control operations such as start, stop, references, monitoring signals, changing parameter values and display collected data.

The setup permits the measurement of currents and voltages of stator and rotor circuits as well. The input power to the generator was measured via control panel of the ACS 611 Frequency Converter and by a LEM NORMA D 4000 power analyzer was obtained the electrical output power.

### 4.4.1. Experimental Results

Experimental results were obtained for steady and transient behavior at different speed and torque.

The test results obtained in super-synchronous mode for the generator to different loads, with a wyes-connected resistance of 1.8 ohms/phase, in parallel with a wyes-connected inductance of 560 mH / phase, are shown in Figs. 4.22-4.25

The power output shows a characteristic of relevance to wind turbine application with an acceptable efficiency.

The stator and rotor currents were measured using LEM Current Probe with an output of 100 mV/A and then acquired by a Tektronix TDS 224 Oscilloscope and a laptop via Wave-Star software tool. The stator and rotor voltages were acquired using a Voltage Transducer with an output of 100 V/V.

#### 4.4.1.1. Steady State Analysis

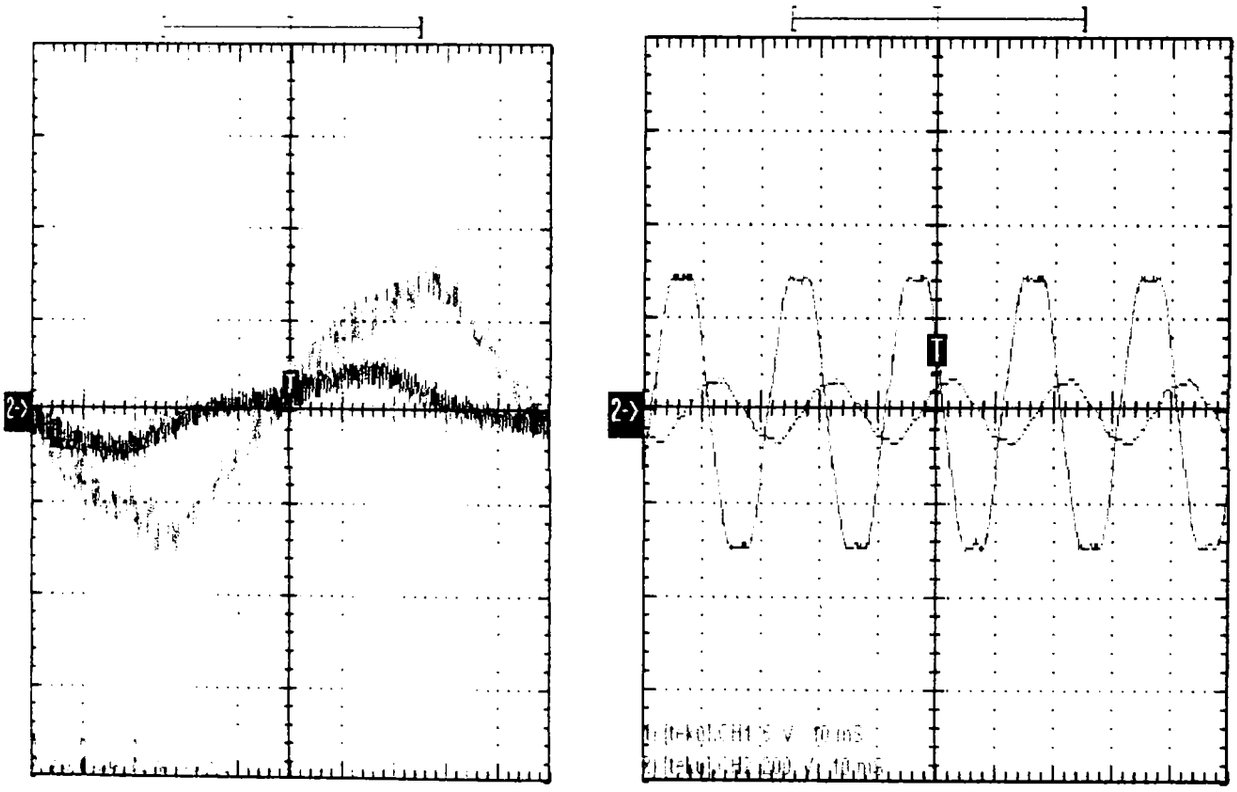

a) b)

**Figure 4.22**. Rotor phase current and voltage (a) and stator phase current and voltage (b) at $P_{IN}$=2.5 kW and $P_{OUT}$=1.5 kW in super-synchronous mode (n=1040 rpm). Scaling factor of the currents is 100 mV/A and scaling factor of the voltages is 100 V/1V. Ir=6A, Vr=6 V and Is=12.5A and Vs=220 V.

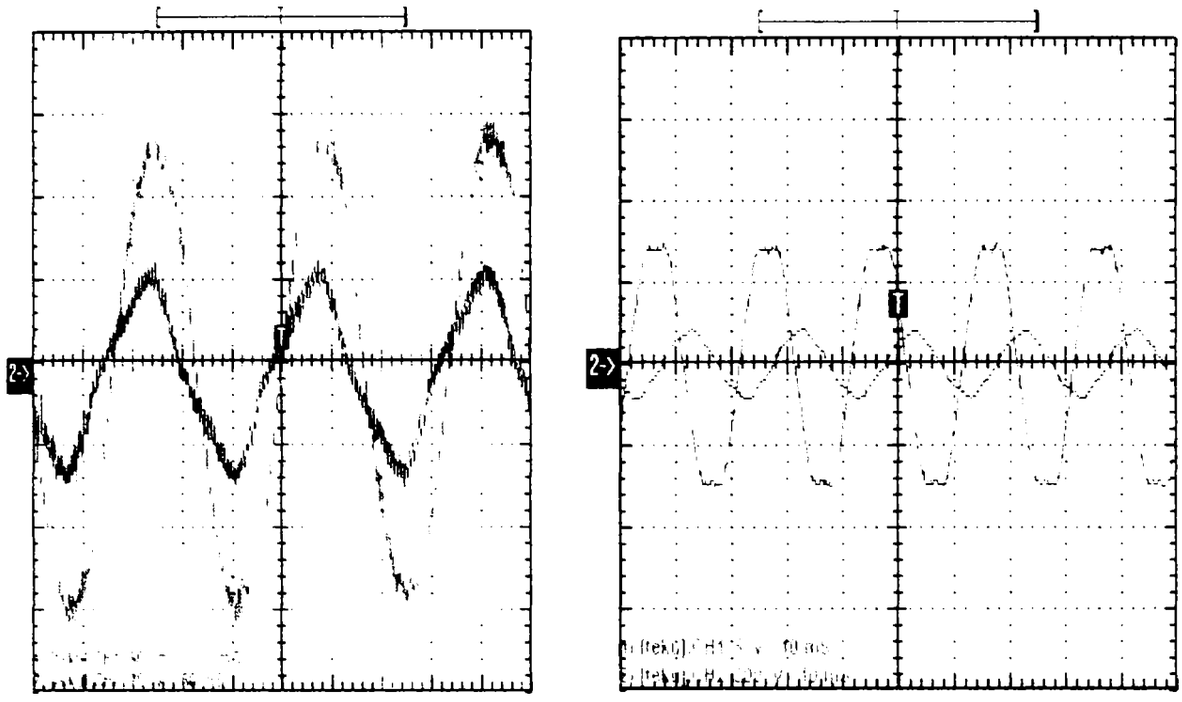

a) b)

**Figure 4.23**. Rotor phase current and voltage (a) and stator phase current and voltage (b) at $P_{IN}$=5 kW and $P_{OUT}$=3.5 kW in super-synchronous mode (n=1100 rpm). Scaling factor of the currents is 100 mV/A and scaling factor of the voltages is 100 V/V. Ir=9.2A, Vr=12.5 V and Is=14.6A and Vs=220 V.

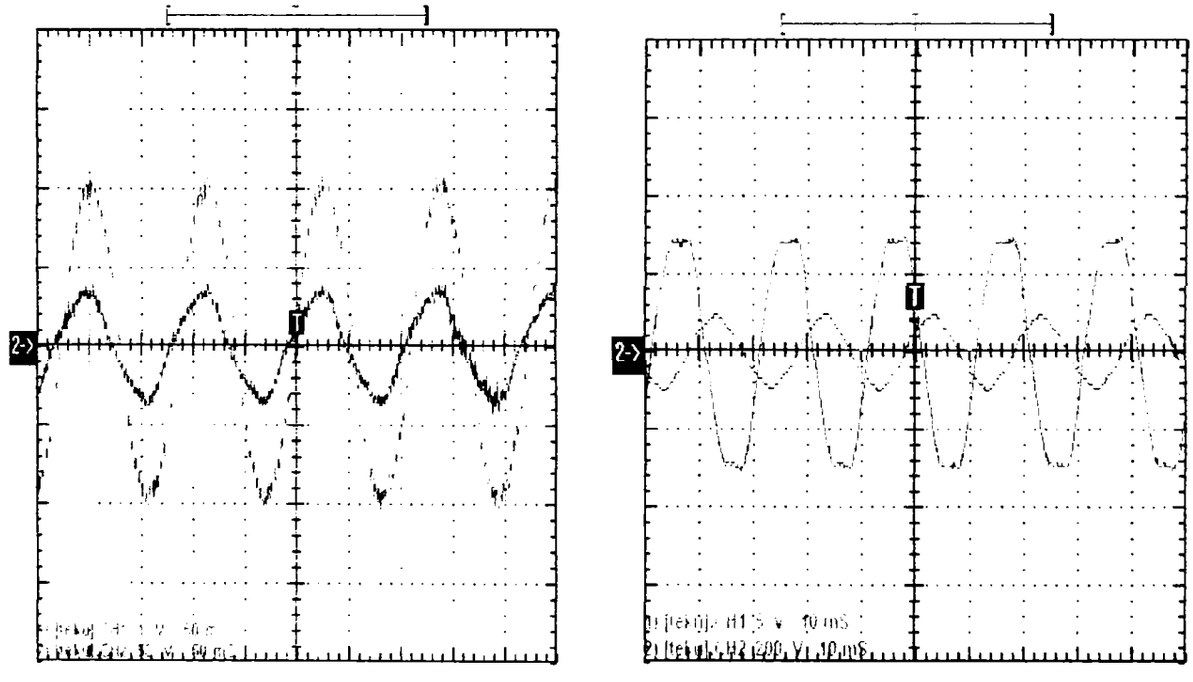

a) b)

**Figure 4.24**. Rotor phase current and voltage (a) and stator phase current and voltage (b) at $P_{IN}$=7.5 kW and $P_{OUT}$=5.6 kW in super-synchronous mode (n=1180 rpm). Scaling factor of the currents is 100 mV/A and scaling factor of the voltages is 100 V/V. Ir=14 A, Vr=23.6 V and Is=17.6A and Vs=220 V.

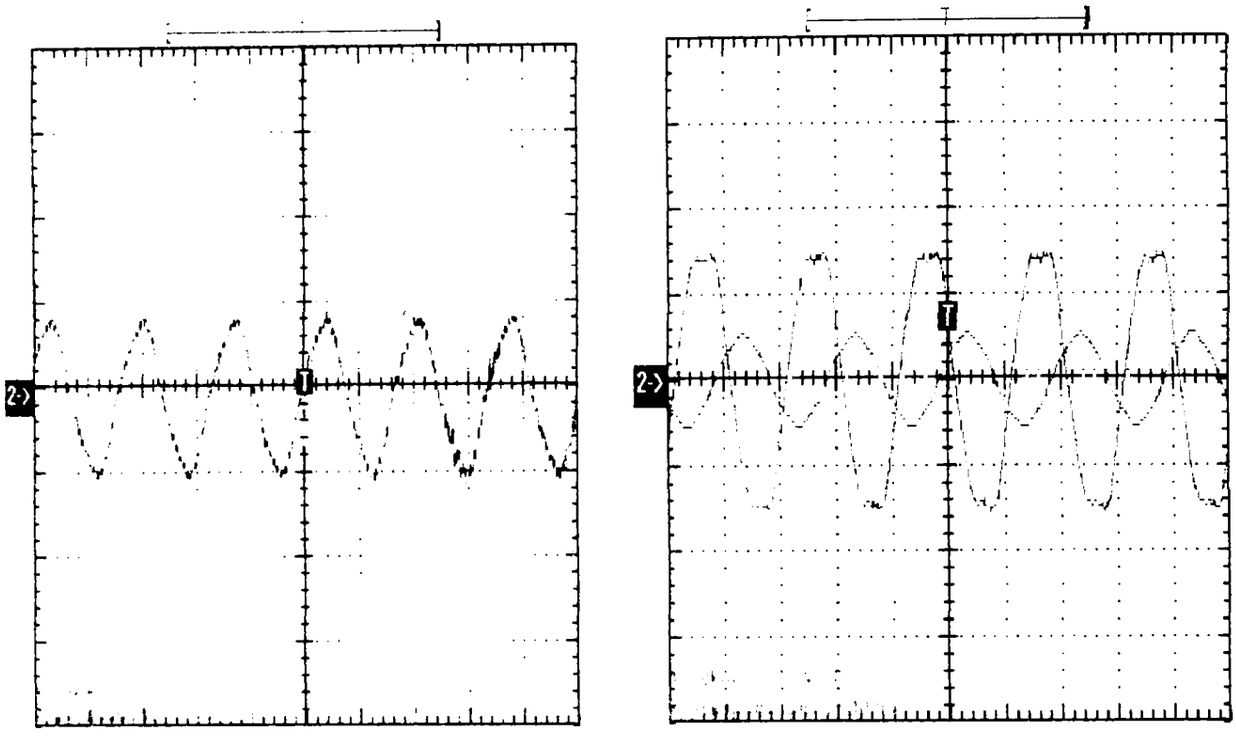

a) b)

**Figure 4.25**. Rotor phase current and voltage (a) and stator phase current and voltage (b) at $P_{IN}$=10 kW and $P_{OUT}$=7.5 kW in super-synchronous mode (n=1240 rpm). Scaling factor of the currents is 100 mV/A and scaling factor of the voltages is 100 V/V. Ir=18 A, Vr=30 V and Is=20 A and Vs=220 V.

Figures 4.22-4.25 illustrate the experimental results obtained in super-synchronous operation mode at different loads ($P_{IN}$=25, 50, 75 and 100 % of Pn=10 kW) with the corresponding values for the output power and rotor speed. The differences between the stator phase current and voltage has 90 degrees indicating that the system is operated in generating mode. These results show good increasing power as a function of speed. It is clear that these will be reasonably compatible with the output of wind turbines.

### *4.4.1.2. Transient conditions*

In order to justify the viability of the proposed system, it has been necessary to extend the testing and analysis and to demonstrate its performance under dynamic conditions such as connections to the power supply at non-synchronous speed and sudden changes in applied torque.

### A. Connections to the grid at non-synchronous speed

Figures 4.26 and 4.27 show a comparison between the stator current transients of DFIG with a parallel inductor-resistor combination connected to the rotor and without additional elements, from a direct connection to the power supply, when the induction machine was working as a generating in super-synchronous mode at 1015 rpm.

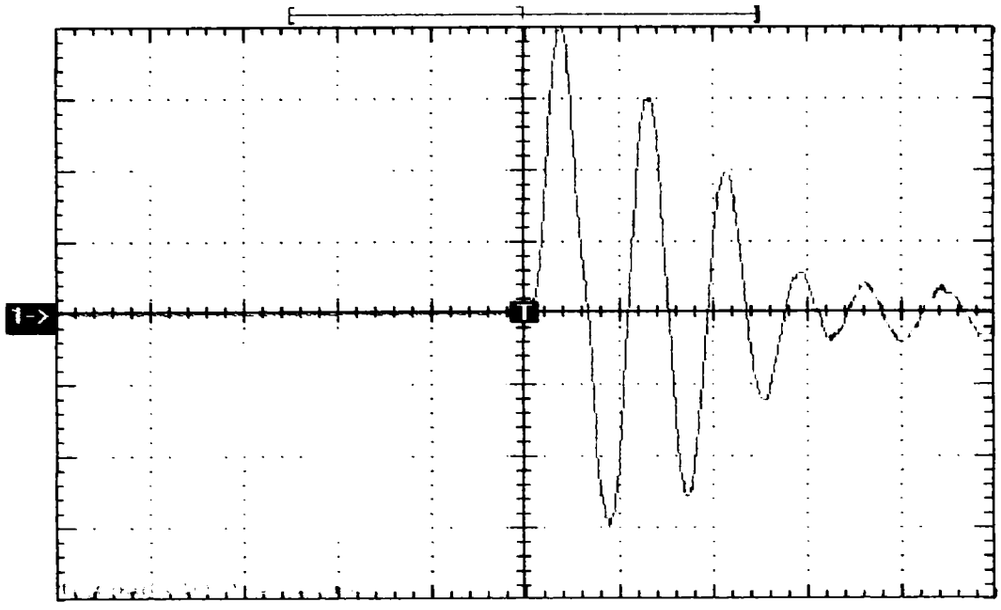

**Figure 4.26**. Measured stator current during start up of DFIG at super synchronous speed of 1015 rpm without additional impedance. Isamax=140 A (6*Isn). Scaling factor is 1V/50A.

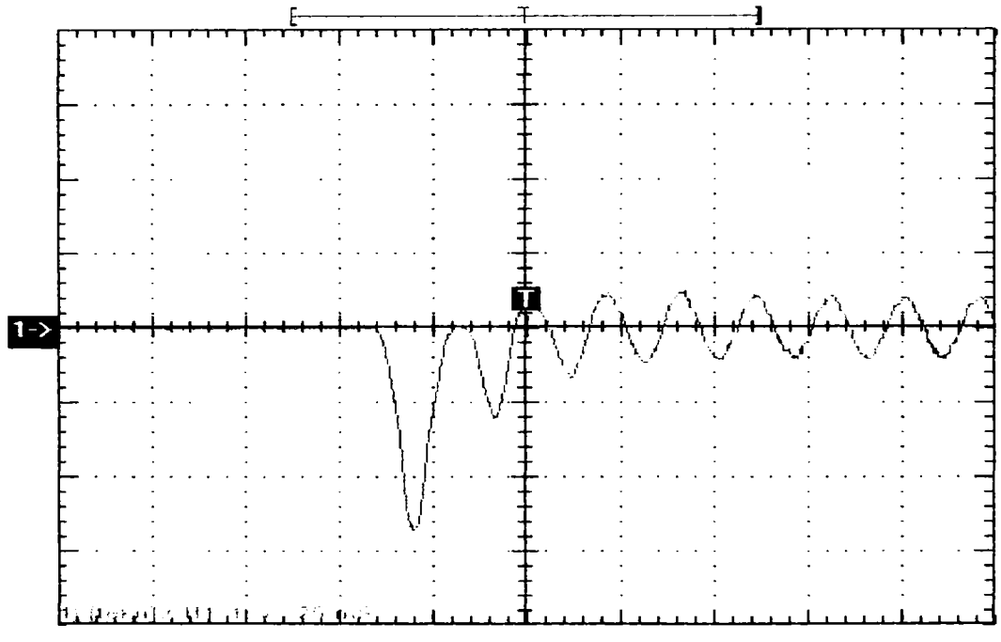

**Figure 4.27.** Measured stator current during start up of DFIG at super synchronous speed of 1015 rpm with Rex and Lex in parallel. Isamax=96 A (4*Isn). Scaling factor is 1V/50A.

The 6-pole, 50 Hz machine used in this study was connected to the 400 rated line-to-line voltages. It should be noted that the transient current peak increased at 140 A (6*In) for a wound rotor machine without passively elements while in the other case the transient current peak increased at 96 A (4*In) and then in steady-state becomes 20 A, as can be seen in Figs. 4.26 and 4.27. Figs. 4.28 and 4.29 also present test results for non-synchronous connection of the DFIG with additional fixed passive elements inserted in the rotor side, to the power supply but in this case in sub-synchronous operation mode at 950 rpm and then at 900 rpm. The

transient stator current peak increased at 70 A (3 times of nominal current) and the transient time is also very short.

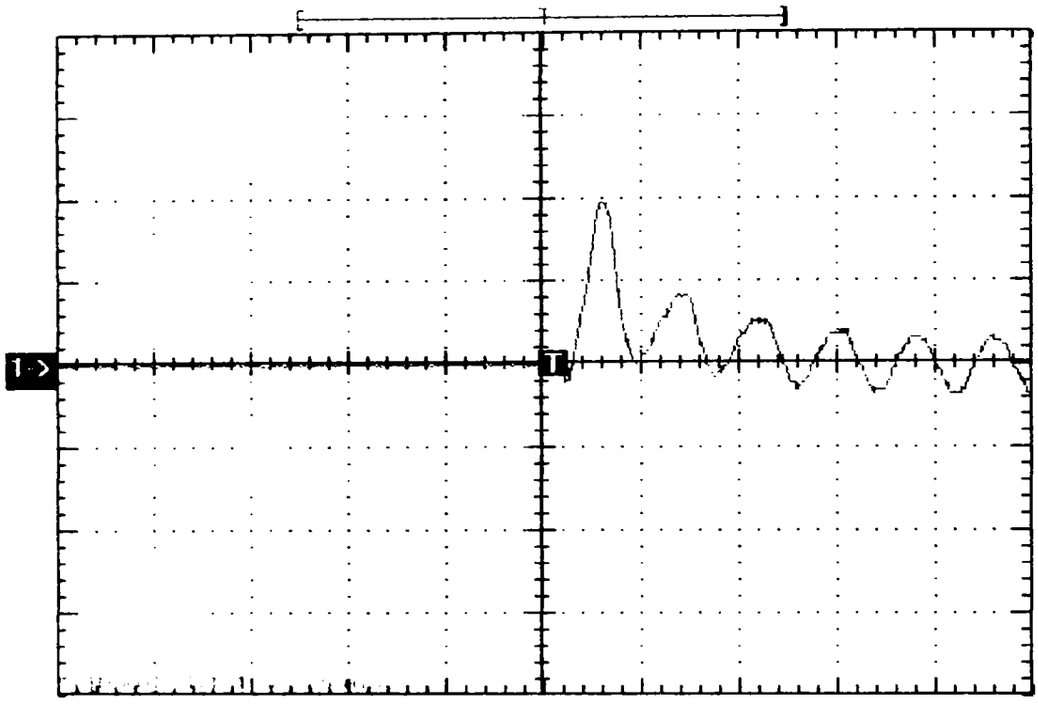

**Figure 4.28**. Stator current during start up of DFIG at sub synchronous speed 950 rpm with Rex and Lex in parallel. $Isa_{max}$=70 A (3*Isn). Scaling factor is 1V/50A.

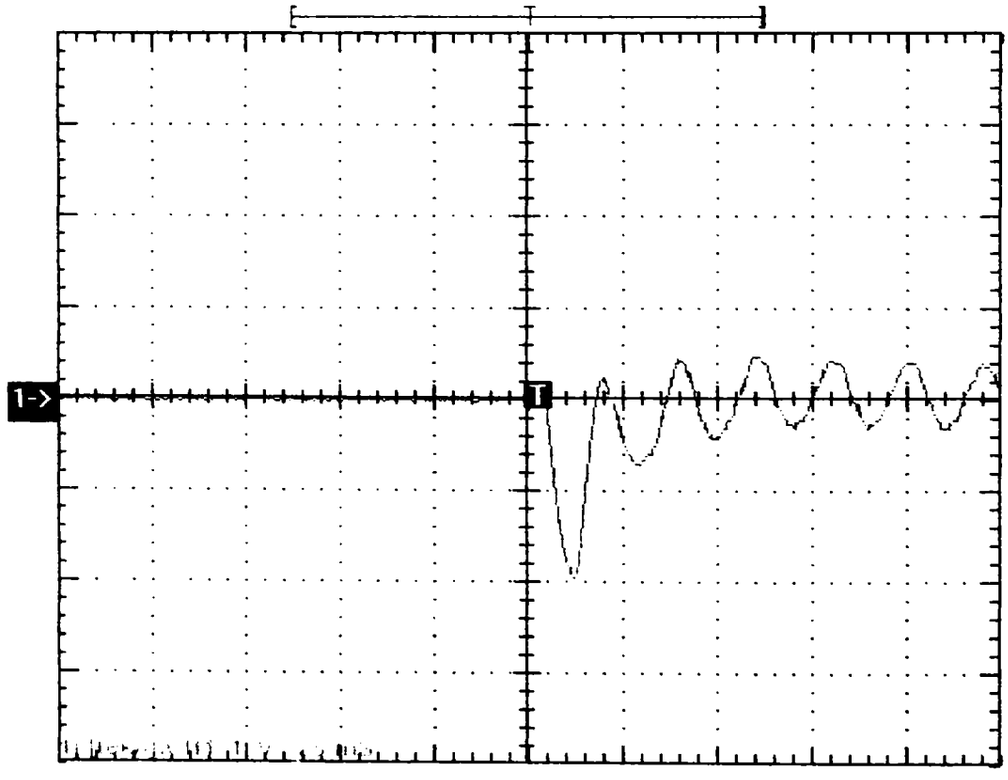

**Figure 4.29**. Stator current during start up of DFIG at sub synchronous speed 900 rpm with Rex and Lex in parallel. Isamax=70 A (3*Isn). Scaling factor 1V/50A.

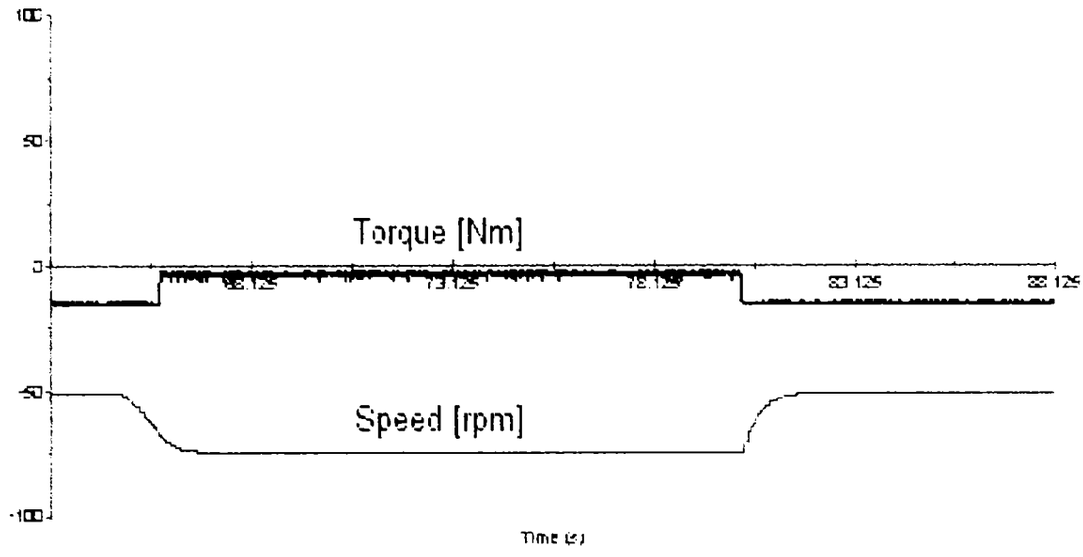


**Figure4.30**. Measured Torque and Speed of DFIG with additional elements during connecting and disconnecting to/from the grid at non-synchronous speed (super synchronous- 1015 rpm). Scaling factor of rotor speed is 0.05. The data were acquired by a laptop via Drive Window PC tool.

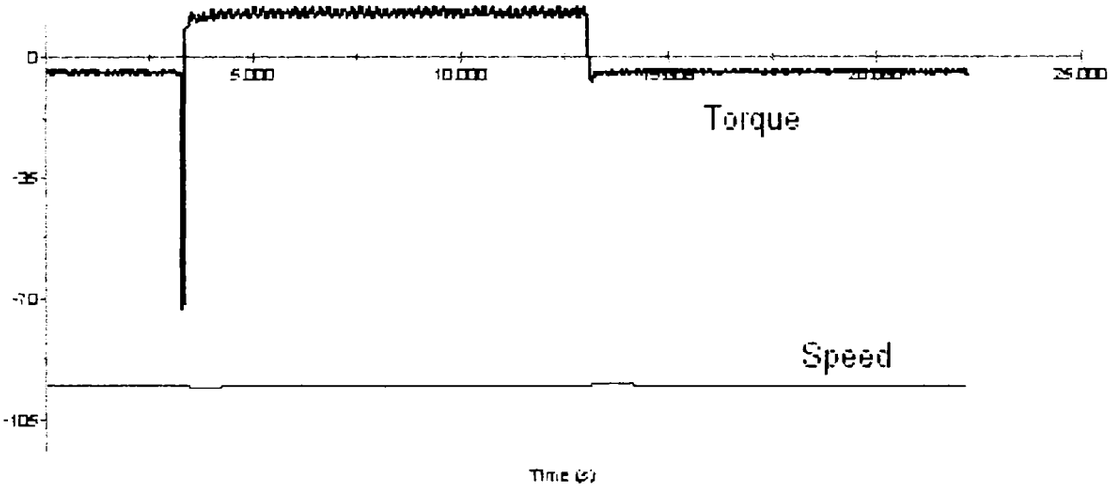


**Figure 4.31**. Measured Torque and Speed of DFIG with additional elements during connecting and disconnecting to/from the grid at non-synchronous speed (sub synchronous - 950 rpm). Scaling factor of rotor speed is 0.1. The data were acquired by a laptop via Drive Window PC tool.

An adequate damping of the system transients is evident in both situations (sub-synchronous and super-synchronous speed) but for the wound rotor induction machine with passive rotor connected elements the system response is relatively "soft" and the transient time is very short. Hence, the passively controlled generator system exhibits adequate stability and natural damping follows the applied torque and rotor speed during connecting and disconnecting the generator to/from the grid, as can be seen in Figs. 4.30-4.31.

## B. Sudden decreases and increases in applied torque (to simulate wind gusts)

The test results with a variable applied torque are intended to represent effects of wind gusts of the wind turbine. The correspondence is good and indicates that the generator system quickly reaches at new stable operating conditions following such changes.

To prove the viability of the proposed system under sudden changes in applied torque the stator phase current, rotor speed and torque of DFIG were recorded for analysis and will be presented in the follow Figures at different dynamic situations. The applied torque has been changed from 50 Nm to 25 Nm and then to 75 Nm, as can be seen in Figs. 4.32-4.35, and from 75 Nm to 50 Nm and then to 100 Nm, as shown Figs. 4.36-4.40. 100 Nm correspond to 100 % of nominal torque of the machine.

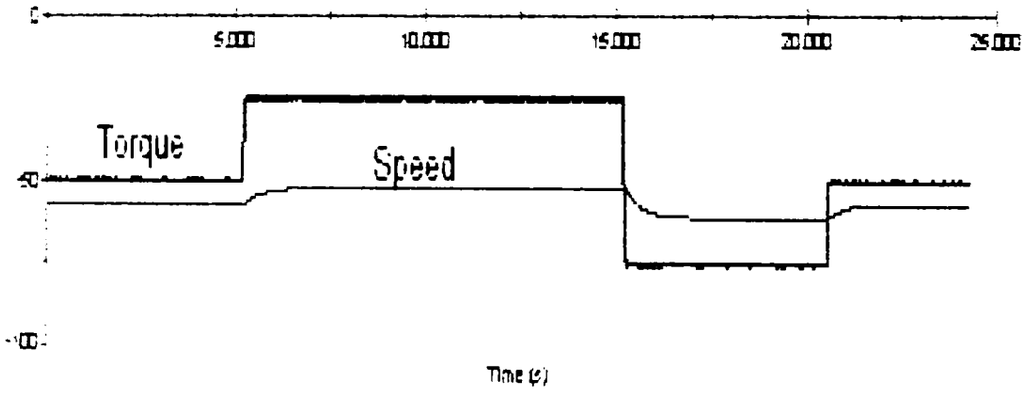


**Figure 4.32** . Effect of wind gusts modifying applied torque T(50-25-75-50) Nm and n(1140-1050-1225-1050) rpm of DFIG with additional impedance. Scaling factor of the rotor speed is 0.05.

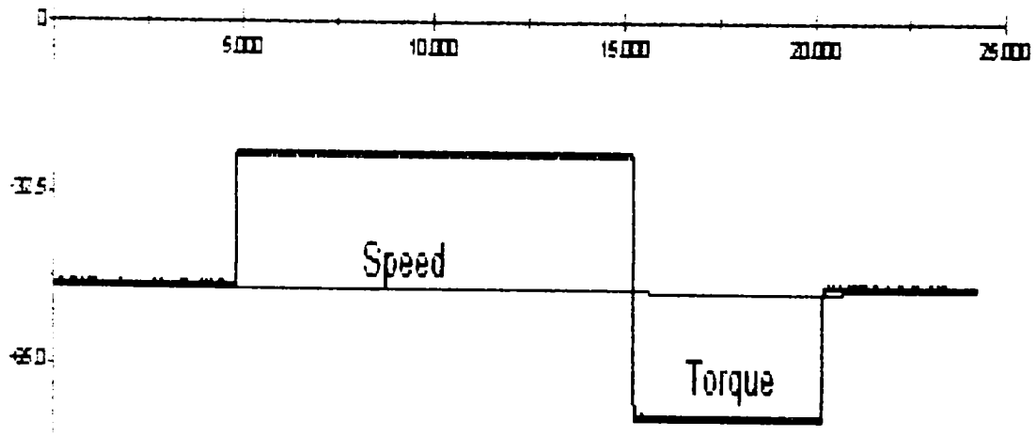


**Figure 4.33**. Sudden changes of applied torque: T(50-25-75-50) Nm and corresponding shaft speed: n(1015-1008-1025) rpm of DFIG without additional impedance. Scaling factor of the rotor speed is 0.05.

When the mechanical torque of DFIG was sudden changed the rotor speed of the generator has been able to follow these changes in both situations as can be seen in Figs.4.32, 4.33 and 4.36, 4.37. Though, due to extended range of the rotor speed for the DFIG with additional passive elements, the corresponding value of rotor speed is much higher in this case, the generator system reached very fast at new stable operating conditions proving a good stability.

Follow the amplitude of stator currents during sudden changes in applied torque (Figs. 4.34, 4.35 and 4.38, 4.39) we may conclude that the generator system with passive elements absorbed the transient current and offer a better stability of the system during transition of dynamic changes.

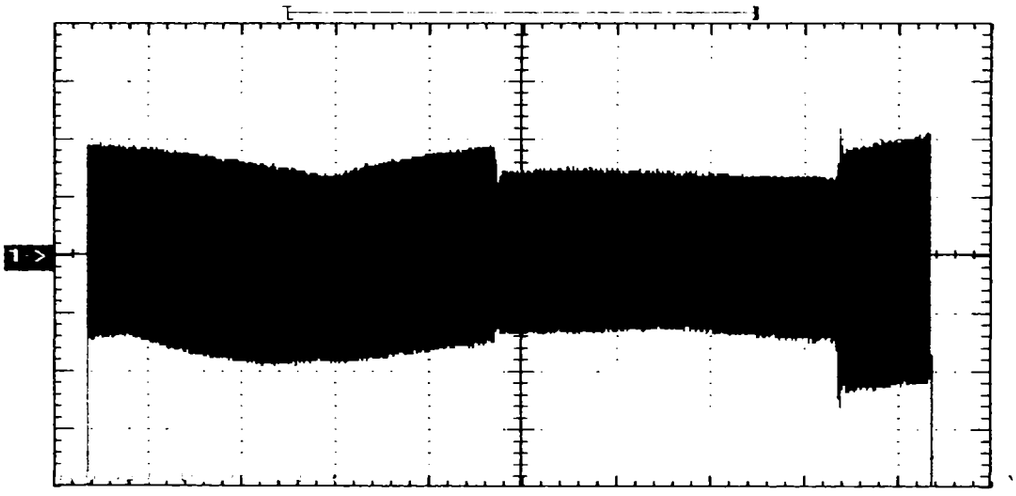

**Figure 4.34**. The stator phase current-$I_{sa}$ measured by a Tektronix Oscilloscope at 50-25-75 % of $T_n$ without additional impedance. Scaling factor is 100 (mV / A).

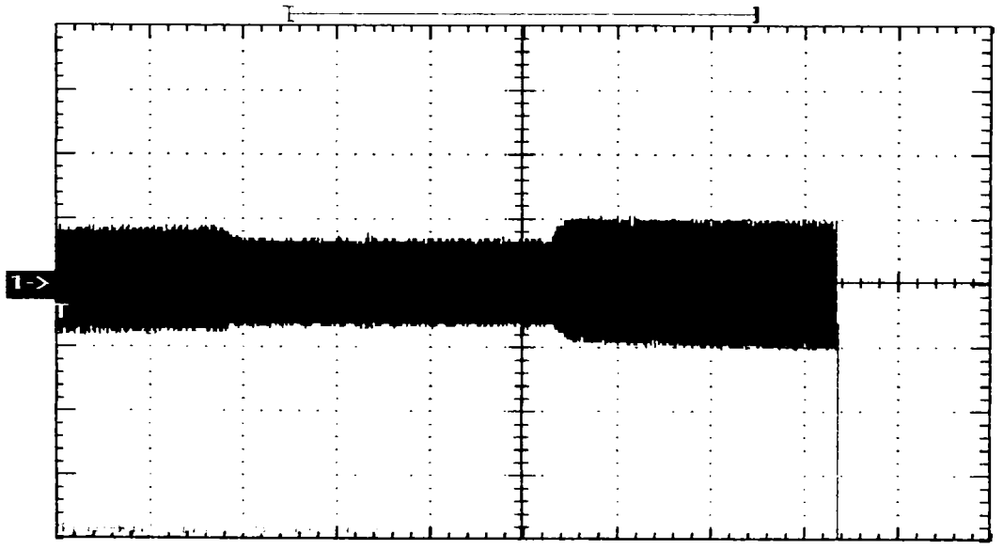

**Figure 4.35**. Stator phase current of DFIG measured by a Tektronix Oscilloscope with additional elements - $R_{ex}$ and $L_{ex}$ in parallel - at sudden increase-decrease torque: (50-25-75) Nm. Scaling factor is 25 (mV / A).

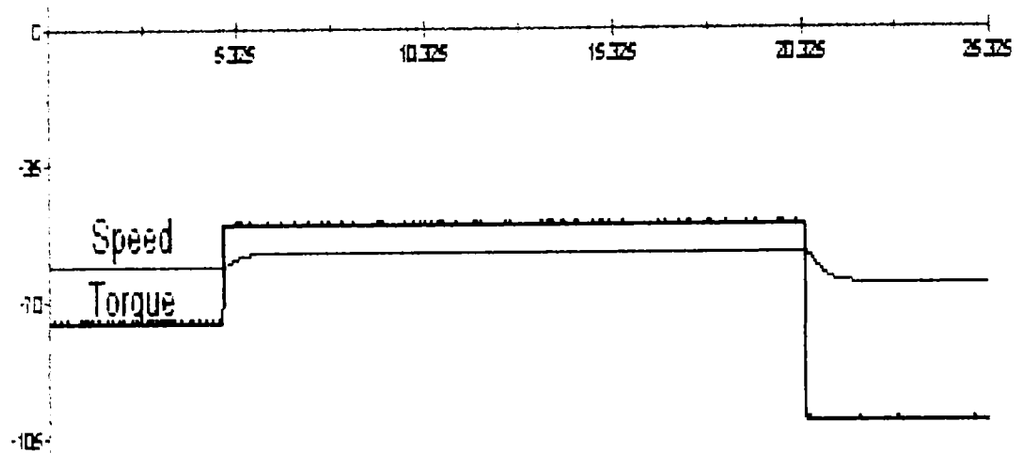


**Figure 4.36**. Sudden changes in applied torque: T(75-50-100) Nm and corresponding shaft speed n(1225-1140-1300) rpm of DFIG with additional impedance. Scaling factor of rotor speed is 0.05

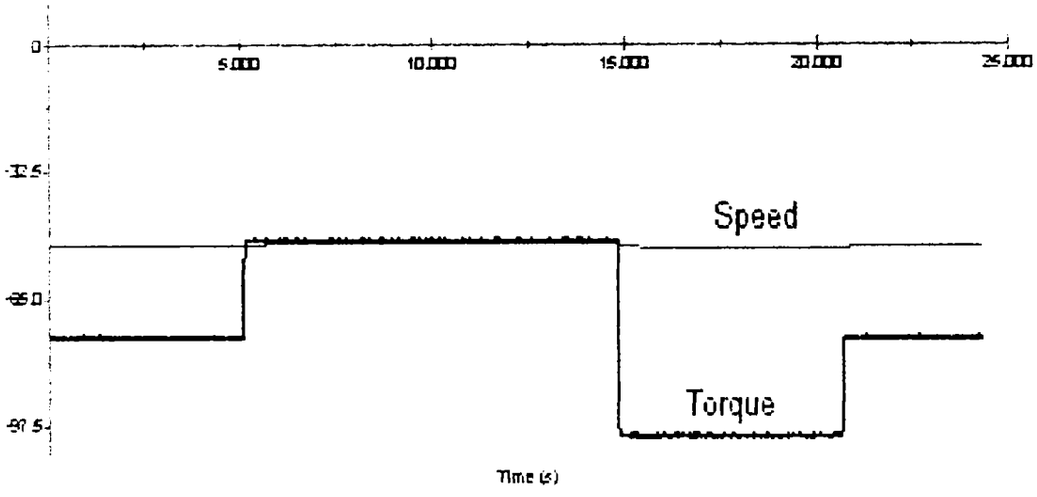


**Figure 4.37**. Variable Torque and Speed: T(75-50-100) Nm and n(1025-1015-1038) rpm of DFIG without additional impedance. Scaling factor of rotor speed is 0.05.

The generator system (Figs. 4.36 and 4.37) is shown to have good response characteristics for a wide range of dynamic changes. A reasonable transients and damping conditions have been observed during the sudden changes in applied torque, intended to represents effects of wind gusts on the turbine.

The acquisition of data and monitoring signals has been done by a Laptop via fiber-optic communication using the dedicated software Drive-Window.

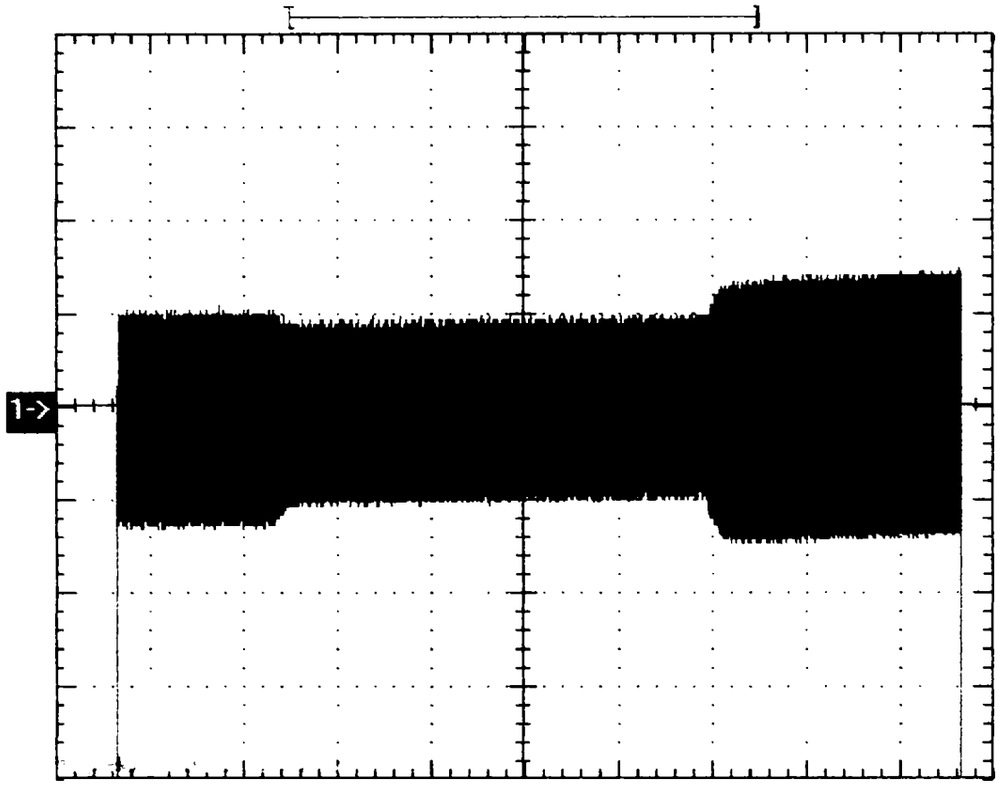


**Fig. 4.38**. Measured stator current of DFIG with passive elements acquired by a Tektronix Oscilloscope via Wave-Star software tool at variable torque (75-50-100) Nm. Scaling factor is 100 (mV / A).

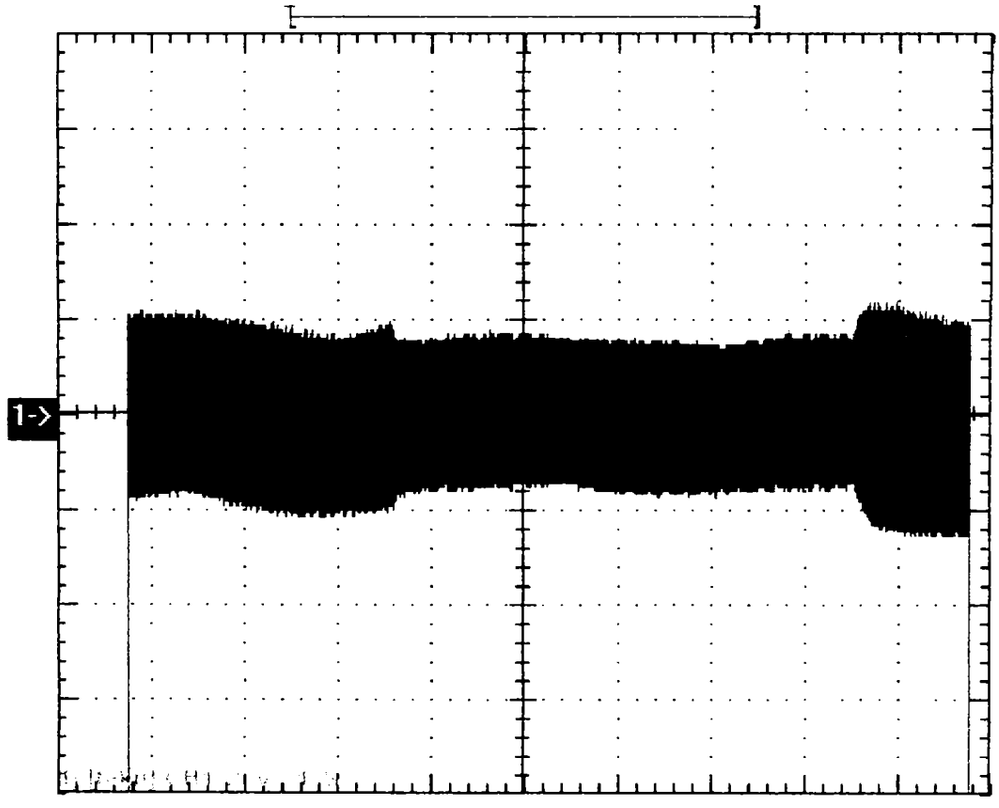


**Fig. 4.39**. Stator current of DFIG without passive elements acquired by a Tektronix Oscilloscope via Wave-Star software tool at variable torque (75-50-100) Nm. Scaling factor of the stator current is 100 (mV / A).

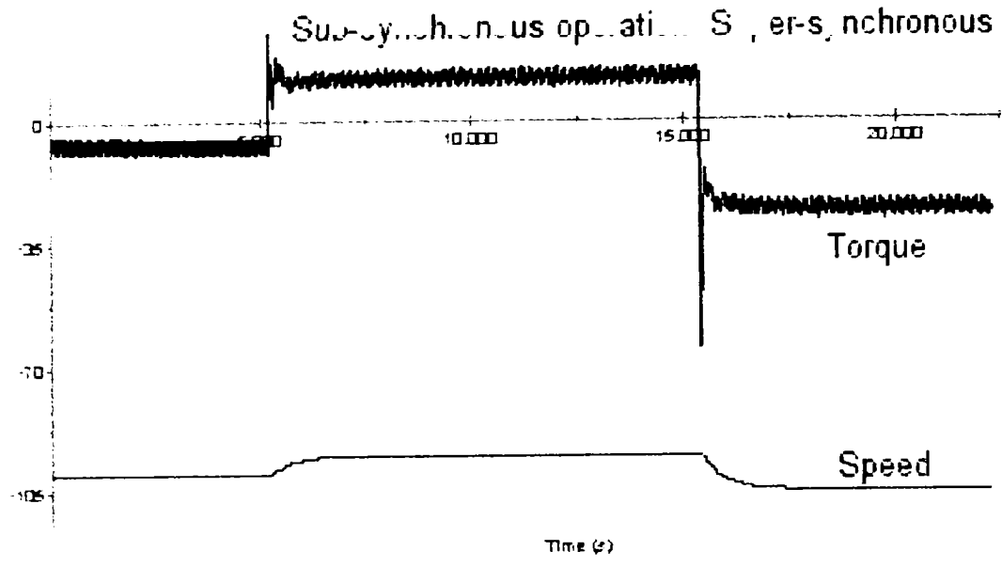


**Figure 4.40**. Measured torque and speed of the DFIG with passive elements during transition from sub-synchronous to super-synchronous operation mode. Scaling factor of rotor speed is 0.1. The data were acquired by a laptop via Drive Window PC tool.

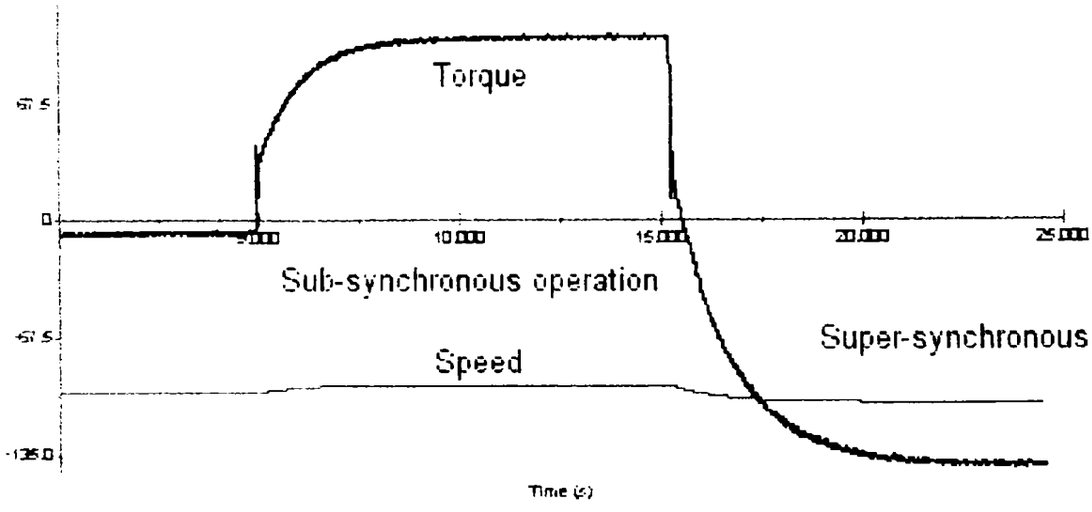


**Figure 4.41**. Measured torque and speed of the DFIG without passive elements during transition from sub-synchronous to super-synchronous operation mode. Scaling factor of rotor speed is 0.1. The data were acquired by a laptop via Drive Window PC tool.

Figs. 4.40-4.41 present the traveling of the torque and speed from synchronous to sub-synchronous and then to super-synchronous operation mode of DFIG with additional rotor passive elements (Fig. 4.40) and without additional elements (Fig. 4.41), which correspond to sudden changes in speed from 1000 rpm to 950 rpm and then to 1050 rpm, in both situations. These Figures also indicate that the generator system with additional passive elements inserted in rotor side, quickly reaches new stable operating conditions following such speed changes while the generator system without additional elements is more slowly.

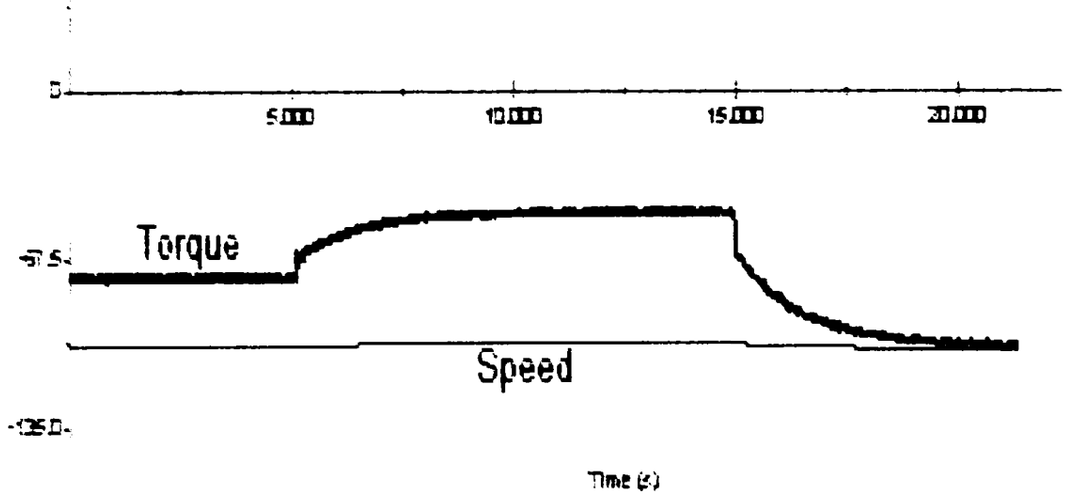


**Fig. 4.42.** Sudden changes of the speed in super-synchronous operation mode: 1025-1015-1035 rpm and corresponding torque: (75-50-100) Nm without additional elements. Scaling factor of rotor speed is 0.1. The data were acquired by a laptop via Drive Window PC tool.

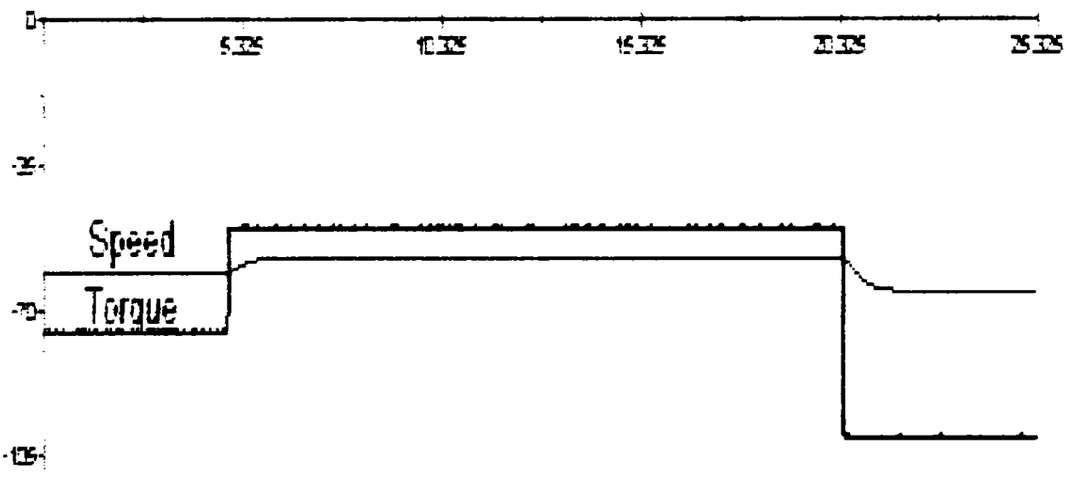


**Fig. 4.43.** Sudden changes in Torque: (75-50-100) Nm and corresponding speed (1225-1140-1300) rpm with additional impedance. Scaling factor of rotor speed is 0.05. The data were acquired by a laptop via Drive Window PC tool.

A comparison of the rotor speed and torque of the same torque values in both situations (with and without passive additional elements), under sudden changes in Figs. 4.42 and 4.43 shows that the generator system with passive element is more stabile than the generator system without passive element, while the machine with passive elements provide an extended speed range as a generator up to 130 %.

### *4.4.2. System Performance Evaluation*

The performance has been measured with external resistance and parallel reactive elements. The input power to the generator was obtained from the control panel of the bidirectional power converter and a power analyzer measured the electrical power output.

The test results obtained for the generator show a good power factor and increasing output power as a function of speeds. The measured efficiency is comparable to that obtained with adjustable frequency control of a similarly rated induction machine.

The speed range of the induction generator (DFIG), while keeping maximum current to the rated values, may be selected by use of appropriate values of additional resistance and inductance, as shown in Table 4.3.

**Table 4.3**. Measured performance of DFIG.

| Pg=0 kW | Pg=2.5 kW | Pg=5 kW | Pg=7.5 kW | Pg=10 kW | Pg=11.5 kW |
|---|---|---|---|---|---|
| Pout=0 | Pout=1.5 kW | Pout=3.5 kW | Pout=5.6 kW | Pout=7.5 kW | Pout=8.3 kW |
| Is=11 A | Is=12.5 A | Is=14.66 A | Is=17.5 A | Is=20 A | Is=20 A |
| Ir=(0-1.2) A | Ir=6.2 A | Ir=9.2 A | Ir=14 A | Ir=18 A | Ir=20 A |
| $Vr_{ext}$=1V | $Vr_{ext}$=6V | $Vr_{ext}$=12.5 V | $Vr_{ext}$=23.6 V | $Vr_{ext}$=30 V | $Vr_{ext}$=34 V |
| n=1000 rpm | n=1040 rpm | n=1100 rpm | n=1180 rpm | n=1240 rpm | n=1250 rpm |

The Fig. 4.44 shows the required input (shaft) powers and the corresponded output powers of the DFIG with the correspondence values of the power factor and efficiency.

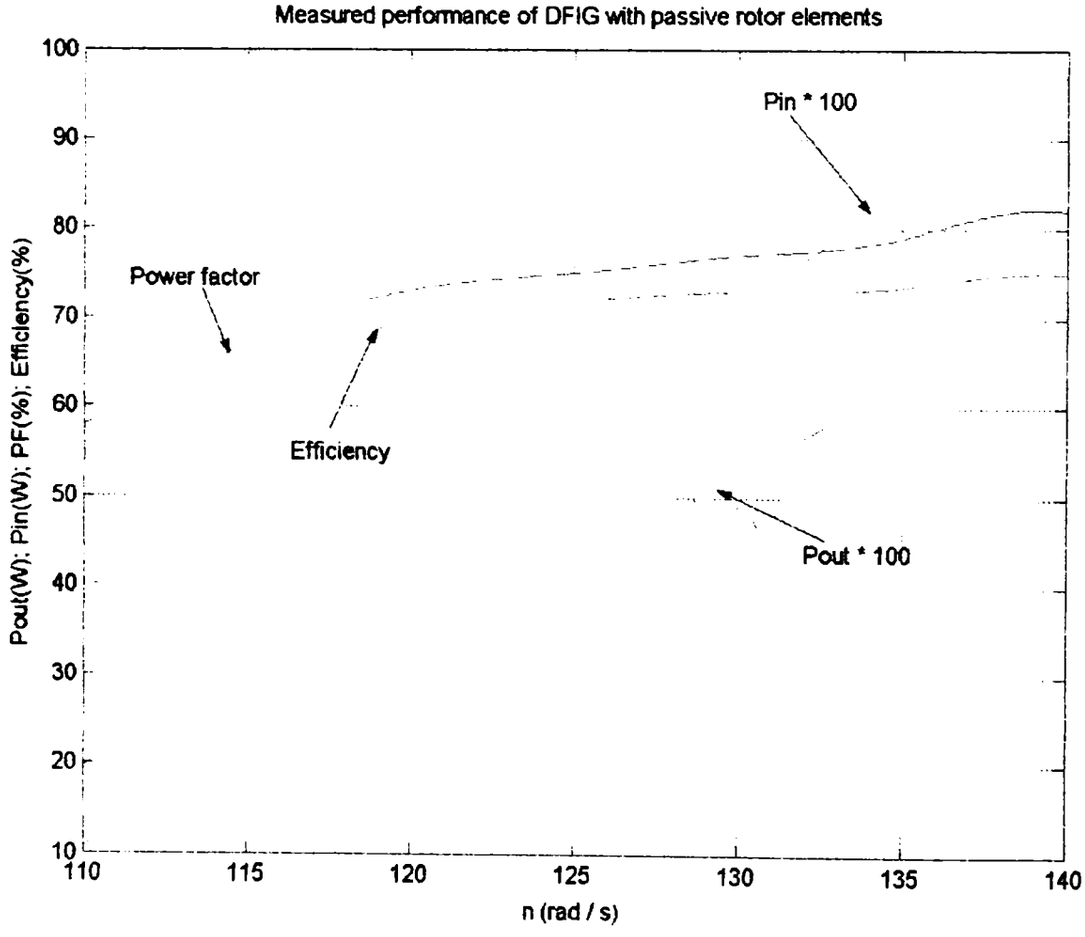


**Fig. 4.44**. Measured performance of DFIG with passive elements controlled system.

It is shown (Fig. 4.44) by laboratory tests on a 10 kW machine that a Doubly-Fed Induction Generator may be used as a variable speed (wind turbine) generator over a relatively large speed range (up to 130 %) with an acceptable efficiency (75 % at full load) and a good power factor (0.81 at full load) by controlling the secondary impedance by passive elements alone.

The power characteristics and the measured efficiency are well suited with the application with similar rated machines in which power converters provide the control.

### *4.4.3. Comparison of Test and Simulated Performance*

The equipment used to obtain the test data was described in the previous sub-chapter.

Tests and simulations were performed to examine the system performance and the effects of non-synchronous connection to the grid and response to changes in applied torque.

The simulations and test results intended to represent that the correspondence is good.

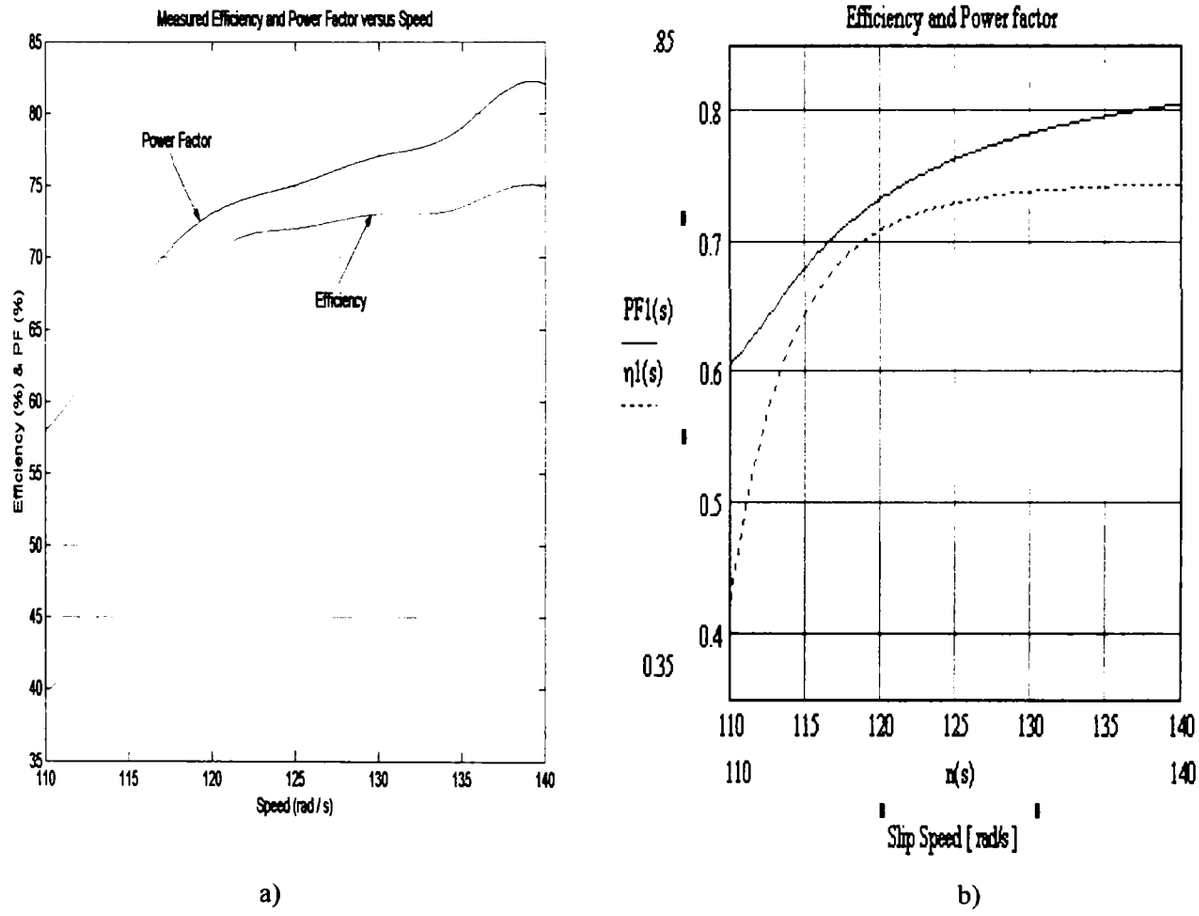


a) b)

**Fig. 4.45.** A Comparison between measured and simulated Efficiency and Power Factor of DFIG with passive elements. Experimental Results (a) and Simulations (b) of DFIG with additional passive elements.

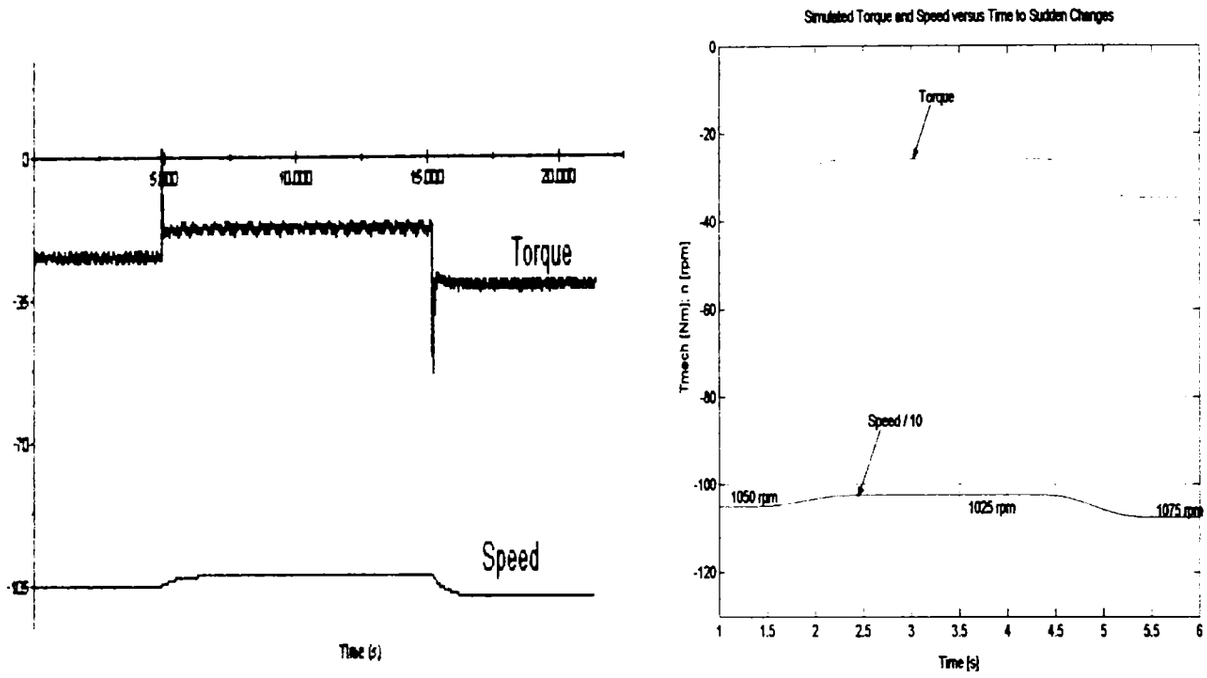


a) b)

**Fig. 4.46.** Measured (a) and simulated (b) mechanical torque and rotor speed of DFIG with additional elements under sudden changes. Scaling factor of measured rotor speed is 0.1. The data were acquired by a laptop via Drive Window PC tool and the simulations were performed using Matlab / Simulink software.

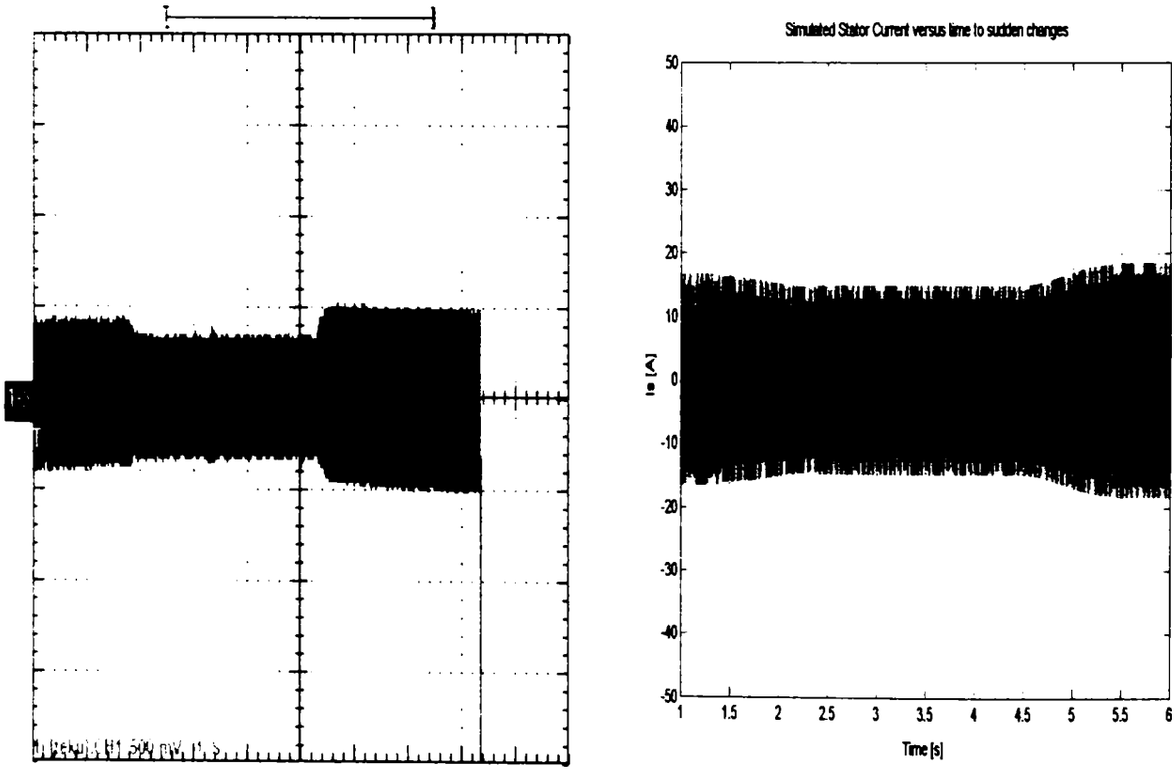


**a)** **b)**

**Fig. 4.47**. Measured (a) and Simulated (b) Stator Current of DFIG with passive elements to sudden changes. Scaling factor of measured stator current is 25 (mV / A).

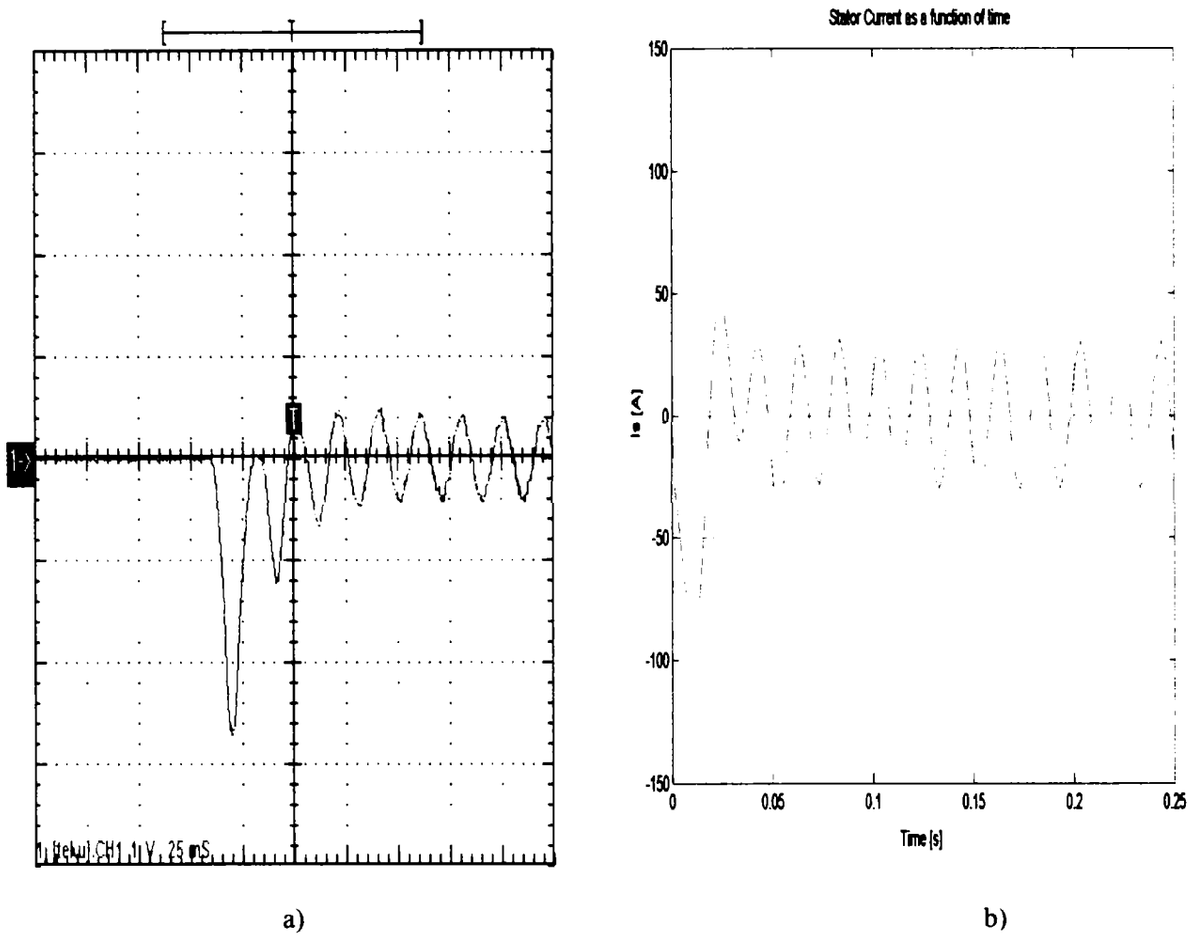


a) b)

**Figure 4.48.** Measured (a) and simulated (b) stator current during start up of DFIG with additional elements at non-synchronous connection to power supply. Scaling factor of measured current is 1V / 50A.

Figures 4.45-4.48 show very good correlation of simulation and test. The test results obtained for the induction generator with passive additional elements correlate acceptably with model predictions and show good power factor and increasing power as a function of speed. The experimental results were acquired by an Oscilloscope and simulation results have been performed by Matlab-Simulink software package.

## 4.5. Summary and Conclusion

In this chapter, the Doubly Fed Induction Generator with limited variable speed generation system is presented. A comparison between two standard topologies of wind systems with dynamic slip control is also shown.

The developed DFIG model with and without additional passive elements is verified through simulations and experiments in steady-state and dynamic conditions as well.

A rotor reference frame model has been developed and implemented using Matlab / Simulink software package for the passively controlled variable-speed generation system. The simulation and experimental results indicate that the induction generator with external rotor passive elements is dynamically stable following three types of transient conditions: connection to the grid at non-synchronous speed, sudden decreases and increases in applied torque (to simulate wind gusts) and repeated cycling of applied torque. It means that the generator system is shown to have good response characteristics for a wide range of dynamic changes.

For steady-state operation, it has been shown that this can be simulated, on a per-phase base, by an equivalent circuit, using Mathcad software package. The single phase equivalent circuit offers an excellent tool to analyze the performance of the induction generator in steady state. The effect of inserting an external resistance in series with the rotor winding was first examined and simulated in MathCAD for both motoring and generating regions. Then the variable resistance ($R_{add}$) was replaced for analysis by an external resistance ($R_{ex}$) in parallel with a reactance ($X_{ex}$).

By laboratory tests on a 10 kW machine that a Doubly-Fed Induction Generator has been used as a variable speed (wind turbine) generator over a relatively large speed range (up to 130 %) with an acceptable efficiency (75 % at full load) and a good power factor (0.81 at full load) by controlling the secondary impedance by passive elements alone.

These results and the good efficiencies obtained by simulations and experiments indicate that the proposed system is a viable low-cost, low maintenance, sensorless, variable-speed generator (wind turbine). Consequently, it is a more practical solution than power electronics for remote locations, for less than (10-20) % of speed variation range.

The passively controlled variable-speed generation system is a simpler and cheaper solution than a similarly rated generator system with power electronic control such as the OptiSlip concept.

## References

[1] Siegfried Heier, "Wind energy conversion systems", book, John Wiley & Sons Inc., New York, 1998.

[2] L.H. Hansen, L. Helle, F. Blaabjerg, E. Ritchie, S. Munk-Nielsen, H. Bidner, P. Sorensen and B. Bak-Jensen, "Conceptual Survey of Generators and Power Electronics for Wind Turbines", Riso-R-1205 (EN), December 2001.

[3] A.K. Wallace and J.A. Oliver, "Variable-speed generation controlled by passive elements", International conference on electric machines, 1998, Istanbul, pp. 1554-1559.

[4] Alan Wallace and Tobias Bathon, "Dynamic operation of passively controlled variable-speed generation system", IEE Ninth International Conference on Electrical Machines and Drives, Conference Publication, No. 468, 1999, pp. 54-59.

[5] M. Boger and A. Wallace, "Performance capability analysis of the brushless doubly fed machine as a wind generator", Electric machines and drives, 11-13 September 1995, Conference publication no 412, pp 458 – 461.

[6] www.Vestas.com, Vestas Wind Systems.

[7] P.C. Krause, O. Wasynczuk and S.D. Sudhoff, „ Analysis of Electric Machinery", IEEE Press, 1995.

[8] C.M. Ong, „Dynamic Simulation of Electrical Machinery using MatLab/SimuLink", Prentice Hall, 1998.

[9] Jimmie J. Cathey, „Electric Machines: Analysis and Design Applying MATLAB", Mc Graw Hill, 2001.

[10] N.Mohan, T.M.Undeland, W.P.Robbins, "Power electronics: Converters, Applications and Design", John Wiley & Sons, 1996.

[11] S.A. Nasar, I. Boldea, "Electric Machines: Steady-State Operation", Hemisphere Publishing Corporation, 1990.

[12] I. Boldea, S.A. Nasar, "The Induction Machine Handbook", CRC Press, 2002.

# Chapter 5

# Variable Speed Wind Generator Systems

## Chapter Contents

## 5.1. Overview of Doubly Fed Induction Generators based Wind Turbines

During the last two decades, the production of wind turbines has grown in size from 20 kW to 3 MW per unit. Due to the rapid development of power electronics, offering both higher power handling capability and lower price per kW, the application of power electronics in wind turbines will increase further.

The doubly fed induction generator can supply power at constant voltage and constant frequency while the rotor speed varies. This makes it suitable for variable speed wind energy applications. Additionally, when a bidirectional AC-AC converter is used in the rotor circuit, the speed range can be extended above synchronous speed and power can be generated both from the stator and the rotor.

Various types of power control strategies have been suggested for application in variable speed wind turbines [1, 2, 10, 12, 13, 17-22]. One possible implementation scheme of adjustable speed generators consist of a synchronous generator and a power converter. The power converter, which has to be rated at 1 p.u. total system power, is expensive. Compared to direct-in-line systems, the doubly fed induction generator (DFIG) systems offer the following advantages [1, 14]

- reduced inverter cost, because inverter rating is typically 25 % of total system power, while the speed range is ± (40-60) % around the synchronous speed
- improved system efficiency
- power factor control can be implemented at lower cost, because the DFIG system basically operates similar to a synchronous generator.

In addition, compared to controlled rectifier based Kramer drives, the DFIG with four quadrant converter in the rotor circuit enables decoupled control of active and reactive power of the generator.

In case of the fully variable speed wind turbine it is possible to produce more mechanical power, using the same wind turbine than in case of fixed speed operation mode [1, 21]. The gain in power production at the wind speed above the most likely wind speed can be higher at variable speed operation as well. The variable speed operation makes it possible to increase the annual power production by approximately 5 % [7, 8].

### *5.1.2. OptiSpeed Control Scheme*

The wind turbine systems that are equipped with OptiSpeed control strategy allows the turbines blades to rotate at varying speeds. OptiSpeed is a further development of the OptiSlip system (described in chapter 4), which allowed the speed of revolution of both the rotor and the generator to vary as much as 10%. With OptiSpeed, the speed of revolution can now vary by up to approx. (60-70) % [6, 7]. This reduces fluctuations in the grid system as well as minimizes the loads on the vital parts of the turbine.

OptiSpeed is an efficient solution because the converter only transforms the energy from the generator rotor, which is only a small part of the total energy generated by the system. The energy generated by the generator rotor is converted back into electricity suitable for the grid by the converter, as can be seen in Fig. 5.1.

OptiSpeed advantages:

- Higher energy production

- Load control
- Flexible noise adjustment
- Improved power quality: controlled reactive power, low flicker, low current harmonics, and fast and soft grid synchronization.

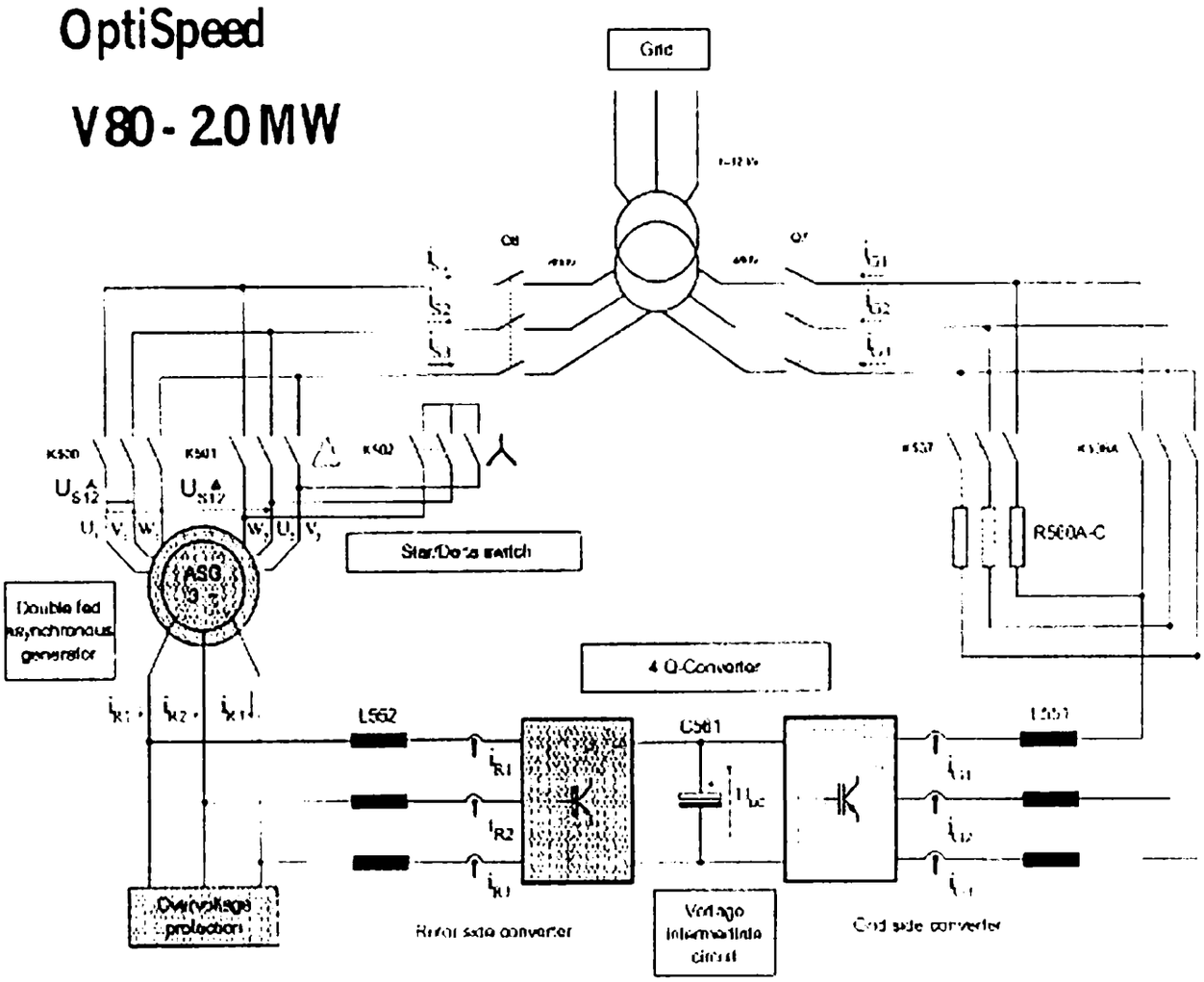


**Figure 5.1.** The block diagram of the OptiSpeed control system of 2 MW Wind Turbine [6, 7].

Figure 5.1 presents a modern high-power wind turbine capable of adjustable speed operation. This topology shows an alternative concept that consists of a doubly fed induction generator with a four quadrant ac-to-ac (back-to-back) converter based on IGBTs connected to the rotor windings. The converter is controlled by the power electronics (switching IGBTs) [1, 6, 7, 8] and its operation corresponds to adding an external voltage phasor in the rotor circuit. The voltage phasor is controlled so that the frequency in the rotor circuit corresponds to the desirable rotational speed of the rotor.

The variable speed wind turbines represent a new technology within wind power for large-scale applications and their models have to be set up for making power stability investigations. Therefore, this concept will be analyzed, modeled and simulated as follows.

## 5.2. Modeling and Simulation of the Doubly Fed Induction Generator

### 5.2.1. Introduction

The Doubly Fed Induction Generator (DFIG) is an induction machine with a wound slip ring rotor. This provides the machine with an additional power port, giving additional control opportunities that may be exploited in the wind power generating systems.

DFIG is implemented as a variable speed, constant frequency scheme, by applying a converter to the rotor terminals of DFIG.

The wind rotor determines the rotor speed, and controlling the rotor currents may control the stator power of the DFIG. If the stator flux is chosen as a reference, the q-rotor current ($I_{qr}$) controls the stator reactive power ($Q_s$), and the rotor d-current ($I_{dr}$) controls the stator active power ($P_s$). Controlling the rotor q- and d-currents respectively may control the stator active and reactive power.

The ability to supply / subtract power to / from the rotor makes it possible to operate the DFIG at sub- and super-synchronous speed, having constant voltage and frequency on the stator terminals. Furthermore it is possible to recover slip power in the rotor and supply it back into the power grid, through which the efficiency of the machine may be increased.

### 5.2.2. DFIG Modeling in Steady-State

The schematic representation of the DFIG with the mechanical power (Pm) port and the stator power (Ps) and the rotor power (Pr) ports are shown in Fig. 5.2 a) and equivalent circuit is depicted in Fig. 5.2 b):

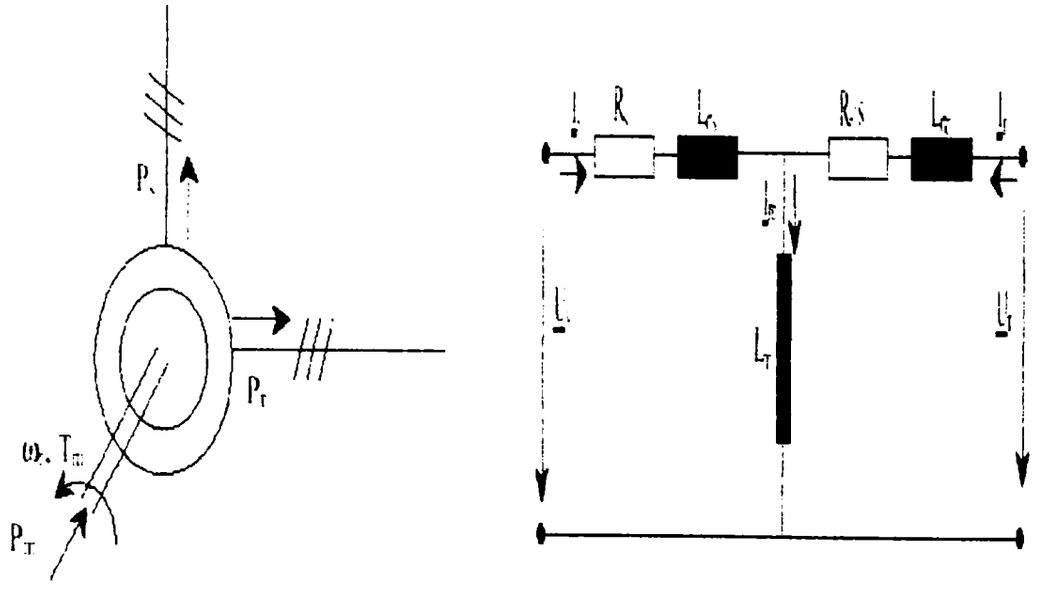

a) b)

**Figure 5.2. a)** Schematic representation of the DFIG with indication of three power ports.
**b)** Standard equivalent circuit of the DFIG.

As can be seen in Fig. 5.2 the power ports of the DFIG are the mechanical power (Pm), which in the wind power systems is provided through the wind rotor and gearbox, the stator power (Ps) and the rotor power (Pr).

The stator windings are connected directly to the AC power grid, while the rotor windings are connected to the power grid through the rotor and grid converter. In order to achieve full controllability i.e. both super- and sub-synchronous speed operation are required.

*Speed control*

The rotor winding yields the option to control the speed of the shaft, enabling compensation for wind speed variations. This means minimizing of the stator power pulsation by storing the mechanical energy supplied to the shaft as a rotational energy. The relationship between mechanical and electrical power is given by equation 5.1, where all losses are neglected.

$$P_m = \omega_m \cdot T_m = P_s + P_r \quad \text{.....(5.1.)}$$

In (5.1) the wind speed variations are expressed by a varying mechanical torque ($T_m$), to variation in the wind energy. In order to keep the electrical power ($P_s$ + $P_r$) unchanged; the mechanical speed of the rotor shaft ($\omega_m$) must be controlled.

*Speed Control via the Rotor Frequency*

By changing the electrical frequency of the rotor it is possible to change the speed of the shaft, as expressed in (5.2):

$$\frac{f_{slip}}{f_s} = \frac{\omega_{slip}}{\omega_s} = \frac{\omega_s - \omega_r}{\omega_s} = \frac{\omega_{syn} - \omega_{slip}}{\omega_{syn}} = s \quad \text{.....(5.2.)}$$

Equation 5.2 presents the definition of the slip and relationship between rotor and stator electrical frequency. By rearranging the equation 5.2 becomes clear that the shaft speed depends on the rotor electrical frequency, as may be seen in equation 5.3:

$$\omega_{slip} = \omega_{syn} \cdot \left(1 - \frac{f_{slip}}{f_s}\right) \quad \text{.....(5.3.)}$$

Control of the rotor speed may be achieved by controlling the electrical frequency of the rotor. The rotor converter controls the electrical frequency on the rotor.

### 5.2.3. Voltage equations

In a three-phase machine, six voltage equations, one for each phase of the stator and rotor circuit, may be set up as [Krause, 1995, pg. 54-57]. The equations are set up in matrix form. The stator voltage equals the supply grid voltage, and the rotor converter controls the rotor voltage. The stator and the rotor phase voltages may be expressed as written in equation:

$$u_s = \begin{bmatrix} u_a \\ u_b \\ u_c \end{bmatrix} = \sqrt{2} * u_{phase} * \begin{bmatrix} \sin(\omega_{syn} t) \\ \sin\left(\omega_{syn} t + \frac{2\pi}{3}\right) \\ \sin\left(\omega_{syn} t + \frac{4\pi}{3}\right) \end{bmatrix}; u_r = \begin{bmatrix} u_k \\ u_l \\ u_m \end{bmatrix} = U_{dc} * D * \begin{bmatrix} \sin(\omega_{slip} t) \\ \sin\left(\omega_{slip} t + \frac{2\pi}{3}\right) \\ \sin\left(\omega_{slip} t + \frac{4\pi}{3}\right) \end{bmatrix}; \quad \text{.....(5.4)}$$

$$u = \begin{bmatrix} u_s \\ u_r \end{bmatrix}$$

Similarly the phase stator and rotor currents are defined in (5.5).

$$i_s = \begin{bmatrix} i_a \\ i_b \\ i_c \end{bmatrix}; i_r = \begin{bmatrix} i_k \\ i_l \\ i_m \end{bmatrix}; i = \begin{bmatrix} i \\ i_r \end{bmatrix} \quad \text{.....(5.5)}$$

The voltage equations describing the DFIG may be set up in the three-phase system. In order to reduce the complexity of the differential equations a change of variables is applied. The three-phase system is therefore transformed into a two-phase representation.
In general, four types of reference frames are widely used. Stator fixed, rotor fixed, flux vector fixed or synchronous rotating reference frame [Krause, 1995, pg. 133-148]. The reduction from three to two-phase reference frame has the advantage that the flux in the two phases or directions does not interact. These gains the advantage that time varying variables of the three-phase system becomes constant when referred to the two-phase system. Those advantages are independent of the choice of the reference system.
The reference system that will be chose depends on what will be investigated. If the investigation deals with the machine interference on the supply net, the choice would be a stator fixed system or a synchronously rotating reference frame, because the stator is connected to the supply net. If an investigation of a rotor phenomenon is to be performed, a rotor fixed system should be chosen. If the machine is to be controlled a flux vector fixed system may be chosen. [Vas, 1990, pg. 122-126]

### 5.2.3.1. D-Q Model of the DFIG (Two Phase Reference Frames)

To control dynamic sequences, the standard equivalent circuit shown in Fig. 5.2 is inadequate, as the model is based on calculations with RMS-values of voltages and currents. A dynamic model is set up in form of the d-q representation in an arbitrary reference frame. Thereby, the complexity of the three-phase differential equations, where some of the machine inductances are functions of the rotor speed and the voltage equations are time varying, is avoided. [Krause, 1986, pg. 53]. The following assumptions are set up to developing the d-q model:

- The stator and rotor windings of the DFIG are assumed symmetric, resistance magnetizing and leakage inductances are equal for all three-phases. This means that the zero-component of the d-q model may be eliminated;

- The windings are assumed sinusoidal distributed around the circumference of the DFIG. Thereby the MMF produced by the windings will be sinusoidal, no harmonic components will be present;
- The air gap is assumed constant, meaning constant air gap reluctance. This means, that the mutual inductances from stator to stator windings and rotor-to-rotor windings are constant. Only the mutual inductance from stator to rotor windings varies.
- Saturation of the mutual inductance, or magnetizing inductance, is neglected i.e. the magnetizing inductance does not vary as a function of the current;
- Skin effect in the stator and rotor is neglected. As the frequency of the current increases, skin effect will increase the resistance, and decrease the inductance due to increased reluctance in the iron of the DFIG;
- Iron losses are neglected. This means that the losses in the DFIG would be larger than simulated;
- Cross saturation effect is neglected. The phenomenon means, that coupling between two perpendicular axes. For the three-phase induction machine neglecting cross saturation effect means that the phase windings are assumed to have inductance in the three-phase direction only.

Essentially, the d-q model is a simple reduction from a three-phase representation to a two-phase representation. The three-axes representing the three-phases in the standard model is projected on two-axes, the d- and q-axes. The arbitrary reference frame is a two-phase system, which reference is arbitrary [Krause, 1995, pg 136-171]. In the stator flux fixed reference frame, both the d- and q-axis is aligned with the stator flux.

The voltage equation in the arbitrary reference frame may be written as in equation (5.6):

$$\begin{bmatrix} u_{qs} \\ u_{ds} \\ u_{qr} \\ u_{dr} \end{bmatrix} = \begin{bmatrix} R_s & 0 & 0 & 0 \\ 0 & R_s & 0 & 0 \\ 0 & 0 & R_r & 0 \\ 0 & 0 & 0 & R_r \end{bmatrix} * \begin{bmatrix} i_{qs} \\ i_{ds} \\ i_{qr} \\ i_{dr} \end{bmatrix} + \begin{bmatrix} L_s & 0 & M & 0 \\ 0 & L_s & 0 & M \\ M & 0 & L_r & 0 \\ 0 & M & 0 & L_r \end{bmatrix} * \begin{bmatrix} \frac{di_{qs}}{dt} \\ \frac{di_{ds}}{dt} \\ \frac{di_{qr}}{dt} \\ \frac{di_{dr}}{dt} \end{bmatrix} + \quad \text{.....(5.6)}$$

$$+ \begin{bmatrix} 0 & \omega_{ref} L_s & 0 & \omega_{ref} M \\ -\omega_{ref} L_s & 0 & -\omega_{ref} M & 0 \\ 0 & (\omega_{ref} - \omega_r) M & 0 & (\omega_{ref} - \omega_r) L_r \\ -(\omega_{ref} - \omega_r) M & 0 & -(\omega_{ref} - \omega_r) L_r & 0 \end{bmatrix}$$

By assembling stator and rotor voltages on matrix form the complete linear model may be illustrated [Krause, 1995, pp 176].

The electrical equivalent circuit is shown in Fig. 5.3 where the matrix expressions are given in equations (5.6) and (5.9), respectively.

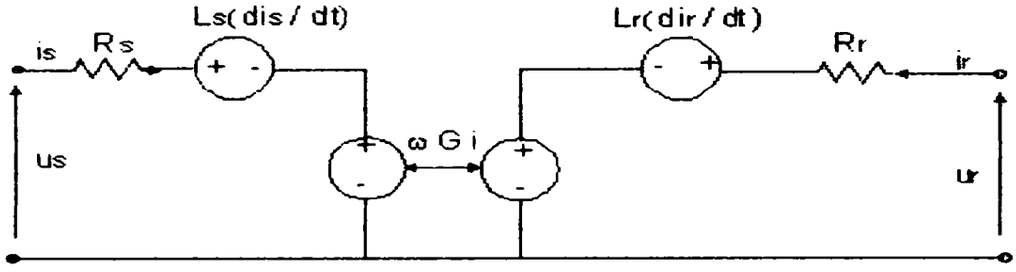


**Figure 5.3.** The d-q equivalent circuit of the symmetrical induction machine in the arbitrary reference frame. Since a symmetric machine is assumed, the zero-components are not included in the model. [4]

The complete system of the DFIG, with arbitrary reference frame, is visualized in Fig. 5.3, where all elements in the equivalent circuit are matrixes. Rotor and stator interact through the voltage sources controlled by **ωG i,** with the assembled **ωG** matrix equation written as in equation (5.7):

$$\omega G = \begin{bmatrix} 0 & \omega_{ref} \cdot L_s & 0 & \omega_{ref} \cdot M \\ -\omega_{ref} \cdot L_s & 0 & -\omega_{ref} \cdot M & 0 \\ 0 & (\omega_{ref} - \omega_r) \cdot M & 0 & (\omega_{ref} - \omega_r) \cdot L_r \\ -(\omega_{ref} - \omega_r) \cdot M & 0 & -(\omega_{ref} - \omega_r) \cdot L_r & 0 \end{bmatrix} \quad \text{.....(5.7)}$$

The voltages and currents equations are defined as shown in (5.8):

$$u = \begin{bmatrix} u_s \\ u_r \end{bmatrix} = \begin{bmatrix} u_{qs} \\ u_{ds} \\ u_{qr} \\ u_{dr} \end{bmatrix}; i = \begin{bmatrix} i_s \\ i_r \end{bmatrix} = \begin{bmatrix} i_{qs} \\ i_{ds} \\ i_{qr} \\ i_{dr} \end{bmatrix} \quad \text{.....(5.8)}$$

The voltage equation derived from the equivalent circuit in Fig. 5.3 may be expressed as in equation (5.9):

$$u = R * i + L * \frac{di}{dt} + \omega * G * i \quad \text{.....(5.9)}$$

The equation (5.9) is the common valid voltage equation of the arbitrary reference system.

The d-q representation is implemented in Simulink, where an overall model of the DFIG is set up. For improvement of the standard linear model, non-linearities may be introduced. The electrical torque may be expressed as equation (5.10) [Krause, 1986, pg. 178]:

$$T_e = \frac{p}{2} * i_s^T * G_{sr} * i_r \quad \text{.....(5.10)}$$

### 5.2.4. Simulink implementation model of the Doubly Fed Induction Generator

A model of the DFIG using the derived equivalent circuit and the equations written before are implemented in Simulink. The model calculates stator and rotor currents, stator and rotor active and reactive power and electrical torque as a function of time, depending on inputs of the stator and rotor voltages and mechanical speed of the shaft. The block representation of the DFIG is depicted in Fig. 5.4:

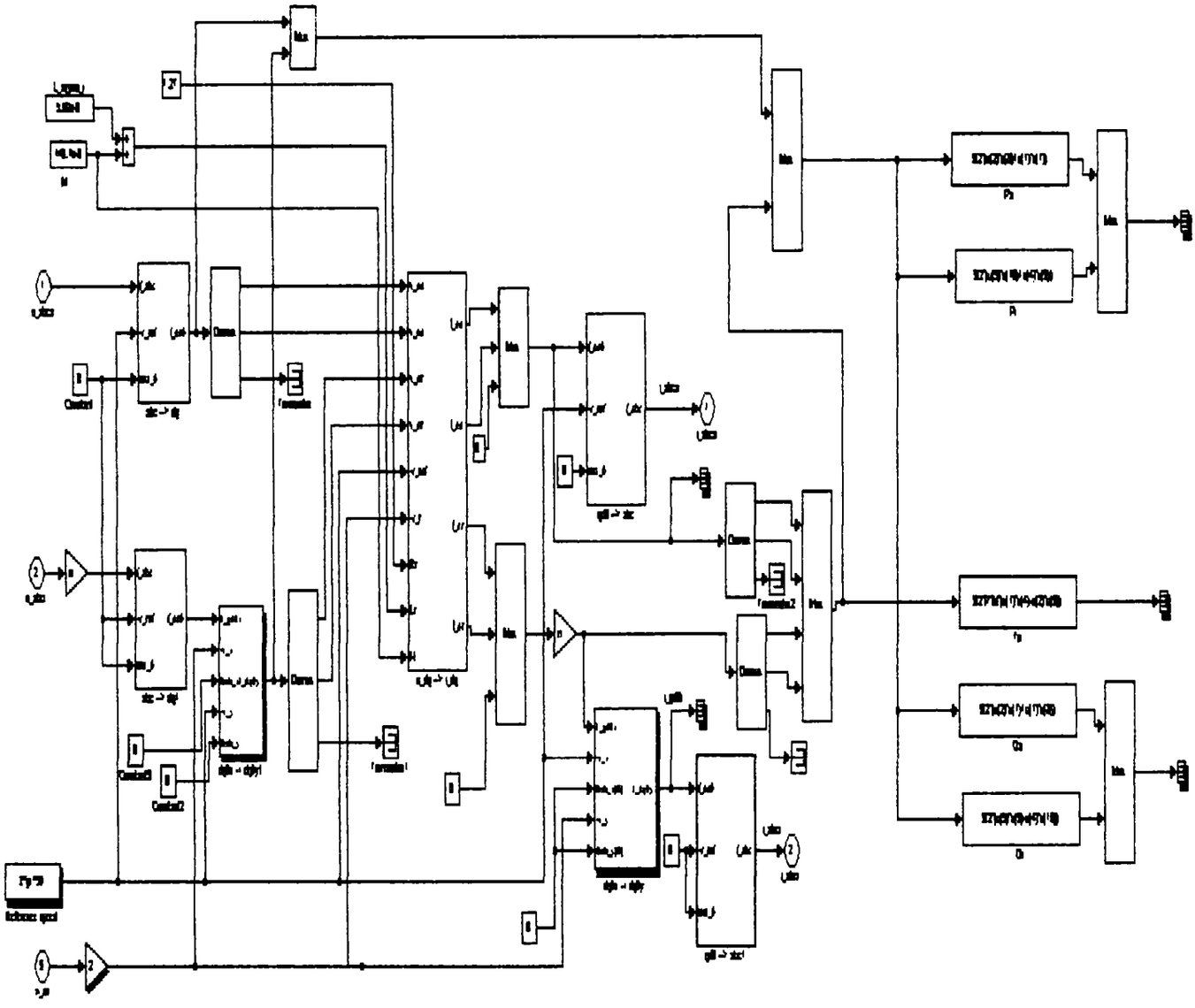

**Figure 5.4.** Block representation of the DFIG model in Simulink. The model is linear without implementation of the parameter variations.

As may also be seen in Fig. 5.4 the Simulink model operates with three phase inputs and returns three phase outputs, both inputs and outputs are transformed to/from the two phase notation used in the model. A more detailed description of the development and implementation of the d-q model may be found in the following section. The equations are rewritten as differential equations in the Laplace plane.

*Flux equations* [Krause. 1995. pp. 173-178]:

$$\lambda_{qs} = \frac{1}{s}\left(u_{qs} - R_s i_{qs} - \omega_{ref}\lambda_{ds}\right) \quad (5.11)$$

$$\lambda_{ds} = \frac{1}{s}\left(u_{ds} - R_s i_{ds} + \omega_{ref}\lambda_{qs}\right) \quad (5.12)$$

$$\lambda_{sr} = \frac{1}{s}\left(u_{qr} - R_r i_{qr} - (\omega_{ref} - \omega_r)\lambda_{ds}\right) \quad (5.13)$$

$$\lambda_{dr} = \frac{1}{s}\left(u_{dr} - R_r i_{dr} - (\omega_{ref} - \omega_r)\lambda_{qr}\right) \quad (5.14)$$

Where s denoted the Laplace operator and the electrical angular velocity of the rotor $\omega_r$ is given by (5.15).

$$\omega_r = \omega_m \frac{p}{2} \quad (5.15)$$

*Current equations:*

$$i_{qs} = \frac{\lambda_{qs} - M.i_{qr}}{L_{qs} + M} = \frac{M \cdot \lambda_{qr} - (L_{or} + M)\cdot \lambda_{qs}}{M^2 - (L_{or} + M)\cdot(L_{os} + M)} \quad (5.16)$$

$$i_{ds} = \frac{\lambda_{ds} - M.i_{dr}}{L_{ds} + M} = \frac{M \cdot \lambda_{qr} - (L_{or} + M)\cdot \lambda_{qs}}{M^2 - (L_{or} + M)\cdot(L_{os} + M)} \quad (5.17)$$

$$i_{qr} = \frac{\lambda_{qr} - M.i_{qs}}{L_{qr} + M} = \frac{M \cdot \lambda_{qs} - (L_{or} + M)\cdot \lambda_{qr}}{M^2 - (L_{or} + M)\cdot(L_{os} + M)} \quad (5.18)$$

$$i_{dr} = \frac{\lambda_{dr} - M \cdot i_{ds}}{L_{dr} + M} = \frac{M\lambda_{qr} - (L_{or} + M)\cdot \lambda_{qs}}{M^2 - (L_{or} + M)\cdot(L_{os} + M)} \quad (5.19)$$

The current and flux equations presented before are implemented in Matlab-Simulink as a subsystem. The subsystem is shown in Fig. 5.5:

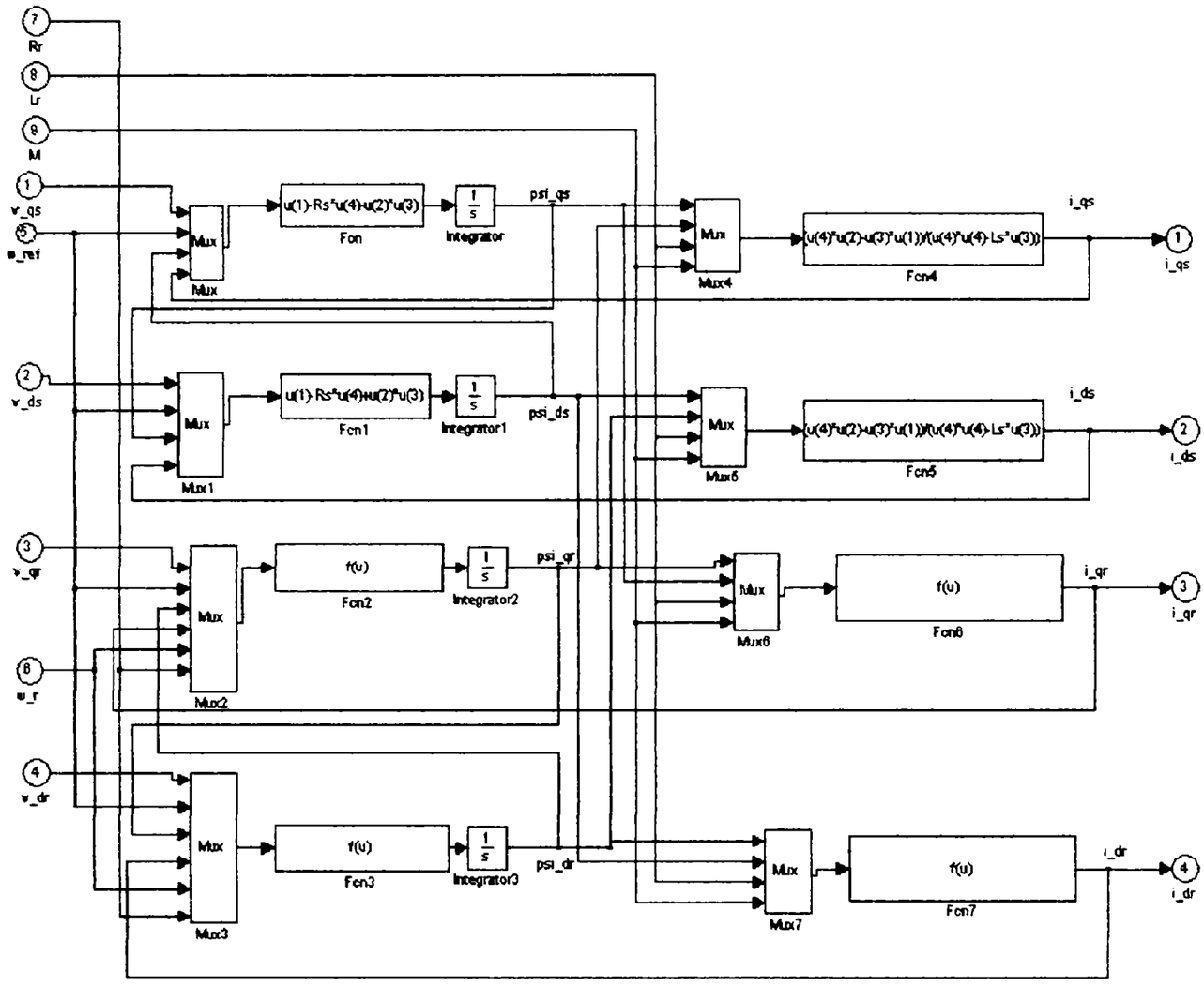


**Figure 5.5.** Block representation of the subsystem u_dq / i_dq. The Fig. 5.5 illustrates the principles of how the flux and current equations are implemented in Matlab-Simulink.

*Torque equation:*

The mutual flux between rotor and stator produces magnetic energy, which is stored in the magnetic field. This energy produces an electrical torque that generates the stator currents. Like the voltages and currents, the electrical torque may be calculated with respect to the arbitrary reference frame. The equation for electrical torque is written in (5.20) [Krause. 1995. pg. 178].

$$Te = -\frac{3}{2}\cdot\frac{p}{2}\cdot M\cdot\left(i_{qs}i_{dr} - i_{ds}i_{qr}\right) = \frac{3}{2}\cdot\frac{p}{2}\cdot\left(\lambda_{ds}i_{qs} - \lambda_{qs}i_{ds}\right) \quad \text{.....(5.20)}$$

*Calculation of Active and Reactive Power*

The stator active power may be calculated by multiplying the voltage and associated current. This means that the active power may be calculated using (5.21)

$$\begin{bmatrix} Ps \\ \Pr \end{bmatrix} = \frac{3}{2}\begin{bmatrix} u_{ds}i_{ds} + u_{qs}i_{qs} \\ u_{dr}i_{dr} + u_{qr}i_{qr} \end{bmatrix} \quad \text{.....(5.21)}$$

The reactive power is calculated by denoted the two axes in the reference frame as a real and imaginary axis in the complex plane. By calculating the apparent power and taking the imaginary part we may obtain the reactive power:

$$\begin{bmatrix} Qs \\ Qr \end{bmatrix} = \frac{3}{2}\begin{bmatrix} u_{ds}i_{qs} - u_{qs}i_{ds} \\ u_{dr}i_{qr} + u_{qr}i_{dr} \end{bmatrix} \quad \text{.....(5.22)}$$

### 5.2.5. Power Control

The purpose of introducing power control is to achieve controllability of both active and reactive stator power and thereby the power factor. In order to investigate the topic of power control and to find essentially control parameters, an analysis of the d-q system is performed and an appropriate reference frame may be chosen.

#### 5.2.5.1. Reference frame for d-q model

With the stator connected to the power supply grid, the stator voltage and frequency may be considered constant and thereby the stator flux may be considered approximately constant. This means that a synchronous rotating reference frame may be advantageous. With a reference frame fixed in the direction of stator flux, the d-q representation simplifies since $\lambda_{qs}=0$ if the q-axis is aligned with the stator flux. This means that the reference frame rotates synchronously at steady state. The reference frame notation is shown in Fig. 5.6.

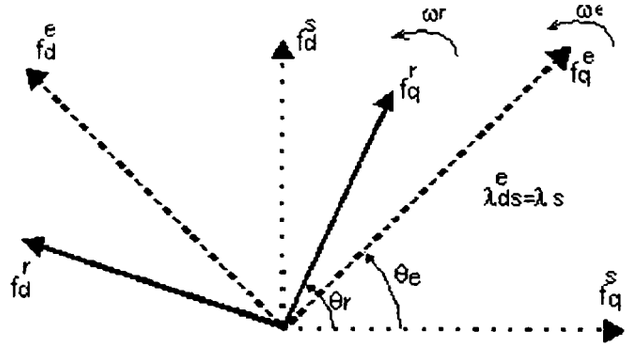


**Figure 5.6.** Reference frame notation used in d-q model for DFIG. $f_d^s, f_q^s$ : stator fixed reference and $f_d^e$, $f_q^e$: stator flux fixed reference [3].

The choice of the reference frame leads to the following important properties:

$$\omega_e = \omega_{ref} \text{ and } \lambda_{qs}=0 \quad \text{.....(5.23)}$$

Where ($\omega_e$) represents the reference frame speed for stationary circuit variables referred to the synchronously rotating reference frame.

### 5.2.5.2. Voltage and flux equations with stator flux fixed reference frame

The dynamic machine equations for voltage and flux in a synchronous rotating reference frame may be expressed as given by equations (5.24)-(5.27) [4]:

$$u_{qs} = R_s i_{qs} + \frac{d\lambda_{qs}}{dt} \quad \text{.....(5.24)}$$

$$u_{ds} = R_s i_{ds} + \omega_e \lambda_{qs} \quad \text{.....(5.25)}$$

$$\lambda_{qs} = L_s i_{qs} + M i_{qr} \quad \text{.....(5.26)}$$

$$\lambda_{ds} = 0 = L_s i_{ds} + M i_{dr} \quad \text{.....(5.27)}$$

### 5.2.6. Power decoupling

To achieve the power decoupling, it means that the active and reactive power may be controlled separately, whereby power factor control may be achieved. By use of the equations (5.24)-(5.27), power control of the DFIG becomes possible. It is important to notice that since the q-axis and the stator flux are aligned and the stator is connected to the supply grid, the flux in the q-axis direction may be considered approximate constant.

The electromagnetic torque and stator active power may be expressed as equations (5.28) and (5.29) respectively ([4], pg.178):

$$Te = -\frac{3}{2}\frac{p}{2}\lambda_{qs} i_{dr} \quad \text{.....(5.28)}$$

$$Pe = -\frac{3}{2}\frac{p}{2}\omega_e \lambda_{qs} i_{dr} \quad \text{.....(5.29)}$$

With $\lambda_{qs}$=constant due to constant stator voltage, electromagnetic torque and the stator active power are controllable via $i_{dr}$. The stator reactive power at the stator side is expressed as equation (5.30):

$$Qs = \frac{3}{2}\frac{p}{2}\left(u_{qs} i_{ds} - u_{ds} i_{qs}\right) \quad \text{.....(5.30)}$$

By substituting equations (5.11) and (5.12) into (5.17) yields:

$$Qs = \frac{3}{2}\frac{p}{2}\omega_e \lambda_{qs} i_{qs} \quad \text{.....(5.31)}$$

From equation 5.31 it is observed, that the stator reactive power is proportional to $i_{qs}$. Rearrangement of the eq. 5.31 shows that the stator q-current is controlled by the rotor q-current as given by (5.32):

$$i_{qs} = \frac{\lambda_{qs} - Mi_{qr}}{L_s} \quad \text{.....(5.32)}$$

Substituting equation (5.31) into equation (5.32) we obtained equation (5.33) for controlling the stator reactive power

$$Qs = \frac{3}{2}\frac{p}{2}\omega_e \lambda_{qs} \frac{\lambda_{qs} - Mi_{qr}}{L_s} \quad \text{.....(5.33)}$$

From equation (5.33) it may be seen that the stator reactive power is controllable via $i_{qr}$.
The above analysis of the DFIG in the d-q system with the q-axis aligned with the stator flux led to the following important properties:

- Stator active power and electromagnetic torque are controlled via $i_{dr}$
- Stator reactive power may be controlled via $i_{qr}$
- By using the power decoupling, stator active and reactive power may be controlled independently.

The knowledge achieved for the control parameters of the DFIG may be summarized as in the Table 5.1:

**Table 5.1.** Control parameters in the d-q system for various control of the DFIG

| ***Control of*** | ***Function of*** |
|---|---|
| Speed [rad / s] | $\omega_m = f(f_{slip})$ |
| Electromagnetic torque [Nm] | $Te = f(i_{dr})$ |
| Active stator power [W] | $Ps = f(i_{dr})$ |
| Reactive stator power [VA] | $Qs = f(i_{qr})$ |

The validity of the model presented before is verified by simulating a step in rotor speed and sample the stator active and reactive power, electromagnetic torque and stator and rotor currents. All simulations are performed with constant DFIG parameters. The DFIG is driven by the drive system at 1125 rpm (sub-synchronous mode-75 % of synchronous speed), and the reference speed is changed at t=2seconds to 1875 rpm (super-synchronous operation mode-125 % of synchronous speed). The speed and torque response are shown in Fig. 5.7 b). The mechanical system is modeled using a first order approximation, where the time constant is determined from a step in rotor speed, more detailed can be found is Appendix $D_2$.

Figures 5.7 a) illustrates the simulated stator active and reactive power of the DFIG as a function of time. The stator active power and stator reactive power are controlled independently, by controlling the rotor currents. If the speed increases so that the machine is operating at super-synchronous speed, the stator active power and electromagnetic torque change direction from the sub-synchronous operation (Fig. 5.7). The rotor and stator currents of the generator during the transition between sub- and super-synchronous operations are shown in Fig. 5.8. As the rotor speed increases, the stator and rotor currents become larger. The transition between sub- and super-synchronous speeds is also reflected in the rotor currents flow, as depicted in Fig. 5.8 a).

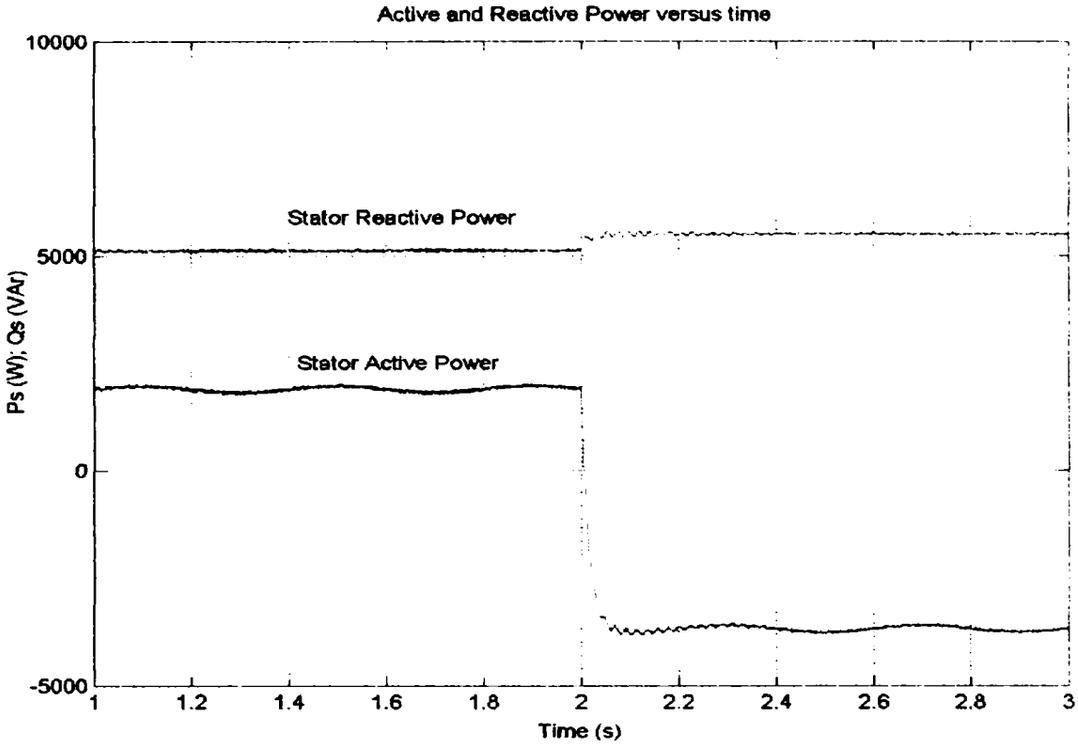


a)

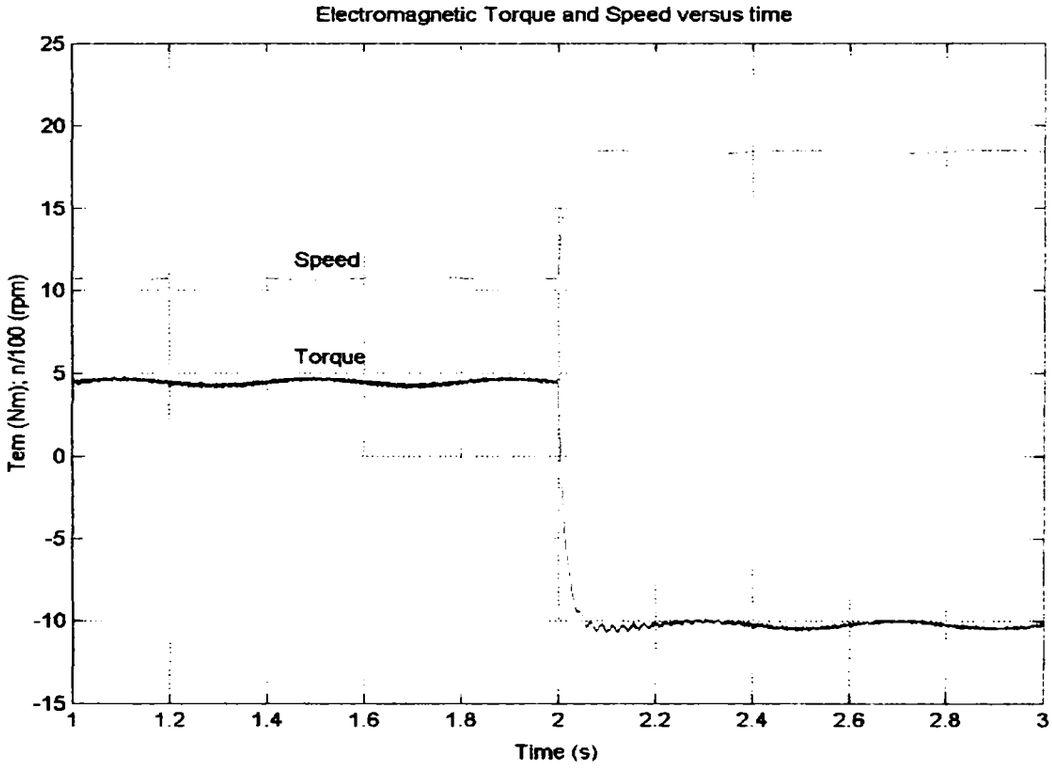


b)

**Figure 5.7**. Simulation of the stator active and reactive power (a) and electromagnetic torque and speed (b) as a function of time. The speed reference of the drive system is changed at t=2 s from 1125 rpm to 1875 rpm.

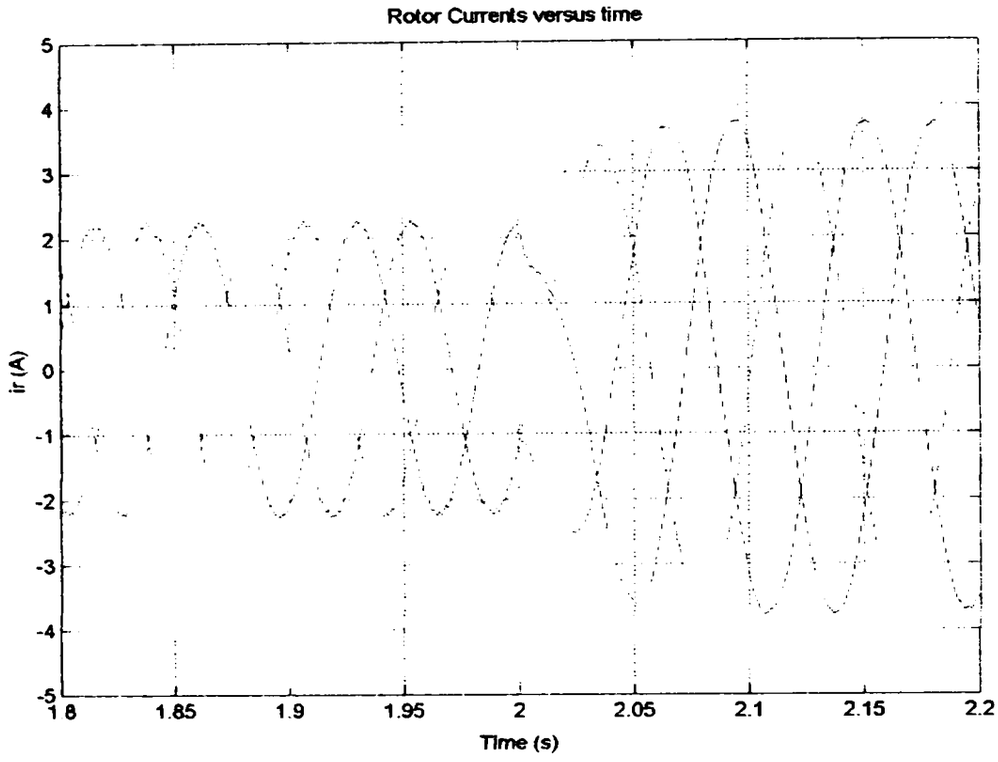


a)

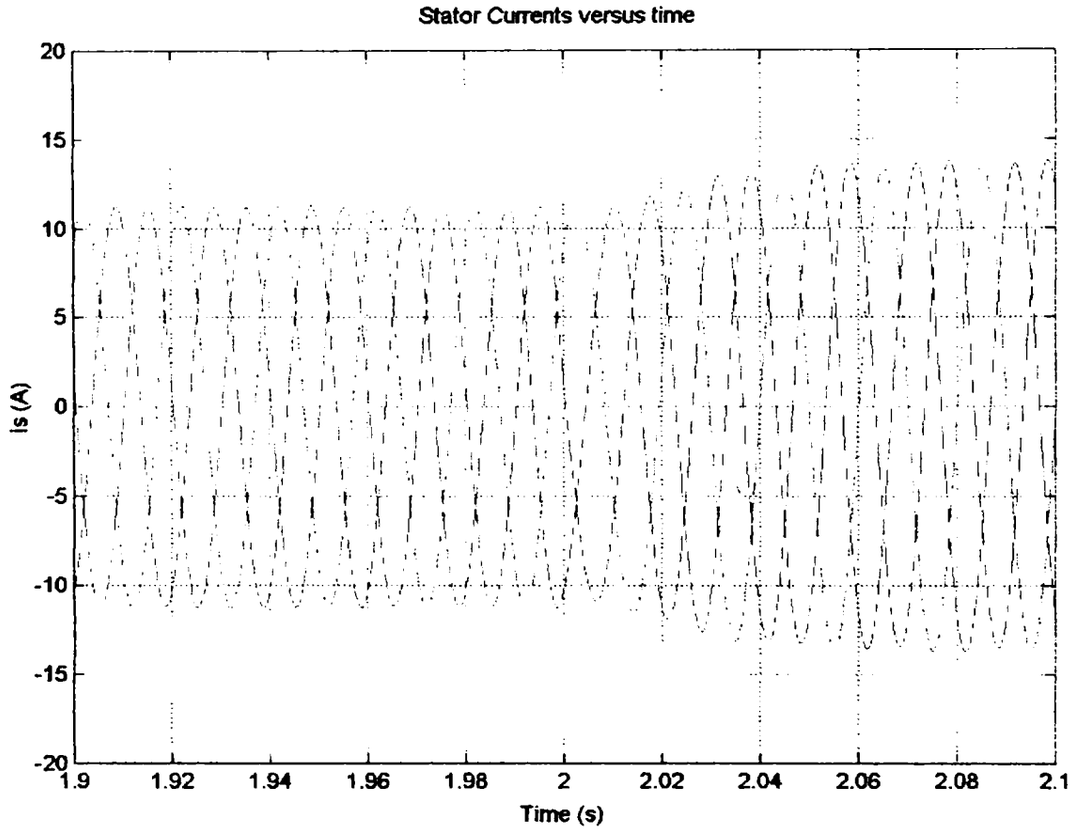


b)

**Figure 5.8.** Simulated stator (b) and rotor (a) currents during the transition from sub-synchronous speed (1125 rpm) to super-synchronous speed (1875 rpm) operation mode.

## 5.3. The rotor converter model

This section contains the development of the rotor converter model, for use during development of the control strategy. Various modulation strategies are presented. Two different models could be developed, an average value model and a non-linear model. It is found that the simplest model, the average value model, gains satisfactory results. Therefore it will be used in the control scheme simulations. Both switch models and modulation strategy are implemented in Matlab-Simulink. More details about the implementation can be found in Appendix D.

For simulating the complete system of wind generator a model of rotor converter is required. The converter is a three-phase four-quadrant converter because bi-directional power-flow of the rotor of the DFIG is required for obtaining full control of the stator power (output power). The structure of the rotor converter is shown in Fig. 5.9.

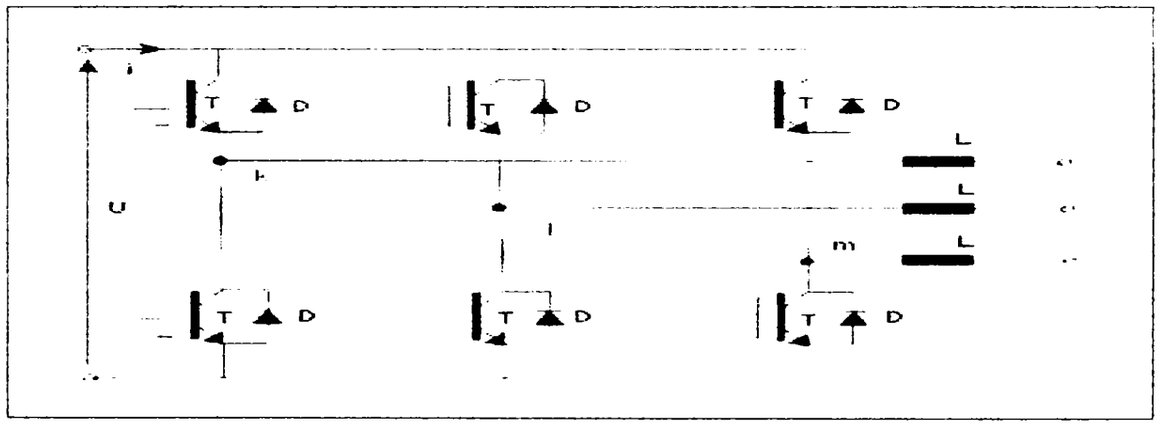

**Figure 5.9.** General structure of the rotor converter.

As may be seen in Fig. 5.9 the converter has six switches and six freewheeling diodes. Each switching element is composed of two parallel-aligned IGBTs and freewheeling diodes for obtaining the appropriate power level. A Digital Signal Processor (DSP) controls the rotor converter. An external timer circuit is used for generating PWM signals required for controlling the gates of IGBTs. The structure of the control is illustrated in Fig. 5.10.

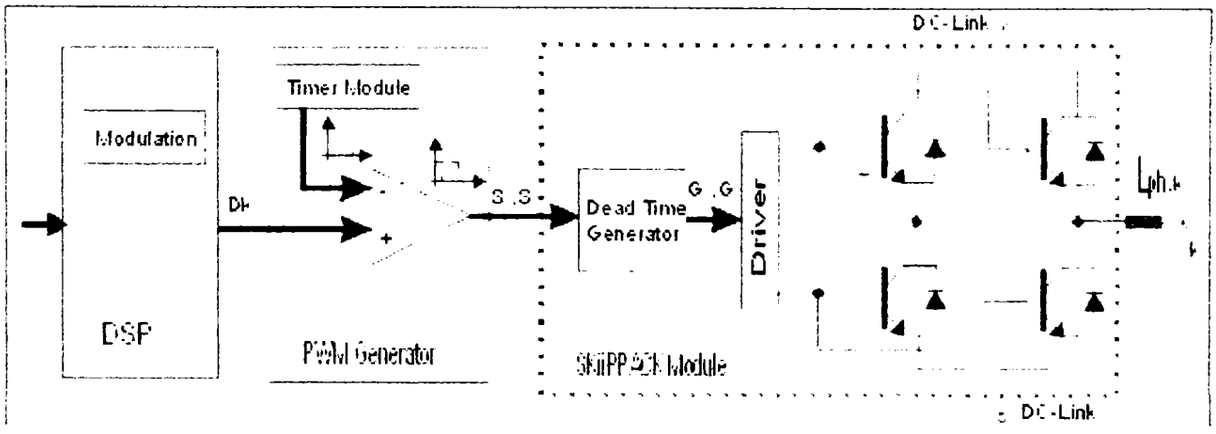


**Figure 5.10**. Schematic illustration of the control structure of the rotor converter for one branch.

The control signals $D_{1\text{-}6}$ are generated by the modulation function, which is implemented in the DSP. The DSP generates the PWM reference signals ($S_1$, $S_2$) on basis of the implemented modulation strategy. The DSP generates the PWM reference signals at 5 kHz switching frequency. The reference signals determine the fundamental rotor frequency and the voltage amplitude.

### 5.3.1. Model implementation

The models set up in the following sections are to be implemented in Simulink.
The converter model is a linear average model. The average model does not model timing blanking time and parasitic elements of the gate signals, but model the outputs of the DC-link voltage times and the duty cycle of each switch.

A modulation strategy is required for generating the desired PWM-pattern in order to optimize the performance of the converter and the control of DFIG.

### 5.3.2. Modulation strategy

For generating the rotor voltages, a PWM strategy is required. Ideally the converter should generate a sinusoidal voltage with no harmonic contents. This is however not possible by use of PWM converters, such as the rotor converter.
For modulation of the output voltage of the flux polygon, the circuit configuration of the rotor converter leaves six active and two zero voltage vectors to be applied to the DFIG.

If the rotor flux is not sinusoidal, a torque ripple is generated resulting in a pulsating stator power. Therefore the torque ripple has to be minimized. As the torque is proportional with $|\lambda_s|*|\lambda_r|*\sin\delta$, where δ is the angle between, $|\lambda_s|$ and $|\lambda_r|$ are the lengths of the stator and rotor flux vectors respectively. The angle and amplitude error of the rotor flux vector has to be minimized. An error in amplitude may generate acoustic noise and an error in angle may generate torque ripple. More details can be found in *Appendix D2*.

#### 5.3.2.1. Requirements of the PWM-strategy

The following requirements of the modulation strategy are stated in order to optimize the performance of the converter and control of the DFIG [9, 24, 25].

- The fundamental frequency of the modulated sinusoidal voltage may be changed from 0-20 Hz;
- A low harmonic content of the rotor voltage is required for reducing torque pulsations, which may influence the stator active and reactive power;
- The number of branch-switch-over should be minimized in order to increase the efficiency of the converter since the switching losses are proportional to the number of switching and the switching frequency;
- The used modulation strategy should be able to yield a torque response faster than the required response of the stator power control;
- The produced torque ripple should be negligible compared to the moment of inertia of the system, no speed ripple should occur;

- The modulation strategy must be simple to reduce the number of real-time calculations in order to minimize the required processor power, and the delay from sampling to control action.

#### 5.3.2.2. Overview of the PWM Strategies

Different PWM-strategies have different properties. However, two basic types of strategies may be defined: feedback (closed loop) PWM and feed forward (open loop) PWM. A comparison of the basic properties of the two strategies may be summarized [25].

*Closed Loop Current Control PWM*

- Direct control of the output current
- Good for repetitive speed reversal
- Operates with small steady state error for space vector amplitude and angle
- Requires current sensors
- Requires current reference
- Normally implemented with hysteresis controllers
- Usually the switching frequency is variable due to hysteresis control

*Open Loop Voltage Control PWM*

- The converter operates as a VSI
- Controls the output voltage of the converter
- Suitable for variable torque operation, due to high bandwidth of the torque control
- Low switching frequency may be used
- No sensors are required
- Needs voltage reference
- May be implemented using Carrier wave or Space-Vector PWM
- The switching frequency is constant

Since the rotor converter is built as a PWM-VSI, an open loop voltage control PWM-strategy is chosen. Two basic principles are available for open-loop PWM control, the Carrier wave or space vector PWM strategies. The Carrier wave PWM modulates the output voltage from the converter based on a modulating function, whereas the Space Vector Modulation (SVM) PWM modulates the flux polygon of the machine. For optimal tracking of the flux polygon, the SVM strategy scheme is necessary. The Stator Flux Asynchronous Vector Modulation (SFAVM) strategy meets most of the requirements to achieve the control strategy for controlling the stator active and reactive power based on the power decoupling [9-14]. Therefore, this PWM strategy is chosen for implementation.

#### 5.3.2.3. Stator Flux Asynchronous Vector Modulation

For modulating the output voltage of the rotor converter and thereby controlling the rotor current, the SFAVM strategy is chosen. The basic idea of the strategy is to track the reference voltage by applying two active and two zero vectors two times in each switching period.

The flux in DFIG has to trace a circle in the complex plane, and a change from one position to another may be performed in a number of different ways using different number of

Branch-Switch-Over (BSO). During each switch period, turn-on and turn-off two BSO, the flux may be changed from one voltage vector to any of the neighboring voltage vectors. This means, that there are six BSO of each switching period.

The problem of the SFAVM is then reduced to the calculation of the time each voltage vector should be applied ($t_0$, $t_1$ and $t_2$).

The most significant properties of the SFAVM modulation strategy may be summarized as follows:

- Asynchronous modulation with constant switching frequency is obtained. This means, that the modulation is independent of the fundamental frequency;
- The flux vector is moved two times during each switching period. The total number of BSO per switching period is six;
- The angle error of the flux vector is minimized by applying the two zero vectors at the start and end of each switching period;
- The amplitude error of flux vector is not controlled directly during each transition, but since only the two neighboring voltage vectors are applied, the amplitude error is moderate ;
- The voltage vectors may be changed from one hexagon to any others from one switching period to another, since switching period starts and ends with a zero voltage vector;
- Compared with standard sinusoidal modulation with 3rd harmonic injection, the SFAVM approach yields up to (10-15) % smaller torque ripple depend on the fundamental frequency [9].

The SFAVM algorithm is implemented in Simulink, by use of a look-up table, for simulation of the rotor converter in the control system and in the control program *DFIG.c* for controlling the rotor converter of the system. The SFAVM algorithm is implemented as a function and is written in the programming language C and then is mixed for use in Matlab-Simulink (Appendix $D_3$).

For rated operation of the DFIG, the amplitude of the modulated voltage should be equal with the DC-link voltage. This means, that the gain of the modulating function should be equal with one. The maximum gain is given for a modulation index of one (m=1) and no zero voltage vectors are applied ($T_{sw} = t_1+t_2$). From these properties, the gain of the modulation strategy may be calculated to be equal with one.

### 5.3.2.4. Average Value Rotor Converter Model

When modeling the converter by means of an average value model (AVM), the parasitic elements of IGBT and freewheeling diodes are ignored. The required control signals for the average value model are $D_k$, $D_l$ and $D_m$. The structure of the average value model for phase k is shown in Fig. 5.11:

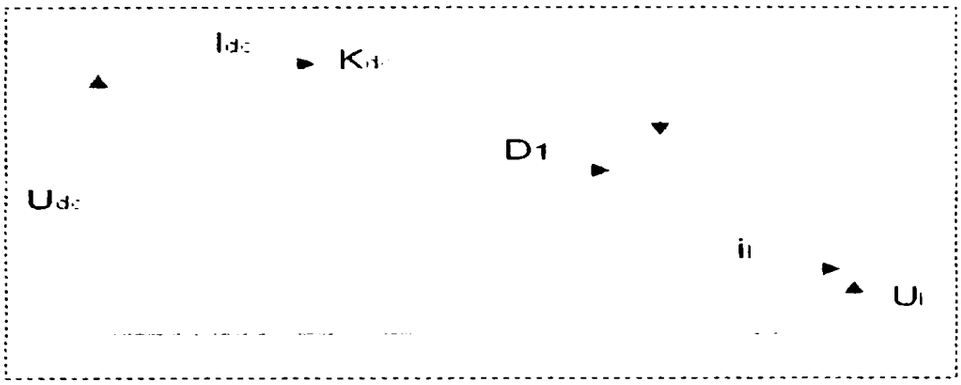


**Figure 5.11.** General structure of the average value model. The illustration shows the model of phase k.

As may be seen in Fig. 5.11, the required input signals for AVM are the reference signals $D_1$, $D_3$ and $D_5$ and the DC-link voltage $U_{DC}$. The output of the model is the phase voltages ($U_k$, $U_l$ and $U_m$) with respect to zero of the DC-link.

Similar structure is required for phase l and m. As may be seen in Fig. 5.11 the average model the voltage of phase k may be written as in (5.34).

$$U_k=U_{dc}*K_{dc}*D_k \quad \text{.....(5.34.)}$$

The constant $K_{dc}$ is applied for scaling the voltage compensating for threshold voltage and voltage drop due to inner resistance of switch and freewheeling diode. As the voltage drop due to inner resistance depends on the rotor current, the AVM is not able to model correct voltages. The constant $K_{dc}$ is scaled for modeling correct voltages at nominal load. The value of $K_{dc}$ is found to equal 0.926. As the modeled voltage is equal to D times $U_{dc}$, the modeled harmonic content is lower than the harmonic content of the real converter and the harmonic content of the non-linear model. The model is implemented in Simulink as can be seen in Fig. 5.12:

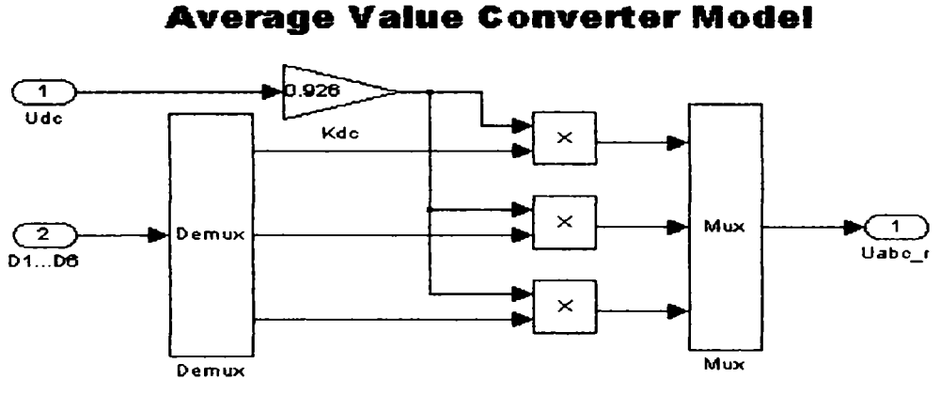


**Figure 5.12.** Average value model of the rotor converter implemented in Simulink.

The modeled rotor voltages are phase voltages with reference to zero of the DC-link. The constant $K_{DC}$ is adjusting for modeling correct voltages at nominal load, the value of $K_{DC}$ is found to be equal with 0.926.

## 5.4. Control Strategy

The main goal of this subchapter is the analysis and implementation of a control scheme for a DFIG in order to achieve the control of output power. The output power must be kept constant during a change in mechanical speed (wind speed). In addition independent control of the active and reactive power must be achieved for obtaining reduced power fluctuations.

The aim of the control strategy is to meet the demands regarding performance and robustness.

The power performance requirements are stated as follows:

- The active power output is to be constant at variable speed operation
- Minimize power fluctuations into the power grid
- The proposed control scheme has to include power factor control
- Higher efficiency may be expected by utilizing the rotor current control by means of a converter in the rotor circuit

The robustness performance requirements must be met under the following conditions:

- Variable rotor speed in the range of 65 % and 140 % of nominal speed
- Robustness against power grid frequency variation in the range of ± 4 % of nominal frequency
- Robustness against power grid voltage variations in the range of ± 10 % of nominal power grid voltage
- It must be robust against unsymmetrical power grid voltages of ± 4 % regarding phase voltages.

The control strategy for controlling the stator active and reactive power is based on the power decoupling described in section 5.2.4. It means that the stator active and reactive power feedback loops are required. The stator and rotor currents and the stator voltages are measured and transformed to the two-phase reference frame with the stator flux as reference axis.

### 5.4.1. Reference Frame Notation

For controlling the DFIG, an appropriate reference frame has to be chosen. As described in section 5.2.4 decoupling of the stator active and reactive power becomes simple if the stator flux is chosen as reference. Therefore, the control strategy is developed in the reference frame with the d-axis aligned along the flux. The relations between the different reference frames are shown in Fig. 5.13:

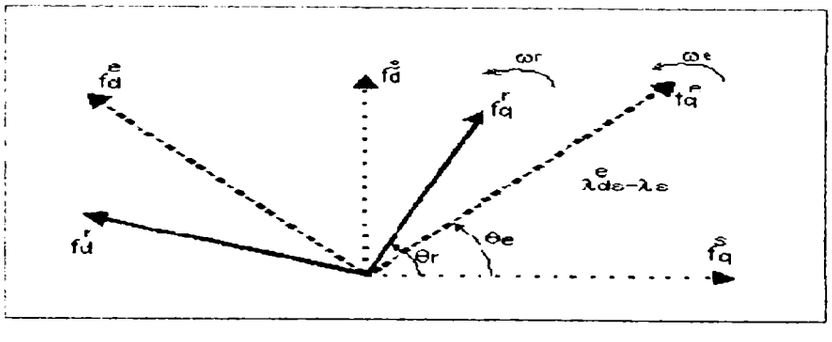


**Figure 5.13.** Illustration of the different reference frame to be used in the control strategy. $f_d^s$, $f_q^s$ : stator fixed reference. $f_d^e$, $f_q^e$: stator flux fixed reference and $f_d^r$, $f_q^r$: reference frame fixed to the rotor using electrical angular speed and angle. The power decoupling is performed using the stator flux fixed reference frame.

As shown in Fig. 5.13, three different reference frames are used in the control strategy. The control strategy is developed in the stator flux fixed reference frame. The input from the stator is in the stator fixed reference frame and rotor input in the rotor fixed reference frame. Rotor voltage output is in the rotor fixed reference frame.

### 5.4.2. Control Strategy

The control system should contain the following components in order to achieved full controllability of the stator power:

- Transformation of the measured stator voltages and currents into the stator fixed reference frame
- Calculation of active and reactive power as well as stator flux in the stator fixed reference frame
- Calculation of the stator flux position to obtain the angle of the stator flux fixed reference frame ($\theta_s$)
- Regulators for controlling the stator active and reactive power
- Calculation of the desired rotor d- and q-axis currents by use of the power decoupling equations
- Transformation of the measured rotor currents into the stator flux fixed reference frame
- Regulators for controlling the rotor currents
- Implementation of the required voltages for obtaining the desired rotor currents
- Implementation of the rotor voltages from the stator flux fixed reference frame to the rotor fixed reference frame
- Calculation of the duty-cycles for the three-phases by use of SFAVM.

To simulate the DFIG, the system shown in Fig. 5.14 will be used. Good results using this scheme are presented by [12, 19, 20 and 22].

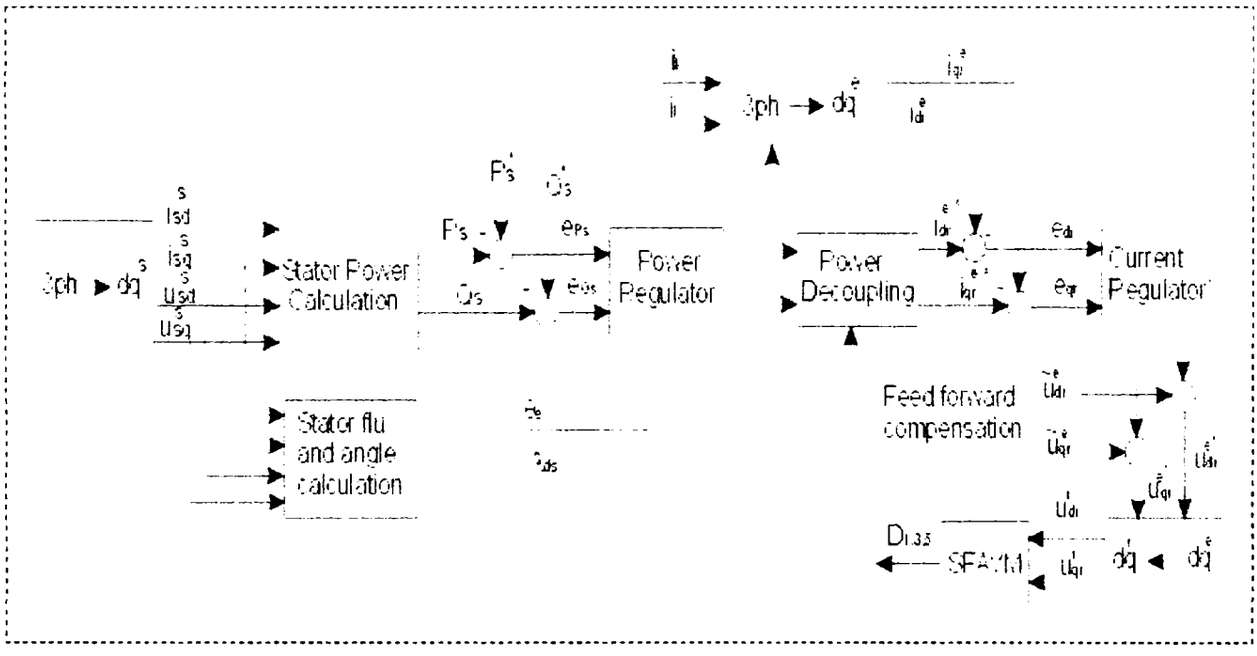


**Figure 5.14.** Proposed control scheme with measurement of stator voltage and stator and rotor currents. The rotor d-and q- axis are compensated by use of feed-forward loop.

The control scheme consists of two control loops: an inner loop for controlling the rotor current, and an outer loop for controlling the stator active and reactive power.
The stator voltages and currents are measured in the stator fixed reference frame. In addition, the stator active and reactive power is calculated in the stator fixed reference frame. From the stator quantities, the stator flux is calculated, and the amplitude and angle of the resulting stator flux is found.

The measured stator power (Ps, Qs) is compared to the power references ($Ps^*$, $Qs^*$), and the errors ($e_{Ps}$, $e_{Qs}$) are fed to the power regulator. From the power regulator the reference values of rotor d- and q-currents are calculated using power decoupling. The reference values of rotor currents are compared to the rotor currents measured in the rotor fixed reference frame and transformed to the stator flux fixed reference frame, and the errors are fed to the current regulators. After the current regulator, feed forward compensation is used for decoupling rotor voltages and currents and then the reference values of rotor voltages are transferred to the rotor fixed reference frame and fed to the SFAVM modulator.

### 5.4.2.1. Stator Flux and Angle Calculation

From the stator voltage and current, the position of the stator flux fixed reference frame is determined.
For determining the position of the stator flux, the two-phase stator voltages are integrated. The stator d-and q-flux vectors are determined in the stator fixed reference frame as given by equations 5.35 [4].

$$\lambda_{ds}^{\ s} = \int \left(u_{ds}^{\ s} - R_s \cdot i_{ds}^{\ s}\right) \cdot dt$$
$$\lambda_{qs}^{\ s} = \int \left(u_{qs}^{\ s} - R_s \cdot i_{qs}^{\ s}\right) \cdot dt \quad \text{.....(5.35)}$$

The stator flux is used as reference, as described in section 5.2.4, the resulting stator flux is determined by equation (5.36) and the reference angle by equation (5.37). The speed of the reference frame is then determined by equation (5.38).

$$\lambda_s = \lambda_{qs}^{\ e} = \sqrt{\lambda_{ds}^{\ s^2} + \lambda_{qs}^{\ s^2}} \quad \text{.....(5.36)}$$

$$\theta_e = \arctan\left(\frac{-\lambda_{ds}^{\ s}}{\lambda_{qs}^{\ e}}\right) \text{ for } \lambda_{qs}^{\ e} \neq 0 \quad \text{.....(5.37)}$$

$$\omega_e = \frac{d\theta_e}{dt} \quad \text{.....(5.38)}$$

Care has to be taken when calculating the reference angle ($\theta_e$) since the output of the *arctan* function is not unique. The following expression may be used for determining the correct angle:

$$\text{If } \lambda_{qs}{}^{e} > 0 \text{ whereupon } \theta_e = \arctan\left(\frac{-\lambda_{ds}{}^{s}}{\lambda_{qs}{}^{e}}\right) \quad \text{.....(5.39)}$$

$$\text{If } \lambda_{qs}{}^{e} < 0 \text{ whereupon } \theta_e = \arctan\left(\frac{-\lambda_{ds}{}^{s}}{\lambda_{qs}{}^{e}}\right) + \pi \quad \text{.....(5.40)}$$

The stator flux in the stator fixed reference frame varies sinusoidal with the stator frequency. As the stator flux is calculated by use of integration, the flux may contain an offset. Therefore, the stator flux may be filtered eliminating the offset error.

### 5.4.2.2. Stator Power Calculation

Since the power is independent of the choice of reference frame, the calculation of stator power may be performed in any reference frame. If the stator power is calculated in the stator fixed reference frame, the number of transformations to be performed may be minimized. The stator power is calculated using equations (5.41) and (5.42):

$$Ps = \frac{3}{2} * \left(u_{ds}{}^{s} i_{ds}{}^{s} + u_{qs}{}^{s} i_{qs}{}^{s}\right) \quad \text{.....(5.41)}$$

$$Qs = \frac{3}{2} * \left(u_{ds}{}^{s} i_{qs}{}^{s} - u_{qs}{}^{s} i_{ds}{}^{s}\right) \quad \text{.....(5.42)}$$

The measured stator power is compared to the reference values of Ps and Qs, and the error signals are fed to the power regulator.

### 5.4.2.3. Power Decoupling

If the stator flux fixed reference frame, the d-axis stator flux is equal with zero and the stator active and reactive power may be expressed as in equations (5.43) and (5.44):

$$Ps = -\frac{3}{2} \cdot \frac{p}{2} \cdot \omega_e \cdot \lambda_{qs}{}^{e} \cdot i_{dr}{}^{e} \quad \text{.....(5.43)}$$

$$Qs = \frac{3}{2} \cdot \frac{p}{2} \cdot \omega_e \cdot \lambda_{qs}{}^{e} \cdot \frac{\lambda_{qs}{}^{e} - M \cdot i_{qr}{}^{e}}{L_s} \quad \text{.....(5.44)}$$

As can be seen in equations 5.43 and 5.44 power decoupling may be obtained by controlling the rotor d- and q-currents. This means that power decoupling is obtained by simply applying to the power rotor regulator output as a reference to the rotor current loop. The output from the power decoupling is the rotor d- and q-current references.

### 5.4.2.4. Rotor Current Controllability

The rotor currents are to be controlled by controlling the rotor voltages. The rotor voltages equations are given by:

$$u_{qr}^{e} = R_r \cdot i_{qr} + M \cdot \frac{di_{qs}^{e}}{dt} + L_r \cdot \frac{di_{qr}^{e}}{dt} + (\omega_e - \omega_r) \cdot M \cdot i_{ds}^{e} + (\omega_e - \omega_r) \cdot L_r \cdot i_{dr}^{e} \quad \text{.....(5.45)}$$

$$u_{dr}^{e} = R_r \cdot i_{dr} + M \cdot \frac{di_{ds}^{e}}{dt} + L_r \cdot \frac{di_{dr}^{e}}{dt} - (\omega_e - \omega_r) \cdot M \cdot i_{qs}^{e} - (\omega_e - \omega_r) \cdot L_r \cdot i_{qr}^{e} \quad \text{.....(5.46)}$$

As may be seen from equations (5.45) and (5.46) the rotor current control via the rotor voltages is complex, since the desired coupling between the rotor axis and the rotor and stator axis is present. For example, the rotor d-voltages depend on both the rotor q-current, and the stator d- and q-currents. This means that a change in rotor d-voltage for changing the rotor d-current will affect the rotor q-voltage and thereby the rotor d- and q-currents. For improving the rotor current control, a decoupling network may be introduced. The decoupling may be performed using feed forward compensation [Vas, 1998, pg. 344], [Tnami, 1995, pg. 553].

### 5.4.2.5. Feed Forward Compensation

The main idea of using feed forward compensation is to add the coupling terms in equations (5.45) and (5.46) after the current regulator as shown in Fig. 5.23. Thereby, the coupling between the axes may be eliminated. For obtaining better controllability of the rotor current by use of the rotor voltages, eq. (5.45) and (5.46) may be written using the equivalent circuits for the d- and q-axis. The rotor voltages in Laplace notation are given by equations (5.47) and (5.48):

$$u_{qr}^{e} = \left[ (R_r + s \cdot L_r) - \frac{s^2 \cdot M^2}{R_s + s \cdot L_s} \right] * i_{qr}^{e} + s \cdot M \frac{u_{qs}^{e} - \omega_{syn} \cdot \lambda_{ds}}{R_s + s \cdot L_s} + (\omega_e - \omega_r) \cdot \lambda_{dr}^{e} \quad \text{.....(5.47)}$$

$$\text{Where } \lambda_{dr}^{e} = L_r i_{dr}^{e} + M i_{sd}^{e}$$

$$u_{dr}^{e} = \left[ (R_r + s \cdot L_r) - \frac{s^2 \cdot M^2}{R_s + s \cdot L_s} \right] * i_{dr}^{e} + s \cdot M \frac{u_{ds}^{e} - \omega_{syn} \cdot \lambda_{qs}}{R_s + s \cdot L_s} - (\omega_e - \omega_r) \cdot \lambda_{qr}^{e} \quad \text{.....(5.48)}$$

$$\text{Where } \lambda_{qr}^{e} = L_r i_{qr}^{e} + M i_{sq}^{e}$$

The couplings terms in equations (5.47) and (5.48) are fed to the control loop as it is depicted in Fig. 5.15:

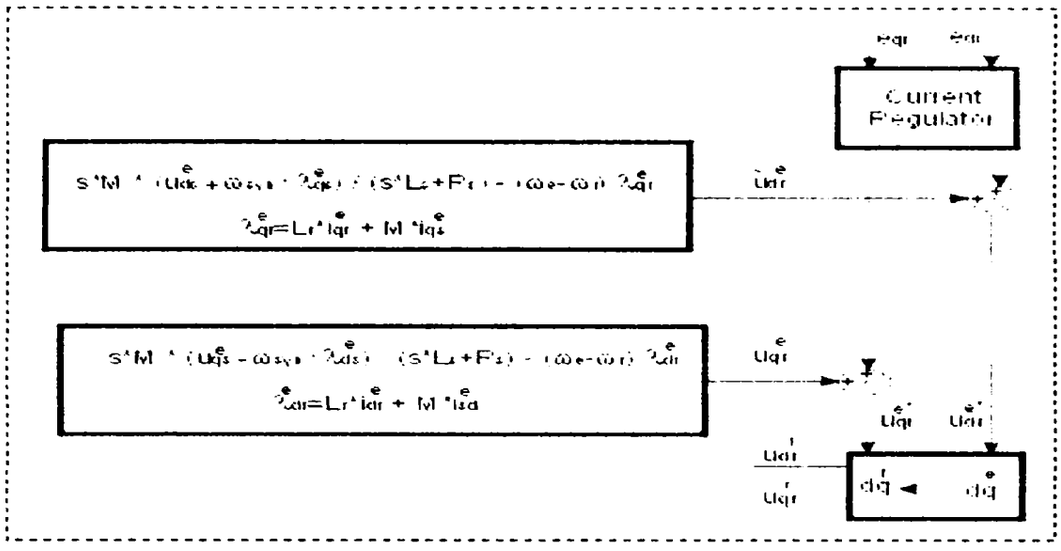


**Figure 5.15.** Illustration of the proposed feed forward decoupling of the rotor currents and voltages. The output from the current regulator is compensated by adding the coupling terms in the rotor voltage equations.

The transfer function for the current loop may be found from equations (5.47) and (5.48) as will be shortly describe in the follows:

The rotor voltages may control the rotor currents by use of feed forward. The undesired couplings between the rotor axes and the rotor and stator axis are decoupled adding signals equivalent to the coupling terms in the voltage equations.

The transfer function of the current loop is shown in Fig. 5.16:

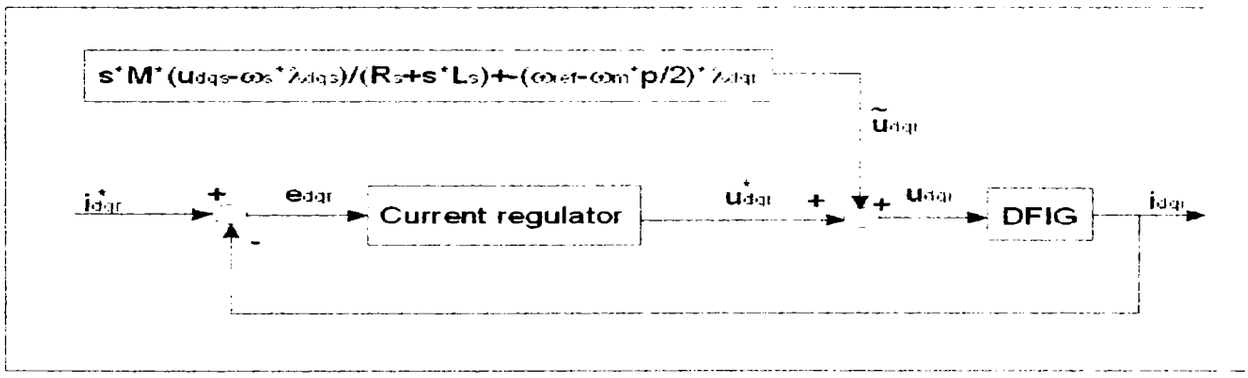


**Figure5.16.** Illustration of the current control loop and the feed forward signal. The decoupling effect gives a linear relation between the rotor voltage and current.

The advantage of the feed forward compensation is the decoupling of the rotor voltages and currents. The transfer function may be written as in equation (5.49):

$$G_i(s) = \frac{i_{dqr}}{u_{dqr}^*} = \left( \frac{R_s + s \cdot L_s}{(R_r + s \cdot L_r) \cdot (R_s + s \cdot L_s) - s^2 \cdot M^2} \right) = \quad \text{.....(5.49)}$$

$$= \frac{R_s + s \cdot L_s}{s^2 \cdot (L_r \cdot L_s - M^2) + s \cdot (L_s \cdot R_r + L_r \cdot R_s) + R_r \cdot R_s}$$

The couplings terms described by equations (5.47) and (5.48) are transferred to the z-plane using ZOH [Franklin, 1990, pg. 419]. In this way we obtain the equations that will be implemented in the control program:

$$u_{qr} = \frac{z-1}{z-e^{-\frac{R_s}{L_s}}} * \frac{M*\left(u_{qs}{}^{e} - \omega_e * \lambda_{ds}{}^{e}\right)}{L_s} + \left(\omega_e - \omega_r\right)* \lambda_{dr}{}^{e} \quad \text{.....(5.50)}$$

$$u_{dr} = \frac{z-1}{z-e^{-\frac{R_s}{L_s}}} * \frac{M*\left(u_{ds}{}^{e} + \omega_e * \lambda_{qs}{}^{e}\right)}{L_s} - \left(\omega_e - \omega_r\right)* \lambda_{qr}{}^{e} \quad \text{.....(5.51)}$$

### 5.4.2.6. Control Scheme

The stator active and reactive power control is to be implemented as a cascade control with an inner rotor current loop and an outer power control loop. The proposed control scheme shown in Fig. 5.14 may be simplified assuming an ideal decoupling between the rotor currents. The simplified control scheme is presented in Fig. 5.17:

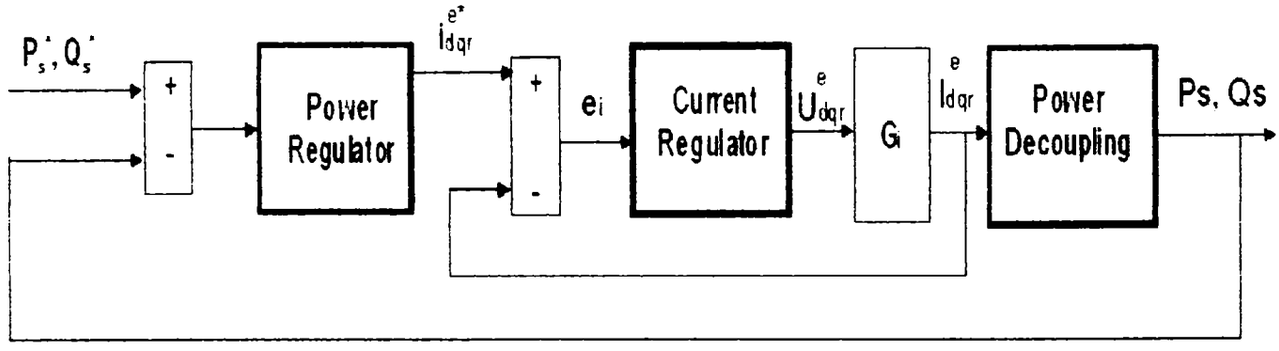


**Figure 5.17.** Simplified control scheme with an inner rotor current control loop, and an outer power control loop. Full decoupling between rotor currents is assumed.

The control scheme is implemented as shown in Fig. 5.17. The current regulator is designed and the closed loop transfer function (Gi) for the current loop is found. The power regulator is also designed and the closed loop performance of the power loop is evaluated.

### 5.4.3. Regulator Types

For controlling the stator power, rotor power and current regulators are required as indicated in Fig. 5.17. Different types of regulators may be implemented, and the best-suited type for control scheme should be chosen. Therefore, the properties of different types of regulators are shortly discussed.

#### 5.4.3.1. Classic Regulators

Classic regulators such as PI, Lag/lead networks or polynomial regulators may be used in the current loops. The advantage of these controllers is standard design methods such as Ziegler-Nicholas tuning, root locus and Nyquist plots. Hysteresis regulators [23] that are simple and robust in design, may be used, but the switching frequency may be variable, and for obtaining the same performance as the classic linear regulators the switching frequency has to be increased. In addition the output will contain small oscillations.

The disadvantages of the classic regulators are constant regulator parameters and the lack of adaptation. Good performance may however be obtained by means of feedback, since parameter variations and non-linearity's are minimized [Ogata, 1992, pg. 225]

#### 5.4.3.2. Choice of Regulator Type

Based on the forgoing sections presenting different types of regulators and their advantages and disadvantages, an appropriate regulator type may be chosen. The type of regulator to be used should have the following properties:

- Should be able to control systems with varying parameters since the rotor resistance varies with temperature and frequency, and the inductances vary with frequency due to skin effect and with current due to saturation. The rotor current variation is however small, and the effect of parameter variation may be small.
- The regulators should be able to stabilize the system at the desired output response concerning rise time, overshoot etc.
- The regulator structure and algorithm should be simple since the control scheme is implemented using real-time calculations.

## 5.5. Regulators Design

This subchapter deals with the analysis and design of the current and power loop of the control scheme presented in subchapter 5.4. The current loop is analyzed, and an appropriate current controller is chosen. The control loop for the stator power is designed and simulated in order to evaluate performance.

### 5.5.1. Current Control Loop

As describe in subchapter 5.4 the control scheme is to be realized using cascade control. This means that the inner current loop is used for controlling the rotor d- and q-currents and an outer loop is used for controlling the stator active and reactive power.

The complete control scheme including both the inner current loop and the outer power loop are shown in Fig. 5.14.

The current loop may be visualized as the schematic diagram in Fig. 5.18:

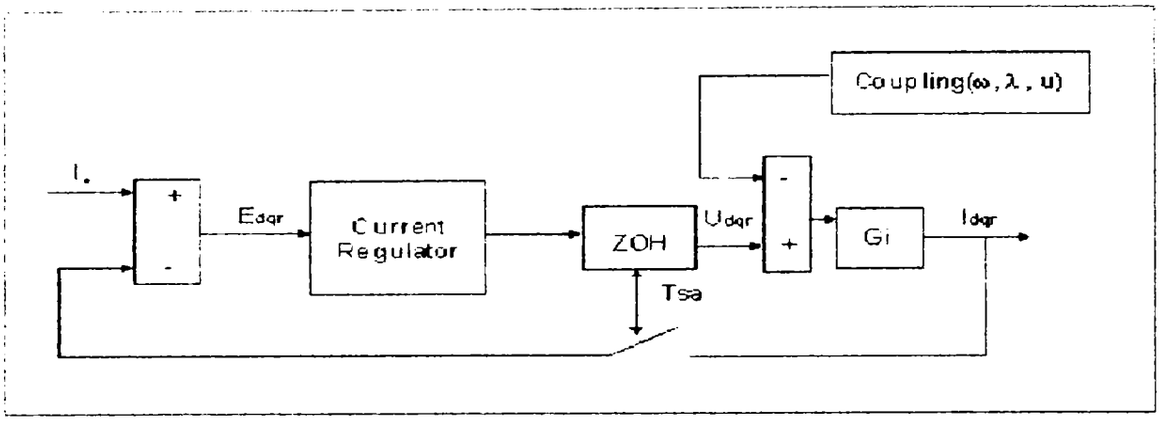


**Figure 5.18.** Schematic diagram of the rotor current loop. The coupling function, coupling (ω, λ, u), represents the coupling terms between the stator and rotor, and d- and q-axis in DFIG. A ZOH-network is inserted after the current regulator, and an AD-converter is inserted in the feedback loop as in the test system. $T_{sa}$ is the sampling time.

As may be seen in the schematic diagram of the rotor current loop (Fig. 5.18), the rotor current coupled with the stator current of the DFIG. This is undesired when controlling the rotor currents due to change in magnetization speed and current level of the other axis invokes non-linearly on the current to be controlled.

An analysis of the current loop is performed for implementing an appropriate control strategy. The analysis of the rotor current is derived into 2 parts:

- An analysis of the ideal rotor current loop is performed. Ideal current loop means, that the feed forward compensates out the coupling between the d- and q-axis in the DFIG
- An analysis of the impact of the parameter variations on the current loop. Stability and performance are taken into consideration.

### 5.5.1.1. Ideal Rotor Current Loop

The analysis of the ideal current loop is performed for determining the optimal dynamic performance of the rotor current loop. Feed forward compensation is used for decoupling the current loop. The feed forward element is to be calculated each time step of the control loop. The rotor ideal current loop is shown in Fig. 5.19:

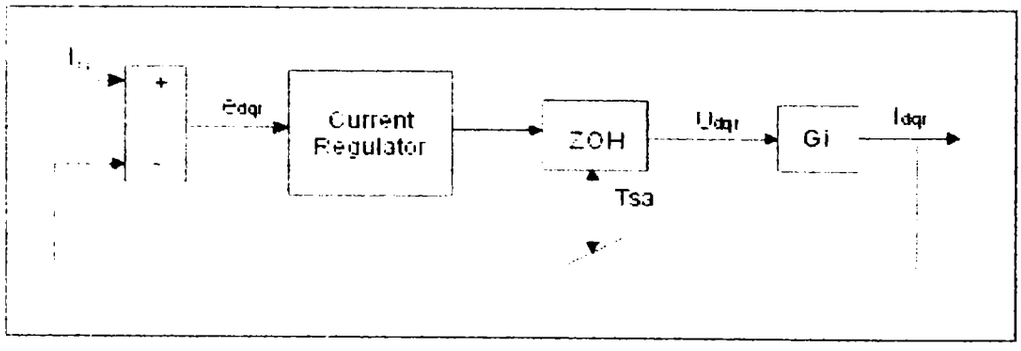


**Figure 5.19.** Schematic diagram of the ideal rotor current loop. It is assumed that the feed forward compensation come out the coupling terms in the DFIG.

To achieve full decoupling, the rotor current transfer function may be expressed by Gi:

$$G_i(s) = \frac{i^e_{dqr}}{u^e_{dqr}} = \frac{s \cdot L_s + R_s}{\left(L_r L_s - M^2\right) \cdot s^2 + \left(L_s R_r + L_r R_s\right) \cdot s + R_r R_s} = \frac{19.05 \cdot (s + 6.83)}{(s + 257) \cdot (s + 3.69)} \quad \text{.....(5.52)}$$

The ideal continuous rotor current transfer function is transferred to the z-plane by use of step invariant transformation using the *Matlab c2dm* function. The discrete transfer function is written in equation (5.53):

$$G_i(z) = \frac{3.842 * 10^{-3}(z-1)}{z^2 - 1.947 * z + 0.947} = \frac{3.842 * 10^{-3}(z-1)}{(z+1) * (z+0.947)} \quad \text{.....(5.53)}$$

It may be noted that the two poles of the continuous transfer function are very different, $s_1$=-257, $s_2$=-3.69. The zero is placed at s=-6.83. This may be explained by examining the electrical equivalent diagram of the DFIG. The rotor current is branched in two, the first part flow through the magnetizing inductance and the second part flow through the stator branch into the power grid. The magnetizing inductance plus the rotor leakage inductance corresponds to a time constant of 119 ms. The time constant of rotor to stator branch is 3.7 ms.

### 5.5.1.2. Current Regulator Design

A closed loop regulator is to be designed. As stated, the rise time should be less than 2 ms. The power control loop may compensate for the error by increasing the reference to the current loop. The current control loop is critical for achieving the desired power control of the DFIG.

*Current Loop Design with P-Regulator*

It is chosen to use a P-regulator due to the capability of a fast response. The proportional current regulator is included in the open loop transfer function of the rotor current as it is shown in equation (5.54):

$$G_{reg}(z) \cdot G_i(z) = \underbrace{K_i}_{Currentregulator} \cdot \underbrace{\frac{3.842 \cdot 10^{-3} \cdot (z-1)}{z^2 - 1.947 \cdot z + 0.947}}_{Current\_loop} \quad \text{.....(5.54)}$$

The calculated duty-cycles is first supplied to the timer / rotor converter after one sample. This means, that an additional delay is introduced. The current components measured by the current transducers are filtered using a first order anti aliasing filter. This has also to be included in the transfer function for the current loop. The discrete transfer function including the anti aliasing filter and timer/calculation delay is described in equation (5.55):

$$G_{reg}(z) \cdot G_i(z) \cdot G_d(z) \cdot G_f(z) = \underbrace{K_i}_{Currentregulator} \cdot \underbrace{\frac{3.842 \cdot 10^{-3} \cdot (z-1)}{z^2 - 1.947 \cdot z + 0.947}}_{Current\_loop} \cdot \underbrace{\frac{1}{z}}_{Timer\ Calc} \cdot \underbrace{\frac{0.8377}{z - 0.1623}}_{Antialiasingfilter} \quad (5.55)$$

The open loop transfer function for the current loop is given by equation (5.55). The complete current loop is shows in Fig. 5.20.

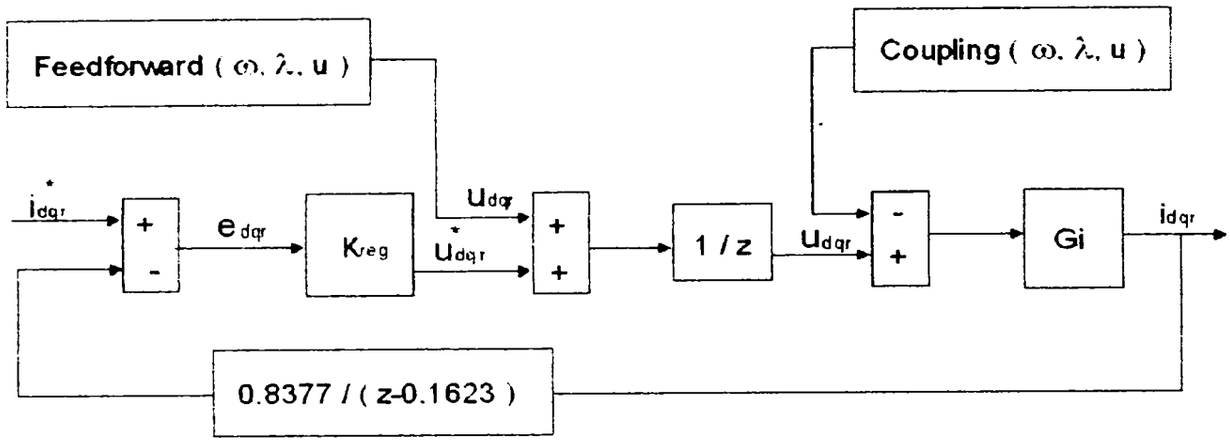


**Figure 5.20.** Complete current loop including ZOH, timer/calculation delay and anti aliasing filter.

The transfer function for the current loop has four poles and one zero. The zero-placement determines the overshoot of the current step response. If the zero moves towards z=1, the system overshoot increases. The additional pole introduced by the timer/calculation delay influences the rise time. As the pole is moved towards z=1, the rise time of the system decreases. [Franklin, 1990, pp. 73-77]

The P-regulator is designed for 25 % overshoot. The gain of the regulator is determined from the root locus diagram and it was found to be equal with 80.

**Table 5.2.** Gain for the proportional current regulator for the current loop including timer/calculation delay, and for the current loop including timer/calculation delay and anti aliasing filter.

| Loop | Current Loop | Current loop with delay | Current loop with delay and filter |
|---|---|---|---|
| *Gain at stability limit* | ∞ | 270 | 160 |
| *Gain for 25 % overshoot* | - | 190 | 80 |

*Current Loop (Regulator) Design with PI-Regulator*

A PI-regulator may be used in the current loop to eliminate the steady state error. The PI-regulator is designed from the requirements concerning rise time, $t_r < 2$ ms, and maximum over-shoot ≈ 25 %. The current loop is shown in Fig. 5.20 and the open loop transfer function including the PI-regulator is given by the next equation (5.56), arising from equation (5.53):

$$G_{PIreg}(z)\cdot G_i(z)\cdot G_f(z) = \underbrace{K_{PI}\cdot\frac{z-N_i}{z-1}}_{CurrentPI-regulator}\cdot\underbrace{\frac{3.842\cdot10^{-3}\cdot(z-1)}{z^2-1.947\cdot z+0.947}}_{Current\_Loop}\cdot\underbrace{\frac{1}{z}}_{Timer/Calc.}\cdot\underbrace{\frac{0.8377}{z-0.1623}}_{Antialiasing\_Filter} \quad ....(5.56)$$

The zero of the PI-Regulator may be used to compensate for the dominating pole of the DFIG transfer function at z=0.95. The problem concerning a PI-regulator is the placement of the zero, which may be used to canceling the dominating pole of the system. Since the dominating system pole moves due to parameter variation, the zero may introduce additional oscillations. In the complete Simulink model, which will be described in section 5.6.1 an option for choosing between the proportional (P) and PI-Regulator is implemented.

The ideal step response using the proportional regulator is compared to the ideal step response using the PI-regulator as is shown in Fig. 5.21.

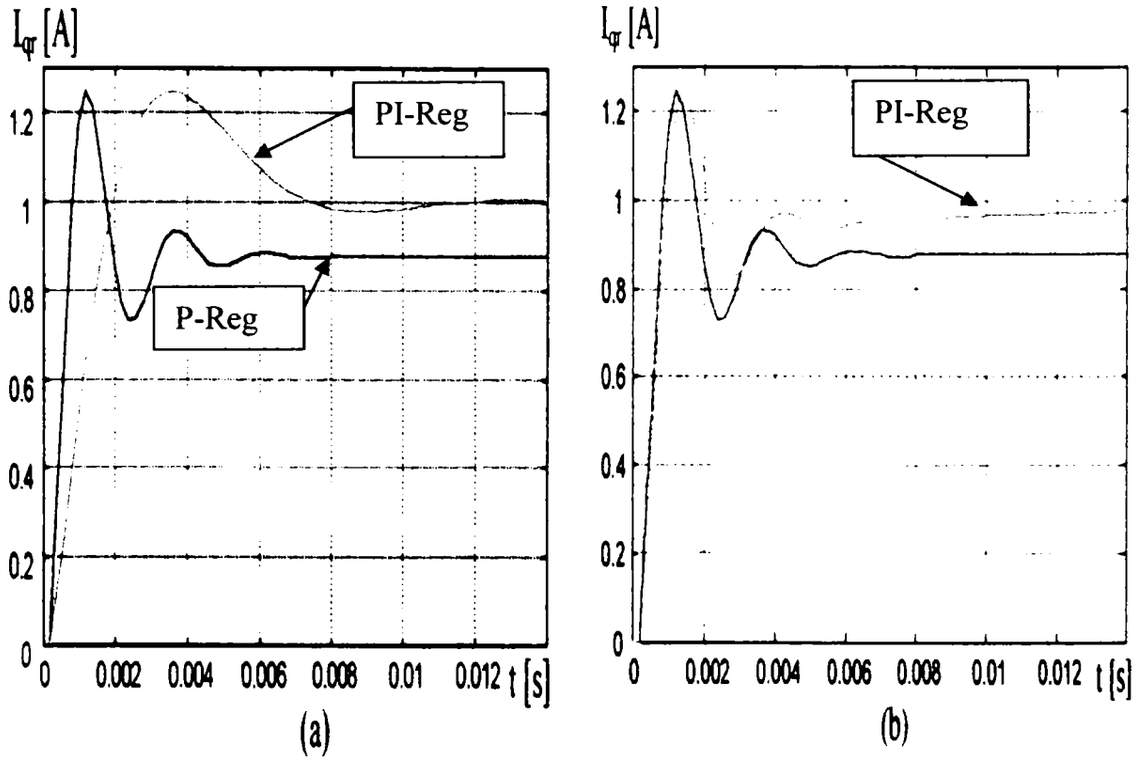


**Figure 5.21.** Step response of the ideal current loop with both the proportional regulator and PI-regulator. a) $K_{PI}$=32, Ni=0.88, b) $K_{PI}$=80, Ni=0.98.

As may be seen in Fig. 5.21 a), the proportional regulator has a smaller rise time than the PI regulator when $K_{PI}$=32 and Ni=0.88. The rise time of the proportional regulator is 0.85 ms and the rise time of the PI regulator is 1.95 ms. The overshoot equals 25% for both regulators. The step response using the PI-regulator has a larger settling time, but the response is more damped than the response using the proportional regulator.

When the PI-regulator is tuned as shown in Fig. 21 b), the PI-regulator behaves close to the proportional regulator. The rise time and overshoot becomes equal, but the settling time for the PI-regulator increases to 20 ms.

In Fig. 5.22 a step response is simulated using both regulators (P and PI).

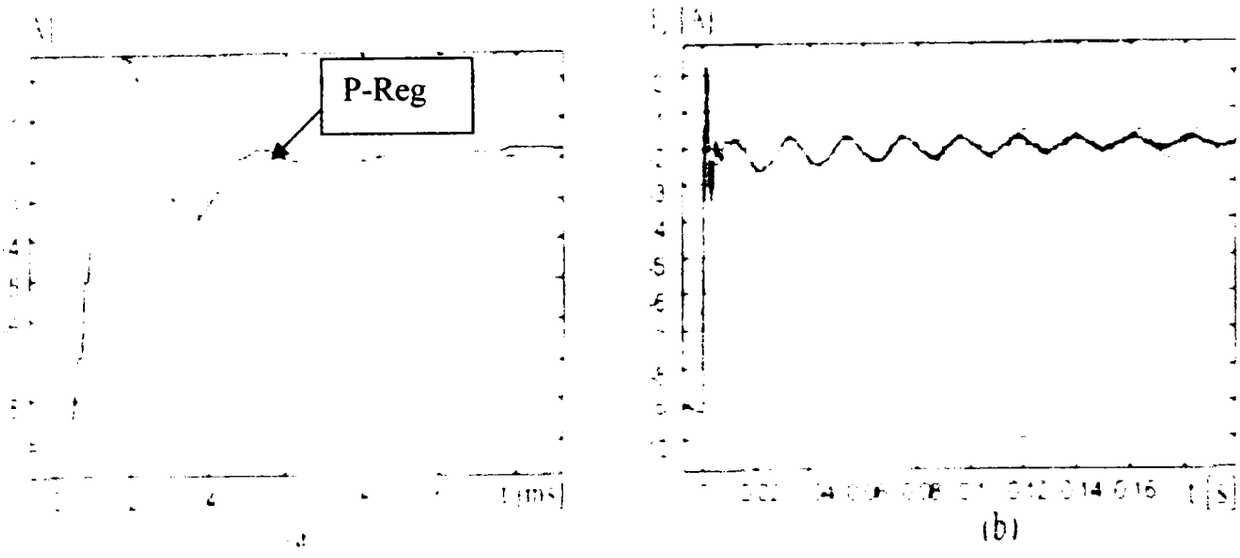


**Figure 5.22.** Simulation of the step response using P and PI-regulators. a) Zoom of the transient behavior in the beginning of the step response; b) Step response including steady-state performance of the regulators.

The step response using the proportional regulator and the PI-regulator yields almost identical results, as can be seen in Fig. 5.22 a). The rise time for the PI-regulator is 1.55 ms, and for P-regulator is 1.25 ms. The overshoot is 16 % for both regulators. Figure 5.22 b) presents the steady-state performance of the regulators. The PI-regulator yields larger ripple amplitude than the P-regulator due to placement of the zero.
Making a comparison between P- and PI-regulators we may conclude that:

- Both the P-and PI-regulator meets the demands concerning rise time and maximum overshoot
- The settling time for the P-regulator is smaller than for the PI-regulator
- At steady-state operation, the oscillations caused by feed forward are larger using the PI-regulator. The oscillations increase at the zero of the regulator is moved to the left
- The transient performances of the regulators are almost the same but the proportional regulator shows superior performance at steady-state.

It is chosen to implement a standard proportional regulator due to its superior performance at steady-state.

### 5.5.2. Power Control Loop

- The power control loop is to be designed for controlling the stator active and reactive power independently. The power control loop generates the reference for the inner rotor current loop designed in the previously subchapter.

A schematic diagram of the power loop is given in Fig. 5.23:

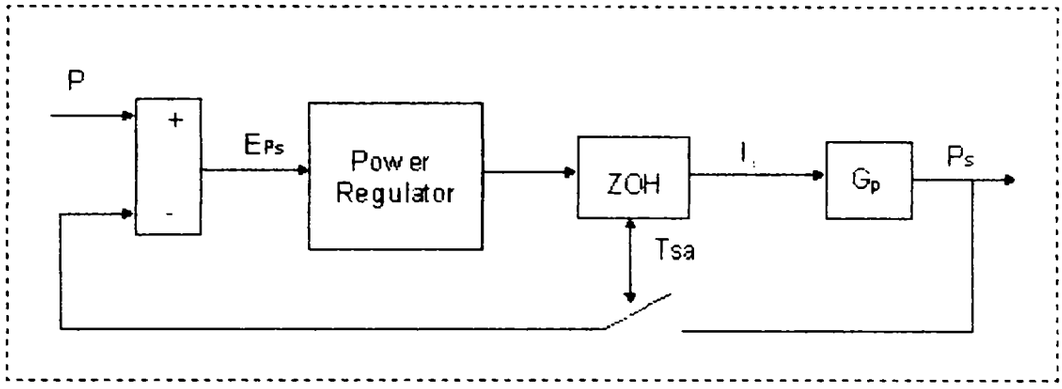


**Figure 5.23.** Schematic diagram of the active power loop. assuming an ideal rotor current loop. The reactive power loop is equivalent.

The power loop is composed of the power regulator, a ZOH-network and the active and reactive power transfer function, as can be seen in Fig. 5.23.

### 5.5.2.1. Ideal Power Control Loop

When designing the power control loop, an ideal rotor current loop is assumed. In addition, the parameters contained in the power loop are assumed constant. The open loop transfer function of the power control loop has to be determined. The rotor currents and stator powers are connected as it is describe in sub-chapter 5.4. The reference to the inner current loop is generated by the power loop, which gives equations (5.57) and (5.58).

$$i_{dr}^{\ e} = -\frac{4 \cdot P_s}{3 \cdot p \cdot \omega_e \cdot \lambda_{qs}^{\ e}} \quad \text{.....(5.57)}$$

$$i_{qr}^{\ e} = \frac{\lambda_{ds}^{\ e}}{M} - \frac{4 \cdot L_s \cdot Q_s}{3 \cdot p \cdot \omega_e \cdot \lambda_{qs}^{\ e} \cdot M} \quad \text{.....(5.58)}$$

$$G_{i,CL} = \frac{i_{dqr}^{\ e}}{i_{dqr}^{\ e^*}} \quad \text{.....(5.59)}$$

By inserting the closed loop transfer function for the rotor currents, the open loop transfer functions of the stator powers are given by equations:

$$\frac{P_s \cdot G_{i,CL}(z)}{G_P(z)} = \frac{4 \cdot P_s}{3 \cdot p \cdot \omega_e \cdot \lambda_{qs}^{\ e}} \text{ for } G_P(z) = \frac{P_s}{i_{dr}^{\ e^*}} \quad \text{.....(5.60)}$$

$$\frac{Q_s \cdot G_{i,CL}(z)}{G_Q(z)} = \frac{\lambda_{ds}^{\ e}}{L_m} - \frac{4 \cdot L_s \cdot Q_s}{3 \cdot p \cdot \omega_e \cdot \lambda_{qs}^{\ e} \cdot L_m} \text{ for } G_Q(z) = \frac{Q_s}{i_{qr}^{\ e^*}} \quad \text{.....(5.61)}$$

By rearranging equations (5.60) – (5.61), the open loop transfer functions of the stator powers are given by equations (5.62) and (5.63):

$$G_P(z) = -\frac{3}{4} \cdot p \cdot \omega_e \cdot {\lambda_{qs}}^e \cdot G_{i.CL}(z) \quad \text{.....(5.62)}$$

$$G_Q(z) = \frac{3 \cdot p \cdot \omega_e}{4 \cdot L_s} \cdot \left( {\lambda_{qs}}^e \cdot L_m \cdot G_{i.CL} - {\lambda_{qs}}^{e^2} \right) \quad \text{.....(5.63)}$$

The open loop transfer functions for the active and reactive power loop are developed and given in equations (5.62) and (5.63).

As may be seen in equations (5.62) and (5.63), the power loop depends on the magnetizing inductance ($M=1.5\ L_m$), stator leakage inductance ($L_s=M + L_{s\sigma}$) and the stator q-axis flux ($\lambda_{qs}$).

With the DFIG parameters from data sheet, inserted into the transfer functions, open loop step response of the active power loop is simulated. The result is shows in Fig. 5.24.

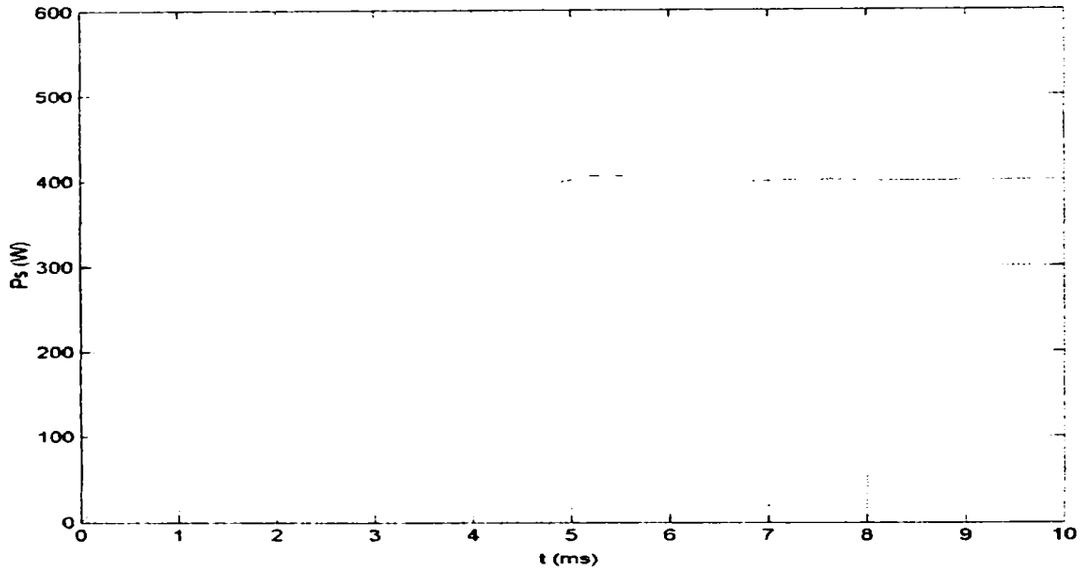


**Figure 5.24.** Open loop step response of the ideal power control loops. Active power - step response with a reference step equal to 1 W. $\lambda_{ds}$=1.04 Wb, $L_m$=147 mH and $L_s$=3.95 mH.

### 5.5.2.2. Regulator Design of the Power Loop

To achieve the desired response and steady state properties of the power control loop, a close loop regulator is to be designed. The rise time should be less than 20 ms, for a 10% step in power reference. The overshoot should be less than 10%, and no steady state error is allowed. As no steady state error is allowed, a well-damped response is required, and due to simplicity a PI-regulator is chosen for implementation. The regulator is composed of two parts, a proportional gain and an integrator. The proportional part of the regulator is the error of the power loop multiplied by the constant gain, $K_P$ for active power and $K_Q$ for reactive power. In general form the proportional part may be written as equation (5.64):

$$y_P(n) = K \cdot \left( x(n) - x(n-1) \right) = K \cdot e(n) \quad \text{.....(5.64)}$$

The integration may be performed using any digital integrator. In this case it is of satisfactory accuracy to employ the Backward-Euler integration. Alternatively, the integration may be performed using the trapezoidal, Runge - Kutta, or other integration methods.
The Backward-Euler integrator may be written as in equations (5.65) and (5.66):

$$y_i(n) = y(n-1) + T_{sa} \cdot \frac{dx}{dt} = y(n-1) + K \cdot \frac{T_{sa}}{T_i} \cdot \left(x(n) - x(n-1)\right) \quad (5.65)$$

$$y_i(n) = y(n-1) + K \cdot \frac{T_{sa}}{T_i} \cdot e(n) \quad (5.66)$$

The PI-regulator may be expressed as the differential equations (5.67) and (5.68) by adding equation (5.65) and (5.66) and subtracting the proportional part from the previous sample. This is done for obtaining a controllable zero.

$$y(n) = K \cdot e(n) - K \cdot e(n-1) + y(n-1) + K \cdot \frac{T_{sa}}{T_i} \cdot e(n) \quad (5.67)$$

$$y(n) = y(n-1) + K \cdot \left( e(n) - \left( 1 - \frac{T_{sa}}{T_i} \right) \cdot e(n-1) \right) \quad (5.68)$$

By transferring the differential equation of the PI-regulator to the z-plane using Zero Order Hold (ZOH), the discrete transfer function may be written as in equation (5.69).

$$\frac{Y}{E} = K \cdot \frac{z + \left( 1 - \frac{T_{sa}}{T_i} \right)}{z+1} \quad (5.69)$$

As may be seen in equation (5.69), the PI-regulator has an integrator pole in z=1, and a zero which may be controlled by the integration time constant $T_i$.

The PI-regulators are implemented in the form shown in equations (5.67) and (5.68). The PI-regulators for controlling the active and reactive power are implemented as in equations (5.70) and (5.71).

$$i_{dr,ref}^{\ e}(n) = i_{dr,ref}^{\ e}(n-1) + K_P \cdot \left( e_P(n) - N_P \cdot e_P(n-1) \right) \quad (5.70)$$

$$i_{qr,ref}^{\ e}(n) = i_{qr,ref}^{\ e}(n-1) + K_Q \cdot \left( e_Q(n) - N_Q \cdot e_Q(n-1) \right) \quad (5.71)$$

Where the constants $N_P$ and $N_Q$ are defined as in equation (5.72):

$$N_P = 1 - \frac{T_{sa}}{T_{i,P}}; N_Q = 1 - \frac{T_{sa}}{T_{i,Q}} \quad (5.72)$$

The PI-regulator is included in the open loop transfer function of the power loop, which gives the equation 5.73 and 5.74, where $K_{PQ}$ is the regulator gain, and $N_{PQ}$ is the regulator zero.

$$G_{Preg}(z)\cdot G_P(z) = K_P \underbrace{\frac{z-N_P}{z-1}}_{PI-regulator} \cdot \underbrace{\frac{3}{4}\cdot p\cdot \omega_e \cdot {\lambda_{ds}}^e \cdot G_{i,CL}(z)}_{activepowerloop} \quad \text{.....(5.73)}$$

$$G_{Qreg}(z)\cdot G_Q(z) = \underbrace{K_Q \cdot \frac{z-N_Q}{z-1}}_{PI-Regulator} \cdot \underbrace{\frac{3\cdot p\cdot \omega_e}{4\cdot L_s}\cdot\left({\lambda_{ds}}^e \cdot L_m \cdot G_{i,CL}(z) - {\lambda_{ds}}^{e^2}\right)}_{Reactive\_Power\_Loop} \quad \text{.....(5.74)}$$

*Anti-aliasing Filter*

The stator voltage and current transducers are equipped with first order anti aliasing filters. These filters have to be included in the transfer function of the power loop. As both the stator voltage and stator currents are filtered, the square of the transfer function of the filters is included in the combined transfer function of the power loop. This gives equations 5.75 and 5.76.

$$G_{Preg}(z)\cdot G_P(z)\cdot {G_f}^2(z) = K_P \underbrace{\frac{z-N_P}{z-1}}_{PI-regulator} \cdot \underbrace{\frac{3}{4}\cdot p\cdot \omega_e \cdot {\lambda_{ds}}^e \cdot G_{i,CL}(z)}_{Activepowerloop} \cdot \underbrace{\frac{0.8377^2}{(z-0.1623)^2}}_{Antialiasing\_Filter} \quad \text{.....(5.75)}$$

$$G_{Qreg}(z)\cdot G_Q(z)\cdot {G_f}^2(z) = \underbrace{K_Q \cdot \frac{z-N_Q}{z-1}}_{PI-Regulator} \cdot \underbrace{\frac{3\cdot p\cdot \omega_e}{4\cdot L_s}\cdot\left({\lambda_{ds}}^e \cdot L_m \cdot G_{i,CL}(z) - {\lambda_{ds}}^{e^2}\right)}_{Reactive\_Power\_Loop} \cdot \underbrace{\frac{0.8377^2}{(z-0.1623)^2}}_{Antialiasing\_Filter} \quad (5.76)$$

*Root Locus Design*

The discrete open loop transfer functions of the power loop are used for determination of the optimal power regulator parameters. The gain and placement of the zero has to be determined. The complete power control loop is depicted in Fig. 5.25.

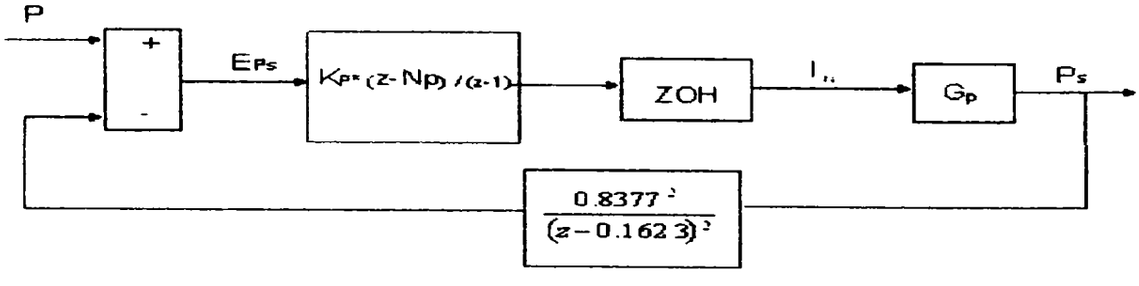


**Figure 5.25.** Complete power control loop including ZOH and stator voltage and current filters. The square of the transfer function of the filter is included since both stator voltage and current is filtered with the first order anti aliasing filter.

The power control loop shown in Fig. 5.33 is reflected very clear by equations (5.75) and (5.76).

The PI-regulators are implemented in the function *Power_Controller()* in the control program *DFIG.c* which can be find in *Appendix* $D_3$.

### 5.5.2.3. Power Decoupling

The stator active and reactive power is to be fully decoupled for obtaining the desired performance of the system.

A simulation may be performed applying a step in active power, and monitoring the reactive power, and visa versa. The results are shown in Fig. 5.26.

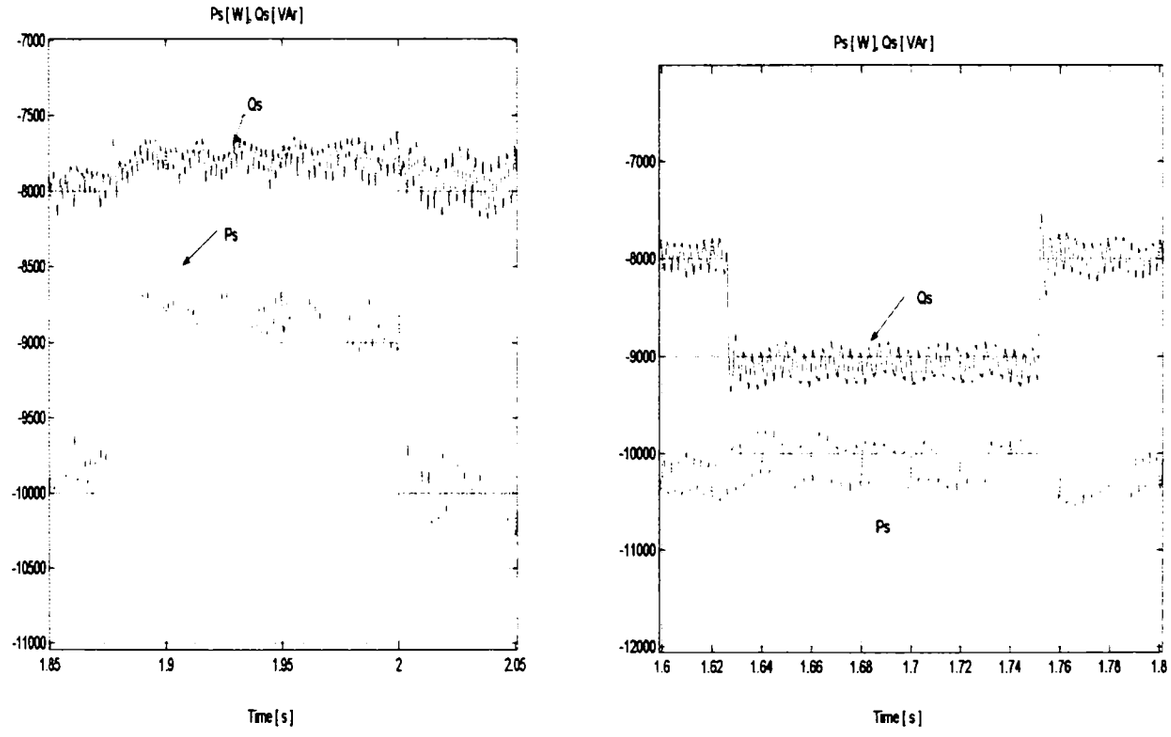


a) b)

**Figure 5.26** a) Step in the stator active power, and the corresponding value of the reactive power; b) Step in reactive power and the corresponding value of the active power.

As can be seen in Fig. 5.26 the simulated active and reactive stator power is fully decoupled. The decoupling of the two stator powers is analyzed from the step responses. A step of 10 % in active power (from 10 kW to 9 kW) causes an oscillation in reactive power with amplitude of 2 % of the set point for the reactive power. A step in reactive power (from 8 kVAr to 9 kVAr) causes the active power to oscillate with maximum amplitude of 2 % of the set point for the active power. Both oscillations are suppressed after 7 ms, which is the time required for the stepping power to settle to its new value. The oscillations of the stator powers are small, and the obtained decoupling of the stator powers are therefore found useable.

## 5.6. Implementation of the system simulation model

The control scheme presented in sub-chapter 5.4 and the regulators designed in sub-chapter 5.5 are implemented in a complete simulation model also including the DFIG model describe in section 5.2, rotor converter model describe in section 5.3 and the control program developed in Ansi C and converted in Matlab-Simulink function, which can be found in Appendix D3.
The implementation of the different components forming the control system is described as follows.

### 5.6.1. Control Processor Unit Components

The control system contains the following components to be modeled:

- TMS320C32 DSP. The control algorithms and I/O declarations have to be modeled.
- AD565 DA-converter. The zero order holds (ZOH) functions of the DA-converters should be implemented.
- AD7891 AD-converter. The quantization error of the ADC has to be included
- Anti aliasing filters. The first order anti aliasing filters on the current and voltage transducers also implemented in the system.

The above listed components are implemented in the Simulink simulation model in the following.

*TMS320C32 DSP*
The DSP and development control board is equipped with several hardware and software tools. The control algorithms are implemented using Ansi-C and the C-file may be executed in Simulink by means of the Matlab MEX-function. The model of the DSP implemented in Simulink is shown in Fig. 5.25:

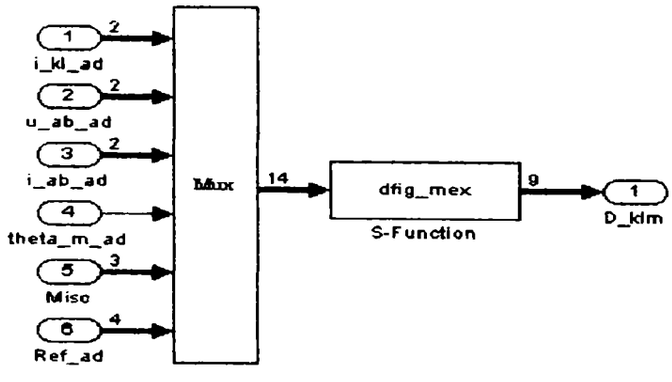


**Figure 5.25.** Model of the TMS320C32 – DSP developed in Simulink. The control algorithms written in the Ansi-C language executed using the Matlab mex S-function.

The advantage of implementing the Ansi-C file in Simulink is the direct connection to the implementation in DSP, and decrease in simulation time.

*AD DA Converters*

The analog signals from the voltage and current transducers are sampled using the AD-converter. The AD 7891 AD-converter is a 12 bit-8 channel converter. The quantization errors are evaluated by assuming a 10 bit resolution for the current transducers and 11 bit resolution for voltage transducers. The AD565 DA-converter is modeled by use of the standard ZOH function from Matlab-Simulink toolbox, as can be seen in Fig. 5.26.

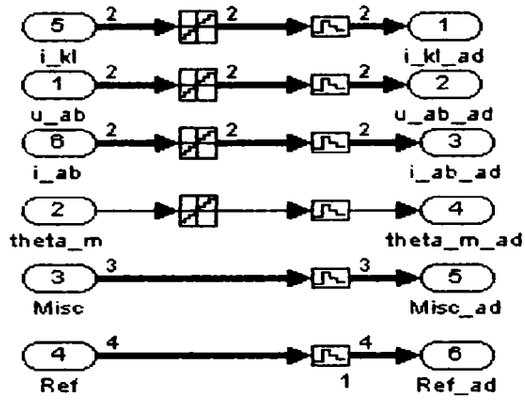


**Figure 5.26.** Simulink representation of the DA-converter using ZOH.

*Anti Aliasing Filters*

The voltage and current transducers are equipped with first order anti aliasing filters. The filters are included in the regulator design as described in section 5.5. The transfer function is given by equation G (z) = 0.8377 / (z-0.1623).

### 5.6.2. The complete Simulation model implemented in Simulink

The complete block diagram of simulation model implemented in Simulink is shown in Fig. 5.27.

The DFIG is driven by the drive system. The drive system in the Matlab - Simulink model contains the speed and angle generation in addition with the mechanical system modeled using the first order transfer function, where the time constant is determined from a step in rotor speed, as can be seen in Fig. 5.27.

When modeling the DFIG and the drive system, the mechanical parameters, moment of inertia, static and viscous friction and ventilation losses are assumed to be placed in the drive system. This means that the DFIG model only contains electrical components.

The speed response of the system is determined mainly by the total moment of inertia, but also by the friction and ventilation losses.

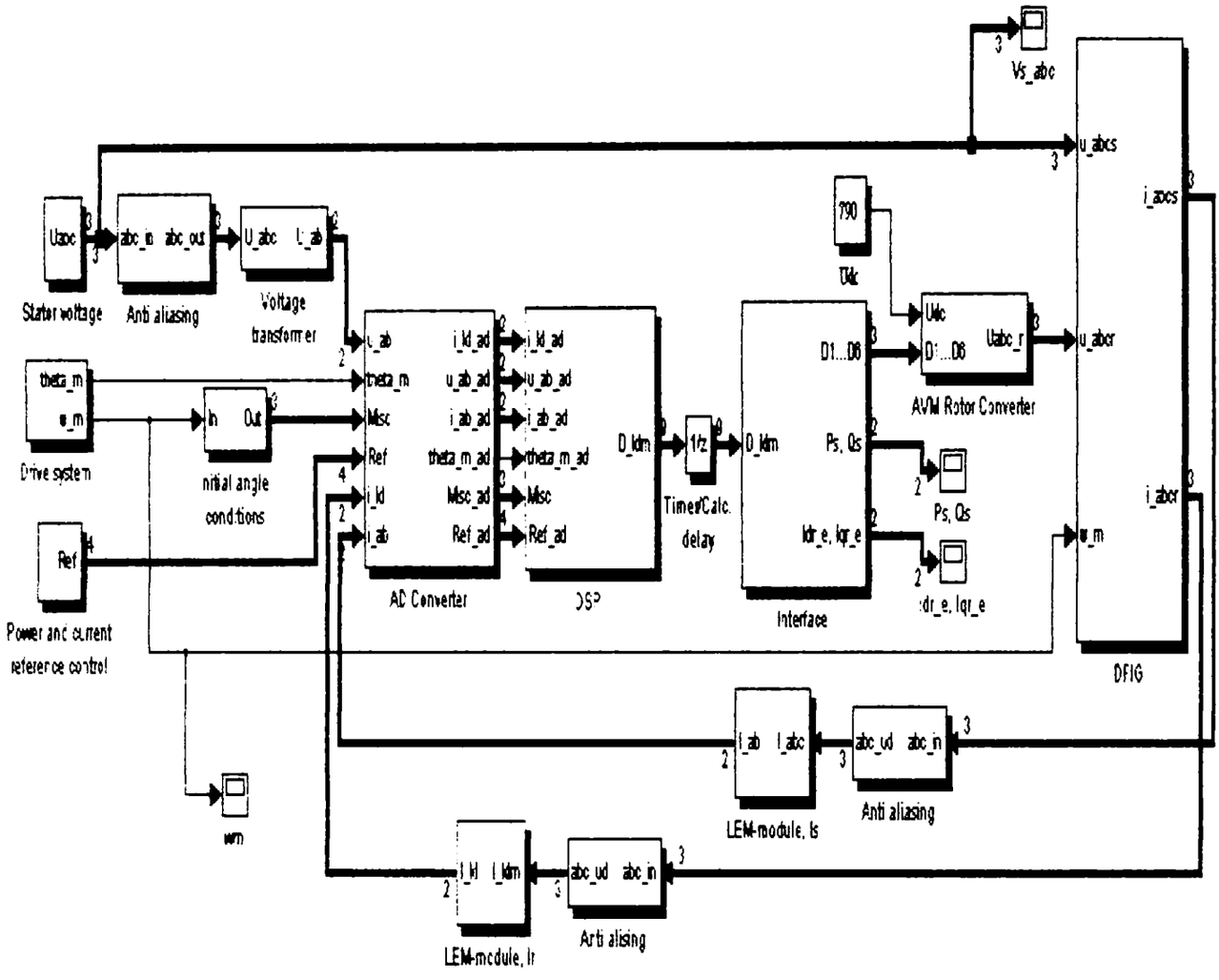


**Figure 5.27.** The complete simulation model of the system.

### 5.6.3. Control System

For controlling the stator active and reactive power of the DFIG, the control algorithm developed in sub-chapters 5.4 and 5.5 are implemented in the DSP control processor unit.

#### 5.6.3.1. Control Algorithm

The control program is developed in Ansi-C, and the structure of the control part of the program is illustrated in Fig. 5.28.

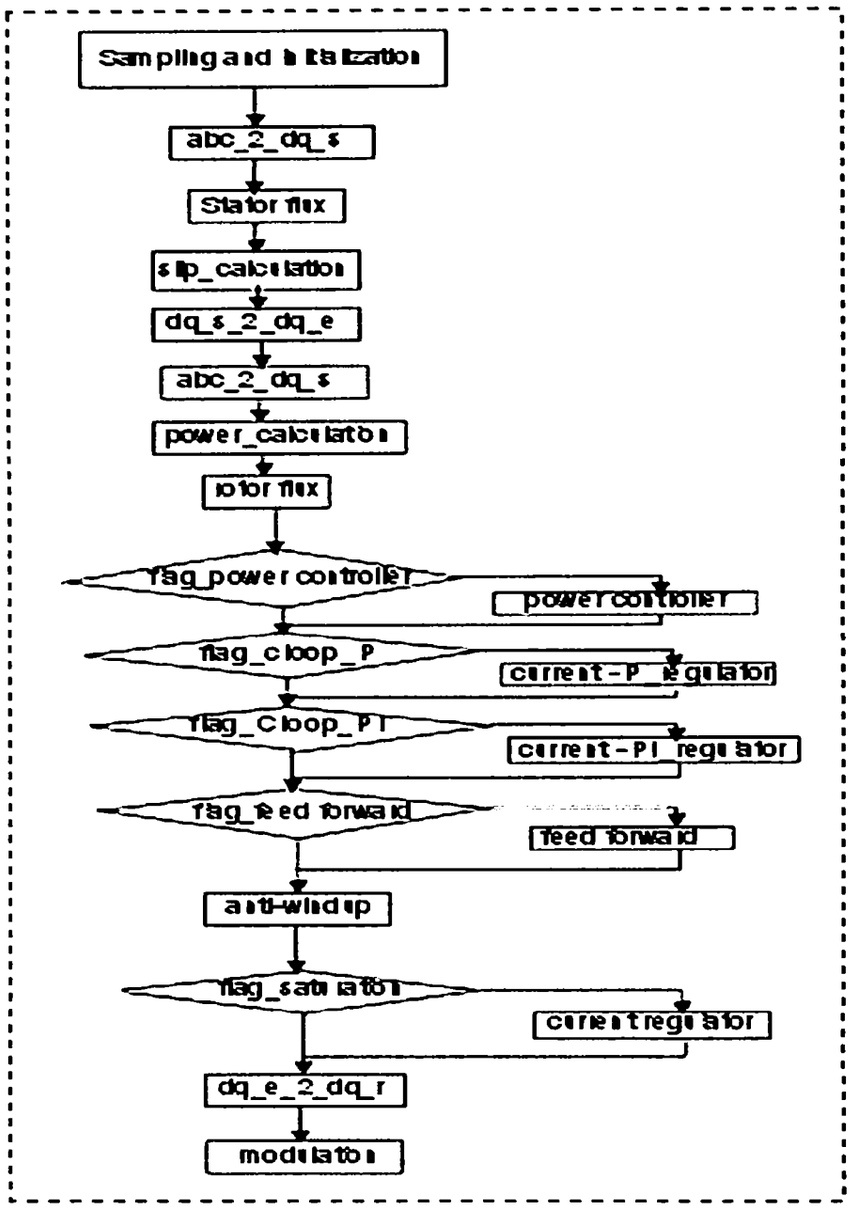


**Figure 5.28.** Program flow for the interrupt routine of the DFIG program.

The complete program structure is described in following:

*Sampling and Initialization*: The stator voltages and currents, and the rotor currents are sampled and scaled.

*Abc_2_dq_s*: the three-phase stator voltages and currents are transferred to the stationary reference frame.

*Stator_flux*: The stator flux is calculated in the stationary reference frame. The resulting stator flux is used as d-axis for the stator flux fixed reference frame.

*Slip_calc*: the slip speed and angle is calculated for transferring the rotor currents to the stator flux reference.

*Dq_s_2_dq_e*: the three-phase stator voltages and currents are transferred to the stator flux reference frame.

*Power_calc*: The stator active and reactive power is calculated.

*Rotor_flux*: Rotor flux calculation in the stator flux reference frame for use in the feed forward compensation.

*Power_controller*: The PI-power regulator algorithm is calculated.

*Current_P_regulator*: The standard proportional regulator is used in the current loop.

*Current_PI_regulator*: The PI current regulator is used in the current loop.

*Feed Forward*: The feed forward compensation algorithm is calculated.

*Anti_windup*: An anti windup algorithm is included since the power regulator is a PI-regulator.

*Dq_e_2_dq_r*: The rotor voltages calculated in the stator flux reference are transferred to the rotor fixed reference frame.

*Modulation*: The rotor voltages are applied to the SFAVM scheme, and the duty-cycles to the rotor converter are calculated, more details can be found in *Appendix D2*.

### 5.6.3.2. Anti Windup

In order to avoid windup of the power regulator, an anti windup function is implemented in the control program. The duty-cycles to the rotor converter is limited in the interval from $0.02<D_{klim}<0.98$, which is limited by the timer. The difference between the limited control signal to the rotor converter and the output signal from the power regulator is calculated and subtracted from the error signal supplied to the power regulator. Thereby, the power regulator is fed with the maximum error, which does not saturate the output signal to the rotor converter. This is illustrated in Fig. 5.29:

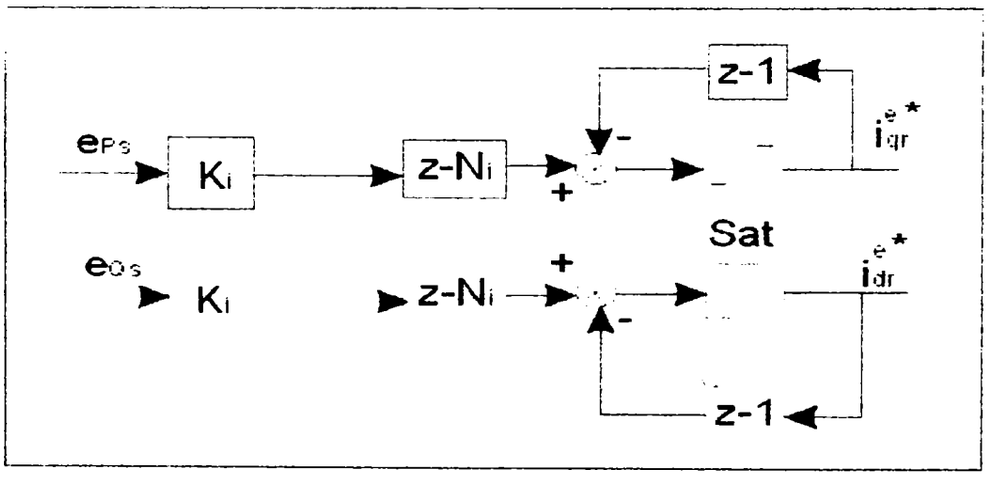


**Figure 5.29**. Illustration of the anti windup algorithm implemented in the control program. The amplitude and angle of the reference voltage vector is calculated, and saturation of the amplitude is implemented [Franklin, pg. 672].

### 5.6.3.3. Simulation Results

In order to evaluate the performance of implemented control strategy presented before and to analyze system response in steady state and transients the DFIG was subject to step changes in active and reactive load power with the machine driven at both sub- and super-synchronous speeds.

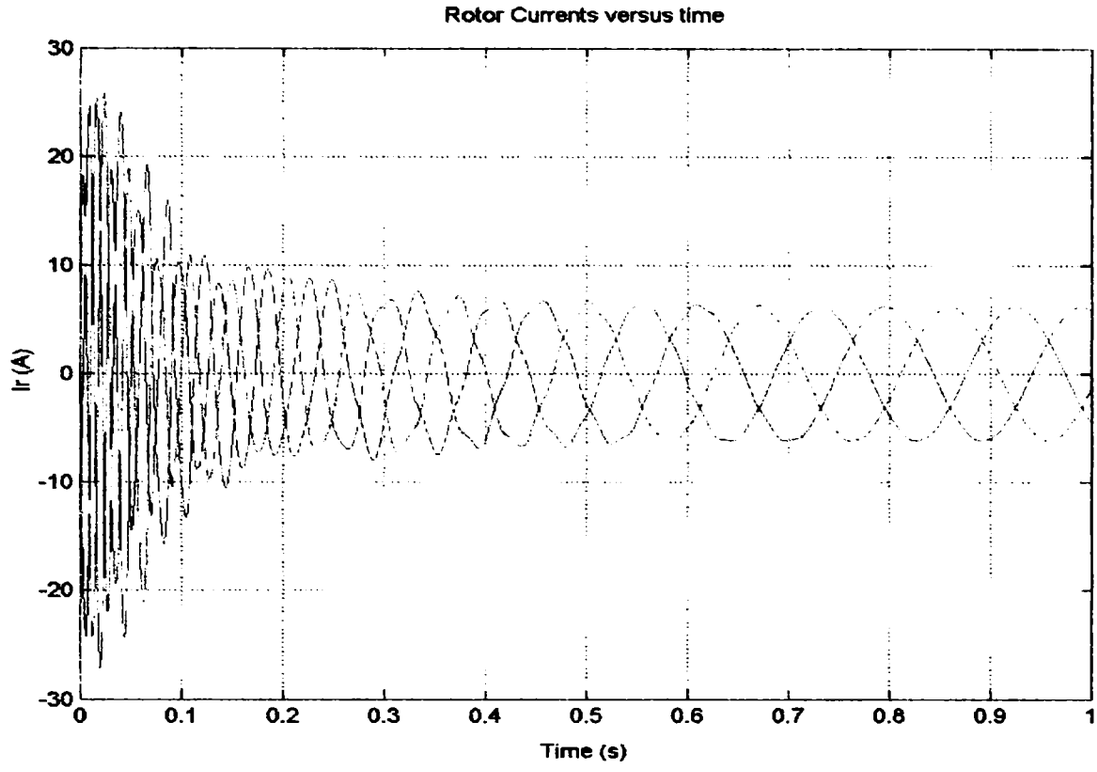
Rotor Currents versus time
Ir (A)
Time (s)
30
20
10
0
-10
-20
-30
0
0.1
0.2
0.3
0.4
0.5
0.6
0.7
0.8
0.9
1

**a)**

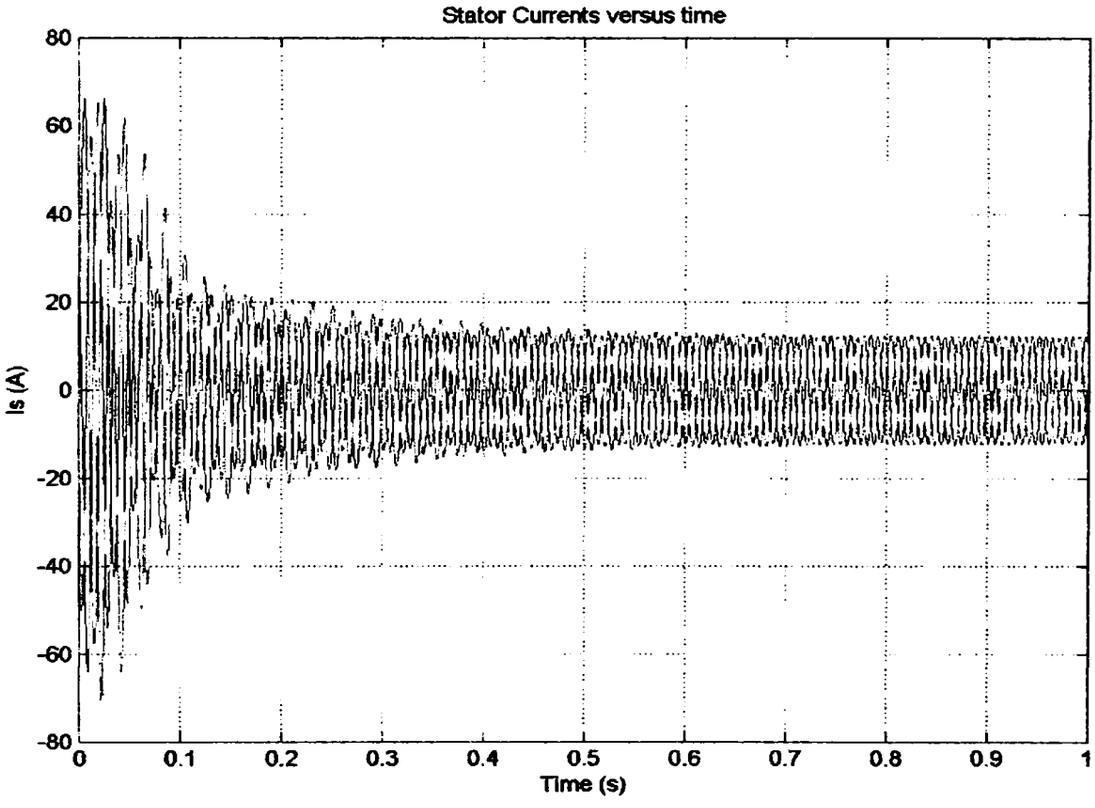
Stator Currents versus time
Is (A)
Time (s)
80
60
40
20
0
-20
-40
-60
-80
0
0.1
0.2
0.3
0.4
0.5
0.6
0.7
0.8
0.9
1

**b)**

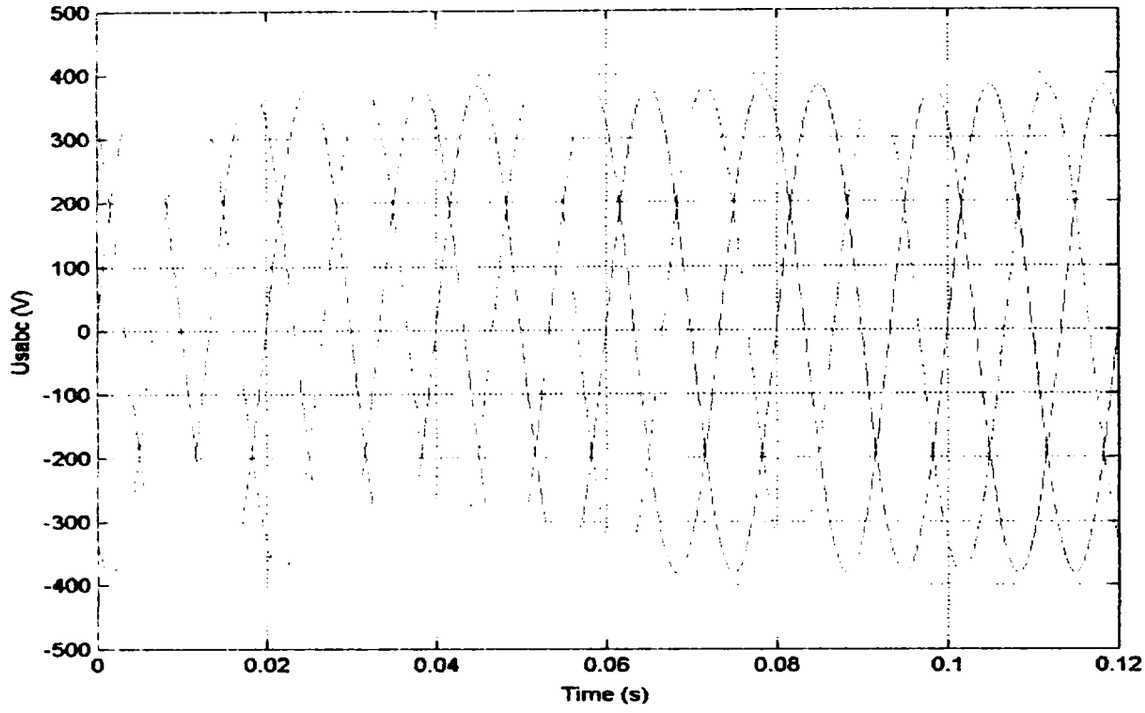


c)

**Figure 5.30. The simulated rotor currents, stator currents and stator voltages as a function of time during a start-up and operation in sub-synchronous mode-$w_m$=1350 rpm (90 % of synchronous speed) at Ps=8 kW.**

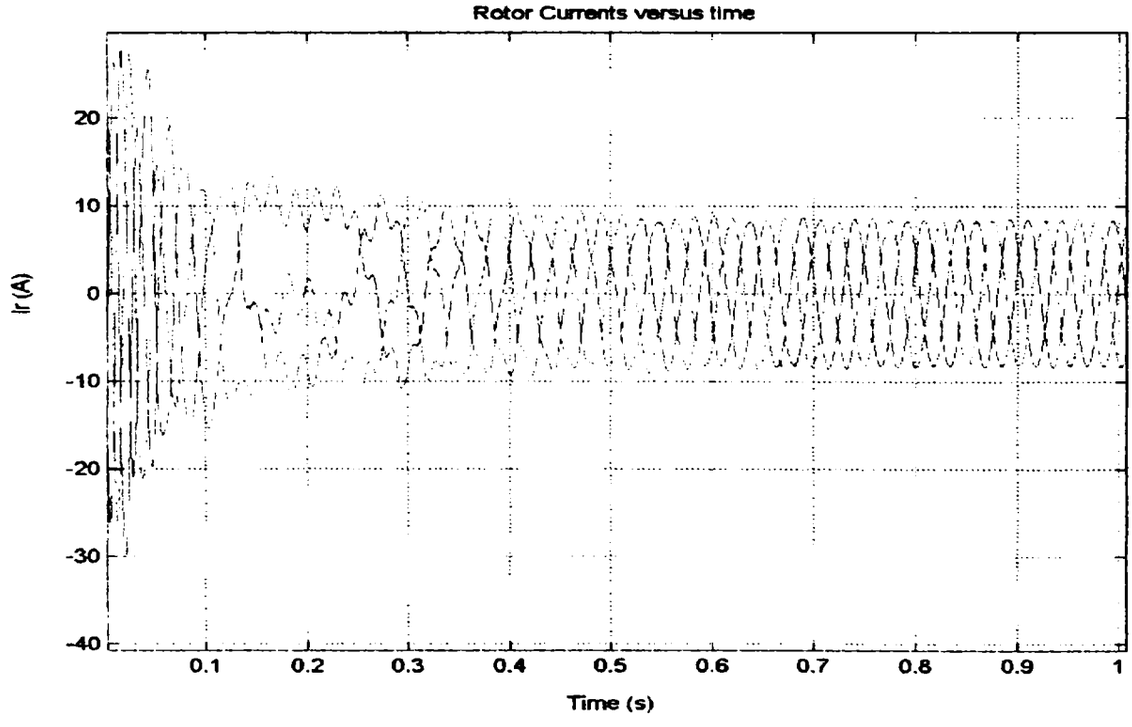


a)

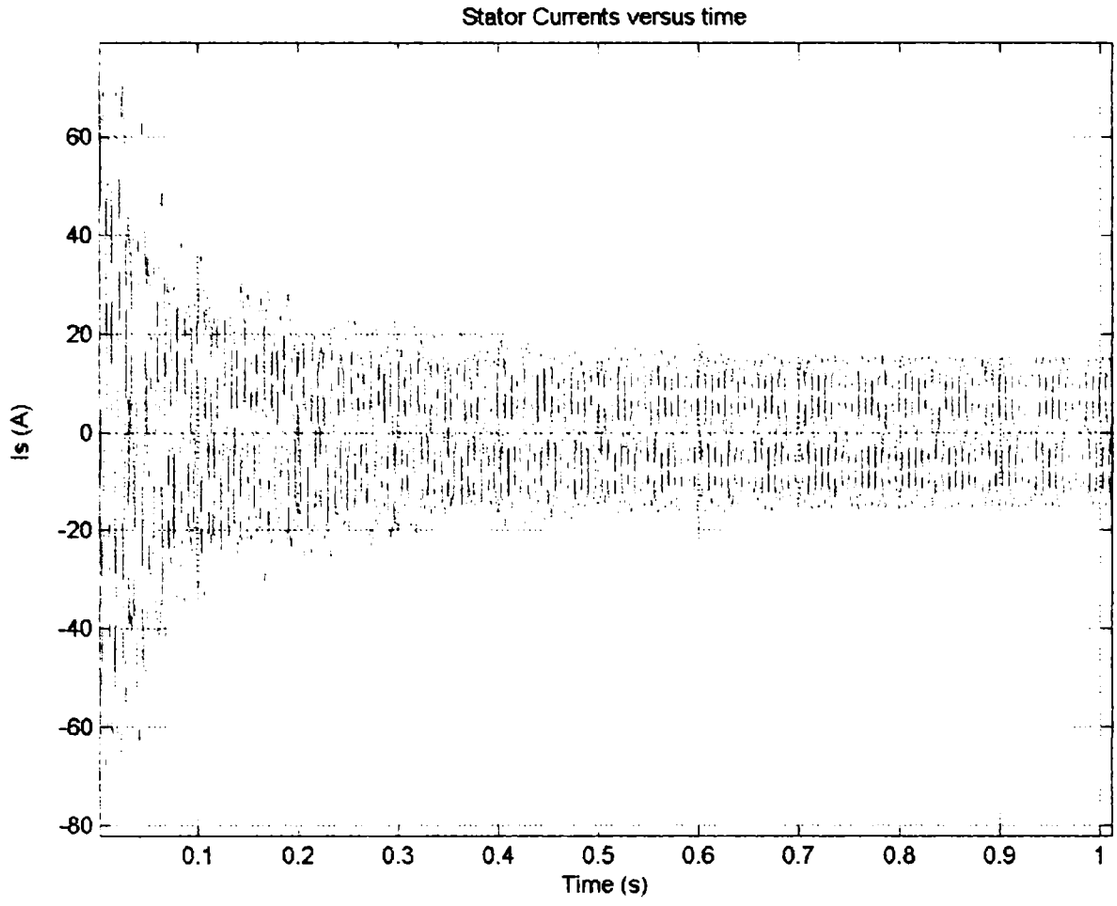


b)

**Figure 5.31.** The simulated rotor currents (a) and stator currents (b) of DFIG as a function of time during a start-up and operation in super-synchronous mode-$w_m$=2100 rpm (140 % of synchronous speed) at Ps=8 kW.

Detailed system simulations were performed using Matlab - Simulink software package to evaluate the performance of the DFIG. The start-up and steady-state operations in sub-synchronous and super-synchronous mode are illustrated in Figs. 5.30-5.31. In Fig. 5.30 is shown a start-up and normal operation in sub-synchronous speed mode with monitoring the DFIG rotor currents (a), stator currents (b) and stator voltages (c). In Fig. 5.31 is depicted a start-up and normal operation of the DFIG in super-synchronous speed operation mode with monitoring of rotor currents (a) and stator currents (b).

The transient response due to a step change in reference active power control is shown in Fig. 5.32. The Fig.5.32 a) shows the response to a step change in the active load power from 0 to 1.5 kW, while the reference of reactive power is maintained at 0 and the corresponding stator active and reactive power of the machine are monitoring. Similar transient response for generating condition is given in Fig. 5.32 b). When a step in active power is applied (t=1sec), the reactive power shows small additional oscillations. It is also observed that (Ps) reaches its set value in approximately 10 ms. The simulation results indicate that the generator follows the reference very fast and is dynamically stable. It may be noted from these waveforms, that the transient responses in (Ps) and (Qs) are perfectly decoupled. The DFIG was driven by the drive system at 1125 rpm (75% of synchronous speed-sub synchronous speed operation mode).

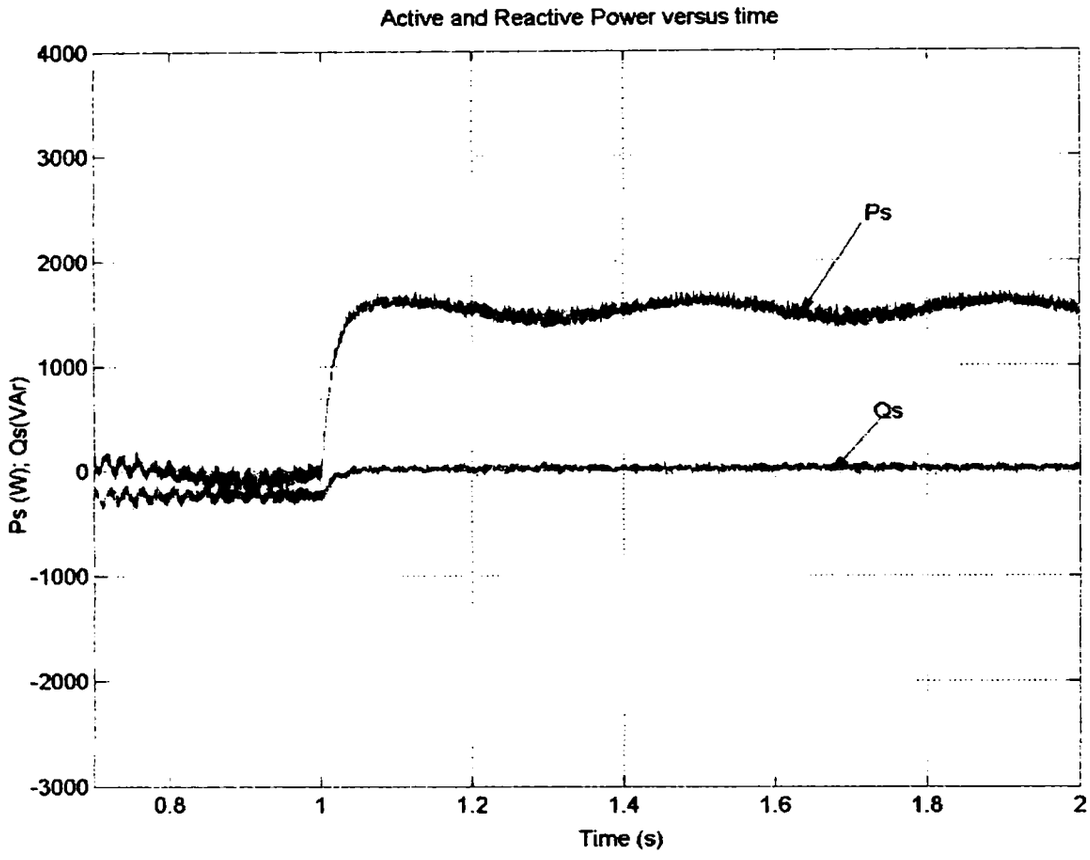


a)

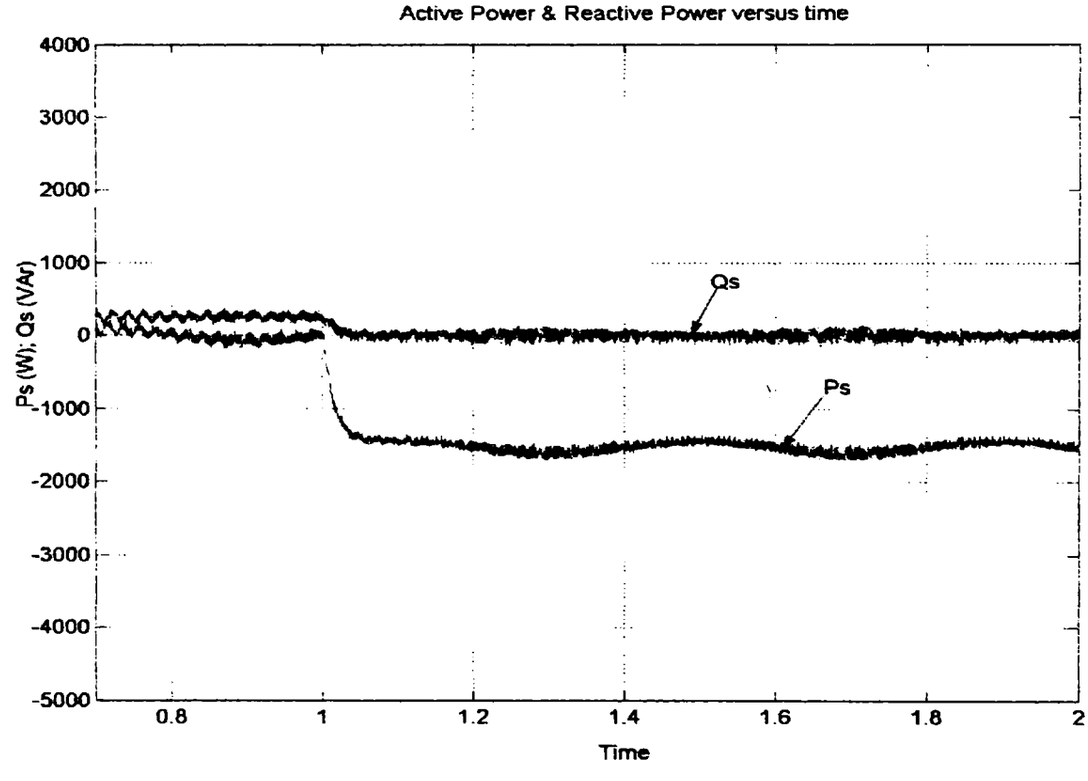


b)

**Figure 5.32.** Simulated stator active and reactive power with a step change in active power command from 0 to 1500 W (a) and with a step change in active power reference from 0 to -1500 W at t=1sec.

# 5.7. Description of the Experimental System

## 5.7.1 Schematic Diagram

The existing experimental system is a model of variable speed wind generator composed of four main components. A DFIG with a four quadrant ac-to-ac converter connected to the rotor windings, a drive system and a control processor unit.

The generator is a wound rotor induction generator (***doubly fed induction generator*** - DFIG), with slip rings, rated at 11 kW provided with a gearbox. The wind turbine rotor is emulated by use of a ***drive system*** scaled for driving the DFIG; the drive system is composed of a 15 kW induction motor and a 22-kVA-frequency converter. Two ***back-to-back PWM-VSI converters*** with a standard control system, with a DC-link including a DC capacitor filter are used to control the rotor currents, active and reactive power flow.

The grid converter is designed to give unity power factor and is controlled by the Control Processor (CP) – board via a PC. It works as an active rectifier supplying the rotor converter with a constant DC voltage. The measurement and control system is composed of a PC with a digital signal processor (TMS320C32 DSP), interfaces and transducers for measuring stator and rotor currents, stator voltages, and rotor speed, as can be seen in Fig. 5.33.

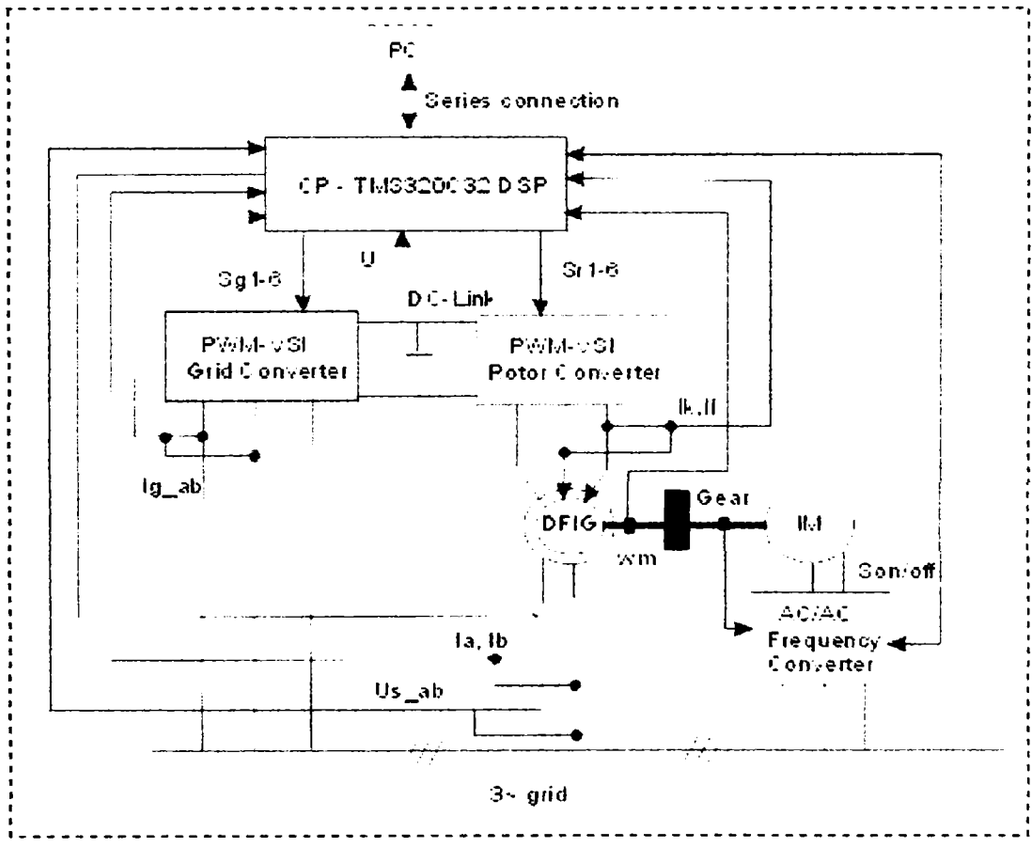


**Figure 5.33.** Schematic diagram of the experimental system.

## 5.7.2. The experimental system components

### 5.7.2.1. DFIG

The DFIG is a LEROY SOMER Induction Generator of 11 kW with a wound rotor. The induction generator is a 3 phases machine (m=3), with 48 number of slots, Ns=48 and number of poles, 2p=4. The number of slots per pole and phase is q = Ns / (2pm) = 4.

The stator of the DFIG is connected to the 50 Hz and 400 V supply grid by the relay $R_1$, as can be seen in Fig. 5.33. The rotor terminals, with rated voltage of 690 V, are connected to the rotor converter. Since the rated voltage is 690 V, the rated power decreases from 11 kW to approx. 9 kW. The DFIG, drive system including drive machine, gear box and back-to-back converter are shown in Fig. 5.34.

The DFIG nameplate data are shown in table 5.3:

**Table 5.3. Nameplate data for LEROY SOMER 11 kW wound rotor slip ring generator.**

| **LEROY SOMER**, MOT. ~ FLSB 180 M4 B3, No. 14618900HG01, kg: 220 | | | | | |
|---|---|---|---|---|---|
| IP55 IK | 1 cl. F | 40 °C | S1 | | |
| V | Hz | 1/min | KW | cosφ | A |
| 690Y | 50 | 1460 | 11 | 0.81 | $I_S$=13 |
| $V_R$=1700 | | | | | $I_R$= 6.1 |
| DE | 6310 | 15cm$^3$ | 11000 | H | 50/60 Hz |
| NDE | 6310 | 15cm$^3$ | 11000 | H | 50/60 Hz |

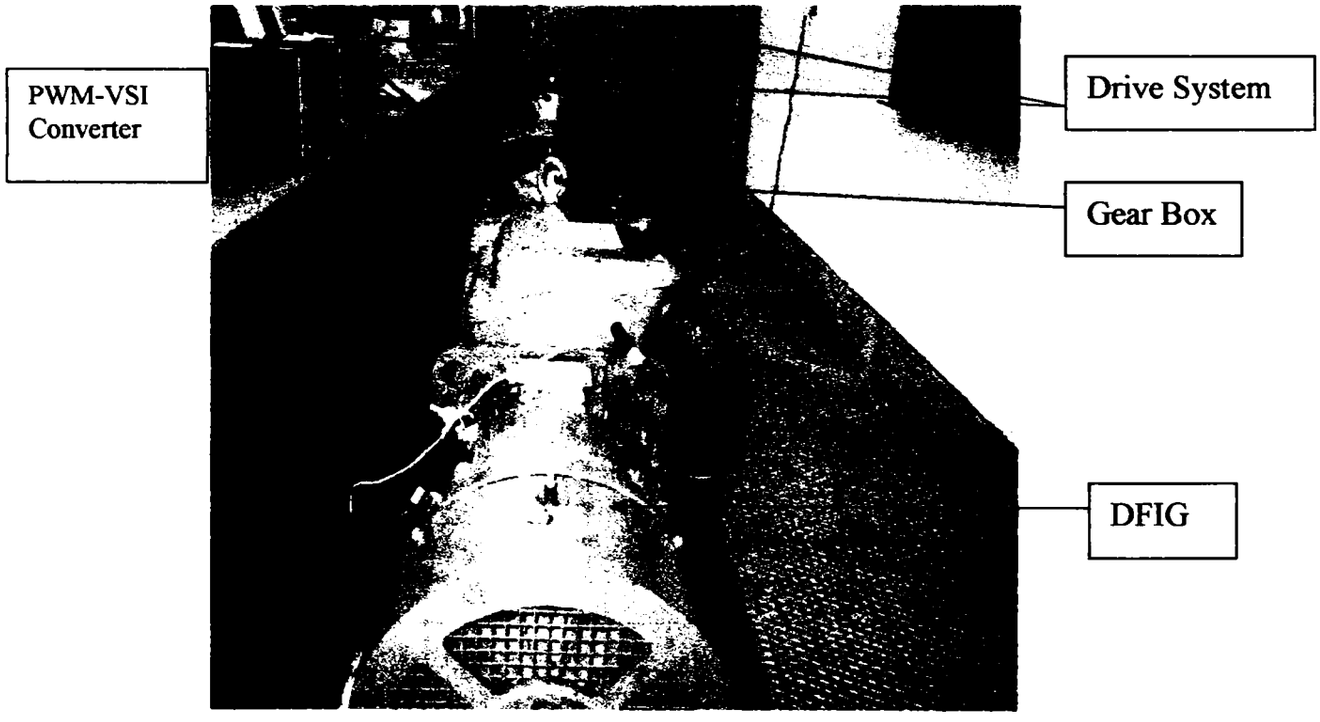


**Figure 5.34**. Picture of the DFIG, gear-box, drive system and PWM-VSI Converter in the test system.

### 5.7.2.2. Drive System

The drive system used for controlling the speed and emulating the variable-speed wind turbine is composed of a three-phase induction machine with a frequency converter. In

addition an encoder is used for measured the speed and position of the rotor. A braking resistance may be used for breaking the DFIG.

The drive motor is a 15 kW squirrel cage induction machine from LEROY SOMER. The converter is a 22-kVA frequency-converter, with speed feedback from the encoder. The resolution of the encoder is 1024 pulses/revolution.

The data for the drive motor and the frequency converter are shown in the tables 5.4 and 5.5:

**Table 5.4. Data sheet for LEROY SOMER 15 kW induction motor**

| **LEROY SOMER**. MOT. 3~LS 160 RB. No 68584HF0002 | | | | | |
|---|---|---|---|---|---|
| IP55 IK 08 | 1 cl. F | 40 °C | | | |
| V | Hz | 1/min | kW | cosφ | A |
| Y380 | 50 | 1440 | 15 | 0.87 | 29.5 |
| D230 | 50 | 1450 | 15 | 0.84 | 50.4 |
| Y400 | | | | | 29.1 |
| Y415 | 50 | 1455 | 15 | 0.81 | 29.2 |
| Y440 | 60 | 1735 | 18 | 0.88 | 30.1 |
| Y460 | 60 | 1740 | 18 | 0.86 | 29.1 |
| AV: 6309ZZ CODEUR 1024 PTS 5V- | | | | | |

**Table 5.5. Data sheet for 22-kVA frequency converters**

| Getriebau NORD Schlich+Kuchenmeister GmbH&Co. D-22941 Bargteheide/Germany | |
|---|---|
| NORDAC Vector | SK 15.00/3 CTD |
| Komm. Nr. | 9731285 |
| Input: | 3 ph 380/460 |
| Output: | 3 ph 0-input-voltage |
| Power | 22.2 kVA |
| Motor: | 15 kW |
| Protection: | IEC 536/VDE 160 |
| | IEC 529 N20 |
| Temp. Range: | 0-40 °C |

The frequency converter is controlled by an analog input proportional to the required speed. To avoid over voltages in the DC-link for generator operation of the drive motor, a braking resistance of 130 Ω and a DC-chopper is added. If an over-voltage would occur, the drive system would be shutdown.

Frequency converter for drive system is shown in Fig. 5.35:

**Figure 5.35**. The frequency converter as a part of drive system.

### 5.7.2.3. The two back to back PWM-VSI converters

The Grid Converter and Rotor Converter are identical. Each converter is composed of three-single phase modules and larger phase inductances of 8-mH for filtering the current, as is shown in Fig. 5.36.

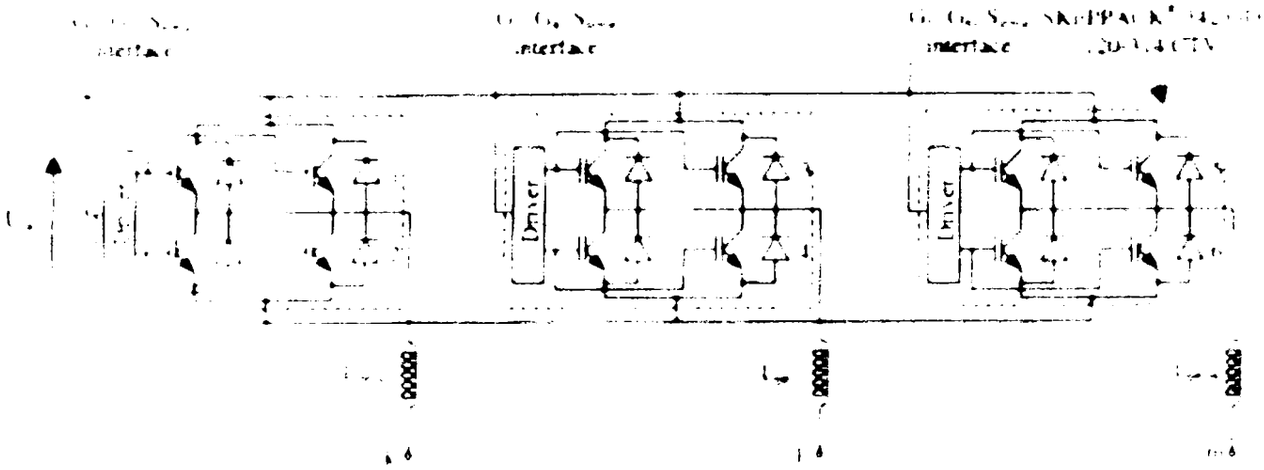

**Figure 5.36.** Circuit configuration of the grid and rotor converters. Each phase contains a SKiiPPACK module and a phase inductance for filtering the current. The signals $S_{1\text{-}6}$ and the error signals are connected to the control system.

Each switch is composed of two parallel IGBTs with freewheeling diodes to obtain the appropriate power level. Therefore each module contains 4 IGBTs and 4 freewheel diodes. The grid and rotor converters are controlled from a digital signal processor (TMS320C32 DSP). An external timer circuit is used for generating the PWM signals required for controlling the gates of IGBTs. The structure of the control of the SKiiPPACK modules has been depicted in Fig. 5.10. An intelligent integrated control module containing the IGBTs, diodes and drive circuit is provided in each phase. The module is a SKiiPPACK 342 GD 120-314 CTV from SEMIKRON. The drive circuit in the SKiiPPACK provides dead time, over voltage protection and over temperature protection. If an error occurs, the error signal from the SKiiPPACK goes low. The driver also provides galvanic isolation between the control system and the IGBTs.

Data for the SKiiPPACK modules are shown in the Table 5.6:

**Table 5.6: Data sheet for SKiiPPACK 342 GD 120-314 CTV modules**

| | | | | | |
|---|---|---|---|---|---|
| $U_{dc}$ [V] | Maximum DC-link voltage | 900 | $U_{DG,\,th}$ [V] | Threshold voltage, IGBT | 1,4 |
| $I_{max}$ [A] | Maximum current | 600 | $U_d$ [V] | Threshold voltage, diode | 0,9 |
| $T_{dead}$ [µs] | Dead time | 3 | $R_{on,\,IGBT}$ [mΩ] | On-resistance, IGBT | 4 |
| $T_{delay}$ [µs] | Driver propagation delay | 1 | $R_{on,\,diode}$ [mΩ] | On-resistance, diode | 2 |

The DC-link filter is composed of 8 times two series capacitors. The total capacitance is equal to 6.8 mF.

### 5.7.2.4. Control Processor Board

The two back-to-back PWM-VSI converters and the DC-link including a DC-link capacitor filter are used for controlling the rotor currents of the DFIG. Both converters are controlled by the CP board-TMS320C32 DSP from a PC. The grid converter maintains a constant DC-link voltage, which may be changed by adjusting the set point. The DC-link voltage is also controlled by the CP-board through the program TERM.EXE via the control PC. The communication between the PC and the CP-board is a serial connection via the PC's COM port. Start and stop of the grid converter and the set point of the DC-link voltage can also be controlled from the PC. The commands for starting and stopping the grid converter are *chargecmd* and *stopcmd* respectively.

The control processor board is shown in Fig. 5.37

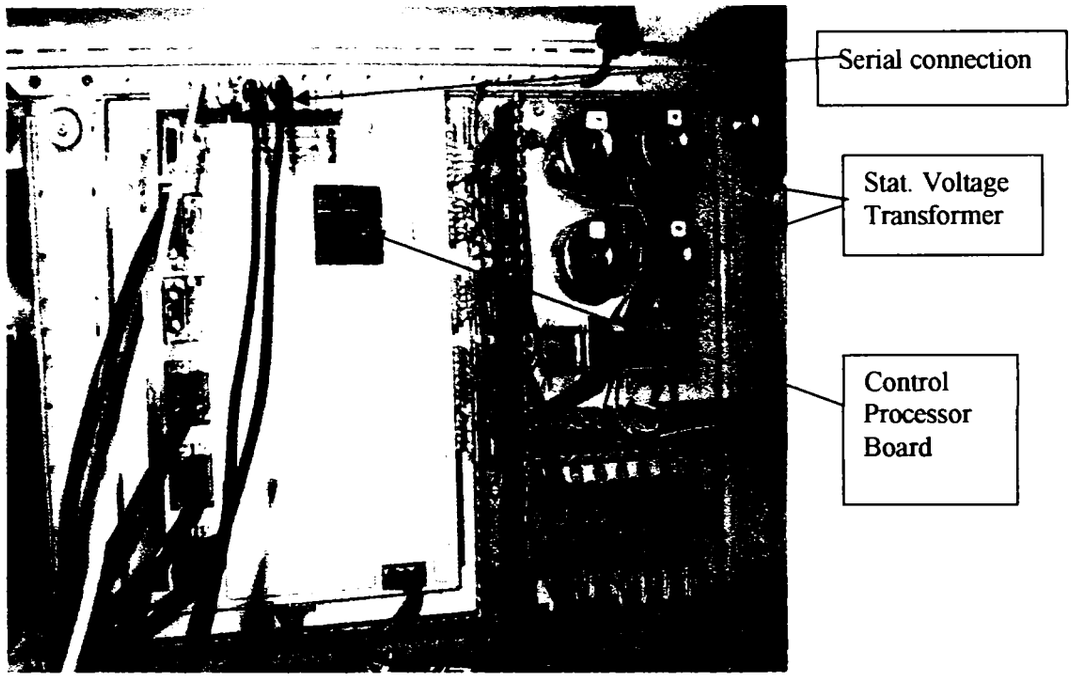


**Figure 5.37**. Control processor board and serial connection between PC and CP.

The control system controls the CP board and thereby the grid converter, the DFIG, the drive system and the rotor converter as well. The modulation and control strategy is implemented by using the TMS320C32 DSP, as shown in Fig. 5.37.

The control system is implemented with the following properties given by the control demands of the two back-to-back converters; the CP board, the DFIG and the drive system.

- Windows based PC for controlling the CP board. Modulation, control and reference parameters may be changed.
- Digital signal processor (DSP) for real-time calculation of the equations given by the control and modulation strategies. In addition, the enable/disable of the drive system and stator relay may be controlled.
- Timer circuit for implementation of the PWM modulation strategy for the grid and rotor converters.
- Transducers for measuring stator voltages and stator currents, rotor currents and rotor speed and position. In addition, filters may be required due to noisy measuring signals and to prevent anti aliasing.

- AD converters for indication of errors in the SKiiPPACK modules, and measurement of the required voltages and currents.
- DA converters for setting the reference speed of the converter to the drive system, and enable/disable settings for the turn-on/off relay and the drive system. In addition, a trigger signal may be generated for synchronization with an oscilloscope.
- Interface circuit for the switch modules in the rotor converter, stator relay and the drive system.

#### 5.7.2.4.1. Control Hardware

The control system is composed of the hardware described in the previous section. A block diagram of the system is shown in Fig. 5.38:

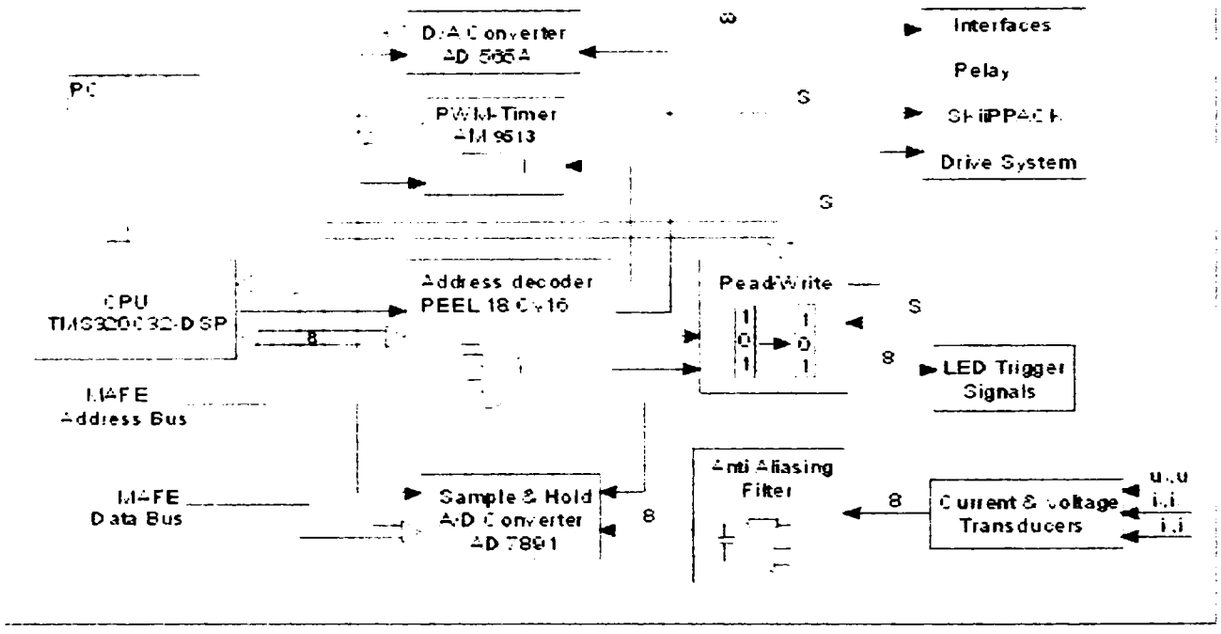


**Figure 5.38.** Block diagram of the control system with indication of the control PC, DSP, timers, DAC filters and transducers with anti aliasing filter.

The different components, illustrated in Fig. 5.38, of the control system are shortly described.

The developer board is connected to the Control PC via the ISA-bus, which makes it possible to control the DSP from the control PC. Control signals and data exchange between the DSP developer boards. The MAFE-bus is composed of an 8-bit address-bus, MA0-7 and a 16 bit parallel data-bus, MD0-15, and the read/write signals MRD and MWR. In addition a number of control signals, enable/disable etc. are controlled by the PC/DSP. The AM9513 timer generates the PWM-pattern.

For measuring the required currents, LEM modules are used since these have a linear characteristics and wide bandwidth. In addition galvanic isolation is obtained. For measuring voltages, voltage transformers are used, which gives high precision measurements and galvanic isolation. The rotor speed and position are obtained from an encoder.

To minimize noise and aliasing in the measured stator and rotor currents, an anti aliasing filter is placed between the measuring resistance of the LEM modules and the ADC. The filter

is a first order standard filter implemented as using differential coupled operational amplifiers and a RC-circuit.

Digitalization of the measured values, is performed using an AD7891 16-bit A/D converter with internal multiplexer. To obtain simultaneous sampling of all measured values, an S/H circuit, AD684 is used. The required output signals are the speed reference of the drive system and the enable/disable signal to the stator relay. The speed reference is written to an AD 565A D/A converter, and the analogue signal is feed to the frequency converter in the drive system.

To obtain the required PWM signals to the converters, an interface is implemented with the $S_1$, $S_3$, and $S_5$ signals as inputs. Each input signal is converted into two output signals for the upper and lower switch in the SKiiPPACK modules.

If the maximum ratings are exceeded or the SKiiPPACK detects an error, the DSP shouts down the system by disabling the drive system, the stator relay and the converter.

### 5.7.3. Experimental Results

This section focuses on experimental results to point out the behavior of DFIG in steady-state and transients as well. The induction generator has been monitoring using measurements of stator current and voltage, rotor current and rotor speed. The stator voltages, stator currents and rotor currents are measured by a Tektronix Oscilloscope at a rotor constant speed of 1475 rpm to a few different stator powers. The stator of DFIG can be connected to the grid in star or delta connection. Then will be presented a few transient conditions of the generator such as the synchronization to the grid and the start-up of the DFIG.

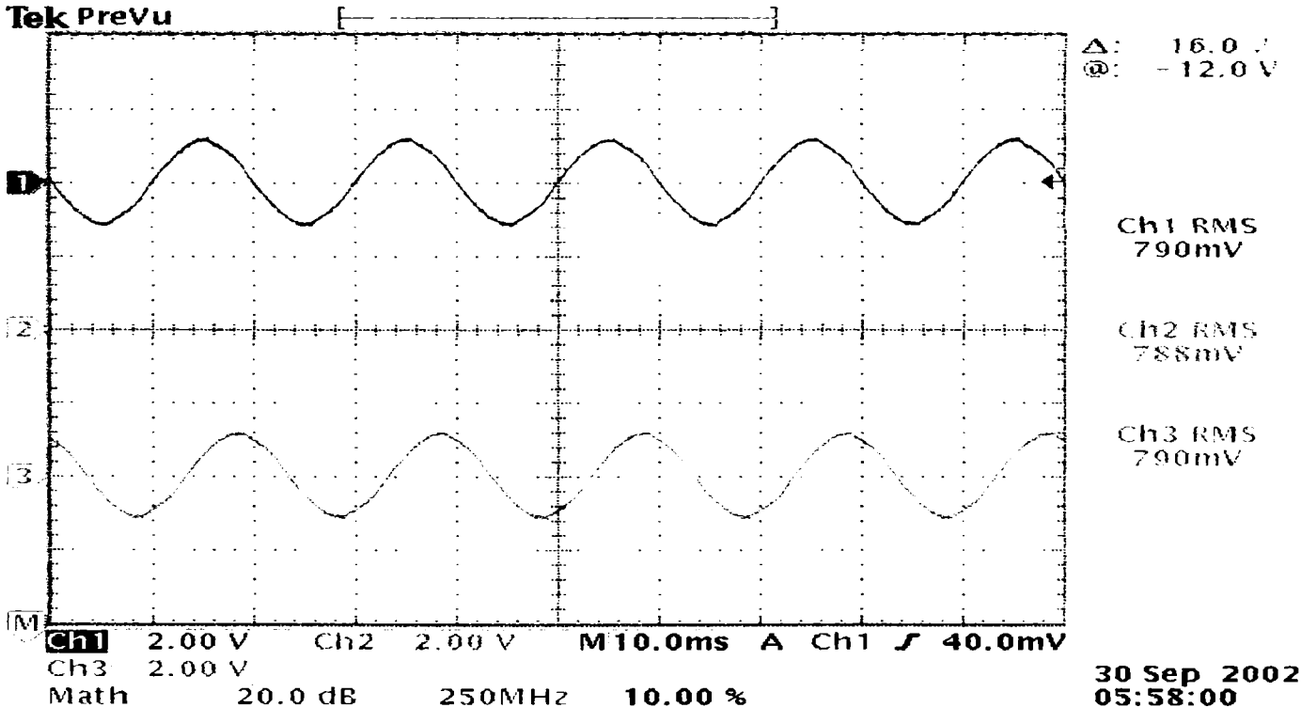


**Figure 5.39.** The stator voltages of DFIG in steady-state measured by an Oscilloscope. The DFIG was driven at 1475 rpm (sub-synchronous speed). Scaling factor is 2 (mV/V).

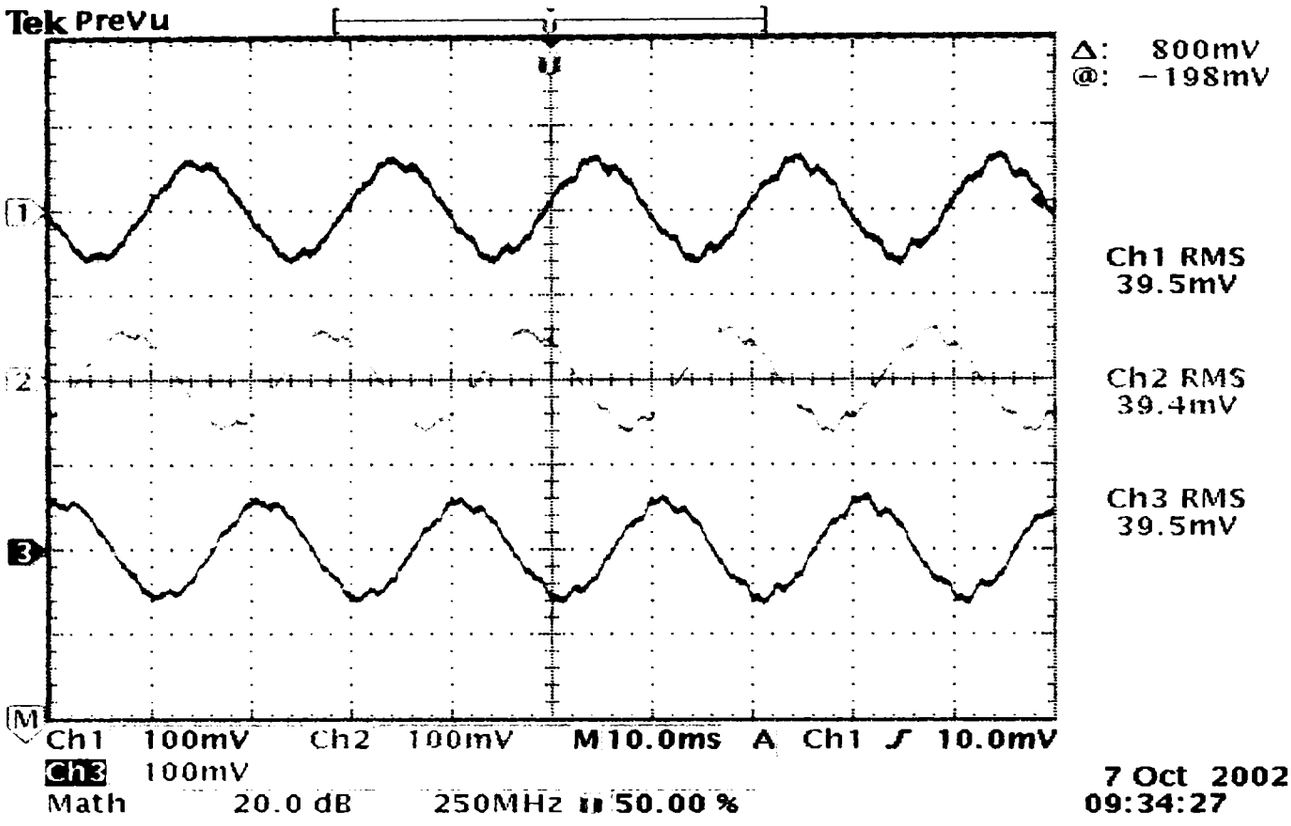


**Figure 5.40.** The stator currents of DFIG in steady-state at $P_s$=7 kW measured by a Tektronix Oscilloscope. Scaling factor is 4 (mV/A).

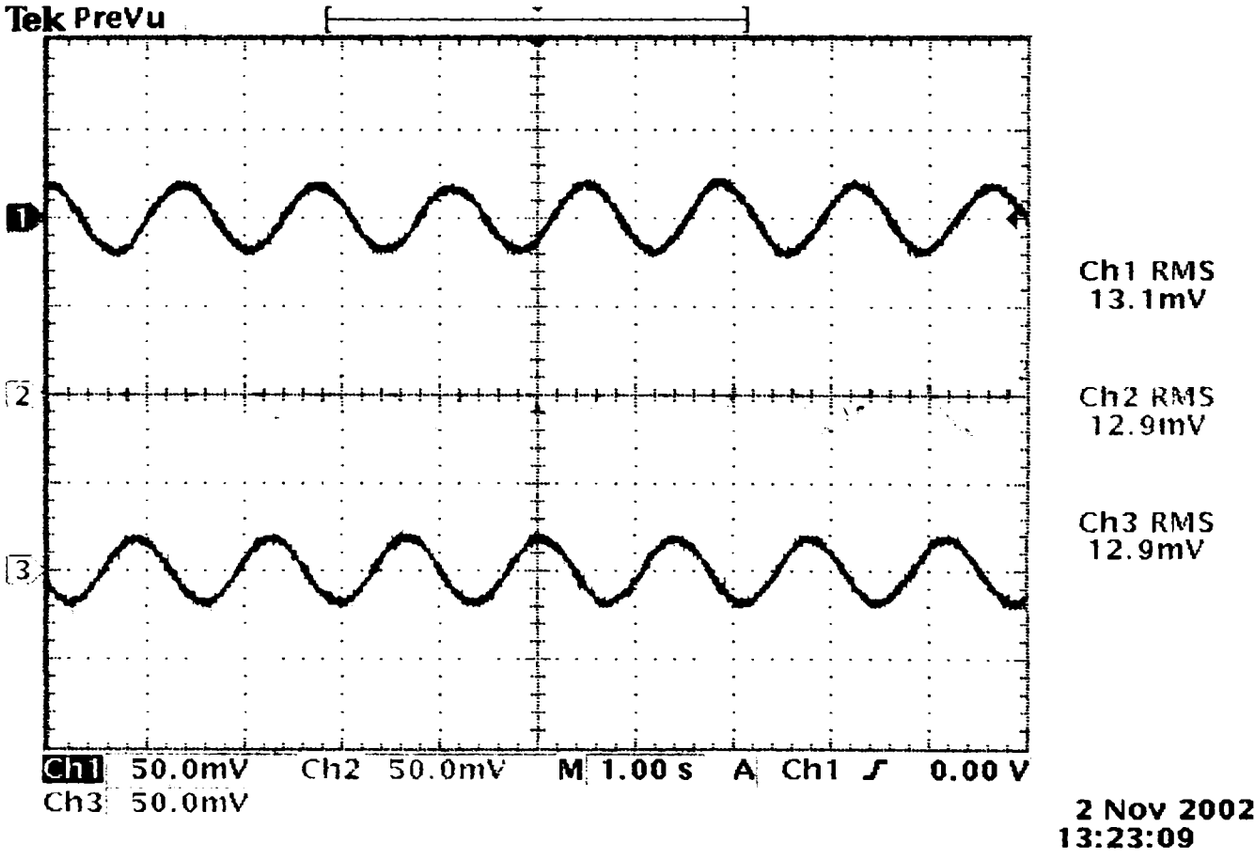


**Figure 5.41.** The rotor currents of DFIG in steady-state at Ps=7 kW acquired by a TDS 540. The scaling factor is 4 (mV/A).

The Figures 5.39, and 5.40 show the stator voltages and currents and the rotor currents of DFIG, assumed to be operating at a constant speed of 1475 rpm (sub-synchronous speed) that corresponding to the stator power of 7 kW. The acquisition of data was acquired by a Tektronix Oscilloscope-TDS 540. The stator of the induction generator was connected to the star connected power source also in star (wyes) connection. In Fig. 5.41 is presented a comparison between the stator current, voltage and stator power when the generator was connected in delta connection (a) and then in star connection (b). The DFIG was operating, during these measurements, at a rotor speed of 1475 rpm corresponding to an active power of 4 kW.

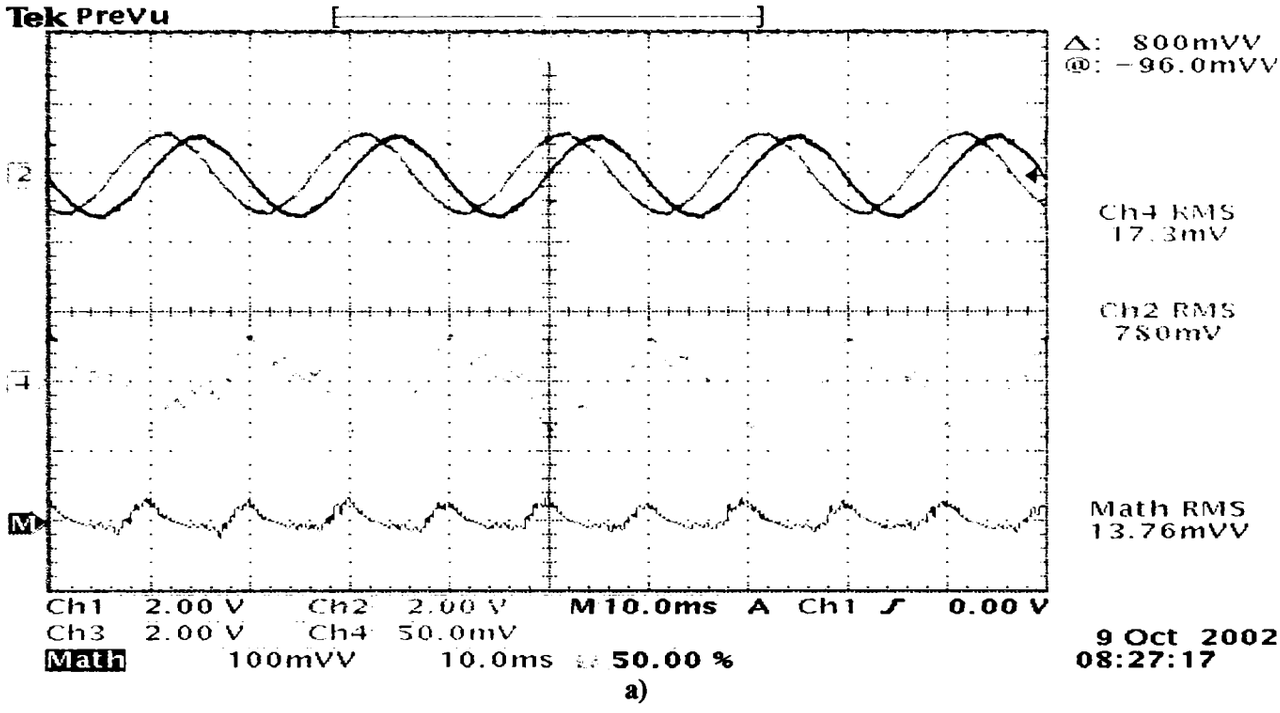


a)

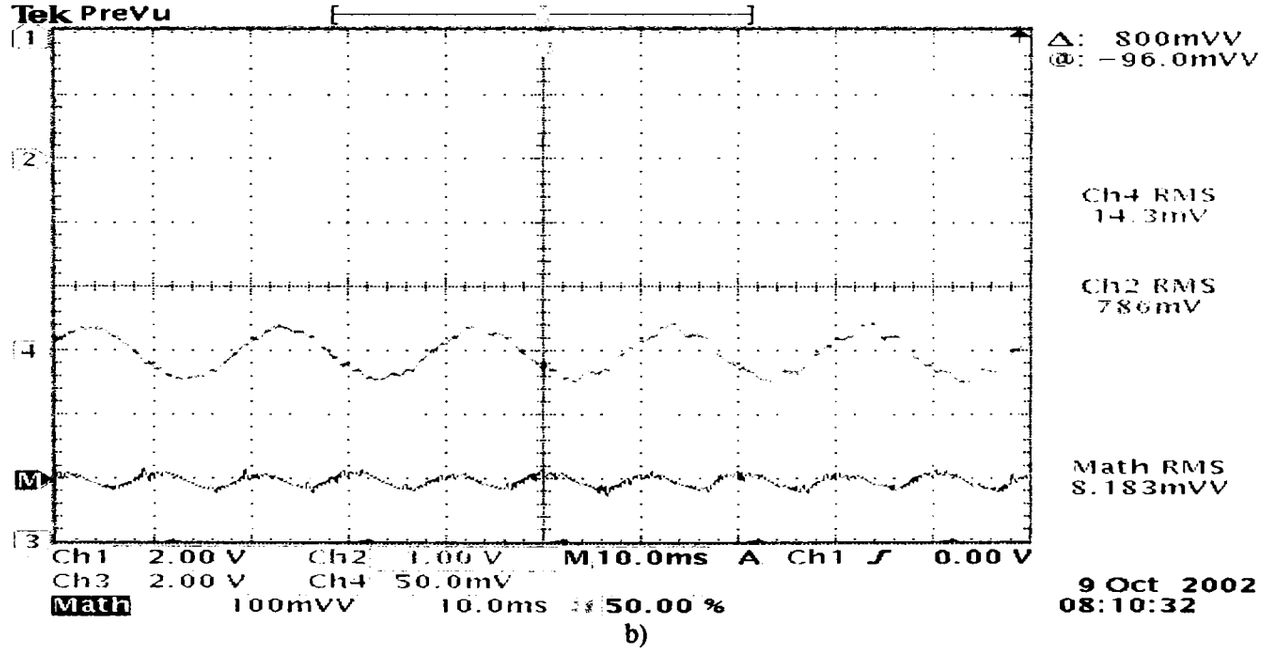


b)

**Figure 5.41**. The stator voltage, current and power of DFIG under steady-state. The stator of the generator is connected in delta-connection (a) and star connection b). CH2: Stator Voltage (2mV/V), CH4-Stator Current (4 mV/A) and M: Stator power (2 mV/V).

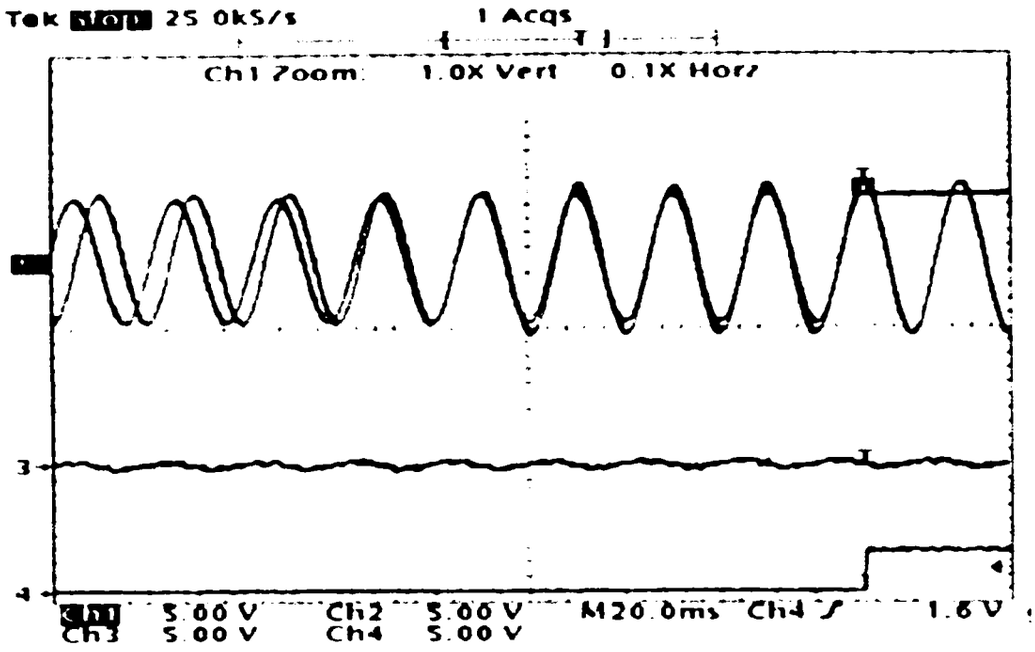


**Figure 5.42.** Grid and stator voltages (ch. 1-2) and grid and stator currents (ch. 3-4) under grid synchronization.

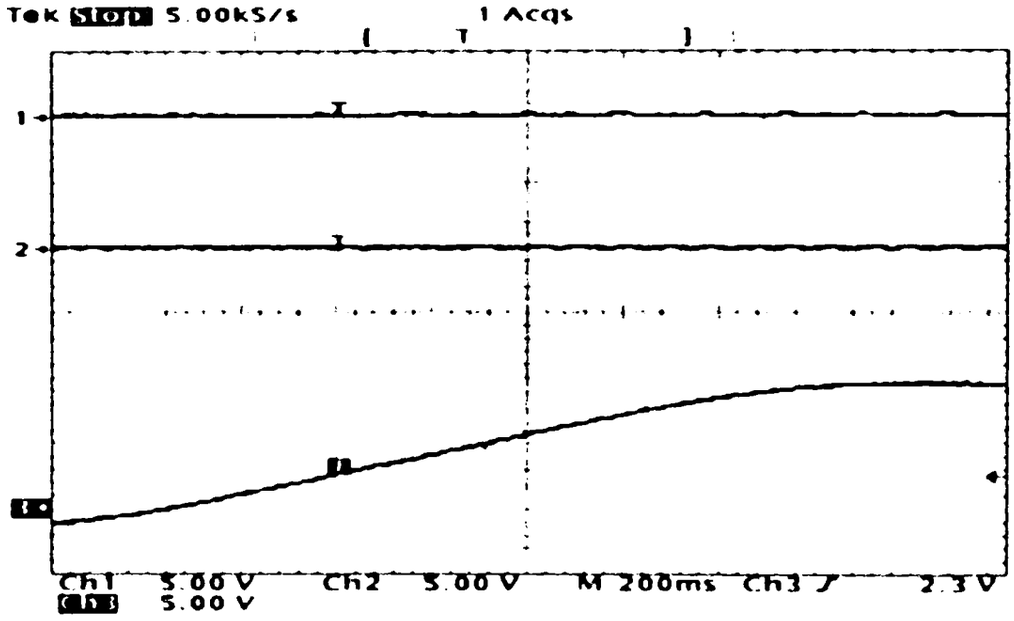


**Figure 5.43.** Active power (ch. 1), reactive power (ch. 2) and rotor speed (ch. 3) during a start-up of DFIG.

In Fig. 5.42 is presented the measured grid and stator voltages and the grid and stator currents during the synchronization on the grid of the DFIG. The control acts to obtain the equality between stator and network voltages and frequencies. The equality of grid and stator voltages is realized after 170 ms when the stator is connected to the grid.

The measured active and reactive power and rotor speed during a start-up of the generator is presented in Fig. 5.43.

The measured data were acquired by an Oscilloscope. The measured active power corresponds to 5 kW / div and the measured reactive power to 5 kVAr / div.

## 5.8. Comparison between simulation and experimental results

The equipment used to obtain the test data was described in the previous sub-chapter.

Tests and simulations were performed to examine the system performance in steady-state and to validate the Matlab-Simulink implemented system developed for a variable speed wind turbine with DFIG.

The simulations and test results intended to represent that the correspondence is good.

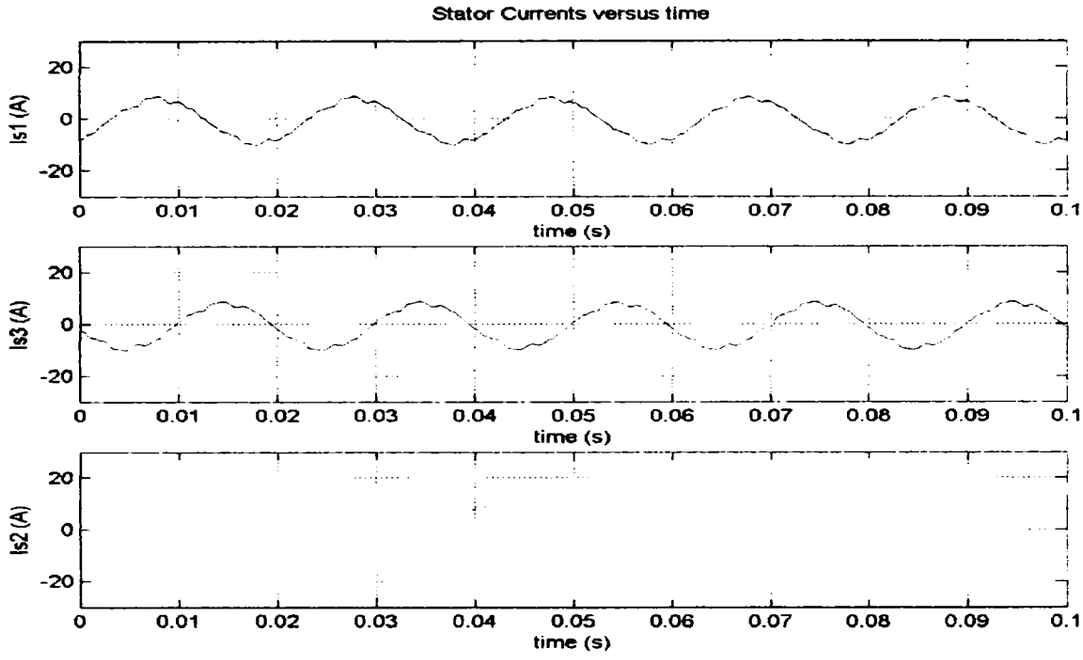


a)

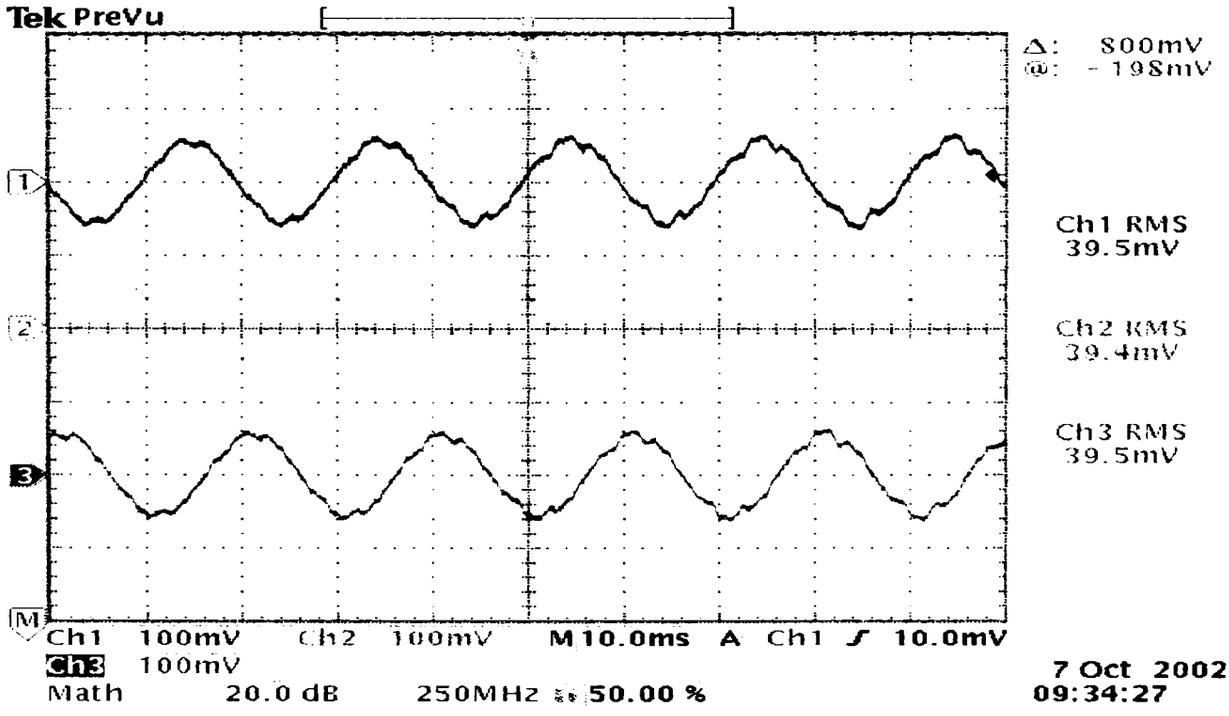


b)

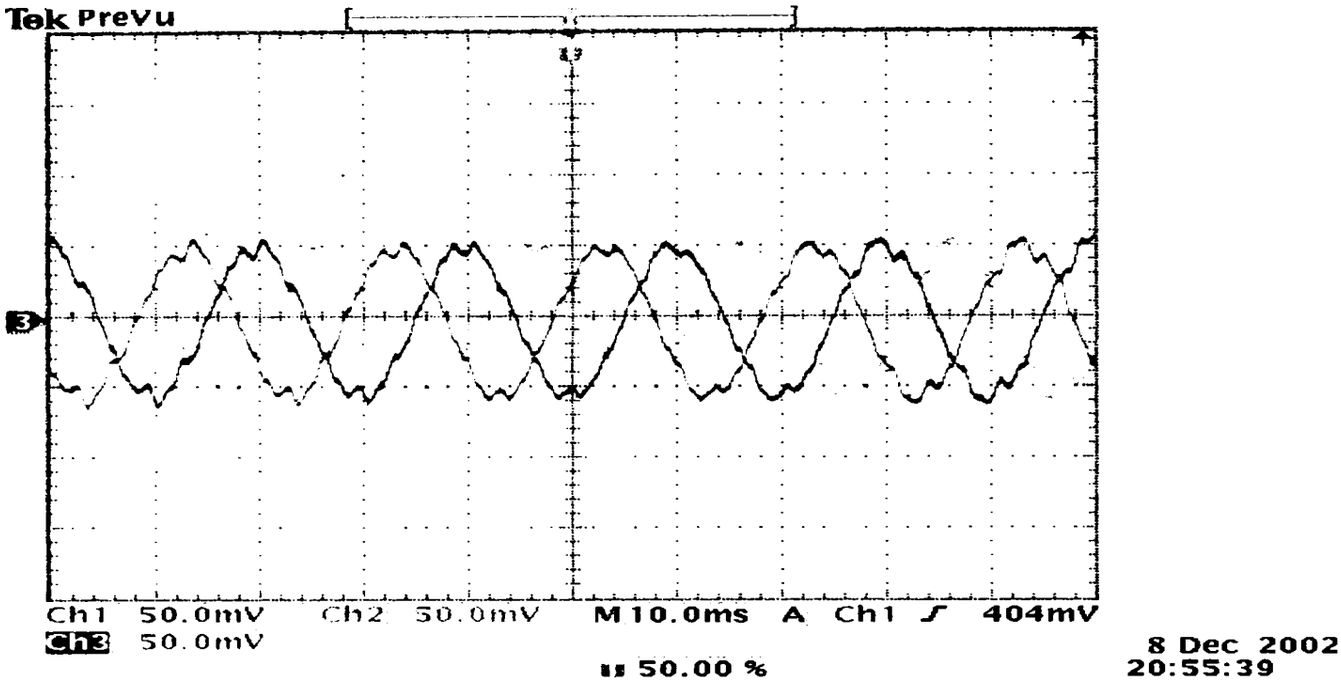


c)

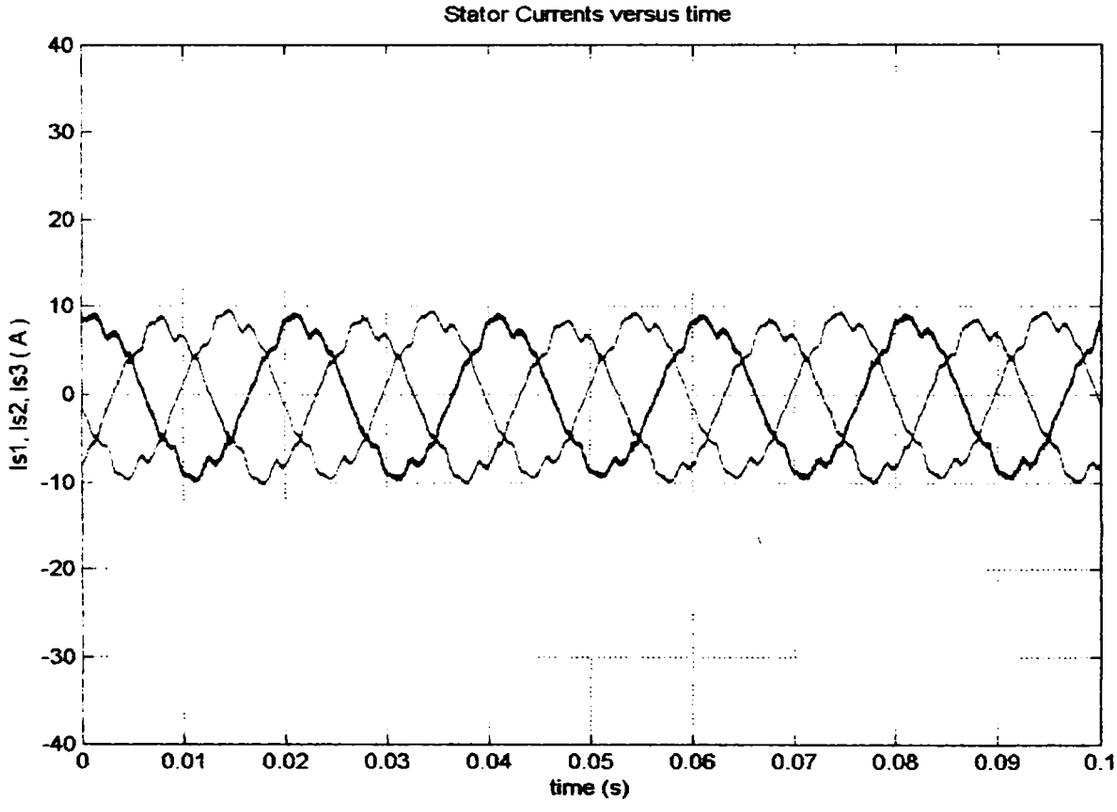


d)

**Figure 5.44.** The simulated stator currents of DFIG (a, d) using Matlab-Simulink and measured stator currents (b, c) by an Oscilloscope in steady-state at P=4 kW and n=1475 rpm (sub-synchronous operation mode). Scaling factor of measured stator currents is 4 (mV/A).

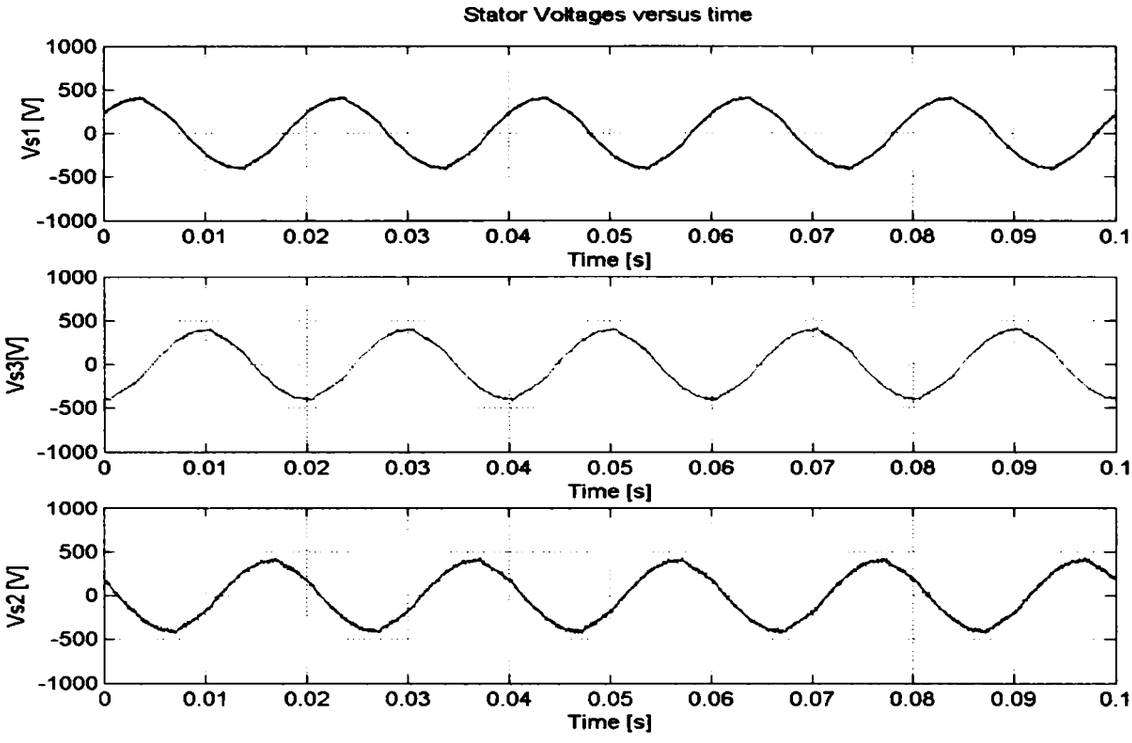


a)

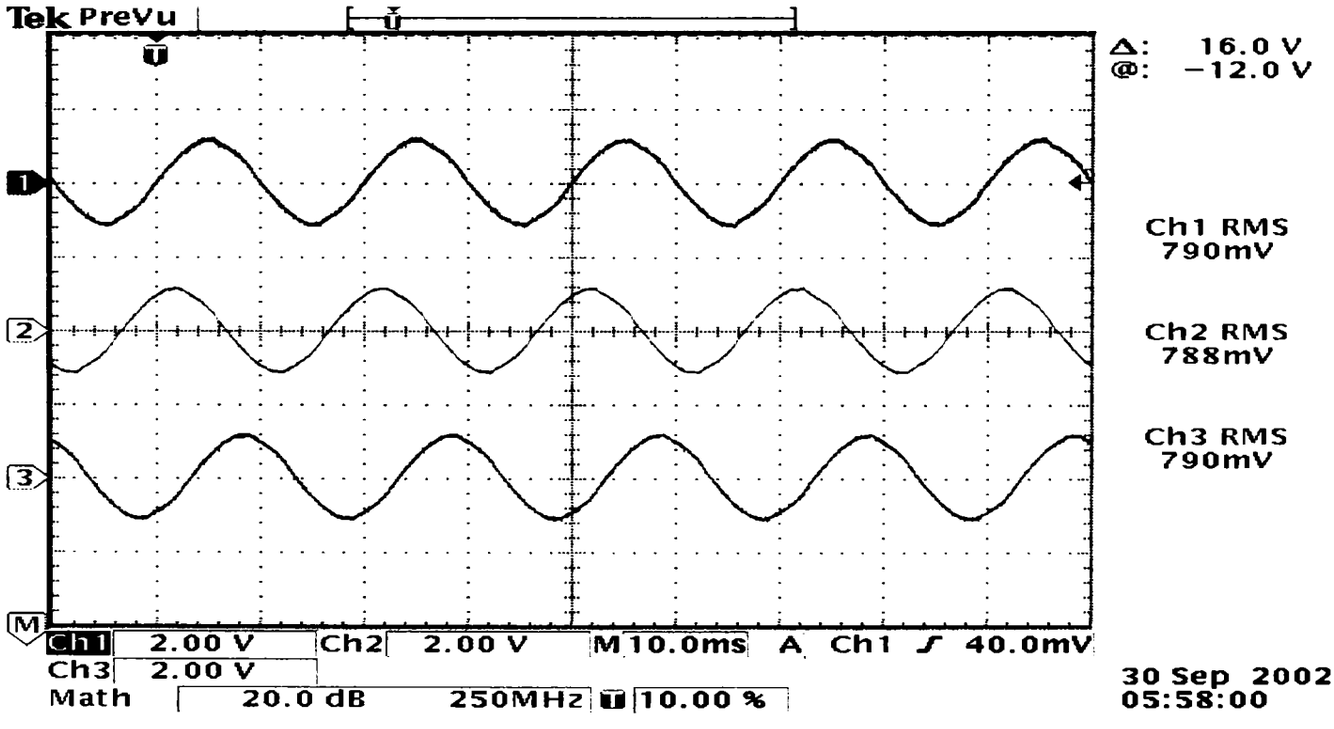


b)

**Figure 5.45.** The Simulation of stator voltages in steady-state (a) and measured line – line stator voltages of DFIG acquired by an Oscilloscope TDS 540. Scaling factor of measured stator voltages is 2 (mV/V).

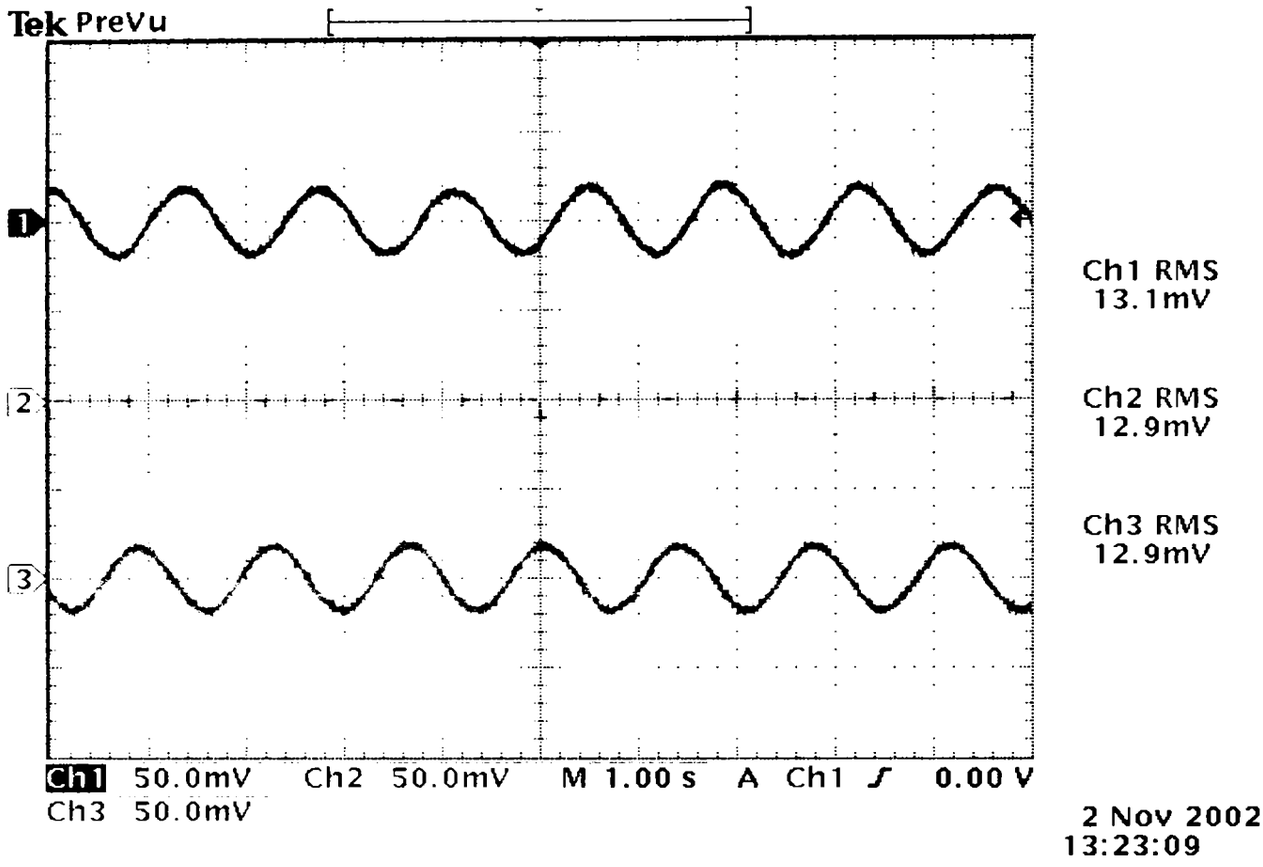


a)

b)

**Figure 5.46.** Measured (a) and Simulated (b) the rotor currents in sub-synchronous mode (1475 rpm) at P=4 kW. The acquisition of measured data was done via an Oscilloscope and the simulations were performed by Matlab-Simulink software package. Scaling factor of measured rotor currents is 4 (mV/A).

Figures 5.44-5.46 show the steady-state waveforms of stator and rotor currents and stator voltages of the DFIG running at 1475 rpm (sub-synchronous speed operation mode) and stator power of 4 kW.

The Figure 5.44 shows a comparison between simulated and measured stator currents of DFIG, while in Fig. 5.45 is presented a comparison between simulated (b) and measured (a) stator voltages of DFIG. Figure 5.46 shown a comparison between simulated (b) and measured (a) rotor currents of DFIG. The generator was running at a constant speed of 1475 rpm at a stator power of 4 kW.

The measured data were acquired by an Oscilloscope, while the simulation results were performed by Matlab / Simulink.

The correspondence between simulation and experiments is very well as can also be seen in Figs. 5.44-5.46.

## Discussion and Conclusion

The variable-speed wind turbine system investigated in this chapter, consist of a DFIG connected to the power grid at the stator terminals, and the rotor are supplied though a back-to-back PWM-VSI converter. A control scheme is developed to decouple active and reactive power control, modeled and implemented using Matlab-Simulink program package.

The modeling of the DFIG is based on the three-phase voltage representation, and the two-phase representation is developed assuming a symmetric three-phase machine. The model is developed in the arbitrary reference frame. The torque and flux equations are also developed and the stator active and reactive power is calculated. The complete Simulink model is presented with DFIG parameters given. The model of DFIG implemented in Matlab-Simulink calculates the stator and rotor currents, stator and rotor active and reactive power and electromagnetic torque as a function of time depending on inputs of the stator and rotor voltages and mechanical speed of the rotor shaft.

The PWM-strategy, Stator Flux Asynchronous Vector Modulation (SFAVM) is applied to control the rotor converter. The SFAVM modulation strategy is presented and equations for calculating the duty-cycles are set up. It is implemented as a modulation function in simulation program. The modulation curve of one phase is calculated for 2 $\pi$ radians and is used as a look up table for generating the duty-cycles for all three rotor phases. As the average value of rotor converter model yields satisfactory results it is decided to employ it due to the decrease time of simulation. The rotor converter is controlled from a DSP. The control signals are generated by the modulation function, which is implemented in the DSP. The DSP generates the PWM reference signals on basis of the implemented modulation strategy (SFAVM). The PWM generator generates the PWM signals at 5 kHz switching frequency. The reference signals determine the fundamental rotor frequency and the voltage amplitude. The grid converter controls the DC-link voltage and the power factor at the grid connection. In Simulink model of the complete system the grid converter is assumed as an ideal converter having a power factor of one, gaining a constant voltage supplying the rotor converter. The power grid is assumed rigid, modeled by an ideal voltage sources. The mechanical system, gear-box, wind turbine rotor are modeled by the drive system. The mechanical system implemented in Simulink is modeled using a first order approximation, where the time constant is determined from a step in rotor speed.

A control scheme is developed for decoupled control of active and reactive stator power of the DFIG. The control strategy is a cascade control, having two control loops. An inner rotor current control loop and an outer stator power control loop. The two-phase d-q reference system with the q-axis aligned along the stator flux is chosen for implementation to realize decoupling of active and reactive power. The simulations show that full power decoupling is obtained in the complete operating range between 65 % and 140 % of nominal speed. The control system contains the following components: transformation of the measured stator voltages and currents into the stator fixed reference frame, calculation of the active and reactive power as well as stator flux in the stator fixed reference frame, calculation of the stator flux position to obtain the angle of the stator flux fixed reference frame, regulators for controlling the stator active and reactive power, calculation of the desired rotor d- and q-axis currents by use of the power decoupling equations, transformation of the measured rotor currents into the stator flux fixed reference frame, regulators for controlling the rotor currents,

implementation of the rotor voltages from the stator flux fixed reference frame to the rotor fixed reference frame and modulation of the duty-cycles for the three phases by use of SFAVM modulation strategy. The simulations show good performance regarding power control therefore the fluctuations into the power grid are reduced compared to the OptiSlip topology or to limited variable speed control scheme.

An analytic analysis of the current loop and the power loop are performed. The appropriate regulators are selected and compared through simulations. Two regulators are implemented in the simulation program. The classical P and PI-Regulators for the current loop and the PI-Regulator for the power loop are tuned using the root locus design method. Both regulators show good performance in the simulations.

The existing experimental system was analyzed, modeled and simulated and tested. The physical system consisting of a drive system, DFIG, rotor converter, DSP, AD/DA converters and transducers are modeled and implemented using Matlab-Simulink. The simulation results were compared with experimental results and good agreement are obtained. The simulation also shows good dynamic performance regarding power control when the rotor speed is varied. Measurements obtained confirm the theoretical results and validate the simulation program of the variable-speed constant frequency system with the DFIG for wind power generation applications.

The doubly fed induction generator system presented in this chapter offers many advantages to reduce cost and has the potential to be built economically at power levels above 1.5 MW, e.g. for off-shore applications. The DFIG can supply power at constant voltage and frequency while the rotor speed varies. This makes it suitable for variable speed wind energy applications. Additionally, when a bidirectional AC-AC converter is used in the rotor circuit, the speed range can be extended above synchronous speed and power can be generated both from the stator and the rotor. The two back-to-back PWM converters in the rotor circuit resulting in low distortion currents, reactive power control and both sub- and super-synchronous operations. Another advantage of this type of DFIG drive is that the rotor converter need only be rated for a fraction of the total output power (25% of the total generator power), the fraction depending on the allowable sub- and super-synchronous speed range.

**Acknowledgements**:
The author would like to thank Ass. Professors Birgitte Bak-Jensen and Ewen Ritchie of Aalborg University-Denmark, for their useful suggestions and for their help to use and improve an existing set-up of variable-speed wind generator system. They hosted my experiments in their laboratory.

# References

[1] Siegfried Heier, "Wind energy conversion systems", book, John Wiley & Sons Inc., New York, 1998.

[2] L.H. Hansen, L. Helle, F. Blaabjerg, E. Ritchie, S. Munk-Nielsen, H. Bidner, P. Sorensen and B. Bak-Jensen, "Conceptual Survey of Generators and Power Electronics for Wind Turbines", Riso-R-1205 (EN), December 2001.

[3] Paul C. Krause, "Analysis of Electric Machinery", Mc Graw-Hill Book Company, 1986.

[4] Paul C. Krause, "Analysis of Electric Machinery", 1995 IEEE Press, ISBN 0-7803-1101-9, 1995.

[5] Gene F. Franklin, Powell J. David, Michael L. Workman, "Digital Control Systems", book, Addison Wesley, ISBN 0-201-51884-8, 1990.

[6] www.vestas.com , Vestas Wind Systems, Denmark.

[7] Vestas, OptiSpeed, Vestas Converter System, General Edition, Item. No. 947543.RO-Class 1, 3rd January 2001.

[8] V. Akhmatov, "Modelling of Variable-Speed Wind Turbines with Doubly-Fed Induction Generators in Short-Term Stability Investigations", 3rd Int. Workshop on Transmission Networks for Offshore Wind Farms, April 1-12, 2002, Stockholm, Sweden.

[9] Paul Thogersen and John K. Pederesen, "Stator Flux Oriented Asynchronous Vector Modulation for AC-Drives", IEEE Transaction on Industry Application, 1990, pp. 641-648.

[10] R. Pena, J.C. Clare, G.M. Asher, "Doubly Fed Induction Generator using Back-to-Back PWM Converters and its Application to Variable Speed Wind Energy Generation", 1996, IEE Proceedings on Electrical Power Applications, vol. 143, no. 3, pp. 231-241.

[11] Katsuhiko Ogata, "Modern Control Engineering", 1995, Prentice Hall, ISBN 981-3026-94-4.

[12] R. Pena, J.C. Clare, G.M. Asher, "A doubly fed induction generator using back-to-back PWM converters supplying an isolated load from a variable speed wind turbine", IEE Proc.-Electr. Power Appl., vol. 143, no. 5, September 1996, pp. 380-387.

[13] Hirofumi Akagi and Hikaru Sato, "Control and Performance of a Doubly-Fed Induction Machine Intended for a Flywheel Energy Storage System", IEEE Transaction on Power Electronics, vol. 17, no. 1, January 2002, pp. 109-116.

[14] S. Muller, M. Deicke and Rik W. De Doncker, "Doubly Fed Induction Generator Systems for Wind Turbines", IEEE Industry Applications Magazine, May-June 2002, pp. 26-33.

[15] V. De Oliveira, E. Monmasson, R. Meuret, J.P. Louis, "Steady State Analysis of a Double Fed Induction Generator for Aircraft Application", Electromotion 2001, June 19-20, pp. 547-551.

[16] B. Robyns, M. Nasser, F. Berthereau, F. Labrique, "Equivalent Continuous Dynamic Model of a Variable Speed Wind Generator", Electromotion 2001, June 19-20, pp. 541-546.

[17] D. Panda, Eric L. Benedict, G. Venkataramanan and Thomas A. Lipo, "A novel Control Strategy for the Rotor Side Control of a Doubly-Fed Induction Machine", IEEE Transactions on Power Electronics, 2001.

[18] Rajib Datta and V.T. Ranganathan, "Direct Power Control of Grid-Connected Wound Rotor Induction Machine Without Rotor Position Sensors", IEEE Transactions on Power Electronics, vol. 16, no. 3, May 2001, pp. 390-399.

[19] P. Vas, "Vector Control of a.c. machines", book, Oxford University Press, 1990.

[20] S. Tnami, S. Diop and A. Berthon, "Novel control strategy of doubly-fed induction machines", EPE, 1995, pp. 553-558.

[21] D.S. Zinger, E. Muljadi, "Annualized wind energy improvement using variable speeds", Industrial & Commercial Power Systems technical Conference, 1997. Conference Records, Papers presented at the 1997 Annual Meeting, IEEE 1997, 11-16 May 1997, pp. 80-83.

[22] P. Vas, "Sensorless vector and direct torque control", book, Oxford University Press, 1998.

[23] A.S. Neris, N.A. Vovos, G.B. Giannakopoulos, "A variable speed wind energy conversion scheme for connection to weak ac systems", IEEE Transactions on Energy Conversion, Vol. 14, No. 1, March 1999, pp. 122-127.

[24] L. Huber, D. Borojevic, "Space Vector Modulated Three-Phase to Three-Phase Matrix Converter with Input Power Factor Correction", IEEE Transactions on Industry Applications, Vol. 31, No. 6, November/December 1995, pp. 1234-1247.

[25] Bimal K. Bose, "Power Electronics and Variable Frequency Drives-Technology and Applications", book, IEEE Press-IEEE IES, IEEE IAS, IEEE PES, ISBN 0-7803-1061-6, New York, 1997.

# Chapter 6

# CONDITION MONITORING OF WIND GENERATORS

**Chapter Contents:**

This chapter deals with the analysis of Condition Monitoring of Wind Generators using Doubly Fed Induction Generators (DFIG). Mainly this paper focuses on the experimental investigation for incipient fault detection and fault detection methods, suitably adapted for use in wind generator systems. The chapter 6 aims is to provide wind generators with an advanced condition monitoring system, monitoring electrical quantities, in order to avoid undesirable operating conditions, to detect and diagnose sensors and incipient electrical faults.

Studies included design and commissioning of a measuring system-comprising signal conditioning box, AD card and transducers for current, voltage, speed and temperature.

## 6.1. An overview of Condition Monitoring.

Most failures (incipient failure) give some warning of the fact that they are about to occur. This warning is called a potential failure, and is defined as an identifiable condition, which indicates that a functional failure is either about to occur, or is in the process of occurring. The objective of condition monitoring is to provide maintenance personnel with reliable information regarding the current condition of the generator system. This will enable maintenance activities to be planned on the basis of the real needs of the apparatus rather than based on an estimated safe time between services. This will keep the machinery operating in acceptable condition for the longest time for the least possible cost.

The principle of Condition Monitoring (CM) of machinery is straightforward:

- The goal is to identify changes in the condition of a machine that will indicate some potential failure
- Physical characteristics are identified that collectively indicate the current condition of the machine
- Each of these characteristics is measured, analysed and recorded so that trends can be recognized

CM is carried out for two main reasons:

- To detect sudden changes in condition that could lead to catastrophic failure
- To identify the early onset of incipient failures so that a prediction can be made about their most likely progress and suitable actions can be planned.

In general, condition-monitoring schemes have concentrated on sensing specific failure modes in one of three induction motor components: the stator, the rotor, or the bearings. Thermal and vibration monitoring have been utilised for decades. Recent research has been directed toward electrical monitoring of the generator with emphasis on inspecting the stator current of the motor. In particular, a large amount of research has been directed toward using the stator current spectrum to sense rotor faults associated with broken rotor bars and mechanical unbalance. Many condition-monitoring methods have been proposed for the detection of different types of rotating machine faults. Vibration sensors based on proximity probes are delicate and expensive. However, in many situations, vibration-monitoring methods are utilised to detect the presence of incipient failure.

A complete condition monitoring system could comprise many subsystems, each monitoring a particular part of the windmill [65-67]. There will be a degree of overlap between the functions of the different subsystems. Development of a single subsystem will comprise several phases:

- Firstly, it will be required to decide which properties to monitor. These could be structural effects and responses, or component damage or ageing.
- Secondly, it must be decided what to measure, in order to monitor these properties. It is extremely important that diagnostic decisions are made, based on reliable monitoring results. It will often be difficult, or even impossible to measure the required properties directly, in operation. Indirect measurement of the required properties is often used.
- The next step is to process the measurement results; on-line or off-line based on a model of the monitored system, to construct a signal containing the required information, the indicator.
- Next, this signal will be analyzed in the diagnosis step, to detect the prevailing condition of the system.
- Finally, a relevant action or control will be decided upon, to maintain the system in acceptable working order.

## 6.2. Faults and fault detection methods of the induction machines

### 6.2.1. A discussion of faults developed in induction machines

The induction machine can operate under asymmetrical stator and/or rotor-winding connections as described in [7, 8, and 10]:

1. Inter-turn fault resulting in the opening or shorting of one or more circuits of a stator phase winding;
2. Abnormal connection of the stator winding;
3. Inter-turn fault of a rotor phase winding and/or brushes;
4. Broken rotor bar or cracked rotor end-rings; (cage rotor)
5. Static and/or dynamic air-gap irregularities;
6. A rub between the rotor and the stator which can result in serious damage to the stator core and windings;
7. Shorted rotor field winding (cage rotor)

*Faults in AC induction machines produce one or more of the following symptoms:*

- Unbalanced air-gap voltages and line currents
- Increased torque pulsation
- Decreased average torque
- Increased losses and reduction in efficiency
- Excessive heating
- Disturbances in the current/voltage/flux etc. waveform

The diagnostic methods available to identify the above faults may involve several different fields of science and technology. They may be described as [9]:

a) Electromagnetic field monitoring, search coils, coils wound around motor shafts (axial flux related detection)
b) Temperature measurements

c) Noise and vibration monitoring
d) Motor current signature analysis (MCSA)
e) Model artificial intelligence and neural network based techniques.

Of the above types of faults, stator or armature faults, broken rotor bar and end ring faults and eccentricity related faults are the most prevalent electrical faults and thus fall into the area of interest of this report.

The most prevalent faults in AC induction machines fall into the following four categories [1, 5, 6, 10, and 53]:

1. ***Bearing fault***: Though almost (40-50) % of all motor failures is bearing related, very little has been reported in the literature regarding bearing related fault detection techniques. Bearings faults may manifest themselves as rotor asymmetry faults from the category of eccentricity related faults. Bearings faults are outside the area of interest of this report and will not be discussed further.
2. ***Stator or armature faults***: These faults start as undetected turn-to-turn faults, which grow and culminate as major faults. Almost (30-40) % of all reported induction machines failures fall in this category. Toliyat and Lipo [7] have shown through both modelling and experiments that these faults can result in asymmetry in the machine impedance causing the machine to draw unbalanced phase currents.
3. ***Broken rotor bar and end ring faults***: Rotor failures now account for (5-10) % of total induction motor failure. The rotor asymmetry, resulting from rotor ellipticity, misalignment of the shaft with the cage, magnetic anisotropy, etc. shows up at the same frequency components as the broken bars. Therefore other features of this fault need to be investigated.
4. ***Rotor faults***: The rotor windings of the induction generators may develop inter turn (turn-to-turn) short-circuits, which can increase in severity over a period of time. Rotor shorts produce damage to the main wall and inter turn insulation at the site of the short due to overheating, and thermal unbalance due to unsymmetrical heating around the rotor.
5. ***Eccentricity related faults.*** Eccentricity related faults cause unequal air-gap between the stator and rotor. It is called static air-gap eccentricity when the position of the minim radial air-gap length is fixed in the space. This may be caused by ovality of the stator core or by the incorrect positioning of the rotor or stator at the manufacturing stage. Dynamic eccentricity occurs when the centre of rotor is not at the centre of rotation, so the position of minimum air-gap rotates with the rotor. A bent rotor shaft, bearing wear, misalignment or mechanical resonance at critical speeds, may cause this. In practice an air-gap eccentricity of up to 10 % of the air-gap length is permissible. Both static and dynamic eccentricities occur in practice. An extreme case of eccentricity will cause a rub between the stator and rotor.

### 6.2.2. Fault Detection Methods

During the past fifteen years there has been a substantial amount of research into the creation of new condition monitoring techniques for electrical machine drives. New methods have been developed which the operators are now using and research is continuing with the development of new and alternative on-line diagnostic techniques. However, it is still the

operators who have to make the selection of the most appropriate and effective monitoring systems to suit their particular electric motor drive systems.

The diagnostic methods to identify the faults may involve several different types of fields of science and technology. They can be described as [53]:

a) Electromagnetic field monitoring, search coils, coils wound around motor shafts (axial flux related detection),
b) Temperature measurements,
c) Infrared recognition,
d) Radio frequency (RF) emissions monitoring,
e) Noise and vibration monitoring,
f) Chemical analysis,
g) Acoustic noise measurements,
h) Motor current signature analysis (MCSA),
i) Model, artificial intelligence and neural network based techniques.

In this context, a variety of sensors could be used to collect measurements from an induction motor for the purpose of failure monitoring. These sensors might measure stator voltages and currents, air-gap and external magnetic flux densities, rotor position and speed, output torque, internal and external temperature, case vibrations, etc. In addition, a failure monitoring system could monitor a variety of machine failures. These failures might include conductor shorts and opens, bearing failures, cooling failures, etc. It is apparent then, that a failure monitoring system should be capable of extracting, in a consistent manner, the evidence of many possible failures from measurements from many physically different sensors, [5, 9, 10, 17, and 54].

The most important methods of detection the faults in induction machines are:

- Motor Current Signature Analysis (MCSA)
- Instantaneous Power
- Negative Sequence
- Partial Discharge (PD) Measurements
- Analysing the axial flux or air-gap flux using search coil method
- Higher Order Spectra (HOS)
- Current space vector analysis
- Wavelets Decomposition Method

All of the presently available techniques require the user to have some degree of expertise in order to distinguish a normal operating condition from a potential failure mode. This is because the monitored spectral components (either vibration or current) can result from a number of sources, including those related to normal operating conditions. This requirement is even more acute when analysing the current spectrum of an induction motor since a multitude of harmonics exists due to both the design and construction of the motor and the variation in the load torque. However, variations in the load torque, which are not related to the health of the motor typically, have exactly the same effect on the load current. Therefore, systems to eliminate induction motors arbitrary load effects in current-based monitoring have been proposed [29, 30].

## 6.3. Description of the Experimental System

The experimental system, useful for achieving the aims of this chapter, is a model of a wind generator, with an advanced condition monitoring system [65]. The generator is a wound rotor induction generator (***doubly fed induction generator*** - DFIG), with slip rings, rated at 11 kW provided with a gearbox. The wind turbine rotor is emulated by use of a ***drive system*** scaled for driving the DFIG; the drive system is composed of a 15 kW induction motor and a 22-kVA-frequency converter. Two ***back-to-back PWM-VSI converters*** with a standard control system, with a DC-link including a DC capacitor filter are used to control the rotor currents, active and reactive power flow. The most important component of the measurement system is a complete ***condition monitoring system***, which comprises many subsystems like transducers, signal conditioning boxes and data acquisition devices, as it is depicted in Fig. 6.1.

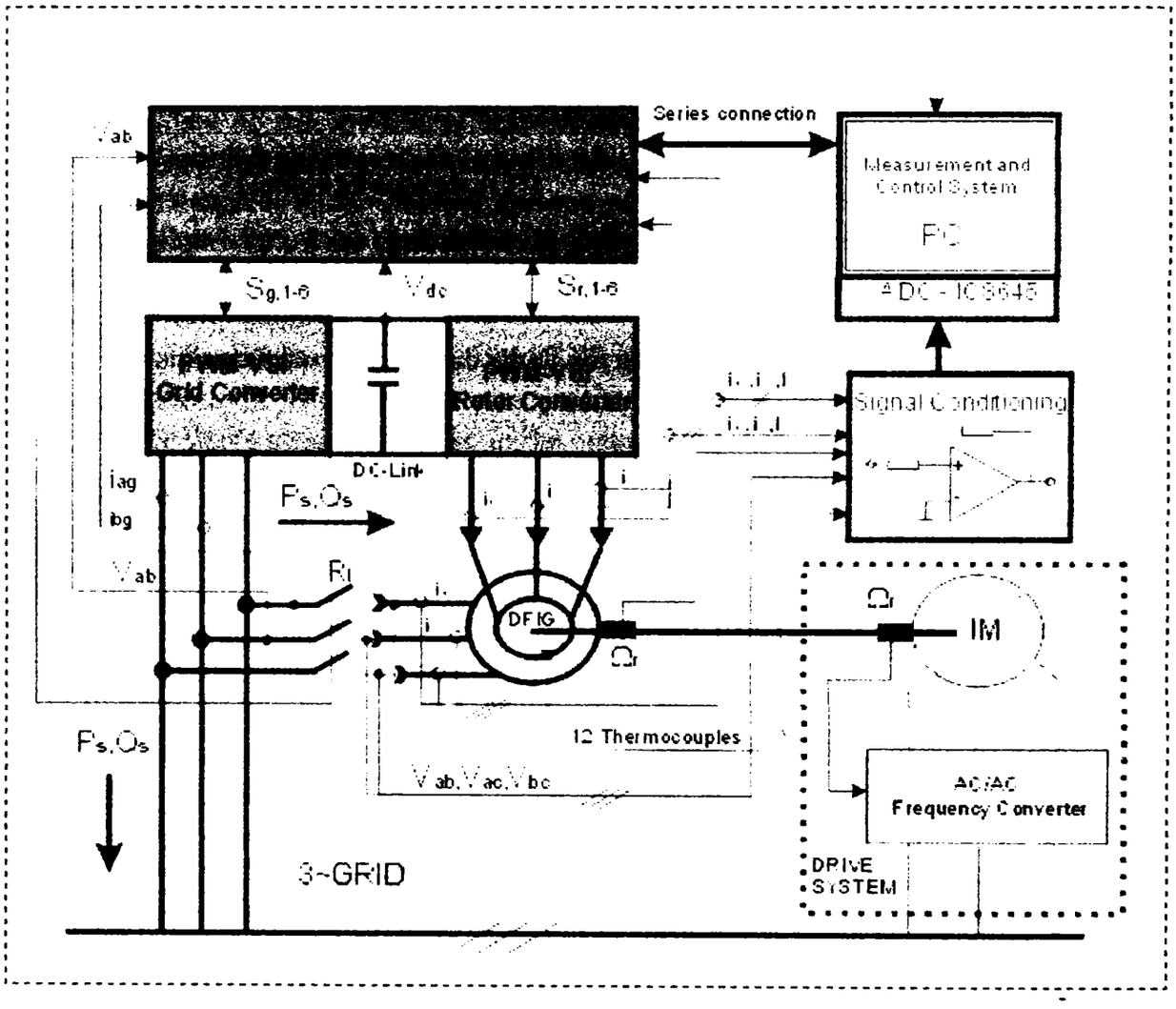


**Figure 6.1.** Schematic diagram of the experimental system.

The grid converter is designed to give unity power factor and is controlled by the CP (Control Processor) –board. It works as an active rectifier supplying the rotor converter with a constant DC voltage. The measurement and control system is composed of a PC with a digital

signal processor (DSP), interfaces and transducers for measuring stator and rotor currents, stator voltage, temperature and rotor speed. From the PC it is possible to control the CP-board, DSP and Analogue Digital Card (ADC) – ICS 645 via software as can be seen in Fig. 6.1.

### 6.3.2. The Condition Monitoring System

A complete condition monitoring system could comprise many subsystems, such as transducers, signal conditioning boxes, data acquisition devices and a PC, each monitoring a particular part of the wind generator, as can be seen in Fig. 6.2. There will be a degree of overlap between the functions of the different subsystems.

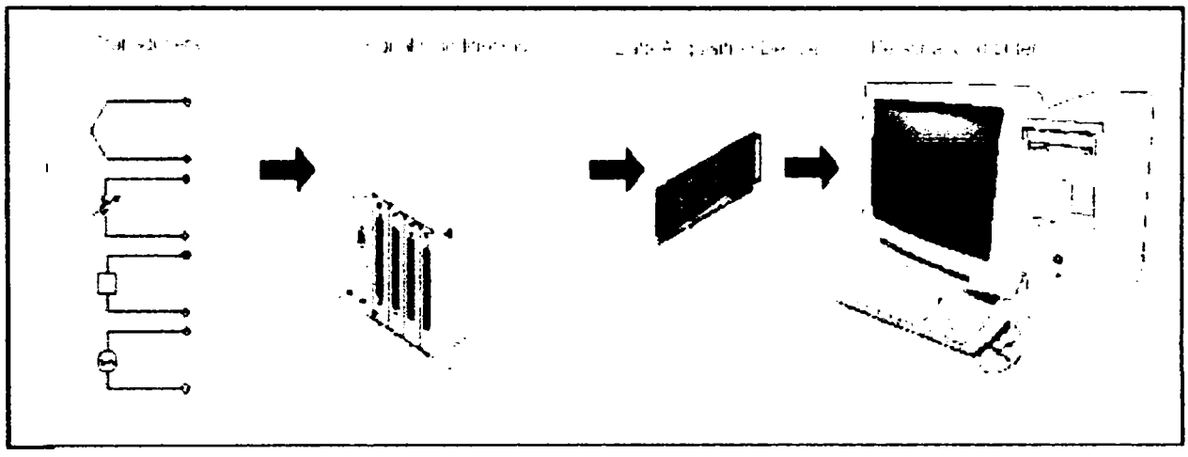

**Figure 6.2.** The block diagram of condition monitoring system.

In this chapter studies included ***design and commissioning of a measuring system*** comprising the AD card and the transducers for current, voltage, shaft speed and temperature.

#### 6.3.2.1. Transducers

Transducers are devices that convert physical phenomena, such as temperature and speed into electrical properties, such as voltage. Transducer characteristics define many of the signal conditioning requirements of a Data Acquisition (DAQ) system.

The induction generator (DFIG) has been monitored using measurements of current, voltage, temperature and shaft speed.

#### A) The Current Transducer.

*The Rogowski Current Transducer – ROGOflex: RGF 75* was selected to measure stator and rotor currents of the generator because of its merits compared to other transducers.

The advantages of Rogowski current transducers compared to other transducers: can measure large current without saturating from a few amps to 2k amps RMS, have a very wide band width extending from 1 Hz at up to 10 MHz (this enables the transducer to measure or reproduce the waveform of very rapidly changing currents - e.g. several thousand A/μs.), are easy to use- the coil is relatively thin and flexible and easy to insert around a conductor or current carrying device without affecting circuit inductance, provide an isolated measurement at around ground potential, accuracy - typically: ± 1 % and linearity – typically ± 0.05 % full scale / 0.1 % actual reading.

A Rogowski current transducer provides an output voltage that is proportional to current (e.g. 2 mV/A). Each transducer comprises a Rogowski coil connected to an electronic integrator by a co-axial cable as shown in Fig. 6.3.

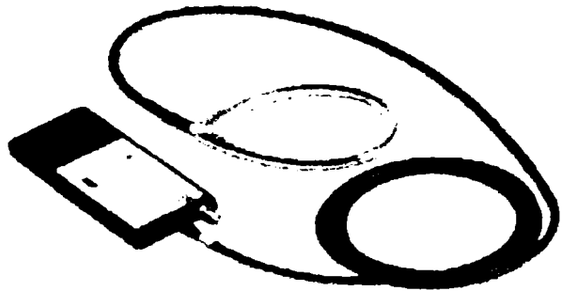

**Fig. 6.3.** The Rogowski coil RGF 75 – AC current probe.

## B) The Voltage Transducer.

Stator voltages were measured using a High Voltage Differential Probe – P5200.

The P5200 High Voltage Differential Probe provides a safe means of measuring circuits with floating potentials up to 1000 $V_{RMS}$ from ground and up to 1300 V (DC + peak AC) differential. The effective volt per division is the attenuation factor of 500 or 50 multiplied by the scale factor of the measurement instrument. The P5200 probe allows clear and accurate measurements of high-speed transitions and provides an excellent common-mode rejection of noisy signals. Both inputs have high impedance and low capacitance.

The BNC output connection to the oscilloscope is calibrated to drive a high impedance (1 MΩ) load. It is specifically designed to operate on Tektronix oscilloscopes with TEKPROBE® interface as can be seen in Fig.6.4.

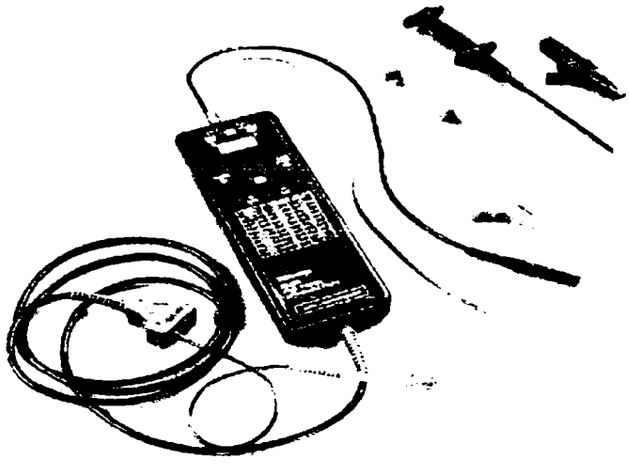

**Fig. 6.4.** P5200 High Voltage Differential Probes.

## C) The Speed Transducer.

Rotor shaft speed was measured using an incremental shaft type encoder made by SCANCON 2R 9000-8M-S.

An absolute encoder is a device that reports the shaft angle within a 360° range. This encoder does not lose its position after a power-down and provides the absolute position upon power-up without requiring a home cycle or any shaft rotation. A traditional absolute encoder has one track per encoder bit, and provides one fixed resolution. Thus, a 1024 position encoder would have 10 tracks (one bit per track).

Incremental Encoders are the most popular choice of sensors in applications where mechanical motion must be processed into digital information. Compared with alternate technologies (such as resolvers, tachometers, etc.), optical encoders represent the best combination of accuracy, resolution, reliability, ruggedness, ease of use, value and variety of solutions in the industry.

## D) The Temperature Transducer.

*Stator winding temperatures were measured by inserting 12 thermocouples* in various winding slots, corresponding to each pole and phase of the induction generator. The thermocouples – Type K are cheap, interchangeable, have standard connectors and can measure a wide range of temperatures.

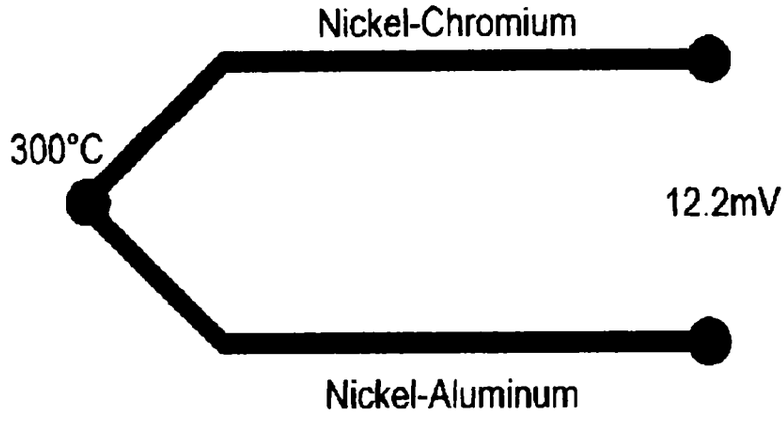


**Fig. 6.5.** The thermocouple junction.

Type K (Chromel-Alumel) is a general-purpose thermocouple with Fe as a positive material and Cu / Ni as a negative one, as it is depicted in Fig. 6.5. It is low cost and, owing to its popularity, it is available in a wide variety of probes. This type of thermocouple offers a – 200 °C to +1000 °C ranges. Sensitivity is approx 41 uV / °C.

### 6.3.2.2. Signal Conditioning

Signal conditioning is one of the most important technologies in measurement and automation systems. It provides the interface between the signals/sensors and the measurement system. Most signals require some form of preparation before they can be digitised. Voltage signals can require special technologies for blocking large common-mode signals or for safely measuring high voltages. For example, thermocouples produce very low voltage signals, which require amplification, filtering and linearization. All of these preparation technologies are forms of signal conditioning.

Signal conditioning improves the performance and reliability of the measurement system with a variety of functions, including: signal amplification, attenuation, isolation, filtering, multiplexing, linearization, sensor conditioning, offsetting and noise reduction.

Many sensors and transducers require special signal conditioning technology, and no instrument has the capability to provide all types of signal conditioning to all sensors. Sensors and transducers generate signals that must be conditioned to provide the correct input to maximum a DAQ device.

The data acquisition device ICS – 645 accepts input signals with peak amplitudes of ± 1.03 V with an input impedance of 500 Ohms. To achieve these requirements it was necessary to adjust the signals from all the transducers used in set up, as can be seen in Fig. 6.6.

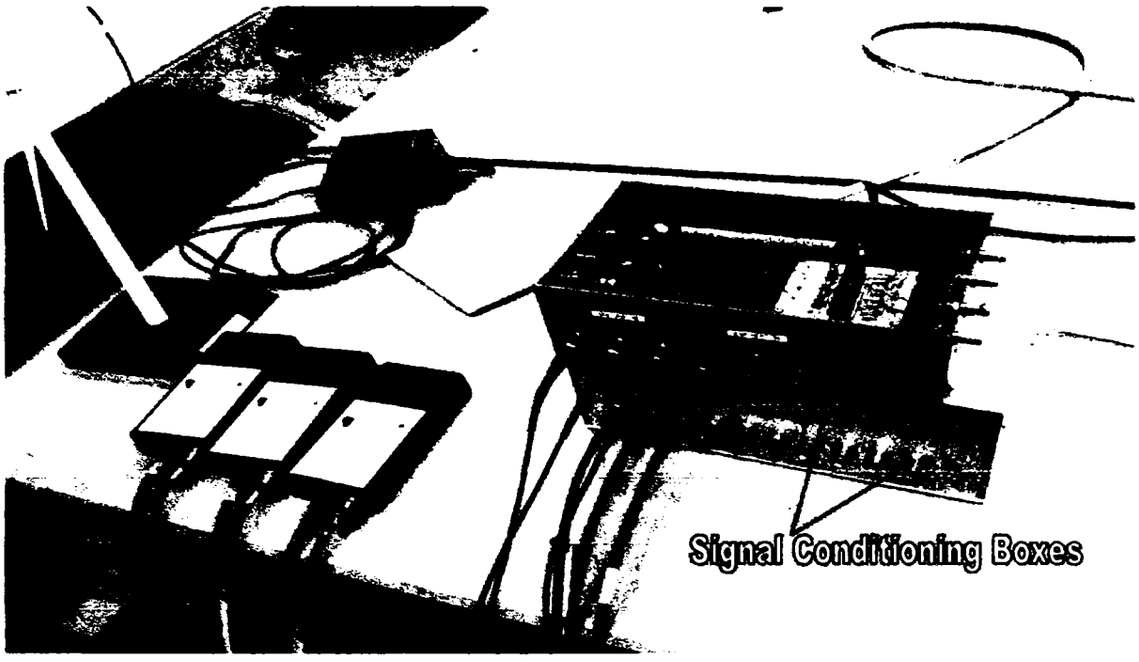


**Fig. 6.6.** Signal conditioning boxes design.

## A) Temperature Signal Conditioning

Thermocouple outputs are very low in level and change only (7 to 50) μV for every 1 °C change in temperature, making the signals very susceptible to the effects of electrical noise. Therefore, a thermocouple requires a transducer-conditioning device, which includes a low pass noise filter for suppressing 50 Hz noise and a high-gain instrumentation amplifier to boost the level of the signal.

The graph below shows the description of signal conditioning design for a single channel thermocouple:

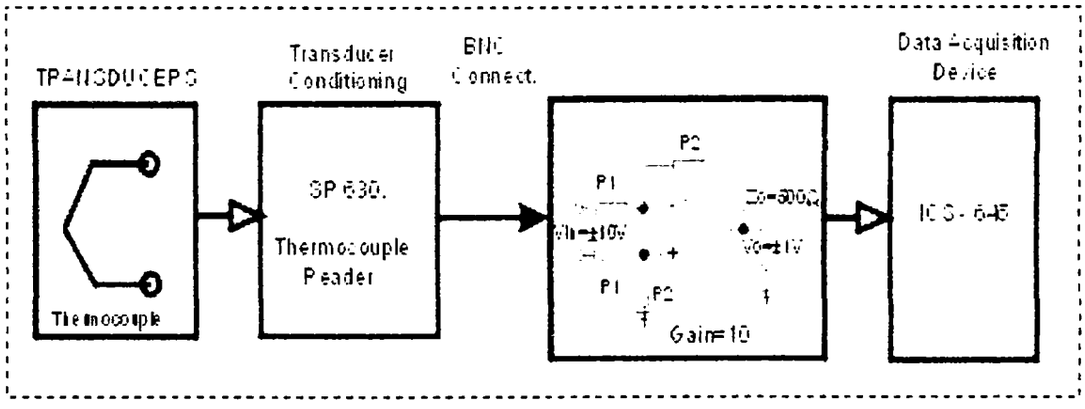


**Fig.6.7.** The block diagram of the single channel thermocouple signal conditioning.

The Model SR630 – 16 Channel Thermocouple Reader (version 1.24) is a device that determines the temperature of a thermocouple junction by measuring the voltage and

computing the temperature from the known characteristics of K type thermocouples. Four analog outputs on the rear panel of the instrument may be used to drive strip chart recorders or to adjust proportional temperature controllers. These four rear panel analog outputs provide dc outputs in the range of ± 10 $V_{DC}$ and were set to track the difference between the nominal and measured temperatures and converted in analog voltage of the corresponding channel.

## B) Voltage Signal Conditioning

Typically, data acquisition devices are general propose instruments that are well suited for measuring voltage signals. Many devices used in monitoring applications generate a voltage signal. Voltage signals require special technologies for blocking large common-mode signals or for safely measuring high voltages. In this case it's necessary to attenuate the signals acquired by high voltage differential probes – P5200, using a differential amplifier with a gain factor of 1/2.6 for each channel, see the figure below.

Attenuation is necessary in general for measuring high voltage. In addition, in our case it is imperative to attenuate the signal from transducers as DAQ – ICS 645 that accepts the input signals with peak amplitudes of ± 1.03 V and the High Voltage Differential Probes that provides an output voltage in the range of ± 2.6, as it can be seen in Fig. 6.8.

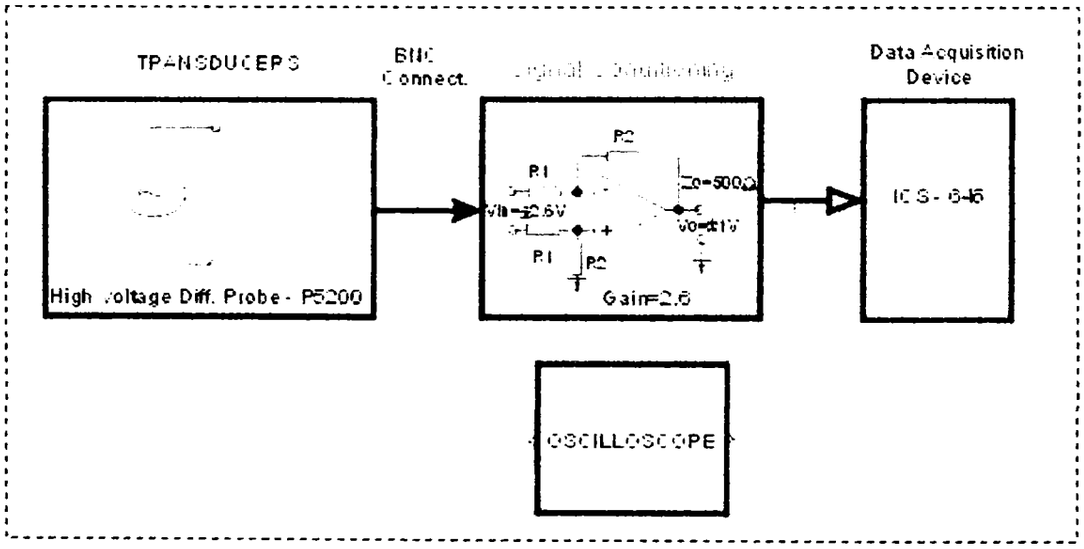


**Figure 6.8.** Block diagram of voltage sensor conditioning.

The voltage signals were acquired in Fig. 6.9 using a TDS 540 - Tektronix oscilloscope. P5200 high voltage differential probes were connected directly to the oscilloscope. On channel 1 is the input of the SC box and on channel 2 is the output signal of the SC box.

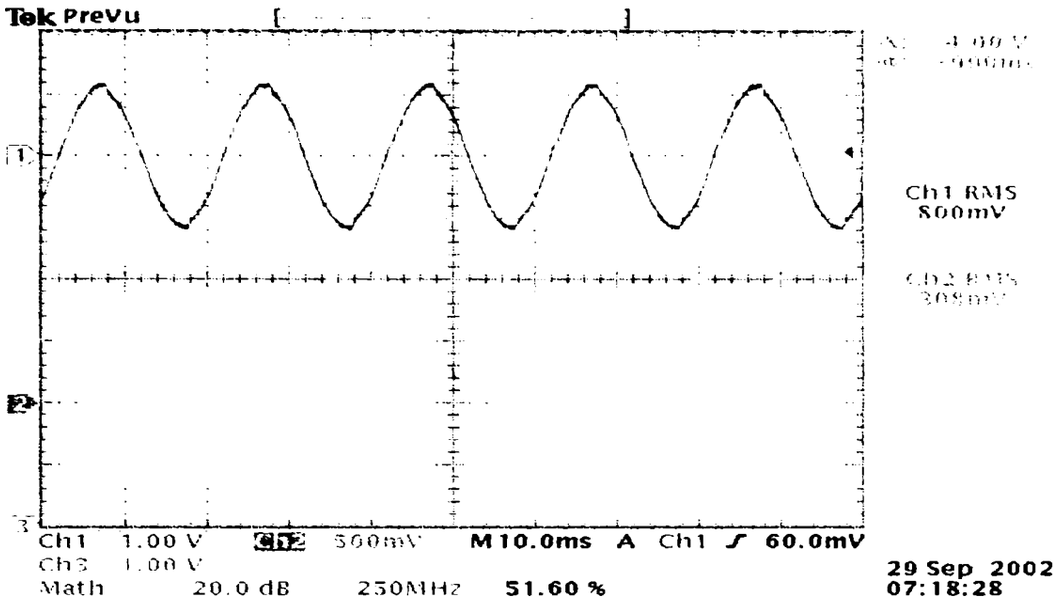


**Fig. 6.9.** IN and OUT of the Voltage SC Box.

The Figure 6.9 also shows that the difference between the input (on ch. 1) and the output (on ch. 2) of the voltage signal conditioning box, corresponds with the gain factor of the voltage SC box, $k_G$=2.6 (e.g. 800 mV / 308 mV = 2.6).

## C) Current Signal Conditioning.

Due to analogue real-world signals are often very small in magnitude, as in this case at low loads, signal conditioning can improve the accuracy of the data, increasing the resolution and sensitivity of the measurement system. The voltage signals obtained from Rogowski coils required filtering and offsetting of the signal, as can be seen in Fig. 6.10.

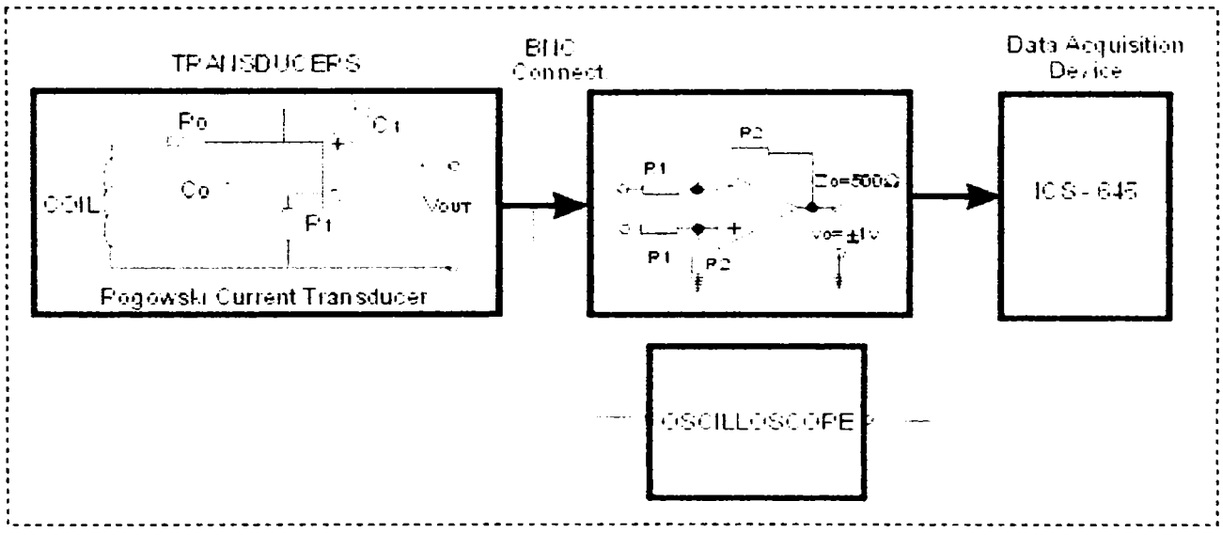


**Figure 6.10.** Single channel block diagram of current sensors conditioning.

In Figure 6.11, can be seen the current signal conditioning box test using Tektronix Oscilloscope – TDS 540. The input of current signal conditioning box is on channel 1 and the output of current signal conditioning box on channel 2. Sometimes there is a small difference between input and output of the current signal-conditioning box because of the amplifier boosts the level of the input signal to better match of the range of the ADC, thus increasing the resolution and sensitivity of the measurement.

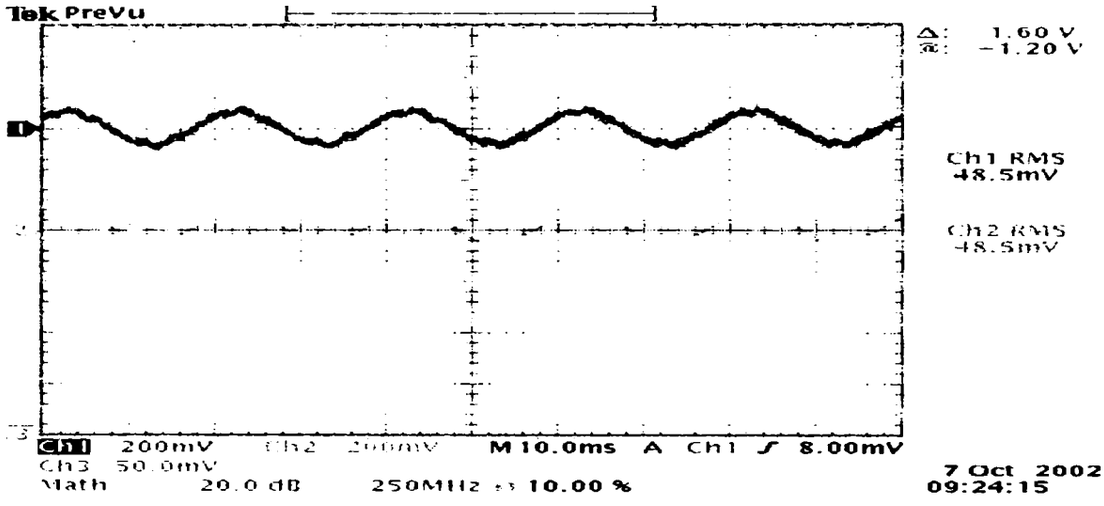


**Fig. 6.11.** IN and OUT of the Current SC Box acquired by Tektronix – TDS 540.
Scaling factor of the stator currents is 4 mV/A.

## D) Encoder Signal Conditioning.

In the case of the Encoder SC box the output signals from incremental encoder must be converted, using a frequency to voltage converter, to fit it with the data acquisition device input, as can be seen in Fig. 6.12.

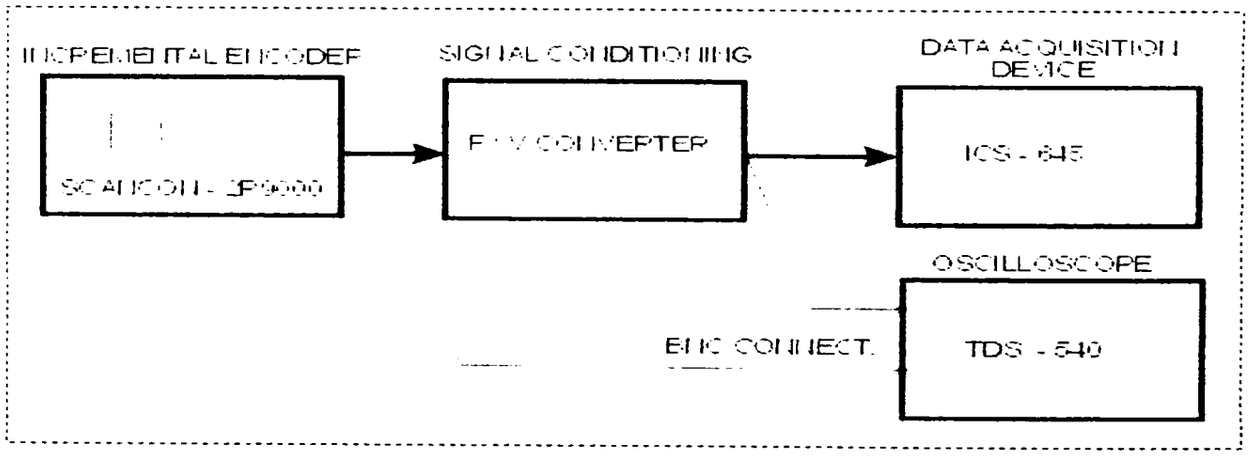


**Figure 6.12.** Simplified block diagram of encoder SC box.

The AD650 is a versatile monolithic voltage to frequency converter (VFC) that utilizes a charge-balanced architecture. Like other charge-balanced VFCs, the AD650 can be used in a reverse mode as a frequency to voltage (F/V) converter as in our case.

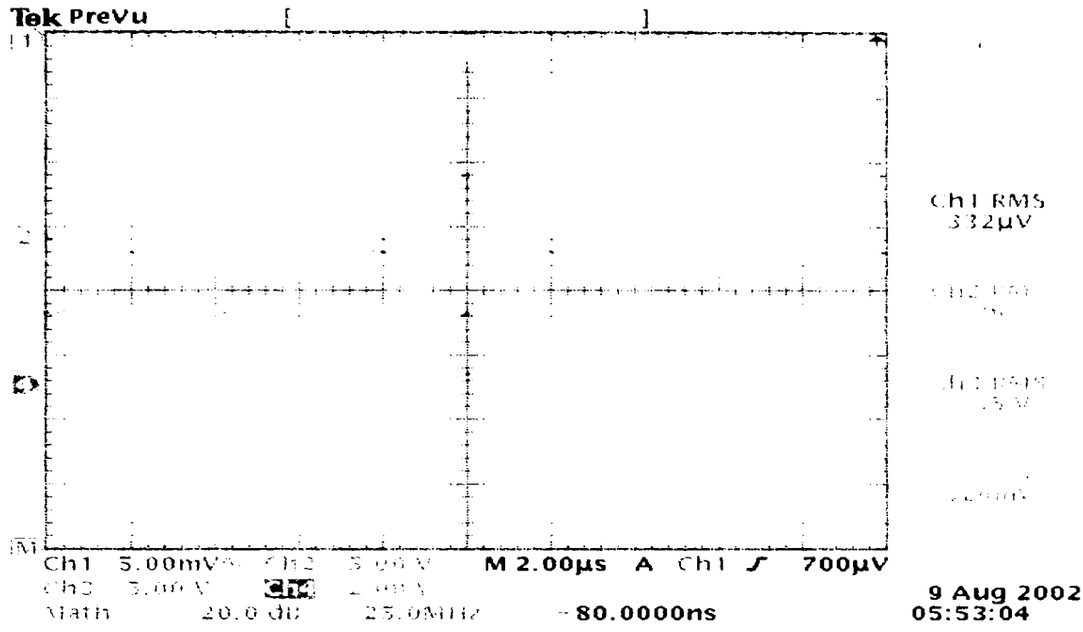


**Fig. 6.13.** IN (ch 2, 3) and OUT of Encoder SC Box acquired using Tektronix – TDS 540.

Figure 6.13 shows a comparison between the inputs on channel 2 and channel 3 and the output on ch.4 of encoder SC box. The Inputs of SC boxes are the output waveforms (rotation clockwise) from the incremental encoder shaft side and the output of the encoder SC box is a $V_{DC}$ value, which corresponds to an rpm value. The encoder Signal Conditioning box was designed so that 600 rpm correspond to – 1.03 V, 1250 rpm correspond to 0 V and 1925 rpm correspond to + 1.03 V.

### 6.3.2.3. Data Acquisition Device

The DAQ ICS-645 is designed for high frequency, high precision, high-density data acquisition and high-speed test and measurement applications (see Fig. 6.14). It combines the ultimate in analog and digital technologies to provide up to 32 channels and sample rates of up to 20 MHz/channel.

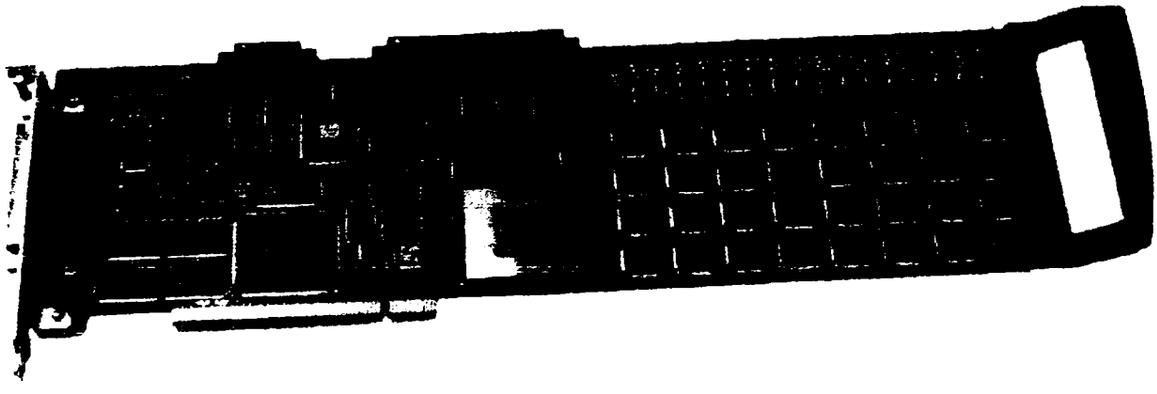

**Figure 6.14.** ICS 645 contains over 1800 components in a single PCI long format board.

The ICS-645 can be configured by the manufacturer for 32 channels with 2.5 MHz / channel, 16 channels with 5 MHz / channel (our case), 8 channels with 10 MHz / channel, or 4 channels with 20 MHz/channel. The over sampling ratio may be programmed to be 2, 4, or 8 depending on the required input signal bandwidth. The output data rate is 10 MHz, 5 MHz or 2.5 MHz for decimation of 2, 4 and 8, respectively. The corresponding signal to noise ratios is 72 dB, 80 dB and 83 dB. The range accuracy of this device is equal to ± 0.02 % in according with data sheets.

Figure 6.15 shows a simplified block diagram of the ICS-645 board. The board uses thirty-two 16-bit ADCs to provide simultaneous sampling at effective rates of up to 20 MSPS/channel.

Based on a new generation of ADC chip that combines Sigma-Delta and flash converter technologies, ICS 645 offers an exceptional dynamic range over a wide bandwidth.

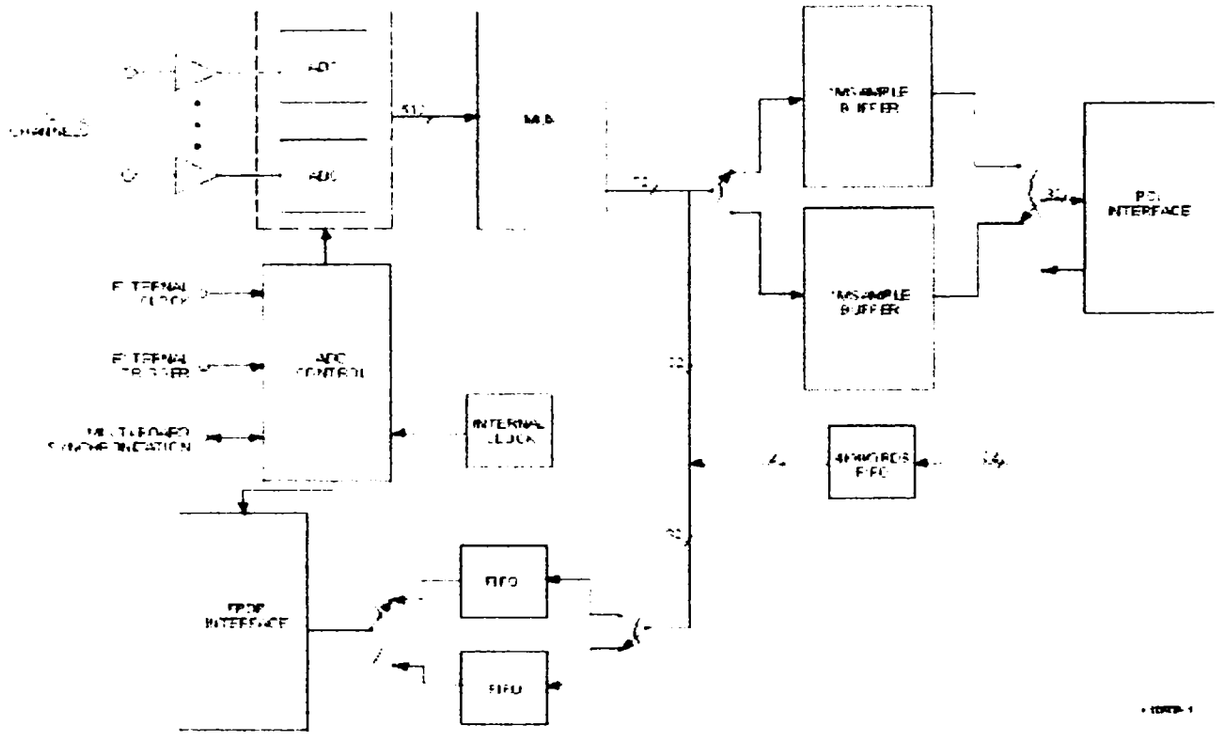


**Fig. 6.15.** Block diagram of the ICS-645.

### 6.3.2.4. PC Configuration – Software device driver

PC-based data acquisition (DAQ) systems are used in a very wide range of applications in the laboratory and on the manufacturing plant floor.

Modern measurement techniques in combination with advanced computerized data processing and acquisition enable new ways in the field of induction machines monitoring by the use of spectral analysis of operational process parameters.

A comprehensive software device driver for the Windows NT operating system supports the ICS-645. Matlab and Lab VIEW drivers are also available. The ICS-645 Matlab Application Software is designed as a starting point from which a user can build application-specific software. The purpose of this software is to quickly configure an ICS-645 card that has been

optimized for applications demanding high speed, precision and ease of integration. This driver software is intended to be used with the Matlab data analysis and graphing software.
To access the ICS-645 Matlab Application Software and implicitly to record and process the data it was necessary to build a program for each task using the Matlab software package tool. This program has been performed to plot the spectrum of signals and then to assess the FFT analysis to diagnostic strategy and will be presented in appendix.

## 6.4. Experimental arrangements for incipient fault detection

Three main experiments (one for stator phase unbalance using a variable resistance or an inductance in series, one for rotor phase unbalance using a resistance in series on one phase and then one for turn-to-turn fault using an inductance in parallel on one stator phase) have been performed to study the electrical behavior of the induction machine.

The input of the machine can be intentionally unbalanced for a short time for several slip conditions using a single-phase inductor and / or by connecting a resistor in one phase. Resistive and inductive unbalance may be used as a fault index for shorted turns in stator windings or may be used to distinguish negative sequence due to unbalanced supply voltage.

Line to line and line to ground conductor faults cause severe unbalance in which voltages and currents may differ drastically among the three-phases, making power system analysis quite complex [34, 35, 41, 42].

### 6.4.1. One stator phase unbalance

Placing an inductance and / or a resistance in series on one phase, as shown in Fig. 6.16, simulated an unbalance (open circuit) in one stator phase.

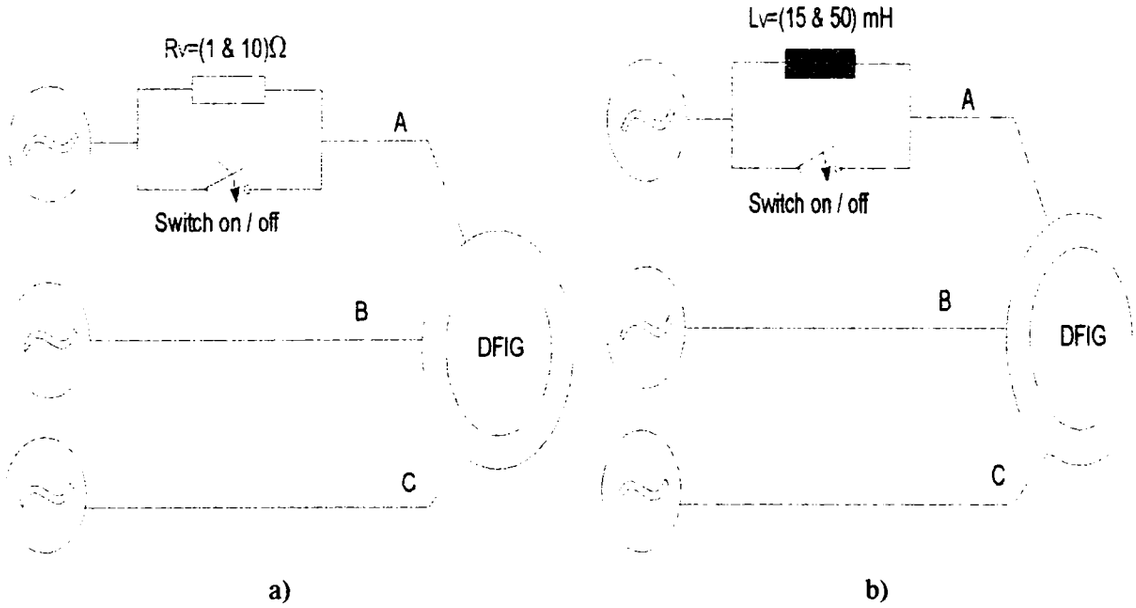


**Figure 6.16.** One stator phase unbalance. a) Resistive unbalance; b) Inductive unbalance.

The stator of the three-phase induction generator was connected to the star connected power source also in star (wyes) connection as can be seen in Figure 6.16.

#### 6.4.1.1. Resistive unbalance

The procedure we used consisted of increasing the *phase a* resistance, and implicitly the impedance, to approximately 1 time and afterwards 10 times than stator phase resistance, as can be seen in Fig. 6.16a). In this way 2 levels of deterioration severity were used during the experiments by inserting these values of variable resistance.

When a variable resistance of $R_{v1}$=10 Ω ≅ 10 * $R_s$ (stator resistance), was inserted between the grid and stator phase terminals on one phase, stator impedance became $Z_{s1}$=11.2 Ω, that mean 7 times larger than in the balance case. When external variable resistance it was set up to $R_{v2}$=1 Ω = $R_s$, stator impedance became $Z_{s2}$=2.5 Ω, that mean 1.5 times larger than in the balance case. In the first case the created unbalance in one stator phase should generate a large currents flow in the others stator phases, as it will be presented in the next section.

#### 6.4.1.2. Inductive unbalance

The procedure, which was used, consisted of increasing the inductance in *phase a* using a variable inductance connected in series on that phase, and implicitly the impedance, to approximately 3 time and afterwards 10 times than stator phase inductance, as can be seen in Figure 6.16b). In this way 2 levels of deterioration severity were used during the experiments as in the resistive unbalance case on one stator phase, presented before.

When a variable inductance of $L_{v1}$=15 mH ≅ 3 * Ls (stator inductance), was inserted between the grid and stator phase terminals on one phase, the stator impedance became $Z_{s1}$=6.4 Ω, that mean 4 times larger than in the balance case. When the external variable inductance it was set up to $L_{v2}$=50 mH = 10*Ls, stator impedance became $Z_{s2}$=17.3 Ω, that mean 10.5 times larger than in the balance case.

### 6.4.2. One rotor phase unbalance

Placing a resistance in series on one rotor phase we may simulate an unbalance (open circuit) in one rotor phase, as can be seen in Fig. 6.17.

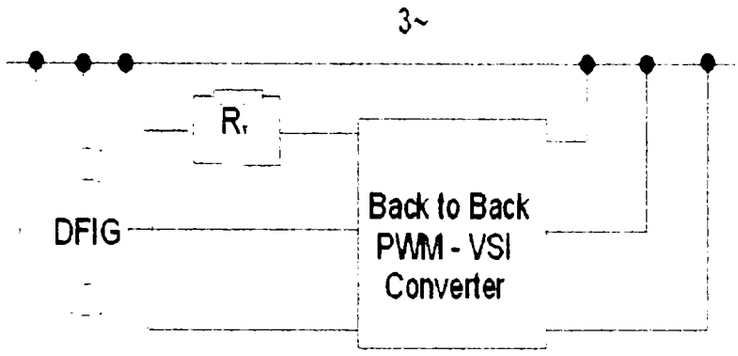


**Figure 6.17.** One rotor phase resistive unbalance.

The procedure, which was used, consisted of increasing the rotor impedance in one phase using a variable resistance connected in series on that phase, to approximately the same value as the rotor phase resistance (Rv=1.2 Ω). In this way the unbalance now is coming from the rotor windings.

### 6.4.3. Turn to turn fault in one stator phase

It is generally believed that most stator failures begin as a minor turn-to-turn fault because turn insulation is susceptible to mechanical stress from end turn movement and electrical stress from voltage transients. It would be advantageous to detect this early stage of deterioration to allow for a timely prediction of incipient failure.

The purpose of this study has been to simulate a low level of turn-to-turn deterioration in one stator phase of DFIG, which may exist well before failure is imminent. Placing an inductance and / or a resistance in parallel on one phase, as shown in Fig. 18, was simulated the deterioration of the turn-to-turn insulation.

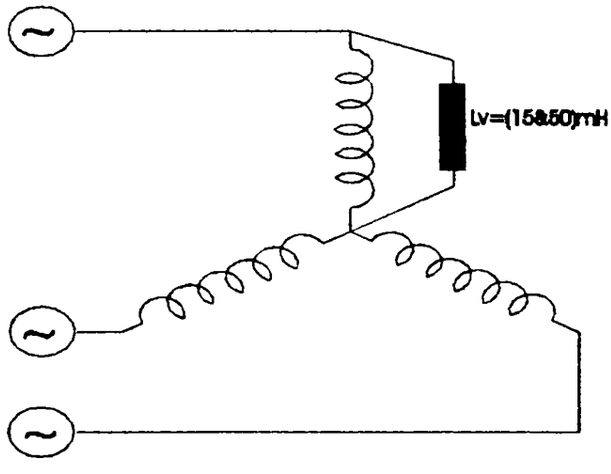


**Figure 6.18.** Turn-to-turn fault in one stator phase windings.

The procedure we used consisted of decreasing (weakening) the impedance of one-stator phase by inserting a variable inductance in parallel on that stator phase.

Through introducing an inductance of 50 mH (10 times more than stator inductance) the stator impedance it was weakening of 1.2 times from Zs=1.65 Ω to Zs1=1.45 Ω. Deterioration is simulated as an inductive connection between a coil end of a single winding and star point, as can be seen in Figs 6.18. In this way we simulated a turn-to-turn fault in one stator phase without to destroy the machine or to build an addition construction as placing taps on the wires of the stator windings and then shorting these taps.

To study this phenomenon it's necessary to monitoring the stator and rotor currents, the stator voltages and the rotor speed of the induction generator.

## 6.5. Experimental Results

Time-domain analysis using characteristic values to determine changes by trend setting and for extracting the amplitude information from current signals will be used in this section as first evaluation tool.

The measurements were acquired by a Tektronix Oscilloscope-TDS 540 and by the DAQ device – ICS 645 via Matlab software package for all situations presented before. The DFIG was operating, during the measurements, at a rotor speed of 1475 rpm corresponding to a stator active power of 2 kW.

The acquisition of data by Oscilloscope has been done to comparison with AD Card acquisition and to verify the accuracy and sensitivity of signal conditioning box.

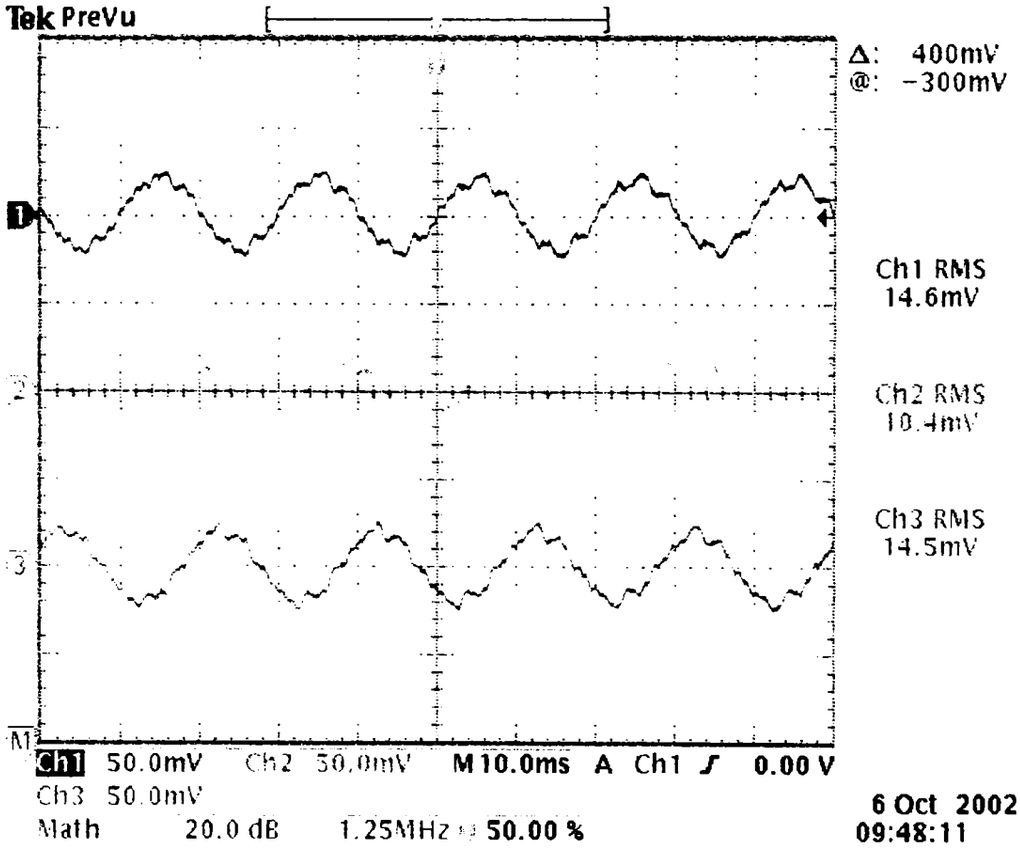


a)

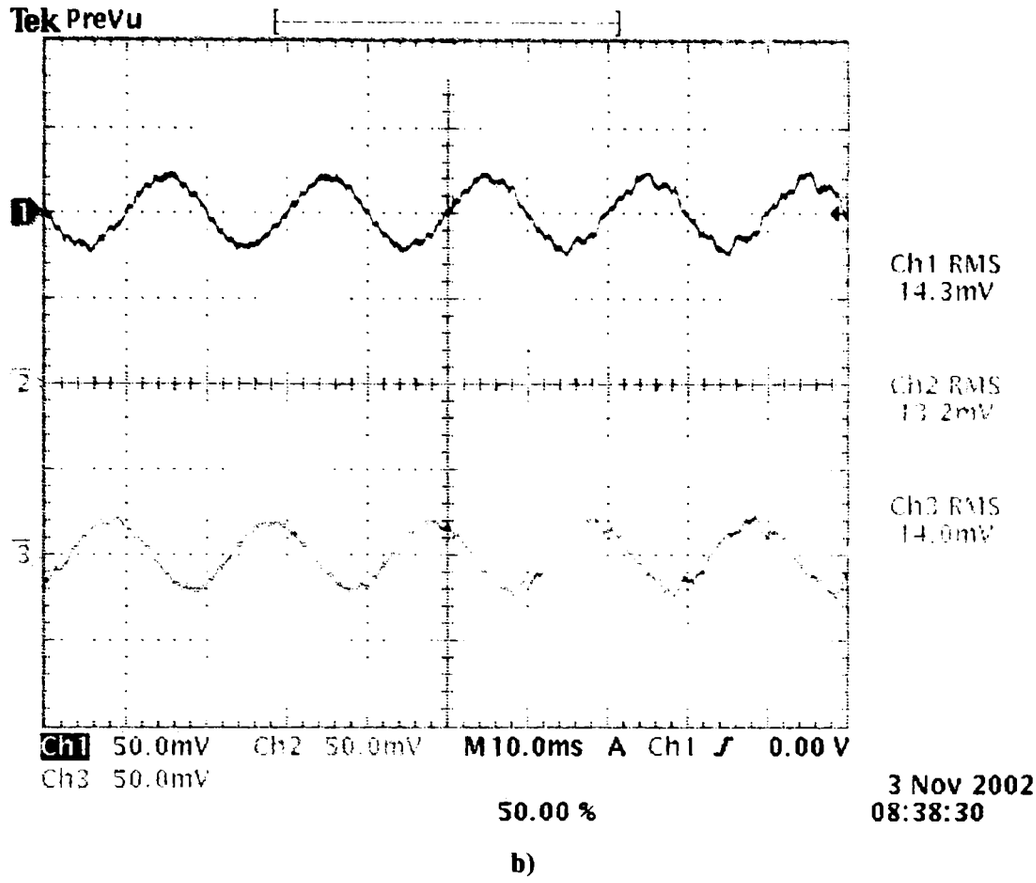


**Figure 6.19.** Stator currents for one stator phase resistive unbalance at P=2kW and n=1475 rpm: a) Rv=10 Ω and b) Rv=1.1 Ω. The unbalance stator current is configured on channel 2. Scaling factor is 4 [mV / A].

Figures 6.19 show the stator currents of the generator, under two levels of resistive unbalance (Rv=10 Ω & Rv=1.1 Ω) in one stator phase, acquired by a Tektronix Oscilloscope-TDS 540. DFIG was running at a rotor speed of 1475 rpm corresponding to a stator power of 2 kW. Comparison of Figs 6.19 a) and b) shows that increasing significantly with a level of the resistive unbalance in one stator phase provoke a decreases of the stator current in that phase (Fig 6.19a on channel 2). It should also be evident that the stator current decreasing on one phase would provoke an increasing of others stator currents.

In Figs 6.20, the stator currents and the rotor speed of IG were acquired by DAQ-ICS 645 for the same conditions as in Figs 6.19. For each variable, $2^{16}$ values were recorded, with the sampling frequency of 2.5 MHz. Is1, Is2 and Is3 denote instantaneous values of the line currents and in addition, Is1 represents the instantaneous stator current of the unbalanced phase. These acquisitions of data using the card ICS 645, has been necessary in addition for current signature analysis (to compute the Fast Fourier Transform - FFT) to diagnostic strategy, which will be presented in the next sub-chapter.

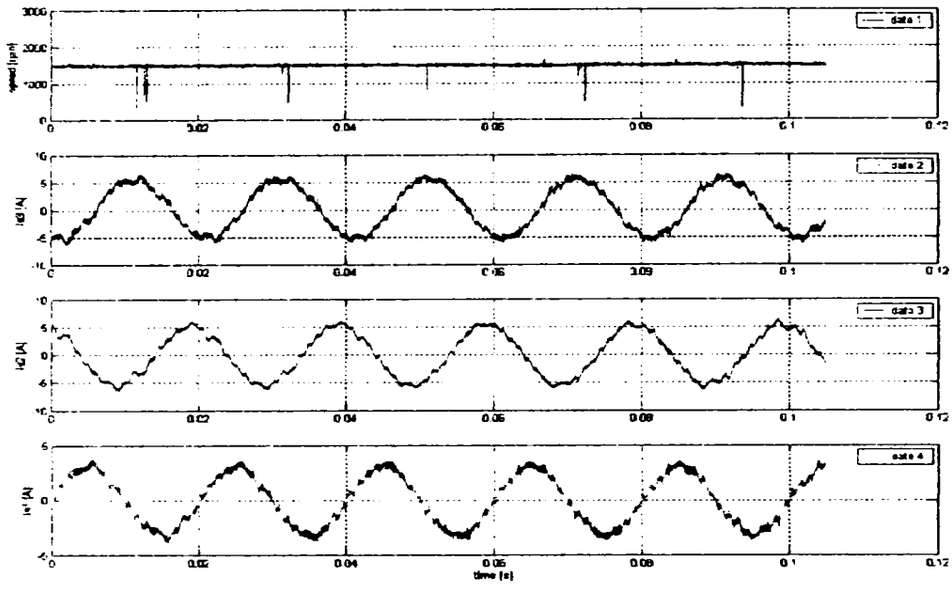

a)

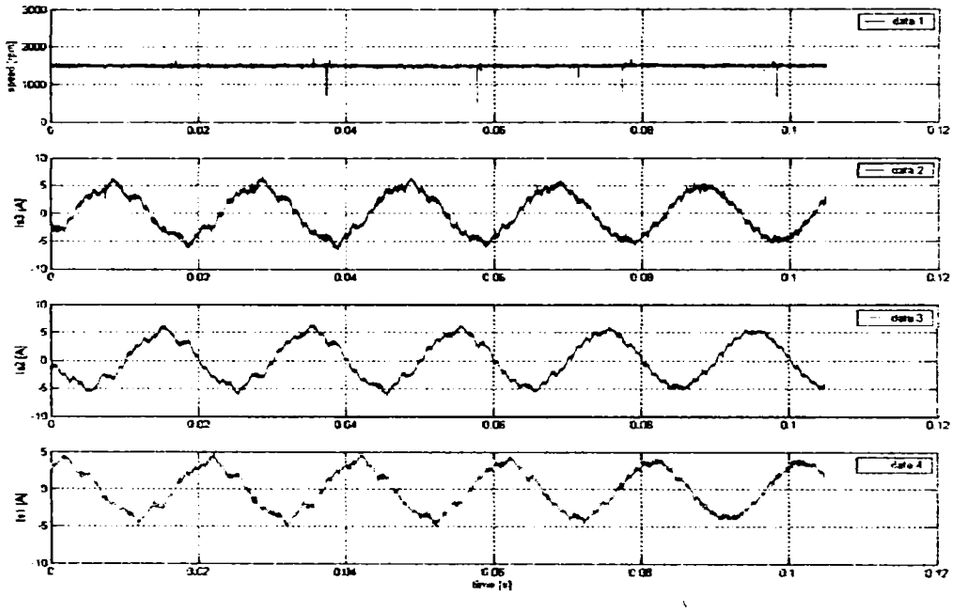

b)

**Fig. 6.20.** The Stator currents under resistive unbalance of Rv=10 Ω (a) and Rv=1 Ω at P=2kW & n=1475 rpm. Is1: instantaneous stator current of the unbalance phase.

Figures 6.21 show an acquisition of data by a Tektronix Oscilloscope-TDS 540 (6.21a) and by ICS-645 (6.21 b) of the stator currents of the induction generator, under a large level of inductive unbalance (Lv=50 mH) developed for one stator phase. Doubly fed induction generator - DFIG was running at a rotor speed of 1475 rpm corresponding to a stator power of 2 kW. Comparisons of Figures 21 show that the degree of unbalance provoked in one stator phase, through introducing the inductive unbalance of 50 mH (10 times more than stator phase inductance), is reflected very clearly in one stator current (Is1 on channel 2).

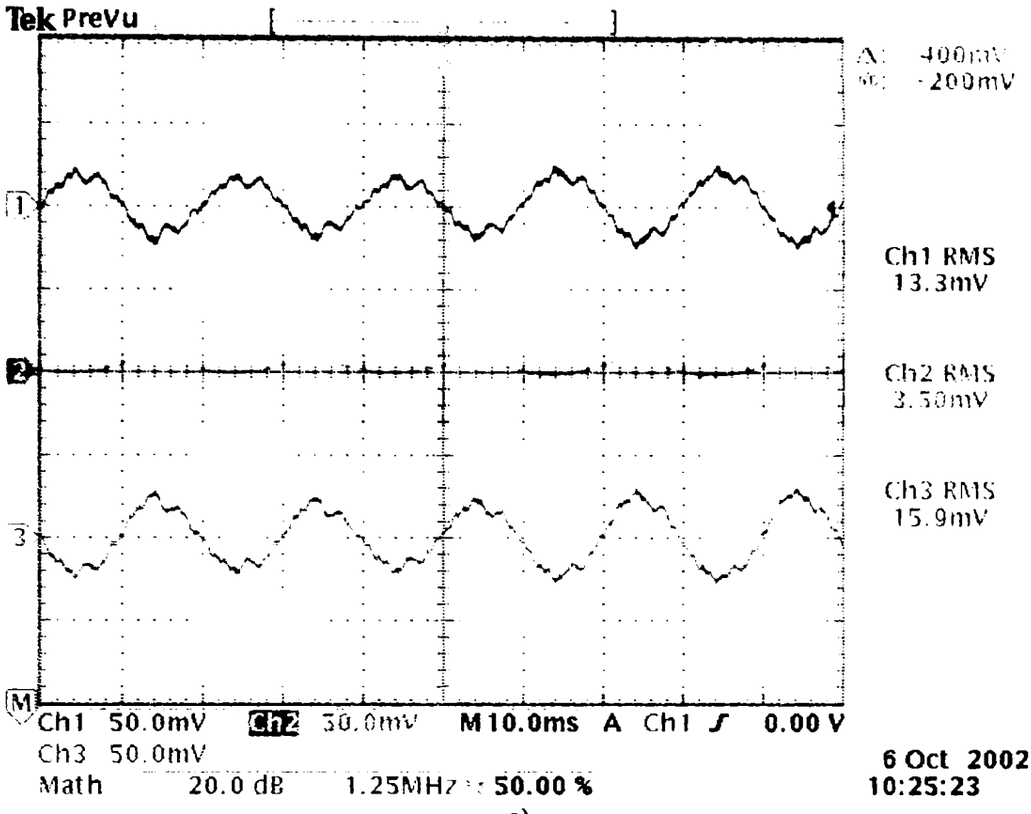


a)

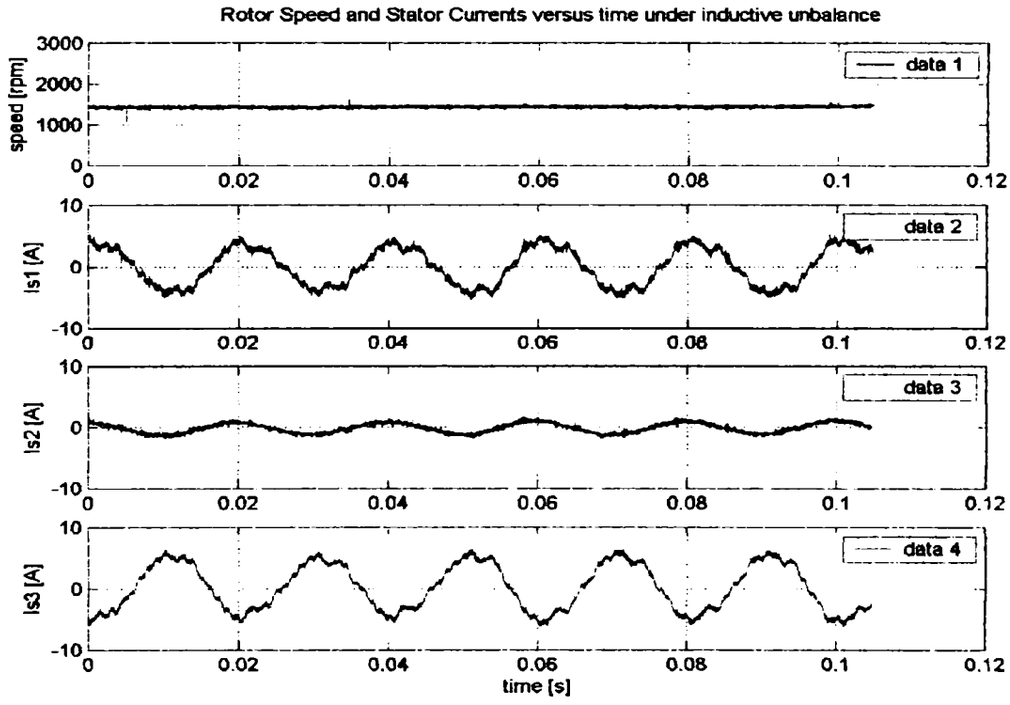


b)

**Fig.6.21.** The stator currents acquired by TDS-540 (a) and by ICS-645 under inductive unbalance-Lv=50 mH at P=2 kW. The unbalance stator current is on channel 2.

The pictures below (Figs. 6.22) show the rotor and stator currents of the generator measured under a resistive unbalance ($R_v$=1.2 Ω) in one rotor phase of the same value as the rotor phase resistance, corresponding to a stator power of 2 kW.

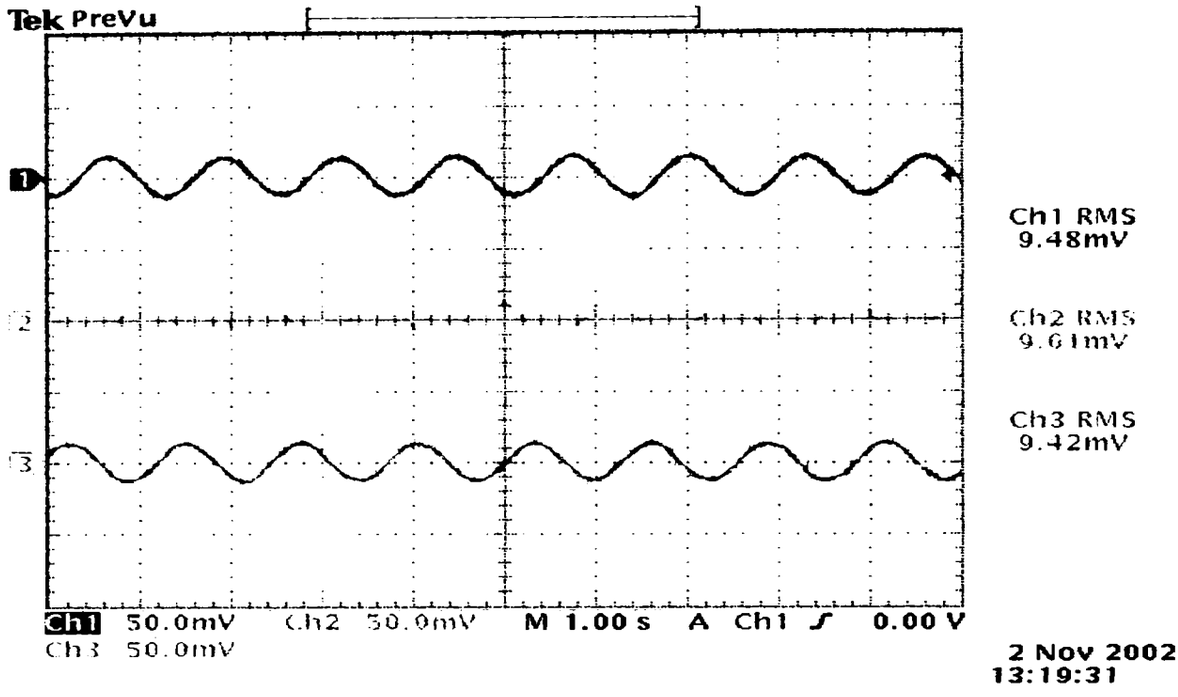


a)

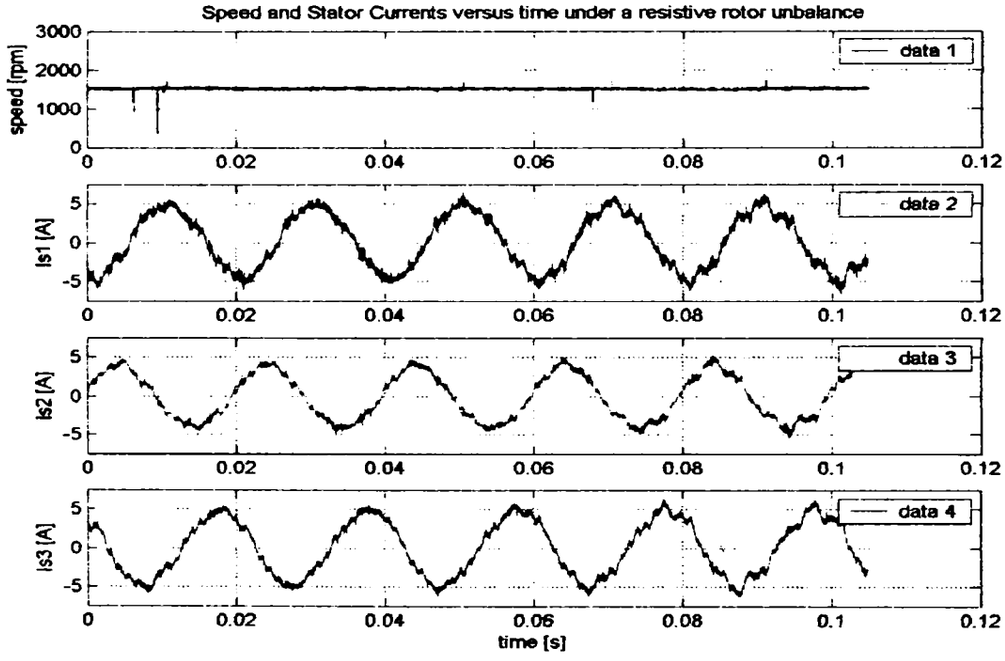


b)

**Fig. 6.22.** The rotor currents of DFIG acquired by TDS 540 (a) and by ICS-645 (b) under the resistive unbalance of 1.2 Ω in one rotor phase at 2 kW. Scaling factor is 4 mV/A.

The measurements were acquired by a Tektronix Oscilloscope-TDS 540 (a) and by the DAQ device – ICS 645 (b) via Matlab software package. The DFIG was operating, during the measurements, at a rotor speed of 1475 rpm corresponding to a stator active power of 2 kW. The comparison between Figs. 22 point out that a very small difference exist in both stator and rotor currents and can only be due to the unbalance provoked in one rotor phase. It means

that the rotor currents are a better indicator than the stator currents under resistive unbalance in one rotor phase.

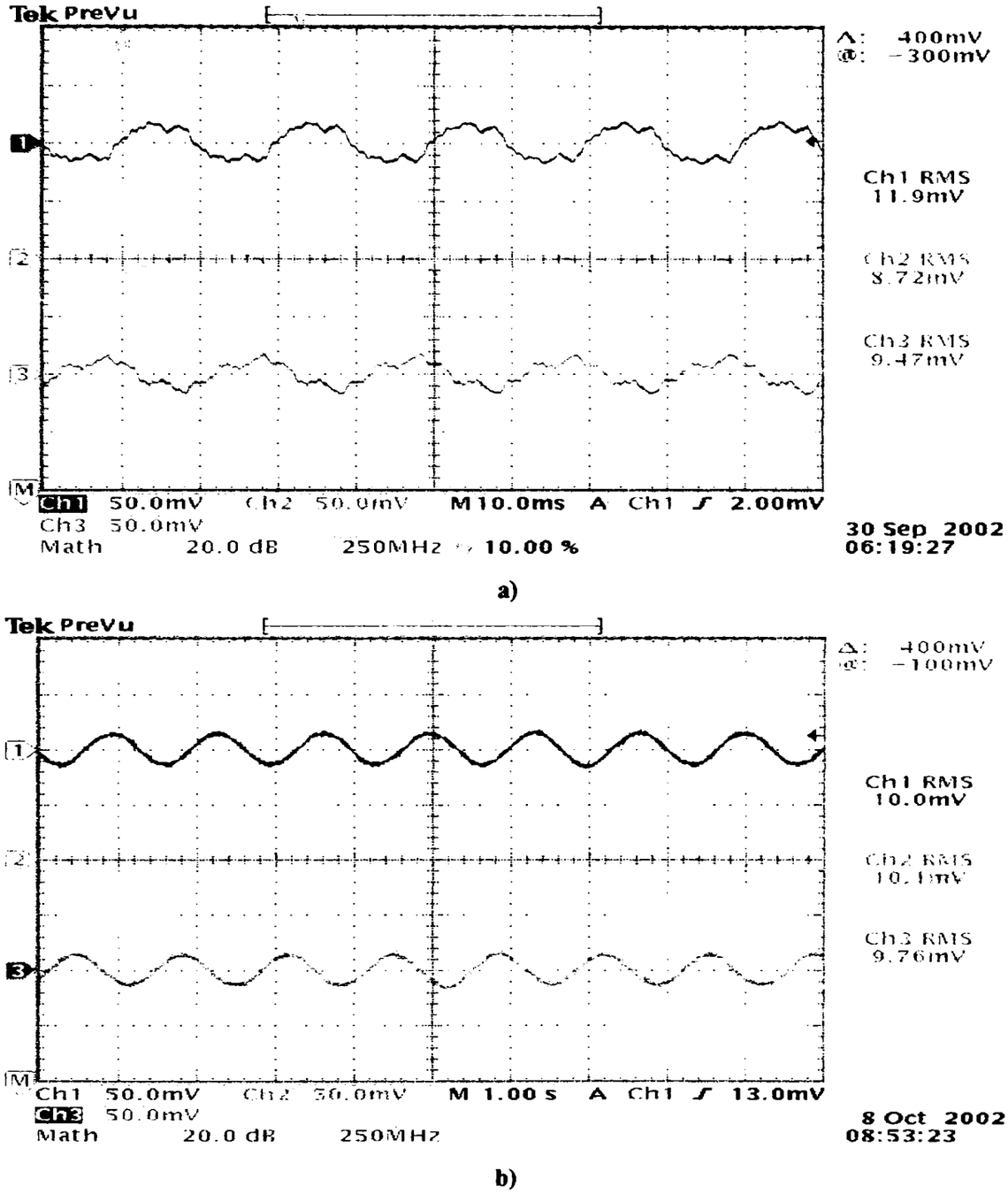


**Fig. 6.23.** The rotor currents acquired by TDS-540 under turn-to-turn fault in one stator phase ($L_v$=50 mH in parallel - Fig. 3c) at P=2 kW and n=1475 rpm. Scaling factor is 4 [mV / A].

Figs. 6.23 show the stator and rotor currents of the generator that corresponds to stator power of 2 kW, under turn-to-turn fault developed in one stator phase, and acquired by a Tektronix Oscilloscope. Comparison of these Figs. illustrate that the rotor currents (rms values) have almost the same value while the imbalance created into the stator currents is more clear. Hence, the stator current could be a good indicator in detection of this type of fault.

## 6.6. FAULT DETECTION METHODS

This sub-chapter presents a theoretical and an experimental result concerning to the fault detection methods of a doubly fed induction generator as a part of a wind generator system.

To obtain a reliable diagnosis of an induction machines it's necessary to recognize both incipient faults and suddenly occurring faults from electrical measurements.

The objective of this paragraph is to test detection methods of condition monitoring, suitable for implementation in wind generator system. This should contribute to increasing the time in which the generator will produce energy, by reducing the time spent in operating in undesirable load or fault conditions, reduce the number of outages and provide and improved background for planning service with relevant, longer, service intervals.

Consequently, a number of techniques have been developed over the years, which monitor specific induction machine parameters with a view to allowing the health of the machine to be determined, and hence maintenance schedules planned. Unnecessary plant failures and consequential damage and / or loss of revenue thus being avoided. These monitoring techniques are all examples of what has become known as CONDITION MONITORING and are presented in the table 1 as an appendix.

Current monitoring techniques are sometimes applied in industry due to their success in the detection of turn-to-turn fault and broken rotor bars. Essentially rotor faults in the machine produce local aberrations in the air-gap magnetic field. It has been shown that a rotor fault such as broken rotor bars will produce specific components within the frequency spectrum of the stator line current. [1, 8, 23]

One parameter, termed the effective negative-sequence impedance, has been identified as an indicator of induction motor stator winding degradation. [34, 35, 41, 42]

Instantaneous power at twice the supply frequency indicates unbalanced conditions of individual stator phases. These maybe: voltage unbalance, constructional unbalance, consisting in non-identical phase impedances in a healthy motor, and stator faults. [36-40]. Measured results must be scaled, converted to digital form and stored, using data acquisition module (ADC – ICS 645). It will be necessary to make many series of measurements and record them for later analysis. The data will first be processed to synthesise suitable indicators. The indicators will then be resolved into spectra, showing the frequency content of the indicators as a stator current, rotor current and stator voltage.

Traditionally, for condition monitoring, Fourier analysis has been employed using the coefficients of the current spectrum or the power spectrum as an indication of how the harmonic content of a signal varies. If the variation of the harmonic content can be related to specific faults then it may be useful as an indicator. If transformations can be found that may distinguish fault conditions with greater ease, their use in conjunction with ANN's (Artificial Neural Networks) or maybe with Wavelet Decomposition would provide a powerful tool for the automated condition monitoring process.

Time-domain analysis using characteristic values to determine changes by trend setting, spectrum analysis to determine trends of frequencies, amplitude and phase relations of spectra are used as an evaluation tools. In many situations, MCSA methods were utilised for incipient fault detection. However, stator current monitoring was found to provide the same indication without requiring access to the machine.

### 6.6.1. Current Signature Analysis to Detect Induction Machine Faults

Machine current signature analysis (MCSA) is a non-invasive, online or offline monitoring technique for the diagnosis of problems in induction machines. The industrial case histories have clearly demonstrated that MCSA is a powerful technique for monitoring the health of three-phase induction machines. The MCSA techniques utilise the results of spectral analysis of the stator current.

MCSA may be implemented using time domain or frequency domain analysis and requires amplitude information of the machine currents.

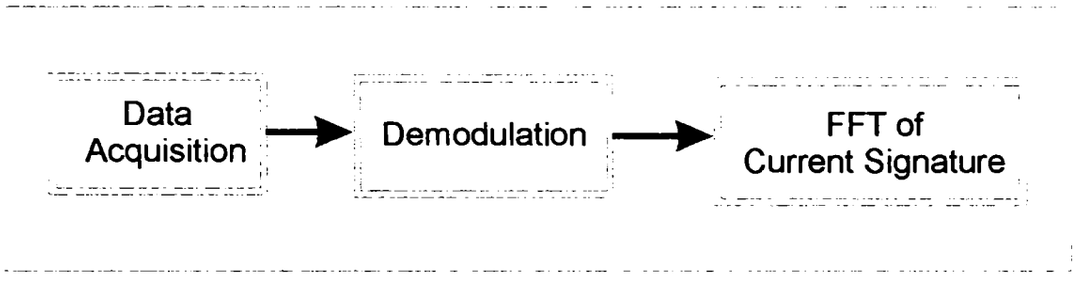


**Figure 6.24.** General procedure for MCSA.

Figure 6.24 shows a general procedure for MCSA. The current signals can be obtained from the outputs of the current transducers (Rogowski coils) that are able to produce voltages proportional to the input currents, which are placed around of the power leads. Computers acquire the resulting raw voltage signals after they go through conditioning circuits and data interfaces. Matlab software processes the signals in the computer after acquisition.

#### 6.6.1.1. Overview of the Monitoring System

The stator and rotor currents monitoring system that has been developed consist of three main sub-systems. These include: signal conditioning, data acquisition and data analysis, Fig. 6.25. Data acquisition and data analysis sections are accessed by Matlab software package run from a PC.

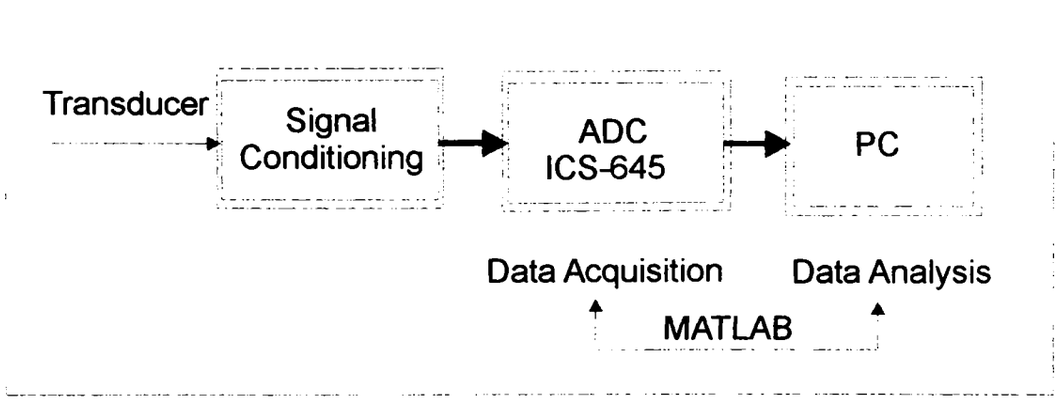


**Figure 6.25.** Single channel acquisition system.

Figure 6.25 shows a diagram of a single channel of hardware required to obtain the indicators for analysis purposes.

The system is capable of acquiring 16 channels simultaneous up to 5 MHz sampling frequency. The controlling software (Matlab) allows the operator of the system to store the data in data files for future processing.

The amount of data points that are displayed on the display screen may be altered, not in our case. The maximum amount of data points to be displayed of the monitoring system is 32 768.

PC based data acquisition (DAQ) systems are used in a very wide range of applications in the laboratory and on the manufacturing plant floor. Modern measurement techniques in combination with advanced computerized data processing and acquisition enable new ways in the field of induction machines monitoring by the use of spectral analysis of operational process parameters.

The ICS-645 Matlab Application Software is designed as a starting point from which a user can build application-specific software. The purpose of this software is to quickly configure an ICS-645 card that has been optimized for applications demanding high speed, precision and easy of integration. This driver software is intended to be used with Matlab data analysis and graphing software. The data acquisition system is designed to be integrated with Matlab software tools.

### 6.6.1.2. MCSA to Diagnose Stator winding faults in Induction Generator

Stator turn-to-turn shorts are one of the more prevalent and potentially destructive electrical faults in induction machines. Arising primarily from insulation degradation, through contamination or abnormal thermal, electrical, mechanical or other environmental stresses, these localized faults produce thermal hot spots that foster progressive degradation that may mature into a more severe turn-to-ground fault [17]. These faults are usually related to *insulation failure*. In common parlance they are generally known as **phase–to-ground** or **phase–to–phase** faults. It is believed that these faults start as undetected **turn-to-turn faults** that finally grow and culminate into major faults. [8. 10]. Almost (30-40) % of all reported induction machines failures fall in this category.

have shown through both modelling and experiments that these faults can result in asymmetry in the machine impedance causing the machine to draw unbalanced phase currents.

The objective of this method is to identify current components in the stator winding that are only a function of shorted turns and are not due to any other problem or mechanical drive characteristic. The following equation gives the components in the air-gap flux waveform that are a function of shorted turns [1. 8. 10. 15. and 20]

$$f_{st} = f_1\left[\frac{n}{p}(1-s)\pm k\right] \quad \text{.....(6.1)}$$

$f_{st}$ = stator frequency components that are a function of shorted turns
$f_1$=supply frequency, $n$=1, 2, 3... $k$=1, 3, 5,...
$p$=pole-pairs, $s$=slip

The diagnosis of shorted turns via MCSA is based on detecting the frequency components given by equation (6.1) in that these rotating flux waves can induce corresponding current components in the stator winding.

From equation (1) there will be a whole series of components for the machine:

With k=1, n=1, $f_{st}$= (3/2) f1*(1-(s/3)) and f1/2(1+s)

With k=1, n=2, $f_{st}$=f1*(2-s) and sf1

With k=1, n=3, $f_{st}$= (5/2) f1*(1-(3s/5)) and f1/2(1-3s)

and so on with combinations of k and n values.

The components that are clearly indicative of shorted turns are 125 Hz and 175 Hz with k=1, n=3 and k=1, n=5

## A. Experimental development

This subchapter focuses on experimental results to prove that current signature analysis (MCSA) may diagnose turn-to-turn fault in stator windings of three-phase induction machines. The line stator currents have been shown to contain frequency components that are indicative of these fault conditions.

The work reported in this paragraph uses the stator line currents, the rotor line currents and the stator line-to-line voltages as the monitored machine parameters.

The procedure we used to simulate a turn-to-turn fault consisted of weakening the impedance of one stator phase by inserting a variable inductance of max 50 mH (10 times greater than the stator winding inductance), between a coil end of a single winding and the star point.

The primary objective is to carry out a high resolution Fourier analysis of the stator and rotor currents to the induction machine to identify current components in the stator and rotor windings that are only a function of shorted turns, in accordance with equation 6.1.

All recorded data were recorded and processed using the Matlab software to plot the currents and voltage spectra and then to compute the FFT for stator and rotor currents and for stator voltages. For each variable, $2^{16}$ values were recorded, with the sampling frequency of 2.5 MHz simultaneously on each channel.

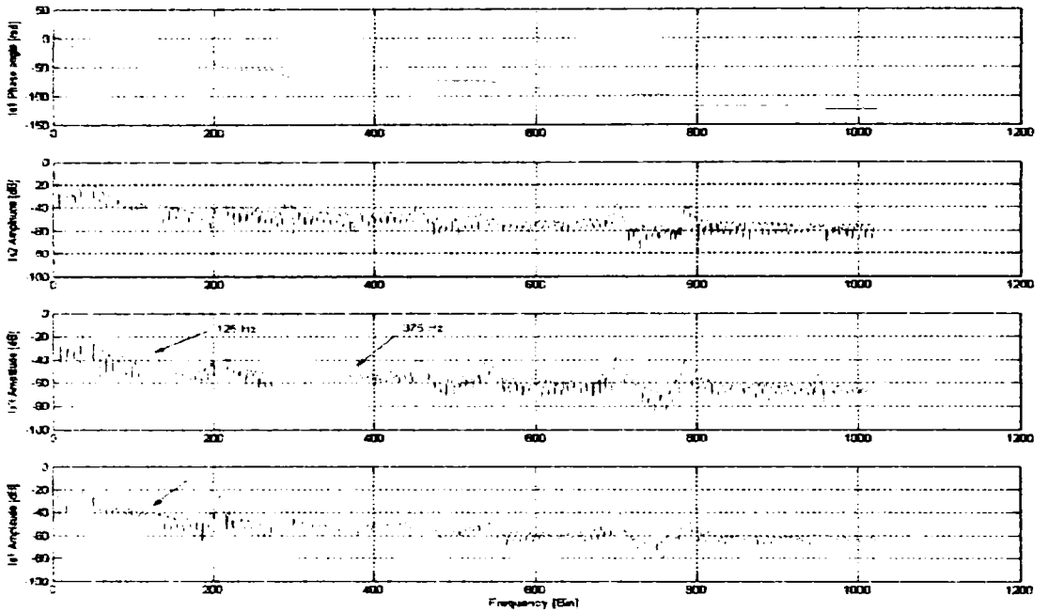


a)

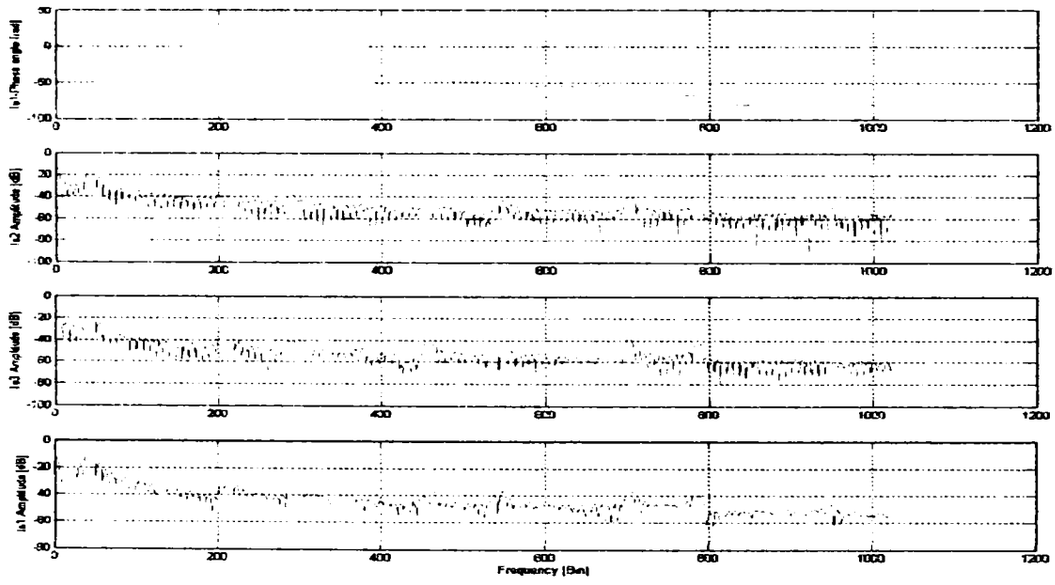


b)

**Fig. 6.26.** FFT and phase angle for turn-to-turn fault (a) and for healthy machine (b) of DFIG at $P_G$=2kW, s=-0.016. $V_S$=390 V, $I_S$=4.7 A. The data were recorded and processed by Matlab and acquired via ICS-645.

Figures 6.26 give the lines current spectrum for all stator phases under turn-to-turn fault (Fig. 6.26 a) and with no stator fault (Fig. 6.26 b). The obvious change, is that completely new current components exist at 125 and 375 Hz and can only be due to the shorted turn, as per theory with k=1, n=3 and k=1, n=13 (equation 6.1). In addition the Figs. 6.26 a) make clear that the difference between balanced operation and under turn-to-turn fault cases follows the phase angle of stator current - Is1. For instance the phase angle is changed around 125 Hz where a new faulty component exist as well. Note that the 125 Hz current components correspond at 40 dB and 375 Hz at 55 dB.

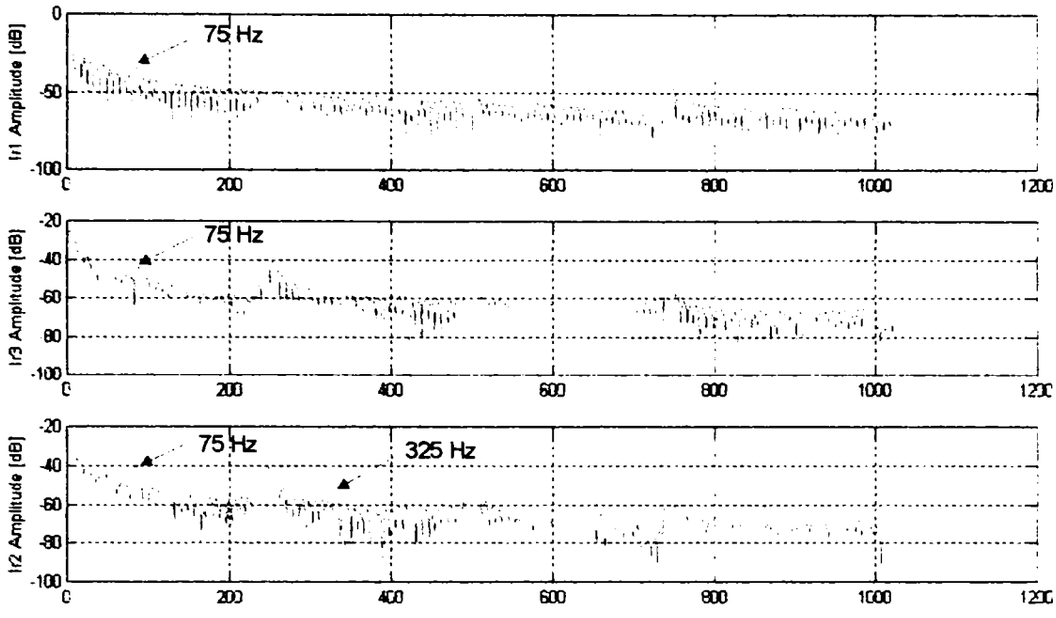


a)

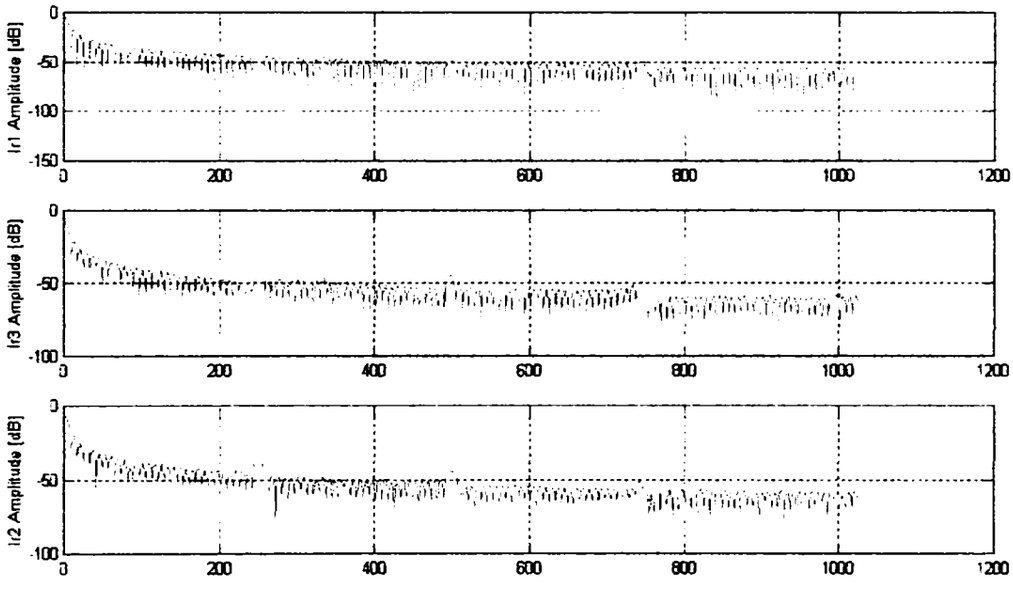


b)

**Figure 6.27.** Spectral content of the rotor line currents at P=2 kW, s=0.016, Ir=3.65 A for turn-to-turn faulty machine (a) and for a Healthy Machine (b).

Figures 6.27 show the rotor line currents spectra under turn-to-turn stator fault by inserted an inductance (Fig. 6.27 a) and for a healthy machine (Fig. 6.27 b). The difference between Figs 6.27 appears in the rotor current components at 75 Hz and sometimes at 325 Hz.

Figs. 6.26 and 6.27 shown that current signature analysis may diagnose turn-to-turn fault developed in stator windings of three-phase induction machines. The line stator and rotor currents have also been shown to contain frequency components that are indicative of these fault conditions. It means that under the turn-to-turn fault in stator windings of the induction generator, the stator line currents spectrum and the rotor line currents spectrum, as well are a proper indicators.

### 6.6.1.3. MCSA to Diagnose Rotor winding unbalance - Experimental development

These tests were carried out to investigate the effect of a resistive unbalance in one rotor phase on the line stator and rotor currents spectra of DFIG. Rotor faults within the machine may produce local aberrations in the air-gap magnetic field and since the stator currents essentially produce this field such anomalies are reflected in these parameters.

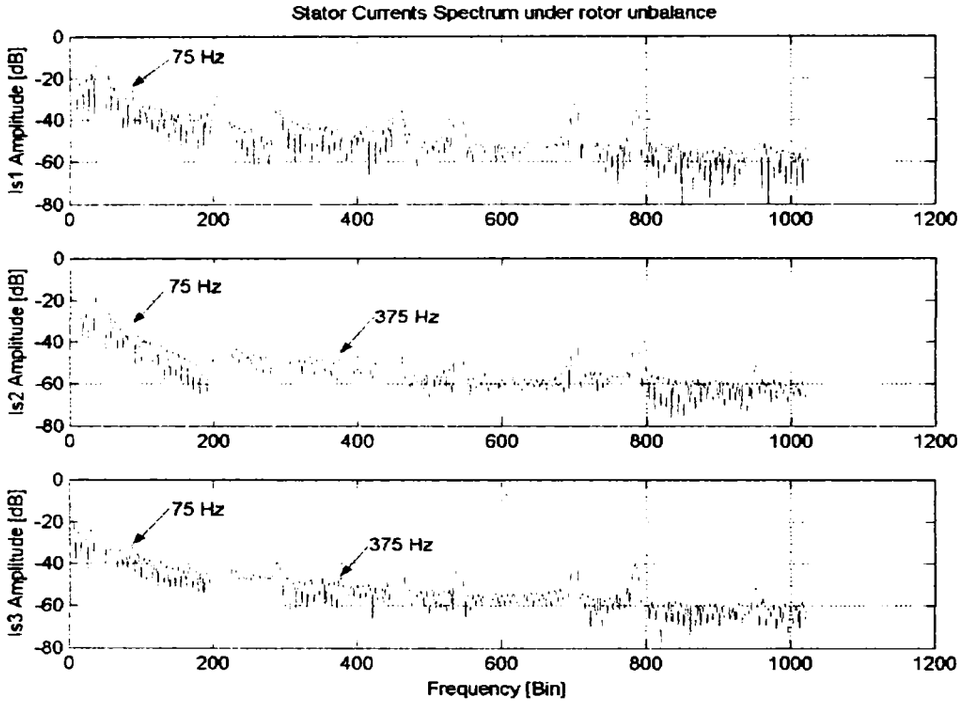


a)

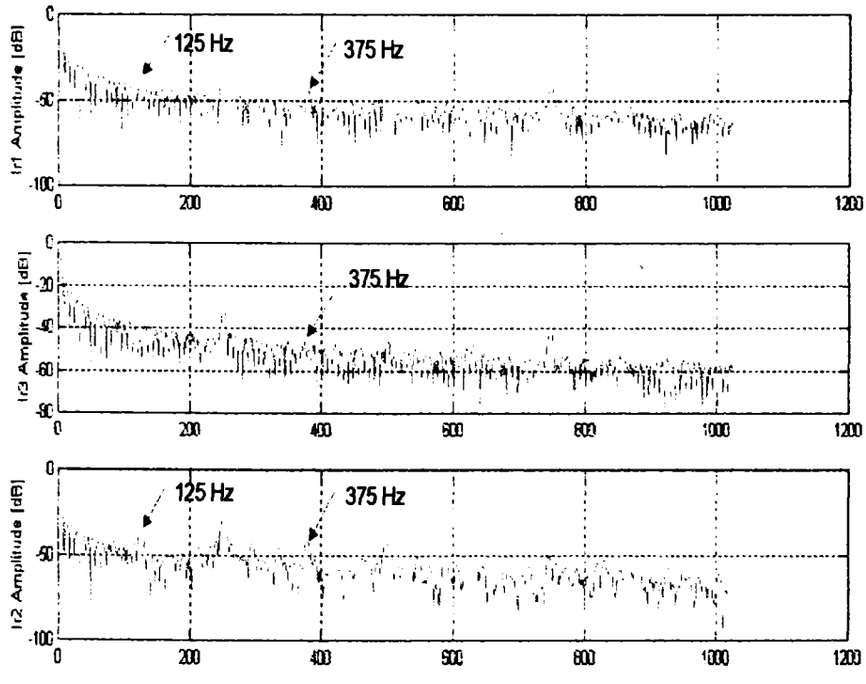


b)

**Fig. 6.28.** Frequency Spectrum of the stator currents (a) and rotor currents (b) under rotor unbalance in one rotor phase at $P_G$=2kW. The data were recorded and processed by Matlab software and acquired by ICS-645.

Figures 6.28 show the stator and rotor line currents spectrum under rotor unbalance in one rotor phase. A clear difference in the spectrum of the stator currents appear at 75 Hz, as can be seen in Fig. 6.28 a). Another new component appears at 375 Hz. The rotor current spectrum offers new faulty components at 375 Hz (k=1 and n=13) and at 125 Hz (k=1 and n=3) as well and sometimes at 325 Hz (k=1 and n=11), as can be seen in Fig. 6.28 b).

It can be concluded that the rotor line current spectrum, under rotor unbalance in one rotor phase, offers more information's about occurrence of this fault than the stator line current spectrum. Anyway, both of them may be used as an indicator in detection of incipient rotor windings unbalance.

### 6.6.1.4. MCSA to Diagnose Stator winding unbalance - Experimental development

This paragraph focuses on experimental results to prove that current signature analysis (MCSA) may diagnose a resistive and an inductive unbalance in the stator windings of a three-phase induction machines.

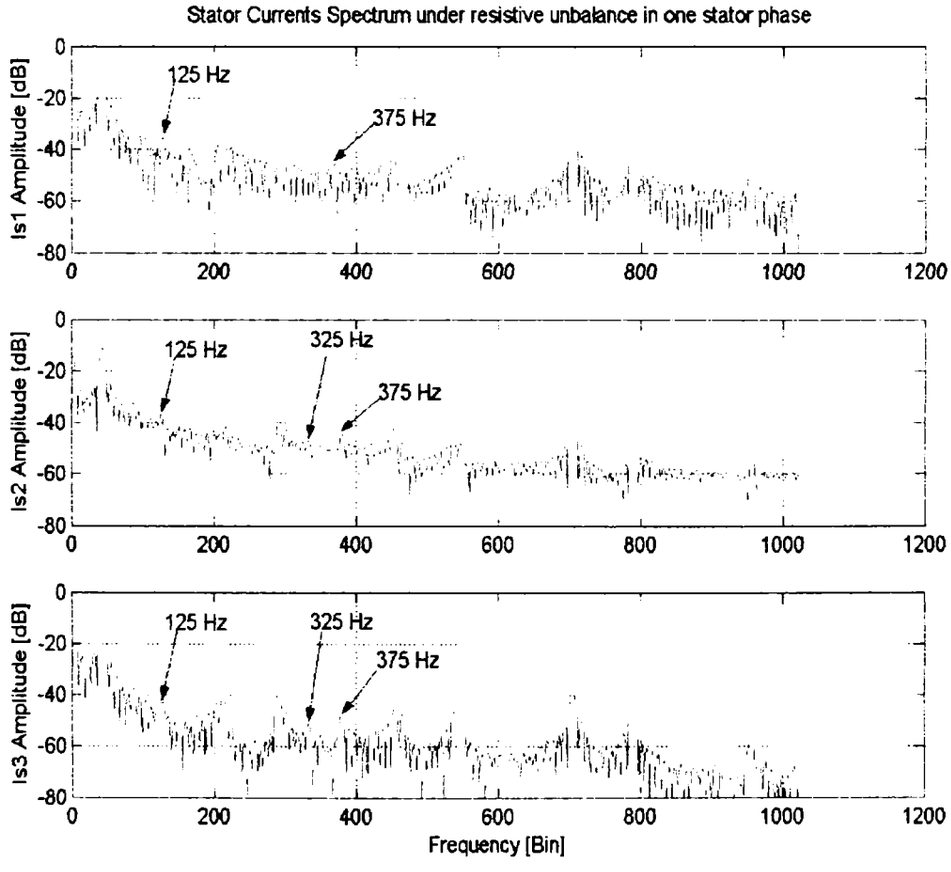


a)

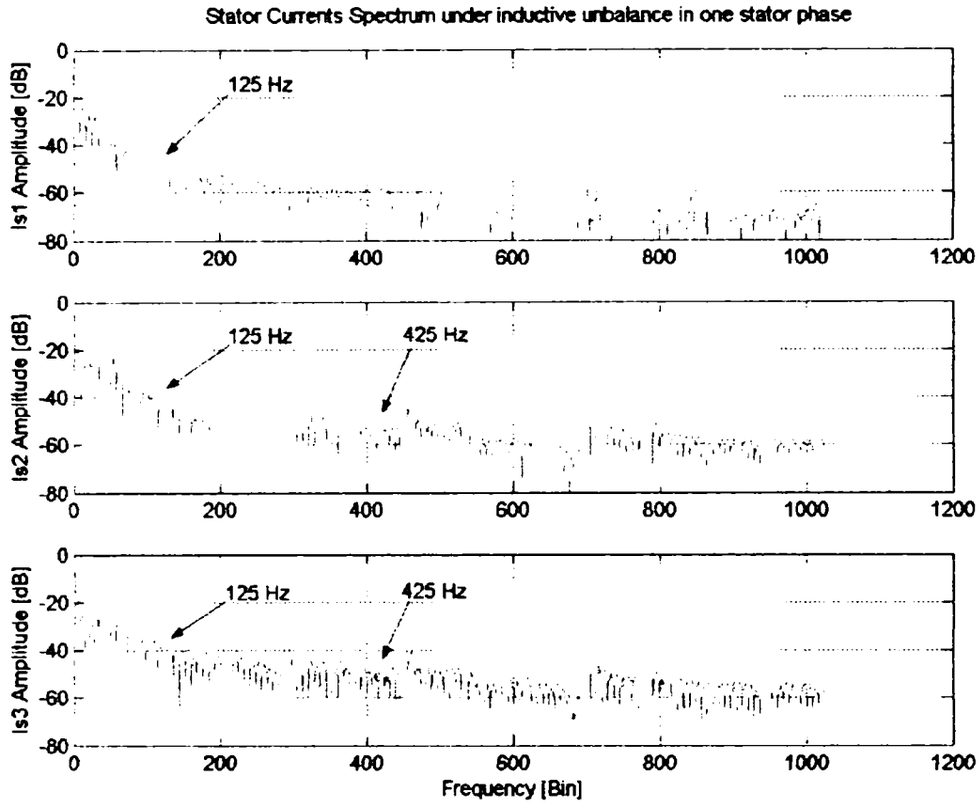


b)

**Fig 6.29.** Stator currents spectrum under resistive (a) and inductive unbalance (b) in one stator phase at $P_G$=2 kW. The data were recorded and processed by Matlab software and acquired by ICS-645.

Figures 6.29 show a comparison between the stator currents spectrum under one stator phase resistive unbalance (R=10 Ω) and one stator phase inductive unbalance (L=50 mH). The inductive unbalance creates the occurrence of new components in the stator current spectrum at 125 Hz (k=1 and n=3) and at 425 Hz (k=1 and n=15) while the resistive unbalance provokes the occurrence of new components in the stator current spectrum at 125 Hz (k=1 and n=3), 325 Hz (k=1 and n=11) and 375 Hz (k=1 and n=13) as well.

These tests were carried out to investigate the effect of a resistive unbalance of Rv=10 Ω placed in series on one stator phase on the line stator currents spectra and the effect of an inductive unbalance of Lv=50 mH.

The current components corresponding to the unbalance phase could decrease in magnitude since the flux components at these frequencies will have decreased due to created unbalance in that phase, as can be seen in Fig. 6.29 (Is1 Amplitude).

### 6.6.2. Instantaneous Partial and Total Power as Diagnostic Media

Sometimes, reliable interpretation of the spectra is difficult, since distortions of the current waveform caused by the abnormalities in the drive system are usually minute. In this situation, an alternative medium for the motor signature analysis, namely the instantaneous power, is used. By theoretical analysis, computer simulations, and laboratory experiments, it was shown that the instantaneous power carries more information than the current itself.

Utilisation of the instantaneous power is thus enhancing the reliability of diagnostics of induction motor drives.

In this case, in place of the stator current, the instantaneous power is used as a medium for the motor signature analysis oriented toward mechanical faults detection in a drive system [37-40] It has been shown that the amount of information carried by the instantaneous power, which is the product of the supply voltage and the motor current, is higher than that deducible from the current alone. In fact, besides the fundamental and the two classical sideband components, the instantaneous power spectrum contains an additional component directly at the modulation frequency. Almost all the fault harmonics are translated into the frequency band 0–100 Hz. This constitutes a great advantage because the fault harmonics domain is well bounded. [53-54]

The diagnostic media include the following:

1. line current $i_A$, in phase A of the supply line;
2. Partial input power $p_{AB}$, calculated as a product of the line-to-line voltage $v_{AB}$ and line current $i_A$.
3. Total instantaneous power $p_{ABC} = p_{AB}+p_{CB}$

For an ideal machine supplied from a balanced three-phase source of sinusoidal voltages, the following waveforms of selected stator voltage and current may be assumed:

$$v_{AB}(t) = \sqrt{2}V_{LL}\cos(\omega t) \quad \text{.....(6.2)}$$

$$i_{A,0}(t) = \sqrt{2}I_L\cos(\omega t - \varphi - \frac{\pi}{6}) \quad \text{.....(6.3)}$$

where $V_{LL}$, $I_L$ are the rms values of line-to-line voltage and line current, $\omega$ is supply frequency and $\varphi$ is power factor angle.

Multiplying $v_{AB}$ by $i_{A,0}$ yields partial instantaneous input power $p_{AB,0}$ given by:

$$p_{AB,0}(t) = V_{LL}I_L\left[\cos\left(\varphi + \frac{\pi}{6}\right) + \cos\left(2\omega t - \varphi - \frac{\pi}{6}\right)\right] \quad \text{.....(6.4)}$$

The two partial powers add up to the total instantaneous power $p_{ABC,0}$, expressed by the well known formula:

$$p_{ABC,0}(t) = \sqrt{3}V_{LL}I_L\cos(\varphi) = P_{ABC,0} \quad \text{.....(6.5)}$$

Thus, in an ideal machine, the total instantaneous power is constant and it is equal to the average real power $P_{ABC,0}$ supplied to the machine.

When an abnormality, such as the stator unbalance, rotor unbalance or turn-to-turn fault develops in the generator system, the current, torque and speed of the machine are affected in

a periodic manner. In the case of periodic disturbances, all three line currents $i_A$, $i_B$ and $i_C$ are simultaneously modulated with the fundamental frequency $f_0$ of the fault induced oscillation of generator variables. Thus, current in phase A of the supply line may now be expresses as:

$$i_1(t) = i_{A,0}(t)\left[1 + m\cos(\omega_0 t)\right] \quad \text{.....(6.6)}$$

where m denotes the modulation index and $\omega_0=2\pi f_0$. The value of the modulation index depends on the severity of the abnormality.

Substituting (6.3) in (6.6) yields:

$$i_A(t) = i_{A,0}(t) + \frac{m}{\sqrt{2}} I_L \left\{ \cos\left[ (\omega + \omega_0)t - \varphi - \frac{\pi}{6} \right] + \cos\left[ (\omega - \omega_0)t - \varphi - \frac{\pi}{6} \right] \right\} \quad \text{....(6.7)}$$

indicating that the spectrum of stator current contains, apart from the fundamental $f_1$ equal to the supply frequency f, two sideband components at frequencies $f_1 \pm f_0$. Corresponding expression for the instantaneous power is:

$$p_{AB}(t) = p_{AB,0}(t) + \frac{m}{2} V_{LL} I_L \left\{ 2\cos(\varphi + \frac{\pi}{6})\cos(\omega_0 t) + \cos\left[ (2\omega + \omega_0)t - \varphi - \frac{\pi}{6} \right] + \cos\left[ (2\omega - \omega_0)t - \varphi - \frac{\pi}{6} \right] \right\} \text{(8)}$$

### 6.6.2.1. Experimental Results

Recorded data were processed using the Matlab software package. The Fast Fourier Transform (FFT) was computed and the power spectra were plotted. For each case, voltage and current measurements were taken for the generator operating. For each variable, $2^{16}$ values were recorded, with the sampling frequency of 2.5 MHz, simultaneously on each channel.

To exemplify the results, selected spectra are shown. Spectra of both diagnostic media with and without fault are shown in Figs. 6.30. The spectrum of line current, instantaneous power and total power are also presented.

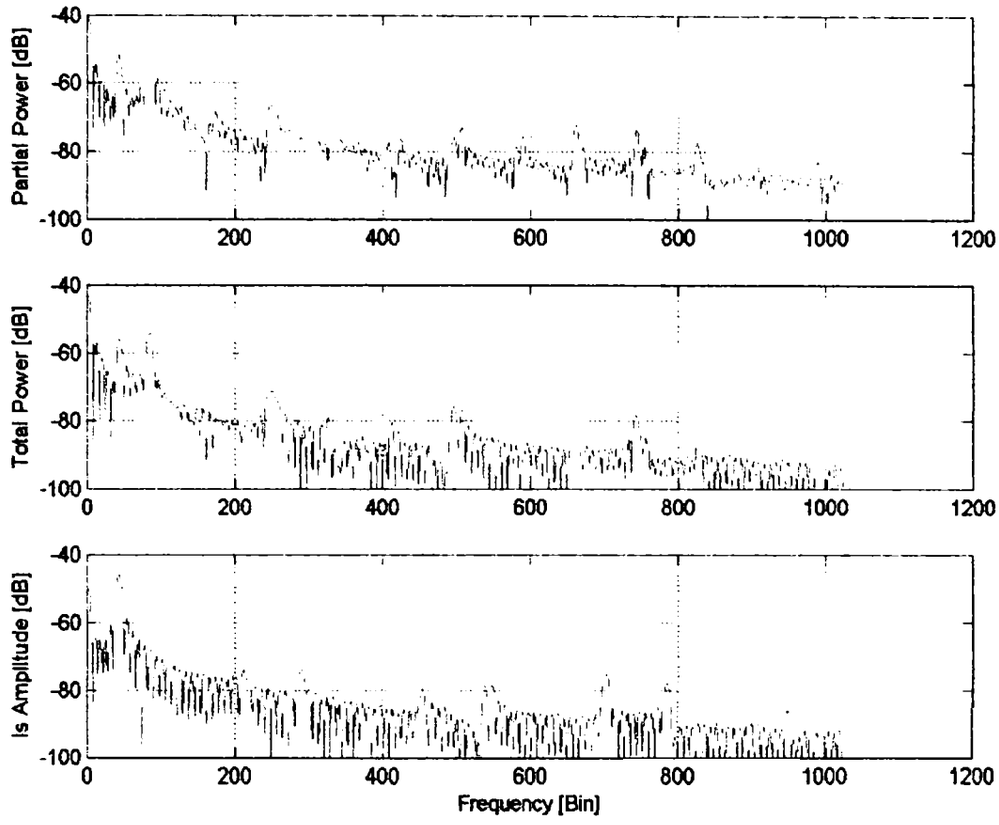
Partial Power [dB]
Total Power [dB]
Is Amplitude [dB]
-40
-60
-80
-100
0
200
400
600
800
1000
1200
Frequency [Bin]

a)

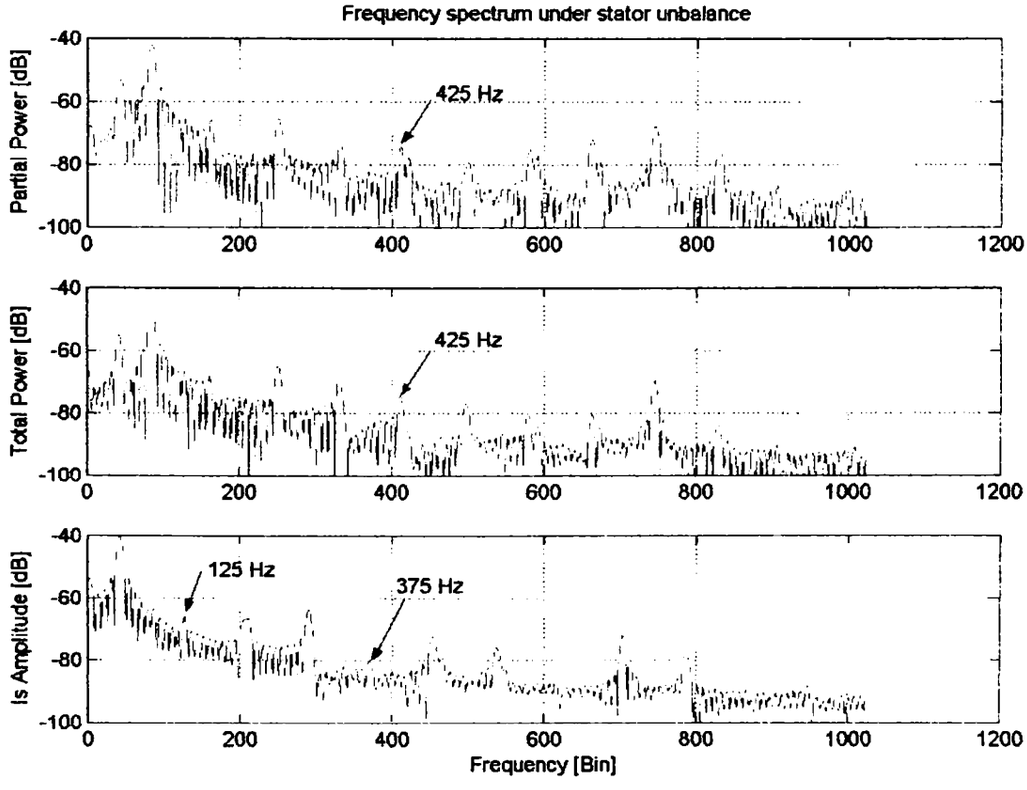
Frequency spectrum under stator unbalance
Partial Power [dB]
Total Power [dB]
Is Amplitude [dB]
425 Hz
425 Hz
125 Hz
375 Hz
-40
-60
-80
-100
0
200
400
600
800
1000
1200
Frequency [Bin]

b)

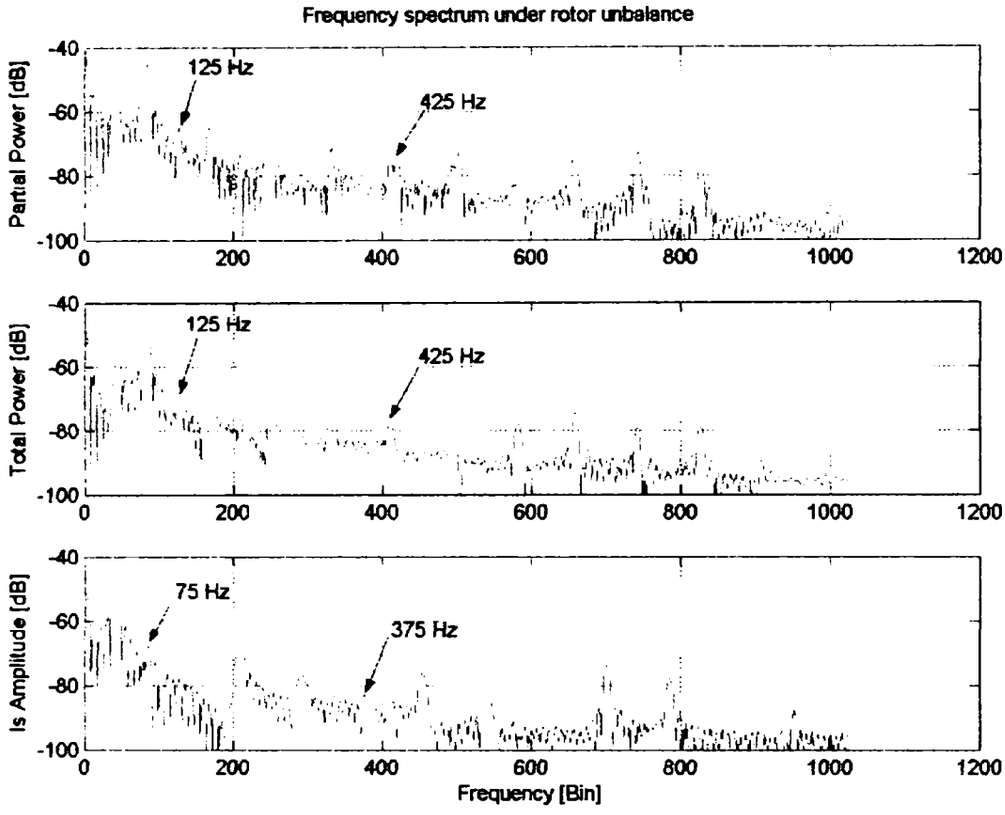


c)

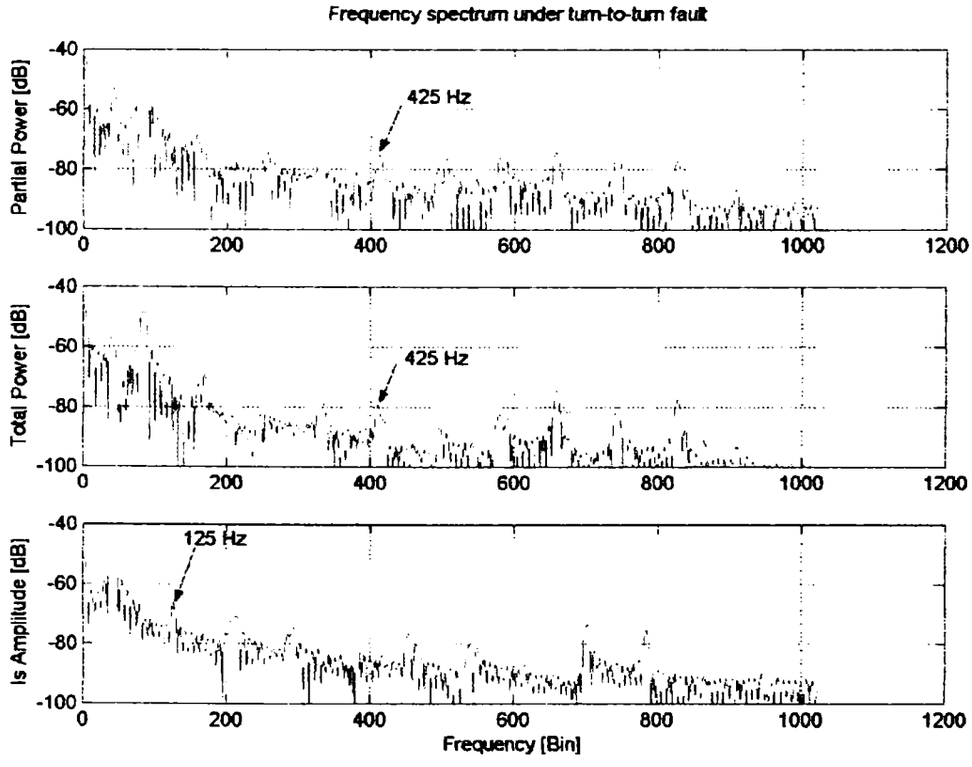


d)

**Figure 6.30.** Spectrum of partial and total instantaneous power and stator current of DFIG at 2 kW for balance machine (a) and under stator unbalance (b), rotor unbalance (c) and turn-to-turn fault (d). The data were recorded and processed by Matlab and acquired via ICS-645.

The sideband components to the left of the fundamental are prominent in all the spectra presented before. The 50 Hz component in the spectra of the power is the result of unbalanced voltages.

The instantaneous partial and total power spectrum offer new faulty components at 125 Hz, 375 Hz and 425 Hz under resistive unbalance in one stator phase, at 125 Hz and 375 Hz under rotor resistive unbalance and at 125 Hz and 425 Hz under turn-to-turn fault provoked in one stator phase. It is concluded that the faulty component at 125 Hz appears in each unbalance situation.

The instantaneous power seems to be a valid alternative diagnostic medium for the machine signature analysis.

## 6.6.3. Negative Sequence Method to Detect Induction Machine Faults

### 6.6.3.1. Theoretical and experimental development.

Symmetrical components are widely used in the analysis of induction machines under unbalance conditions. The method of symmetrical components simplifies the theoretical analysis during fault conditions by defining specific sequence components include the positive, negative and zero sequence components.

Unbalance in the three-phase voltage supply causes unbalance (negative sequence) currents in a healthy machine. The presence of a negative sequence component indicates some levels of unbalance, with the magnitude of this unbalance commonly represented as a percent unbalance based on the positive-sequence value.

Methods for the prediction of electrical behavior in deteriorating induction machines allow a number of winding deterioration processes to be simulated on the stator and / or the rotor. Forms of deterioration might include high or low impedance between grid and machine, between phases, between coils in a single phase, or between a phase and ground.

The theory of symmetrical components provides powerful analysis techniques for simplifying calculation on unbalanced or faulted power systems. Symmetrical component quantities of three-phase systems include the positive, negative and zero-sequence components. The phase value is the vector sum of its zero, positive and negative-sequence components.

On-line monitoring of symmetrical component as the inverse voltage and the inverse current can provide a simple and effective method for detecting voltage power supply unbalance. Moreover, the use of this method is simple and the interpretation of the results does not require specific knowledge.

The negative sequence method for detecting an incipient failure could contain the following steps:

1. Periodically measuring or continuously monitoring voltage and current at each machine input
2. Determining negative sequence voltage and current for each measurement
3. Calculating an effective negative sequence impedance phasor value angle for each value of 2)

4. Comparing the calculate negative sequence impedance phasor values and components to detect changes indicative of incipient failure modes

A method for stator turn fault detection involve measured and digitised of current and voltage waveforms and then these are transformed using a weighted discrete Fourier transform to obtain negative sequence current and voltage phasor. These are then used to detect the existence of a turn fault. Employing one of several techniques can perform the use of the negative sequence current and voltage phasors:

a) In a first embodiment, apparent negative sequence impedance is estimated by dividing the negative sequence voltage phasor by the negative sequence current phasor for comparison with threshold negative sequence impedance.

b) In a second embodiment, dividing the negative sequence voltage phasor by characteristic negative sequence impedance and subtracting the result from the negative sequence current phasor for comparison with a threshold current differential estimate.

c) In a third, related embodiment, a voltage differential is estimated by multiplying the negative sequence current phasor by characteristic negative sequence impedance and subtracting the result from the negative sequence voltage phasor for comparison with a threshold voltage differential. In either of the second or third embodiments, the characteristic negative sequence impedance can be obtained by inserting a calibration device into one phase of the machine.

According to Fortescue's theorem, three unbalance phasors of a three-phase system can be resolved into three phase balance systems of phasors. Symmetrical components quantities of three phase system include the positive, negative and zero-sequence components.

1. The positive sequence components consisting of three phasors equal in magnitude, displaced from each other by 120° in phase, and having the same phase sequence as the original phasors.
2. The negative sequence components consisting of three phasors equal in magnitude, displaced from each other by 120° in phase, and having the phase sequence opposite to that of the original phasors.
3. Zero sequence components consisting of three phasors equal in magnitude and with zero phase displacement from each other.

Since each of the original unbalanced phasors is the sum of its components, the phase value is the vector sum of its zero, positive and negative sequence component as expressed in (6.9):

$$V_A = V_{A0} + V_{Ap} + V_{An}; V_B = V_{B0} + V_{Bp} + V_{Bn}; V_C = V_{C0} + V_{Cp} + V_{Cn} \quad \text{.....(6.9)}$$

The expressed in (6.9) are also true for current if $I$ is substituted for $V$. These equations can be simplified by representing the unit vector $a = e^{j120^0} = e^{j\frac{2\pi}{3}}$ and making the proper substitutions, as expressed in (6.10) in matrix notation.

$$[A_{0pn}] = \frac{1}{3}\begin{bmatrix} 1 & 1 & 1 \\ 1 & a^2 & a \\ 1 & a & a^2 \end{bmatrix} \quad \text{.....(6.10)}$$

$A$ is called the symmetrical components transformation matrix.
In this way we may write the phase voltage equations as a function of zero, positive and negative sequence:

$$[V_{ABC}] = [A_{0pn}] * [V_{0pn}] or [V_{0pn}] = [A_{0pn}]^{-1} * [V_{ABC}] \quad \text{.....(6.11)}$$

or in matrix notation:

$$\begin{vmatrix} V_A \\ V_B \\ V_C \end{vmatrix} = \begin{vmatrix} 1 & 1 & 1 \\ 1 & a^2 & a \\ 1 & a & a^2 \end{vmatrix} * \begin{vmatrix} V_{A0} \\ V_{Ap} \\ V_{An} \end{vmatrix} \quad \text{.....(6.12)}$$

and solving for the sequence components yields,

$$\begin{vmatrix} V_{A0} \\ V_{Ap} \\ V_{An} \end{vmatrix} = \frac{1}{3}\begin{vmatrix} 1 & 1 & 1 \\ 1 & a & a^2 \\ 1 & a^2 & a \end{vmatrix} * \begin{vmatrix} V_A \\ V_B \\ V_C \end{vmatrix} \quad \text{.....(6.13)}$$

This relationship between line and sequence values also exists for currents if $I$ is substituted for $V$. The sequence components in (6.13) represent more than mathematical conveniences, and their presence can be indicative of specific power systems problems [41, 42, 64]. For example, the zero-sequence component of current is directly proportional to the level of neutral current flowing during a line-to-line fault; the presence of a negative-sequence component indicates some levels of unbalance, with the magnitude of this unbalance commonly represented as a percent unbalance based on the positive sequence value (Voltage Unbalance Factor-VUF of 0.5 percent indicates that the negative sequence voltage is 1/200 of the positive sequence [42]).

Although negative-sequence components indicate system unbalance, small supply unbalances are frequently caused by single-phase loading, and the resulting voltage unbalance generates the flow of negative-sequence current [41, 42].

Let's calculate the positive and negative sequence current for a balance machine and for each unbalance case presented before.

$$I = |I| * e^{\pm j\varphi} = |I| * (\cos\varphi \pm j\sin\varphi) = |I| \angle \varphi \quad \text{.....(6.14)}$$

Where $|I|$ is the magnitude, given by $|I| = \sqrt{a^2 + b^2}$ and φ is the phase angle or argument given by $\varphi = \tan^{-1}\left(\frac{b}{a}\right)$; Where the real numbers $a$ and $b$ are real and imaginary part of $I$.

$$\underline{I}_s = \underline{I}_{sp} + \underline{I}_{sn}; \underline{I}_r = \underline{I}_{rp} + \underline{I}_{rn} \quad \text{.....(6.15)}$$

$$\begin{aligned} I_s &= |I_{sp}| * \angle\varphi_1 + |I_{sn}| * \angle\varphi_2 = |I_{sp}|[\cos(\varphi_1) + j\sin(\varphi_1] + |I_{sn}|[\cos(\varphi_2) + j\sin(\varphi_2] \\ I_r &= |I_{rp}| * \angle\varphi_3 + |I_{rn}| * \angle\varphi_4 = |I_{rp}|[\cos(\varphi_1) + j\sin(\varphi_1] + |I_{rn}|[\cos(\varphi_2) + j\sin(\varphi_2] \end{aligned} \quad \text{.....(6.16)}$$

Where $\varphi_1$ is phase angle of the positive sequence stator current, $\varphi_2$ is phase angle of the negative sequence stator current, $\varphi_3$ is phase angle of the positive sequence rotor current and $\varphi_4$ is phase angle of the negative sequence rotor current.

According to Fortescue's theorem, three unbalance phasors of a three-phase system can be resolved into three phase balance systems of phasors.

$$\begin{vmatrix} 0 \\ I_p \\ I_n \end{vmatrix} = \frac{1}{3}\begin{vmatrix} 1 & 1 & 1 \\ 1 & a & a^2 \\ 1 & a^2 & a \end{vmatrix} * \begin{vmatrix} I_A \\ I_B \\ I_C \end{vmatrix} \quad \text{.....(6.17)}$$

From equation (6.17) we can deduce that:

$$I_p = \frac{1}{3}\left(I_A + aI_B + a^2 I_C\right) \quad \text{.....(6.18)}$$

$$I_n = \frac{1}{3}\left(I_A + a^2 I_B + aI_C\right) \quad \text{.....(6.19)}$$

*Experimental results: (resistive unbalance of Rv=10 Ω)*

P=2kW, $I_C$=3.75 A, $I_B$=3.7A, $I_A$=2.75A;

$I_p = 2.43A, I_n = 0.33A$

P=4kW, $I_A$=7.04, $I_B$=7A, $I_C$=5.15A

$I_p = 4.5A; I_n = 0.67A$

*Experimental results: (inductive unbalance of Lv=50 mH)*

P=2kW, $I_A$=0.87A, $I_B$=3.35 A, $I_C$=4A

$I_p = 0.77A; I_n = 0.095A$

P=3kW, Is1=1.07A, Is2=4.1A, Is3=5.05A

$I_p = 0.92A; I_n = 0.17A$

*Experimental results: (rotor resistive unbalance of Rv= 1.2 Ω in one phase)*

P=2 kW, $I_A$=3.75 A, $I_B$=3.8 A and $I_C$=3.9 A

$I_p = 3.86A; I_n = 0.036A$

*Experimental results: (turn-to-turn fault - Lv=50 mH in parallel on one stator phase)*

P=2 kW, $I_A$=2.57 A, $I_B$=2.38 A and $I_C$=3.32 A

$I_p = 3.06A; I_n = 0.28A$

The experimental results have clearly demonstrated that the presence of a negative-sequence component indicates some levels of unbalance, with the magnitude of this unbalance commonly represented as a percent unbalance based on the positive sequence value. The negative-sequence components indicate system unbalance that is frequently caused by single-phase loading and the resulting voltage unbalance generates the flow of negative-sequence current, as can be seen in all unbalance situations presented before.

## 6.7. Conclusions

The objective of this chapter was to develop different type of faults and to test detection methods of condition monitoring, previously reported in the literature, and suitable adapted for implementation in wind generator systems. The results presented have shown that the objective was achieved.

An induction machine condition monitoring system has also been developed to tests these methods. The software which controls both the acquisition and analysis of the signals is written in Matlab and has been developed as a sub-part of the monitoring system. The chapter has shown that the detection of these faults is also possible by time and frequency domain analysis. The frequency spectrum of the stator and rotor line currents was found to give the best results.

Placing an inductance and / or a resistance in series on one phase, between the grid and stator phase terminals on one phase, an unbalance in one stator phase was simulated. Inserting

a resistance in series on one rotor phase we also simulated an unbalance in one rotor phase. Placing an inductance in parallel on one phase, the deterioration of the turn-to-turn insulation in one stator phase of the induction generator was simulated. In this way we simulated a turn-to-turn fault in one stator phase without destroying the machine or building an additional construction such as placing taps on the wires of the stator windings and then shorting these taps.

The experimental results show the efficiency of line stator and rotor currents monitoring in identifying the presence of an unbalance in one stator and rotor phase and confirm the presence of harmonics as described by equation (6.1).

The theoretical and experimental results in this chapter have clearly demonstrated that MCSA can diagnose turn-to-turn faults. MCSA is a powerful technique for monitoring the health of three-phase induction machines.

The line stator currents have been shown to contain frequency components that are indicative of these fault conditions. The obvious change, is that completely new current components exist at 125 and 375 Hz and can only be due to the shorted turn, as per theory with k=1, n=3 and k=1, n=13, in according to equation 1.

MCSA can also diagnose other problems in induction generators such as inductive and resistive unbalance in one stator and rotor phase. It was shown that the rotor current spectrum might be a good indicator, as the stator currents spectrum, under inductive and resistive unbalance. The obvious change is that new rotor current components exist at 75 Hz, 325 Hz, and 675 Hz and the new stator current components appear at 125 Hz, 175 Hz and 375 Hz as well. The magnitude of the faulty currents and phase angle is different in comparison with the healthy machine currents magnitude.

The instantaneous partial and total power seems to be a valid alternative diagnostic medium for the machine signature analysis. It is worth mentioning, that the instantaneous power constitutes an attractive medium for diagnosis of stator and rotor unbalance or turn-to-turn fault in one stator or rotor phase in induction generator systems. This has been demonstrated in many papers.

Hopefully, results of the presented study will enhance the insight into application of various variables in diagnostics of abnormalities in induction machine drives.

## References

[1] W.T.Thomson and M.Fenger, "Current Signature Analysis to Detect Induction Motor Faults", IEEE Industry Applications Magazine, pp. 26-34, July/August 2001.

[2] R.Burnett, J.F.Watson, S.Elder, "The Application of Modern Signal Processing Techniques to Rotor Fault Detection and Location within Three Phase Induction Motors", IEEE, pp.426-431, June 1995.

[3] R.Burnett and J.F.Watson, "The Current Analysis Program-A Software Tool for Rotor Fault Detection in Three Phase Induction Motors", Electrical Machines and Drives, pp.156-160, 11-13 September 1995.

[4] F.Filippetti, G.Franceschini, C.Tassoni and P.Vas, "Recent Developments of Induction Motor Drives Fault diagnosis Using AI Techniques", IEEE Transactions on Industrial Electronics, vol.47, no.5, pp.994-1004, October 2000.

[5] A.H.Bonnet and G.C.Soukup, "Cause and analysis of stator and rotor failures in three-phase squirrel-cage induction motors", IEEE Trans. Ind. Applicat., vol. 28, pp. 921-937, July/August 1992.

[6] M.Haji, H.A.Toliyat, "Pattern Recognition-A Technique for Induction Machines Rotor Fault Detection Eccentricity and Broken Bar Fault", 36th IAS Annual Meeting, IEEE Ind. 2001, September 30th – October 4th, Chicago, Illinois, USA.

[7] H.A.Toliyat, T.A.Lipo, "Transient Analysis of Cage Induction Machines under Stator, Rotor Bar and End Ring Faults", IEEE Trans. On Energy Conv., Vol. 9, No. 4, June 1995.

[8] S.Nandi and H.A.Toliyat, "Fault Diagnosis of Electrical Machines – A Review", IEEE Industry Applications Conference, 1999. Thirty-Fourth IAS Annual Meeting. Vol. 1, 1999, pp. 197-204.

[9] P.Vas, "Parameter Estimation, Condition Monitoring, and Diagnosis of Electrical Machines", Clarendon Press, Oxford, 1993.

[10] G.B.Kliman, W.J.Premerlani, R.A.Koegl and D.Hoeweler, "A new approach to online fault detection in ac motors", IEEE-IAS Annual Meeting Conference, pp. 687-693, San Diego, CA, 1996.

[11] N.M.Elkasabgy, A.R.Eastham, G.E.Dawson, "Detection of broken bars in the cage rotor on an induction machine", IEEE Trans. Ind. Applns, vol. IA-22, no. 6, pp. 165-171, Jan./Feb. 1972.

[12] W.T.Thomson, M.Fenger, "Industrial application of current signature analysis to diagnose fault in 3-phase squirrel cage induction motors", IEEE 2000.

[13] W.T.Thomson, "On-line current monitoring to detect electrical and mechanical faults in three-phase induction motor drives", Proc. IEE and IMECHE (London), Int. Conf. Proc on Life Management of Power Plants, Heriot-Watt University, Edinburgh, 12-14 December 1994, pp. 66-73.

[14] W.T.Thomson and I.D.Stewart, "On-line current monitoring for fault diagnosis in inverter fed induction motors", In 3rd International Conference on Power Electronics and Variable Sped Drives, 1998, pp. 432-435.

[15] J.Penman, H.G.Sedding, B.A.Lloyd, W.T.Fink, "Detection and location of interturn short circuits in the stator windings of operating motors", IEEE Trans. Energy Conv., Vol. 9, no. 4, Dec. 1994,pp. 652-658.

[16] S.Williamson and P.Mirzoian, "Analysis of cage induction motor with stator winding faults", IEEE-PES, Summer Meeting, July 1994.

[17] G.B.Kliman, W.J.Premerlani, B.Yazici, R.A.Koegl and J.Mazereeuw, "Sensorless Online Motor Diagnostics", IEEE Computer Applications in Power, April 1997, pp. 39-43.

[18] Li Yonggang, Li Heming, Zhu Ling and Zhao Hua, "Inter turn short-circuit fault research on generator rotor windings", ICEMS'2001. Proceedings of the fifth International Conference on Electrical Machines and Systems, August 18-20, Shenyang-China, Vol. 1 pp. 357-361.

[19] Robin Smith, "Monitoring for Rotor Shorted Turns", Siemens Power Generation Limited Newcastle upon Tyne, 1990. pp. 8/1-8/20.

[20] William T.Thomson, "On-line MCSA to diagnose shorted turns in low voltage stator windings of 3-phase induction motors prior to failure", Electric Machines and Drives Conference, 2000. IEMDC 2001. IEEE International, 2001, pp. 891-898.

[21] K.Delaere, K.Hameyer, R.Belmans, "Static eccentricity as a cause for audible noise of induction motors", ICEM September 2-4, 1998, Vol. 1, pp. 502-506.

[22] J.M.Aller, J.A.Restrepo, A.Bueno, M.I.Gimenez, R.Alves, "Dynamic models of induction motor including the rotor eccentricities and the slot effect using the spatial vector transform", ICEM September 2-4, 1998, Vol. 1, pp. 597-602.

[23] Xiaolan Deng, "Detection of rotor faults on induction motors by investigating the flux linkage of the stator winding", Ph.D. Thesis, December 1994, I 1494S0076.

[24] A.Stavrou, J.Penman, "Modelling dynamic eccentricity in smooth air-gap induction machines", IEEE 2001.pp. 864-871.

[25] D.G.Dorrell, W.T.Thomson, and S.Roach, "Analysis of air-gap flux, current, and vibration signals as a function of the combination of static and dynamic air-gap eccentricity in 3-phase induction motors", IEEE Trans. On IA, Vol. 33, nr. 1,1997, pp. 24-34.

[26] W.T.Thomson, D.Rankin, D.G.Dorrell, "On-line current monitoring to diagnose air-gap eccentricity in large three-phase induction motors-industrial case histories verify the predictions", IEEE Transactions on Energy Conversion, vol. 14, no. 4, December 1999, pp. 1372-1378.

[27] W.T.Thomson and A.Barbour, "The on-line prediction of air-gap eccentricity levels in large (MW Range) 3-phase induction motors", Electric Machines and Drives, International Conference IEMD, 1999, pp. 383-385.

[28] R.Ong, J.H.Dymond and R.D.Findlay, "Bearing damage analysis in a large oil-ring-lubricated induction machine", IEEE Transactions on Industrial Electronics, vol. 47, no. 5, October 2000.

[29] Randy R.Schoen and Thomas G.Habetler, "Effects of time-varying loads on rotor fault detection in induction machines", IEEE Transactions on Industry Applications, vol. 31, no. 4, July/August 1995,pp. 900-906.

[30] Randy R.Schoen and Thomas G.Habetler, "Evaluation and implementation of a system to eliminate arbitrary load effects in current-based monitoring of induction machines", IEEE Transactions on Industry Applications, vol. 33, no. 6, November/December 1997,pp. 1571-1577.

[31] S.Nandi, S.Ahmed, H.A.Toliyat, R.Bharadwaj, "Selection criteria of induction machines for speed-sensorless drive applications", 36th IAS Annual Meeting, IEEE Ind. 2001, September 30th – October 4th, Chicago, Illinois, USA.

[32] G.B.Kliman, J.Stein and R.D.Endicott, "Non-invasive detection of broken rotor bars in operating induction motors", IEEE Transactions Energy Conversion, vol. 3, no. 4, December 1988, pp. 873-879.

[33] A.Stavrou and J.Penman, "The on-line quantification of air-gap eccentricity in induction machines", Proc. International Conference on Electrical Machines '94 Paris, France, 5-8 Sept. 1994, pp. 261-266.

[34] J.Sottile, F.C.Trutt and J.L.Koher, "Experimental investigation of on-line methods for incipient fault detection", IEEE 2000, pp. 2682-2687.

[35] J.L.Koher, J.Sottile and F.C.Trutt, "Condition based maintenance of electrical machines", IEEE 1999, pp. 205-211.

[36] Bin Huo and Andrzej M. Trzynadlowski, "Simple stator fault detector for ac motors", Electric Machines and Drives Conference, 2000. IEMDC 2001. IEEE International, 2001,pp. 192-194.

[37] Andrzej M. Trzynadlowski and Ewen Ritchie, "Comparative investigation of diagnostic media for induction motors: a case of rotor cage faults", IEEE Transactions on industrial electronics, vol. 47, no. 5, October 2000, pp. 1092-1099.

[38] Andrzej M. Trzynadlowski and Ewen Ritchie, "Comparative investigation of diagnostic media for induction motors: a case of rotor cage faults", Industry Applications Conference, 1999.Thirty-Fourth IAS Annual Meeting. Conference Record of 1999 IEEE, vol. 3, pp. 1935-1941.

[39] S.F. Legowski, A.H.M. Sadrul Ula and A.M. Trzynadlowski, "Instantaneous power as a medium for the signature analysis of induction motors", IEEE Transactions on Industry Applications, Vol. 32, no. 4, July/August 1996, pp. 904-909.

[40] S.F. Legowski, A.H.M. Sadrul Ula and A.M. Trzynadlowski, "Instantaneous stator power as a medium for the signature analysis of induction motors", Industry Applications Conference, 1995.Thirtieth IAS Annual Meeting, Vol. 1, pp. 619-624.

[41] J. Sottile and J.L. Kohler, "An on-line method to detect incipient failure of turn insulation in random-wound motors", IEEE Transactions on Energy Conversion, vol. 8, no. 4, December 1993,pp. 762-768.

[42] F.C. Trutt, J. Sottile and J.L. Kohler, "On-line monitoring of induction motors", Industry Applications Conference, 2001. Thirty-Sixth IAS Annual Meeting. Conference Record of the 2001 IEEE, Volume: 2, 2001, Page(s): 1369 -1375.

[43] M.Alex Cash, Thomas G. Habetler and Gerald B. Kliman, "Insulation failure prediction in induction machines using line-neutral voltages", Industry Applications Conference, 1997, Thirty-Second IAS Annual Meeting, Conference Record of the 1997 IEEE, Vol. 1, pp. 208-212.

[44] M.Alex Cash and Thomas G. Habetler, "Insulation failure detection in the stator windings of ASD-Driven induction machines using standard deviation of line currents", Industry Applications Conference, 1998, Thirty-Third IAS Annual Meeting, Vol. 1, pp. 299-303.

[45] M.Alex Cash, Thomas G. Habetler and Gerald B. Kliman, "Insulation failure prediction in ac machines using line-neutral voltages", IEEE Transactions of Industry Applications, vol. 34, no. 6, November/December 1998, pp. 1234-1239.

[46] F. Filippetti, G.Franceschini, G.Gentile, S.Meo, A.Ometto, N.Rotondale, C.Tassoni, "Current pattern analysis to detect induction machine non rotational anomalies", ICEM 98, International Conference on Electrical Machines, September 2-4, 1998, Istambul-Turkey, Vol. 1, pp. 448-453.

[47] I.J.Kemp, H.Zhu, H.G.Sedding, J.W.Wood, W.K.Hogg, "Towards a new partial discharge calibration strategy based on the transfer function of machine stator windings", IEE Proc. – Sci. Meas. Technol., Vol. 143, No. 1, January 1996, pp. 57-62.

[48] M. Fenger, G.C. Stone and B.A. Lloyd, "Experience with continuous partial discharge monitoring of stator windings", Electrical Insulation Conference and Electrical Manufacturing & Coil Winding Conference, 2001, pp. 417-421.

[49] D.G. Edwards, "On-line diagnosis of defects in the stator winding insulation structures of high voltage rotating machines", ICEM'92, Manchester, UK (15-17 September, Vol. 3, pp. 1299-1303.

[50] S. Nandi and H.A. Toliyat, "Novel frequency domain based technique to detect incipient stator inter-turn faults in induction machines", Industry Applications Conference, 2000. Conference Record of the 2000 IEEE, Vol. 1, pp. 367-374.

[51] Paul Gipe, "Wind energy comes of age", book, Wiley & Sons Inc., New York, 1995.

[52] Siegfried Heier, "Wind energy conversion systems", book, John Wiley & Sons Inc., New York, 1998.

[53] El Hachemi Benbouzid, M., "A review of induction motors signature analysis as a medium for faults detection", Industrial Electronics, IEEE Transactions on, Volume: 47 Issue: 5, Oct. 2000, Page(s): 984 –993.

[54] Benbouzid, M.E.H.; Vieira, M.; Theys, C., "Induction motors faults detection and localisation using stator current advanced signal processing techniques", Power Electronics, IEEE Transactions on, Volume: 14 Issue: 1, Jan. 1999, Page(s): 14 –22.

[55] A. A. Da Silva et al., "Rotating machinery monitoring and diagnosis using short-time Fourier transform and wavelet techniques," in Proc. 1997 Int. Conf. Maintenance and Reliability, vol. 1, Knoxville, TN, pp. 14.01–14.15.

[56] A. W. Galli et al., "Exploring the power of wavelet analysis," IEEE Comput. Appl. Power, vol. 9, pp. 37–41, Oct. 1996.

[57] W. J. Wang et al., "Application of wavelets to gearbox vibration signals for fault detection," J. Sound Vib, vol. 192, no. 5, pp. 927–939, 1996.

[58] H.A Tolyiat, M.S. Arefeen, A.G. Parlos "A method for dynamic simulation of air-gap eccentricity in induction machines", IEEE-Trans. Ind. Applns., pp. 910-918, vol. 32, no.4, July/Aug., 1996.

[59] H.A Tolyiat, A. Al-Nuaim, "A novel method for modelling dynamic air-gap eccentricity in synchronous machines based on modified winding function theory", IEEE-PES Summer Meeting, July 1997.

[60] A.J.M Cardoso, E.S. Saraiva, "Computer-aided detection of air gap eccentricity in operating three-phase induction motors by Park's Vector Approach", IEEE Trans. Ind. Appls., pp. 897-901, vol. 29, no. 5, Sept./Oct. 1993.

[61] J.R. Cameron, W.T. Thomson, A.B. Dow, "Vibration and current monitoring for detecting air gap eccentricity in large induction motors", IEE Proceedings, pp. 155-163, vol. 133, pt. B, no. 3, May, 1986.

[62] M. Arkan, D.K. Perovic and P.J.Unsworth, "Closed rotor slot effect on negative sequence impedance", IEEE 2001, pp. 751-753.

[63] M. Arkan, D.K. Perovic and P.J.Unsworth, "Online stator faults diagnosis in induction motors", IEE Proc.-Electr. Power Appl., Vol. 148, No. 6, November 2001, pp. 537-547.

[64] I. Boldea and Nasar, "The Induction Machine Handbook", book, CRC Press, 2002.

[65] Lucian Mihet-Popa, "Condition Monitoring of Wind Generators", Internal report, Institute of Energy Technology, Aalborg University, Denmark, 2002.

[66] Lucian Mihet-Popa, Birgitte-Bak Jensen, Ewen Ritchie and Ion Boldea, "Condition Monitoring of Wind Generators", Record of IEEE-IAS 38th Annual Meeting, 2003, 12-16 October.

[67] Lucian Mihet-Popa, Birgitte-Bak Jensen, Ewen Ritchie and Ion Boldea, "Current Signature Analysis to Diagnose Incipient Faults in Wind Generator Systems", ELECTROMOTION 2003, 26-28 November.

# Chapter 7

# Conclusion

**Chapter Contents**

## 7.1. Summary

This thesis builds on the previous work of wind energy conversion systems by presenting and implementing the new wind turbine generator control configurations with constant speed and variable speed induction generators, connected to the grid.

The thesis is structured in seven chapters and five appendices. It starts by presenting various wind turbine generator configurations pointing out the principal components of a modern wind generator system and the basics of wind energy conversion systems. ***Chapter 2*** presents the development in the area of electric machines and power electronics with respect to wind turbine generators, highlighting the generator and power electronics configurations most commonly applied in wind turbines. Also, the control strategies and trends in wind turbine design are shortly presented.

***Chapter 3*** presents details about modeling and simulation of a constant-speed wind turbine using cage rotor induction generators. The model developed also includes control of soft-starter, power factor compensation and relatively new alternative control strategies of large constant-speed wind generator systems. ***Chapter 4*** proposes a wound rotor induction generator with limited variable-speed generation system for a viable low-cost, low maintenance, variable-speed wind generator system. This system provides acceptable efficiency over a reasonable speed range.

***Chapter 5*** is devoted to modeling, simulation and testing of a variable-speed wind turbine with doubly-fed induction generator. A control strategy of decoupling active and reactive power and a PWM modulation strategy to control the rotor converter are developed. An analytic analysis of the current loop and the power loop are performed, and the appropriate regulators are selected and compared through simulations. The comparison between simulations and experiments show a good similarity.

***Chapter 6*** presents the analysis of Condition Monitoring of Wind Generators using Doubly Fed Induction Generators (DFIG). Mainly this study focuses on the experimental investigation for incipient fault detection and fault detection methods, suitably adapted for use in wind generator systems. Studies also include design and commissioning of a measuring system, comprising signal conditioning box, AD card and transducers for current, voltage, speed and temperature.

## 7.2. Contributions of the thesis

Chapters 3-6 are based on original material, published previously in four scientific papers, which have as first author the author of this thesis. The papers have been presented at International Conferences and one of them has been accepted to be published in IEEE-IAS Transactions-January / February 2004.

The following contributions are believed to be new:

- Modeling and simulation of a constant-speed wind turbine generators with cage rotor induction generators of (0.5 and 2) MW using DIgSILENT and Matlab-Simulink software packages, including: modeling and implementing of the wind turbine components, such as wind model, transmission model, induction generator model, transformer, soft-starter controller and power factor compensation unit that include the switching strategy of capacitors as a function of average value of reactive power (chapter 3).
- This thesis introduces a relatively recent innovation in the power control strategy of large constant-speed wind turbines that is the active-stall constant speed concept. This alternative control strategy, involves the combined interaction between wind model, pitch control and the aerodynamics of wind turbine rotor blades (chapter 3 & [64, 65]);
- Modeling, simulation, building and testing a highly reliable, low maintenance, and low capital cost alternative of wind generator system with acceptable efficiency over a reasonable speed range. Digital simulations using Mathcad and Matlab-Simulink are developed to analyze the performance of wind turbine generators with passive rotor elements and limited variable-speed, in steady-state and transients, such as non-synchronous connection to power system, mechanical input torque cycling and sudden changes. A rotor reference frame model has also been developed and implemented in Matlab-Simulink (chapter 4). It has been shown by laboratory tests and simulation results that a wound rotor induction machine with passive elements inserted in the rotor side may be used as a variable-speed wind generator systems over a relatively large speed range (up to 130 %) with an acceptable efficiency at full load (75 %) and a relatively good power factor (0.81);

- Modeling and simulation of an existing set-up of variable-speed wind turbine using doubly-fed induction generator that include: modeling and implementation of doubly-fed induction generator, modeling and implementation of rotor converter, which include Stator Flux Asynchronous Vector Modulation Strategy. Control system design contains power decoupling, current and power regulators design, voltage and current transducers with anti-aliasing filters, AD-DA converters and DSP system block and modeling of drive system (chapter 5). Experimental results, in steady-state and transients, have been done in order to verify and validate the simulation model developed in Matlab-Simulink.
- Design and commissioning of a measuring system-comprising signal conditioning box, AD card and transducers for current, voltage, speed and temperature, used for an experimental investigation for incipient fault detection and fault detection methods, suitably adapted for use in wind generator systems. Investigations have been performed to provide wind generator with an advanced condition monitoring system, in order to avoid undesirable operating conditions, to detect and diagnose sensors and incipient electrical faults. The software which controls both the acquisition and analysis of the signals has been written in Matlab and has also been developed as a sub-part of the monitoring system (chapter 6, [66-68]).

Digital simulations and experimental results presented in this paper have shown that the objectives of thesis have been successfully achieved. Hopefully, results of the presented study will enhance the insight into applications of wind energy conversion systems.

## 7.3. Future work

A great volume of work has to be carried out in order to investigate all possible applications of the wind energy conversion systems. The rapid development of power electronics, which offers high power handling capability at lower price per kW, can benefit both the wind generator development and the integration of wind farms into the power system. More research is also necessary in the classical solutions using power electronics. Especially, it is important to be able to predict the losses in order to keep a high reliability of wind generators.

Variable speed wind turbines, especially with doubly fed induction generators, have progressed dramatically in recent years. They are a spreading, dominating design principle of power converters applied in wind power turbines today. The doubly fed induction generator is now widely used but still research is needed in diagnosis, control and optimized design in order to reduce the overall price of the generator system.

The future work on this subject should contain improvements of the proposed solutions and study and development of new power control system alternatives. A simulation software for variable-speed wind turbine applications using rotor cage induction generators with experiments on an existing test rig implemented using dSPACE DS1103 development tool, will be presented in a new paper.

# Appendix A: Author's papers

[64] **Lucian Mihet-Popa**, F. Blaabjerg and I. Boldea, "Simulation of Wind Generator Systems for the Power Grid", Record of OPTIM 2002, vol. 2, pp. 423-428, 16-18 May, 2002.

[65] **Lucian Mihet-Popa**, F. Blaabjerg and I. Boldea, "Wind Turbine Generator Modeling and Simulation where Rotational Speed is the Controlled Variable", paper accepted to be publish in IEEE Transactions on Energy Conversion, January / February 2004.

[66] **Lucian Mihet-Popa**, "Condition Monitoring of Wind Generators", Internal report, Institute of Energy Technology, Aalborg University, Denmark, 2002.

[67] **Lucian Mihet-Popa**, Birgitte-Bak Jensen, Ewen Ritchie and Ion Boldea, "Condition Monitoring of Wind Generators", Record of IEEE-IAS 38$^{th}$ Annual Meeting, 2003, 12-16 October.

[68] **Lucian Mihet-Popa**, Birgitte-Bak Jensen, Ewen Ritchie and Ion Boldea, "Current Signature Analysis to Diagnose Incipient Faults in Wind Generator Systems", ELECTROMOTION 2003, 26-28 November.

[69] **Lucian Mihet-Popa** and Ion Boldea, "Variable speed electric generators for the distributed power systems of the future?", Paper accepted to be publish in EMPS 2002;

# Appendix B: Wind Turbine Generator System implemented in DIgSILENT and Matlab-Simulink.

## *Appendix B1. Details about Wind Turbine model implemented in DIgSILENT:*

| | | |
|---|---|---|
| **Wind turbine model** | **Composite Model** | 1 |
| Block Definition | Composite frames\Wind turbine composite | |
| **Slots** | **Net Elements** | |
| Hub wind slot | Hub wind model | |
| Rotor wind slot | Rotor wind model | |
| Aerodynamic | Aerodynamic Model | |
| Structure slot | Transmission Model | |
| G2000 | G2000 | |
| Wind filter Slot | Wind filter | |
| Cp table | Two Dimensional Characteristic | |
| Product Slot | Product model | |
| Measurement | G2000 | |
| Noise 1 Slot | Sample and Hold noise generator | |
| Noise 2 Slot | Sample and Hold noise generator | |
| Noise 3 Slot | Sample and Hold noise generator | |
| Pitch control slot | Pitch control block | |
| f5 | f5 | |
| f6 | f6 | |
| f4 | f4 | |
| G500 | G500 | |
| Common shaft slot | Common shaft | |
| Speed conversion | Speed conversion to rpm | |
| G500 measurement | G500 | |
| Power calculation | Power calculation | |
| Command slot | Command DSL | |
| Start_pitch_from_table | StartPitch | |
| Softstarter state | Soft starter state | |
| MaxPitch2200 | Maxpitch_2200kW | |
| --- **wind model** | **Common Model** | |
| --- Definition | Additional macros\Hub wind block | |
| Parameter | | |
| ti Turbulence intensity [%] | | 12.0000 |
| u0 Mean wind speed [m/s] | | 12.0000 |
| L Lengh scale [m] | | 600.0000 |
| Tsampl Sampling time [1/s] | | 0.0500 |

| | | |
|---|---|---|
| **Rotor wind model** | **Common Model** | |
| Parameter | | |
| u0 Mean wind speed [m/s] | | 12.0000 |
| rotdiam Rotor diameter [m] | | 72.0000 |
| ti Turbulence intensity [%] | | 12.0000 |
| L Lengh scale [m] | | 600.0000 |
| Tsampl Sampling time [1/s] | | 0.0500 |
| t3p Const tower shadow [ ] | | 0.0150 |

| | | |
|---|---|---|
| **Aerodynamic Model** | **Common Model** | |
| Parameters | | |
| rho Air Density [kg/m^3] | | 1.2250 |
| rotdiam Rotor diameter [m] | | 72.0000 |

```
|
Transmission Model                          Common Model                    |
| Parameter                                                                 |
|   Jr    Rotor shaft inertia [kgm^2]                        4392000.0000   |
|   n_gear Ratio of the gear box [ ]                              83.5310   |
|   K_stiff Torsional stiffness [Nm/rad]                     59700000.0000   |

|G2000                                      Asynchronous Machine            |
|Type                                ...\Library\Generators\ABB 2MW - 5-0L4/6 |
|Generator/Motor                          Generator                         |
---nd filter                                 Common Model                    |
T                                                                  20.0000   |
u0                                                                 12.0000   |
yi                                                                           |
yo                                                                           |
|Two Dimensional Characteristic    Two Dimensional Characteristic           |
\Wind generators\Table_cp.tx.....................................................
w1-Value of first Line                                              0.0000   |
w1-Step Size (Dist. of Lines)                                       1.0000   |
w2-Value of first Column                                          -30.0000   |
w2-Step Size (Dist. of Columns)                                     1.0000   |
|Conversion for Output y = a*f(w1,w2)+b                                      |
|   Factor a                                                        1.0000   |
|   Factor b                                                        0.0000   |
|Automatic Calculation of Initial Conditions                                 |
|   Calculate Signal                    2                                    |
|  Sample and Hold noise generator       Sample and Hold noise generator     |
|Frequency                                                         20.0000  Hz |
|Power                                                              1.0000  W  |
!      control block                        Common Model                     |
-----l Definition                          Control Macros\Pitch control block |
| Parameter                                                                 |
T1    Time constant [s]                                                0.1000 |
IC_speed - Initial condition [ ]                                       0.0000 |
DT1                                                                    0.6000 |
Ta                                                                     0.1000 |
T3    Time constant [s]                                              200.0000 |
IC_power - Initial condition [ ]                                    2000.0000 |
Tp                                                                   100.0000 |
T4    Time constant [s]                                                0.0400 |
IC_hydr - Initial condition [ ]                                        0.0000 |
P_init                                                                 0.0000 |
acc_res Constant K1 [ ]                                                0.0000 |
power_res Constant K1 [ ]                                              0.0000 |
valid_start_pitch Constant K1 [ ]                                     -1.0000 |
ya_min                                                              -120.0000 |
yp_min                                                              -100.0000 |
ya_max                                                                -0.5000 |
yp_max                                                                 0.0000 |
|
|f5                                          Common Model
| Parameter          racteristics                                           |
|            ref_x          ref_y                                           |
|   Size       24.0000       24.0000                                       |
|    1          0.0000       -0.5000                                       |
|    2          9.0000       -0.5000                                       |
|    3         10.0000       -2.0000                                       |
|    4         11.0000       -3.0000                                       |
|    5         12.0000       -4.0000                                       |
|    6         13.0000       -4.5000                                       |
|    7         14.0000       -4.5000                                       |
```

| | | |
|---|---|---|
| 8 | 15.0000 | -4.5000 |
| 9 | 16.0000 | -4.5000 |
| 10 | 17.0000 | -4.5000 |
| 11 | 18.0000 | -4.4000 |
| 12 | 19.0000 | -4.3000 |
| 13 | 20.0000 | -4. |
| 14 | 21.0000 | -4.1000 |
| 15 | 22.0000 | -4.0000 |
| 16 | 23.0000 | -3.9000 |
| 17 | 24.0000 | -3.8000 |
| 18 | 25.0000 | -3. |
| 19 | 26.0000 | -3.7000 |
| 20 | 27.0000 | -3.6000 |
| 21 | 28.0000 | -3.6000 |
| 22 | 29.0000 | -3.5000 |
| 23 | 30.0000 | -3.5000 |
| 24 | 31.0000 | -3.5000 |

wind
f5_out

**Common Model**

Characteristics

| | ref_x | ref_y |
|---|---|---|
| Size | 24.0000 | 24.0000 |
| 1 | 0.0000 | 0.0125 |
| 2 | 9.0000 | 0.0125 |
| 3 | 10.0000 | 0.0125 |
| 4 | 11.0000 | 0.0125 |
| 5 | 12.0000 | 0.0094 |
| 6 | 13.0000 | 0.0038 |
| 7 | 14.0000 | 0.0027 |
| 8 | 15.0000 | 0.0019 |
| 9 | 16.0000 | 0.0018 |
| 10 | 17.0000 | 0.0017 |
| 11 | 18.0000 | 0.0016 |
| 12 | 19.0000 | 0.0015 |
| 13 | 20.0000 | 0.0015 |
| 14 | 21.0000 | 0.0014 |
| 15 | 22.0000 | 0.0014 |
| 16 | 23.0000 | 0.0014 |
| 17 | 24.0000 | 0.0014 |
| 18 | 25.0000 | 0.0013 |
| 19 | 26.0000 | 0.0013 |
| 20 | 27.0000 | 0.0013 |
| 21 | 28.0000 | 0.0013 |
| 22 | 29.0000 | 0.0012 |
| 23 | 30.0000 | 0.0012 |
| 24 | 31.0000 | 0.0012 |

wind

**G500** **Asynchronous Machine**

| | |
|---|---|
| Type | Library\Generators\ABB 500kW - 500L4/6 |
| Generator/Motor | Generator |

**Power calculation** **Common Model**

P2000
P500

**Command DSL** **Common Model**

| | | |
|---|---|---|
| n1 | Cut in speed [p.u.] | 1.0026 |
| n2 | Maximum speed [p.u.] | 1.1000 |

Tpick Pick up time for events, can be 0s [s] 0.0000

| Characteristics

**StartPitch** **Common Model**

| Model Definition | Control Macros\startpitch_block |
|---|---|

| Characteristics | ref_x | ref_y |
|---|---|---|
| Size | 24.0000 | 24.0000 |
| 1 | 0.0000 | -1.0000 |
| 2 | 9.0000 | -1.0000 |
| 3 | 10.0000 | -2.0000 |
| 4 | 11.0000 | -3.0000 |
| 5 | 12.0000 | -1.0000 |
| 6 | 13.0000 | -2.6000 |
| 7 | 14.0000 | -3.0000 |
| 8 | 15.0000 | -3.1000 |
| 9 | 16.0000 | -3.2000 |
| 10 | 17.0000 | -3.2000 |
| 11 | 18.0000 | -3.2000 |
| 12 | 19.0000 | -3.2000 |
| 13 | 20.0000 | -3.1000 |
| 14 | 21.0000 | -3.0000 |
| 15 | 22.0000 | -2.9000 |
| 16 | 23.0000 | -2.8000 |
| 17 | 24.0000 | -2.6000 |
| 18 | 25.0000 | -2.5000 |
| 19 | 26.0000 | -2.4000 |
| 20 | 27.0000 | -2.3000 |
| 21 | 28.0000 | -2.2000 |
| 22 | 29.0000 | -2.1000 |
| 23 | 30.0000 | -2.0000 |
| 24 | 31.0000 | -2.0000 |

**Maxpitch_2200kW** **Common Model**

| Characteristics | ref_x | ref_y |
|---|---|---|
| Size | 24.0000 | 24.0000 |
| 1 | 0.0000 | -0.5000 |
| 2 | 9.0000 | -0.5000 |
| 3 | 10.0000 | -2.0000 |
| 4 | 11.0000 | -3.0000 |
| 5 | 12.0000 | -1.0000 |
| 6 | 13.0000 | -1.0000 |
| 7 | 14.0000 | -2.1000 |
| 8 | 15.0000 | -2.1000 |
| 9 | 16.0000 | -2.5000 |
| 10 | 17.0000 | -2.6000 |
| 11 | 18.0000 | -2.6000 |
| 12 | 19.0000 | -2.6000 |
| 13 | 20.0000 | -2.6000 |
| 14 | 21.0000 | -2.5000 |
| 15 | 22.0000 | -2.4000 |
| 16 | 23.0000 | -2.3000 |
| 17 | 24.0000 | -2.2000 |
| 18 | 25.0000 | -2.1000 |
| 19 | 26.0000 | -2.0000 |
| 20 | 27.0000 | -1.9000 |
| 21 | 28.0000 | -1.8000 |
| 22 | 29.0000 | -1.7000 |
| 23 | 30.0000 | -1.6000 |

```
|   24        31.0000       -1.6000                                          |
|
|SS_Controller                          Common Model
|
| Parameter                                                                  |
|   T                                                          4.0000        |
|   start                                                      0.0000        |
|   a1                                                       120.0000        |
|   a2                                                        70.0000        |
| Characteristics                                                            |
|   Size       0.0000        0.0000                                        |
|    Interface                                                               |
|    Kin                                                                     |
|    alpha                                                                   |
-----------------------------------------------------------------------------
|Nominal Voltage                                          0.9600  kV         |
|Nominal Current                                          1.4000  kA         |
|Bypass                                 Off                                  |
|Amplification                                            0.0000             |

|PFC composite                    Composite Model                 1   /1    |
-----------------------------------------------------------------------------
|Block Definition                ...        Capacitor Switching composite |

|C_Switching                            Common Model                        |
-----------------------------------------------------------------------------
|Model Definition                ...\Macros\PFC macros\Switching logic 10 |
| Parameter                                                                  |
|   Qlim1                                                      0.0500        |
|   Qlim2                                                      0.1500        |
|   Qlim3                                                      0.2500        |
|   Qlim4                                                      0.3500        |
|   Qlim5                                                      0.4500        |
|   Qlim6                                                      0.5500        |
|   Qlim7                                                      0.6500        |
|   Qlim8                                                      0.7500        |
|   Qlim9                                                      0.8500        |
|   Qlim10                                                     0.9500        |
|   Tpick                                                      1.0000        |
|   start_PF                                                   0.0000        |
|   T1    Time constant (1s average) [s]                      0.3300    |
|   T2    Time constant (1min average) [s]                    20.0000       |
|
```

## *B1.2. Wind turbine composite model:*

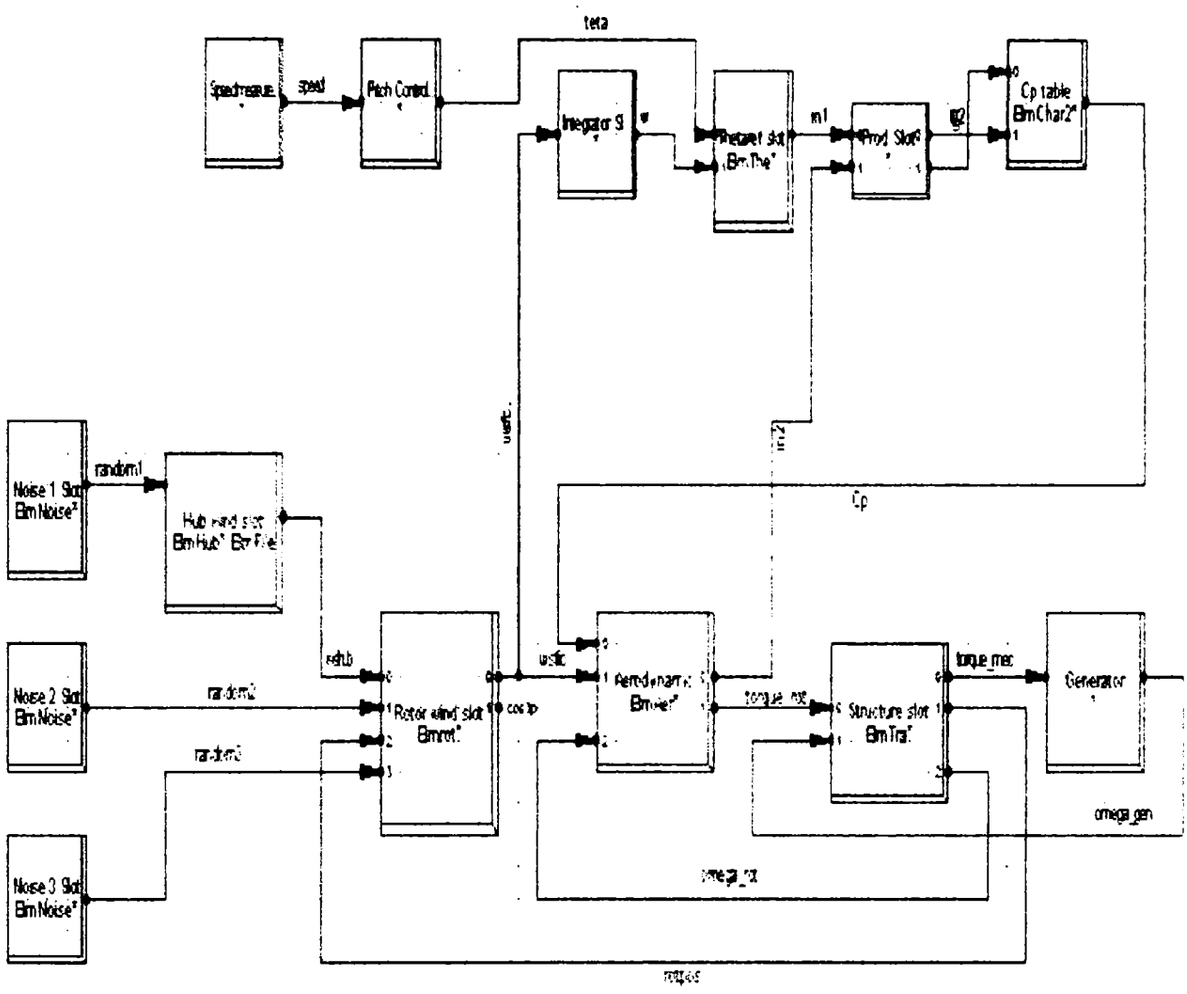


**Figure B1**. Block diagram of complete model of constant speed wind turbine using induction generators developed in DIgSILENT.

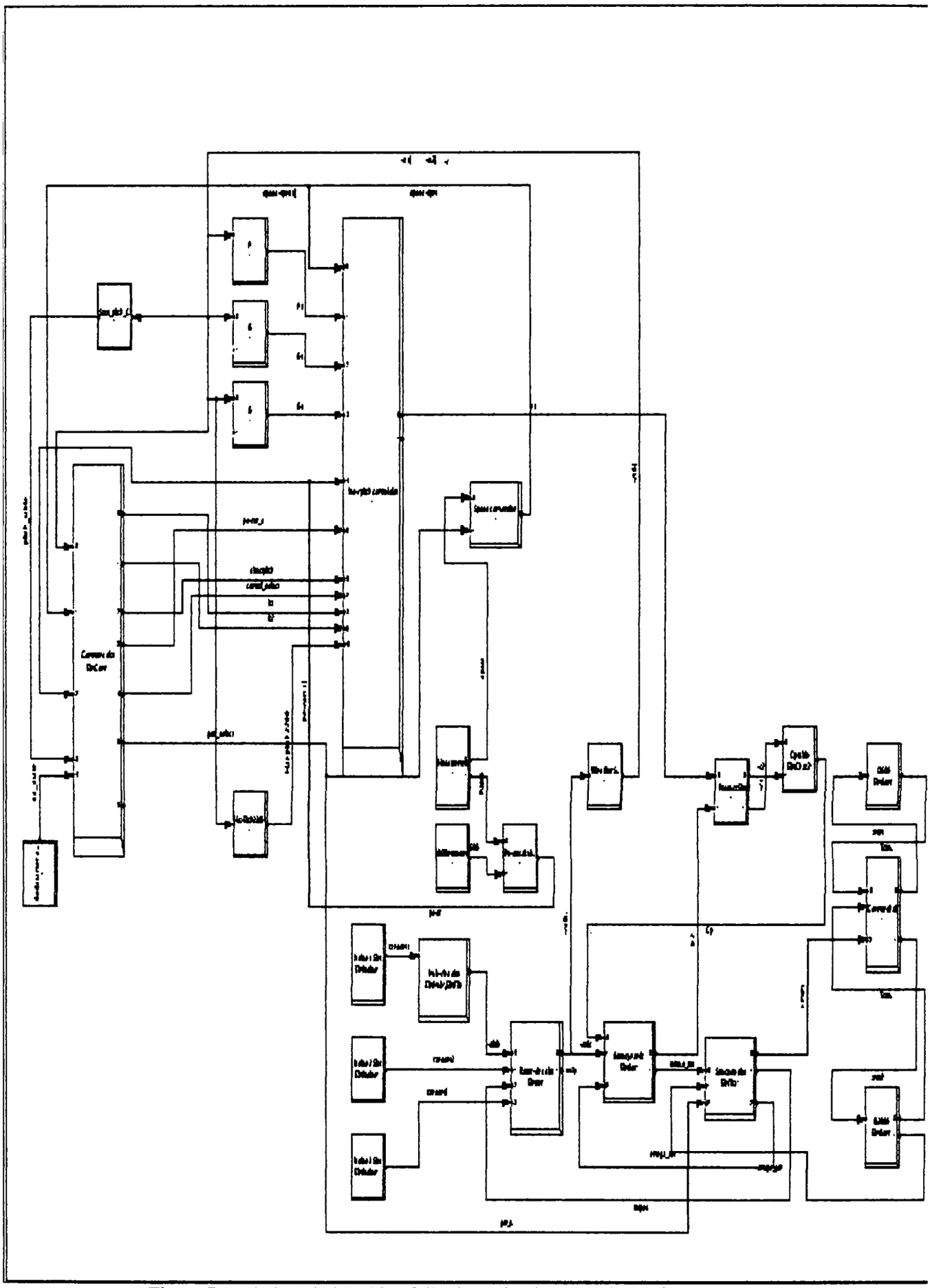

**Figure B2**. 2 MW Wind Turbine-full scheme implemented in DIgSILENT.

## Command DSL block description:

```
! HS generation mode from freewheel -> high-speed-startup
!**************************
!Inputs: wind,speed,power,pitch_table,ss_state
!Outputs: K1,K2,directpitch,power_d,control_select,gen_select
! Initialization of internal variables/state variables:
inc(x1)=0;inc(y1)=0;inc(o1)=0;inc(ss_state)=0;inc(wind)=0;inc(power)=0;inc(speed)=0;inc(control_select)=0;in
c(directpitch)=0;inc(K1)=0;inc(K2)=0;inc(PF_start)=0
!**************************
!Conditions - transition from direct pitch control to acceleration control
!if speed is above 1504 then y1 is integrated and o1 will be different than 0, moment when 2rpm/s acceleration
demand is set by K1 and K2 during soft start.

y1=select(speed>1504,1,0); x1=y1; o1=select(x1>0,1,0)
K1=select(o1>0,0,-0.0147); K2=select(o1>0,2,25)
!**************************

!Selection of control mode.
!1 - acceleration control
!2 - power control
!3 - direct pitch control

control_select=select(speed<1000,3,select(ss_state>0.98,2,1))
!**************************
!acceleration loop is reseted before speed<1000rpm
acc_r=select(speed>1000,and,ss_state<=0.99,1,0)
fault(acc_r=1,'name=start_acc_control dtime=0.0')
!**************************
!control_select=3
!**************************
!pitch value at direct pitch signal is -0.5deg until soft start ends
!anyway direct pitch is active until speed<1000rpm
direct pitch=select(ss_state<0.98,-0.5,pitch_table)
!**************************
!Power factor compensation starts after soft start by closing the breaker
!of SVS unit or capacitors
PF_start=select(ss_state<0.98,0,1);fault(PF_start=1,'name=PF_compensation dtime=0.0')
!power filter reset to 2MW
!after soft start power control loop is reseted
fault(PF_start=1,'name=reset_P_filter dtime=0.0');fault(PF_start=1,'name=start_power_control dtime=0.0')
!start pitch is active 60s after power control starts
fault(PF_start=1,'name=valid_limit_PI dtime=60.0');fault(PF_start=1,'name=power_PI_state dtime=59.0')
!**************************
!G2000 is selected;inc(gen_select)=2;gen_select=2
!Power demand 2000[kW] is selected;inc(power_d)=2000;power_d=2000
!**************************
!Generator cut in logic:
inc(sc)=0;inc(so)=0;vardef(n1)='p.u.';'Cut in speed'; vardef(n2)='p.u.';'Maximum speed'
vardef(Tpick)='s';'Pick up time for events, can be 0s'
sc=picdro(abs(speed)>n1*50*60/gen_select,Tpick,1.1*Tpick)
so=picdro(abs(speed)>n2*50*60/gen_select,Tpick,1.1*Tpick)

!Softstarter main switch close/open events
fault(sc=1,'name=SCloseMain dtime=0.0');fault(so=1,'name=SOpenMain dtime=0.0')
!start of softstarter, see SS_controller DSL code
fault(sc=1,'name=StartSS dtime=0.0')

!Generator 2000kW main switch close/open events
fault(sc=1,'name=SCloseG2000 dtime=0.0');fault(so=1,'name=SOpenG2000 dtime=0.0')
!**************************
```

!Wind step at 100s
fault(time()>100,'name=Hub_wind_change dtime=0.0');fault(time()>100,'name=Rotor_wind_change dtime=0.0')

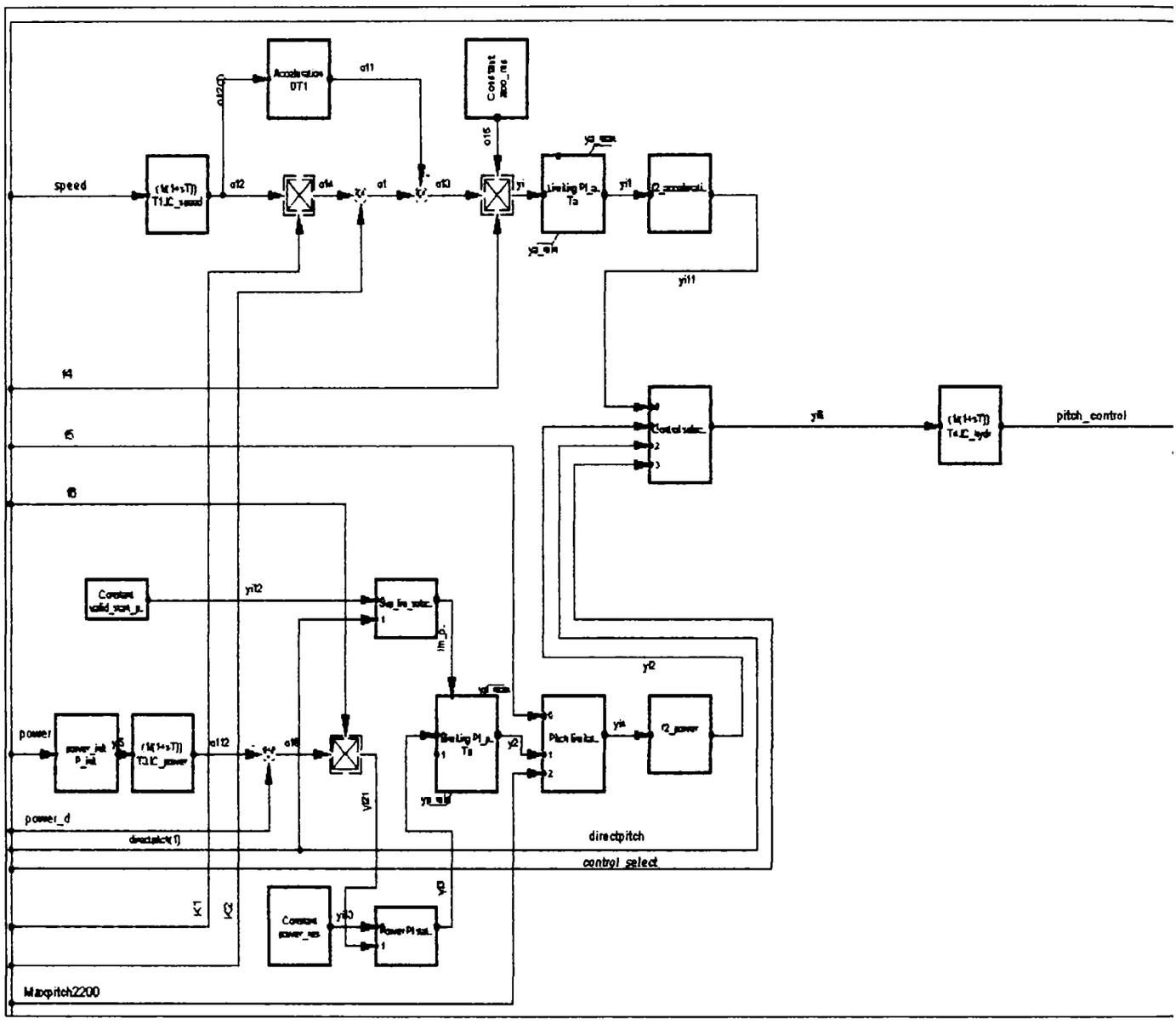


**Figure B3**. Pitch control block implemented in DIgSILENT.

**! Aerodynamic Model**
! Inputs: Cp, wsfic (wind speed), omega_rot,
! Outputs: lambda, torque_rot

! Unit and name of internal variables/parameters
!-----------------------------------------
vardef(rho)='kg/m^3';'Air Density', vardef(rotdiam)='m';'Rotor diameter'
omega_aero=select(omega_rot<0.8,0.8,omega_rot)
lambda=omega_aero*rotdiam/(2*wsfic)
torque_rot=1/8*rho*pi()*sqr(rotdiam)*pow(wsfic,3)*Cp/omega_aero
lambda=omega_rot*rotdiam/(2*wsfic)
torque_rot=1/8*rho*pi()*sqr(rotdiam)*pow(wsfic,3)*Cp/omega_rot
inc(omega_rot)=0;inc(lambda)=0;inc(torque_rot)=0;inc(wsfic)=0;inc(Cp)=0

**! Transmission macro**
! 1) It generates as output the mechanic power to the generator

```
! 2) In the torsional torque, only stiffness is taken into account
! gen_select is 2 for G2000 or 3 for G500

! Unit and name of internal variables/parameters
!---------------------------------------
vardef(Jr)='kgm^2';'Rotor shaft inertia'
vardef(n_gear)=' ';'Ratio of the gear box'
vardef(K_stiff)='Nm/rad';'Torsional stiffness'

! Definition of states and inputs
!-----------------------------
! States: x1 = theta_rot; x2 = omega_rot; x3 = mechanical torque left side
! Inputs: rotor torque (torque_rot); generator speed (omega_gen)
omega_rad=omega_gen*pi()*100/gen_select; omega_rad=omega_gen
x1.=x2; x2.=torque_rot/Jr-x3/Jr; x3.=K_stiff*(x2-omega_rad/n_gear)

! Definition of outputs
!--------------------

torque_mec=select(gen_select=2,x3/n_gear*pi()*100/gen_select/2000000,x3/n_gear*pi()*100/gen_select/50000
0)
rotpos=x1                    ! the position of the rotor
omega_rot=x2                   ! rotor speed omega_rot
inc(x1)=0; inc(x2)=pi()*50/n_gear; inc(x2)=0
inc(x3)=torque_mec*n_gear; inc(x3)=0; inc(torque_rot)=x3; inc(torque_mec)=0

!Wind filter block
limits(T)=(0,]; x.=(yi-x)/T; yo=x; inc(x)=u0
!
f5 block – for more details see DSL model
ww=floor(wind); f5_out=lapprox(ww,array_ref); inc(f5_out)=0; inc(ww)=0
```

## *B.1.3. Soft-starter control implementation*

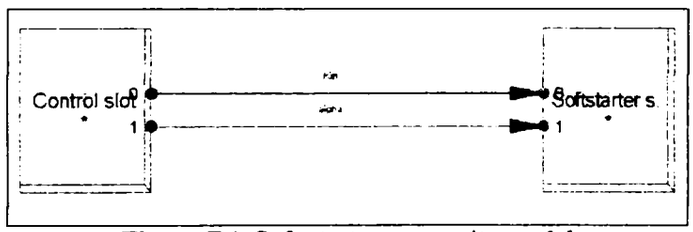


**Figure B4.** Soft-starter composite model

---

**Control slot DSL code:** `Soft starter control block`

```
!Inputs:
! Outputs: Kin, alpha (amplification factor, firing angle)
! Kin for RMS simulation and alpha for EMT simulation
! Integration is performed on variable x from 0 to 1 as Kin
!alpha is calculated according to Kin between !maximum and minimum angles (a1,a2 are parameters in degrees)
!bypass and ss_state events occurs when Kin>0.99; inc(byp)=0;inc(Kin)=0;inc(x)=0;inc(alpha)=a1
dx=select(x>1,1,start/T); x.=dx; Kin=lim(x,0,1);alpha=pi()/180*(a2+(a2-a1)*(Kin-1))
byp=select(Kin>0.99,1,0)
fault(byp=1,'name=bypass dtime=0.0'); fault (byp=1,'name=ss_state dtime=0.0')
```

**Additional comments:**

1. parameter start has initial value 0, it is set to 1 when soft start starts by an event of Command DSL block.

2. alpha is calculated so that if Kin varies between 0 and 1 then alpha will take values starting from a1 down to a2.
3. byp is a variable to enable bypass of soft starter through an event of SS_controller block.

## B.1.4. Power factor compensation

```
inc(Q)=0;inc(x1)=0;inc(x2)=0; vardef(T1)='s';'Time constant (1s average)';x1.=(Q-x1)/T1; y1=x1
vardef(T2)='s';'Time constant (1min average)'; x2.=(y1-x2)/T2;y2=x2
sc1=20*picdro(abs(y2)>Qlim1.and.start_PF,Tpick,10*Tpick)-10
sc2=20*picdro(abs(y2)>Qlim2.and.start_PF,2*Tpick,9*Tpick)-10
sc3=20*picdro(abs(y2)>Qlim3.and.start_PF,3*Tpick,8*Tpick)-10
sc4=20*picdro(abs(y2)>Qlim4.and.start_PF,4*Tpick,7*Tpick)-10
sc5=20*picdro(abs(y2)>Qlim5.and.start_PF,5*Tpick,6*Tpick)-10
sc6=20*picdro(abs(y2)>Qlim6.and.start_PF,6*Tpick,5*Tpick)-10
sc7=20*picdro(abs(y2)>Qlim7.and.start_PF,7*Tpick,4*Tpick)-10
sc8=20*picdro(abs(y2)>Qlim8.and.start_PF,8*Tpick,3*Tpick)-10
sc9=20*picdro(abs(y2)>Qlim9.and.start_PF,9*Tpick,2*Tpick)-10
sc10=20*picdro(abs(y2)>Qlim10.and.start_PF,10*Tpick,1*Tpick)-10
so1=20*picdro(abs(y2)<Qlim1.and.start_PF.and.sc1,10*Tpick,2*Tpick)-10
so2=20*picdro(abs(y2)<Qlim2.and.start_PF.and.sc2,9*Tpick,2*Tpick)-10
so3=20*picdro(abs(y2)<Qlim3.and.start_PF.and.sc3,8*Tpick,2*Tpick)-10
so4=20*picdro(abs(y2)<Qlim4.and.start_PF.and.sc4,7*Tpick,2*Tpick)-10
so5=20*picdro(abs(y2)<Qlim5.and.start_PF.and.sc5,6*Tpick,2*Tpick)-10
so6=20*picdro(abs(y2)<Qlim6.and.start_PF.and.sc6,5*Tpick,2*Tpick)-10
so7=20*picdro(abs(y2)<Qlim7.and.start_PF.and.sc7,4*Tpick,2*Tpick)-10
so8=20*picdro(abs(y2)<Qlim8.and.start_PF.and.sc8,3*Tpick,2*Tpick)-10
so9=20*picdro(abs(y2)<Qlim9.and.start_PF.and.sc9,2*Tpick,2*Tpick)-10
so10=20*picdro(abs(y2)<Qlim10.and.start_PF.and.sc10,Tpick,2*Tpick)-10
inc(sc1)=0;inc(sc2)=0;inc(sc3)=0;inc(sc4)=0;inc(sc5)=0;inc(sc6)=0;inc(sc7)=0;inc(sc8)=0;inc(sc9)=0;inc(sc10)=
0;inc(so1)=0;inc(so2)=0;inc(so3)=0;inc(so4)=0;inc(so5)=0;inc(so6)=0;inc(so7)=0;inc(so8)=0;inc(so9)=0;inc(so1
0)=0
event(0,sc1,'name=S1Close dtime=0.0');event(0,so1,'name=S1Open dtime=0.0')
event(0,sc2,'name=S2Close dtime=0.0');event(0,so2,'name=S2Open dtime=0.0')
event(0,sc3,'name=S3Close dtime=0.0');event(0,so3,'name=S3Open dtime=0.0')
event(0,sc4,'name=S4Close dtime=0.0');event(0,so4,'name=S4Open dtime=0.0')
event(0,sc5,'name=S5Close dtime=0.0');event(0,so5,'name=S5Open dtime=0.0')
event(0,sc6,'name=S6Close dtime=0.0');event(0,so6,'name=S6Open dtime=0.0')
event(0,sc7,'name=S7Close dtime=0.0');event(0,so7,'name=S7Open dtime=0.0')
event(0,sc8,'name=S8Close dtime=0.0');event(0,so8,'name=S8Open dtime=0.0')
event(0,sc9,'name=S9Close dtime=0.0');event(0,so9,'name=S9Open dtime=0.0')
event(0,sc10,'name=S10Close dtime=0.0');event(0,so10,'name=S10Open dtime=0.0')
```

**Details:**

Two PT1 filters ($T_1$=0.33s, $T_2$=20s) are implemented for 1s and 1min averaging of reactive power "measured" at soft starter terminals (Qsum:bus1).

sc1, sc2, ..., sc10 and so1, so2, ... so10 internal variables are defined for each step of connection of capacitors. They can have values of +/- 10 as function, comparing the filtered Q and $Qlim_i$ and respectively a start_PF flag. This flag is set on 1 when the power control starts (see Command DSL events).

delays are implemented in picdro functions to assure that between two connections of capacitors there is at least 1s delay.

"event" function implements the triggering of switching events. Attention this function is available just from DigSilent version **12.126**

*syntax: **event**(maxtrig, input, 'name=xxx dtime=...')*

*function: emits event named xxx if input signal changes sign from - to +*

*function triggers maxtrig times;*

*set maxtrig to 0 to get unlimited triggering*

name=xxx is S1Open, S1Close, ...S10Open, S10Close

see event list (close/open) in DSL model for $S_i$Close/$S_i$Open event implementation on capacitors.

# Appendix B2: Matlab - Simulink Programs

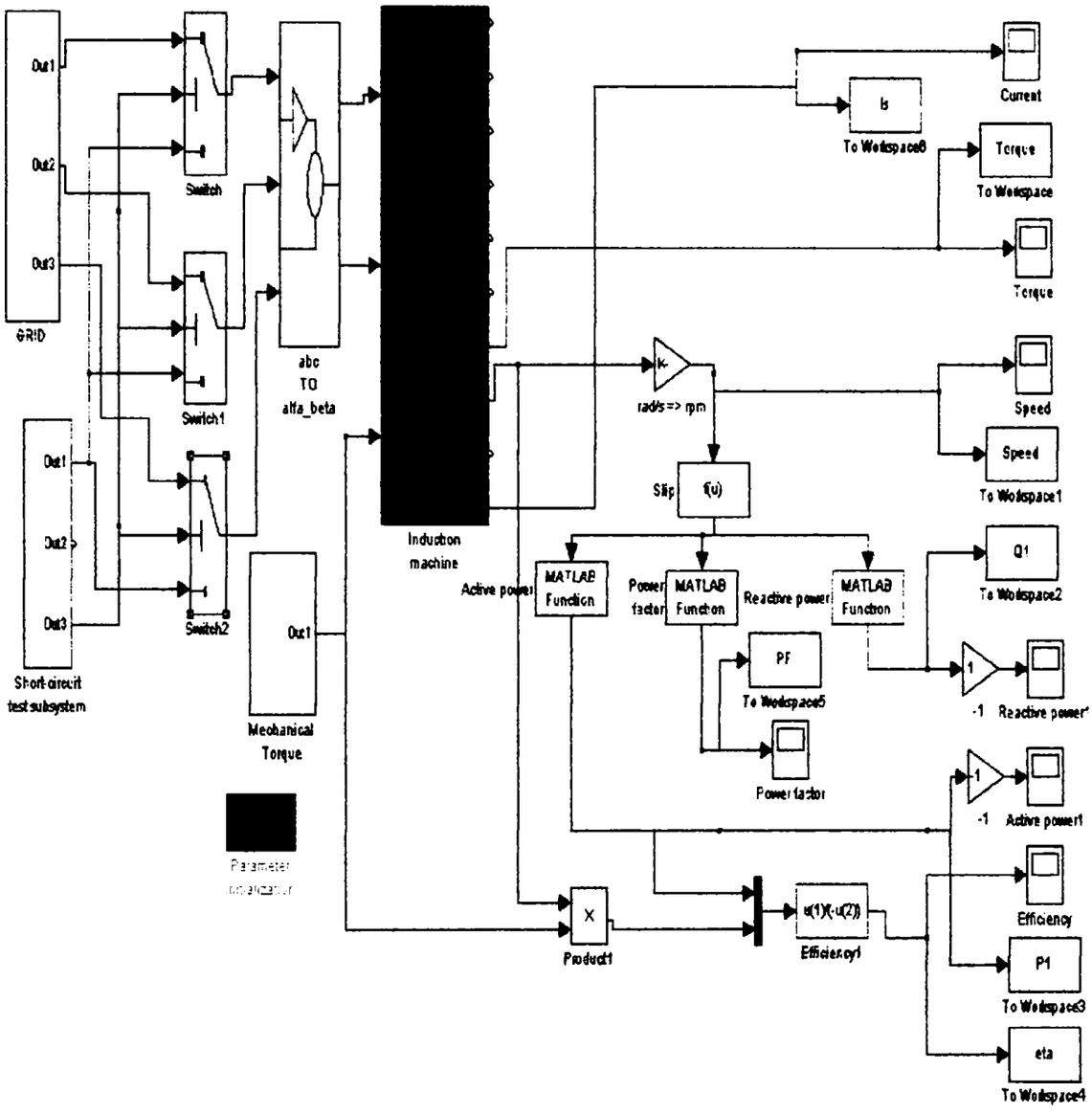


**Figure B5.** Wind generator model implemented in Simulink.

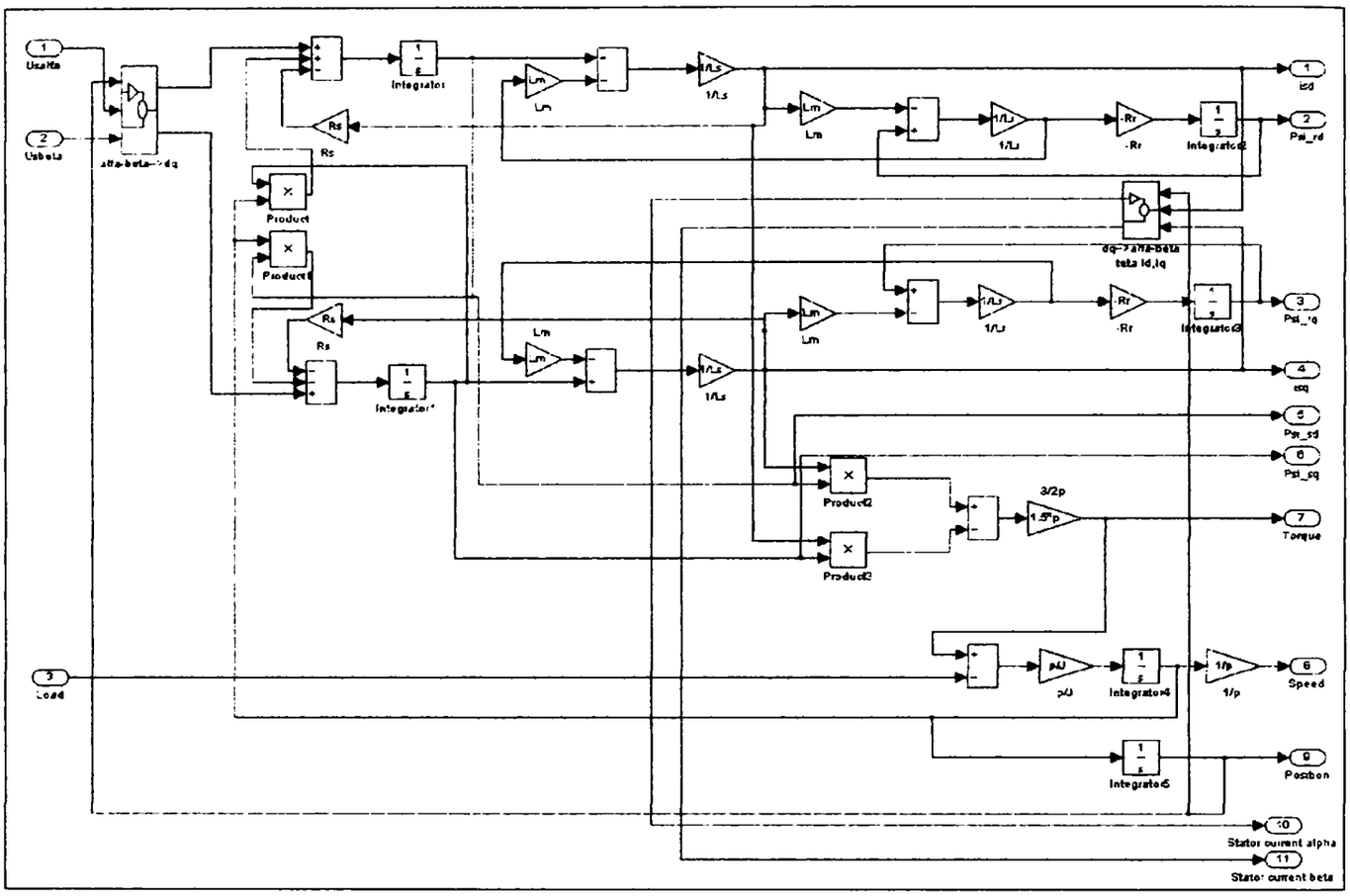


**Figure B6**. *D-Q Model of induction machine implemented in Simulink.*

**%Induction Generator parameters**

```
U=960;Rs=0.0064/3;Rr=0.0104/3;Ls=0.14/100/pi/3+5.728/100/pi/3;%Lss+Lm;
Lr=0.105/100/pi/3+5.728/100/pi/3;%Lrs+Lm
Lm=5.728/100/pi/3; J=90; p=2; s=-0.008; Pm=2058000;U1=960; p=2;
R1=0.005;R2=0.0089;Xs1=0.128;Xs2=0.094;Xm=5.04;Rm=135;
```

**%IG calculations;**

```
C1=abs(1+(R1+Xs1*i)/(Rm+Xm*i));
Zeg_c=R1+Xs1*i+Rm*Xm*i/(Rm+Xm*i);Zeg=abs(Zeg_c);
Ze_c=(R1+Xs1*i)+(Rm*Xm*i/(Rm+Xm*i))*(R2+Xs2*i+R2*(1-
s)/s)/((Rm*Xm*i/(Rm+Xm*i))+R2+Xs2*i+R2*(1-s)/s);
Ze=abs(Ze_c);
T=3*U1*U1*p/(2*pi*50)*R2/s/((R1+C1*R2/s)*(R1+C1*R2/s)+(Xs1+C1*Xs2)*(Xs1+C1*Xs2));
I=U1/Ze*sqrt(3);
Ir=-I*abs((Rm*Xm*i/(Rm+Xm*i))/(R2+Xs2*i+R2*(1-s)/s+(Rm*Xm*i/(Rm+Xm*i))));
T0=3*R2/s*Ir*Ir*p/(2*pi*50)/3;%Ir is line current!
PF=sqrt(1/(1+imag(Ze_c)/real(Ze_c)*imag(Ze_c)/real(Ze_c)));
S1=sqrt(3)*U1*I;P1=sqrt(3)*U1*I*PF;I1g=U1/Zeg*sqrt(3);eta=P1/Pm;
k=1;s=-1;while s<0,
Ze_c=(R1+Xs1*i)+(Rm*Xm*i/(Rm+Xm*i))*(R2+Xs2*i+R2*(1-
s)/s)/((Rm*Xm*i/(Rm+Xm*i))+R2+Xs2*i+R2*(1-s)/s);
Ze=abs(Ze_c);PF=sqrt(1/(1+imag(Ze_c)/real(Ze_c)*imag(Ze_c)/real(Ze_c)));
  sv(k)=s; PFv(k)=PF; k=k+1; s=s+0.0001;
end
plot(sv,PFv);grid;
```

```
%Torque caracteristics for IM_GENERATOR - 2MW
clear all;close all;hold off;
s=-1;j=1;i=1;k=1;sn=-0.009267;
U1=960/sqrt(3); p=2; R1=0.0064/3;
while j<=1,
R2=0.0104/3;Xs1=0.14/3;Xs2=0.105/3;Xs2v(k)=Xs2;Xm=5.728/3;C1=1+Xs1/Xm;
sk=-C1*R2/sqrt(R1*R1+(Xs1+C1*Xs2)*(Xs1+C1*Xs2));
Tk(k)=3*p/(2*pi*50)*U1*U1/(2*C1*(R1+sqrt(R1*R1+(Xs1+C1*Xs2)*(Xs1+C1*Xs2))));
i=1;while s<=0,
T(i)=3*U1*U1*p/(2*pi*50)*R2/s/((R1+C1*R2/s)*(R1+C1*R2/s)+(Xs1+C1*Xs2)*(Xs1+C1*Xs2));
s1(i)=s; s=s+0.001; i=i+1;
end
s=-1;j=j+0.1;k=k+1; s=sn;
Tn=3*U1*U1*p/(2*pi*50)*R2/s/((R1+C1*R2/s)*(R1+C1*R2/s)+(Xs1+C1*Xs2)*(Xs1+C1*Xs2));
plot(s1,T/Tn,'b');hold on;grid;zoom;
pause;
end
figure;
plot(Xs2v/0.094,Tk/13050,'r');hold on;grid;zoom;
```

# Appendix C: Matchad and Matlab / Simulink files used for steady-state and transients analysis of the DFIG with passive elements.

This appendix contains details about the parameters of three phase wound rotor induction machine and the programs developed in Mathcad for steady-state analysis and in Matlab for dynamic analysis. Also, the complete Simulink scheme are presented.

## *Appendix C1: MathCad file for the steady state analysis*

**Three Phase Wound Rotor Induction Generator**

Ratings: 10 kW; 920 rpm; 380 V; 23.5 A; 50 Hz;

Stator Turns Ratio: 1.46

External Elements: Lex=560 mH; Rex=1.8 Ω

PHASE VOLTAGE: $V := \frac{400}{\sqrt{3}}$ $V = 230.94$

STATOR PARAM: $Rs := 1.4$ $Xs := 7.5j$ $POLES := 6$

$f := 50$

CORE PARAM: $Rc := 10.5$ $Xm := 25j$

ROTOR PARAM: $Rr1 := 0.45$ $Xr := 6.66j$ SLIP RANGE:

$Rr2 := Rr1 \cdot 2$ $s := (-.999, -.997 .. .999)$

$Rr3 := Rr1 \cdot 3$

$Rext := \frac{1.80}{1.46^2}$ $Xext := \frac{175j}{1.45^2}$ $Xext = 83.234i$

$$n(s) := (1 - s) \cdot 4 \cdot \pi \cdot \frac{f}{POLES}$$

$$Z1(s) := Rs + Xs + \frac{\left(\frac{Rext \cdot Xext}{Rext + Xext} + Xr + \frac{Rr1}{s}\right) \cdot \left(\frac{Xm \cdot Rc}{Xm + Rc}\right)}{\frac{Xm \cdot Rc}{Xm + Rc} + \left(Xr + \frac{Rr1}{s}\right) + \frac{Rext \cdot Xext}{Rext + Xext}}$$

$$Z(s) := Rs + Xs + \frac{\left(Xr + \frac{Rr1}{s}\right) \cdot \left(\frac{Xm \cdot Rc}{Xm + Rc}\right)}{\frac{Xm \cdot Rc}{Xm + Rc} + \left(Xr + \frac{Rr1}{s}\right)}$$

**Rotor induced voltage:**

$$V21(s) := \frac{V\cdot\left[\dfrac{\left(\dfrac{Rext\cdot Xext}{Rext+Xext}+Xr+\dfrac{Rr1}{s}\right)\cdot\left(\dfrac{Xm\cdot Rc}{Xm+Rc}\right)}{\dfrac{Xm\cdot Rc}{Xm+Rc}+\left(Xr+\dfrac{Rr1}{s}\right)+\dfrac{Rext\cdot Xext}{Rext+Xext}}\right]}{\left[Rs+Xs+\dfrac{\left(\dfrac{Rext\cdot Xext}{Rext+Xext}+Xr+\dfrac{Rr1}{s}\right)\cdot\left(\dfrac{Xm\cdot Rc}{Xm+Rc}\right)}{\dfrac{Xm\cdot Rc}{Xm+Rc}+\left(Xr+\dfrac{Rr1}{s}\right)+\dfrac{Rext\cdot Xext}{Rext+Xext}}\right]}$$

**Rotor current:**

$$I21(s) := \frac{V21(s)}{\left(Xr+\dfrac{Rr1}{s}\right)+\dfrac{Rext\cdot Xext}{Rext+Xext}}$$

$$I2(s) := \frac{V21(s)}{\left(Xr+\dfrac{Rr1}{s}\right)}$$

**Input power:**

$$P1(s) := 3\left(\frac{V^2}{Z1(s)}\right)$$

**Output Power [W]:**

$$P21(s) := 3\left(|I21(s)|\right)^2\cdot Z1(s)$$

**Input power factor:**

$$PF1(s) := \cos(\arg(P1(s)))$$

**Efficiency :**

$$\eta 1(s) := \frac{((P21(s)))}{(P1(s))}$$

## *Appendix C2: Matlab files for dynamic analysis of the induction machine.*

*% Parameters of machine used in simulations*

```
Vrated = 3800;              % rated line to line voltage in V
phi = 1/15*pi;              % Starting phase angle of stator voltage
p = 6;                      % number of poles
frated = 50;                % rated frequency in Hz
a = 1.46;                   % rotor/stator turn ration
Vm = Vrated*sqrt(2/3);      % magnitude of phase voltage
Tfactor = (3*p)/4;          % factor for torque expression
rs = 1.2;                   % stator wdg resistance in ohms
Lls = 0.042;                % stator leakage reactance in ohms
Lm = 0.07074;               % stator magnetizing reactance
rpr = 0.45;                 % referred rotor wdg resistance in ohms
Lplr = 0.018;               % rotor leakage reactance
rpex = 1.8/(a*a);           % external (passive) resistor
rpLex = 0.28/(a*a);         % external (passive) resistance of the coil
Lpex = 0.56/(a*a);          % external (passive) inductance
LM = 1/(1/Lm + 1/Lls + 1/Lplr);
J = 0.5;                    % rotor inertia in kg*m^2
B = 0.05;                   % rotor damping coefficent.
```

% M-file for 10 kW induction machine simulations when connecting it to the power grid at a speed of 1015 rpm

% It sets up the machine parameters, initial conditions, and speed input in the MATLAB workspace for simulation, and plots the results of the simulation.

*% Load three-phase induction machine parameters*

```
ap10 kW                 % load 10 kW motor parameters from ap10 kW.m
% initialize to start from standstill with machine unexcited

flqs = 0;       % stator q-axis total flux linkage; flqr = 0;     % rotor q-axis total flux linkage
flds = 0;       % stator d-axis total flux linkage; fldr = 0;     % rotor d-axis total flux linkage
iqrLex = 0;     % external q-axis inductance current; idrLex = 0; % external d-axis inductance current
tstop = 1.5;    % use 1.5 sec simultion time for Fig. in text

% program time and output arrays of repeating sequence signal for Tmech

% Transfer to keyboard for simulation
disp('Set up for running as_g10 kW.m');
```

```
as_g10 kW; sim('as_g10 kW'); close all; figure(20);
subplot(5,1,1); plot(y(:,1),y(:,2),'-'); axis([-inf inf -500 500]);
ylabel('Va (V)'); title('a: Stator Voltage Va in Rotor Coordinates'); grid on;
subplot(5,1,2); plot(y(:,1),y(:,3),'-')
axis([0 1.5 -50 50]); ylabel('Tem (Nm)'); title('b: Electromagnetic Torque');grid on;
subplot(5,1,3); plot(y(:,1),y(:,3),'-')
axis([0.5 1.5 0 80]); ylabel('Tem (Nm)');title('c: Zoomed in Electromagnetic Torque'); grid on;
subplot(5,1,4); plot(y(:,1),y(:,5),'-')
axis([0 1.5 -20 20]); ylabel('Ia (A)'); title('d: Stator Current Ia'); grid on;
subplot(5,1,5); plot(y(:,1),y(:,5),'-')
axis([1 1.5 -30 30]); ylabel('Ia (A)') ; xlabel('time in sec');title('e: Zoomed in Stator Current Ia'); grid on;
```

## *Appendix C3: Matlab-Simulink files for dynamic analysis of the induction machine with passive elements.*

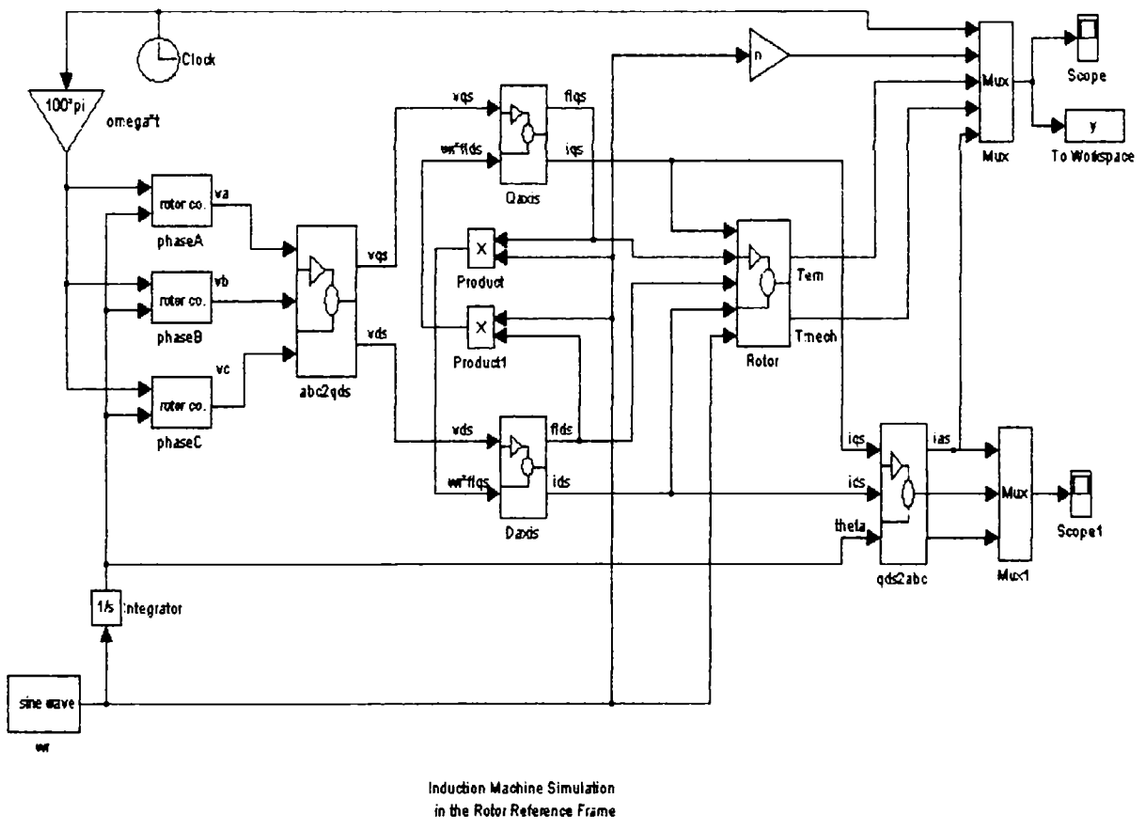


**Figure C1**. Induction machine with passive elements simulation in the rotor reference frame.

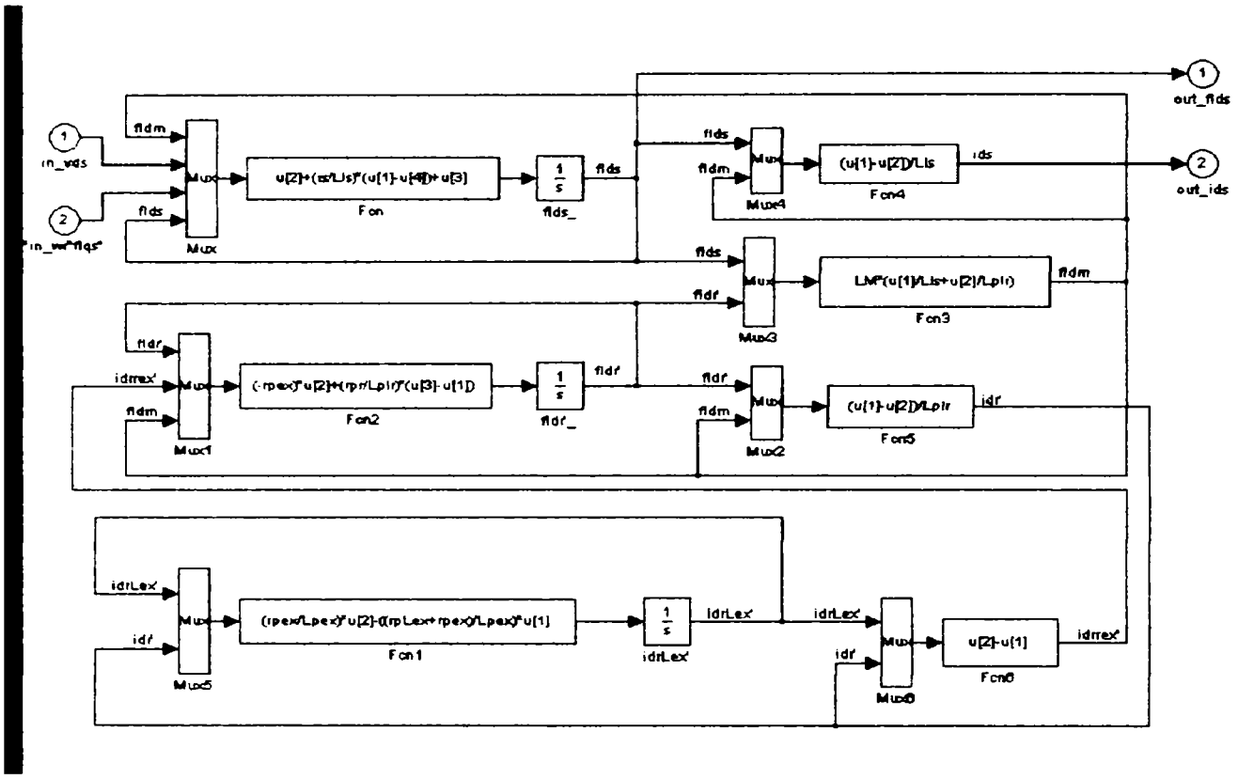


**Figure C2.** Block representation of the subsystem D-axis. The Figure illustrates the principle of how the flux and current equations are implemented in Simulink.

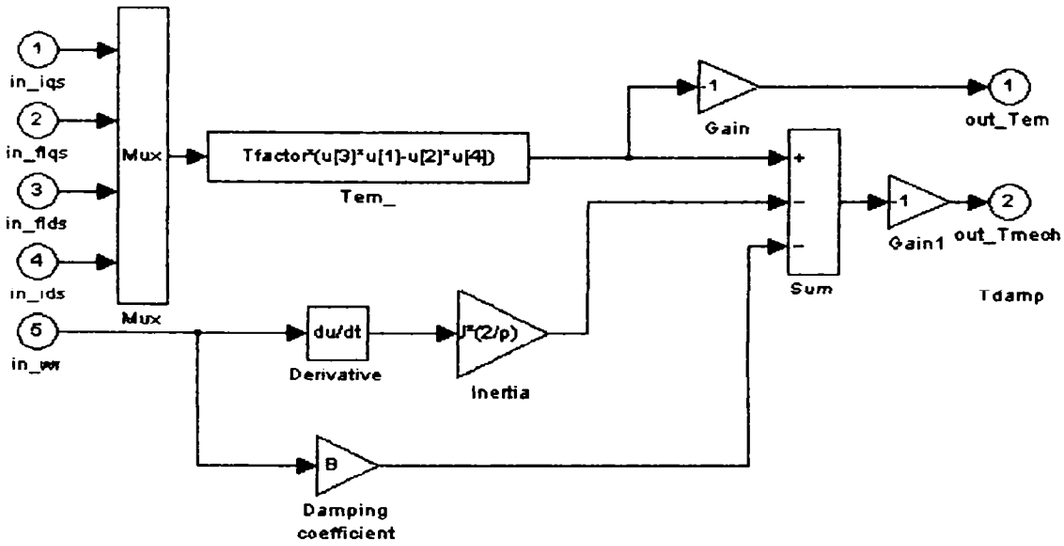


**Figure C3**. Details about rotorl equation implemented in Simulink.

# Appendix D: Details about machine parameters and simulation model

This appendix contains more details about DFIG parameters, complete simulation model implemented in Matlab/Simulink, including rotor converter model with details about the control modulation strategy-SFAVM and the control program developed in Ansi C used to control the rotor converter.

## *Appendix D1: DFIG data*

### D1.1. Nameplate data:

3-phase, wye/delta connected, 50 Hz
Stator: 220 V/phase, 13 A
Rotor: 220 V/phase, 6.1 A
Nominal speed=1460 rpm
Nominal power: 11 kW, cosφ=0.81

### D1.2. Machine parameters:

Rs=0.95 Ω, Rr=1.2 Ω, $L_{\sigma s}$=3.95 mH, $L_{\sigma r}$=5 mH, $L_m$=149.7 mH
All values are referred to the stator.

## *D2: Simulation Model implemented in Matlab-Simulink*

This appendix section contains a description of the complete simulation model including the drive system, the DFIG model, the current and voltage transducers with anti-aliasing filters, the rotor converter model and the control system implementation in Matlab-Simulink software-package.

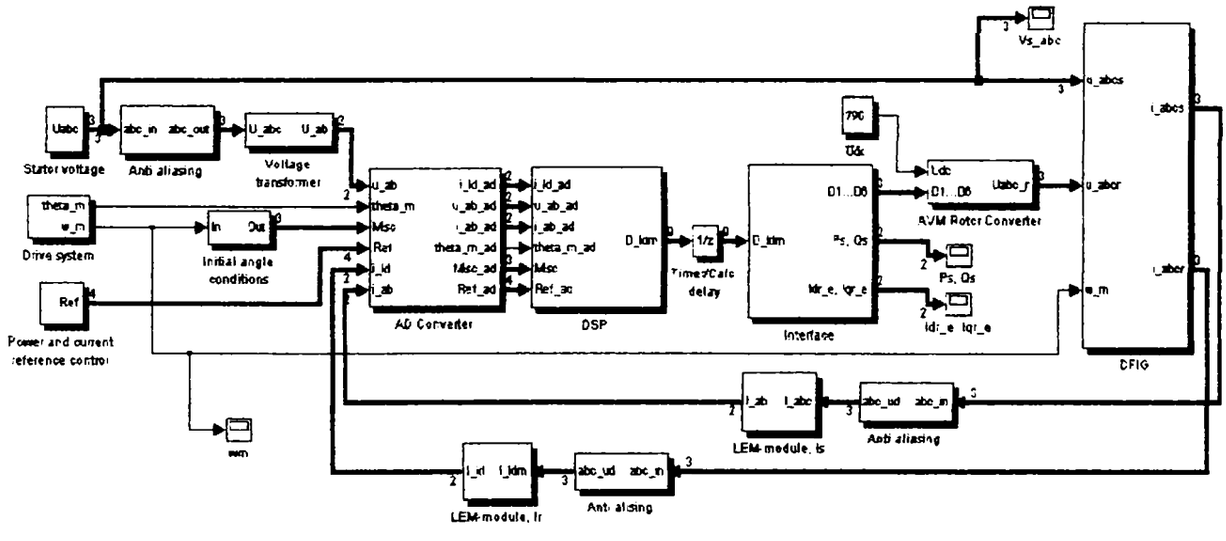


**Fig. D1**. The complete simulation model implemented in Matlab-Simulink.

The mechanical system, gear-box, wind turbine rotor are modeled by the drive system. The mechanical system implemented in Simulink is modeled using a first order approximation, where the time constant is determined from a step in rotor speed, as illustrate in Fig. D2.

The Fig. D3 shows the applied subsystems, and the calculation of torque and power. Three-phase inputs are transformed to two-phase quantities and the current equations are solved in the u_dq > i_dq block. The power, electromagnetic torque and three-phase currents are outputs of the simulation model.

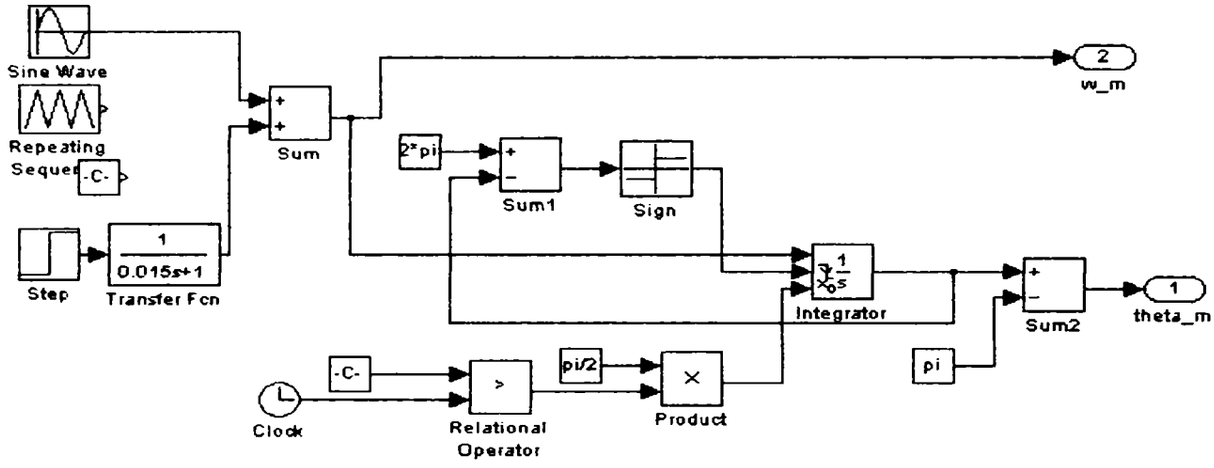


**Fig. D2**. The drive system implemented in Simulink.

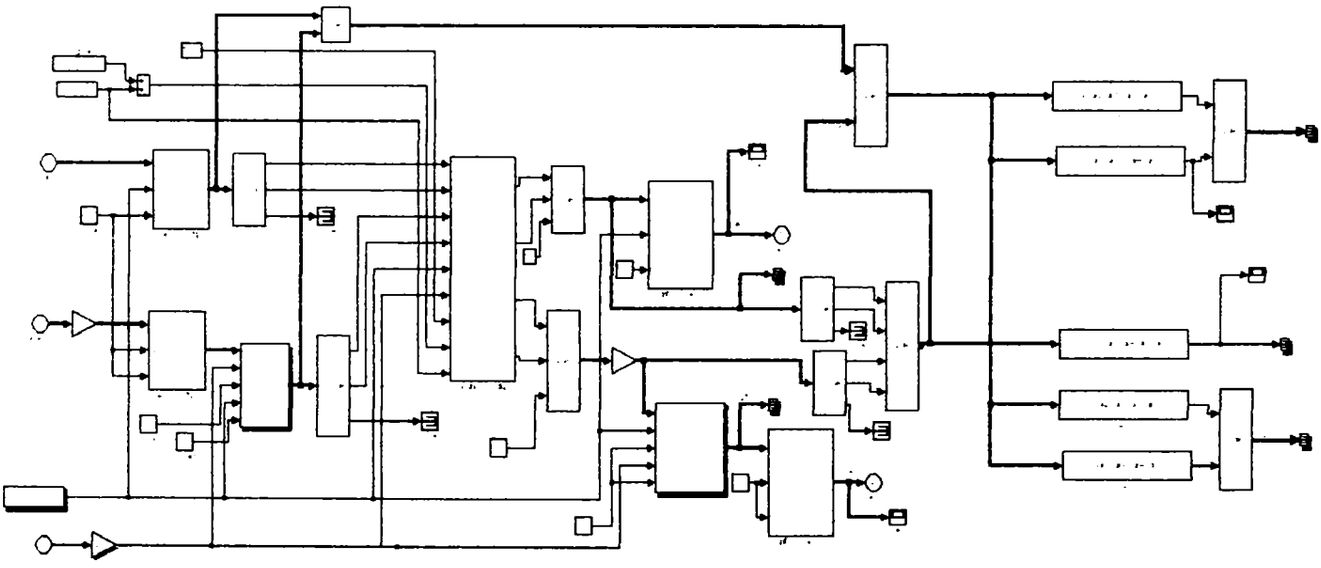

**Fig. D3**. The DFIG model implemented in Simulink.

## *D2.1. Implementation of the Rotor Converter.*

An average value model for rotor converter is implemented. The SFAVM approach is chosen for implementation.

## D2.1.1. Stator Flux Asynchronous Vector Modulation (SFAVM)

For modulating the output voltage of the rotor converter and thereby controlling the rotor current, the SFAVM strategy is chosen. As the converter has three-phases, the converter voltages are gained from six available active

vectors. The six-voltage vectors are given by the configuration of the rotor converter shown in Fig. D.1. The basic idea of the strategy is to track the reference voltage by applying two active and two zero vectors two times each switching period. For calculating the duty cycles the voltage vector is turned into the first hexagon as may be seen in figure, which shows the six active voltage vectors and the reference voltage vector.

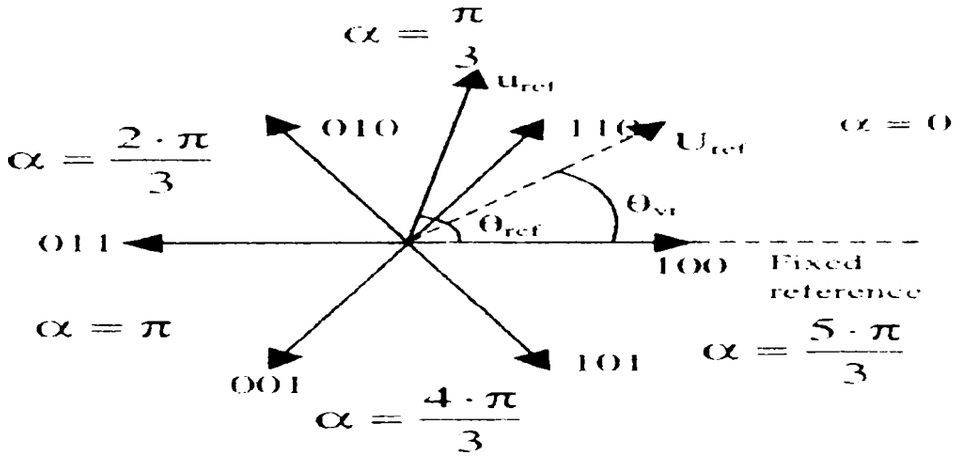


**Figure D.4**. Illustration of the vectors of the three-phase converter and the voltage vector ($u_{ref}$) to be gained from the vectors.

As may be seen in Fig. D.4 the voltage vector is turned into the first hexagon for calculating the duty cycles because the equations for calculating the duty cycles only are developed for the first hexagon. The generation of the reference voltage vector, and the corresponding flux vector are shows in Figure D.5:

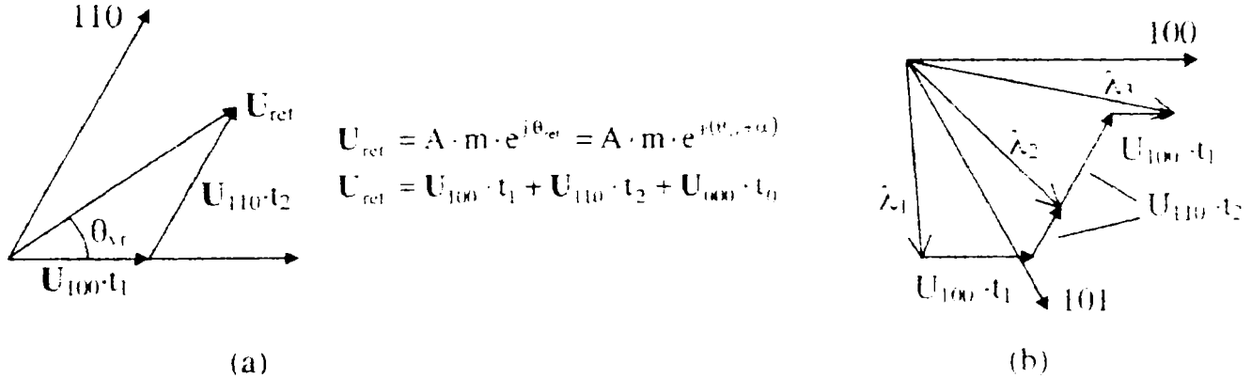


**Figure D.5.** a) Illustration of the components, $U_{100}\, t_1$, $U_{110}\, t_2$ and $U_{000}\, t_0$ required for generating the reference voltage vector. b) Illustration of the flux vectors displaced $90^0$ behind the voltage vectors.

## D2.1.2. Angle and Torque Error Minimization

For minimizing the amplitude and angle error, the zero voltage vectors may be used. This is illustrated in Fig. D.6, where the transition from $\lambda_1$ to $\lambda_2$ to $\lambda_3$ shown in figure 2 are compared with the reference flux path.

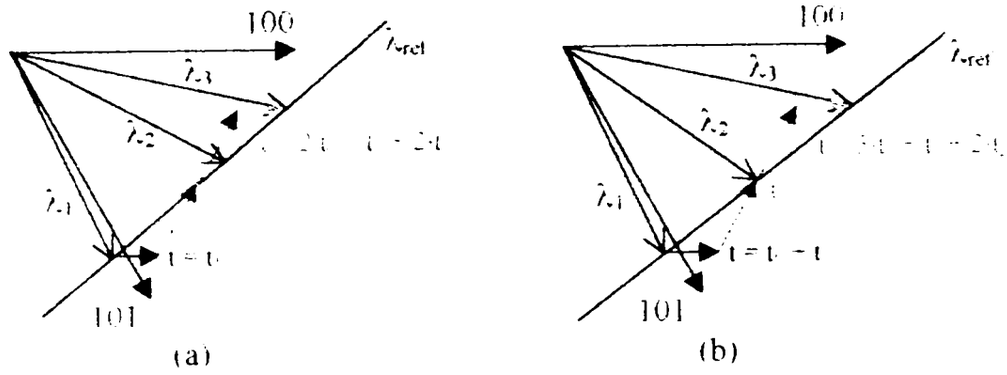


**Figure D.6**. Comparison of the modulated flux vector path and the reference flux vector path.

The maximum angle and amplitude error of the modulated flux is smallest in Fig. D6 b). This means, that the active vectors are to be placed in the middle of the switching period, and the zero voltage vectors should be applied at the beginning and end of the switching period.

For implementation of the SFAVM strategy, the duty cycles of each phase or converter branch has to be calculated. The zero voltage vectors should be applied for an equally time duration in the beginning and end of each switching period $T_{sw}=2(t_0+t_1+t_2)$.

## D2.1.3. Calculating of Duty cycles

For calculation of the duty-cycles of each phase, the reference voltage vector and the actual average voltage vector are expressed in the complex notation as given by eq. (D.1)

$$U_{ref} = A \cdot m \cdot \left(\cos(\theta_{ref}) + j \cdot \sin(\theta_{ref})\right) = \\ = \frac{2}{3} \cdot U_{k,ref} + U_{l,ref} \cdot e^{j\cdot\frac{2\pi}{3}} + U_{m,ref} \cdot e^{j\cdot\frac{4\pi}{3}} \quad \text{....(D.1)}$$

Equation 1 may be rewritten expressing the exponential term as, $e^{j2\pi/3}=1/2+j*\sqrt{3}/2$, and using the condition, that $U_{m0,ref}=0$ since only voltage vectors $U_{100}$ and $U_{110}$ are used.

$$U_{ref} = \frac{2}{3} \cdot U_{dc} \cdot \frac{t_1}{T_{sw}} + \frac{2}{3} \cdot U_{dc} \cdot \frac{t_2}{T_{sw}} \cdot \left(\frac{1}{2} + j \cdot \frac{\sqrt{3}}{2}\right) \quad \text{.....(D.2)}$$

By combining eq D.1 and D.2, and equalize the real part of eq D.1 and eq D.2 and similarly equalize the imaginary parts, $t_1$ and $t_2$ may be calculated as eq D.3 and D.4. The time duration for applying the zero voltage vectors is calculated from eq D.5

$$t_1 = \frac{3 \cdot T_{sw} \cdot A \cdot m}{2 \cdot U_{dc}} \cdot \left(\cos(\theta_{vr}) - \frac{1}{\sqrt{3}} \cdot \sin(\theta_{vr})\right) = \frac{\sqrt{3} \cdot T_{sw} \cdot A \cdot m}{U_{dc}} \cdot \left(\cos\left(\theta_{vr} - \frac{\pi}{6}\right)\right) \quad \text{.....(D.3)}$$

$$t_2 = \frac{\sqrt{3} \cdot T_{sw} \cdot A \cdot m}{U_{dc}} \cdot \left(\sin(\theta_{vr})\right) \quad \text{.....(D.4)}$$

$$t_0 = T_{sw} - t_2 - t_1 \quad \text{.....(D.5)}$$

When calculating the voltage vector, $U_{ref}$, it is assumed that the voltage in phase equals zero, since only the voltage vectors $U_{100}$ and $U_{110}$ are4 used in the first hexagon. The time $t_1$ is then regarded as the time for applying the voltage vector behind the average voltage vector, and $t_2$ is regarded, as the time required for applying the voltage vector in front of the average voltage vector. Therefore a detection of the reference angle $\theta_{vr}$ is required to determine which two active voltage vectors is to be applied.

The equations for calculating the duty-cycles of each phase are set up by use of Fig. 1a, and eq D.3-5, as given by eq D. 6-8.

$$D_k = U_1 \cdot \frac{t_1}{T_{sw}} + U_2 \cdot \frac{t_2}{T_{sw}} + \frac{1}{2} \cdot \left(1 - \frac{t_1}{T_{sw}} - \frac{t_2}{T_{sw}}\right) \quad \text{.....(D.6)}$$

$$D_l = U_3 \cdot \frac{t_1}{T_{sw}} + U_4 \cdot \frac{t_2}{T_{sw}} + \frac{1}{2} \cdot \left(1 - \frac{t_1}{T_{sw}} - \frac{t_2}{T_{sw}}\right) \quad \text{.....(D.7)}$$

$$D_m = U_5 \cdot \frac{t_1}{T_{sw}} + U_6 \cdot \frac{t_2}{T_{sw}} + \frac{1}{2} \cdot \left(1 - \frac{t_1}{T_{sw}} - \frac{t_2}{T_{sw}}\right) \quad \text{.....(D.8)}$$

It is important to realize that $U_{ref}$ is the phase reference voltage whereby the calculation of $t_1$ and $t_2$ reduces since, $U_{dc} = \sqrt{3} * A$.

### D.2.1.4. Maximum Amplitude

Ordinary modulation strategies such as sinusoidal modulation needs either over modulation or injection of a 3rd harmonic in the modulation function to obtain the desired amplitude of the output voltage. The maximum amplitude of the SFAVM strategy may be calculated using the following conditions:

m=1 and $t_1+t_2=T_{sw}$ i.e. $t_0=0$.

By using eq D.3 equal to eq D.4, the following expression for the amplitude of the output voltage, A, may be set up as eq. D.9

$$A = \frac{U_{dc}}{\sqrt{3} \cdot \sin(\theta_{vr}) + \frac{3}{2} \cdot \left(\cos(\theta_{vr}) - \frac{1}{\sqrt{3}} \sin(\theta_{vr})\right)} \quad \text{.....(D.9)}$$

The maximum of the amplitude is found by calculating the derivative of the amplitude with respect to $\theta_{vr}$. The angle of maximum amplitude is found, and substituted into eq 6 as expressed in eq. D.7

$$\frac{dA}{d\theta_{vr}} = 0 \Rightarrow \theta_{vr} = \frac{\pi}{6} \Rightarrow A_{\max} = \frac{U_{dc}}{\sqrt{3}} \quad \text{.....(D.10)}$$

As may be seen from equation D.10, the maximum amplitude of the line-to-line output voltage will equal the DC-link voltage, and a unity gain of the converter is obtained.

## D2.1.5. Implementation of SFAVM

The SFAVM algorithm is implemented in Simulink as a function is written in the programming language C and is mixed for use in Matlab-Simulink.

The SFAVM modulation curve is calculated in the following steps letting $\theta_{ref}$ vary $2\pi$ radians:

- the amplitude of the voltage vector is calculated
- the current hexagon and the offset angle $\alpha$ are determined from the reference angle $\theta_u$
- the two neighboring voltage vectors for generating the reference voltage vector are selected
- the times for applying the two active vectors ($t_1$ and $t_2$) are calculated from eq. D.3 and D.4
- the time for applying the zero vectors ($t_0$) is calculated from equation D.5
- the modulation curve for phase k is saved for an array in the file *mod.h* that may be read of the C-compiler.

For calculating the reference voltage vector, the current hexagon is to be determined. The angle of the reference voltage vector is calculated, and an offset angle ($\alpha$) dependent on the hexagon number is subtracted from the reference angle as may be seen in Fig. D.7.

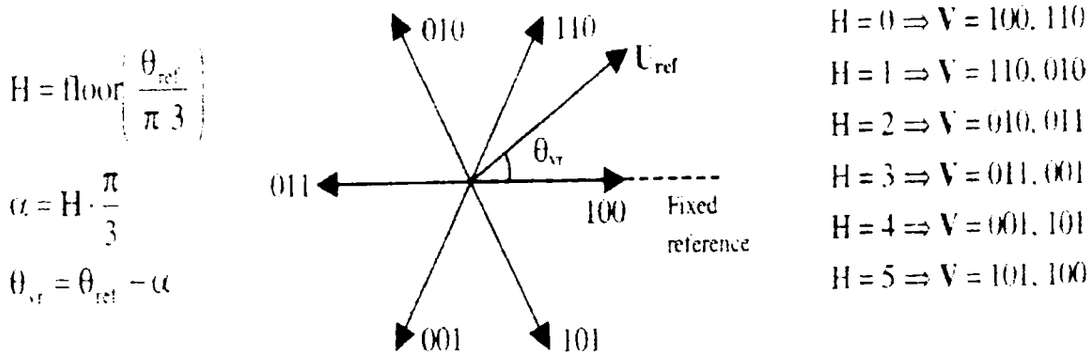


**Figure D.7**. Calculation of the current hexagon by evaluation of the sign of the phase-to-phase voltages.

The reference voltage vector is moved to the first hexagon, since the calculation of $t_1$ and $t_2$ is derived for the first hexagon only. The actual hexagon (H) and the offset angle are determined as is shown in Figure D.7 and the actual vectors corresponding to the hexagons are determined. The angle and amplitude of the voltage vector is used for calculating the times for applying the two active voltage vectors and the zero voltage vectors.

For minimizing the calculating time of the control program, the modulation function is implemented as a 1024 element table containing the modulation curve for rotor phase k for $2\pi$ radians electrical degrees. The table is named mod.h. The duty cycle of phase k is calculated as a the point of the table corresponding the angle of voltage reference $u_{ref}$. The time for applying the two active voltage vectors and the zero vectors are calculated using eq. D.3-D.5 by inserting the maximum amplitude and modulation index of one. The duty cycle for phase k is calculated from eq. D.6. The modulation curve for rotor phase k is shown in Fig. D.8:

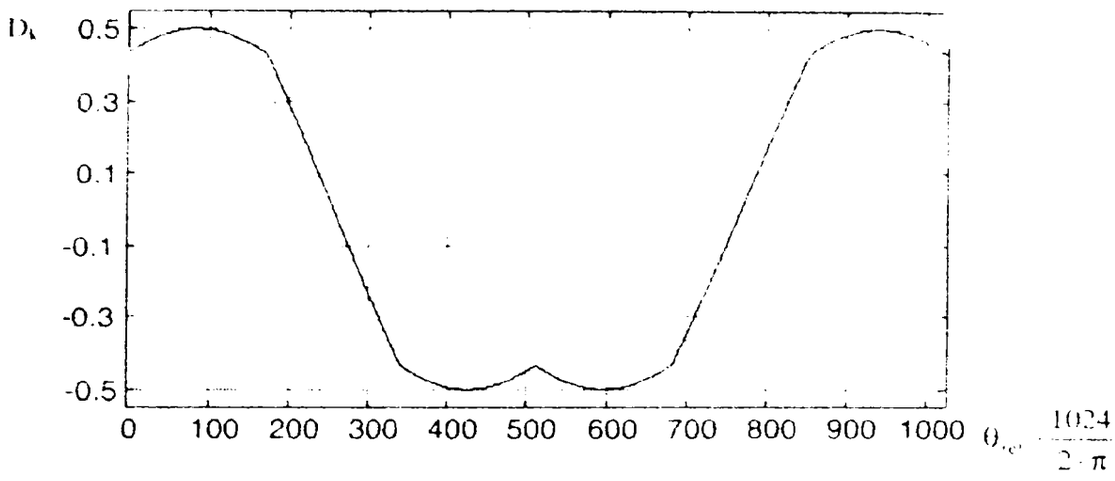


**Figure D.8.** Modulation curve to be implemented in Simulink. The input to the array is the voltage reference vector angle ($\theta_{ref}$), and the output is the duty cycle.

The duty cycles of each phase are to be centered on 0.5. The modulation curve is generated symmetric around zero. Therefore 0.5 is added for getting duty cycles symmetric around 0.5 when calculating the duty cycles as described in the following.

The voltage vector in rotor co-ordinates is input to the modulation function. First the amplitude and the modulation index are calculated. The modulation index is calculated as written in equation D.11, as the maximum is equal the DC-link voltage divided by the square root of three.

$$m = \frac{\sqrt{3} \cdot U_{r,amp}}{U_{dc}} \quad \text{.....(D.11)}$$

For calculating the duty cycle for phase k, the element of the array in *mod.h* containing the duty cycle for phase k is determined as written in equation D.12:

$$P_k = floor\left(\frac{1024 \cdot \theta_{vr}}{2 \cdot \pi}\right) \quad \text{.....(D.12)}$$

The function floor is automatically used at the data conversion when $P_k$ is defined as an integer variable and $\theta_{vr}$ is a float. As the element of the array for calculating $D_k$ is determined the duty cycle for phase k is calculated as written in equation D.13

$$D_k = m \cdot \text{mod}(P_k) + 0.5 \quad \text{.....(D.13)}$$

For calculating the duty cycles of phase l and m elements are picked displaced 341 elements corresponding to a displacement of $120^0$ as is written in equations D.14-D.15:

$$P_l = P_k - 341 \quad \text{.....(D.14)}$$

$$P_m = P_k - 683 \quad \text{.....(D.15)}$$

The duty cycles for phase l and m are calculated as equations D.16-D.17:

$$D_l = m \cdot \text{mod}(P_l) + 0.5 \quad \text{.....(D.16)}$$

$$D_m = m \cdot \mathrm{mod}(P_m) + 0.5 \quad \text{.....(D.17)}$$

The function is implemented in the simulation control program as the function *modulation()*.

## D2.1.7. PWM Generator

The function of the PWM generator is to convert the modulation signals ($D_k$, $D_l$ and $D_m$) from the DSP into the PWM signals $S_{1\text{-}6}$. For modeling the PWM generator, the switching frequency has to be determined. The performance of the control loop is dependent on the switching frequency. The PWM signals are generated at a switching frequency of 5 kHz. The timer operation is modeled by a triangular signal gaining the required switching frequency as can be seen in Fig. D.9. The advantage of using a triangular PWM signal is that the gate signals to the converter are placed in the middle of the switching period.

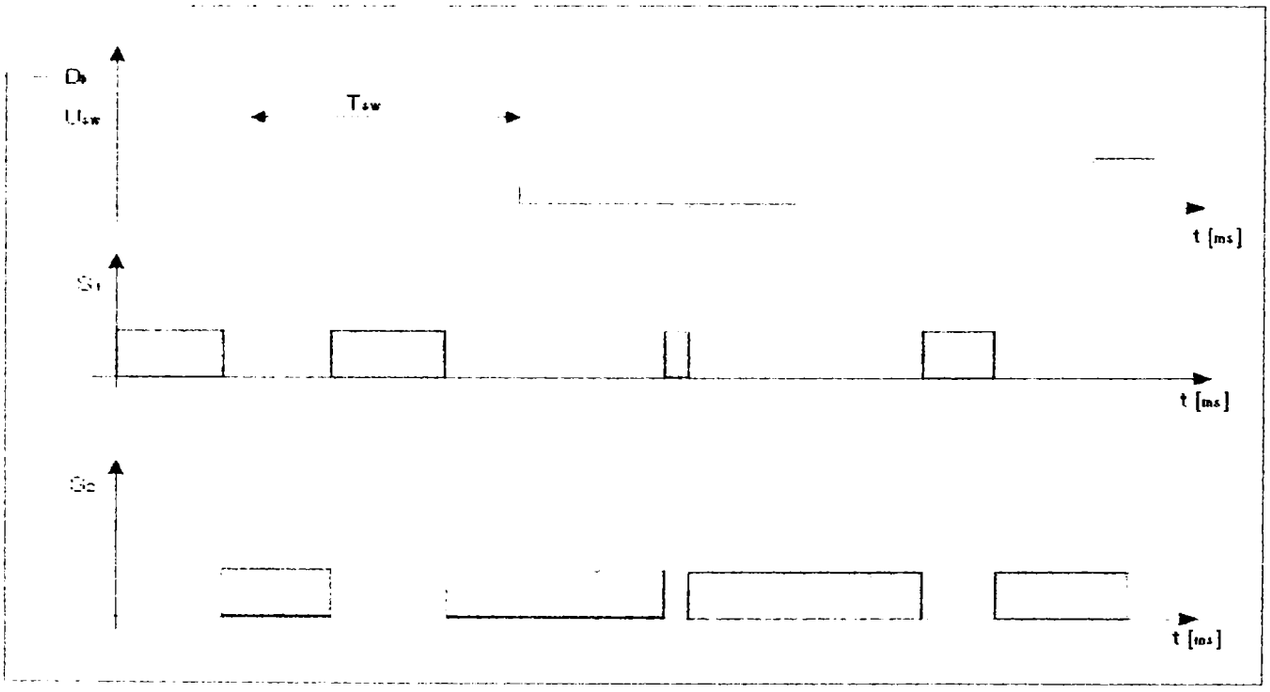


**Figure D.9.** Illustration of the generation of PWM signal $S_1$ from the DSP output $D_l$ and the timer generated function $U_{sw}$. The signal $S_2$ is the complimentary signal of $S_1$.

Comparing the voltage modulation duty-cycles $D_k$, $D_l$ and $D_m$ with the triangular PWM signal generates the gate signals $S_{1\text{-}6}$. $S_1$ is high when $D_l$ is larger than $U_{sw}$ as may be seen in Fig. 5.13. $S_2$, $S_4$ and $S_6$ are generated as complimentary signals of $S_1$, $S_3$ and $S_5$.

## D2.1.8. Blanking Time Modulation

The blanking time of the SKiiPACK module when switching between upper and lower IGBT has to be modeled. The principal of blanking time is illustrated in Fig.D.10:


**Fig. D.10.** Illustration of blanking time. The gate signals $G_1$ and $G_2$ are generated from PWM signals $S_1$ and $S_2$.

As may be seen in Fig. D.10, the blanking time is modeled as a turn on delay. The blanking time of the SKiiPACK module is $\tau = 3$ μs, as can be seen in experimental set-up description.
The control implementation of rotor converter is divided into the following blocks: timer interface, blanking time and switch modulation, as can be seen in Fig.D.11.

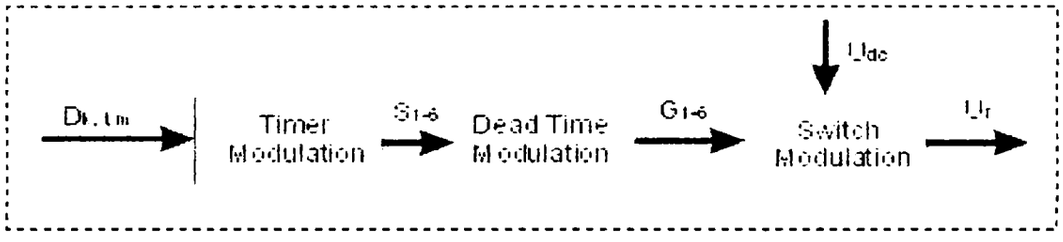


**Figure D.11.** Control implementation of the rotor converter model.

The subsystems are connected in the rotor converter models shown in Fig. D.11; where $D_{k,Lm}$ represent the duty-cycles for rotor converter and $S_{1-6}$ represent trigger signals for IGBTs.

*Timer Interface*
In this section the timer interface Simulink model is describe. The reference signal for generating the PWM pulses is modeled as well. A reference signal is required for generating the PWM signals. In this case a triangular reference signal is chosen. The advantage of the triangular signal is that it is a symmetrical signal and may be modeled by use of less simulation steps as a saw tooth signal. The function for generating the triangular reference signal is illustrated in Fig. D.12:

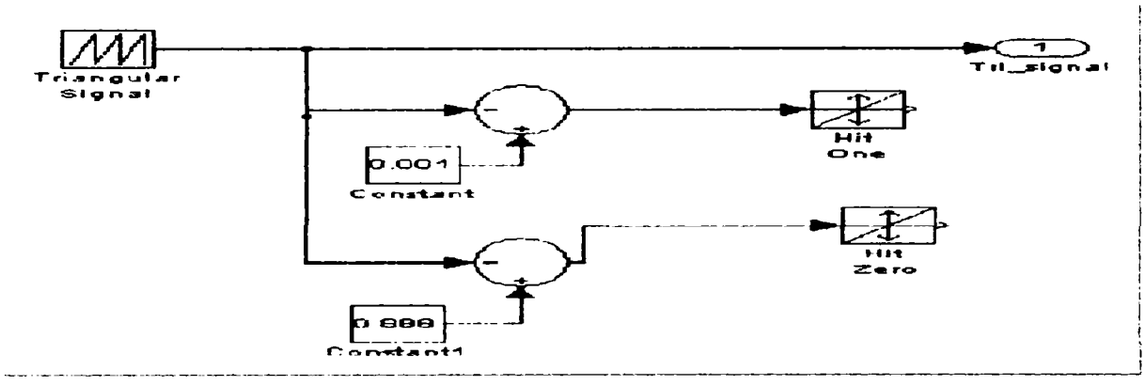


**Figure D.12.** Triangular reference signal generator implemented in Simulink.

For generating the triangular signal the standard "triangular signal" block from the Simulink toolbox is used. For decreasing the simulation time it is advantages to use variable time step. The hit zero crossing function is used for forcing Simulink to perform simulation points at the maximum and minimum of the trace.
For generating the PWM signals, the modulation reference $D_{\_1}$ is compared to the triangular signal as shown in Fig. D.13.

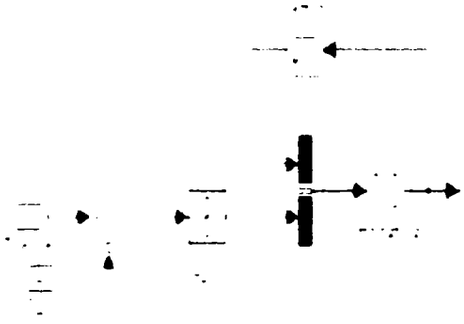

| Zero-crossing¤ | Last·output¤ | Output¤ |
|---|---|---|
| 0¤ | 0¤ | 0¤ |
| 0¤ | 1¤ | 1¤ |
| 1¤ | 0¤ | 1¤ |
| 1¤ | 1¤ | 0¤ |

a) b)

**Figure D.13.** a) Function for generating PWM signals S1. b) Truth table for the combinatorial logic block.

The hit zero crossing function is set up for generating pulses on both negative and positive zero crossing function. The inputs to the combinatorial logic block are the actual output and the last output of the hit zero crossing function.

$S_1$, $S_3$ and $S_5$ are generated as explained above. $S_2$, $S_4$ and $S_6$ are not generated since they are inverse functions of $S_1$, $S_3$ and $S_5$.

*Blanking Time*

The PWM signals require blanking time to avoid short-circuiting the DC-link voltage during switching. The gate signals must be separated before adding blanking time. The gate signals including blanking time for gate one and two are illustrated in Fig. D.14:

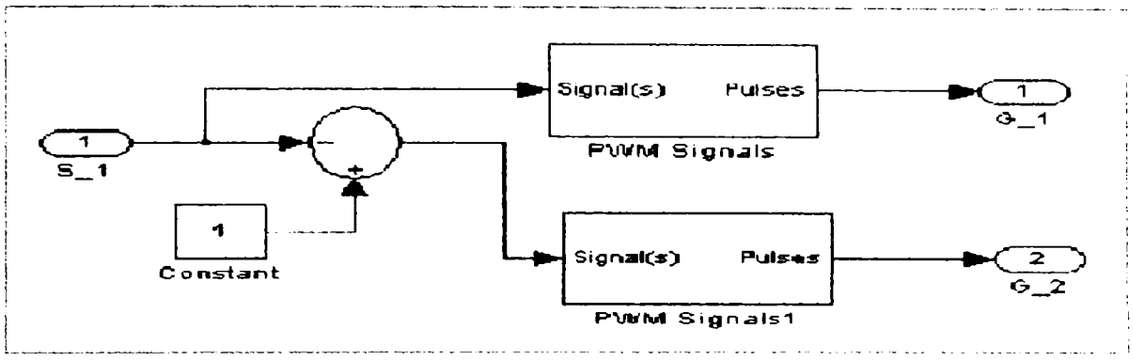


**Figure D.14.** Separation of gate signal one ($G_{\_1}$) and two ($G_{\_2}$) and addition of blanking time.

$S_1$ and $S_2$ are fed to a function for generating blanking time as may be seen in Fig. D.14. The blanking time function for gate signals ($G_{1\text{-}6}$) is shown in Fig. D.15.

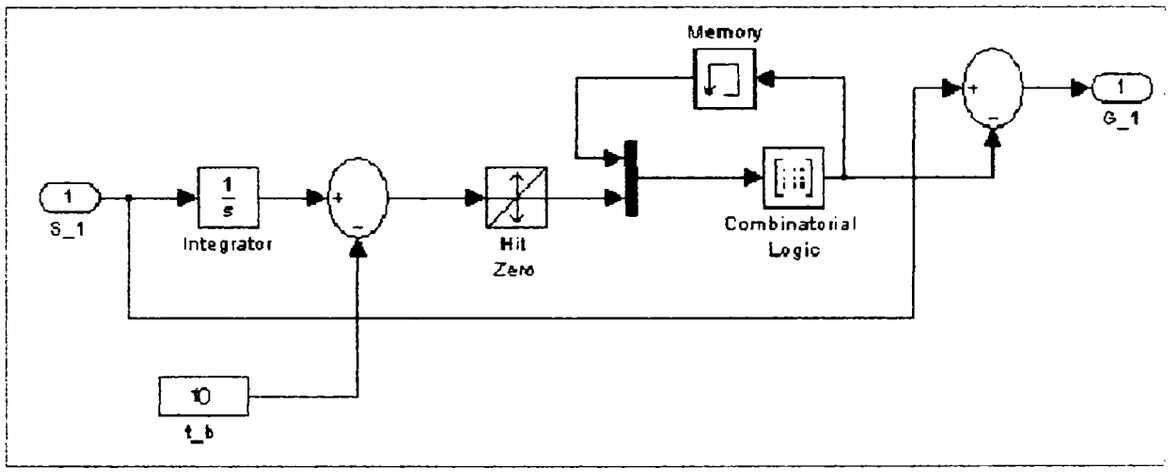


**Figure D.15.** Function for adding blanking time $t_b$ to the PWM signal $S_1$ gaining the gate signals $G_1$. The function is equal for all gate signals.

*Switch Modulation*

The IGBTs and the freewheeling diodes are modeled by use of an S-function programmed in Borland C. The C file is compiled by use of the Matlab MEX-compiler.

For determining the correct operating point of the switches "if" expression (command) are used. The determination of the operating point is performed from the input data. The input data are rotor current, gate signals and the parameters of IGBTs and diodes. The model structure is shown in Fig. D.16:

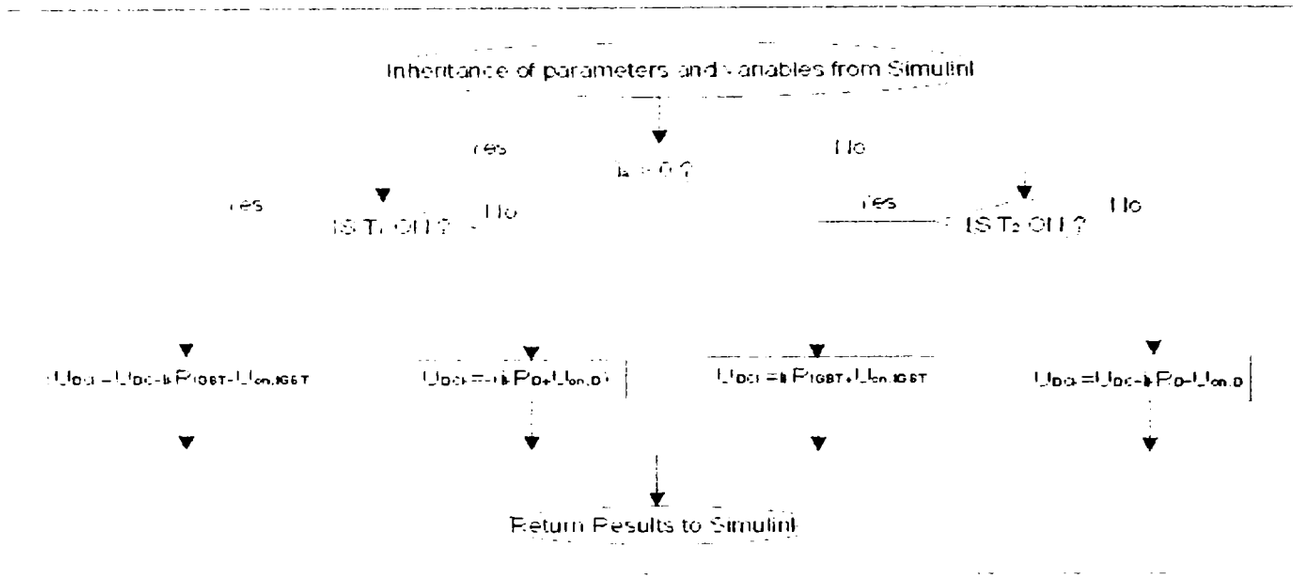


**Figure D.16.** Model structure of the function for calculating the voltage on phase k. The voltage is calculated as is shown in the boxes. Similar functions are set up for calculating the voltages of phase l and phase m.

As can be seen in Fig. D.16 "*if*" expressions are used for determining which of the components are conducting. As the conducting component is determined the voltage is calculated by use of the equations shown in boxes. The voltages are calculated with respect to zero of the DC-link.

## *D3 – The control program developed in Ansi C used to control the rotor converter.*

DFIG.c file is compiled and applied to the DSP in Simulink simulation model.

### DFIG.c

```
//* MEX Function *
#define S_FUNCTION_NAME dsp_mex
#include "simstruc.h"
#include "mod.h"
#include <stdio.h>
#include <math.h>
#include <stdlib.h>
//* DSP:   Macro and variable definition//*Frequency constants*
#define f_sa 5000//5000.4951f#define T_sa 2e-4//1.999802e-4f#define f_sw 2500//.2475f
#define T_sw 4e-4//3.999604e-4f
//*Trigonometric and diverse*
#define cos0 1.0f#define cos_min2pi3 0.5*(-1.0)#define cos_2pi3      0.5*(-1.0)#define sin0 0.0f
#define sin_min2pi3 866.0254e-3*(-1.0)#define sin_2pi3 866.0254e-3f#define pi 3.141593f
#define _2pi 6.283185f#define _1pi3 1.047198f#define _2pi3 2.094395f#define _4pi3 4.188790f
#define _3pi2 4.712389f#define _pi2 1.570796f#define _5pi3 5.235988f#define sqrt2 1.414214f
#define sqrt3 1.732051f#define _2_3 666.6667e-3f#define _3_2 1.5f//* Motor parameters *
#define R_s      5.766645f#define M_Ls   9.751127e-1f # define M 9.084591e-1f # define L_r .363406e-1f
#define L_s 9.316453e-1f
//*Flux-filter constants*
#define A1       8.496827e-2f#define A0   8.496827e-2*(-1.0) # define B1      1.9112f*(-1.0)
#define B0       9.149758e-1f#define D_max       0.98f # define offset_b      341
# define offset_c     683 # define K 1024 # define Udc 790
```

```
//** TMZ0_isr() **
int       flag_sw;int flag_regulator;int flag_effect regulator;int flag_afkobling;
float u_reA;float u_rePI;float u_imA;float u_imPI;
//** SH_AD_Converter() **
float     i_k=0;float i_l=0;float w_rm=0;float u_a=0;floatu_b=0;
float     i_a=0;float i_b=0;float theta_rm;
float w_re;float w_slip;float w_e;float i_m;float u_c;float i_c;float Dtheta_re;
float theta_re;
//** abc_2_qd_s() **
float u_ds_s;float u_qs_s;float i_ds_s;float i_qs_s;
float u_ds_s_old;float u_qs_s_old;float i_ds_s_old;float i_qs_s_old;
StatorFlux() **
float psi_ds_s;float psi_qs_s;float ppsi_ds_s;float ppsi_qs_s;float psi_ds_s_old;float psi_qs_s_old;float
psi_ds_s_old_old;float psi_qs_s_old_old;float ppsi_ds_s_old;float ppsi_qs_s_old;
float theta_e;w_e_slip() **
float theta_e_old;float w_e;float w_slip;float theta_slip;float Dtheta_slip;float Dtheta;
//** qd_s_2_qd_e() **float psi_qs_e;float psi_ds_e;float ppsi_qs_e;float ppsi_ds_e;
//** abc_2_qd_e **float u_qs_e;float u_ds_e;float i_qs_e;float i_ds_e;float i_qr_e;float i_dr_e;
float i_qr_r;float i_dr_r;
Effect() **
float P_s;float Q_s;//*Rotorflux() **float psi_qr_e;float psi_dr_e;
//** Effectregulator() **
float E_P_s;float E_Q_s;float E_P_s_old;float E_Q_s_old;float P_s_ref;float Q_s_ref;
float K_p;float N_p;float K_q;float N_q;
//** regulator() **
float E_i_qr_e;float E_i_dr_e;float E_i_qr_e_old;float E_i_dr_e_old;float i_qr_e_ref;float i_dr_e_ref;float
u_qr_e_ref_PI = 0;float u_dr_e_ref_PI = 0;float K_i;float N_i;float u_qr_e_ref;float u_dr_e_ref;float
Kp_idr_reg;float Kp_iqr_reg;float Reg_select;float uwpsi_q_old;float uwpsi_d_old;float uwpsi_q;float uwpsi_d;
float wpsi_q_old;float wpsi_d_old;float wpsi_q;float wpsi_d;float A;float u_qrA_old_old;float
u_drA_old_old;float u_qrA_old;float u_drA_old;float u_qrA;float u_drA;float u_qrA_new;float u_drA_new;
//** Antiwindup() **
float u_ref;float theta_ref;float E_qAWU;float E_dAWU;float u_qAWU;float u_dAWU;
//** qd_e_2_qd_r() **
float u_qr_r_ref;float u_dr_r_ref;
//** rect_2_pol() **
float u_mod_ref;float theta_mod_ref;
//** Modulation() **
float theta_mod_sync=0;float u_k;
float u_l; float u_m; float M_Index;float  T_2=0,T_1=0,T_0=0;float Duty_k=0.1;float Duty_l=0.1;
float Duty_m=0.1;float Dmax;float b, m, Da, Db, Dc, Ur_amp, theta_vr, Udr, Uqr;int Pa, Pb, Pc;
sqrt;sin;cos;atan;
constant _pi2 osv
K_i;N_i;K_p;N_p;K_q;N_q
//* MEX      Function definition                    *
void SH_AD_Converter_MEX();
//* END  MEX      Function definition                    *
//*       Declaration of functions                    *
void abc_2_qd_s(void);void StatorFlux(void);void w_e_slip(void);void qd_s_2_q_e(void);
void abc_2_qd_e(void);void Effect(void);void Begin_Rotorflux(void);void Effect_Regulator(void);
void Stream_Regulator(void);void Current_regulator(void);void qd_s_2_qd_e(void);
void qd_e_2_abc_r(void);void qd_e_2_qd_r(void);void Antiwindup(void);
void qd_e_2_qd_r(void);void rekt_2_pol(void);void Modulation2(void);
//* END       Function definition                    *
//MEX ******************* On-line Input i MEX ***************************
        #define reg_select                  ssGetArg(S,0)
        #define K_idr_reg                       ssGetArg(S,1)
        #define K_iqr_reg                       ssGetArg(S,2)
  #define Ki                    ssGetArg(S,3)
        #define Ni                  ssGetArg(S,4)
        #define Kp_Preg                 ssGetArg(S,5)
```

```
        #define N_Preg                  ssGetArg(S,6)
        #define Kp_Qreg                 ssGetArg(S,7)
        #define N_Qreg                  ssGetArg(S,8)
        #define f_afkob                 ssGetArg(S,9)
        #define f_PQ_reg                        ssGetArg(S,10)
//END MEX *************** On-line Input i MEX ***************************
//MEX
static void mdlInitializeSizes(SimStruct *S)
{
   ssSetNumContStates(    S, 0);     // number of continuous states
   ssSetNumDiscStates(    S, 50);    // number of discrete states
   ssSetNumInputs(        S, 14);    // number of inputs
   ssSetNumOutputs(       S, 9);     // number of outputs
   ssSetDirectFeedThrough(S, 0);     // direct feed through flag
   ssSetNumSampleTimes(   S, 0);             // number of sample times
   ssSetNumSFcnParams(    S, 0);     // number of input arguments
   ssSetNumInputArgs(     S, 11);    // argument
   ssSetNumRWork(         S, 0);     // number of real work vector elements
   ssSetNumIWork(         S, 0);     // number of integer work vector elements
   ssSetNumPWork(         S, 0);     // number of pointer work vector elements
}// END MEX
static void mdlInitializeSampleTimes(SimStruct *S)
{
   ssSetSampleTime(S, 0, T_sa); ssSetOffsetTime(S, 0, 0);
}//END MEX
//MEX static void mdlInitializeConditions(double *x0, SimStruct *S)
{
        x0[0] = 0;x0[1] = 0;x0[2] = 0;x0[3] = 0;x0[4] = 0;x0[5] = 0;x0[6] = 0;
        x0[7] = 0;x0[8] = 0;x0[9] = 0;x0[11] = 0;x0[12] = 0;x0[13] = 0;
        x0[14] = 0;x0[15] = 0;x0[16] = 0;x0[17] = 0;x0[22] = 0;//439.823*(-1.0)*T_sa; // theta_re
        x0[29] = 0;//314.159*(-1.0)*T_sa;//0.15*(-1);//pi;  theta_e, x0[30] = 1;
}//END MEX
//MEX static void mdlOutputs(double *y, double *x, double *u, SimStruct *S, int tid)
{
  if(x[30])
  {
y[0] = x[0];  //Da;y[1] = x[1];  //Db;y[2] = x[2];  //Dc
}
y[3] = x[3]; //i_qr_e;y[4] = x[4];  /i_dr_e;y[5] = x[5];   //P_s;y[6] = x[49];    //Q_s
 y[7] = x[27];//x[27] is i_qr_e_ref; y[8] = x[28];     //x[28] is i_dr_e_ref
        }
//END MEX
//MEX DSP ***************************************************************
//static void mdlUpdate(double *x, double *u, SimStruct *S, int tid)
static void mdlUpdate(double *x, double *u, SimStruct *S, int tid)
{
Duty_k  = x[0];Duty_l     = x[1];Duty_m    = x[2];u_qs_s      = x[6];   u_ds_s   = x[7];i_qs_s      = x[8];
i_ds_s   = x[9];psi_qs_s_old= x[10];psi_ds_s_old = x[11];ppsi_qs_s_old = x[12];
ppsi_ds_s_old = x[13];u_qrA_old= x[14];u_drA_old= x[15];theta_mod_ref= x[16];
theta_ref = x[17];ppsi_qs_s x[18];ppsi_ds_s= x[19];psi_qs_s_old_old   = x[20];psi_ds_s_old_old  =
x[21];theta_re= x[22];E_i_qr_e      = x[23];E_i_dr_e = x[24];u_qr_e_ref_PI      = x[25];u_dr_e_ref_PI=
x[26];i_qr_e_ref= x[27];i_dr_e_ref= x[28];theta_e x[29];flag_sw= x[30];E_qAWU = x[31];E_dAWU =
x[32];E_P_s= x[33];E_Q_s= x[34];u_qrA    = x[35];u_drA= x[36];w_e= x[37];uwpsi_q= x[38];uwpsi_d=
x[39];wpsi_q      = x[40]; wpsi_d= x[41];Q_s= x[49];
//END
// ********************** On-line Input i MEX *******************************
        flag_effectregulator = mxGetPr(f_PQ_reg)[0];K_i = mxGetPr(Ki)[0];Kp_idr_reg=
mxGetPr(K_idr_reg)[0];Kp_iqr_reg= mxGetPr(K_iqr_reg)[0];N_i = mxGetPr(Ni)[0];
        Reg_select = mxGetPr(reg_select)[0];K_p= mxGetPr(Kp_Preg)[0];//5
        N_p= mxGetPr(N_Preg)[0];//6;K_q= mxGetPr(Kp_Qreg)[0];//7;N_q= mxGetPr(N_Qreg)[0];//8
```

```
        flag_afkobling      = mxGetPr(f_afkob)[0];  //12;flag_regulator = 1;
//* MEX    Sample                                  *
i_k = u[0];i_l = u[1];u_a = u[2];u_b  = u[3];i_a = u[4];
i_b = u[5];theta_rm = u[6];w_rm= u[7];Dtheta_slip = u[8];
if(!flag_effektregulator)
{
i_qr_e_ref  = u[10];
i_dr_e_ref  = u[11];
}
P_s_ref  = u[12];Q_s_ref  = u[13];
        //**END ****************** sample ******************************************
  //END MEX *************** On-line Input i MEX ***************************
//* MEX (DSP)   Function TMZ0_isr()                      *
//void TMZ0_isr()
//        {
        SH_AD_Converter_MEX();abc_2_qd_s();StatorFlux();w_e_slip();qd_s_2_qd_e();abc_2_qd_e();
Effect(); Rotorflux();if(1)//if (flag_sw )
{
        if (flag_effektregulator)
        {
                Effect_Regulator();
                }
        if(!flag_afkobling)
        {
                K_i = 75;N_i = 0.9867;
                }
    if(Reg_select)
        {
      Stream_Regulator();
      }
    if(!Reg_select)
        {
      Current_regulator();
}
{
u_qrA_new = 0;u_drA_new = 0;
        }
        u_qr_e_ref = u_qr_e_ref_PI + u_qrA_new;u_dr_e_ref = u_dr_e_ref_PI + u_drA_new;
Antiwindup();qd_e_2_qd_r();//rect_2_pol();
        Modulation2();
                }
        flag_sw = 1;//!flag_sw;
//}
// MEX  // {******************
  x[0] = Duty_k; x[1] = Duty_l; x[2] = Duty_m;x[3]  = i_qr_e;//u_qrA; // test
  x[4]  = i_dr_e;//u_drA; // test x[5]  = P_s; //u_qr_e_ref;// test
 x[6]  = u_qs_s; x[7]  = u_ds_s; x[8]  = i_qs_s; x[9]   = i_ds_s;
  x[10] = psi_qs_s_old; x[11] = psi_ds_s_old; x[12] = ppsi_qs_s_old; x[13] = ppsi_ds_s_old;
  x[14] = u_qrA_old; x[15] = u_drA_old;x[16] = theta_mod_ref; x[17] = theta_ref;
  x[18] = ppsi_qs_s; x[19] = ppsi_ds_s; x[20] = psi_qs_s_old_old; x[21] = psi_ds_s_old_old;
  x[22] = theta_re; x[23] = E_i_qr_e; x[24] = E_i_dr_e;
  x[25] = u_qr_e_ref_PI; x[26] = u_dr_e_ref_PI;x[27] = i_qr_e_ref; x[28] = i_dr_e_ref;
  x[29] = theta_e; x[30] = flag_sw; x[31] = E_qAWU; x[32] = E_dAWU;
  x[33] = E_P_s; x[34] = E_Q_s; x[35] = u_qrA; x[36] = u_drA; x[37] = w_e;
  x[38] = uwpsi_q; x[39] = uwpsi_d; x[40] = wpsi_q; x[41] = wpsi_d; x[49] = Q_s;
/ {END*************** }

 mdlUpdate
// DSP ***************** Procedure ****************************************
//* MEX       Function SH_AD_Converter_MEX()                *
```

```
void SH_AD_Converter_MEX(){
 i_a = i_a/2.463768; i_b = i_b/2.463768; u_a = u_a*2.463768; u_b = u_b*2.463768; i_m = (i_k + i_l)*(-1);
 u_c = (u_a + u_b)*(-1); i_c = (i_a + i_b)*(-1);w_re = w_rm*2.0; theta_re = theta_rm*2 + pi + Dtheta_re;
} // END Function SH_AD_Converter_MEX()
//*      Function abc_2_qd_s()                              *
void abc_2_qd_s(void){
 u_qs_s_old = u_qs_s; u_ds_s_old = u_ds_s; u_qs_s = (cos0*u_a + cos_min2pi3*u_b + cos_2pi3*u_c)*_2_3;
 u_ds_s = (sin0*u_a + sin_min2pi3*u_b + sin_2pi3*u_c)*_2_3;
 i_ds_s_old = i_ds_s; i_qs_s_old = i_qs_s; i_qs_s = (cos0*i_a + cos_min2pi3*i_b + cos_2pi3*i_c)*_2_3;
 i_ds_s = (sin0*i_a + sin_min2pi3*i_b + sin_2pi3*i_c)*_2_3;} // END Function abc_2_qd_s()
//*      Function StatorFlux()                              *
void StatorFlux(void){
 psi_qs_s = A1*ppsi_qs_s + A0*ppsi_qs_s_old - B1*psi_qs_s_old - B0*psi_qs_s_old_old;
 psi_ds_s = A1*ppsi_ds_s + A0*ppsi_ds_s_old - B1*psi_ds_s_old - B0*psi_ds_s_old_old; psi_qs_s_old_old =
psi_qs_s_old; psi_ds_s_old_old = psi_ds_s_old; psi_qs_s_old = psi_qs_s; psi_ds_s_old = psi_ds_s;
 ppsi_qs_s_old = ppsi_qs_s; ppsi_ds_s_old = ppsi_ds_s; ppsi_qs_s = ppsi_qs_s + T_sa*(u_qs_s_old -
R_s*i_qs_s_old); ppsi_ds_s = ppsi_ds_s + T_sa*(u_ds_s_old - R_s*i_ds_s_old); theta_e_old = theta_e; if
(psi_qs_s){
        theta_e = atan2(psi_ds_s*(-1),psi_qs_s); }
} // END Function StatorFlux()
//*      Function w_e_slip()
void w_e_slip(void){
 if ((theta_e_old - theta_e) > 1){
        w_e = w_e;
 }
 else{
        w_e = (theta_e - theta_e_old)*f_sa;
 }
w_slip = w_e - w_re;
theta_slip = theta_e - theta_re;
} // END Function w_e_slip()
//*      Function qd_s_2_qd_e()                             *
void qd_s_2_qd_e(void){
//      psi_qs_e = cos(theta_e)*psi_qs_s - sin(theta_e)*psi_ds_s;psi_ds_e = sin(theta_e)*psi_qs_s +
cos(theta_e)*psi_ds_s;    ppsi_qs_e = cos(theta_e)*ppsi_qs_s - sin(theta_e)*ppsi_ds_s;  ppsi_ds_e =
sin(theta_e)*ppsi_qs_s + cos(theta_e)*ppsi_ds_s;
} // END Function qd_s_2_qd_e()
//*      Function abc_2_qd_e()                              *
void abc_2_qd_e(void){
        i_qs_e = (cos(theta_e)*i_a + cos(theta_e - _2pi3)*i_b + cos(theta_e + _2pi3)*i_c)*_2_3;
 i_ds_e = (sin(theta_e)*i_a + sin(theta_e - _2pi3)*i_b + sin(theta_e + _2pi3)*i_c)*_2_3;
 u_qs_e = (cos(theta_e)*u_a + cos(theta_e - _2pi3)*u_b + cos(theta_e + _2pi3)*u_c)*_2_3;
 u_ds_e = (sin(theta_e)*u_a + sin(theta_e - _2pi3)*u_b + sin(theta_e + _2pi3)*u_c)*_2_3;
 i_qr_e = (cos(theta_slip)*i_k + cos(theta_slip - _2pi3)*i_l + cos(theta_slip + _2pi3)*i_m)*_2_3;
 i_dr_e = (sin(theta_slip)*i_k + sin(theta_slip - _2pi3)*i_l + sin(theta_slip + _2pi3)*i_m)*_2_3;
} // END Function abc_2_qd_e()
///*      Function Effect()                              *
void Effect(void){
        P_s = (u_ds_s*i_ds_s + u_qs_s*i_qs_s)*1.5;
 Q_s = (u_qs_s*i_ds_s - u_ds_s*i_qs_s)*1.5;
} // END Function Effect()
//*      Function Rotorflux()                           *
void Rotorflux(void){
 psi_qr_e = i_qr_e*L_r + i_qs_e*M;
 psi_dr_e = i_dr_e*L_r + i_ds_e*M;
} // END Function Rotorflux()
//*      Function Effect_Regulator()                        *
void Effect_Regulator(void)
        {
E_P_s_old = E_P_s; E_Q_s_old = E_Q_s; E_P_s = P_s_ref - P_s; E_Q_s = Q_s - Q_s_ref;
```

```
i_dr_e_ref = i_dr_e_ref + K_p*(E_P_s - N_p*E_P_s_old);i_qr_e_ref = i_qr_e_ref + K_q*(E_Q_s -
N_q*E_Q_s_old);
        } // END Function Effect_Regulator()
//*      Function Stream_Regulator()                              *
void Stream_Regulator(void)
        {
        E_i_qr_e_old = E_i_qr_e; E_i_dr_e_old = E_i_dr_e;
//E_i_qr_e = i_qr_e_ref + psi_qs_e*psi_qs_e*w_e/L_s*1.5 - i_qr_e;
 E_i_qr_e = i_qr_e_ref - i_qr_e;E_i_dr_e = i_dr_e_ref - i_dr_e;u_qr_e_ref_PI = u_qr_e_ref_PI + K_i*(E_i_qr_e
- N_i*E_i_qr_e_old) + E_qAWU*T_sw/(1 - N_i)*0.2; u_dr_e_ref_PI = u_dr_e_ref_PI + K_i*(E_i_dr_e -
N_i*E_i_dr_e_old) + E_dAWU*T_sw/(1 - N_i)*0.2;//*(N_i*(-1) + 1)/0.2;
} // END Function Stream_Regulator()
//*      Function Current_regulator()                             *
void Current_regulator(void)
        {
        E_i_qr_e_old = E_i_qr_e;E_i_dr_e_old = E_i_dr_e;
        //E_i_qr_e = i_qr_e_ref + psi_qs_e*psi_qs_e*w_e/L_s*1.5 - i_qr_e;
  E_i_qr_e = i_qr_e_ref - i_qr_e;E_i_dr_e = i_dr_e_ref - i_dr_e;
 u_qr_e_ref_PI = Kp_iqr_reg*E_i_qr_e;u_dr_e_ref_PI = Kp_idr_reg*E_i_dr_e;
} // END Function Current_Regulator()
//*      Function ()                                              *
void Afkobling(void){
  uwpsi_q_old = uwpsi_q; uwpsi_d_old = uwpsi_d;
  uwpsi_q = (u_qs_e - w_e*ppsi_ds_e)*M_Ls; uwpsi_d = (u_ds_e + w_e*ppsi_qs_e)*M_Ls;
  wpsi_q_old = wpsi_q; wpsi_d_old = wpsi_d; wpsi_q = w_slip*psi_dr_e;wpsi_d = w_slip*psi_qr_e;
  A = 9.975272e-1; A = 1; u_qrA_old_old = u_qrA_old; u_drA_old_old = u_drA_old;
  u_qrA_old = u_qrA; u_drA_old = u_drA; u_qrA = u_qrA*A + uwpsi_q - uwpsi_q_old + wpsi_q -
wpsi_q_old*A; u_drA = u_drA*A + uwpsi_d - uwpsi_d_old - wpsi_d + wpsi_d_old*A;
//  u_qrA = wpsi_q;//  u_drA = wpsi_d; u_qrA_new = u_qrA*3.0 - u_qrA_old*3.0 + u_qrA_old_old;
  u_drA_new = u_drA*3.0 - u_drA_old*3.0 + u_drA_old_old;
} // END Function ()
//*      Function qd_e_2_abc_r()                                  *
void qd_e_2_abc_r(void){
u_qr_e_ref = u_qr_e_ref_PI + u_qrA_new; u_dr_e_ref = u_dr_e_ref_PI + u_drA_new;
Duty_k = cos(theta_slip)*u_qr_e_ref + sin(theta_slip)*u_dr_e_ref;
Duty_l = cos(theta_slip - _2pi3)*u_qr_e_ref + sin(theta_slip - _2pi3)*u_dr_e_ref;
Duty_m = cos(theta_slip + _2pi3)*u_qr_e_ref + sin(theta_slip + _2pi3)*u_dr_e_ref;
} // END Function qd_e_2_abc_r()
//*      Function Antiwindup()                                    *
void Antiwindup(void){
  u_qr_e_ref = u_qr_e_ref_PI + u_qrA_new;u_dr_e_ref = u_dr_e_ref_PI + u_drA_new;
  u_ref = sqrt(u_qr_e_ref*u_qr_e_ref + u_dr_e_ref*u_dr_e_ref);
  if (u_qr_e_ref){
            theta_ref = atan2(u_dr_e_ref*(-1),u_qr_e_ref);
  }
 Dmax = (D_max - 0.50)*2.0;
if (u_ref > Dmax*790.0/sqrt3){
          u_ref = Dmax*790.0/sqrt3;
  }
  u_qr_e_ref = cos(theta_ref)*u_ref; u_dr_e_ref = sin(theta_ref)*u_ref*(-1.0); u_qAWU = u_qr_e_ref -
u_qrA_new; u_dAWU = u_dr_e_ref - u_drA_new; E_qAWU = u_qAWU - u_qr_e_ref_PI;  E_dAWU =
u_dAWU - u_dr_e_ref_PI;
//  if (abs(E_qAWU) > abs(u_qr_e_ref_PI)){
//    E_qAWU = u_qr_e_ref_PI;
//  }
//  if (abs(E_dAWU) > abs(u_dr_e_ref_PI)){
//    E_dAWU = u_dr_e_ref_PI;
//  }
} // END Function Antiwindup()
//*      Function qd_e_2_qd_r();                                  *
```

```
void qd_e_2_qd_r(void){
 u_qr_r_ref = cos(Dtheta_slip - theta_slip)*u_qr_e_ref - sin(Dtheta_slip - theta_slip)*u_dr_e_ref;
 u_dr_r_ref = sin(Dtheta_slip - theta_slip)*u_qr_e_ref + cos(Dtheta_slip - theta_slip)*u_dr_e_ref;
} // END Function qd_e_2_qd_r()
//*      Function rect_2_pol()                                    *
//*************************************************************************
void rect_2_pol(void){
 u_mod_ref = sqrt(u_qr_r_ref*u_qr_r_ref + u_dr_r_ref*u_dr_r_ref);
 if (u_qr_r_ref){
          theta_mod_ref = atan2(u_dr_r_ref*(-1),u_qr_r_ref);
 }
} // END Function rect_2_pol()
//*      Function Modulation();                                   *
void Modulation2(void)              //The modulation function is SFAVM modulation
        {
  Udr  = u_dr_r_ref;
  Uqr  = u_qr_r_ref;
//Transformation from rectangular to polar coordinates
  Ur_amp = u_mod_ref;
        Ur_amp = sqrt(Udr*Udr + Uqr*Uqr);
  theta_vr = theta_mod_ref; theta_vr = atan2(Udr*(-1),Uqr);
  if(theta_vr<0)
        {
    theta_vr = theta_vr + 6.283185;
    }
//Calculation of Dutycycles
  m = Ur_amp*1.73205/790;                                  //Modulation index for SFAVM
        Pa = theta_vr*1024/6.283185;                       /Pa is the element of "mod" including Da
  if (Pa>=1024)
        {
    Pa = Pa - 1024;
        }
  Pb = Pa + 341;     //Pb is the element of "mod" including Db
  if (Pb>=1024)
        {
    Pb = Pb - 1024;
        }
  Pc = Pa + 683;  /Pc is the element of "mod" including Dc
  if (Pc>=1024)
        {
    Pc = Pc - 1024;
        };
  Duty_k = m*mod[Pa] + 0.5;                                //Da
  Duty_m = m*mod[Pb] + 0.5;                                 //Db
  Duty_l = m*mod[Pc] + 0.5;                                //Dc
        }
//**** End of Function Modulation () ****************************************
// END DSP ************* Procedure ****************************************
// MEX ***************************************
* mdlDerivatives - compute the derivatives
static void mdlDerivatives(double *dx, double *x, double *u, SimStruct *S, int tid)
{}
* mdlTerminate - called when the simulation is terminated.
static void mdl Terminate(SimStruct *S)
{}
#ifdef    MATLAB_MEX_FILE    /* Is this file being compiled as a MEX-file? */
#include "simulink.c"      /* MEX-file interface mechanism */
#else
#include "cg_sfun.h"       /* Code generation registration function */
#end
```

## Appendix E. The software used to set up the ICS 645-Data Acquisition Card

The ICS-645 Matlab Application Software is designed as a starting point from which a user can build application-specific software. The purpose of this software is to quickly configure an ICS-645 card that has been optimized for applications demanding high speed, precision and ease of integration. This driver software is intended to be used with the Matlab data analysis and graphing software. To access the ICS-645 Matlab Application Software and implicitly to record and process the data it was necessary to build a program for each task using the Matlab software package tool. This program has been performed to plot the spectrum of signals and then to assess the FFT analysis to diagnostic strategy and will be presented in appendix.

### Open645.m

triggerselect=0; clocksource=0; diagenable=0;Enable=1; FPDPenable=0; FPDPwidth=1; ADCmaster=1;ADCterm=1; FPDPmaster=1; IFPDPterm=1; ACQmode=1; internaltrigger=1; decimation=4; fftlength=2^(11); Channels=16; sample-frequency=5; %MHz

c=[triggerselect clocksource diagenable Enable FPDPenable FPDPwidth ADCmaster ADCterm FPDPmaster IFPDPterm ACQmode internaltrigger Decimation fftlength Channels sample frequency] [h,e]=mldevopn; [e,m]=mldevcfg(h,c');

%Trigger select=0 correspond with internal settings %ACQmode=1 correspond to capture mode and 0 to continuous

%Internal trigger=1 - begin acquisition and 0-no effect %ADC over sampling or decimation - these bits select the over sampling ratio of the converters

%Decimation 4 will operate with max 16 channels (8 with 32)

%The minimum sampling rate for the ADCs is 1 kHz, giving a min output rate of 125Hz in 8 over sampling ratio. %FFT length-the number of samples that ICS may acquire is ch/2*f

### Go645.m

close all

e=mldevtrg(h);

timeout=100;

e=mladcint(h,timeout);

**% data acquisition**

d1=ones(1,fftlength); [e, d1]=mldatard(h, fftlength, channels, 2, m);

d2=ones(1,fftlength); [e, d2]=mldatard(h, fftlength, channels, 1, m);

d3=ones(1,fftlength); [e, d3]=mldatard(h, fftlength, channels, 4, m);

d4=ones(1,fftlength); [e, d4]=mldatard(h, fftlength, channels, 3, m);

d5=ones(1,fftlength); [e, d5]=mldatard(h, fftlength, channels, 6, m);

d6=ones(1,fftlength); [e, d6]=mldatard(h, fftlength, channels, 5, m);

d7=ones(1,fftlength); [e, d7]=mldatard(h, fftlength, channels, 8, m);

d8=ones(1,fftlength); [e, d8]=mldatard(h, fftlength, channels, 7, m);

```
d9=ones(1,fftlength); [e, d9]=mldatard(h, fftlength, channels, 10, m);
d10=ones(1,fftlength); [e, d10]=mldatard(h, fftlength, channels, 9, m);
d11=ones(1,fftlength); [e, d11]=mldatard(h, fftlength, channels, 12, m);
d12=ones(1,fftlength); [e, d12]=mldatard(h, fftlength, channels, 11, m);
d13=ones(1,fftlength); [e, d13]=mldatard(h, fftlength, channels, 14, m);
d14=ones(1,fftlength); [e, d14]=mldatard(h, fftlength, channels, 13, m);
d15=ones(1,fftlength); [e, d15]=mldatard(h, fftlength, channels, 16, m);
d16=ones(1,fftlength); [e, d16]=mldatard(h, fftlength, channels, 15, m);
d0=ones(1,fftlength); [e, d0]=mldatard(h, fftlength, channels, 2, m);
n=(length(d1))/(channels/2);
time=zeros(1,n);
sampletime=decimation/(samplefrequency*10^6); %MHz
for aa=1:n
time(aa)=aa*sampletime;
end
scal=2*1.03/(2^(16));
figure
subplot(411); plot(time,d1(1,1:n)*scal,'k'),grid; ylabel('CH1')
subplot(412); plot(time,d2(1,1:n)*scal,'b'),grid
ylabel('CH2')
subplot(413); plot(time,d3(1,1:n)*scal,'r'),grid
ylabel('CH3')
subplot(414); plot(time,d4(1,1:n)*scal,'g'),grid
ylabel('CH4'); xlabel('time [s]')
zoom, figure;subplot(411); plot(time,d5(1,1:n)*scal,'k'),grid
ylabel('CH5'); subplot(412)
plot(time,d6(1,1:n)*scal,'b'),grid
ylabel('CH6');subplot(413); plot(time,d7(1,1:n)*scal,'r'),grid
ylabel('CH7'); subplot(414); plot(time,d8(1,1:n)*scal,'g'),grid
ylabel('CH8');xlabel('time [s]'); zoom, figure
subplot(411); plot(time,d9(1,1:n)*scal,'k'),grid
ylabel('CH9'); subplot(412); plot(time,d10(1,1:n)*scal,'b'),grid
ylabel('CH10'); subplot(413); plot(time,d11(1,1:n)*scal,'r'),grid
ylabel('CH11')
subplot(414); plot(time,d12(1,1:n)*scal,'g'),grid; ylabel('CH12'),xlabel('time [s]'),
zoom, figure;subplot(411);plot(time,d13(1,1:n)*scal,'k'),grid
ylabel('CH13');subplot(412);plot(time,d14(1,1:n)*scal,'b'),grid
ylabel('CH14');subplot(413);plot(time,d15(1,1:n)*scal,'r'),grid
ylabel('CH15');subplot(414);plot(time,d16(1,1:n)*scal,'g'),grid;ylabel('CH16');xlabel('time [s]').
```

```
% Plot the FFT of the data
triggerselect=0; clocksource=0; diagenable=0;
enable=1; FPDPenable=0; FPDPwidth=1; ADCmaster=1;
ADCterm=1; FPDPmaster=1;
IFPDPterm=1; ACQmode=1;
internaltrigger=1; decimation=8; fftlength=2^(15);
channels=16; samplefrequency=2.50; %MHz
l=(length(d1)/16)/channels;
f1=abs((fft(d1))); f1=f1*(2^-17); f1=20*log10(f1);
f2=abs((fft(d3))); f2=f2*(2^-25); f2=20*log10(f2);
f3=abs((fft(d7))); f3=f3*(2^-25); f3=20*log10(f3);
f4=abs((d1)); %f4=f4*(2^-25); f44=angle(d1);%*360/(2*pi));
f4=unwrap(f44);%*360/(2*pi); %f4=20*log10(f4);
figure
subplot(311)
plot(f1(1:l)),grid
axis([0 1200 -80 0])
ylabel ('Is1 Amplitude [dB]');
subplot(312)
plot(f2(1:l)),grid
axis([0 1200 -80 0])
ylabel ('Is2 Amplitude [dB]');
subplot(313)
plot(f3(1:l)),grid
axis([0 1200 -80 0])
ylabel ('Is3 Amplitude [dB]');
%subplot(414)
%plot(f4(1:l)),grid
%ylabel ('Is1-Phase Angle [rad]');
xlabel ('Frequency [Bin]');
```

# Complete List of References

[1] H. Akagi and H. Sato, "Control and Performance of a Doubly-Fed Induction Machine Intended for a Flywheel Energy Storage System", IEEE Transactions on Power Electronics, Vol. 17, No. 1, January 2002, pp. 109-116.

[2] V. Akhmatov, "Modelling of Variable-Speed Wind Turbines with Doubly-Fed Induction Generators in Short-Term Stability Investigations", 3rd Int. Workshop on Transmission Networks for Offshore Wind Farms, April 1-12, 2002, Stockholm, Sweden.

[3] J.M.Aller, J.A.Restrepo, A.Bueno, M.I.Gimenez, R.Alves, "Dynamic models of induction motor including the rotor eccentricities and the slot effect using the spatial vector transform", ICEM September 2-4, 1998, Vol. 1, pp. 597-602.

[4] D.C. Aliprantis, S.A. Papathanassiou, M.P. Papadopoulos and A.G. Kladas, "Modeling and control of a variable-speed wind turbine equipped with permanent magnet synchronous generator", ICEM 2000, 28-30 August, Espoo-Finland, pp. 558-562.

[5] M. Arkan, D.K. Perovic and P.J.Unsworth, "Online stator faults diagnosis in induction motors", IEE Proc.-Electr. Power Appl., Vol. 148, No. 6, November 2001, pp. 537-547.

[6] M. Arkan, D.K. Perovic and P.J.Unsworth, "Closed rotor slot effect on negative sequence impedance", IEEE 2001, pp. 751-753.

[7] http://www.awea.com, The American Wind Energy Association, Wind Turbine Configurations.

[8] M.E.H Benbouzid, M. Vieira, Theys, C., "*Induction motors faults detection and localisation using stator* current advanced signal processing techniques", Power Electronics, IEEE Transactions on, Volume: 14 Issue: 1, Jan. 1999, Page(s): 14 –22.

[9] M. Boger and A. Wallace, "Performance capability analysis of the brushless doubly fed machine as a wind generator", Electric machines and drives, 11-13 September 1995, Conference publication no 412, pp 458 – 461.

[10] I. Boldea and S.A. Nasar, "The Induction Machine Handbook", CRC Press, 2002.

[11] I. Boldea and S.A. Nasar, "Electric Machines: Steady-State Operation", Hemisphere Publishing Corporation, 1990.

[12] A.H.Bonnet and G.C.Soukup, "Cause and analysis of stator and rotor failures in three-phase squirrel-cage induction motors", IEEE Trans. Ind. Applicat., vol. 28, pp. 921-937, July/August 1992.

[13] Bimal K. Bose, "Power Electronics and Variable Frequency Drives-Technology and Applications", book, IEEE Press-IEEE IES, IEEE IAS, IEEE PES, ISBN 0-7803-1061-6, New York, 1997.

[14] R.Burnett, J.F.Watson, S.Elder, "The Application of Modern Signal Processing Techniques to Rotor Fault Detection and Location within Three Phase Induction Motors", IEEE, pp.426-431, June 1995.

[15] R.Burnett and J.F.Watson, "The Current Analysis Program-A Software Tool for Rotor Fault Detection in Three Phase Induction Motors", Electrical Machines and Drives, pp.156-160, 11-13 September 1995.

[16] J.R. Cameron, W.T. Thomson, A.B. Dow, "Vibration and current monitoring for detecting air gap eccentricity in large induction motors", IEE Proceedings, pp. 155-163, vol. 133, pt. B, no. 3, May, 1986.

[17] A.J.M Cardoso, E.S. Saraiva, "Computer-aided detection of air gap eccentricity in operating three-phase induction motors by Park's Vector Approach", IEEE Trans. Ind. Appls., pp. 897-901, vol. 29, no. 5, Sept./Oct. 1993.

[18] R.Cardenas, R. Pena, G.M. Asher and J.C. Clare, "Experimental emulation of wind turbines and flywheels for wind energy applications", Proceedings of IEEE-EPE 2001, Graz.

[19] M.Alex Cash, Thomas G. Habetler and Gerald B. Kliman, "Insulation failure prediction in induction machines using line-neutral voltages", Industry Applications Conference, 1997, Thirty-Second IAS Annual Meeting, Conference Record of the 1997 IEEE, Vol. 1, pp. 208-212.

[20] M.Alex Cash and Thomas G. Habetler, "Insulation failure detection in the stator windings of ASD-Driven induction machines using standard deviation of line currents", Industry Applications Conference, 1998, Thirty-Third IAS Annual Meeting, Vol. 1, pp. 299-303.

[21] M.Alex Cash, Thomas G. Habetler and Gerald B. Kliman, "Insulation failure prediction in ac machines using line-neutral voltages", IEEE Transactions of Industry Applications, vol. 34, no. 6, November/December 1998, pp. 1234-1239.

[22] Z. Chen, E. Spooner, "Grid Interface for a Variable-Speed, Permanent-Magnet, Wind Turbine Generator", International Conference on Electric Machine-ICEM'96, Vol. 3, pp. 347-352.

[23] Z. Chen, E. Spooner, "Wind Turbine Power Converters: A comparative study", IEE International Conference – PEVD'98, London, September, pp. 471-476.

[24] Z. Chen, S. Arnalte Gomez and M. Mc Cormick, "A fuzzy logic controlled power electronic system for variable speed wing wind energy conversion systems", Power Electronics and Variable Speed Drives, 18-19 September 2000, Conference Publication No. 475, IEE 2000, pp. 114-119.

[25] Rajib Datta and V.T. Ranganathan, "Direct Power Control of Grid-Connected Wound Rotor Induction Machine without Rotor Position Sensors", IEEE Transactions on Power Electronics, vol. 16, no. 3, May 2001, pp. 390-399.

[26] W. Deleroi, J.B. Woudstra, "Connecting an asynchronous generator on the grid using a thyristor switch", IEEE Transactions on Industry Application, vol. 2, March 1991, pp. 55-60.

[27] W. Deleroi, J.B. Woudstra and A.A. Fahim, "Analysis of thyristor controlled three-phase induction motor with alternation of symmetrical and unsymmetrical operation", EM&PS, vol. 16, 1989, pp. 59-76.

[28] K.Delaere, K.Hameyer, R.Belmans, "Static eccentricity as a cause for audible noise of induction motors", *ICEM September 2-4, 1998, Vol. 1, pp. 502-506.*

[29] Xiaolan Deng, "Detection of rotor faults on induction motors by investigating the flux linkage of the stator winding", Ph.D. Thesis, December 1994, I 1494S0076.

[30] - DiGSILENT Power Factory user manuals, *DiGSILENT GmbH, Germany.*

[31] D.G.Dorrell, W.T.Thomson, and S.Roach, "Analysis of air-gap flux, current, and vibration signals as a function of the combination of static and dynamic air-gap eccentricity in 3-phase induction motors", IEEE Trans. On IA, Vol. 33, nr. 1,1997, pp. 24-34.

[32] N.M.Elkasabgy, A.R.Eastham, G.E.Dawson, "Detection of broken bars in the cage rotor on an induction machine", IEEE Trans. Ind. Applns, vol. IA-22, no. 6, pp. 165-171, Jan./Feb. 1972.

[33] - http://www.eren.doe.gov/wind/feature.html, Wind Energy Program-How Do Wind Turbines Work?, US Department of Energy.

[34] D.G. Edwards, "On-line diagnosis of defects in the stator winding insulation structures of high voltage rotating machines", ICEM'92, Manchester, UK (15-17 September, Vol. 3, pp. 1299-1303.

[35] M. Fenger, G.C. Stone and B.A. Lloyd, "Experience with continuous partial discharge monitoring of stator windings", Electrical Insulation Conference and Electrical Manufacturing & Coil Winding Conference, 2001, pp. 417-421.

[36] F. Filippetti, G.Franceschini, G.Gentile, S.Meo, A.Ometto, N.Rotondale, C.Tassoni, "Current pattern analysis to detect induction machine non rotational anomalies", ICEM 98, International Conference on Electrical Machines, September 2-4, 1998, Istambul-Turkey, Vol. 1, pp. 448-453.

[37] F.Filippetti, G.Franceschini, C.Tassoni and P.Vas, "Recent Developments of Induction Motor Drives Fault diagnosis Using AI Techniques", IEEE Transactions on Industrial Electronics, vol.47, no.5, pp.994-1004. October 2000.

[38] Gene F. Franklin, Powell J. David, Michael L. Workman, "Digital Control Systems", book, Addison Wesley, ISBN 0-201-51884-8, 1990.

[39] A. W. Galli et al., "Exploring the power of wavelet analysis," IEEE Comput. Appl. Power, vol. 9, pp. 37–41, Oct. 1996.

[40] Francois Giraud and Ziyad M. Salameh, "Wind-Driven, Variable-Speed, Variable-Frequency, Double-Output, Induction Generators", Electric Machines and Power Systems, vol. 26, 1998, pp. 287-297.

[41] Paul Gipe, "Wind energy comes of age", book, Wiley & Sons Inc., New York, 1995.

[42] Anders Grauers, "Efficiency of three wind energy generator systems", IEEE Transactions on Energy Conversion, Vol. 11, No. 3, September 1996, pp. 650-657.

[43] El Hachemi and Benbouzid, M., "A review of induction motors signature analysis as a medium for faults detection", Industrial Electronics, IEEE Transactions on, Volume: 47 Issue: 5, Oct. 2000, Page(s): 984 –993.

[44] M.Haji, H.A.Toliyat, "Pattern Recognition-A Technique for Induction Machines Rotor Fault Detection Eccentricity and Broken Bar Fault", 36th IAS Annual Meeting, IEEE Ind. 2001, September 30th – October 4th, Chicago, Illinois, USA.

[45] L.H. Hansen, P. Sorensen, U.S. Paulsen, "Variable Speed Wind Turbine using Full Conversion", *Contribution to the NORpie-2000, Aalborg, Denmark*, pp. 115-119, June 13th to 16th, 2000.

[46] L.H. Hansen, L. Helle, F. Blaabjerg, E. Ritchie, S. Munk-Nielsen, H. Bidner, P. Sorensen and B. Bak-Jensen, "Conceptual Survey of Generators and Power Electronics for Wind Turbines", Riso-R-1205 (EN), December 2001.

[47] Anca D. Hansen, Poul Sorensen, L. Janosi and J. Bech, "Wind farm modelling for power quality", *IECON'01: The 27th Annual Conference of the IEEE Industrial Electronics Society*, vol. 3, pp.1959-1964.

[48] Siegfried Heier, "Wind energy conversion systems", book, John Wiley & Sons Inc., New York, 1998.

[49] L. Helle and S. Nielsen, "Comparison of Converter Efficiency in Large Variable Speed Wind Turbines", IEEE Transaction on Power Electronics, Vol. , No. , 2001, pp. 628-634.

[50] L. Huber, D. Borojevic, "Space Vector Modulated Three-Phase to Three-Phase Matrix Converter with Input Power Factor Correction", IEEE Transactions on Industry Applications, Vol. 31, No. 6, November/December 1995, pp. 1234-1247.

[51] Bin Huo and Andrzej M. Trzynadlowski, "Simple stator fault detector for ac motors", Electric Machines and Drives Conference, 2000. IEMDC 2001. IEEE International, 2001,pp. 192-194.

[52] International Wind Energy Development, "World Market Update 1999". *BTM Consults Aps. Ringkobing, Denmark 2000 ISBN 87-987788-0-3.*

[53] I.J.Kemp, H.Zhu, H.G.Sedding, J.W.Wood, W.K.Hogg, "Towards a new partial discharge calibration strategy based on the transfer function of machine stator windings", IEE Proc. – Sci. Meas. Technol., Vol. 143, No. 1, January 1996, pp. 57-62.

[54] G.B.Kliman, J.Stein and R.D.Endicott, "Non-invasive detection of broken rotor bars in operating induction motors", IEEE Transactions Energy Conversion, vol. 3, no. 4, December 1988, pp. 873-879.

[55] G.B.Kliman, W.J.Premerlani, B.Yazici, R.A.Koegl and J.Mazereeuw, "Sensorless Online Motor Diagnostics", IEEE Computer Applications in Power, April 1997, pp. 39-43.

[56] G.B.Kliman, W.J.Premerlani, R.A.Koegl and D.Hoeweler, "A new approach to online fault detection in ac motors", IEEE-IAS Annual Meeting Conference, pp. 687-693, San Diego, CA, 1996.

[57] J.L.Koher, J.Sottile and F.C.Trutt, "Condition based maintenance of electrical machines", IEEE 1999, pp. 205-211.

[58] Paul C. Krause, "Analysis of Electric Machinery", Mc Graw-Hill Book Company, 1986.

[59] Paul C. Krause, "Analysis of Electric Machinery", 1995 IEEE Press, ISBN 0-7803-1101-9, 1995.

[60] S.F. Legowski, A.H.M. Sadrul Ula and A.M. Trzynadlowski, "Instantaneous power as a medium for the signature analysis of induction motors", IEEE Transactions on Industry Applications, Vol. 32, no. 4, July/August 1996, pp. 904-909.

[61] S.F. Legowski, A.H.M. Sadrul Ula and A.M. Trzynadlowski, "Instantaneous stator power as a medium for the signature analysis of induction motors", Industry Applications Conference, 1995.Thirtieth IAS Annual Meeting, Vol. 1, pp. 619-624.

[62] P. Madsen and J. Rasmussen, "Rotor loading on a three-bladed wind turbine", European Wind Energy Conference, Glasgow EWEC, 1989.

[63] Jakob Mann, "Wind field simulation", Prob. Eng. Mech., Vol. 13, no. 4, Elsevier 1998.

[64] **Lucian Mihet-Popa**, F. Blaabjerg and I. Boldea, "Simulation of Wind Generator Systems for the Power Grid", Record of OPTIM 2002, vol. 2, pp. 423-428, 16-18 May, 2002.

[65] **Lucian Mihet-Popa**, F. Blaabjerg and I. Boldea, "Wind Turbine Generator Modeling and Simulation where Rotational Speed is the Controlled Variable", paper accepted to be publish in IEEE Transactions on Energy Conversion, January / February 2004.

[66] **Lucian Mihet-Popa**, "Condition Monitoring of Wind Generators", Internal report, Institute of Energy Technology, Aalborg University, Denmark, 2002.

[67] **Lucian Mihet-Popa**, Birgitte-Bak Jensen, Ewen Ritchie and Ion Boldea, "Condition Monitoring of Wind Generators", Record of IEEE-IAS 38th Annual Meeting, 2003, 12-16 October.

[68] **Lucian Mihet-Popa**, *Birgitte-Bak Jensen, Ewen Ritchie and Ion Boldea*, "*Current Signature Analysis to* Diagnose Incipient Faults in Wind Generator Systems", ELECTROMOTION 2003, 26-28 November.

[69] **Lucian Mihet-Popa** and Ion Boldea, "Variable speed electric generators for the distributed power systems of the future?", *Paper accepted to be publish in EMPS 2002*;

[70] A. Miller, E. Muljadi and D.S. Zinger, "A variable speed wind turbine power control", IEEE/PESC Summer Meeting, Denver-CO, July 1996.

[71] A. Miller, E. Muljadi, D.S. Zinger, "A Variable Speed Wind Turbine Control", *IEEE Trans. on Energy Conversion*, vol.12, no 2, June 1997, pp. 181-186.

[72] N.Mohan, T.M.Undeland, W.P.Robbins, "Power electronics: Converters, Applications and Design", John Wiley & Sons, 1996.

[73] S. Mpekos, E. Tsimplostephanakis, E. Tatakis and A. Safacas, "Control technique for a variable speed WECS using a synchronous generator", ICEM 2000, 28-30 August, Espoo-Finland, pp. 1092-1096.

[74] S. Muller, M. Deicke and Rik W. De Doncker, "Doubly Fed Induction Generator Systems for Wind Turbines", IEEE Industry Applications Magazine, May-June 2002, pp. 26-33.

[75] E. Muljadi, P.C. Butterfield, "Pitch controlled variable-speed wind turbine generator", *Industry Applications Conference, 1999. IAS Annual Meeting. Conference Record*, Vol. 1, pp. 323 – 330.

[76] www.NREL.gov, National Renewable Energy Lab.

[77] A.S. Neris, N.A. Vovos and G.B. Giannakopoulos, "A variable speed wind energy conversion scheme for connection to weak ac systems", IEEE Transactions on Energy Conversion, Vol. 14, No. 1, March 1999, pp. 122-127.

[78] S.Nandi and H.A.Toliyat, "Fault Diagnosis of Electrical Machines – A Review", IEEE Industry Applications Conference, 1999. Thirty-Fourth IAS Annual Meeting. Vol. 1, 1999, pp. 197-204.

[79] S.Nandi, S.Ahmed, H.A.Toliyat, R.Bharadwaj, "Selection criteria of induction machines for speed-sensorless drive applications", 36th IAS Annual Meeting, IEEE Ind. 2001, September 30th – October 4th, Chicago, Illinois, USA.

[80] S. Nandi and H.A. Toliyat, "Novel frequency domain based technique to detect incipient stator inter-turn faults in induction machines", Industry Applications Conference, 2000. Conference Record of the 2000 IEEE, Vol. 1, pp. 367-374.

[81] Katsuhiko Ogata, "Modern Control Engineering", 1995, Prentice Hall, ISBN 981-3026-94-4.

[82] V. De Oliveira, E. Monmasson, R. Meuret, J.P. Louis, "Steady State Analysis of a Double Fed Induction Generator for Aircraft Application", Electromotion 2001, June 19-20, pp. 547-551.

[83] R.Ong, J.H.Dymond and R.D.Findlay, "Bearing damage analysis in a large oil-ring-lubricated induction machine", IEEE Transactions on Industrial Electronics, vol. 47, no. 5, October 2000.

[84] C.M. Ong, „Dynamic Simulation of Electrical Machinery using MatLab/SimuLink", Prentice Hall, 1998.

[85] D. Panda, Eric L. Benedict, G. Venkataramanan and Thomas A. Lipo, "A novel Control Strategy for the Rotor Side Control of a Doubly-Fed Induction Machine", IEEE Transactions on Power Electronics, 2001.

[86] S.A. Papathanassious, M.P.Papadopoulus, "Dynamic Behaviour of Variable Speed Wind Turbines under Stochastic Wind", *IEEE Trans. on Energy Conversion*, vol. 14, no.4 1999, pp. 1617-1623.

[87] R. Pena, R. Cardenas, R. Blasco, G. Asher, J. Clare, "A Cage Induction Generator using back-to-back PWM Converters for Variable Speed Grid Connected Wind Energy System", Proceedings of IECON'01, pp. 1376-1381.

[88] R. Pena, J.C. Clare, G.M. Asher, "Doubly Fed Induction Generator using Back-to-Back PWM Converters and its Application to Variable Speed Wind Energy Generation", 1996, IEE Proceedings on Electrical Power Applications, vol. 143, no. 3, pp. 231-241.

[89] R. Pena, J.C. Clare, G.M. Asher, "A doubly fed induction generator using back-to-back PWM converters supplying an isolated load from a variable speed wind turbine", IEE Proc.-Electr. Power Appl., vol. 143, no. 5, September 1996, pp. 380-387.

[90] J.Penman, H.G.Sedding, B.A.Lloyd, W.T.Fink, "Detection and location of interturn short circuits in the stator windings of operating motors", IEEE Trans. Energy Conv., Vol. 9, no. 4, Dec. 1994,pp. 652-658.

[91] Saifur Rahman, "Green Power. What is it and where can we find it?", IEEE power & energy magazine, January/February 2003, pp. 30-37.

[92] B. Robyns, M. Nasser, F. Berthereau, F. Labrique, "Equivalent Continuous Dynamic Model of a Variable Speed Wind Generator", Electromotion 2001, June 19-20, pp. 541-546.

[93] C. Rombaut, G. Seguier and R. Bausiere, "Power Electronic Converters", McGraw-Hill Book Company, vol. 2 AC-AC Conversion, 1987.

[94] P.A.C. Rosas, P. Sorensen and H. Bindner, "Fast wind modelling of wind turbines". *Special topic conference. Wind power for the 21st Century.* Kassel, Germany, September 2000.

[95] Randy R.Schoen and Thomas G.Habetler, "Effects of time-varying loads on rotor fault detection in induction machines", IEEE Transactions on Industry Applications, vol. 31, no. 4, July/August 1995,pp. 900-906.

[96] Randy R.Schoen and Thomas G.Habetler, "Evaluation and implementation of a system to eliminate arbitrary load effects in current-based monitoring of induction machines", IEEE Transactions on Industry Applications, vol. 33, no. 6, November/December 1997,pp. 1571-1577.

[97] I. Schiemenz and M. Stiebler, "Maximum power point tracking of a wind energy system with a permanent-magnet synchronous generator", ICEM 2000, 28-30 August, Espoo-Finland, pp. 1083-1086.

[98] Dejan Schreiber, "Applied Designs of Variable Speed Wind Turbines and New Approaches", PCIM 2002.

[99] G. Seguier, *Power Electronic Converters-AC/DC Conversion*, New York; McGraw-Hill, 1986.

[100] J.G. Slootweg., S. W. H De Haan., H. Polinder, and W.L. Kling, "Voltage Control Methods with Grid Connected Wind Turbines: a tutorial review", *Wind Engineering*, Vol. 25, no. 6, 2001, pp. 353-365

[101] J.G Slootweg, and W.L. Kling, "Modelling and Analysing Impacts of Wind Power on Transient Stability of Power Systems", *Wind Engineering*, Vol. 26, no. 1, 2002, pp. 3-20.

[102] Robin Smith, "Monitoring for Rotor Shorted Turns", Siemens Power Generation Limited Newcastle upon Tyne, 1990, pp. 8/1-8/20.

[103] J.Sottile, F.C.Trutt and J.L.Koher, "Experimental investigation of on-line methods for incipient fault detection", IEEE 2000, pp. 2682-2687.

[104] R. Spee, S. Bhowmik and J.H.R. Eslin, "Adaptive control strategies for variable speed doubly-fed wind power generation systems", Proc. IEEE-IAS Annual Meeting, 1995, pp. 545-552.

[105] A.Stavrou, J.Penman, "Modelling dynamic eccentricity in smooth air-gap induction machines", IEEE 2001,pp. 864-871.

[106] A.Stavrou and J.Penman, "The on-line quantification of air-gap eccentricity in induction machines", Proc. International Conference on Electrical Machines '94 Paris, France, 5-8 Sept. 1994, pp. 261-266.

[107] J. Sottile and J.L. Kohler, "An on-line method to detect incipient failure of turn insulation in random-wound motors", IEEE Transactions on Energy Conversion, vol. 8, no. 4, December 1993,pp. 762-768.

[108] A. A. Da Silva et al., "Rotating machinery monitoring and diagnosis using short-time Fourier transform and wavelet techniques," in Proc. 1997 Int. Conf. Maintenance and Reliability, vol. 1, Knoxville, TN, pp. 14.01–14.15.

[109] A. Tapia, G. Tapia, J.X. Ostolaza, J.R. Saenz and J.L. Berasategui, "Reactive Power Control of a Wind Farm made up with Doubly Fed Induction Generators", Paper accepted for presentation at PPT (Porto Power Tech Conference)-IEEE 2001, 10th - 13th September, Porto-Portugal.

[110] Paul Thogersen and John K. Pederesen, "Stator Flux Oriented Asynchronous Vector Modulation for AC-Drives", IEEE Transaction on Industry Application, 1990, pp. 641-648.

[111] W.T.Thomson, M.Fenger, "Industrial application of current signature analysis to diagnose fault in 3-phase squirrel cage induction motors", IEEE 2000.

[112] W.T.Thomson, "On-line current monitoring to detect electrical and mechanical faults in three-phase induction motor drives", Proc. IEE and IMECHE (London), Int. Conf. Proc on Life Management of Power Plants, Heriot-Watt University, Edinburgh, 12-14 December 1994, pp. 66-73.

[113] W.T.Thomson and I.D.Stewart, "On-line current monitoring for fault diagnosis in inverter fed induction motors", In 3rd International Conference on Power Electronics and Variable Sped Drives, 1998, pp. 432-435.

[114] William T.Thomson, "On-line MCSA to diagnose shorted turns in low voltage stator windings of 3-phase induction motors prior to failure", Electric Machines and Drives Conference, 2000. IEMDC 2001. IEEE International, 2001, pp. 891-898.

[115] W.T.Thomson, D.Rankin, D.G.Dorrell, "On-line current monitoring to diagnose air-gap eccentricity in large three-phase induction motors-industrial case histories verify the predictions", IEEE Transactions on Energy Conversion, vol. 14, no. 4, December 1999, pp. 1372-1378.

[116] W.T.Thomson and A.Barbour, "The on-line prediction of air-gap eccentricity levels in large (MW Range) 3-phase induction motors", Electric Machines and Drives, International Conference IEMD, 1999, pp. 383-385.

[117] Torbjorn Thiringer and Jan Linders, "Control by Variable Rotor Speed of a Fixed-Pitch Wind Turbine Operating in a Wide Speed Range", IEEE Transactions on Energy Conversion, Vol. 8, No. 3, September 1993, pp. 520-526.

[118] Torbjorn Thiringer, "Grid-Friendly Connecting of Constant-Speed Wind Turbines Using External Resistors", IEEE Transactions on Energy Conversion, vol. 17, no. 4, pp. 537-542. December, 2002.

[119] S. Tnami, S. Diop and A. Berthon. "Novel control strategy of doubly-fed induction machines", EPE, 1995, pp. 553-558.

[120] W.T.Thomson and M.Fenger, "Current Signature Analysis to Detect Induction Motor Faults", IEEE Industry Applications Magazine, pp. 26-34, July/August 2001.

[121] H.A.Toliyat, T.A.Lipo, "Transient Analysis of Cage Induction Machines under Stator, Rotor Bar and End Ring Faults", IEEE Trans. On Energy Conv., Vol. 9, No. 4, June 1995.

[122] Torbjorn Thiringer, Jan Linders, "Control by variable rotor speed of a fixed-pitch wind turbine operating in a wide speed range", IEEE Transactions on Energy Conversion, September 1993, vol. 8, no. 3, pp. 520-526.

[123] H.A Tolyiat, M.S. Arefeen, A.G. Parlos "A method for dynamic simulation of air-gap eccentricity in induction machines", IEEE-Trans. Ind. Applns., pp. 910-918, vol. 32, no.4, July/Aug., 1996.

[124] H.A Tolyiat, A. Al-Nuaim, "A novel method for modelling dynamic air-gap eccentricity in synchronous machines based on modified winding function theory", IEEE-PES Summer Meeting, July 1997.

[125] Andrzej M. Trzynadlowski and Ewen Ritchie, "Comparative investigation of diagnostic media for induction motors: a case of rotor cage faults", IEEE Transactions on industrial electronics, vol. 47, no. 5, October 2000, pp. 1092-1099.

[126] Andrzej M. Trzynadlowski and Ewen Ritchie, "Comparative investigation of diagnostic media for induction motors: a case of rotor cage faults", Industry Applications Conference, 1999.Thirty-Fourth IAS Annual Meeting. Conference Record of 1999 IEEE, vol. 3, pp. 1935-1941.

[127] F.C. Trutt, J. Sottile and J.L. Kohler, "On-line monitoring of induction motors", Industry Applications Conference, 2001. Thirty-Sixth IAS Annual Meeting. Conference Record of the 2001 IEEE, Volume: 2, 2001, Page(s): 1369 -1375.

[128] P. Vas, "Sensorless vector and direct torque control", book, Oxford University Press, 1998.

[129] P. Vas, "Vector Control of a.c. machines", book, Oxford University Press, 1990.

[130] P.Vas, "Parameter Estimation, Condition Monitoring, and Diagnosis of Electrical Machines", Clarendon Press, Oxford, 1993.

[131] www.vestas.com, Vestas Wind Systems, Denmark.

[132] Vestas, OptiSpeed, Vestas Converter System, General Edition, Item. No. 947543.RO-Class 1, 3rd January 2001.

[133] A.K. Wallace and J.A. Oliver, "Variable-speed generation controlled by passive elements", International conference on electric machines, 1998, Istanbul, pp. 1554-1559.

[134] Alan Wallace and Tobias Bathon, "Dynamic operation of passively controlled variable-speed generation system", IEE Ninth International Conference on Electrical Machines and Drives, Conference Publication, No. 468, 1999, pp. 54-59.

[135] Q. Wang and L. Chang, "An Independent Maximum Power Extraction Strategy for Wind Energy Conversion Systems", Proceedings of the 1999 IEEE Canadian Conference on Electrical and Computer Engineering Shaw Conference Center, Edmonton-Alberta, Canada, May 9-12, 1999, pp.1142-1147.

[136] W. J. Wang et al., "Application of wavelets to gearbox vibration signals for fault detection," J. Sound Vib, vol. 192, no. 5, pp. 927–939, 1996.

[137] S.Williamson and P.Mirzoian, "Analysis of cage induction motor with stator winding faults", IEEE-PES, Summer Meeting, July 1994.

[138] www.windpower.org, Danish Wind Industry Associations, Guided Tour on Wind Energy.

[139] www.windpower.org/tour/wres/eurspeed.html, Guided Tour on Wind Energy, Danish Wind Industry Association.

[140] Li Yonggang, Li Heming, Zhu Ling and Zhao Hua, "Inter turn short-circuit fault research on generator rotor windings", ICEMS'2001, Proceedings of the fifth International Conference on Electrical Machines and Systems, August 18-20, Shenyang-China, Vol. 1 pp. 357-361.

[141] D.S. Zinger, E. Muljadi, "Annualized wind energy improvement using variable speeds", Industrial & Commercial Power Systems technical Conference, 1997. Conference Records, Papers presented at the 1997 Annual Meeting, IEEE 1997, 11-16 May 1997, pp. 80-83.

[142] Donald S. Zinger and Eduard Muljadi, "Annualized Wind Energy Improvement using Variable Speeds", IEEE Transactions on Industry Applications, Vol. 33, No. 6, November/December 1997, pp. 1444-1447.

[143] D.S. Zinger, E. Muljadi and A. Miller, "A simple control scheme for variable speed wind turbines", IEEE-IAS Annual Meeting, October 1996, pp. 1613-1618.